VOLUME 76 DECEMBER 21, 1972 NUMBER 26

JPCHA x

THE JOURNAL OF PHYSICAL CHEMISTRY

PUBLISHED BIWEEKLY BY THE AMERICAN CHEMICAL SOCIETY

THE JOURNAL OF
PHYSICAL CHEMISTRY

BRYCE CRAWFORD, Jr., *Editor*
STEPHEN PRAGER, *Associate Editor*
ROBERT W. CARR, Jr., FREDERIC A. VAN-CATLEDGE, *Assistant Editors*

EDITORIAL BOARD: A. O. ALLEN (1970–1974), J. R. BOLTON (1971–1975),
F. S. DAINTON (1972–1976), M. FIXMAN (1970–1974),
H. S. FRANK (1970–1974), R. R. HENTZ (1972–1976), J. R. HUIZENGA (1969–1973),
W. J. KAUZMANN (1969–1973), R. L. KAY (1972–1976), W. R. KRIGBAUM (1969–1973),
R. A. MARCUS (1968–1972), W. J. MOORE (1969–1973), J. A. POPLE (1971–1975),
B. S. RABINOVITCH (1971–1975), H. REISS (1970–1974), S. A. RICE (1969–1975),
F. S. ROWLAND (1968–1972), R. L. SCOTT (1968–1972),
R. SEIFERT (1968–1972), W. A. ZISMAN (1972–1976)

CHARLES R. BERTSCH, *Manager, Editorial Production*

AMERICAN CHEMICAL SOCIETY, *1155 Sixteenth St., N.W., Washington, D. C. 20036*

Books and Journals Division
JOHN K CRUM, *Director*
JOSEPH H. KUNEY, *Head, Business Operations Department*
RUTH REYNARD, *Assistant to the Director*

©Copyright, 1972, by the American Chemical Society. Published biweekly by the American Chemical Society at 20th and Northampton Sts., Easton, Pa. 18042. Second-class postage paid at Washington, D. C., and at additional mailing offices.

All manuscripts should be sent to *The Journal of Physical Chemistry,* Department of Chemistry, University of Minnesota, Minneapolis, Minn. 55455.

Additions and Corrections are published once yearly in the final issue. See Volume 75, Number 26 for the proper form.

Extensive or unusual alterations in an article after it has been set in type are made at the author's expense, and it is understood that by requesting such alterations the author agrees to defray the cost thereof.

The American Chemical Society and the Editor of *The Journal of Physical Chemistry* assume no responsibility for the statements and opinions advanced by contributors.

Correspondence regarding accepted copy, proofs, and reprints should be directed to Editorial Production Office, American Chemical Society, 20th and Northampton Sts., Easton, Pa. 18042. Manager: Charles R. Bertsch. Assistant Editor: Edward A. Borger. Editorial Assistant: Joseph E. Yurvati.

Advertising Office: Centcom, Ltd. (formerly Century Communications Corporation), 142 East Avenue, Norwalk, Conn. 06851.

Business and Subscription Information

Remittances and orders for subscriptions and for single copies, notices of changes of address and new professional connections, and claims for missing numbers should be sent to the Subscription Service Department, American Chemical Society, 1155 Sixteenth St., N.W., Washington, D. C. 20036. Allow 4 weeks for changes of address. Please include an old address label with the notification.

Claims for missing numbers will not be allowed (1) if received more than sixty days from date of issue, (2) if loss was due to failure of notice of change of address to be received before the date specified in the preceding paragraph, or (3) if the reason for the claim is "missing from files."

Subscription rates (1972): members of the American Chemical Society, $20.00 for 1 year; to nonmembers, $60.00 for 1 year. Those interested in becoming members should write to the Admissions Department, American Chemical Society, 1155 Sixteenth St., N.W., Washington, D. C. 20036. Postage to Canada and countries in the Pan-American Union, $5.00; all other countries, $6.00. Single copies for current year: $3.00. Rates for back issues from Volume 56 to date are available from the Special Issues Sales Department, 1155 Sixteenth St., N.W., Washington, D. C. 20036.

This publication and the other ACS periodical publications are now available on microfilm. For information write to: MICROFILM, Special Issues Sales Department, 1155 Sixteenth St., N.W., Washington, D. C. 20036.

Notice to Authors last printed in the issue of November 23, 1972

THE JOURNAL OF
PHYSICAL CHEMISTRY

Volume 76, Number 26 December 21, 1972

JPCHAx 76(26) 3911–4042 (1972)

Rate Constants for the Reactions of Deuterium Atoms with Silanes . . . **K. Obi, H. S. Sandhu, H. E. Gunning, and O. P. Strausz*** 3911

Chemical Ionization Mass Spectrometry. XVII. Effect of Pressure on the Decomposition of Protonated *tert*-Amyl Acetate . . . **W. A. Laurie and F. H. Field*** 3917

Ion–Molecule Reactions in Ethane . . . **S. L. Bennett, S. G. Lias, and F. H. Field*** 3919

Kinetics and Mechanism of Decafluorobenzophenone Photochemical Reactions in Cyclohexane, Benzene, and Alkyl Aromatics . . . **Jonas Dedinas* and T. H. Regan** 3926

Sensitization and Quenching of the Cis → Trans Isomerization of Bis(glycinato)platinum(II) . . . **Fabrizio Bolletta, Mario Gleria, and Vincenzo Balzani*** 3934

Triplet ← Triplet Absorption and Intersystem Crossing in Phthalazine . . . **Vernon L. Alvarez and Steven G. Hadley*** 3937

Mechanism of Hydrogen–Deuterium Exchange of Propylene over a Brønsted Zeolite Catalyst . . . **Z. M. George and H. W. Habgood*** 3940

Electron Spin Resonance Studies of Dialkoxydialkylbenzenes. Evidence for Some Unusual Rearrangements in Sulfuric Acid . . . **Paul D. Sullivan** 3943

An Electron Spin Resonance Investigation of the Reactions in Irradiated Aqueous Solutions of Hydrogen Cyanide and Cyanide Ion . . . **D. Behar and Richard W. Fessenden*** 3945

Electron Paramagnetic Resonance Line Widths of Vanadyl(IV) α-Hydroxycarboxylates . . . **N. Dennis Chasteen and Melvin W. Hanna*** 3951

An Electron Spin Resonance Study of the Geometry of 9-Phenylacridine . . . **Ann Lomax, L. S. Marcoux, and A. J. Bard*** 3958

Electronic and Electron Spin Resonance Spectra of the Anion Radicals of Phenyl- and Diphenylethylenes . **A. Gamba, V. Malatesta, G. Morosi, and M. Simonetta*** 3960

Infrared Spectra of S_4 . . . **B. Meyer* and T. Stroyer-Hansen** 3968

Hypochromism and Exciton Interaction in Halofluorescein Dyes . . . **K. K. Rohatgi* and A. K. Mukhopadhyay** 3970

Tetracyanomethane. X-Ray Diffraction and Differential Scanning Calorimetry Study from −150 to +160° . . . **Kerry Rubin and Reuben Rudman*** 3973

High-Resolution X-Ray Emission Study of Central Atom–Ligand Bonding in Phosphorus Oxy Anions . . . **K. Myers and G. Andermann*** 3975

Fluorescence and Absorption Spectra of Polyphenyls. Theoretical Study on the Band Shape . . . **Fabio Momicchioli,* Maria C. Bruni, and Ivan Baraldi** 3983

Charge-Transfer Properties of the Hydrogen Bond. II. Charge-Transfer Theory and the Relation between the Enhancement of Dipole Moment and the Ionization Potential of Hydrogen-Bonded Systems . . . **Henryk Ratajczak** 3991

First-Order Perturbation Theory in the LCAO Approximation. The Case of an Ionic Crystal in a Magnetic Field . . . **T. Vladimiroff** 3993

Ion Transport through Layered Ion Exchange Membranes . . . **Ain A. Sonin* and Gershon Grossman** 3996

Factors Influencing Reverse Osmosis Rejection of Organic Solutes from Aqueous Solution . . . **J. E. Anderson,* S. J. Hoffman, and C. R. Peters** 4006

Specific Interactions of Anilines with Water . . . **A. Gomez, J. Mullens, and P. Huyskens*** 4011

Electrokinetic Salt Rejection in Hyperfiltration through Porous Materials. Theory and Experiment . . . **G. Jacazio, R. F. Probstein,* A. A. Sonin, and D. Yung** 4015

Kinetics of Acid Dissociation–Ion Recombination of Aqueous Methyl Orange . . . **Richard G. Sandberg, Gary H. Henderson, Robert D. White, and Edward M. Eyring*** 4023

Equilibrium Sedimentation Studies of the Aggregation of Methylene Blue . **Emory H. Braswell** 4026

Influence of a Hard-Sphere Solute on Water Structure . . . **Michel Lucas** 4030

Solutions of *N*-Substituted Amino Acids. IV. Tautomerism in *N,N*-Di-*n*-butyl-α-, β-, and γ-amino Acids . . . **Joseph W.-O. Tam and Charles P. Nash*** 4033

Molecular Movements and Phase Transitions in Solids. Tetrakis(trimethylsilyl)methane . . . **J. M. Dereppe and J. H. Magill*** 4037

Additions and Corrections . . . 4040

Author Index for Volume 76, 1972 . . . 1A

Keyword Index for Volume 76, 1972 . . . 1K

AUTHOR INDEX

Alvarez, V. L., 3937
Andermann, G., 3975
Anderson, J. E., 4006

Balzani, V., 3934
Baraldi, I., 3983
Bard, A. J., 3958
Behar, D., 3945
Bennett, S. L., 3919
Bolletta, F., 3934
Braswell, E. H., 4026
Bruni, M. C., 3983

Chasteen, N. D., 3951

Dedinas, J., 3926
Dereppe, J. M., 4037

Eyring, E. M., 4023

Fessenden, R. W., 3945
Field, F. H., 3917, 3919

Gamba, A., 3960
George, Z. M., 3940
Gleria, M., 3934
Gomez, A., 4011
Grossman, G., 3996
Gunning, H. E., 3911

Habgood, H. W., 3940
Hadley, S. G., 3937
Hanna, M. W., 3951
Henderson, G. H., 4023
Hoffman, S. J., 4006
Huyskens, P., 4011

Jacazio, G., 4015

Laurie, W. A., 3917
Lias, S. G., 3919
Lomax, A., 3958
Lucas, M., 4030

Magill, J. H., 4037
Malatesta, V., 3960
Marcoux, L. S., 3958
Meyer, B., 3968
Momicchioli, F., 3983
Morosi, G., 3960
Mukhopadhyay, A. K., 3970
Mullens, J., 4011
Myers, K., 3975

Nash, C. P., 4033

Obi, K., 3911

Peters, C. R., 4006
Probstein, R. F., 4015

Ratajczak, H., 3991
Regan, T. H., 3926
Rohatgi, K. K., 3970
Rubin, K., 3973
Rudman, R., 3973

Sandberg, R. G., 4023
Sandhu, H. S., 3911
Simonetta, M., 3960
Sonin, A. A., 3996, 4015
Strausz, O. P., 3911
Stroyer-Hansen, T., 3968
Sullivan, P. D., 3943

Tam, J. W.-O., 4033

Vladimiroff, T., 3993

White, R. D., 4023

Yung, D., 4015

In papers with more than one author the name of the author to whom inquiries about the paper should be addressed is marked with an asterisk in the by-line.

THE JOURNAL OF
PHYSICAL CHEMISTRY

Registered in U. S. Patent Office © Copyright, 1972, by the American Chemical Society

VOLUME 76, NUMBER 26 DECEMBER 21, 1972

Rate Constants for the Reactions of Deuterium Atoms with Silanes

K. Obi, H. S. Sandhu, H. E. Gunning, and O. P. Strausz*

Department of Chemistry, University of Alberta, Edmonton, Alberta, Canada (Received June 26, 1972)

Publication costs assisted by the National Research Council of Canada

The absolute rate constants for the abstraction reactions of deuterium atoms, produced by the photolysis of C_2D_4 with SiH_4, Si_2H_6, CH_3SiH_3, $(CH_3)_2SiH_2$, and $(CH_3)_3SiH$, have been determined at room temperature in competition with addition to ethylene. Silanes are more reactive than their hydrocarbon counterparts and the reactivities have the same order of magnitude as ethylene. The reactivity per Si–H bond is in the order $Si_2H_6 > (CH_3)_3SiH > (CH_3)_2SiH_2 > CH_3SiH_3 > SiH_4$. Potential energies of activation of these reactions have been computed using a modified BEBO method.

Introduction

Quantitative kinetic data for the gas-phase hydrogen atom transfer reactions of alkyl radicals with a variety of silicon compounds have become available during the past 5 years.[1-18] In general, these reactions proceed at much faster rates than those with carbon analogs and the increased reactivity has been shown to be due to lower activation energy requirements, the *A* factors being essentially identical. Quantitative data involving H atoms, however, are still sparse and are restricted to a study of the H plus $(CH_3)_3SiH$[16] and H plus SiH_4[17] systems.

It has been shown recently from this laboratory[19] that the hydrogen atoms produced in the mercury photosensitization of disilane undergo a displacement type reaction with the substrate to give SiH_4 and SiH_3, parallel to the more common abstraction reaction producing H_2 and Si_2H_5. The rates of these two processes are comparable at room temperature. No such displacement reaction has been observed with methylated silanes.[20,21]

In previous publications[5-8] from this laboratory Arrhenius parameters and kinetic isotope effects have been reported for the reactions of alkyl radicals with monosilane, disilane, and methyl- and phenyl-substituted silanes which were compared to theoretical values derived on the basis of transition state theory. The present article reports the rate constants of the reactions of D atoms with monosilane, disilane, and methyl-substituted silanes.

Experimental Section

A conventional cylindrical quartz reaction cell, 35 mm × 140 mm and 168 cc volume, was attached to a grease-free high-vacuum system. The quartz iodine lamp,[22] filled with *ca.* 10 Torr of Ne and excess iodine crystals, was dis-

---

[1] J. A. Kerr, D. H. Slater, and J. C. Young, *J. Chem. Soc. A*, 104 (1966).
[2] J. A. Kerr, D. H. Slater, and J. C. Young, *J. Chem. Soc. A*, 134 (1967).
[3] T. N. Bell and B. B. Johnson, *Aust. J. Chem.*, **20**, 1545 (1967).
[4] W. J. Cheng and M. Szwarc, *J. Phys. Chem.*, **72**, 494 (1968).
[5] O. P. Strausz, E. Jakubowski, H. S. Sandhu, and H. E. Gunning, *J. Chem. Phys.*, **51**, 552 (1969).
[6] E. Jakubowski, H. S. Sandhu, H. E. Gunning, and O. P. Strausz, *J. Chem. Phys.*, **52**, 4242 (1970).
[7] R. E. Berkley, Ph.D. Thesis, University of Alberta, Edmonton, Canada, 1970; R. E. Berkley, I. Safarik, H. E. Gunning, and O. P. Strausz, to be submitted for publication.
[8] I. Safarik, R. E. Berkley, and O. P. Strausz, *J. Chem. Phys.*, **54**, 1919 (1971).
[9] E. R. Morris and J. C. J. Thynne, *J. Phys. Chem.*, **73**, 3294 (1969).
[10] E. R. Morris and J. C. J. Thynne, *Trans. Faraday Soc.*, **65**, 183 (1970).
[11] A. U. Chaudhry and B. G. Gowenlock, *J. Organometal. Chem.*, **16**, 221 (1969).
[12] J. A. Kerr, A. Stephens, and J. C. Young, *Int. J. Chem. Kinet.*, **1**, 339, 371 (1969).
[13] T. N. Bell and U. F. Zucker, *J. Phys. Chem.*, **74**, 979 (1970); *Can. J. Chem.*, **48**, 1209 (1970).
[14] T. N. Bell and A. E. Platt, *Int. J. Chem. Kinet.*, **2**, 299 (1970); *J. Phys. Chem.*, **75**, 603 (1971).
[15] J. A. Kerr and D. M. Timlin, *Int. J. Chem. Kinet.*, **3**, 1, 69 (1971).
[16] M. A. Contineanu, D. Mihelcic, R. N. Schindler, and P. Potzinger, *Ber. Bunsenges. Phys. Chem.*, **75**, 426 (1971).
[17] G. K. Moortgat, *Diss. Abstr. B*, **31**, 1879 (1970).
[18] H. E. O'Neal, S. Pavlou, T. Lubin, M. A. Ring, and L. Batt, *J. Phys. Chem.*, **75**, 3945 (1971).
[19] T. L. Pollock, H. S. Sandhu, A. Jodhan, and O. P. Strausz, *J. Amer. Chem. Soc.*, in press.
[20] M. A. Nay, G. N. C. Woodall, O. P. Strausz, and H. E. Gunning, *J. Amer. Chem. Soc.*, **87**, 179 (1965).
[21] A. G. Alexander, Ph.D. Thesis, University of Alberta, Edmonton, Canada, 1972; A. G. Alexander, R. W. Fair, and O. P. Strausz, to be submitted for publication; A. G. Alexander and O. P. Strausz, to be submitted for publication.

TABLE I: Product Yields in the Photolysis of Ethylene-d_4 at 25°[a]

$P(C_2D_4)$, Torr	Products, μmol				Material balance
	D_2	C_2D_2	C_2D_6	n-C_4D_{10}	
50	2.94	4.05	0.21	1.37	$C_2D_{4.1}$
50.4	2.86	3.48	0.21	1.26	$C_2D_{4.3}$
50.2	2.89	3.91	0.20	1.37	$C_2D_{4.2}$
50.4[b]	2.84	3.20	0.18	1.10	$C_2D_{4.4}$
50.7[c]	1.23	1.71	0.09	0.59	$C_2D_{4.2}$
10.4[c]	0.60	0.77	0.04	0.29	$C_2D_{4.2}$
50.0[c,d]	0.66	0.72	0.04	0.34	$C_2D_{4.0}$

[a] Exposure time 5 min. [b] 660 Torr of Xe added. [c] Screen filter used. [d] Exposure time 2 min.

charged by a 2450 MHz/sec microwave generator. Constant iodine pressure (40 μ) was maintained by an ice-water bath. Of the nine emission lines between 2062 and 1618 Å the 2062-Å line was the strongest and the shorter wavelength lines were effectively eliminated by keeping the lamp 1 cm away from the cell. Fresh air was flushed through continuously in order to cool the lamp and to remove ozone produced during the irradiation. When Si_2H_6 was present, a screen filter (28% transparency) was used to reduce the light intensity.

Ethylene-d_4 (Merck) was purified by gas chromatography on medium activity silica gel column. Using mass spectrometry it was found that 4.5% ethylene-d_3 was present as an impurity. Monosilane, disilane, methylsilane, and dimethylsilane (Peninsular) were purified by low-temperature distillations. Trimethylsilane (Procurement) was first purified by preparative gas chromatography on a medium activity silica gel column and then subjected to distillation.

Results

The deuterium atoms were generated by the photolysis of C_2D_4. Effective light intensities were calculated from the published relative emission intensities[23] and the extinction coefficient of oxygen[24] assuming the transparency of the reaction cell windows to be independent of wavelength. About 80% of the absorbed radiation was in the 2062–1830-Å region.

The primary and secondary processes occurring in the photolysis of C_2H_4 are reasonably well understood.[25-27] Analogous reactions of C_2D_4 are

$$C_2D_4 + h\nu \rightarrow C_2D_2 + D_2 \qquad (1)$$

$$C_2D_4 + h\nu \rightarrow C_2D_2 + 2D \qquad (2)$$

$$D + C_2D_4 \rightarrow C_2D_5 \qquad (3)$$

$$C_2D_5 + C_2D_5 \rightarrow n\text{-}C_4D_{10} \qquad (4)$$

$$C_2D_5 + C_2D_5 \rightarrow C_2D_6 + C_2D_4 \qquad (5)$$

The importance of primary process 2, relative to 1, increases with increasing photonic energy.[25] The enthalpy change of reaction 2 is ~143 kcal/mol and consequently little excess translational energy can be associated with the D atoms. In addition a concurrent study[21] has shown that excess translational energy up to 35 kcal/mol has no discernible effect on the reaction of H or D atoms with silanes.

The major products of the reaction, D_2, C_2D_2, C_2D_6, and n-C_4D_{10}, and the experimental conditions employed are given in Table I. Their formation can be explained in terms of steps 1-5. In addition, small amounts of 1-butene, n-hexene, and 1-pentane were also detected. These minor products, which could be completely suppressed in the presence of nitric oxide, probably arise from addition reactions of ethyl radicals to the olefins and/or secondary radical reactions of products. They have been neglected in the following kinetic treatments.

The ratio of the primary quantum yields is given by the relation

$$\frac{\phi(1)}{\phi(2)} = \frac{\text{rate}(D_2)}{\text{rate}(n\text{-}C_4D_{10}) + \text{rate}(C_2D_6)}$$

The value of 1.84 ± 0.03, calculated from the data given in Table I, is identical with that determined by Akimoto and Tanaka[27] for C_2H_4 at 1931 Å.

If a silicon compound containing abstractable hydrogen is introduced into the system, the abstraction, displacement, and exchange reactions will compete with the addition step 3.

$$D + \text{silane} \rightarrow HD + \text{silyl radical} \qquad (6)$$

$$D + \text{silane} \rightarrow \text{silane-}d_1 + \text{radical} \qquad (7)$$

$$D + \text{silane} \rightarrow H + \text{silane-}d_1 \qquad (8)$$

Steady-state treatment of reactions 1–3 and 6–8 leads to the following rate expression

$$\frac{\text{rate}(D_2)}{\text{rate}(HD)} = \frac{\phi(1)}{2\phi(2)}\left[1 + \frac{k_7 + k_8}{k_6} + \frac{k_3[C_2D_4]}{k_6[\text{silane}]}\right] \qquad (I)$$

Thus, a plot of the left-hand side of this equation against ethylene-d_4/silane concentration should give a straight line, from the slope of which k_3/k_6 values can be determined. The importance of steps 7 and 8 relative to step 6 can be estimated from the intercept.

Monosilane. The isotopic composition of hydrogen formed in the presence of SiH_4 is shown in Table II. The values have been corrected for the presence of ethylene-d_3 in ethylene-d_4.

Monosilane is transparent to wavelengths longer than 1850 Å;[28] consequently its photolysis is slow and the yield of H_2 is less than 5% of the total hydrogen yield from equimolar concentrations of C_2D_4 and SiH_4. A plot of eq I using the data presented in Table II for SiH_4 is shown in Figure 1. From $\phi(1)/\phi(2)$ and the slope, the ratio of the rate constants for addition reaction 3 to that of abstraction reaction 9

$$D + SiH_4 \rightarrow HD + SiH_3 \qquad (9)$$

k_3/k_9 = 1.88 ± 0.07. From the intercept, an upper limit of less than 0.3 can be obtained for k_{10}/k_9

$$D + SiH_4 \rightarrow H + SiH_3D \qquad (10)$$

and we believe that step 10 does not occur at all.[21]

Disilane. Disilane absorbs strongly up to 2100 Å and can be readily decomposed in this region[29] whereas significant absorption by ethylene occurs only below 1850 Å.[30] In

---

(22) P. Harteck, R. R. Reeves, and B. A. Thompson, *Z. Naturforsh. A*, **19**, 2 (1964).

(23) K. Obi, Ph.D. Thesis, Tokyo Institute of Technology, 1966.

(24) K. Watanabe, E. C. Y. Inn, and M. Zelikoff, *J. Chem. Phys.*, **21**, 1026 (1953).

(25) J. R. McNesby and H. Okabe, *Advan. Photochem.*, **3**, 228 (1964).

(26) R. A. Back and D. W. L. Griffiths, *J. Chem. Phys.*, **46**, 4839 (1967).

(27) H. Akimoto and I. Tanaka, *Z. Electrochem.*, **72**, 134 (1968).

(28) V. R. Scharz and F. Heinrich, *Z. Anorg. Chem.*, **221**, 277 (1935).

(29) T. L. Pollock, H. S. Sandhu, and O. P. Strausz, to be submitted for publication.

(30) R. McDiarmid and E. Charney, *J. Chem. Phys.*, **47**, 1517 (1967).

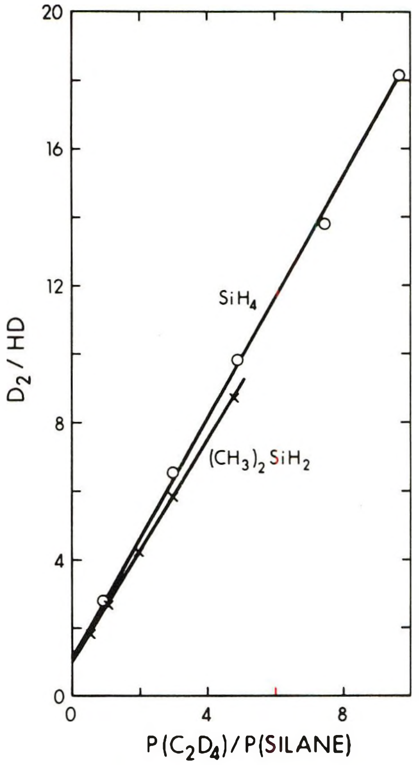

Figure 1. Plot of D_2/HD as a function of $P(C_2D_4)/P$(silane).

TABLE II: Isotopic Composition of Hydrogen Formed in the Photolysis of C_2D_4 in the Presence of SiH_4 at 25°[a]

$P(C_2D_4)$, Torr	$P(SiH_4)$, Torr	Hydrogen, μmol		
		D_2	HD	H_2
50.5	50.7	3.14	1.13	0.14
50.9	17.0	3.20	0.49	0.10
50.0	10.2	3.16	0.32	0.07
51.2	6.9	3.05	0.22	0.05
50.4	5.2	2.91	0.16	0.03

[a] Exposure time 5 min.

TABLE III: Isotopic Composition of Hydrogen Formed in the Photolysis of C_2D_4 in the Presence of Si_2H_6 at 25°[a,b]

$P(C_2D_4)$, Torr	$P(Si_2H_6)$, Torr	Hydrogen, μmol		
		D_2	HD	H_2
50.9	5.2	0.16	0.06	1.34
50.7	2.6	0.35	0.07	1.26
50.7	1.7	0.45	0.06	1.13
50.1	1.3	0.57	0.07	1.10
50.6	0.97	0.63	0.06	0.94

[a] Exposure time 5 min. [b] Screen filter used.

order to reduce absorption by disilane, low disilane concentrations were used and the light intensity was attenuated by a screen filter. The results of isotopic analyses are shown in Table III. It can be seen that disilane is the major absorbing species even at 2% concentrations, since H_2 constitutes 58% of total hydrogen yield. From the plot of D_2/HD as a function of $P(C_2D_4)/P(Si_2H_6)$, shown in Figure 2, the relative rate constant for abstraction reaction 11

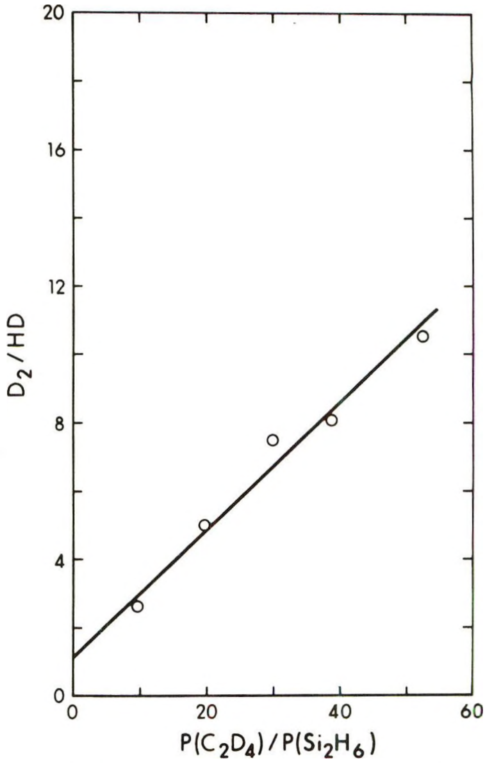

Figure 2. Plot of D_2/HD as a function of $P(C_2D_4)/P(Si_2H_6)$.

$$D + Si_2H_6 \rightarrow HD + Si_2H_5 \quad (11)$$

$k_3/k_{11} = 0.20 \pm 0.04$. For the displacement and exchange reactions

$$D + Si_2H_6 \rightarrow SiH_3D + SiH_3 \quad (12)$$

$$D + Si_2H_6 \rightarrow H + Si_2H_5D \quad (13)$$

the upper limit of $(k_{12} + k_{13})/k_{11}$ is estimated to be 0.4. Since step 13 is unlikely to occur[21] this leads to an upper limit of $k_{12}/k_{11} = 0.4$. From independent studies[19] the measured value of k_{12}/k_{11} for the attack by H atoms is 0.52.

Methylsilane. The isotopic composition of hydrogen obtained in the presence of CH_3SiH_3 is given in Table IV. For a fourfold excess of methylsilane, H_2 is 15% of the total hydrogen yield. Thus, although methylsilane is known to decompose at 1783 Å[31] its absorption at longer wavelengths is much weaker than that of ethylene-d_4. As methane was not observed among the products, the displacement reaction

$$D + CH_3SiH_3 \rightarrow CH_3 + SiH_3D$$

does not occur. It should be mentioned here that exchange reaction 8 does not occur with the methylated silanes.[16,20] A plot of D_2/HD ratios as a function of $P(C_2D_4)/P(CH_3SiH_3)$ is displayed in Figure 3. For the abstraction reaction

$$D + CH_3SiH_3 \rightarrow HD + CH_3SiH_2 \quad (14)$$

$k_3/k_{14} = 1.72 \pm 0.02$.

Dimethylsilane. The isotopic composition of hydrogen formed in the presence of $(CH_3)_2SiH_2$ is shown in Table V. Since the H_2 yield is only 5% of total hydrogen yield

---

(31) A. G. Alexander, O. P. Strausz, R. Pottier, and G. F. Semeluk, *Chem. Phys. Lett.*, **13**, 608 (1972).

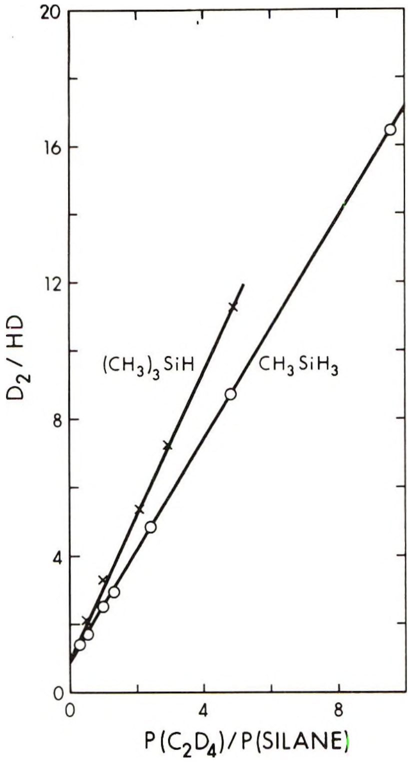

Figure 3. Plot of D_2/HD as a function of $P(C_2D_4)/P$(silane).

TABLE IV: Isotopic Composition of Hydrogen Formed in the Photolysis of C_2D_4 in the Presence of CH_3SiH_3 at 25°[a]

$P(C_2D_4)$, Torr	$P(CH_3SiH_3)$, Torr	Hydrogen, μmol D_2	Hydrogen, μmol HD	Hydrogen, μmol H_2
50.8	203.0	2.38	1.70	0.72
51.1	100.3	2.78	1.62	0.47
49.9	50.8	2.83	1.11	0.28
50.2	39.5	2.81	0.96	0.23
50.2	21.2	3.02	0.62	0.07
49.8	10.3	2.98	0.34	0.06
100.0	10.5	3.62	0.22	0.06

[a] Exposure time 5 min.

for a twofold excess of dimethylsilane the amount of absorption by dimethylsilane must be minimal. Only small amounts of methane (0.004 μmol at the highest dimethylsilane concentration) were present in the products. A plot of D_2/HD as a function of $P(C_2D_4)/P((CH_3)_2SiH_2)$ is shown in Figure 1. From the slope the ratio of the rate constant of addition reaction 3 to that of the abstraction reaction

$$D + (CH_3)_2SiH_2 \rightarrow HD + (CH_3)_2SiH \qquad (15)$$

is $k_3/k_{15} = 1.75 \pm 0.04$.

A possible source of methane formation is the displacement reaction

$$D + (CH_3)_2SiH_2 \rightarrow CH_3 + CH_3SiHD$$

followed by H atom abstraction by methyl. However, this mechanism can be discounted since the Hg $6(^3P_1)$ plus dimethylsilane reaction, which leads to exclusive Si–H bond cleavage, does not give rise to the production of CH_4.[20] Consequently the small amount of CH_4 formed in the present system must arise from the direct photolysis of $(CH_3)_2SiH_2$.

TABLE V: Isotopic Composition of Hydrogen Formed in the Photolysis of C_2D_4 in the Presence of $(CH_3)_2SiH_2$ at 25°[a]

$P(C_2D_4)$, Torr	$P((CH_3)_2SiH_2)$, Torr	Hydrogen, μmol D_2	Hydrogen, μmol HD	Hydrogen, μmol H_2
50.1	100.5	2.40	1.31	0.20
50.1	50.1	2.64	0.99	0.12
49.4	25.3	2.65	0.63	0.06
50.0	17.0	2.62	0.45	0.05
49.0	10.3	2.78	0.32	0.03

[a] Exposure time 5 min.

TABLE VI: Isotopic Composition of Hydrogen and Methane Formed in the Photolysis of C_2D_4 in the Presence of $(CH_3)_3SiH$ at 25°[a]

$P(C_2D_4)$, Torr	$P((CH_3)_3SiH)$, Torr	Hydrogen, μmol D_2	Hydrogen, μmol HD	Hydrogen, μmol H_2	Methane, μmol
50.6	99.8	1.88	0.88	0.09	0.22
50.4	49.7	2.26	0.68	0.06	0.04
50.1	24.9	2.46	0.46	0.03	0.01
50.2	17.3	2.69	0.37	0.02	
50.4	10.4	2.92	0.26	0.01	

[a] Exposure time 5 min.

Trimethylsilane. The results on this sytem are given in Table VI. Small amounts of H_2 and methane indicate that absorption by trimethylsilane is much weaker than that by ethylene-d_4 in the region above 1783 Å. At the highest trimethylsilane concentration used, *ca.* 92% of methane product was CH_4 and the remaining was CH_3D. The only possible source of CH_4 formation is the direct photolysis of $(CH_3)_3SiH$. Both molecular and radical abstraction steps for methane formation have been shown to occur in the photolysis of methylsilane[32] and dimethylsilane.[21] The small amount of CH_3D could arise from the disproportionation reactions of CH_3, formed in the direct photolysis, with C_2D_5

$$CH_3 + C_2D_5 \rightarrow CH_3D + C_2D_4$$

A plot of D_2/HD ratios as a function of $P(C_2D_4)/P((CH_3)_3SiH)$ is shown in Figure 3. The slope of this plot yields

$$D + (CH_3)_3SiH \rightarrow HD + (CH_3)_3Si \qquad (16)$$

for the rate constant ratio $k_3/k_{16} = 2.28 \pm 0.07$.

Bond Energy Bond Order (BEBO) Calculations. According to this method,[33,34] the potential energy of the system, V, along the line of constant bond order, $m = 1 - n$, is given by

$$V = E_{1s}(1 - n^p) - E_{2s}m^q + V_{tr} \qquad (II)$$

where

$$V_{tr} = 0.5E_{3s}\{[\exp(-\beta r_3)][1 + 0.5\exp(-\beta r_3)]\} \qquad (III)$$

$$r_3 = R_1 + R_2 - R_{3s}$$

$$R_1 = R_{1s} - 0.26\ln n$$

$$R_2 = R_{2s} - 0.26\ln m$$

---

[32] K. Obi, A. Clement, H. E. Gunning, and O. P. Strausz, *J. Amer. Chem. Soc.*, **91**, 1622 (1969).
[33] H. S. Johnston and C. Parr, *J. Amer. Chem. Soc.*, **85**, 2544 (1963).
[34] H. S. Johnston, "Gas Phase Reaction Rate Theory," Ronald Press, New York, N. Y., 1966, p 339.

TABLE VII: Bond Properties for BEBO Calculations[a]

Bond	D_e,[b] kcal mol^{-1}	ω_e,[c] cm^{-1}	R_e,[d] Å	β,[e] Å^{-1}
H–H	109.4[f]	4395[f]	0.74[f]	1.940[f]
SiH_3–H	98.3[g]	2182	1.48	1.408
Si_2H_5–H	93.0[h]	2159	1.48	1.433
CH_3SiH_2–H	89.0[i]	2167	1.48	1.470
$(CH_3)_2SiH$–H	87.0[i]	2143	1.48	1.470
$(CH_3)_3Si$–H	84.1[j]	2125	1.48	1.483
CH_3–H	108.3[k]	2914[f]	1.09[f]	1.780

[a] The bond energy indices used are H–H = 1.041 and C–H = 1.087 (ref 34); and Si–H = 1.004 (ref 5). [b] Includes zero point energy. [c] Weighted average of Si–H stretching frequencies taken from R. P. Hollandsworth and M. A. Ring, *Inorg. Chem.*, 7, 1635 (1968). [d] R. E. Wilde, *J. Mol. Spectrosc.*, **8**, 424 (1962). [e] Calculated from the expression $\beta = 1.2177 \times 10^7\ \omega_e(\mu/D_e)^{1/2}$. [f] Reference 34, p 82. [g] Reference 41. [h] Estimated from the relationship $D(CH_3\text{–}H)/D(C_2H_5\text{–}H) \simeq D(SiH_3\text{–}H)/D(Si_2H_5\text{–}H)$. [i] Estimated using the relationship $[D(SiH_3\text{–}H) - D(Me_xSiH_{3-x}\text{–}H)]/[D(CH_3\text{–}H) - D(Me_xCH_{3-x}\text{–}H)] = [D(SiH_3\text{–}H) - D(Me_3Si\text{–}H)]/[D(CH_3\text{–}H) - D(Me_3C\text{–}H)]$. [j] Reference 42. [k] Reference 40.

TABLE VIII: Potential Energies of Activation and Experimental Activation Energies of Hydrogen Abstraction by H Atoms

Substrate	V,[a] kcal mol^{-1}	E_a, kcal mol^{-1}
CH_3–H	14.0	12.0[b]
C_2H_5–H	10.6	9.4[c]
$(CH_3)_2CH$–H	9.0	8.2[c]
$(CH_3)_3C$–H	7.6	6.8[c]
SiH_3–H	9.1 (6.2)	2.5–3.9,[d] 4.1[e]
Si_2H_5–H	7.0 (4.6)	1.4–2.8[d]
CH_3SiH_2–H	5.6 (3.6)	2.3–3.7[d]
$(CH_3)_2SiH$–H	5.1 (3.3)	2.1–3.4[d]
$(CH_3)_3Si$–H	4.4 (2.80)	1.8–3.2,[d] 2.30[f]

[a] In parentheses are the values calculated using modified V_{tr}, eq IV. [b] K. J. Laidler, "Chemical Kinetics," McGraw-Hill, New York, N. Y., 1965, p 129. [c] B. A. Thrush, *Progr. React. Kinet.*, **3**, 89, 95 (1965). [d] Estimated assuming an A factor in the range 5×10^{12}–5×10^{13} cc mol^{-1} sec^{-1} per Si–H bond. [e] Reference 17. [f] Reference 16.

p and q are the bond energy indices, E_{1s}, E_{2s}, and E_{3s} are the single bond energies, R_{1s}, R_{2s}, and R_{3s} denote the single bond distances, R_1 and R_2 are the progress distances, β is the Morse parameter of the R–R′ bond in the triatomic transition state R---H---R′ (see ref 34 for a detailed discussion and notation), and V_{tr} represents the triplet interaction energy between the end atoms. This expression has been widely used to predict the activation energies for a variety of H atom abstraction reactions and the calculated values are found to agree with experiment to within ±2 kcal mol^{-1}. Table VII lists the bond properties needed in the computations. The final results are given in Table VIII which also contains the estimated values for silanes *(vide infra)* and the literature values for alkane reactions.

Discussion

In order to calculate absolute rate constants from relative rate measurements, k_3 must be estimated. For the analogous reaction

$$H + C_2H_4 \rightarrow C_2H_5 \quad (17)$$

the high-pressure rate constants reported in the literature[35–38] are in good agreement, yielding an average value of 6.7×10^{11} cc mol^{-1} sec^{-1}. The rate of the H plus C_2D_4 reaction is reported to be 10% higher than reaction 17.[36] Although primary and secondary isotope effects will contribute to the overall isotope effect in the D plus C_2D_4 reaction, the major contribution to the k_H/k_D ratio will probably arise from the stretching frequency of the newly created C–D bond in the activated complex. Neglecting tunneling effects then, the minimum value of the primary isotope effect will be ~1.4. Taking into account these considerations a value of 5.3×10^{11} cc mol^{-1} sec^{-1} is adopted for k_3. Table IX lists the absolute rate constants derived for the D plus silane reactions, along with those for CH_3 and CF_3 radicals.

The absolute rate constants derived in the present study for reactions 9, 11, and 16 are in reasonable agreement with the literature values, considering the different experimental techniques employed in the measurements. The reactions of deuterium atoms with silanes are much faster than those with carbon analogs; the approximate values of the rate constants[39] for the analogous reactions with methane and isobutane are ~10^4 and 10^9 cc mol^{-1} sec^{-1}, respectively. Enhanced reactivities have also been reported for the reactions of methyl and trifluoromethyl radicals with silanes.[5–10] For paraffins, it is now well established that the reactivities for hydrogen atom abstraction are intimately related to the strength of the bonds being broken and formed, that is, to the enthalpy changes of the reactions. An examination of Table IX reveals that the reactivities of monosilanes, per Si–H bond, increase with increasing the number of methyl substituents on the Si atom. This trend is the same as in the corresponding hydrocarbons: $(CH_3)_3C\text{–}H > (CH_3)_2CH\text{–}H > CH_3CH_2H > CH_3\text{–}H$.

The difference in reactivities between alkanes and silanes in their hydrogen transfer reactions is due largely to activation energy differences since the preexponential factors are almost identical.[5–10] Lower activation energies result from lower Si–H bond energies. The bond dissociation energies of paraffins are[40] $D(CH_3\text{–}H) = 104.0$, $D(C_2H_5\text{–}H) = 98.0$, $D((CH_3)_2CH\text{–}H) = 94.5$, and $D((CH_3)_3C\text{–}H) = 91.0$ kcal mol^{-1}. Similar data for silanes are scarce and values are available only for monosilane,[41] 95.2 kcal mol^{-1}, and trimethylsilane,[42] 81.0 kcal mol^{-1}. Clearly, a difference of about 10 kcal mol^{-1} between the Si–H and C–H bond strengths manifests itself in the enhanced reactivities of silane reactions.

The reported[39] preexponential factors of the hydrogen atom reactions with alkanes vary from 10^{11} to 10^{14} cc mol^{-1} sec^{-1}. The latest values of Parsamyan, *et al.*,[43,44] are 6.6×10^{13}, 5.4×10^{13}, and 4.5×10^{13} cc mol^{-1} sec^{-1} for ethane, propane, and butane, respectively. The only study reported on the temperature dependence of the silicon hydride reactions was made on the D plus $(CH_3)_3Si$–H system[16] which has an A factor of 5.4×10^{12} cc mol^{-1}

---

(35) W. Braun and M. Lenzi, *Discuss. Faraday Soc.*, **44**, 252 (1967).
(36) R. D. Penzhorn and B. deB. Darwent, *J. Chem. Phys.*, **55**, 1508 (1971).
(37) J. A. Eyre, T. Hikida, and L. M. Dorfman, *J. Chem. Phys.*, **53**, 1281 (1970).
(38) M. J. Kurylo, N. C. Peterson, and W. Braun, *J. Chem. Phys.*, **53**, 2776 (1970).
(39) A. F. Trotman-Dickenson, *Advan. Free-Radical Chem.*, **1**, 1 (1965).
(40) J. A. Kerr, *Chem. Rev.*, **66**, 465 (1966).
(41) F. E. Saafeld and J. J. Svec, *J. Phys. Chem.*, **70**, 1753 (1966).
(42) S. J. Band, I. M. T. Davidson, and C. A. Lambert, *J. Chem. Soc. A*, 2068 (1968).
(43) N. I. Parsamyan, E. A. Arakelyan, V. V. Azatyan, and A. B. Nalbandyan, *Izv. Akad. Nauk SSSR, Ser. Khim.*, 496 (1968).
(44) N. I. Parsamyan and A. B. Nalbandyan, *Izv. Akad. Nauk SSSR, Ser. Khim.*, 750 (1968).

TABLE IX: Kinetic Data of Hydrogen Transfer Reactions of Silanes

		D[b]		CH_3		CF_3	
		$k_{abstr} \times 10^{-11}$ cc mol^{-1} sec^{-1}					
Substrate	k_3/k_{abstr}[a]	Total	Per Si-H bond	Log A, cc mol^{-1} sec^{-1}	E_a, kcal mol^{-1}	Log A, cc mol^{-1} sec^{-1}	E_a, kcal mol^{-1}
SiH_3-H	1.88 ± 0.07	2.82, 1.32[c]	0.71	11.80,[f] 11.82[g]	6.99,[f] 6.89[g]	11.90,[h] 11.90[i]	4.93,[h] 5.11[i]
CH_3SiH_2-H	1.72 ± 0.02	3.08	1.03				
$(CH_3)_2SiH$-H	1.75 ± 0.04	3.03	1.51				
$(CH_3)_3Si$-H	2.28 ± 0.04	2.94, 1.11[d]	2.32	11.34[g]	7.83[g]	12.26[i]	5.56[i]
SiH_3SiH_2-H	0.20 ± 0.04	26.5, 13.0[e]	4.41	11.96[f]	5.63[f]		

[a] Errors quoted are based on 90% confidence limit. [b] Present work, temperature 25°. Absolute rate constants calculated with $k_3 = 5.3 \times 10^{11}$ cc mol^{-1} sec^{-1} (see text). [c] Lower limit for H plus SiH_4 reaction, ref 17. [d] Reference 16, log A = 12.73 (cc mol^{-1}), E_a = 2.3 kcal mol^{-1}. [e] H plus Si_2H_6 reaction, ref 19. [f] Reference 5. [g] Reference 9. [h] Reference 6. [i] Reference 10.

sec^{-1}. This is an order of magnitude smaller than those of the alkane reactions. On the other hand, the A factors for the reactions of methyl and trifluoromethyl radicals with several silanes have been found to have values essentially identical with those of the alkanes. The cause of this discrepancy is not understood but clearly more experimental work will be required for the elucidation of the problem.

If we now arbitrarily assign a value to the A factor of the H plus silane systems then it is possible to estimate the magnitude of the activation energies involved. The values derived this way by taking a range of A from 5×10^{12} to 5×10^{13} cc mol^{-1} sec^{-1} per Si-H bond are listed in Table VIII in comparison with the measured activation energies of the alkane reactions and calculated potential energies of activation for both systems. As seen from the table, the measured and calculated values are in good agreement for the alkanes; for the silanes, however, the computed values are persistently too high. The discrepancies, which were also found before in the CH_3 and CF_3 plus silane systems,[5-8] cannot be attributed to possible inaccuracies in the input parameters because the spectroscopic and bond energy data for the monosilane molecule are reasonably well established, and it is highly unlikely that they could lead to a 5-6 kcal mol^{-1} error.

One crucial point in the BEBO method is the estimation of the triplet repulsion term, V_{tr}. In the original formulation of the method, Johnston and Parr[33] assumed Sato's[45] anti-Morse function with a coefficient of 0.5, eq III, to represent the triplet repulsion between two H atoms. This same function, however, would not be expected to provide a satisfactory description of the repulsive term in cases where one or both end atoms are different from hydrogen. Also, Matsen[46] has questioned, on quantum mechanical grounds, the hypothesis that the repulsive term arises only from spin-spin interactions. Thus, the overestimation of the activation energy in the hydrogen transfer reactions of silicon hydrides is probably related to the inadequacy of the anti-Morse function in the description of the repulsive potentials. Since, apart from the case of the H_2 molecule, neither experimental nor computed repulsive potential data are available, we modified the potential energy function, V_{tr}, on empirical grounds by introducing a coefficient α into the exponential factors

$$V_{tr} = 0.5E_{3s}\{[\exp(-\alpha\beta r_3)][1 + 0.5\exp(-\alpha\beta r_3)]\} \quad (IV)$$

The value of α was determined from the measured activation energy of the $CH_3 + SiH_4$ reaction.

The potential energies of activation computed with this modified potential function, listed in Table VIII, are in reasonable agreement with the experimentally estimated values of the action energies. It should be mentioned that other modifications of V_{tr} have also been suggested recently in the literature.[47-49]

Acknowledgment. The authors thank the National Research Council of Canada for financial support.

(45) S. Sato, *J. Chem. Phys.*, **23**, 2465 (1955).
(46) F. A. Matsen, *J. Amer. Chem. Soc.*, **92**, 3525 (1970).
(47) S. W. Mayer, L. Schieler, and H. S. Johnston, *Proc. Int. Symp. Combust., 11th*, 387 (1967).
(48) S. W. Mayer, *J. Phys. Chem.*, **73**, 3941 (1969).
(49) C. M. Previtali and J. C. Scaiano, *J. Chem. Soc. B*, 2317 (1971).

Chemical Ionization Mass Spectrometry. XVII. Effect of Pressure on the Decomposition of Protonated *tert*-Amyl Acetate

W. A. Laurie and F. H. Field*

The Rockefeller University, New York, New York 10021

(Received February 17, 1972)

Publication costs assisted by the National Science Foundation

The kinetics of the decomposition of protonated *tert*-amyl acetate have been investigated mass spectrometrically under chemical ionization conditions at pressures of isobutane (the reactant gas) between 0.5 and 4.0 Torr. Within the limits of experimental error, the rate constant (k_{300} = 2 × 10^3 sec^{-1}), activation energy (12 kcal/mol), and frequency factor (6 × 10^{11} sec^{-1}) are independent of pressure in this range, and it is concluded that thermal equilibrium is essentially established in the ionization chamber of the mass spectrometer.

It has been shown[1-5] that the chemical ionization mass spectra of organic esters are strongly dependent on temperature. The gaseous ionic reactions occurring under chemical ionization conditions have therefore been studied as a function of temperature in an attempt to derive meaningful kinetic data about the reactions. To date the results obtained have shown satisfactory correlations between reactivity and structure of the ions being studied. However, one of our continuing concerns is whether sufficient collisions occur in the ion chamber so that the reactions of the decomposing ions are activated completely or nearly completely (except for a small electrical contribution) by thermal collisions, *i.e.*, whether thermal equilibrium conditions are essentially achieved in the ion source. In order further to investigate this problem, we have extended our measurements[1,5] of the decomposition of protonated *tert*-amyl acetate in isobutane to pressures up to 4 Torr. This is a matter of some importance because gas-phase investigations of the chemistry of ions permit in principle the determination of the chemical properties of the ions in the absence of solvent. To the extent that we are able to demonstrate that reliable quantitative and physically meaningful kinetic measurements can be made for gaseous ionic reactions, we shall be able to parallel in the gas phase the extensive condensed-phase studies (solvolysis studies, for example) of the reactions and kinetics of ions.

Experimental Section

The experiments were made with the Esso Chemical Physics mass spectrometer[6-8] modified as follows. The original 300 l./sec source diffusion pump was replaced by a Norton Vacuum VHS-4 pump, which has a capacity of 1200 l./sec. A new power supply for the electron accelerating voltage was installed, and with it variable electron voltages to 600 V can be achieved. The higher voltages are needed to provide the higher electron penetration requisite for adequate sensitivity at the higher source pressures. The accelerating voltages actually used were those which maximized the ion production. Duplicate determinations were made of the effect on rate constants of varying the source pressure, and duplicate or triplicate determinations were made of the temperature variations of the rate constants at the several different source pressures. The rate constants were obtained using previously described[1] calculational procedures.

Measurements and Results

The reaction studied is the alkyl oxygen cleavage of protonated *tert*-amyl acetate with isobutane as the reactant gas

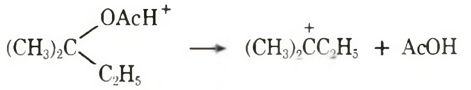 (1)

$$(CH_3)_2C(OAcH^+)(C_2H_5) \longrightarrow (CH_3)_2\overset{+}{C}C_2H_5 + AcOH \qquad (1)$$

The following two kinds of experiments were made: (1) measurements of the rate constants at different temperatures holding the isobutane pressure constant (experiments made at $P(i\text{-}C_4H_{10})$ = 0.70, 2.0, and 3.1 Torr), and (2) measurements of the rate constants at different isobutane pressures between 0.5 and 4.0 Torr holding the temperature constant at (T = 350°K).

In making the pressure studies we found that the magnitude of the repeller voltage significantly influences the results obtained. We have previously shown[1] that the rate constants for dissociation of protonated esters increase as the repeller voltage is increased, and this may be attributed to collision-induced dissociations produced by the drift of the ions under the influence of the repeller field gradient. We find in the present study that for certain ranges of the repeller voltage and the source pressure, an inverse relationship exists at constant repeller voltage between the rate constant for decomposition and the pressure. Our mass spectrometer requires the presence of a repeller field for the extraction of ions from the ion source. Below a certain minimum repeller voltage no ion current is observed, and increasing the repeller voltage above the minimum value causes the ion current to rise and approach an asymptote. Of interest here is the fact that the value of the minimum repeller voltage needed for the appearance of an ion current is dependent upon the particle

---

(1) F. H. Field, *J. Amer. Chem. Soc.*, **91**, 2827 (1969).
(2) F. H. Field, *J. Amer. Chem. Soc.*, **91**, 6334 (1969).
(3) D. P. Weeks and F. H. Field, *J. Amer. Chem. Soc.*, **92**, 1600 (1970).
(4) F. H. Field and D. P. Weeks, *J. Amer. Chem. Soc.*, **92**, 6521 (1970).
(5) W. A. Laurie and F. H. Field, *J. Amer. Chem. Soc.*, **94**, 2913 (1972).
(6) F. H. Field, *J. Amer. Chem. Soc.*, **83**, 1523 (1961).
(7) M. S. B. Munson and F. H. Field, *J. Amer. Chem. Soc.*, **88**, 2621 (1966).
(8) D. P. Beggs and F. H. Field, *J. Amer. Chem. Soc.*, **93**, 1567 (1971).

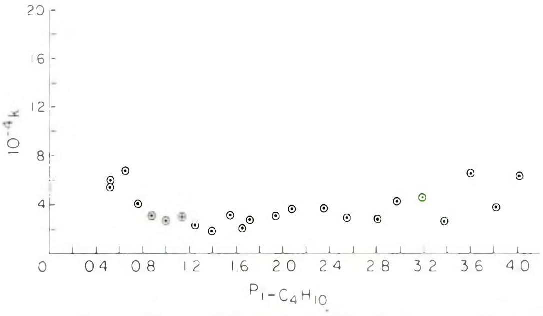

Figure 1. k(sec^{-1}) *vs.* $P(i\text{-}C_4H_{10})$ (Torr) for reaction 1: T = 350°K.

density in the ion source, and specifically the minimum repeller voltage needed becomes larger as the particle density becomes larger. The threshold for the appearance of ion current seems to occur at approximately the same value of E/P at the several different pressures (E = repeller field strength, P = source pressure). The quantity E/P is a measure of the mean energy the ions acquire from the electric field, and it seems reasonable to investigate the effect of pressure on the kinetics of ionic reactions at approximately constant values of E/P. We did this indirectly by adjusting the repeller voltage at each pressure so that the total ion current issuing from the ionization chamber was the same at each pressure (other experimental conditions maintained constant). The E/P values involved lay in the range 10 ± 2 V/cm Torr. By contrast, if the pressure studies are made at a fixed repeller, the variation in E/P is as large as the variation in pressure, which on the basis of our past experience should give rise to an appreciable variation in rate constants, but one which is of little or no significance for the intrinsic chemistry of the system.

The rate constants obtained at various isobutane pressures at fixed temperature (350°K) and quasi-constant E/P are given in Figure 1. One does well to achieve an accuracy of a factor of 2 in the determination of the absolute values of rate constants for these gaseous ionic reactions, and within this limit of accuracy we conclude that the rate constants in Figure 1 exhibit no meaningful trend. Thus the rate constants are essentially unchanged by increasing the pressure of isobutane from 0.7 to 4 Torr, which is in agreement with more restricted experiments (0.5–1.3 Torr) carried out on substituted benzyl acetates.[2]

Determinations of the temperature variation of the rate constants were made at three different isobutane pressures, namely, 0.70, 2.0, and 3.1 Torr. The values of the repeller voltage used in the measurements at the different pressures corresponded roughly to those used at the same pressures in the pressure study depicted in Figure 1. A typical Arrhenius plot is given in Figure 2, and the kinetic results obtained are given in Table I. Our experience has been that we can measure a rate constant at a given temperature more accurately than we can measure activation energies or frequency factors, and thus we first examine the values of log k_{300} given in Table I. The variation to be observed for this quantity corresponds to a variation in k_{300} of a factor of 3, which we consider to be small in the context of the overall accuracy generally found with these measurements. Moreover, one is most often concerned with the effect of molecular structure on the kinetics of the reactions, and for such studies one considers as significant differences in rate constants appreciably larger than a factor of 3.

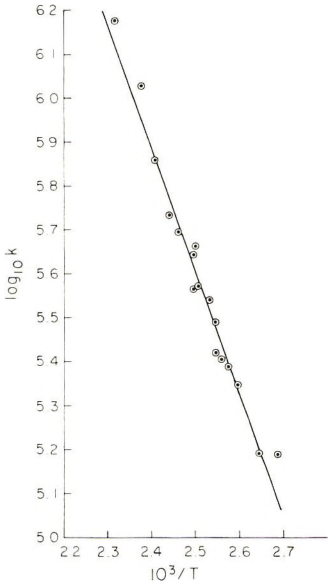

Figure 2. Arrhenius plot for reaction 1.

The values found for the activation energies and the frequency factors show variations, but here particularly we feel that the variations lie within the appreciable experimental uncertainties in determining these quantities. Comparing the present results with those obtained previously (all in the same mass spectrometer but with somewhat different configurations and conditions), we see that poor agreement exists with the results of ref 5 and good agreement with results of ref 1. The higher rate constant obtained in ref 5 can be attributed at least in part to the significantly higher E/P value used in that experiment.

Since the modification of our instrument enables us to vary the electron voltage over a much wider range than previously, we determined the rate constant for reaction 1 at four electron voltages between 200 and 600 V ($P(i\text{-}C_4$

TABLE I: Effect of Source Pressure on Rate Parameters[a] for *t*-AmAcOH$^+$ → *t*-Am$^+$ + AcOH

$P(i\text{-}C_4H_{10})$, Torr	Repeller, V	E/P, V/cm Torr	E_a, kcal/mol	Log A	Log k_{300}
0.70	2	7.2	11.0 ± 1.0	11.0 ± 0.6	2.9 ± 0.2
2.0	8	10.0	11.9 ± 0.4	11.7 ± 0.2	3.1 ± 0.1
2.0	10	12.5	12.7 ± 0.5	12.4 ± 0.2	3.4 ± 0.4
3.1	10	8.3	11.8 ± 1.2	12.0 ± 0.7	3.4 ± 0.2
		Previous Results			
0.70[b]	8	27.4	9.3	11.3	4.5
0.70[c]	5	17.9	12.4	12.4	3.3

[a] The uncertainties given in the kinetic quantities are the average deviation from average of replicate measurements. [b] Reference 5. [c] Reference 1.

H_{10}) = 1 Torr) and found it to be independent of electron voltage (10% average deviation from average).

An increase in pressure effects a proportional increase in the number of collisions per second experienced by an ion. In our experiment the pressure is varied by a factor of approximately 6, and this change in pressure and collision rate has no significant effect on the kinetic quantities obtained. This result indicates that thermal equilibrium conditions are essentially achieved in our chemical ionization source and that meaningful comparative kinetic data can be obtained by this method. However, it must be noted from both present and past experience[2] that the results are dependent upon repeller voltage. Since we are obliged to use this voltage, the results obtained should properly be considered as relative values, and all data should be obtained under the same experimental conditions where practically possible.

Acknowledgments. We wish to thank Mr. A. S. Viscomi for carrying out many of the measurements involved in this work. We have held profitable discussions concerning the work with Mrs. S. G. Lias. We acknowledge with thanks the gift of the Esso Chemical Physics mass spectrometer by Esso Research and Engineering Co., Linden, N. J. The work was supported in part by a grant from the National Science Foundation.

Ion-Molecule Reactions in Ethane

S. L. Bennett, S. G. Lias,[1a] and F. H. Field*

Rockefeller University, New York, New York 10021

(Received July 20, 1972)

Publication costs assisted by the National Science Foundation

The ion-molecule reactions in ethane have been investigated in a mass spectrometer at pressures from 0.1 to 5 Torr and at temperatures ranging from 189 to 410°K. The major primary ions, $C_2H_4^+$, $C_2H_5^+$, and $C_2H_6^+$, react with ethane to form the respective addition ions, $C_4H_{10}^+$, $C_4H_{11}^+$, and $(C_2H_6)_2^+$. Under these conditions, the addition ions dissociate to give all the product ions which have been attributed to reactions of these primary ions in previous studies. The major product ions resulting from these dissociation reactions are the $C_3H_7^+$ and $C_4H_9^+$ ions, formed by dissociations of the $C_4H_{10}^+$ and $C_4H_{11}^+$ ions, respectively. The rate constants for disappearance of the primary ions decrease as the temperature is raised from 189 to 410°K, from 2×10^{-10} to 0.9×10^{-10} cm^3/molecule sec for the ethylene ion, from 2.5×10^{-10} to 0.5×10^{-10} cm^3/molecule sec for the ethyl ion, and from 2×10^{-10} to 0.5×10^{-10} cm^3/molecule sec for the ethane ion. There is no evidence that any of the product ions react further with ethane to give higher molecular weight addition ions under these conditions of temperature and pressure. When H_2O is added to ethane the ethylene ion is intercepted in a rapid reaction to form the $C_2H_4 \cdot H_2O^+$ complex, which reacts further with water to add a second, a third, and a fourth molecule of water.

Introduction

Recent studies of ion-molecule reactions in saturated hydrocarbon systems have called attention to the fact that under conditions of low temperature and high pressure, many ions will form persistent complexes or condensation ions[1b] in reactions with alkane molecules. It has been demonstrated, for example, that the "unreactive" CH_5^+ and $C_2H_5^+$ ions formed in methane will associate with a molecule of methane at temperatures in the range 77-370°K, and at pressures of 0.1-1 Torr.[2a]

$$CH_5^+ + CH_4 \rightleftarrows CH_5 \cdot CH_4^+ \quad (1)$$

$$C_2H_5 + CH_4 \rightleftarrows C_2H_5 \cdot CH_4^+ \quad (2)$$

Furthermore, it was seen that the $CH_5 \cdot CH_4^+$ ion formed in reaction 1 would associate with still another molecule of methane

$$CH_4 \cdot CH_5^+ + CH_4 \rightleftarrows (CH_4)_2CH_5^+ \quad (3)$$

In each case, the lifetime of the adduct ion increased as the temperature was lowered.

Other recent studies have shown that at 300°K and pressures in the range 0.01-0.1 Torr, the ethane,[2b] propane,[3,4] and isobutane[5] parent ions will react with their respective parent molecules to form dimer ions. The ethane ion, for instance, reacts with ethane as follows

---

(1) (a) Visiting Assistant Professor, 1971-1972, National Bureau of Standards Training Act. (b) According to the usual usage, a condensation reaction is taken to be the addition of an ion to a molecule to form a new species which is held together by chemical bonds, while an association reaction is pictured as a combination of an ion with a molecule through attractive forces of a physical nature. Obviously there is not a sharp dividing line between condensation and association, and there will be many reactions which will seem to belong to both categories. In the results discussed here we will not attempt to make such distinctions, but will simply refer to all product ions formed in such reactions as "adducts" or "complexes."

(2) (a) F. H. Field and D. P. Beggs, *J. Amer. Chem. Soc.*, **93**, 1585 (1971); (b) S. K. Searles, L. W. Sieck, and P. Ausloos, *J. Chem. Phys.*, **53**, 849 (1970).

(3) L. W. Sieck, S. Searles, and P. Ausloos, *J. Chem. Phys.*, **54**, 91 (1971).

(4) D. P. Beggs and F. H. Field, *J. Amer. Chem. Soc.*, **93**, 1576 (1971).

(5) L. W. Sieck, S. K. Searles, and P. Ausloos, *J. Res. Nat. Bur. Stand., Sect. A*, **75**, 147 (1971).

$$C_2H_6^+ + C_2H_6 \rightarrow (C_2H_6)_2^+ \quad (4)$$

The addition of the vinyl to ethane has also been observed[6-8]

$$C_2H_3^+ + C_2H_6 \rightarrow C_4H_9^+ \quad (5)$$

With the exception of reactions 4 and 5, however, the occurrence of addition reactions between the major ions formed in ethane and ethane itself has not been demonstrated, although in a recent study of the radiolysis of ethane at pressures of 100 Torr and above,[6] experiments utilizing deuterium labeling gave evidence that a large fraction of the *n*-butane product originated from the $C_4H_{11}^+$ ion formed by addition of the ethyl ion to ethane. For example, about 70% of the partially deuterated butane formed in a C_2D_6-C_2H_6 (1:1) mixture was $C_4D_5H_5$

$$C_2H_5^+(C_2D_5^+) + C_2D_6(C_2H_6) \rightarrow C_4H_5D_6^+(C_4D_5H_6) \quad (6)$$

$$C_4H_5D_6^+(C_4D_5H_6^+) + A \rightarrow C_4H_5D_5 + AD^+(AH^+) \quad (7)$$

(where A is a proton acceptor).

We have here examined the ion chemistry of ethane in a mass spectrometer at pressures ranging from 0.1 to 5 Torr and at temperatures from 189 to 410°K, with particular emphasis on detecting and following the chemistry of the addition complexes of the various ions with ethane. In the discussion which follows, we shall relate our results to the ion chemistry reported to occur in ethane at pressures in the range 10^{-4}-10^{-5} Torr (where stabilization of such complexes does not occur), as well as to the radiolytic results[6] obtained at pressures above 100 Torr.

Experimental Section

The experiments were performed with the Esso chemical physics mass spectrometer, equipped with the ion source designated as Source III. The apparatus and technique have been described in previous papers.[1,4,9-11] The repeller and focus electrodes were maintained at minimum operating potentials (5 V repeller and 6 V focus) needed to achieve a useable sensitivity. The maximum pressures which could be attained in the pressure variation experiments were a function of the temperature of the source. That is, under these approximate field-free conditions, at 410°K, a source pressure of 5 Torr could be used, but at 189°K, the maximum pressure which could be attained was only 3 Torr. In terms of particle density, however, these pressures are roughly equivalent.

The ethane used in this study was Phillips Research Grade. Gas chromatographic analysis indicated that it contained 0.0003% methane, 0.011% ethylene, 0.0036% propylene, 0.034% propane, and 0.011% butane. No analysis was made for higher molecular weight impurities. Traces of water in the ethane were substantially reduced by passing the ethane through a refrigerated bath at 196°K.

Results and Discussions

In ethane, the major primary and secondary fragmentation processes will lead to the formation of $C_2H_2^+$, $C_2H_3^+$, $C_2H_4^+$, and $C_2H_5^+$ fragment ions. The reactions which these ions and the parent $C_2H_6^+$ ion undergo with ethane at pressures below about 0.1 Torr have been thoroughly documented,[2,7-8,12-19] especially by recent cyclotron resonance studies[7,18,19] which have unambiguously established the numerous parent-daughter relationships for these reactions. The exothermic or thermoneutral reactions which have been established, as well as the reactions observed for the first time in this study, are summarized in Table I (eq 9-32). With the exception of reaction 8 (which may proceed through a direct transfer of an H atom or proton), we make the assumption that each reactant ion forms a collision complex with ethane which may be collisionally deactivated to give the addition ion, or may dissociate in various ways to give the overall reactions which have been observed. We neglect the numerous reactions which are endothermic for ground-state ions but which energetic ions have been observed to undergo with ethane, since it is reasonable to assume that at the pressures used in this study, collisional deactivation of the intermediate complex ion will preclude the occurrence of these reactions to any significant extent.

All of the product ions reported in previous studies (Table I) were observed in our experiments. Ions at masses corresponding to all of the adduct ions were observed in significant quantities. Of especial interest is the observation of ions at masses 58 and 56 which, as will be shown in more detail below, seem to correspond to the adduct ions formed in the reactions

$$C_2H_4^+ + C_2H_6 \rightarrow C_4H_{10}^+ \quad (17)$$

and

$$C_2H_2^+ + C_2H_6 \rightarrow C_4H_8^+ \quad (26)$$

These reactions have not been reported before. Our results also provide the first direct observation of the formation of the adduct $C_4H_{11}^+$ in reaction 13.

$$C_2H_5^+ + C_2H_6 = C_4H_{11}^+ \quad (13)$$

The only other ions observed in amounts as great as 1% of the total ion current were at masses 70 ($C_5H_{10}^+$), 71 ($C_5H_{11}^+$), 85 ($C_6H_{13}^+$), and 99 ($C_7H_{15}^+$). These ions, each of which comprises about 1-2% of the total ion current under most experimental conditions, probably originate in reactions with small amounts of impurities as will be demonstrated below. Finally, low-intensity ions were observed at *m/e* 46, 47, 48, 49, 54, 64, 65, 72, 73, 74, 75, 83 and 84. These include many ions produced by reactions of various ions with small amounts of water which is always present as a minor impurity in the ion source. The sum of the intensitites of these ions was less than 1% of the total ion intensity.

The effects of varying pressure on the intensities of all the ion currents of interest are shown in Figures 1-4 for

---

(6) P. Ausloos, R. E. Rebbert, and L. W. Sieck, *J. Chem. Phys.*, **54**, 2612 (1971).

(7) S. Wexler and L. G. Pobo, *J. Amer. Chem. Soc.*, **93**, 1327 (1971).

(8) A. S. Blair, E. J. Heslin, and A. G. Harrison, *J. Amer. Chem. Soc.*, **94**, 2935 (1972).

(9) F. H. Field, *J. Amer. Chem. Soc.*, **83**, 1523 (1961).

(10) D. P. Beggs and F. H. Field, *J. Amer. Chem. Soc.*, **93**, 1567 (1971).

(11) S. L. Bennett and F. H. Field, *J. Amer. Chem. Soc.* **94**, 5188 (1972). lished

(12) M. S. B. Munson, J. L. Franklin, and F. H. Field, *J. Phys. Chem.*, **68**, 3098 (1964).

(13) G. A. Derwish, A. Galli, A. Giardini-Guidoni, and G. G. Volpi, *J. Chem. Phys.*, **40**, 5 (1964).

(14) R. Fuchs, *Z. Naturforsch. A*, **16**, 1026 (1961).

(15) F. H. Field and F. W. Lampe, *J. Amer. Chem. Soc.*, **81**, 3242 (1959).

(16) A. Henglein and G. A. Muccini, *Z. Naturforsch. A*, **17**, 452 (1962).

(17) V. L. Talroze and E. L. Frankevich, *J. Amer. Chem. Soc.*, **80**, 2344 (1958).

(18) R. C. Dunbar, J. Shen, and G. A. Olah, *J. Chem. Phys.*, **56**, 3794 (1972).

(19) T. McAllister, *J. Chem. Phys.*, **56**, 5192 (1972).

TABLE I: Exothermic or Thermoneutral Ion-Molecular Reactions in Ethane

Reaction	Ref	Eq no.
$(C_2H_6^+)^* + C_2H_6 \rightarrow C_2H_7^+ + C_2H_5$	6-8, 12, 13	(8)
$C_2H_6^+ + C_2H_6 \rightarrow (C_2H_6)_2^+$	2b	(4)
$\rightarrow C_4H_{11}^+ + H$	2b	(9)
$\rightarrow C_4H_9^+ + H_2 + H$	2b, 18	(10)
$\rightarrow C_3H_8^+ + CH_4$	2b, 7, 18	(11)
$\rightarrow C_3H_9^+ + CH_3$	2b, 7, 18	(12)
$C_2H_5^+ + C_2H_6 \rightarrow C_4H_{11}^+$	6, 18[a]	(13)
$\rightarrow sec\text{-}C_4H_9^+ + H_2$	6-8, 13, 18	(14)
$\rightarrow C_3H_7^+ + CH_4$	7, 8, 12	(15)
$\rightarrow C_2H_5^+ + C_2H_6$	6	(16)
$C_2H_4^+ + C_2H_6 \rightarrow C_4H_{10}^+$	This work	(17)
$\rightarrow C_3H_7^+ + CH_3$	7, 8, 13, 14	(18)
$\rightarrow C_3H_6^+ + CH_4$	7, 18	(19)
$\rightarrow C_4H_8^+ + H_2$	18	(20)
$\rightarrow C_4H_9^+ + H$	18	(21)
$\rightarrow C_2H_4^+ + C_2H_6$	6	(22)
$C_2H_3^+ + C_2H_6 \rightarrow i\text{-}C_4H_9^+$	6-8	(5)
$\rightarrow C_2H_5^+ + C_2H_4$	7, 8	(23)
$\rightarrow C_3H_5^+ + CH_4$	7	(24)
$\rightarrow C_4H_7^+ + H_2$	7, 8	(25)
$C_2H_2^+ + C_2H_6 \rightarrow C_4H_8^+$	This work	(26)
$\rightarrow C_2H_4^+ + C_2H_4$	7, 8	(27)
$\rightarrow C_3H_3^+ + CH_3 + H_2$	7	(28)
$\rightarrow C_3H_5^+ + CH_3$	7, 18	(29)
$\rightarrow C_4H_7^+ + H$	7, 8, 18	(30)
$\rightarrow C_4H_5^+ + H_2 + H$	8	(31)
$C_3H_3^+ + C_2H_6 \rightarrow C_3H_5^+ + C_3H_4$	7	(32)

[a] $C_4H_{11}^+$ was observed but not attributed to any particular reaction.

experiments performed at 189, 327, and 410°K. We have found that at pressures above about 1 Torr, the variations of the intensities of the ion currents of the primary ions ($C_2H_6^+$, $C_2H_5^+$, $C_2H_4^+$, $C_2H_3^+$, and $C_2H_2^+$) cannot easily be interpreted in terms of the kinetics of the reactions occurring in the system. Material balance considerations between ions thought to be involved in reactant-product relationships are oftentimes inexact at the higher pressures. It is clear that our understanding of the details of the reactions occurring is far from complete, but in spite of this, the overall trends shown in the figures yield meaningful information about the ion chemistry of ethane at high pressures.

We discuss separately the reaction sequences initiated by the various primary ions.

Ethyl Ion Reactant. As the results given in Figure 1 show $C_4H_{11}^+$ is formed in significant quantities in ethane at pressures from 1 to 5 Torr, particularly at temperatures of around 300°K or lower. This ion corresponds to that which would be formed in the addition of $C_2H_5^+$ to $C_2H_6^+$.

$$C_2H_5^+ + C_2H_6 \rightarrow C_4H_{11}^+ \qquad (13)$$

The formation of $C_4H_{11}^+$ in reaction 13 was verified in an experiment in which methane was used as the reactant gas in a chemical ionization experiment with ethane as the additive at 336°K. In such an experiment, the ethyl ion formed in methane will react with the added ethane through reactions 13-16, and the CH_5^+ ion will transfer a proton to ethane

$$CH_5^+ + C_2H_6 \rightarrow C_2H_7^+ + CH_4 \qquad (33)$$

to give $C_2H_7^+$, which, if it dissociates, will form a $C_2H_5^+$ ion. That is, such an experiment, in which small amounts (1-10%) of ethane are added to methane, effectively allows us to observe the reaction sequence initiated by reaction of the ethyl ion with ethane, in the absence of other reactive ions which are present in the pure ethane system. The results, shown in Figure 5, confirm that the $C_4H_{11}^+$ species originates from reaction of the ethyl ion. A fraction of the $C_4H_{11}^+$ in the pure ethane system may originate from reaction 9.

The results of the chemical ionization experiment also indicate that the $C_4H_{11}^+$ ion dissociates primarily to give a $C_4H_9^+$ ion (reaction 14), but also undergoes a dissociation to form a $C_3H_7^+$ ion (reaction 15, Table I) to a much lesser extent. This is in agreement with results obtained in earlier studies.[6-8,12,13,18]

The $C_4H_9^+$ formed in these experiments (Figure 1) does not necessarily all originate from reaction of the ethyl ion. As shown in Table I, it has been demonstrated[6,7] that the condensation reaction between the vinyl ion and ethane results in the formation of an i-$C_4H_9^+$ ion (reaction 5). Furthermore, the dissociation of the ethane dimer ion results in the formation of some $C_4H_9^+$ (reaction 10), and it has recently been suggested[18] that $C_4H_9^+$ is formed in a reaction of the $C_2H_4^+$ ion (reaction 21). However, it has been demonstrated[7] that at low pressures (where contributions from reactions 10 and 21 would be most important) the ethyl ion is the precursor of most of the butyl ions observed. At the pressures of the experiments reported here, the stabilized i-$C_4H_9^+$ ion formed in the condensation reaction between the $C_2H_3^+$ ion and ethane (reaction 5) undoubtedly contributes to the observed ion current, but the diminution of the $C_2H_3^+$ ion current as the pressure is increased in these experiments amounts to not more than 5-7% of the total ion current (Figure 4) while the increase in $C_4H_9^+$ is four-six times greater, so the contribution to $C_4H_9^+$ from this source cannot be large. We may therefore conclude that most of the $C_4H_9^+$ originates from reaction 14, the dissociation of the $C_4H_{11}^+$ ion. On this basis it can be seen that under all conditions,

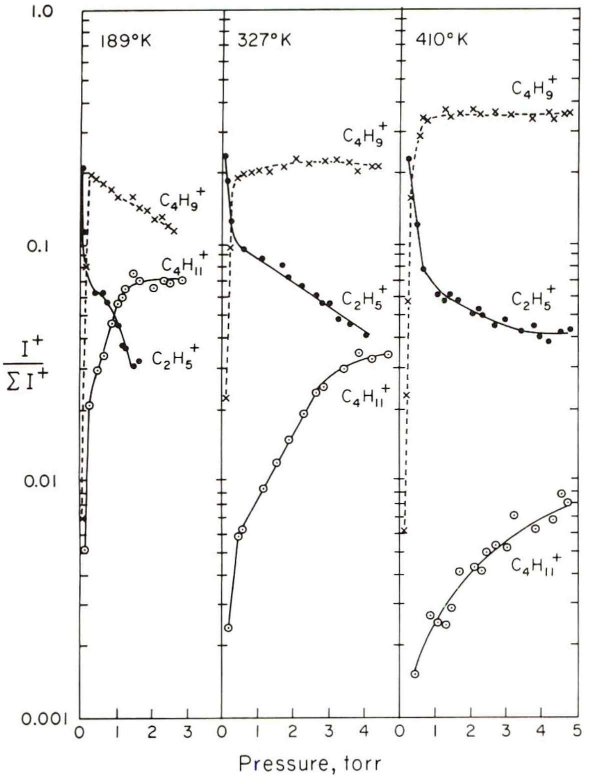

Figure 1. Abundances of the $C_2H_5^+$, $C_4H_{11}^+$, and $C_4H_9^+$ ions as a function of pressure at 189, 327, and 410°K.

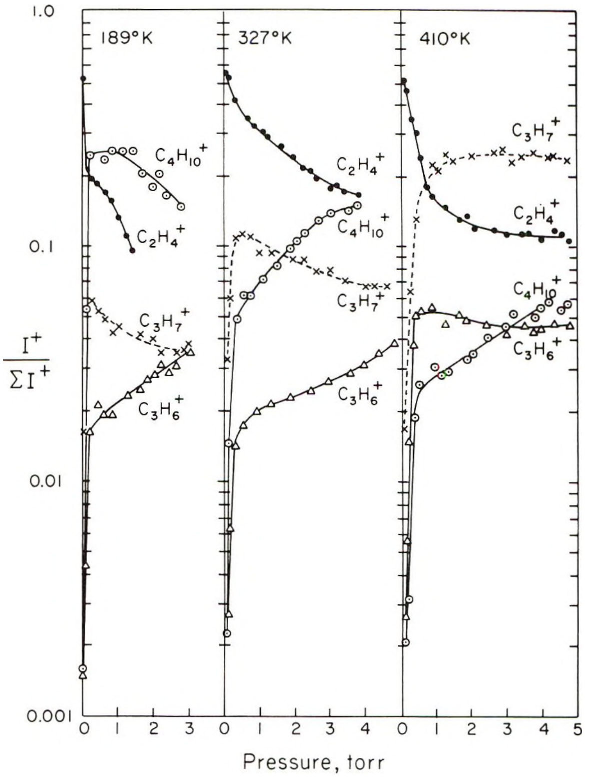

Figure 2. Abundances of the $C_2H_4^+$, $C_4H_{10}^+$, $C_3H_7^+$, and $C_3H_6^+$ ions as a function of pressure at 189, 327, and 410°K.

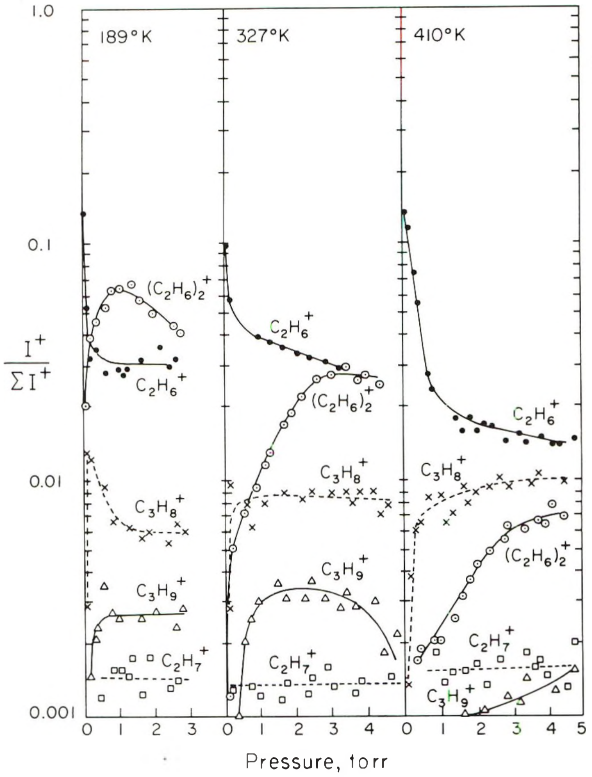

Figure 3. Abundances of the $C_2H_6^+$, $C_2H_7^+$, $(C_2H_6)_2^+$, $C_3H_8^+$, and $C_3H_9^+$ ions as a function of pressure at 189, 327, and 410°K.

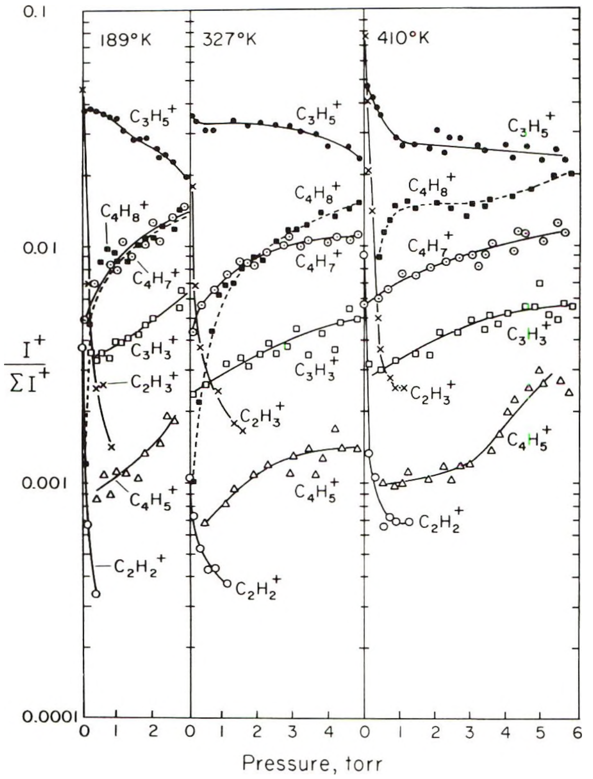

Figure 4. Abundances of the $C_2H_2^+$ (○), $C_2H_3^+$ (×), $C_3H_3^+$ (□), $C_3H_5^+$ (●), $C_4H_5^+$ (△), $C_4H_7^+$ (⊙), and $C_4H_8^+$ (■) ions as a function of pressure at 189, 327, and 410°K.

reaction 14 is the most probable dissociation of the $C_4H_{11}^+$ ion. As would be expected, this dissociation becomes more important at higher temperatures.

It may be seen from a careful examination of Figure 1 that the overall rate of disappearance of the ethyl ion, and the overall rate of formation of the $C_4H_{11}^+$ and $C_4H_9^+$ ions, are strongly temperature dependent, being much

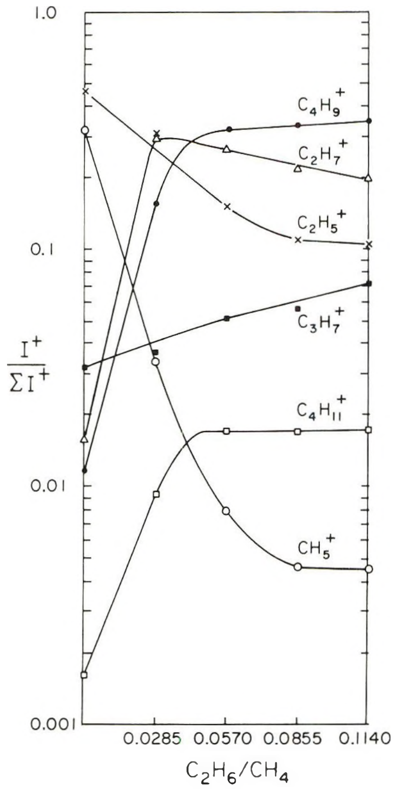

Figure 5. Abundances of the CH_5^+, $C_2H_5^+$, $C_4H_{11}^+$, $C_3H_7^+$, $C_4H_9^+$, and $C_2H_7^+$ ions in methane as a function of added ethane concentration at 336°K and 1.5 Torr.

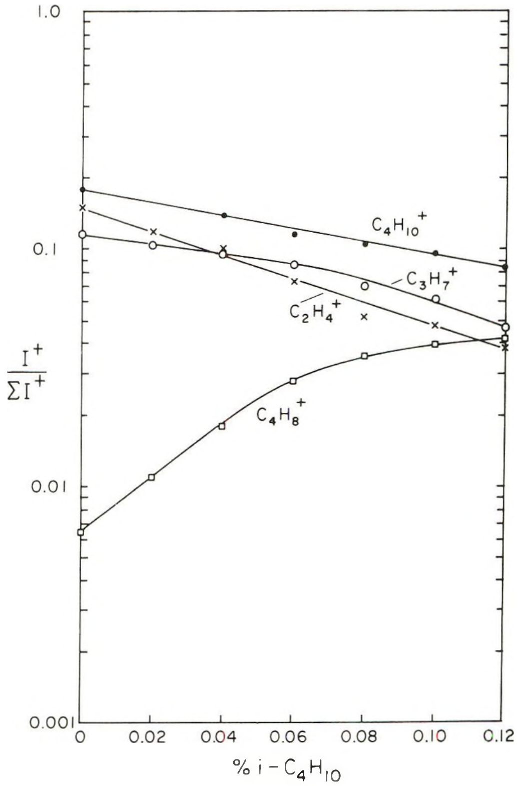

Figure 6. Abundances of the $C_2H_4^+$, $C_4H_{10}^+$, $C_3H_7^+$, and $C_4H_8^+$ ions as a function of added isobutane concentration at 1 Torr and 334°K.

faster at low temperatures. This undoubtedly reflects the fact that the dissociation of $C_4H_{11}^+$ to regenerate the ethyl ion (reaction 16) is much slower at the lower temperatures. If we accept the earlier estimate[6] of 1×10^{-10} cm^3/molecule sec as the rate constant for the reaction of the ethyl ion with ethane to give products other than the original reactants at temperatures of about 300°K (and assume that at low pressures, the distribution of ion residence times is not strongly temperature dependent), we can estimate from the initial slopes of the curves in Figure 1 that at 189°K, this rate constant is about 2.5×10^{-10} cm^3/molecule sec, and at 410°K, the value is about 0.5×10^{-10} cm^3/molecule sec. These experiments were conceived of and executed as being essentially qualitative in nature. However, we found that rough quantitative analyses of the data could be made, and the rate constant values given above resulted. These values are not highly accurate, but they do indicate trends.

Ethylene Ion Reactant. The addition of an ethylene ion to ethane would result in the formation of a product ion of the formula $C_4H_{10}^+$

$$C_2H_4^+ + C_2H_6 \rightarrow C_4H_{10}^+ \qquad (17)$$

At the high pressures and relatively low temperatures used in the experiments reported here, the $C_4H_{10}^+$ ion is a significant ion in all experiments, as shown by the results given in Figure 2. Although $C_4H_{10}^+$ from reaction 17 has never before been observed in the mass spectrometer, it has been shown[7,8,13,14] that the major products coming from reaction of an ethylene ion with ethane (other than the regeneration of the original reactants) at low pressures are the propyl ion and the propylene ion. These are exactly the product ions which would result from the dissociation of a $C_4H_{10}^+$ ion formed with about 20-kcal excess energy[20-22] (as it would most probably have if formed in reaction 17).

In order to demonstrate that the $C_4H_{10}^+$ ion does not originate in any reaction sequence involving the small amount (0.011%) of butane impurity present in the starting material, experiments were performed in which small amounts of butane or isobutane were added to ethane in the ion source. Similar results were obtained in these two experiments, and the results of the isobutane additive experiment are given in Figure 6. These results show that as the $C_2H_4^+$ ion is intercepted by the isobutane to form $C_4H_8^+$

$$C_2H_4^+ + i\text{-}C_4H_{10} \rightarrow C_2H_6 + C_4H_8^+ \qquad (34)$$

the abundances of the $C_4H_{10}^+$ and $C_3H_7^+$ ions diminish, as would be expected if these ions originate primarily in reactions 17 and 18.

It should be mentioned that $C_4H_{10}^+$ ions were observed in low yield in a recent ion cyclotron study of ethane,[18] but double resonance experiments demonstrated that they originated in a slow reaction ($k = 4 \times 10^{-12}$ cm^3/molecule sec) of the $C_2H_6^+$ ion

$$C_2H_6^+ + C_2H_6 \rightarrow C_4H_{10}^+ + H_2 \qquad (35)$$

In the results reported here, the fact that at low or moderate temperatures the intensity of the $C_4H_{10}^+$ ion current is much greater than the maximum intensity of the ion current of the parent ion essentially precludes this reaction as a significant source of the butane ions.

We conclude, then, that the $C_4H_{10}^+$ observed in our experiments originates in reaction 17, the addition of the ethylene ion to ethane. The intensities of the $C_2H_4^+$, $C_4H_{10}^+$, $C_3H_7^+$, and $C_3H_6^+$ ions at pressures of 0.1–5 Torr

(20) W. A. Chupka and E. Lindholm, *Ark. Fys.*, **25**, 349 (1963).

(21) V. Cermak and Z. Herman, *Collect. Czech. Chem. Commun.*, **30**, 169 (1965).

(22) B. Steiner, C. F. Giese, and M. G. Inghram, *J. Chem. Phys.*, **34**, 189 (1961).

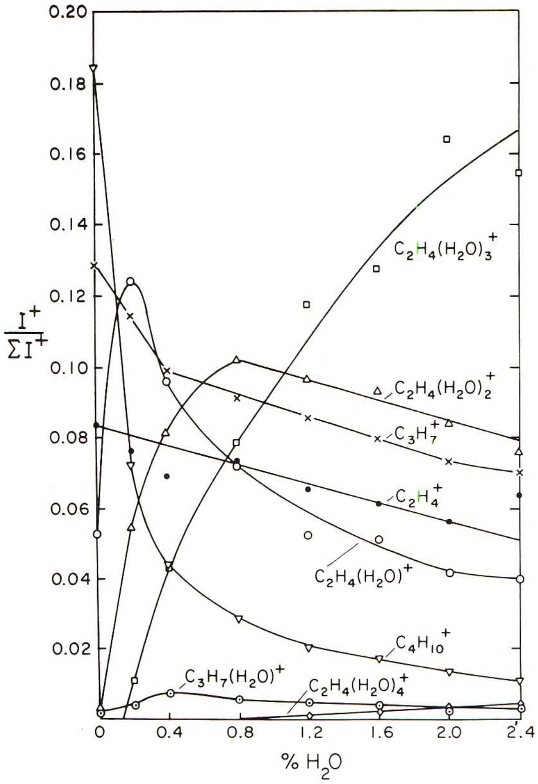

Figure 7. Abundances of the $C_2H_4^+$, $C_4H_{10}^+$, $C_3H_7^+$, $C_2H_4(H_2O)^+$, $C_2H_4(H_2O)_2^+$, $C_2H_4(H_2O)_3^+$, $C_2H_4(H_2O)_4^+$, and $C_3H_7(H_2O)^+$ ions as a function of the concentration of added water at 1 Torr and 334°K.

and at temperatures of 189, 327, and 410°K are shown in Figure 2. Ion cyclotron experiments[7] have shown that reaction 18 is the major source of $C_3H_7^+$ ions in ethane, and that at low pressures, about half of the $C_3H_6^+$ ions originate from reaction 19 of the ethylene ion. In a recent study of ethane,[18] it was observed that reactions of $C_2H_4^+$ also led to the formation of $C_2H_5^+$, $C_3H_5^+$, $C_3H_3^+$, $C_4H_8^+$, $C_4H_7^+$, and $C_4H_9^+$. The reactions to form $C_2H_5^+$, $C_3H_5^+$, and $C_4H_7^+$ are endothermic by 11, 16, and 22 kcal, respectively, indicating that the $C_2H_4^+$ ions which reacted in the experiments reported must have had considerable excess energy. In view of this, one must view with some suspicion the authors' contention that their observation of the reaction

$$C_2H_4^+ + C_2H_6 \rightarrow C_3H_3^+ + CH_3 + H_2 \qquad (36)$$

constitutes evidence for the existence of a $C_3H_3^+$ ion with a heat of formation of about 200 kcal/mol. Finally, although exothermic reactions between $C_2H_4^+$ and C_2H_6 leading to the formation of $C_4H_8^+$ and $C_4H_9^+$ can be written, the fact that these ions are not observed as dissociation products[20-23] of n-$C_4H_{10}^+$ or i-$C_4H_{10}^+$ formed with about 1-eV excess energy argues against their occurrence to any important extent in these experiments.

The overall trends with pressure and temperature observed for reactions 17-19 are similar to those discussed above for the reaction sequences of the ethyl ion. That is, the adduct ion, $C_4H_{10}^+$, becomes less important as the temperature is increased, while the fragment ions become more important. Making the same assumptions as were made above for the reactions of the ethyl ion, it can be estimated that the rate constant for the overall disappearance of the ethylene ion increases by about an order of magnitude when the temperature is lowered from 410°K, where the rate constant is about 0.1×10^{-10} cm^3/molecule sec, to 189°K, where the rate constant is about 2×10^{-10}. The high-temperature rate constant for disappearance of the ethylene ion in ethane is in agreement with earlier estimates[12,13] for this rate constant of $1\text{-}3 \times 10^{-11}$ cm^3/molecule sec. The effect of temperature on the overall rate of disappearance of the ethylene ion may be explained in terms of an increased probability for the collision complex to fall apart to regenerate the original reactants (reaction 22) as the temperature is increased. Reaction 22 includes dissociations which regenerate the original ethylene ion and ethane molecule, as well as the resonance H_2^- transfer reaction which can be detected only through labeling experiments. In the recent radiolytic study[6] of ethane, a rate constant of 1.1×10^{-10} cm^3/molecule sec was measured for the resonance D_2^- transfer (reaction 37) at a temperature of about 300°K.

$$C_2H_4^+ + C_2D_6 \rightarrow C_2H_4D_2 + C_2D_4^+ \qquad (37)$$

The results given in Figure 7 show the effects of added water on the reaction sequence initiated by reaction of $C_2H_4^+$ with ethane. As H_2O is added, the ethylene ion is intercepted to form a complex

$$C_2H_4^+ + H_2O \rightarrow C_2H_4 \cdot H_2O^+ \qquad (38)$$

which, as the concentration of water is increased, adds a second, a third, and a fourth molecule of water

$$C_2H_4 \cdot H_2O^+ + H_2O \rightarrow C_2H_4(H_2O)_2^+ \qquad (39)$$

$$C_2H_4(H_2O)_2^+ + H_2O \rightarrow C_2H_4(H_2O)_3^+ \qquad (40)$$

$$C_2H_4(H_2O)_3^+ + H_2O \rightarrow C_2H_4(H_2O)_4^+ \qquad (41)$$

The $C_4H_{10}^+$ and $C_3H_7^+$ ions show a strong decrease as the $C_2H_4^+$ precursors are intercepted, although in the case of $C_3H_7^+$, some of the decrease occurs because the ions form a complex[4] with H_2O

$$C_3H_7^+ + H_2O \rightarrow C_3H_7(H_2O)^+ \qquad (42)$$

The $C_3H_7^+$ ion will add a second and a third molecule of water.[4]

Ethane Ion Reactant. As mentioned above, it has been reported[2a] that ethane ions, formed by ionizing ethane with 11.6-11.8-eV photons, will react with ethane to form the ethane dimer ion, $(C_2H_6)_2^+$ (reaction 4). The failure to observe the ethane dimer in a recent mass spectrometric study[18] led to the suggestion that $C_2H_6^+$ ions produced by electron impact are formed with too much internal energy to form the dimer ion. The results presented here show that at sufficiently high pressures, a stable ethane dimer ion is indeed formed. As shown in Table I, the dissociation of an unstabilized dimer complex is expected to lead to the formation of $C_4H_{11}^+$, $C_4H_9^+$, $C_3H_9^+$, and $C_3H_8^+$. The first two of these product ions are, of course, formed in much greater abundance through reactions 13 and 14, as discussed above, and the relative importance of reactions 9 and 10 cannot be assessed in these experiments. Figure 3, therefore, shows the relative abundances of the $C_2H_6^+$, $(C_2H_6)_2^+$, $C_3H_9^+$, and $C_3H_8^+$ ions observed in these experiments, as well as the $C_2H_7^+$ formed in reaction 8.

Again, as in the cases of the ethyl and ethylene ions discussed above, it is seen that the relative importance of the adduct ion is much greater at the lower temperatures, but this is the only straightforward phenomenon to be observed in Figure 3. Beyond this, we call attention to the variations with pressure of the intensities of $C_3H_8^+$ and $C_3H_9^+$. One can conclude that these ions are formed from $C_2H_6^+$, but the pressure variations do not seem to be easily compatible with the sequential reactions.

$$C_2H_6^+ + C_2H_6 \rightarrow (C_2H_6)_2^+ \rightarrow C_3H_8^+ + CH_4 \quad (11)$$

$$\rightarrow C_3H_9^+ + CH_3 \quad (12)$$

The earlier study of the ethane dimer ion[2a] indicated that reaction 12, the formation of the $C_3H_9^+$ ion, was readily quenched by increasing pressure; the dimer ions formed in these experiments (a fraction of which possibly have more initial internal energy than those formed in the earlier photoionization study) still undergo this dissociation at pressures as high as 5 Torr, although the yield of $C_3H_9^+$ is low in all experiments. It should be mentioned that there is no evidence that the $C_3H_9^+$ ion undergoes a fast ($k = 1 \times 10^{-10}$ cm^3/molecule sec) reaction with ethane as suggested in a recent study.[18]

Making the same assumptions as those made above for the ethyl ion, one can derive from the initial slopes of the curves describing the abundance of the $C_2H_6^+$ ion as a function of pressure (Figure 3) an estimate that the rate constant for the disappearance of the parent ethane ion is about 0.5×10^{-10} cm^3/molecule sec at 410°K, 0.7×10^{-10} cm^3/molecule sec at 327°K, and 2×10^{-10} cm^3/molecule sec at 189°K. The value derived for the 327°K experiment is in excellent agreement with the value of 1×10^{-10} cm^3 molecule sec reported for this rate constant[2a] at 300°K. (Values of 1.85×10^{-11} and 3.2×10^{-11} cm^3/molecule sec have also been reported for this rate constant at an unspecified temperature,[8] presumably higher than 300°K.) Again, the fact that the rate of disappearance of the ion increases as the temperature is lowered undoubtedly reflects the fact that the dissociation to regenerate the original reactants becomes less important as the energy of the complex is lowered.

Other Ionic Reactants. Figure 4 shows the intensities of the ion currents of the $C_2H_2^+$ and $C_2H_3^+$ ions as a function of pressure in the experiments carried out at 189, 327, and 410°K. For the sake of clarity in the figure, the abundances of these two primary ion currents are not shown at pressures above about 1 Torr. In each case the ion currents of these primary ions reach a minimum value, then increase with increasing pressure. As pointed out above, in the pressure region above about 1 Torr, variations in the ion currents of the primary ions do not accurately reflect the kinetics occurring in the system.

Figure 4 also shows the relative abundances of the $C_3H_3^+$, $C_3H_5^+$, $C_4H_5^+$, $C_4H_7^+$, and $C_4H_8^+$ ions as a function of pressure. As the reactions listed in Table I show, results obtained in previous studies[7,8,13,18] have shown that the first four of these ions are formed in reactions of the $C_2H_2^+$ and $C_2H_3^+$ ions. The $C_4H_8^+$ could result from the addition of $C_2H_2^+$ to ethane (reaction 26), from reaction 20, or from reaction 34 between the ethylene ion and the small amount of butane impurity (0.011%) which is present in the starting material. A rough calculation indicates that reaction with the impurity could probably not account for all of the $C_4H_8^+$ which we observe.

Previous results[7,8,12-19] have indicated that none of the C_3 or C_4 ions, except possibly $C_3H_3^+$ and $C_3H_5^+$ [7] or $C_3H_9^+$ [18] show any reactivity toward ethane. Therefore, several experiments were performed in an attempt to trace the sources of the higher molecular weight ions observed in these experiments at masses 70, 71, 85, and 99. These results are given in Figures 8 and 9 which show the yields of the higher molecular weight ions, as well as their possible precursors, as a function of added propane or butane. It is seen (Figure 8) that the $C_3H_5^+$ ion reacts with propane and with butane (Figure 9). The abundance of the $C_6H_{13}^+$ ion increases in the presence of propane and decreases as butane is added. This ion may be formed as a

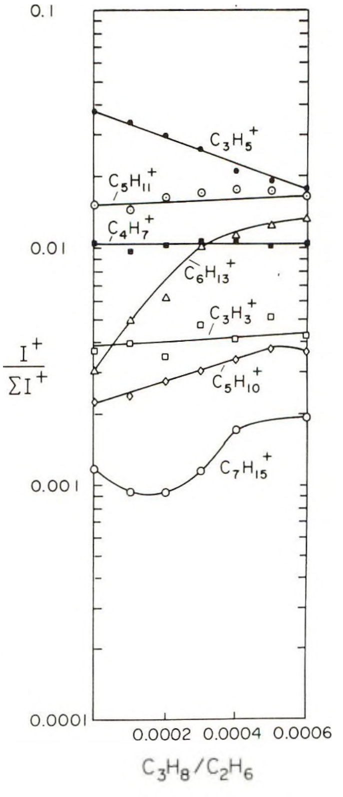

Figure 8. Abundances of the $C_3H_5^+$, $C_5H_{11}^+$, $C_4H_7^+$, $C_6H_{13}^+$, $C_3H_3^+$, $C_5H_{10}^+$, and $C_7H_{15}^+$ ions as a function of the concentration of added propane at 2 Torr and 333°K.

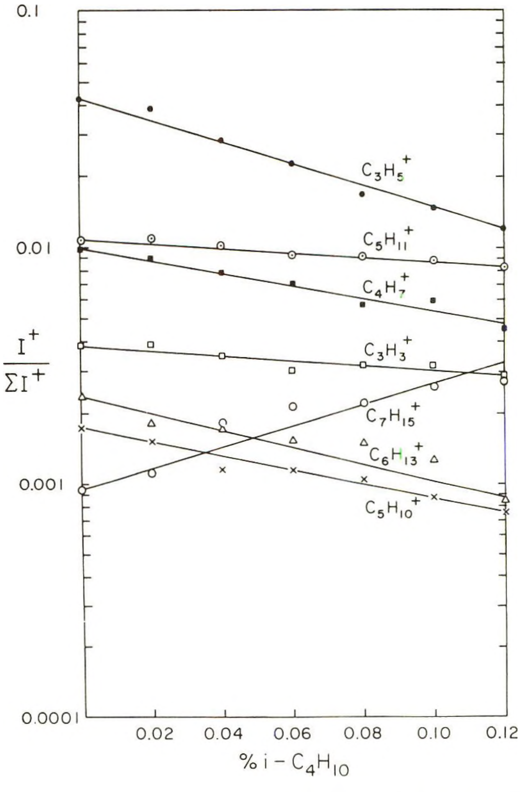

Figure 9. Abundances of the $C_3H_5^+$, $C_5H_{11}^-$, $C_3H_3^+$, $C_6H_{13}^+$, $C_5H_{10}^+$, $C_4H_7^+$, and $C_7H_{15}^+$ ions as a function of the concentration of added isobutane at 1 Torr and 334°K.

result of a reaction between $C_3H_5^+$ and propane

$$C_3H_5^+ + C_3H_8 \rightarrow C_6H_{13}^+ \quad (43)$$

Propane is the major impurity present in the starting material (0.034%). The ion current at mass 99 ($C_7H_{15}^+$) increases with the concentration of added butane, suggesting that the reaction of $C_3H_5^+$ with butane may be

$$C_3H_5^+ + C_4H_{10} \rightarrow C_7H_{15}^+ \quad (44)$$

under these conditions.

The same reasoning may be applied to the ion current at mass 70 ($C_5H_{10}^+$) and, to a lesser extent, that at mass 71 ($C_5H_{11}^+$), which may also originate from reactions involving the propane impurity to some extent. The relative insensitivity of the ion current at mass 71 to the added propane and butane, however, suggests that this ion may originate largely from some other source, probably a fast reaction with some other impurity, possibly a small amount of C_5H_{12}.

We must conclude that although several higher molecular weight ions were observed in our experiments at high pressures, there is no firm evidence for further reaction of any of the product ions with ethane itself to form these higher molecular weight ions, and their presence is probably best explained by the occurrence of fast reactions with minute amounts of alkane impurities.

It is worthy of mention that when propane and butane are added to ethane, no ions corresponding to the $C_2H_6 \cdot C_3H_8^+$ or $C_2H_6 \cdot C_4H_{10}^+$ addition ions are observed. In order to check on this point, large amounts of propane (up to 10%) were added to ethane, and the product ions were observed at temperatures from room temperature down to 188°K, but no adduct ion was observed.

When butane or isobutane is added to ethane, an ion current is observed at mass 113, indicating the occurrence of the reaction

$$C_4H_7^+ + C_4H_{10} \rightarrow C_8H_{17}^+ \quad (45)$$

Acknowledgment. This work was supported in part by a grant from the National Science Foundation. The Esso Chemical Physics mass spectrometer is a gift from Esso Research and Engineering Co., Linden, N. J.

Kinetics and Mechanism of Decafluorobenzophenone Photochemical Reactions in Cyclohexane, Benzene, and Alkyl Aromatics

Jonas Dedinas* and **T. H. Regan**

Research Laboratories, Eastman Kodak Company, Rochester, New York 14650

(Received May 4, 1972)

Publication costs assisted by Eastman Kodak Company

The photochemistry of decafluorobenzophenone was investigated in degassed solutions of cyclohexane, benzene, toluene, and *p*-xylene using 366-nm irradiation. In cyclohexane the primary photochemical step is hydrogen abstraction by triplet decafluorobenzophenone, $^3(n,\pi^*)$, with a rate constant of 7.5×10^6 M^{-1} sec^{-1}. The primary radicals formed undergo two types of radical-radical reactions, (a) combination and (b) an aromatic substitution reaction. At high concentrations (C) and at low light intensities (I_a), aromatic substitution of decafluorobenzophenone by cyclohexyl radical is also observed. Thus, the quantum yield (Φ) is dependent on C and I_a. In cyclohexane using $C = 0.01$ M and by extrapolating I_a to ∞, $\Phi = 0.41$ for decafluorobenzophenone disappearance, the major products of which are cyclohexyldi(pentafluoro)phenylcarbinol (24%) and *o*- and *p*-cyclohexylnonafluorobenzophenone (22 and 54%). Benzene quenches the triplet state with a rate constant k_q of 1.6×10^8 M^{-1} sec^{-1}. There is no conversion of decafluorobenzophenone to products in pure benzene. In toluene and *p*-xylene, $\Phi = 0.055$ and 0.096, respectively, indicating that both hydrogen abstraction and direct quenching by the aromatic ring is taking place. The rates of hydrogen abstraction from cyclohexane and quenching by benzene are much higher than those obtained in the photochemistry of benzophenone. These higher rates must be due to the inductive effect of fluorine substitution, which increases the charge polarization of the $^3(n,\pi^*)$ state. The quenching mechanism by benzene thus can be explained by a charge-transfer complex or an exciplex between the ketone in the $^3(n,\pi^*)$ state and benzene.

Introduction

The reactivity of the aromatic ketones in hydrogen-donating solvents depends on the nature of the lowest energy triplet state. The order of reactivity of the three known triplet states is as follows: $^3(n,\pi^*) > {}^3(\pi,\pi^*) > {}^3(CT)$. The reactivity has been correlated[1] qualitatively with the partial charge distribution of the carbonyl group in the excited state. The partial charge on oxygen has been indicated to be positive in the $^3(n,\pi^*)$ state, neutral in the $^3(\pi,\pi^*)$ state, and negative in the ^{3}(CT) state. A wide range of reactivity is also anticipated within a particular class of the triplet states as the partial charge can be varied by substituent groups.

---

[1] G. Porter and P. Supan, *Trans. Faraday Soc.*, **61**, 1664 (1965).

To determine the effect of substituent groups on the reactivity of the $^3(n,\pi^*)$ states, exploratory photochemical investigation of a series of fluorine-substituted benzophenones has been initiated. The preliminary results indicated that decafluorobenzophenone is the most unusual and therefore further investigation has been pursued using several solvents to determine the mechanism of the photochemical reactions of this compound.

Recently some photochemical[2,3] and spectroscopic[4,5] studies have been reported on this subject by other investigators. Of these, the most pertinent is the flash photolysis[2] study reported at the XXXIIIrd International Congress of IUPAC. In this study the decafluorobenzophenone ketyl radical generated in 2-propanol was identified and the lifetime of the triplet state at room temperature using inert solvents (CCl_4, Freon E4, and perfluoromethylcyclohexane) was determined to be 20 μsec. The lifetime of the benzophenone triplet[6] at similar conditions is 0.71 msec. The esr spectra of the decafluorobenzophenone ketyl and anion radicals have been reported by Sargent and Bailey.[4] The phosphorescence spectrum of decafluorobenzophenone has been reported by Simpson and Offen.[5] It is interesting that the lowest energy excited state is $^3(n,\pi^*)$ and that the energy of this state in nonpolar solvents is essentially the same as that of benzophenone. The sole photochemical study reported by Filipescu, Pinion, and Minn[3] indicates that decafluorobenzophenone in 2-propanol is converted to decafluorobenzhydrol with a quantum yield of 0.60 ± 0.01. These authors recommend decafluorobenzophenone dissolved in 2-propanol as an actinometer in the uv region from 290 to 370 nm.

Experimental Section

1. *Reagents.* Decafluorobenzophenone (Aldrich), when recrystallized from cyclohexane, did not contain any reactive impurities. Spectro Grade (Eastman Kodak) cyclohexane, benzene, toluene, *p*-xylene, and 1,2-dichloroethane were used without further purification. Perfluorodimethylcyclobutane was obtained from the Pierce Chemical Co., zone-refined benzene and benzophenone from James Hinton, and *trans*-stilbene from Eastman Kodak Co.

2. *Procedure.* The light source (1000-W xenon-mercury arc lamp), actinometry, and preparations of degassed samples for irradiation have been previously described.[7] Monochromatic light, 366 nm, was used. Cylindrical spectrophotometer cells made of either Pyrex or quartz were attached to degassing tubes and were used as reactors. The irradiated samples were analyzed by glc using ⅛ in. by 8 ft columns packed with 10% silicone gum rubber (UC98) supported on silanized diatomaceous earth. A thermal conductivity detector and temperature programming up to a maximum temperature of 300° were used for quantitative determination or product yields. The minor products were identified by glc-mass spectrometric (LKB-9000) analysis using a glass column (⅛ in. by 8 ft) packed with 2% Dexil supported on Chromosorb W(AW-DMCS).

The major components were isolated by tlc using Chrom-AR sheets (Mallinckrodt) and a solvent containing 80% cyclohexane and 20% benzene. The compounds were identified on the basis of mass spectrometry and proton and fluorine nmr analysis. The spectroscopic data included in the Appendix will appear in the microfilm edition of the journal.[8] The uv absorption spectrum was obtained using a Cary Model 14 recording spectrophotometer. Phosphorescence measurements were made using a setup consisting of 1000-W xenon arc lamp, two Bausch & Lomb monochromators, a light beam chopper, and a photomultiplier connected to an x-y recorder. The phosphorescence quantum yield was determined using a degassed 0.02 *M* solution of decafluorobenzophenone in perfluorodimethylcyclobutane.

The intersystem crossing efficiency was determined by the method of Lamola and Hammond[9] using *trans*-stilbene isomerization. The yield of *cis*-stilbene was determined in several experiments using a 1,2-dichloroethane solution containing 0.02 *M* concentration of decafluorobenzophenone and *trans*-stilbene concentration in the range from 0.005 to 0.3 *M*. Similar experiments were performed for comparison with benzophenone. The conversion of *trans*-stilbene was <5%.

Results and Discussion

1. *Intersystem Crossing Efficiency.* Decafluorobenzophenone exhibited only phosphorescence and no detectable fluorescence. The phosphorescence spectrum[5] indicates that the lowest energy triplet state is the reactive $^3(n,\pi^*)$ state. The triplet energy measured in both polar and nonpolar solvents is presented in Table I and is approximately the same as that of benzophenone. The absorption spectrum, shown in Figure 1, indicates that the forbidden $n \rightarrow \pi^*$ band is in the 325–390-nm region. Although this band does not show a maximum, it overlaps the corresponding band of the benzophenone $n \rightarrow \pi^*$ absorption. Since the lowest triplet energy of both ketones is essentially the same, as shown in Table I, it is apparent that the energy difference between $^1(n,\pi^*)$ and $^3(n,\pi^*)$ states should be approximately the same as in benzophenone and thus a high value of intersystem crossing efficiency can be predicted. This was confirmed experimentally by the method of Lamola and Hammond[9] using *trans*-stilbene isomerization. It was found from a direct comparison presented in Figure 2 that the maximum yield of *cis*-stilbene was the same as that obtained with benzophenone. Thus, the intersystem crossing efficiency of these two compounds is the same and is equal to 1.00 ± 0.03.

It should be mentioned that the yield of *cis*-stilbene, shown in Figure 2, decreases with increasing *trans*-stilbene concentration in the range from 0.04 to 0.3 *M* when using decafluorobenzophenone. This is unusual in view of the study by Hammond, DeMeyer, and Williams[10] who found that *trans*-stilbene concentration had no effect on

---

(2) A. Singh, M. G. Jonasson, F. C. Sopchyshyn, and F. P. Sargent, XXXIIIrd International Congress of Pure and Applied Chemistry, Boston, Mass., July 25–30, 1971.

(3) N. Filipescu, J. P. Pinion, and F. L. Minn, *Chem. Commun.*, 1413 (1970).

(4) F. P. Sargent and M. G. Bailey, *Can. J. Chem.*, **49**, 2350 (1971).

(5) J. Simpson and J. Offen, *J. Chem. Phys.*, **55**, 4832 (1971).

(6) C. A. Parker and T. A. Joyce, *Chem. Commun.*, 749 (1968).

(7) J. Dedinas, *J. Phys. Chem.*, **75**, 181 (1971).

(8) The spectroscopic data included in the Appendix will appear following these pages in the microfilm edition of this volume of the journal. Single copies may be obtained from the Business Operations Office, Books and Journals Division, American Chemical Society, 1155 Sixteenth St., N.W., Washington, D. C. 20036. Remit check or money order for $4.00 for photocopy or $2.00 for microfiche, referring to code number JPC-72-0000.

(9) A. A. Lamola and G. S. Hammond, *J. Chem. Phys.*, **43**, 2129 (1965).

(10) H. A. Hammond, D. E. DeMeyer, and J. L. R. Williams, *J. Amer. Chem. Soc.*, **91**, 5180 (1969).

TABLE I: Comparison of Triplet Decafluorobenzophenone and Benzophenone

	Solvent	$(C_6F_5)_2CO$	Ref	$(C_6H_5)_2CO$	Ref
$E_{triplet}$, kcal/mol	Nonpolar	68.4 ± 0.1	*a*	68.1 ± 0.1	*a*
	Nonpolar	68.4	4	68.4	5
	Polar, EPA	70.0	4	69.3	5
Phosphorescence lifetime at 77°K, msec	Polar, EPA	3.8		5.2	
	Polar, EPA	4.0	4	5.8	5
$\Phi_{phosphorescence}$ 77°K		0.21	*b*	0.74	*d*
Φ_{isc}		1.00 ± 0.03	*c*	1.0	8
Triplet lifetime at 23°, msec		0.020	2	0.71	6

[a] This work, solvent 20% isopentane, 80% methylcyclohexane. $E_{triplet}$ determined from phosphorescence spectrum obtained at −196°. [b] This work, results obtained in collaboration with L. F. Costa. [c] This work, results obtained by comparison with benzophenone. [d] W. D. K. Clark, A. D. Litt, and C. Steel, *J. Amer. Chem. Soc.*, **91**, 5413 (1969).

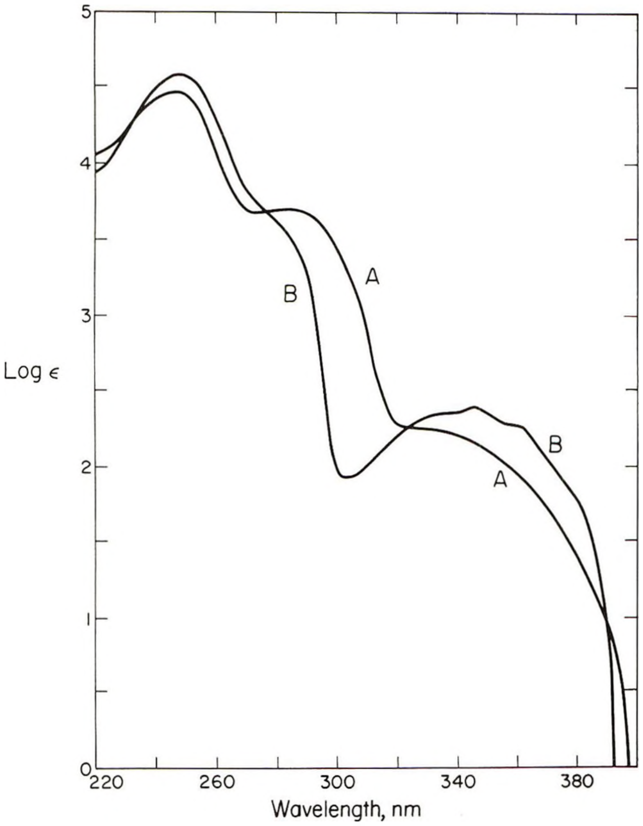

Figure 1. Uv absorption spectrum in cyclohexane of (A) decafluorobenzophenone and (B) benzophenone.

the quantum yield of isomerization for several substituted benzophenones. Their results were confirmed in this study with benzophenone. This anomaly is apparently due to singlet quenching by *trans*-stilbene. However, it should be pointed out that the determination of the intersystem crossing efficiency is not affected by this anomaly since it was determined at a *trans*-stilbene concentration of 0.01 M, whereas the anomaly is observed at concentrations $>0.04\ M$.

2. *Photochemistry in Cyclohexane. (a) Products and Yields.* Three major products are obtained in the photochemical reaction of decafluorobenzophenone in degassed cyclohexane solution when 366-nm irradiation is used. They are cyclohexyldi(pentafluoro)phenylcarbinol (**1**) and *o*- and *p*-cyclohexylnonafluorobenzophenone (**2** and **3**).

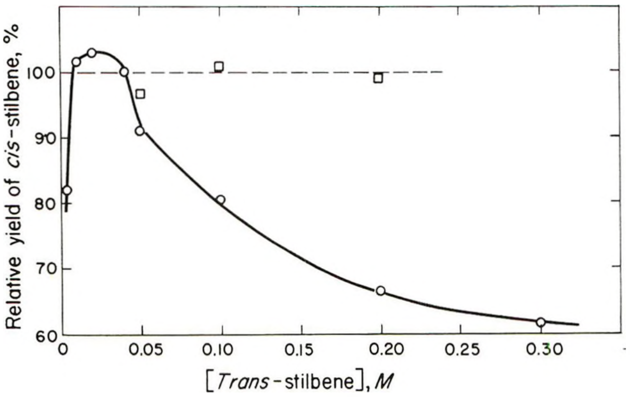

Figure 2. Determination of intersystem crossing efficiency by sensitized *trans*-stilbene isomerization in degassed solution of 1,2-dichloroethane: □, 0.02 M benzophenone; ○, 0.02 M decafluorobenzophenone.

The overall reaction for the formation of these products is shown in eq 1–3. The yield of HF has not been determined. The quantum yields of products **1**, **2**, and **3** depend on the reaction conditions and are presented in Table II for the cases where high light intensity (extrapolated to infinity) and two concentrations of decafluorobenzophenone, 0.01 and 0.05 M, were used. Additional yield data related to the intensity of absorbed light (I_a) and concentrations are presented in Figures 3–5. Light intensity affects the values Φ(**2**) and Φ(**3**) and has no effect on the value of Φ(**1**).

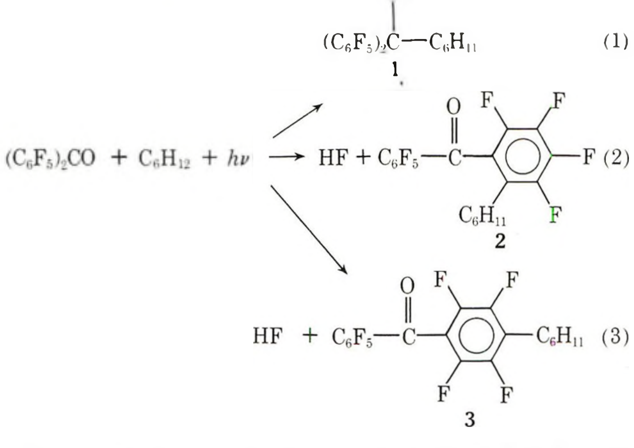

The effect of concentration was investigated at I_a = 2.2

TABLE II: Quantum Yields of Products Obtained in Cyclohexane at High Light Intensity (Extrapolated to ∞)

	Concn of decafluorobenzophenone	
Compd	0.01 *M*	0.05 *M*
1	0.10	0.07
2	0.09	0.09
3	0.22	0.22
4	<0.005	0.005
5	<0.005	0.005
6	0.01	0.01
7	<0.001	<0.001
8	*a*	*a*

[a] Product not detected.

× 10^{17} quanta min^{-1} ml^{-1}. In these experiments (Figure 5) the incident light intensity (I_i) was varied in inverse proportion to concentration, so as to maintain I_a approximately constant. The effect is greatest on $\Phi(3)$, which increases with concentration; $\Phi(1)$ and $\Phi(2)$ are only slightly affected by concentration. These data were obtained primarily to elucidate the reaction mechanism; a further discussion of interpretation is presented in the following section. The minor products were *m*-cyclohexylnonafluorobenzophenone (**4**), dicyclohexyloctafluorobenzophenones (**5**), decafluorobenzhydrol (**6**), and bicyclohexyl (**7**). It is interesting that there was no eicosafluorobenzopinacol (**8**) formed in this reaction and that the quantum yield of bicyclohexyl was very low, <0.001. The quantum yields of the minor products are also reported in Table II.

(b) Mechanism. Spectroscopic results obtained by flash photolysis[2] indicate that in a hydrogen-donating solvent such as 2-propanol, decafluorobenzophenone ketyl radical is formed from triplet decafluorobenzophenone. These results, in conjunction with uv absorption and phosphorescence[5] spectra, indicate that the initial photochemical processes, light absorption, intersystem crossing, and quenching of the triplet state by hydrogen abstraction should occur by the same mechanism as in the photochemistry of benzophenone.

$$\mathrm{K_0} \xrightarrow{h\nu} \mathrm{K^{1*}} \xrightarrow{k_{isc}} \mathrm{K^{3*}} \qquad (4)$$

$$\mathrm{K^{3*}} \xrightarrow{k_d} \mathrm{K_0} \qquad (5)$$

$$\mathrm{K^{3*} + RH} \xrightarrow{k_r} \mathrm{KH\cdot + R\cdot} \qquad (6)$$

$$\mathrm{KH\cdot + R\cdot} \xrightarrow{k_b} \mathrm{K_0 + RH} \qquad (7a)$$

$$\mathrm{KH\cdot + R\cdot} \xrightarrow{k_p} \text{products} \qquad (7b)$$

$\mathrm{K_0}$, $\mathrm{K^{1*}}$, and $\mathrm{K^{3*}}$ represent ketone in the ground, singlet excited, and triplet state, respectively; KH· is a ketyl radical, RH is a hydrogen donor, and R· is a radical.

Combination of the ketyl and the cyclohexyl radicals is apparently the mechanism of the formation of product **1**, *e.g.*

$$\mathrm{(C_6F_5)_2\dot{C}OH + C_6H_{11}\cdot} \xrightarrow{k_1} \mathrm{(C_6F_5)_2C(OH)C_6H_{11}} \qquad (8)$$

This mechanism is derived from the observation that $\Phi(1)$ is independent of I_a and is only slightly dependent on concentration.

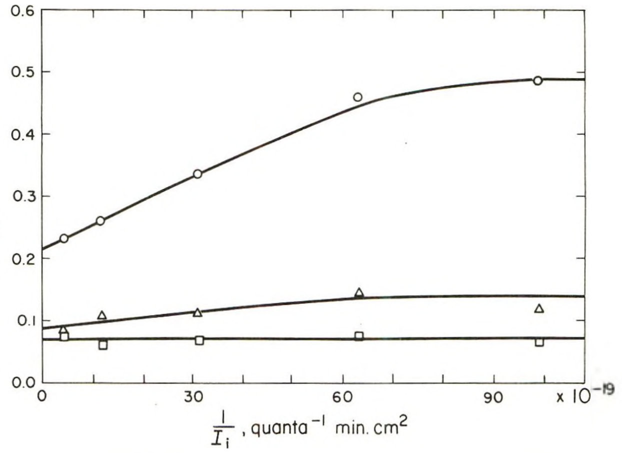

Figure 3. Effect of light intensity at decafluorobenzophenone concentration of 0.05 *M* in cyclohexane: □, $\Phi(1)$; △, $\Phi(2)$; ○, $\Phi(3)$.

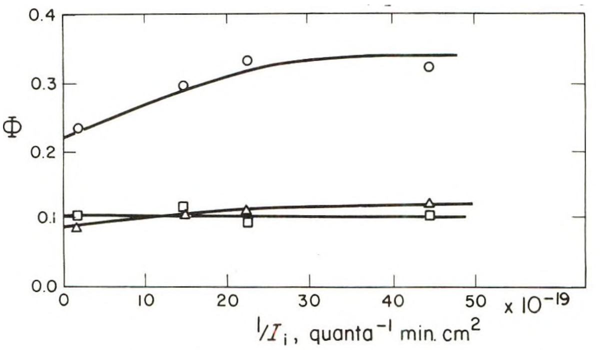

Figure 4. Effect of light intensity at decafluorobenzophenone concentration of 0.01 *M* in cyclohexane: □, $\Phi(1)$; △, $\Phi(2)$; ○, $\Phi(3)$.

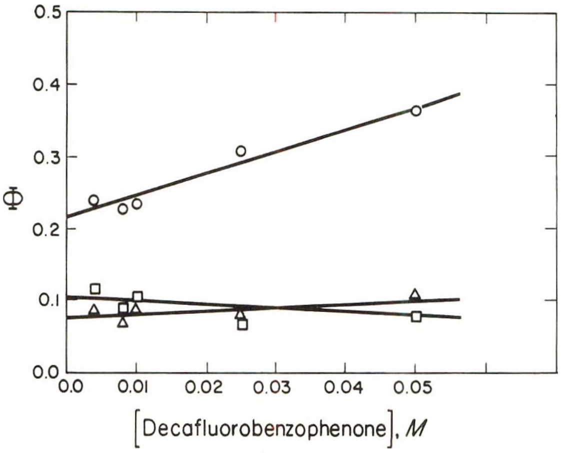

Figure 5. Effect of decafluorobenzophenone concentration in cyclohexane: □, $\Phi(1)$; △, $\Phi(2)$; ○, $\Phi(3)$. $I_a = 2.2 \times 10^{17}$ quanta min^{-1} ml^{-1}.

The quantum yields of products **2** and **3** increase linearly with increase of concentration (Figure 5) and in the region of high light intensity they also increase linearly as a function of $1/I_a$ (Figures 3 and 4). Thus, in the regions where linear relationship holds, the following equation describes the effects of concentration (*C*) and of absorbed light intensity (I_a)

$$\Phi = A + BC/I_a \qquad (9)$$

where Φ is the quantum yield of ketone disappearance and *A* and *B* are constants. It is interesting that the intercepts in Figures 3–5 for compound **3** are essentially the same. They are also the same for compound **2**; however, this is not very surprising since $\Phi(2)$ is much less affected by the operating variables than $\Phi(3)$. On the basis of these relationships two mechanisms must be involved in the formation of products **2** and **3**. At the conditions where $BC/I_a \approx 0$ ($I_a \approx \infty$ or $C \approx 0$), solely radical–radical reactions should be important, while at the other conditions, $BC/I_a > 0$, both radical–radical and ground-state decafluorobenzophenone-radical reactions may be present. The reactions involving ground-state decafluorobenzophenone are indicated by the results in Figure 5, where the concentration effect shows a significant increase of $\Phi(\mathbf{3})$ with increasing concentration. This effect is much smaller on $\Phi(\mathbf{2})$, but nevertheless is unequivocally evident.

Thus, two mechanisms of aromatic substitution are proposed for the formation of products 2 and 3, (1) reaction between cyclohexyl and decafluorobenzophenone ketyl radicals and (2) reaction between cyclohexyl radical and decafluorobenzophenone in the ground state. The cyclohexyl–ketyl radical aromatic substitution (mechanism I) is indicated by reaction 10. The product should be relatively unstable, as it can undergo enolization by reaction 11, and a unimolecular decomposition leading to the formation of *p*-cyclohexylnonafluorobenzophenone, as shown by reaction 12. Analogous reactions to 10–12 can be written for the formation of *o*-cyclohexylnonafluorobenzophenone. Reaction 10 is similar to that proposed by Schenck and coworkers[11] to explain the formation of isopinacol in the photochemical reaction of benzophenone and 2-propanol. Reaction 12 is feasible on the basis that HF elimination should be highly exothermic and that the final product is much more stable than the precursor. Although reaction 12 shows HF elimination from the enol form, it should be mentioned that the keto form (reaction 11) or both forms may be involved in the aromatization step. Because of the inductive effect of the perfluorophenyl group, the hydroxylic proton should be highly acidic; and thus HF elimination by reaction 12 is facilitated by that effect.

Mechanism I

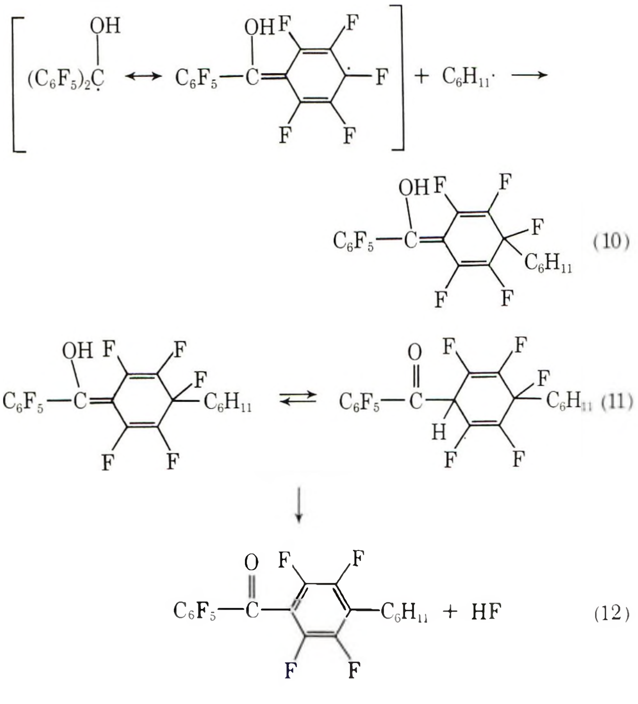
(10)

(11)

(12)

In mechanism II aromatic substitution of decafluorobenzophenone by cyclohexyl radical is shown by means of reactions 13–15. Cyclohexyl radical addition to benzene is well known[7]. The rate of addition increases with halide substitution;[12] thus it is not unusual that cyclohexyl radical addition to decafluorobenzophenone competes with radical–radical reactions. The importance of reaction 13 depends on the decafluorobenzophenone concentration and also on the concentration of the cyclohexyl radical. Similar reactions to 13 and 14 are envisioned for the formation of *o*- and *m*-cyclohexylnonafluorobenzophenone.

Mechanism II

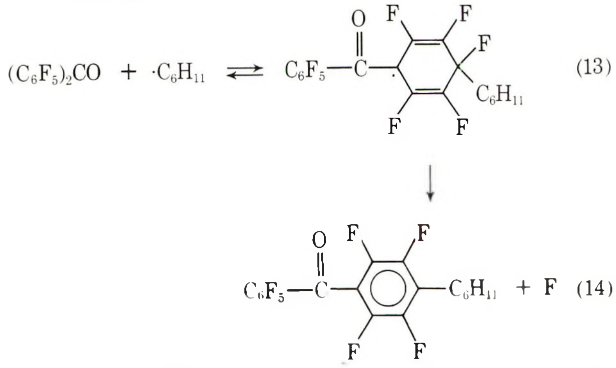
(13)

(14)

$$C_6H_{12} + F \longrightarrow \cdot C_6H_{11} + HF \qquad (15)$$

This mechanism differs from aromatic substitution by mechanism I in two respects. First, it is a chain propagation reaction. Second, the radical formed by reaction 13 can undergo consecutive radical combination and disproportionation reactions, for example, as in reaction 16.

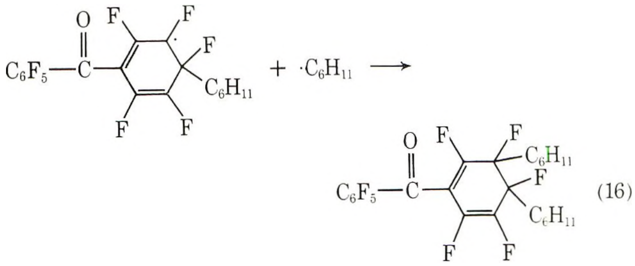
(16)

Reaction 16 and analogous reactions account for the formation of dicyclohexyl-substituted compounds found to be present in small yields (~1%) even at very low conversions when consecutive reactions of the monosubstituted products are unlikely.

The para/ortho isomer ratio in products resulting from mechanism I is 2.44 as measured by the ratio of $\Phi(\mathbf{3})/\Phi(\mathbf{2})$ at $I_a \approx \infty$. The para/ortho isomer ratio in the products obtained by mechanism II is estimated as approximately 6. The yield of the meta isomer is low (<5%) in both cases; however, mechanism II favors a higher yield of meta substitution than does mechanism I.

It should be mentioned that decafluorobenzophenone ketyl and cyclohexyl radicals, with the exception of reaction 8, do not undergo the usual radical combination and disproportionation reactions, as observed in the photochemistry of benzophenone. Thus, the yield of bicyclohexyl is very low, <1% of the total product. This indicates

---

(11) (a) G. O. Schenck and G. Matthias, *Tetrahedron Lett.*, 699 (1967); (b) G. O. Schenck, M. Cziesla, K. Eppinger, G. Matthias, and M. Pape, *ibid.*, 193 (1967).

(12) D. H. Hey and G. H. Williams, *J. Chem. Phys.*, **23**, 757 (1955).

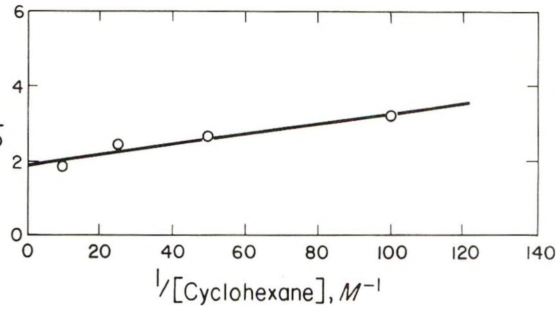

Figure 6. Φ *vs.* reciprocal cyclohexane concentration in perfluorodimethylcyclobutane. Decafluorobenzophenone concentration = 0.01 *M*; I_i = 3.96 × 10^{18} quanta min^{-1} cm^{-2}; light absorption = 46.2%.

that the rates of reactions 8 and 10 are higher by at least an order of magnitude than reaction 17a. The yield of de-

$$2\cdot C_6H_{11} \begin{array}{l} \xrightarrow{k_{17a}} C_{12}H_{22} \qquad (17a) \\ \xrightarrow{k_{17b}} C_6H_{10} + C_6H_{12} \qquad (17b) \end{array}$$

cafluorobenzhydrol is also very low, 2.5%, and there was no eicosafluorobenzopinacol detected in the reaction products. The low yield of these compounds indicates that the rates of reactions 8 and 10 are also much higher than the competing reactions 18a and 18b. The ratio of the rate

$$2(C_6F_5)_2\underset{\cdot}{C}OH \begin{array}{l} \xrightarrow{k_{18a}} (C_6F_5)_2COHCOH(C_6F_5)_2 \qquad (18a) \\ \xrightarrow{k_{18b}} (C_6F_5)_2CO + (C_6F_5)_2HCOH \qquad (18b) \end{array}$$

constants is k_{17b}/k_{17a} = 1.3[13] and the combined rate constant,[14] $k_{17a} + k_{17b} = 3.4 \times 10^9\ M^{-1}\ sec^{-1}$. From this, it follows that $k_{17a} = 1.5 \times 10^9\ M^{-1}\ sec^{-1}$. Assuming that k_{18a} is approximately the same as the rate constant[15] for the formation ot benzopinacol, *e.g.*, $k_{18a} \approx 3.1 \times 10^7\ M^{-1}\ sec^{-1}$, the combined rate of the cyclohexyl and the decafluorobenzophenone ketyl radical leading to products 1, 2, and 3 (reactions 8 and 10) can be estimated to be of the order of $1 \times 10^{10}\ M^{-1}\ sec^{-1}$, which is essentially equal to a diffusion-controlled rate. This rate constant is approximately two orders of magnitude greater than the corresponding rate constant of the reaction between the cyclohexyl and the benzophenone ketyl radicals. However, it should be pointed out that the assumption that $k_{18a} \approx 3.1 \times 10^7\ M^{-1}\ sec^{-1}$ may be invalid, and thus a definite conclusion cannot be drawn about the reactivity of the decafluorobenzophenone ketyl radical with the cyclohexyl radical. It is clear, however, that the unusual reactivity of the two primary radicals generated in this system can be caused either by a very high rate constant for the reaction between the decafluorobenzophenone ketyl and the cyclohexyl radicals, or alternatively, by a very low value for the rate constant k_{18b}, which should be at least two orders of magnitude lower than the corresponding rate constant for the reaction of benzophenone ketyl radicals. The importance of these two factors is being investigated, and the results will be reported elsewhere.

The slight decrease of Φ(1) with increasing decafluorobenzophenone concentration can be explained by radical–radical disproportionation reactions. Cyclohexyl radical addition to ground-state decafluorobenzophenone, reaction 13, is concentration dependent; thus reaction 19 which involves the radical formed by reaction 13 and the ketyl radical should be also concentration dependent. The diene formed by reaction 19a should aromatize by elimination of HF, as shown by reaction 12. The compound $(C_6F_5)_2C(OH)F$, if formed, would be very unstable and would decompose rapidly to decafluorobenzophenone and HF. Reactions 19a and 19b would decrease the concentration of the ketyl radical and thus the yield of 1 by reaction 8 would decrease with increasing decafluorobenzophenone concentration.

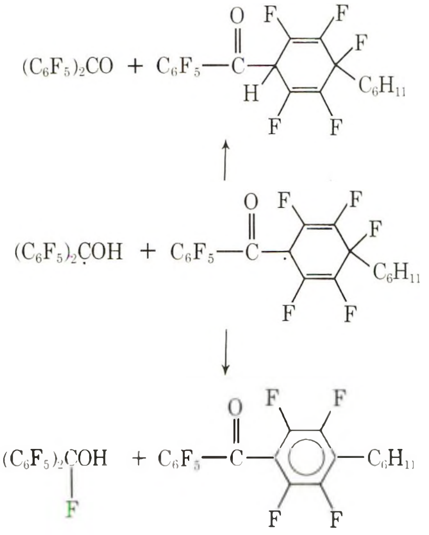

(19a)

(19b)

Finally, it should be mentioned that the quantum yield of decafluorobenzophenone at high light intensity being less than unity (Φ = 0.41 at *C* = 0.01 *M*) may be entirely due to back reaction 7a which converts the primary radical intermediates to the starting reactants. This is expected, since it was shown in the flash photolysis of benzophenone[16] that the yield of benzophenone ketyl radical was the same in several hydrogen-donating solvents, although the quantum yield of the final products varied by as much as fourfold.

(c) Rate of Hydrogen Abstraction. The triplet half-lifetime of decafluorobenzophenone in inert solvents (perfluoromethylcyclohexane, Freon E4, and CCl_4) at room temperature has been reported to be 14 μsec on the basis of flash photolysis investigation.[2] Thus, the decay constant, $k_d = 0.693/14 \times 10^{-6} = 4.95 \times 10^4\ sec^{-1}$. The rate of hydrogen abstraction, k_r, (reaction 6) can be related to Φ and cyclohexane concentration based on reactions 4–7b.

$$\Phi = \Phi_{isc}\left(\frac{k_p}{k_p + k_b}\right)\left[\frac{k_r(K^{3*})(RH)}{k_r(K^{3*})(RH) + k_d(K^{3*})}\right] \qquad (20)$$

where Φ and Φ_{isc} are the quantum yields of the disappearance of decafluorobenzophenone and of intersystem crossing efficiency, respectively.

$$\frac{1}{\Phi} = \frac{1}{\Phi_{isc}}\left(\frac{k_p + k_b}{k_p}\right)\left[1 + \frac{k_d}{k_r(RH)}\right] \qquad (21)$$

$$\frac{1}{\Phi} = \frac{1}{a}\left[1 + \frac{k_d}{k_r(RH)}\right] \qquad (22)$$

where $a = [(k_p + k_b)/k_p](1/\Phi_{isc})$. A linear plot of 1/Φ *vs.* 1/(RH) is shown in Figure 6 for the disappearance of decafluorobenzophenone dissolved in perfluorodimethylcyclobutane. The ratio of k_d/k_r is 0.00657 (determined from

---

[13] J. Y. Yang, F. M. Servedio, and R. A. Holroyd, *J. Chem. Phys.*, **48**, 1331 (1968).

[14] (a) W. G. Burns and C. R. V. Reed, *Trans. Faraday Soc.*, **66**, 2159 (1970); (b) W. G. Burns, M. J. Hopper, and C. R. V. Reed, *ibid.*, **66**, 2183 (1970).

[15] (a) C. C. Wamser, G. S. Hammond, C. T. Chang, and C. Baylor, Jr., *J. Amer. Chem. Soc.*, **92**, 6362 (1970); (b) A. Beckett and G. Porter, *Trans. Faraday Soc.*, **59**, 2038 (1963).

TABLE III: Comparison of Rate Constants of Decafluorobenzophenone and Benzophenone

Reaction	$(C_6F_5)_2CO$	Ref	$(C_6H_5)_2CO$	Ref
$K^{3*} \xrightarrow{k_d} K_0$	4.95×10^4 sec^{-1}	2	1.41×10^3 sec^{-1}	6
$K^{3*} + C_6H_{12} \xrightarrow{k_r} KH\cdot + \cdot C_6H_{11}$	$7.5 \times 10^6\ M^{-1}$ sec^{-1}	*a*	$3.6 \times 10^5\ M^{-1}$ sec^{-1}	16
$K^{3*} + C_6H_6 \xrightarrow{k_q} K_0 + C_6H_6$	$1.6 \times 10^8\ M^{-1}$ sec^{-1}	*a*	$0.8 \pm 0.1 \times 10^5\ M^{-1}$ sec^{-1}	19

[a] This work.

the slope/intercept ratio). Thus, $k_r = 7.5 \times 10^6\ M^{-1}$ sec^{-1}.

Porter and Topp[16] reported a decay constant for benzophenone triplet in cyclohexane of 3.3×10^6 sec^{-1}. Assuming that the triplet is quenched essentially by hydrogen abstraction (reaction 6), the second-order rate constant is $(3.3 \times 10^6)/9.27 = 3.6 \times 10^5\ M^{-1}$ sec^{-1} (concentration of cyclohexane is 9.27 M). Thus, the rate of hydrogen abstraction by decafluorobenzophenone is 22 times as great as that by benzophenone. The higher rate of hydrogen abstraction provides an explanation why the photochemical reaction in this case is not nearly so much affected by oxygen as in the case of benzophenone. For example, a long irradiation of a nondegassed solution of benzophenone in cyclohexane does not result in any appreciable conversion; on the other hand, decafluorobenzophenone under similar conditions is converted at a moderate rate, which is approximately ⅓ as fast as that obtained under irradiation conditions using degassed solutions.

3. *Quenching by Benzene.* Hammond, Baker, and Moore[17] showed that benzene and toluene quench the triplet state of benzophenone and calculated the approximate rate constants of the quenching reactions. Bell and Linschitz[18] showed by flash photolysis that the triplet lifetime of benzophenone in benzene is relatively short. In this laboratory using continuous irradiation[7] and flash photolysis[19] it was shown that photoreduction of benzophenone triplet by hydrogen abstraction from benzene takes place, but at such a slow rate that the short lifetime of the triplet state cannot be explained by the hydrogen abstraction reaction, and thus a direct quenching of the benzophenone triplet by benzene is indicated. Saltiel, Curtis, and Jones[20] also determined the quantum yield of the photoreduction reaction. It was found by Porter and Topp[16] and by Schuster, *et al.*,[21] that benzophenone triplet is quenched faster by perfluorobenzene than by benzene. Since a direct energy transfer would be endothermic by 13 kcal/mol, it appears that the mechanism of quenching should involve an intermediate derived from benzophenone triplet and benzene. The intermediate may be a charge-transfer complex, an exciplex, or a diradical adduct.[22]

In view of these findings, it was of interest to study the photochemical reactions of decafluorobenzophenone in benzene. The results showed no conversion of decafluorobenzophenone after a long period of irradiation and there was no indication of any products formed on the basis of tlc, glc, and uv absorption analysis. These results indicated a rapid quenching of the triplet state by benzene. Therefore, a study was carried out using decafluorobenzophenone dissolved in perfluorodimethylcyclobutane (0.01 M) containing 0.04 M cyclohexane and varying amounts of benzene. A Stern-Volmer plot based on eq 23 is presented in Figure 7, which shows a linear relationship for the disappearance of decafluorobenzophenone.

$$\Phi_0/\Phi = 1 + [k_q[Q]/(k_d + k_r[RH])] \qquad (23)$$

In this equation, k_q is the rate constant for quenching by benzene and [Q] is benzene concentration. The slope of the plot = 470; thus $k_q = 1.6 \times 10^8\ M^{-1}$ sec^{-1}. This rate constant is three orders of magnitude greater than that of benzophenone quenching by benzene, as can be seen from the comparison of the rate constants for decafluorobenzophenone and benzophenone presented in Table III.

In general, both the rate of hydrogen abstraction from cyclohexane and the rate of quenching of the $^3(n,\pi^*)$ state by benzene are greater in the case of decafluorobenzophenone than in benzophenone. Since the $^3(n,\pi^*)$ energy of these two compounds is essentially the same, the only explanation that is consistent with the experimental results is that both the difference in the rate of hydrogen abstraction and the rate of quenching by benzene must be dependent on the degree of charge polarization of the $^3(n,\pi^*)$ state. The decafluorobenzophenone because of the inductive effect of fluorine substitution should have a much higher degree of charge polarization in the $^3(n,\pi^*)$ state than benzophenone and thus, a higher rate of hydrogen abstraction. This is in agreement with the experimental results. A higher degree of charge polarization should also facilitate the rate of formation of a charge-transfer complex or an exciplex between ketone in the $^3(n,\pi^*)$ state and benzene. Since the quenching rate of the decafluorobenzophenone triplet by benzene is 10^3 times greater than that of benzophenone triplet, these results indicate that the intermediate in the energy transfer mechanism must be a charge-transfer complex, or an exciplex, formed between the ketone in the $^3(n,\pi^*)$ state and benzene.

---

(16) G. Porter and M. R. Topp, *Proc. Roy. Soc., Ser. A*, **315**, 163 (1970).

(17) G. S. Hammond, W. P. Baker, and W. M. Moore, *J. Amer. Chem. Soc.*, **83**, 2795 (1961).

(18) J. A. Bell and H. Linschitz, *J. Amer. Chem. Soc.*, **85**, 528 (1963).

(19) A. V. Buettner and J. Dedinas, *J. Phys. Chem.*, **75**, 187 (1971).

(20) J. Saltiel, H. C. Curtis, and B. Jones, *Mol. Photochem.*, **2**, 331 (1970).

(21) D. I. Schuster, T. M. Weil, and M. R. Topp, *Chem. Commun.*, 1212 (1971).

(22) Schuster, *et al.*,[21] claim evidence for a diradical intermediate on the basis that the benzophenone triplet is quenched by perfluorobenzene at a faster rate than by benzene. This observation cannot constitute a proof for the existence of a diradical intermediate and is essentially a reiteration of the earlier hypothesis of Saltiel, *et al.*,[23] and of Schuster, *et al.*[24]

Some of the statements pertaining to experimental procedures may be misleading. The selective photochlorination procedure, an unpublished technique of Saltiel and Metts, is claimed to produce benzene of higher purity[21] than that obtained by alternative procedures. The test for maximum purity was the finding of the lowest observed rate of benzophenone triplet decay (k_q), the value of which reported by Schuster, *et al.*,[21] is $1.0 \pm 0.1 \times 10^5$ sec^{-1}. Buettner and Dedinas,[19] using zone-refined benzene (99.997%) and zone-refined benzophenone (99.9%), determined k_q to be $0.8 \pm 0.1 \times 10^5$ sec^{-1}. Since these values are the same within experimental error, they cannot be used as a test for determining which technique for purifying benzene is superior.

Schuster, *et al.*,[21] imply that more accurate results were obtained using a laser flash than the microsecond flash employed in the previous investigations.[18,19] This is hardly the case because the results within experimental error were the same using both techniques.[19,21]

(23) J. Saltiel, H. C. Curtis, L. Metts, J. W. Miley, J. Winterle, and M. Wrighton, *J. Amer. Chem. Soc.*, **92**, 410 (1970).

(24) D. I. Schuster and D. F. Brizzolara, *J. Amer. Chem. Soc.*, **92**, 4357 (1970).

TABLE IV: Photolysis[a] of Decafluorobenzophenone in Toluene and *p*-Xylene

Solvent	Toluene	*p*-Xylene
Φ (ketone disappearance)	0.055	0.096
Product[b] yields, %		
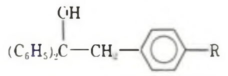	68 ± 5	68 ± 5
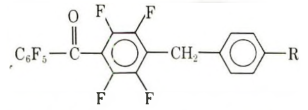	30 ± 5	30 ± 5
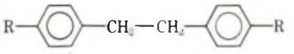	<2	<2
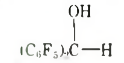 $(C_6F_5)_2C(OH)H$	<1	<1

[a] Conditions: 0.01 *M* decafluorobenzophenone concentration, 23°, 366-nm light, $I_i = 5.84 \times 10^{17}$ quanta min^{-1} cm^{-2}. [b] R = H in toluene, R = CH_3 in *p*-xylene.

4. Photochemistry in Toluene and p-Xylene. In view of the rapid rate of decafluorobenzophenone triplet quenching by benzene and, *via* a hydrogen abstraction mechanism, by cyclohexane, it was of interest to investigate the photochemistry in toluene. As expected, in this solvent the triplet state was quenched by both mechanisms: (a) hydrogen abstraction of the benzylic hydrogen and (b) energy transfer by the aromatic ring. This is concluded from the very low quantum yield, 0.055 of decafluorobenzophenone disappearance and a good agreement between this value and an estimated quantum yield (0.045). The latter was deduced from an assumption that the rate constant of hydrogen abstraction of the benzylic hydrogen is approximately the same as that ot the cyclohexane hydrogen, and that the rate of direct triplet quenching by toluene is the same as by benzene, *e.g.*

$$\Phi_{\text{estimated}} \approx k_r/(k_r + k_q) = 0.045$$

The reaction mechanism, based on the products identified, is similar but not quite the same as described for the photochemistry in cyclohexane. The difference of product distribution is attributed to a lower reactivity of the benzyl radical in comparison to the cyclohexyl radical. The product yields are summarized in Table IV. The principal product (68%) is benzyldi(pentafluoro)phenylcarbinol. The other major product (30%) is *p*-benzylnonafluorobenzophenone. These products are analogous to those formed by reaction 8 and by mechanism I (reactions 10–12), respectively, obtained when using cyclohexane solvent. There is only the para-substituted ketone formed and there is no ortho product when toluene is used as a solvent. The lack of substitution at the ortho position indicates that the decafluorobenzophenone ketyl radical has the unpaired electron essentially localized on the carbon atom containing the hydroxyl group, and thus the preferred reaction with a benzyl radical is a radical combination (reaction 8) rather than a radical substitution (reaction 10). Similarly, it appears that the rate of benzyl radical addition to the ground-state decafluorobenzophenone should be much slower than the rate of addition of the cyclohexyl radical. From this it follows that the product distribution (although not tested experimentally) using toluene as a solvent should be much less dependent on light intensity and on decafluorobenzophenone concentration than in the case of cyclohexane solutions.

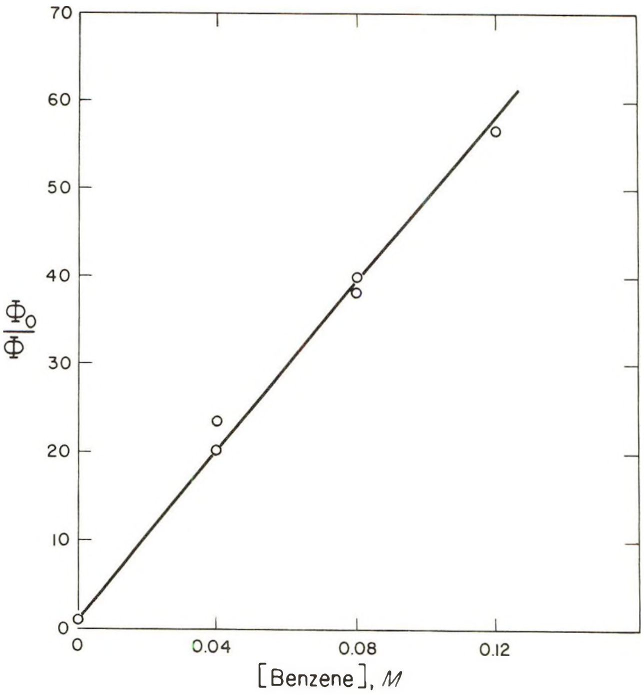

Figure 7. Stern–Volmer plot showing the effect of benzene quenching. Decafluorobenzophenone and cyclohexane concentrations are 0.01 and 0.04 *M*, respectively, in perfluorodimethylcyclobutane.

The decafluorobenzophenone disappearance in *p*-xylene was measured under the same conditions as in toluene. Φ = 0.096, indicating that the rate of hydrogen abstraction, as expected, should be greater by a factor of 2 than in toluene. The results summarized in Table IV indicate that the products were of the same type and essentially of the distribution as obtained in the photochemistry of toluene.

Conclusion

The initial photochemical steps, including intersystem crossing efficiency and the mechanism of hydrogen abstraction by the reactive $^3(n,\pi^*)$ state, are the same as in the photochemistry of benzophenone. The primary radical intermediates undergo a recombination reaction and a radical–radical aromatic substitution reaction. The latter reaction, when one of the radicals is the cyclohexyl radical, leads to the formation of both ortho and para alkyl-substituted nonafluorobenzophenone; when it is the benzyl radical, only the corresponding para-substituted compound is formed. At high concentrations and at low light intensities, an aromatic substitution reaction involving the cyclohexyl radical and decafluorobenzophenone in the ground state is also significant. A summary of the rate constants presented in Table III indicates that the rate constants of hydrogen abstraction from cyclohexane and quenching by benzene are much higher than those obtained in the photochemistry of benzophenone. These higher rates must be due to the inductive effect of fluorine substitution, which increases the charge polarization of the $^3(n,\pi^*)$ state. The quenching mechanism by benzene must involve a charge-transfer complex or an exciplex between the $^3(n,\pi^*)$ state and benzene.

Acknowledgment. Reviewing of the manuscript by Dr. C. D. DeBoer is gratefully acknowledged.

Sensitization and Quenching of the Cis → Trans Isomerization of Bis(glycinato)platinum(II)

Fabrizio Bolletta, Mario Gleria, and Vincenzo Balzani*

Istituto Chimico "G. Ciamician" dell' Università, Laboratorio di Fotochimica e Radiazioni d'Alta Energia del CNR, 40126 Bologna, Italy

(Received June 27, 1972)

The possibility of sensitizing and quenching the cis → trans intramolecular isomerization of $Pt(gly)_2$ has been investigated using various triplet donors and acceptors. Pyrazine (26.2 kK) and xanthone (26 kK) were found to sensitize the cis → trans isomerization ($\Phi_{\lim} \sim 0.03$ and ~ 0.1, respectively), whereas no sensitization was found when thioxanthone (22.9 kK), quinoline (22 kK), naphthalene (21.2 kK), and biacetyl (19.2 kK) were used. Ni_{aq}^{2+} ions (8.9 kK) were found to quench the photoisomerization, whereas no quenching effect was obtained with Mn_{aq}^{2+} ions (18.9 kK). The lack of sensitization by the donors in the 22.9–19.2 kK range *and* the lack of quenching by Mn_{aq}^{2+} (18.9 kK) are interpreted on the basis of unfavorable Franck–Condon factors due to the distortion of the excited state that is responsible for the cis → trans isomerization.

Introduction

Sensitization and quenching techniques have profitably been used in organic photochemistry to individualize the state(s) responsible for the observed photoreactivity.[1]

In the last few years, the use of these techniques has also become popular in the photochemistry of coordination compounds and some interesting results have already been obtained concerning the role played by the various excited states in the photoaquation of Cr(III) complexes[2] and in the redox decomposition of Co(III) complexes.[3] However, to our knowledge no example of sensitized or quenched isomerization of coordination compounds has so far been reported. In the field of organic photochemistry, on the contrary, sensitization and quenching of isomerization reactions have extensively been investigated,[1,4] and the results so obtained have given important information on the involvement of distorted excited states and have also generated stimulating discussions on nonvertical energy transfer and related problems.[1] It seems obvious that the extension of such investigations to the intramolecular isomerization of coordination compounds may also offer interesting information as far as the excited state distortions and the energy transfer processes are concerned.

We wish to report here a study concerning the sensitization and quenching of the cis → trans isomerization of $Pt(gly)_2$ (gly = glycinato anion). The choice of this complex was based on the fact that, at present, it is the sole coordination compound which has been shown to undergo a geometrical photoisomerization *via* an intramolecular mechanism.[5a] The participation of distorted excited states in such an intramolecular isomerization reaction has already been discussed in some detail.[5,6]

Experimental Section

Materials. *cis*-Bis(glycinato)platinum(II), *cis*-$Pt(gly)_2$, was prepared following the indications given in ref 5a. *trans*-$Pt(gly)_2$ was obtained by the methods of Pinkard, *et al.*[7] Xanthone (xanthen-9-one), thioxanthone (thioxanthen-9-one), biacetyl (2,3-butanedione), and naphthalene "suitable for sensitizer use" were obtained from the Baker Chemical Co. and used without further purifications. Reagent grade pyrazine was purified by vacuum sublimation. All of the other chemicals were of reagent grade.

Apparatus. Radiations of 254 nm were obtained as previously described.[8] Those of 313, 334, and 365 nm were obtained from a Hanau Q 400 mercury vapor lamp by using Schott and Genossin interference filters.[9] Radiations of 401 nm were obtained as described in ref 10. The intensity of the incident light was measured by means of the ferric oxalate actinometer,[11] and was of the order of 10^{-7} $Nh\nu$/min for all of the wavelengths used. The fraction of the absorbed light was calculated on the basis of the transmittance of the solutions. Spectrophotometric measurements were performed with an Optica CF4 NI spectrophotometer and the emission spectra were recorded with a Turner Spectro 210 spectrofluorimeter.

Procedures. The general procedure for the study of the sensitization and quenching of the *cis*-$Pt(gly)_2$ isomerization was as follows. Weighed amounts of the complex and of the potential sensitizer or quencher were dissolved in the selected medium (water or water–ethanol 50% v/v). A sample (3 ml) of the solution was put into a spectrophoto-

---

(1) A. A. Lamola, "Energy Transfer and Organic Photochemistry," A. A. Lamola and N. J. Turro, Ed., Interscience, New York, N. Y., 1969, p 17.

(2) (a) G. B. Porter, S. N. Chen, H. L. Schläfer, and H. Gausmann, *Theor. Chim. Acta*, **20**, 81 (1971); (b) C. H. Langford and L. Tipping, *Can. J. Chem.*, **50**, 887 (1971); (c) N. Sabbatini and V. Balzani, *J. Amer. Chem. Soc.*, in press.

(3) M. A. Scandola and F. Scandola, *J. Amer. Chem. Soc.*, **92**, 7278 (1970).

(4) (a) N. J. Turro, *Photochem. Photobiol.*, **9**, 555 (1969); (b) J. Saltiel and E. D. Magarit, *J. Amer. Chem. Soc.*, **94**, 2742 (1972), and references cited therein.

(5) (a) F. Scandola, O. Traverso, V. Balzani, G. L. Zucchini, and V. Carassiti, *Inorg. Chim. Acta*, **1**, 76 (1967); (b) V. Balzani and V. Carassiti, *J. Phys. Chem.*, **72**, 383 (1968); (c) F. S. Richardson, D. D. Shillady, and A. Waldrop, *Inorg. Chim. Acta*, **5**, 279 (1971).

(6) V. Balzani and V. Carassiti, "Photochemistry of Coordination Compounds," Academic Press, London, 1970.

(7) F. W. Pinkard, E. Sharrat, and W. Wardlaw, *J. Chem. Soc.*, 1012 (1934).

(8) V. Balzani, V. Carassiti, L. Moggi, and F. Scandola, *Inorg. Chem.*, **4**, 1243 (1965).

(9) V. Balzani, R. Ballardini, N. Sabbatini, and L. Moggi, *Inorg. Chem.*, **7**, 1398 (1968).

(10) V. Balzani, R. Ballardini, M. T. Gandolfi, and L. Moggi, *J. Amer. Chem. Soc.*, **93**, 339 (1971).

(11) C. G. Hatchard and C. A. Parker, *Proc. Royal Soc., Ser. A*, **235**, 518 (1956).

metric cell that was placed in the thermostated (25°) cell holder of the irradiation equipment. All of the experiments were carried out at a pH of 6–7 since it has been shown that in this pH range *cis*-$Pt(gly)_2$ only undergoes intramolecular cis → trans photoisomerization.[12] After a suitable irradiation period, the irradiated solution was poured into a chromatographic column in order to separate the two isomers whose concentration was then determined spectrophotometrically at 230 nm. For more details on this procedure see ref 12. Since xanthone, thioxanthone, naphthalene, and biacetyl were found to interfere with the chromatographic separation, they were extracted with ether or chloroform before pouring the irradiated solution into the column. Irradiation of deaerated solutions was carried out on a special spectrophotometric cell connected to a side-arm bulb where the solution was degassed with freeze–pump–thaw cycles. For solutions containing biacetyl, this deaeration method could not be used since it gave some turbidity. In these cases, deoxygenation was performed by bubbling a stream of purified N_2. The observed ratio of phosphorescent to fluorescent emission was about 8:1.

Results

The maximum solubility of *cis*-$Pt(gly)_2$ in water at 25° was about 2×10^{-3} *M* and the trans isomer was about five times less soluble. In all of the other solvents suitable for photochemical studies both the complexes were much less soluble. For this reason, and because of the small extinction coefficients of *cis*-$Pt(gly)_2$ above 230 nm, only water or water–ethanol 50% v/v mixtures could be used as a solvent. This, of course, somewhat limited the possibility of using standard donors since many of them are water insoluble organic molecules.[1,13,14] Moreover, some of the organic donors that were soluble in water or water–ethanol mixtures (specifically, diphenylamine, β-naphthylamine, 3-pentanone, *p*-toluenesulfonic acid, and naphthalene-1-sulfonic acid) were found to undergo photodecomposition reactions, and other donors, like acetone and biphenyl, were found to give some photoreaction with *cis*-$Pt(gly)_2$. All of these compounds had thus to be discarded.

As far as the quenching of the isomerization reaction was concerned, the small absorption coefficient and the low solubility of *cis*-$Pt(gly)_2$ did not allow us to use any of the standard organic quenchers. However, the hydrated ions of some transition metals proved to be suited for these experiments, as had already been shown for the quenching of $Cr(en)_3{}^{3+}$.[15]

None of the potential donors or acceptors that we systematically investigated (see Table I) gave any disturbing thermal or photochemical reactions under our experimental conditions (see below). We would also like to mention that, contrary to what was reported in ref 16, we were unable to obtain any luminescence emission from room temperature methanolic solutions of *cis*- or *trans*-$Pt(gly)_2$. No emission was also found to occur for aqueous or ethanolic solutions of the two isomers.

A summary of the results obtained from the sensitization and quenching experiments is given in Table I.

Sensitization Experiments. Pyrazine. Aqueous solutions containing 4×10^{-3} *M* pyrazine and 2×10^{-4}–1.8×10^{-3} *M cis*-$Pt(gly)_2$ were used. The excitation was carried out at 313 nm. Under such conditions, most of the incident light was absorbed by pyrazine. Chromatographic separation of the irradiated solutions showed that the light absorbed by pyrazine led to the formation of *trans*-$Pt(gly)_2$ and to the concomitant disappearance of *cis*-$Pt(gly)_2$. After correcting for the small contribution of the direct photoisomerization, the experimental quantum yield for the sensitized isomerization was found to increase with increasing complex concentration. The results obtained, however, were limited for solubility reasons and were also affected by a large experimental error (≤30%[12]) owing to the complicated analytical procedure that had to be adopted. Therefore, only an approximate value could be obtained for the limiting quantum yield ($\Phi_{\lim} \sim 0.03$). No quenching of the pyrazine fluorescence was observed.

TABLE I: Sensitization and Quenching of the Cis → Trans Isomerization of $Pt(gly)_2$

Potential donor or acceptor	E,[a] kK	Sensitization	Quenching
Pyrazine	26.2	Yes	
Xanthone	26.0	Yes	
Thioxanthone	22.9	No	
Quinoline	22.0	No	
Naphthalene	21.2	No	
Biacetyl	19.2	No[b]	
$Mn_{aq}{}^{2+}$	18.9[c]		No
$Ni_{aq}{}^{2+}$	8.5		Yes

[a] Energy of the lowest triplet excited state unless otherwise noted. [b] The biacetyl phosphorescence is quenched (see text). [c] This excited state, which is the lowest one for $Mn_{aq}{}^{2+}$, is a quartet.

Xanthone. Deaerated hydroalcoholic solutions containing 2×10^{-4} *M* xanthone and 6×10^{-4}–1×10^{-3} *M cis*-$Pt(gly)_2$ were used. The excitation was carried out with 334-nm radiations. Under such conditions, most of the incident light (≥98%) was absorbed by xanthone and a sensitized isomerization of the complex was found to occur. The experimental quantum yield of the photosensitized isomerization increased with increasing complex concentration and an approximate value of ~0.1 was obtained for the limiting quantum yield.

Other Potential Donors. When thioxanthone, quinoline, naphthalene, and biacetyl were used as donors, no photosensitization effect was observed on the *cis*-$Pt(gly)_2$ isomerization. The experimental conditions used were as follows: *thioxanthone* 1×10^{-4} *M*, *cis*-$Pt(gly)_2$ 6×10^{-4}–1×10^{-3} *M*, λ_{exc} 365 nm, irradiation times up to 8 hr, deaerated hydroalcoholic solutions; *quinoline* 3×10^{-4} *M*, *cis*-$Pt(gly)_2$ 6×10^{-4}–1.8×10^{-3} *M*, λ_{exc} 313 nm, irradiation times up to 6 hr, deaerated aqueous solutions; *naphthalene* 2×10^{-4} *M*, *cis*-$Pt(gly)_2$ 2×10^{-4}–1×10^{-3} *M*, λ_{exc} 254 nm, irradiation times up to 8 hr, deaerated hydroalcoholic solutions, no quenching of the naphthalene fluorescence was observed; *biacetyl* 1×10^{-1} *M*, *cis*-$Pt(gly)_2$ 6×10^{-4}–1.8×10^{-3} *M*, λ_{exc} 401 nm, irradiation times up to 8 hr, deoxygenated aqueous solutions. It is interesting to note that, in spite of the lack of any sensitization effect of biacetyl on the isomerization reaction, its phosphorescence was quenched by *cis*-$Pt(gly)_2$. The Stern–Volmer

---

(12) F. Bolletta, M. Gleria, and V. Balzani, *Mol. Photochem.*, **4**, 205 (1972).

(13) N. J. Turro, J. C. Dalton, and D. S. Weiss, "Organic Photochemistry," Vol. 2, O. L. Chapman, Ed., Marcel Dekker, New York, N. Y., 1969, p 1.

(14) P. S. Engel and B. M. Monroe, *Advan. Photochem.*, **8**, 245 (1971).

(15) R. Ballardini, G. Varani, L. Moggi, and V. Balzani, to be submitted for publication.

(16) Private communication quoted in P. D. Fleischauer and P. Fleischauer, *Chem. Rev.*, 70, 199 (1970).

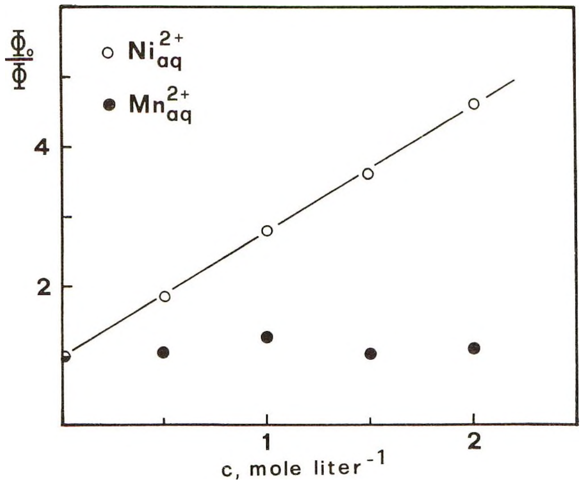

Figure 1. Stern–Volmer plots for the quenching of the cis → trans isomerization of $Pt(gly)_2$.

quenching constant obtained from a plot of I_0/I *vs.* [*cis*-$Pt(gly)_2$] was 6×10^4 M^{-1}. Since prolonged irradiation (up to 8 hr) of solutions containing biacetyl and *cis*-$Pt(gly)_2$ did not cause any consumption of *cis*-$Pt(gly)_2$ within our experimental errors, it resulted that no more than 1% of the biacetyl triplet excited states generated by irradiation were quenched *via* an irreversible chemical mechanism involving the complex. We have also found that the biacetyl phosphorescence was not quenched by 8×10^{-3} M glycine, both at pH 2 and 6.

Quenching Experiments. When aqueous solutions of *cis*-$Pt(gly)_2$ were irradiated at 254 nm in the presence of various amounts of $MnSO_4 \cdot H_2O$ (up to 2 M), no quenching effect was observed on the quantum yield of the photoisomerization reaction. On the contrary, the presence of $NiSO_4 \cdot 7H_2O$ was found to exhibit a quenching effect. For 2 F Ni_{aq}^{2+}, the quantum yield of the photoisomerization was reduced to about 20% of its Φ_0 value. After appropriate corrections were made for the fraction of light absorbed by the quencher, a linear Stern–Volmer plot was obtained as is shown in Figure 1.

Discussion

The results obtained show that the cis → trans isomerization of $Pt(gly)_2$ can be sensitized and quenched when suitable donors and acceptors are used. Since the pyrazine fluorescence was unquenched by *cis*-$Pt(gly)_2$ and since xanthone is known to act as a triplet donor,[1] the sensitization process can formally be described as a triplet–triplet intermolecular energy transfer. However, it must be recalled that in platinum complexes, owing to the large degree of spin–orbit coupling, it may be meaningless to talk about discrete spin states.

Considering that the intersystem crossing efficiency of pyrazine is lower than unity (~0.3 in n-hexane at 25° [17]) and assuming that the intersystem crossing effficiency of xanthone is near unity, the approximate values obtained for the limiting quantum yield (~0.03 and ~0.1, respectively) seem to indicate that the quantum yield is roughly the same for the sensitized and the direct[5a] photoisomerization.

The results obtained with the donors and acceptors used (see Table I) show that the states responsible for the isomerization of *cis*-$Pt(gly)_2$ must be located between 8.5 and 26 kK. At first sight, it may seem surprising that there is lack of sensitization by donors in the 22.9–19.2 kK range *and* a lack of quenching by Mn_{aq}^{2+} (18.9 kK). As a matter of fact, such a result is exactly that expected for sensitization and quenching of intramolecular isomerization which involve distorted excited states.[1] We would like to discuss briefly this feature as well as some other interesting ones of our system.

Generally speaking, the lack of energy transfer between a donor and an acceptor may be due to (i) a low concentration of the acceptor, (ii) a short lifetime of the donor excited state, τ, and (iii) a low value of the energy transfer rate constant, k_{et}. The minimum value for the quantum yield of the sensitized isomerization detectable with our analytical procedure was $\sim 10^{-3}$. Since the maximum value for the acceptor concentration was $\sim 10^{-2}$ M, it can be shown that, in order to observe some sensitized isomerization, the product τk_{et} had to be of the order of 10 M^{-1}. Since all of the triplet states of the donors used are expected to have $\tau > 10^{-7}$ sec,[18] we can conclude that the lack of sensitization when thioxanthone, quinoline, naphthalene, and biacetyl were used must be due to the fact that the rate constant for energy transfer from the donor triplets *to any excited state of cis-*$Pt(gly)_2$*, which can be a precursor to the isomerization,* is much lower than the diffusion controlled rate constant.[23,24] Such a low value of the energy transfer rate constant may be due to two main reasons: (i) the energy transfer is endothermic; (ii) there are unfavorable Franck–Condon factors. However, the lack of quenching by Mn_{aq}^{2+} shows that the Franck–Condon factors certainly play an important role (Figure 2, see below).

From the results concerning the quenching of the photoisomerization by Ni_{aq}^{2+} (Figure 1), we can obtain a value of about 2 M^{-1} for the product $k_q\tau$ (k_q = quenching constant, τ = lifetime of the excited state that is responsible for the cis → trans isomerization). Since the quenching constants for transition metal ions are known to be $\sim 10^7$ M^{-1} sec^{-1} in the case of aromatic triplets[26] and even lower ($\sim 10^5$ M^{-1} sec^{-1}) for metal-centered excited states,[15] the lifetime of the excited state responsible for the cis → trans isomerization must be $> 10^{-7}$ sec.[27]

Finally, we would like to point out that the lack of

---

(17) B. J. Cohen and L. Goodman, *J. Chem. Phys.*, **46**, 713 (1967).

(18) This is a conservative estimate. The values reported in the literature are as follows: 7.7×10^{-5} sec for thioxanthone in benzene;[19] $\sim 10^{-4}$ sec for quinoline in 20% ethanol–water;[20] 3.6×10^{-3} sec for naphthalene in ethanol;[21] $\sim 10^{-4}$ sec for biacetyl in water.[22]

(19) W. G. Herkstroeter and G. S. Hammond, *J. Amer. Chem. Soc.*, **88**, 4769 (1966).

(20) H. D. Gafney and A. W. Adamson, *J. Phys. Chem.*, **76**, 1105 (1972).

(21) C. A. Parker, "Photoluminescence of Solutions," Elsevier, New York, N. Y., 1968, p 315.

(22) M. Almgren, *Photochem. Photobiol.*, **6**, 829 (1967).

(23) J. C. Calvert and N. J. Pitts, Jr., "Photochemistry," Wiley, New York, N. Y., 1966, p 627.

(24) The lack of any sensitized isomerization using biacetyl and the concomitant quenching of the biacetyl phosphorescence by *cis*-$Pt(gly)_2$ can be attributed either (i) to an intramolecular deactivation of the biacetyl triplets catalyzed by the complex,[3] or (ii) to an energy transfer process from the biacetyl triplets to *cis*-$Pt(gly)_2$ excited state that cannot be a precursor to the isomerization. A chemical mechanism for the quenching of the biacetyl phosphorescence by *cis*-$Pt(gly)_2$ can most probably be excluded for the reasons exposed under Results. Of course, a chemical quenching mechanism involving *reversible* hydrogen or electron abstraction[25] cannot be ruled out. In the case of hydrogen abstraction, however, free glycine would also be expected to quench the biacetyl phosphorescence, but this did not happen (see Results). As far as the reversible electron abstraction is concerned, there does not seem to be any obvious reason for the involvement of *cis*-$Pt(gly)_2$ in such a mechanism.

(25) N. J. Turro and R. Engel, *Mol. Photochem.*, **1**, 143 (1969).

(26) G. Porter and M. R. Wright, *Discuss. Faraday Soc.*, **27**, 18 (1959).

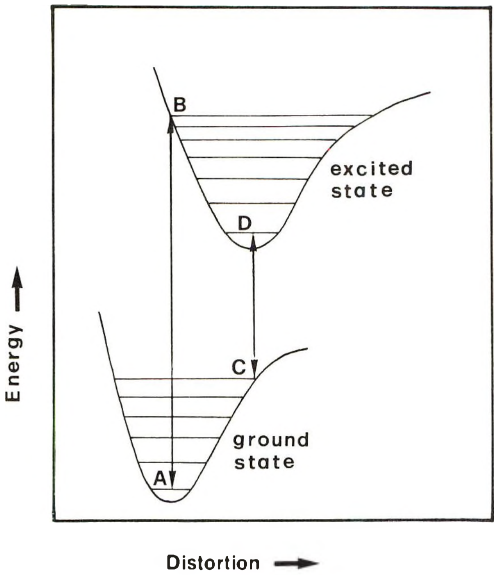

Figure 2. Schematic representation of the importance of excited state distortion in the sensitization and quenching of *cis*-Pt(gly)$_2$ isomerization. Our results suggest that AB is between ~23 and ~26 kK, and CD between ~9 and ~19 kK.

sensitization by the donors in the 22.9–19.2 kK range *and* the lack of quenching by Mn_{aq}^{2+} (18.9 kK) indicate that, as happens for the organic molecules which are capable of undergoing cis → trans intramolecular isomerization,[1] the energy of the state responsible for the isomerization cannot be "localized" by sensitization and quenching experiments, owing to the distortion of this state with respect to the ground state. Our data (see Table I) only indicate that, as far as the excited state responsible for the *cis*-Pt(gly)$_2$ isomerization is concerned, the vertical excitation energy (AB in Figure 2) is between ~23 and ~26 kK, and the vertical deactivation energy (CD in Figure 2) is between ~9 and ~19 kK.

Note also that this quenchable excited state must be a "cisoid" excited state as, for example, that shown in Figure 5 of ref 5c; it cannot be the "transoid" excited state proposed in ref 5a, 5b, and 6, although it could be a cisoid precursor of that state.

(27) Since the quenching constant is much lower than the diffusion constant, static quenching cannot be important even if very high quencher concentrations were used.[28] This is also confirmed by the linearity of the Stern–Volmer plot (Figure 1).

(28) P. J. Wagner, "Creation and Detection of the Excited State," Vol. 1A, A. A. Lamola, Ed., Marcel Dekker, New York, N. Y., 1971, p 201.

Triplet ← Triplet Absorption and Intersystem Crossing in Phthalazine

Vernon L. Alvarez and Steven G. Hadley*

Department of Chemistry, University of Utah, Salt Lake City, Utah 84112

(Received June 6, 1972)

Publication costs assisted by the National Science Foundation

The extinction coefficient for triplet–triplet absorption and the value of the intersystem crossing quantum yield, Φ_{ISC}, were measured for phthalazine in a rigid glass at the temperature of boiling nitrogen. The value of the extinction coefficient was found to be ϵ_{max} 4.45(±0.2) × 10^3 M^{-1} cm^{-1} measured at 420.5 nm. The value of the oscillator strength for this transition was determined to be $f = 0.11$. The intersystem crossing quantum yield was measured using excitation radiation corresponding to both $\pi \rightarrow \pi^*$ excitation (240–300 nm) and n → π^* excitation (310–350 nm). The value of the intersystem crossing quantum yield, $\Phi_{ISC} = 0.99 \pm 0.07$, was found to be independent of the excitation region within the experiment uncertainty. The lifetime of the phosphorescent state was also measured and was found to be independent of the excitation region. The phosphorescent lifetime was measured to be $\tau_p = 0.42 \pm 0.04$ sec.

Introduction

Phthalazine (2,3-diazanaphthalene) has recently been the subject of much study[1-4] because of the possibility of strong interaction between the nonbonding electron pairs. It is now generally accepted that the lowest excited singlet[3] is of type $^1A_2(n,\pi^*)$ which in the pure crystal is located 23,577 cm^{-1} above the ground state. The next higher excited singlet is of type $^1A_1(\pi,\pi^*)$, 32,250 cm^{-1} above the ground state. The lowest triplet state[1,2] is of type $^3B_2$ (π,π^*), with energy 22,780 cm^{-1} above the ground state. Little information is available concerning the dependence (if any) of the luminescent and radiationless processes such as fluorescence, phosphorescence, and intersystem crossing on the wavelength of absorption. Li and Lim[4] report that the phosphorescence quantum yield of phthalazine changes by a factor of 3 upon change in excitation wavelength. They reported that the phosphorescent quantum yield for excitation wavelengths less than 310 nm was three times greater than the quantum yield for excitation

(1) E. C. Lim and J. Stanislaus, *J. Chem. Phys.*, **53**, 2096 (1970).

(2) H. Baba, I. Yamazaki, and T. Takemura, *Spectrochim. Acta, Part A*, **27**, 1271 (1971).

(3) R. M. Hochstrasser and D. A. Wiersma, *J. Chem. Phys.*, **56**, 528 (1972).

(4) Y. H. Li and E. C. Lim, *J. Chem. Phys.*, **56**, 1004 (1972).

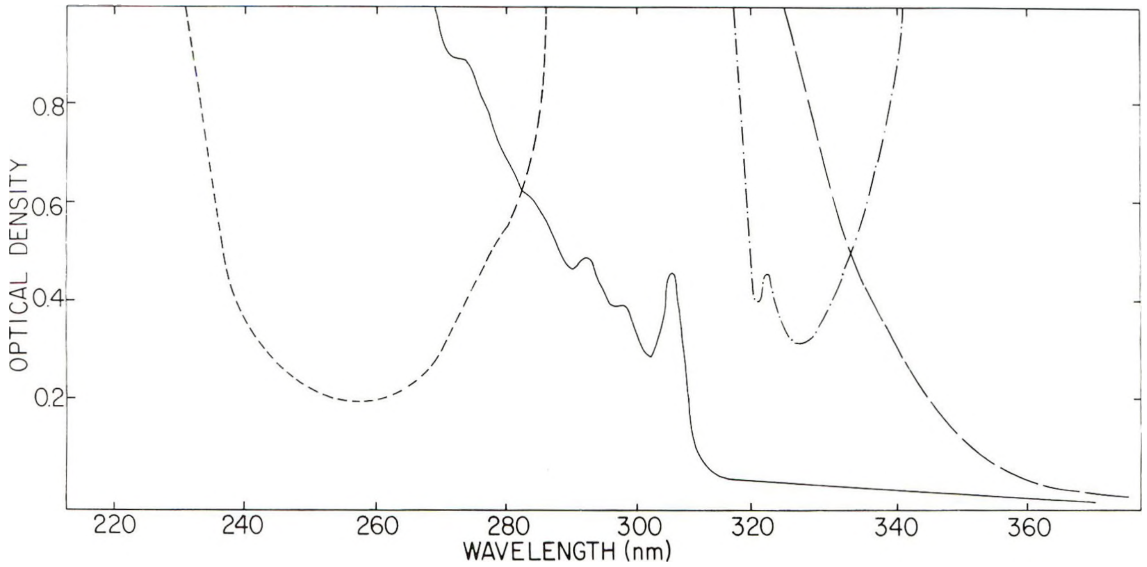

Figure 1. Absorption spectrum (——) of a 3.19×10^{-5} *M* solution of phthalazine at the temperature of boiling nitrogen. Absorption spectrum (– – –) of a 2.97×10^{-3} *M* solution of phthalazine at the temperature of boiling nitrogen. Transmitance (- - - -) of the filter used to isolate the excitation radiation in the $\pi \rightarrow \pi^*$ absorption region of phthalazine. Transmitance (–·–·–) of the filter combination used to isolate the excitation radiation in the $n \rightarrow \pi^*$ absorption region of phthalazine.

wavelengths greater than 310 nm. They suggested that this behavior was due to a fast intersystem crossing rate from higher excited singlet levels, compared with the rate of internal conversion to the lowest (n,π^*) singlet.

In this paper we report measurement of the value of the extinction coefficient for triplet-triplet absorption. We have used this value to determine the intersystem crossing quantum yield for excitation in both the $\pi \rightarrow \pi^*$ and the $n \rightarrow \pi^*$ excitation regions. We also report the triplet-triplet absorption spectrum and the oscillator strength. These results are of interest when compared with other diazanaphthalenes.

Experimental Section

I. T. ← T Absorption Extinction Coefficients. Phthalazine was purchased from Aldrich Chemical Co. and was used after recrystallization from ethanol followed by vacuum sublimation. Phenanthrene, which was used as a check on our experimental procedure, was obtained as 99.999% pure from James Hinton, and was used as received. The concentrations were adjusted so that the optical density was between 0.5 and 0.7 in the region where the singlet ← singlet depletion was measured. Typical phthalazine concentrations were on the order of 10^{-3}–10^{-4} *M*. The solvents used consisted of 30% *n*-butyl alcohol and 70% isopentane by volume. Both solvents were spectroquality and purchased from Matheson Coleman and Bell. These solvents formed a clear rigid glass when cooled to the temperature of boiling nitrogen.

The apparatus and experimental techniques were very similar to those described by Hadley[5] and by Hadley and Keller.[6] The sample was contained in a metal dewar, which has been previously described. Singlet ← singlet absorption spectra were measured with a Cary 14 spectrophotometer. The triplet ← triplet absorption spectrum was determined point by point using a flash lamp which dissipated 18,000 J, generating a 100-μsec pulse of light. The absorption of the metastable triplet was measured using an interrogating light beam dispersed by a JACO 0.5-m monochromator with a 1P28A photomultiplier. The signals were displayed on a Tektronix 544 oscilloscope using a type W preamplifier.

The procedure used to calculate the extinction coefficient for triplet ← triplet absorption was very similar to that described by Hadley and Keller.[6] Values for the optical density of the T ← T absorption at its maximum and the optical density at three points in the singlet–singlet region were obtained immediately following the discharging of the lamp, and then (following the method outlined in ref 6) the initial concentration of triplets, C_T^0, was calculated. The extinction coefficient for T ← T absorption was calculated from Beer's law using this value of C_T^0. Phenanthrene was used as a check on our experimental procedure. In all cases, the values of ϵ_T obtained for phenanthrene agreed with reported values.[6,7]

II. Quantum Yields. For the quantum yield measurement, it was necessary to increase the concentration of phthalazine to about 10^{-2} *M*. This was done to ensure that all of the light passing through the sample was absorbed by the solute. Samples with an OD ≥ 2 in the singlet ← singlet region (as measured on the Cary 14 spectrophotometer) were considered to fulfill this requirement.

The apparatus used was very similar to that discussed in the previous section, and to that described by Hadley.[7] Since we specifically wanted to measure the quantum yields for intersystem crossing resulting from excitation in two distinct wavelength regions, two different filter systems were used. The $\pi \rightarrow \pi^*$ bands, originating at about 310 nm, have an $\epsilon_{\max}$ of about 10^2 greater than the n,π^* bands which originate at about 380 nm. To study the intersystem crossing originating from the $^1(\pi,\pi^*)$ state we used an interference filter whose transmittance is shown in Figure 1. In order to study the intersystem crossing originating from the $n \rightarrow \pi^*$ absorption system it was necessary to isolate the 310–350-nm spectral region. We used a 310-nm interference filter combined with a naphthalene filter (10 g/200 ml ethanol) and the Corning 7-54 filter to

---

(5) S. G. Hadley, *J. Phys. Chem.*, **74**, 3551 (1970).

(6) S. G. Hadley and R. A. Keller, *J. Phys. Chem.*, **73**, 4351 (1969).

(7) D. Lavalette, *et al.*, *Chem. Phys. Lett.*, **10**, 331 (1971).

isolate this region. The transmittance of this filter is shown relative to the absorption of phthalazine in Figure 1.

The experimental procedure followed, essentially that of Hadley,[8] consisted of measuring the optical density at the maximum of the T ← T absorption, followed by actinometric measurement of the intensity of the flash lamp. For flash excitation, the intersystem crossing quantum yield was then calculated from the equation

$$\Phi_{ISC} = OD/\epsilon_T i_0$$

The procedure for the actinometry has been described by Hatchard and Parker.[9] We followed this procedure, except that bathophenanthroline was used in the determination of iron(II). Typical values of i_0 determined in this manner were $i_0 = 2 \times 10^{-9}$ einstein cm^{-2} flash^{-1}.

Care was taken to ensure that the actinometry was performed under conditions identical with those used in the optical density determinations. In the $\pi \rightarrow \pi^*$ absorption region, only 10 flashes of the lamp were required to determine accurately the value of i_0, while 15 flashes were required in the $n \rightarrow \pi^*$ absorption region. This was due to the difference in transmittance of the two filters.

The light from the flash lamp was generally defocused to ensure that the same amount of light was incident on both the sample and the actinometer cell. For measurement in the $n \rightarrow \pi^*$ absorption region, however, it was necessary to focus the light into a circle about 2 cm in diameter at the front of the sample to ensure sufficient intensity for accurate measurement of the T ← T absorption.

A separate determination of Φ_{ISC} for phenanthrene was performed for each set of experimental conditions. In all cases, the values for the extinction coefficients, quantum yields, and phosphorescence lifetimes were consistent with reported values.[6,7,8,10]

Results

The values of the triplet ← triplet absorption extinction coefficient and the oscillator strength are presented in Table I. The intersystem crossing quantum yields for both excitation regions and the phosphorescence lifetime for excitation in both regions are presented in Table II. All values are for rigid glass solutions of 30% *n*-butyl alcohol–70% isopentane at the temperature of boiling nitrogen.

The triplet ← triplet absorption spectrum of phthalazine is shown in Figure 2. The value of the oscillator strength was computed from the equation

$$f = 4.32 \times 10^{-9} \int_{\nu_1}^{\nu_2} \epsilon d\nu$$

and was found to be $f = 0.11$.

Discussion

The triplet ← triplet absorption spectrum of phthalazine is characteristic of aza-substituted naphthalenes. It is broad and shows little structure in rigid glass solutions at the temperature of boiling nitrogen.[5] The absorption maximum in the visible region occurs at 420.5 nm, which is the same spectral region as other aza-substituted naphthalenes. The maximum extinction coefficient, ϵ_{max} (4.45 ± 0.2) × 10^3 M^{-1} cm^{-1}, is smaller than the other aza-substituted naphthalenes thus far studied. The oscillator strength, $f = 0.11$, is typical of values previously determined for naphthalene and its aza-substituted derivatives. Thus, this transition is probably the same as has been assigned as $^3K_a \leftarrow {}^3L_a$ in naphthalene.[11]

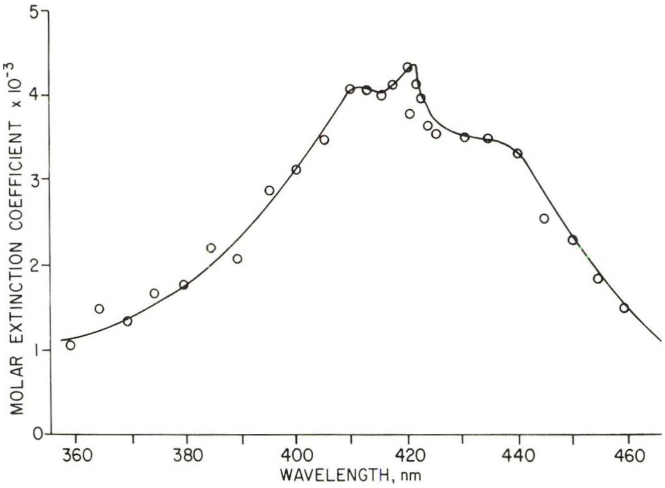

Figure 2. Triplet → triplet absorption spectrum of phthalazine at the temperature of boiling nitrogen.

TABLE I: Value of T ← T Extinction Coefficient and f Number for Phthalazine

Molecule	$\epsilon_T \times 10^{-3}$, M^{-1} cm^{-1} ^{a}	f_T^{b}	λ, nm^c
Phthalazine	4.45 (± 0.02)	0.11	420.5

^{a}Estimated error. ^{b}Computed from $f = 4.32 \times 10^{-9} \int_{\nu_1}^{\nu_2} \epsilon d\nu$. ^{c}Wavelength of maximum triplet ← triplet absorption.

TABLE II: Values of the Intersystem Crossing Quantum Yield and the Phosphorescent Lifetime for Phthalazine in Two Different Excitation Regions Measured at the Temperature of Boiling Nitrogen

Excitation region	Φ_{ISC}^{a}	τ_p^{a}
$n \rightarrow \pi^*$	0.95 ± 0.09	0.41 ± 0.03
$\pi \rightarrow \pi^*$	1.04 ± 0.06	0.42 ± 0.04

^{a} Estimated error.

The intersystem crossing quantum yield of 0.99 ± 0.07 demonstrates that the internal conversion, $S_1 \rightsquigarrow S_0$, is an unimportant relaxation path in phthalazine. No fluorescence has been reported for phthalazine. The intersystem crossing quantum yield of phthalazine has been reported by Baba, Yamazaki, and Takemura[2] as being as great as 0.7, which is in fair agreement with the value we report.

Recently Takemura, Yamamoto, Yamazaki, and Baba[12] have reported a value of the intersystem crossing quantum yield of phthalazine dissolved in EPA at 77°K of 0.45 ± 0.05. This value was determined using a T ← T energy transfer technique. It required independently determined values of the phosphorescence quantum yield of phthalazine (0.04), phosphorescence quantum yield of naphthalene(0.03), and the intersystem crossing quantum yield of naphthalene (0.25). The overall uncertainty in each of these values could be as great as 25%. Thus we believe that the values reported in the present work are more reli-

(8) S. G. Hadley, *J. Phys. Chem.*, **75**, 2083 (1971).

(9) C. G. Hatchard and C. A. Parker, *Proc. Roy. Soc., Sec. A*, **220**, 104 (1953); **235**, 518 (1956).

(10) S. G. Hadley and R. A. Keller, *J. Phys. Chem.*, **73**, 4356 (1969).

(11) M. A. El-Sayed and T. Pavlopoulos, *J. Chem. Phys.*, **39**, 834 (1963).

(12) T. Takemura, K. Yamamoto, I. Yamazaki, and H. Baba, *Bull. Chem. Soc. Jap.*, **45**, 1639 (1972).

able because they rely only upon a value of the extinction coefficient of the triplet ← triplet absorption and the quantum yield of a well-characterized chemical actinometer.

Our results show that the intersystem crossing quantum yield does not depend upon whether phthalazine is excited in the n → π^* or $\pi \rightarrow \pi^*$ absorption regions. Because the quantum yield is unity, within our experimental error, we are unable to decide whether the intersystem crossing occurs from upper vibronic levels of the $^1(n,\pi^*)$ and $^1(\pi,\pi^*)$ states or whether the path to the triplet relies upon internal conversion in the singlet manifold, followed by intersystem crossing from the $^1(n,\pi^*)$ state. From our work the wavelength dependence of the phosphorescence quantum yield reported by Li and Lim[4] cannot be ascribed to a wavelength dependence of the intersystem crossing quantum yield. The discrepancy may arise from the erroneous value of the n → π^* extinction coefficient reported by Li and Lim. The lifetime of the emitting triplet state, $\tau_p = 0.42 \pm 0.4$ sec, was found to be independent of the singlet excitation region, indicating that the emitting state is probably independent of excitation region.

Conclusions

Until values of the lifetimes of the excited singlet states of phthalazine and other aza aromatic heterocycles such as quinoxaline, quinoline, and isoquinoline are known, a direct comparison of their radiative and radiationless processes is difficult. However, it appears that there are no simple generalizations that can explain the radiative and radiationless properties of these aromatic heterocycles. The triplet ← triplet absorption spectrum of phthalazine is quite similar to those reported[5] for other aza-substituted naphthalenes.

Acknowledgment. We acknowledge the support of this work by the National Science Foundation through Grant No. GP 19750 and the Ford Foundation for fellowship support of V. Alvarez.

Mechanism of Hydrogen–Deuterium Exchange of Propylene over a Brønsted Zeolite Catalyst

Z. M. George and H. W. Habgood*

Research Council of Alberta,[1] Edmonton 7, Alberta, Canada

(Received May 11, 1972)

Publication costs assisted by the Research Council of Alberta

Propylene has been shown to exchange with the hydrogen of a Brønsted acid catalyst (NaY zeolite containing traces of Ca^{2+} and H^+) at 400°. Significant exchange was found on the C2 carbon in addition to the expected exchange at C1 and C3. The relative rates of exchange and of isomerization to cyclopropane rule out the possibility of any appreciable participation of protonated cyclopropane in the reaction under these conditions.

Introduction

The structures and relative stabilities of the various possible propyl and protonated cyclopropane cations are still a subject of considerable interest as indicated by recent theoretical studies from the laboratories of Pople[2] and of Dewar.[3] Bodor and Dewar[3] concluded that edge-protonated cyclopropane cation should be the most stable form in the gas phase, even slightly more stable than 2-Pr^+. On the other hand, Radom, *et al.*,[2] decided that corner-protonated cyclopropane and 1-Pr^+ are about equal in stability and at a level 17–20 kcal above that of 2-Pr^+. In the course of our studies of the catalytic isomerization of cyclopropane to propylene over various X- and Y-zeolite protonic acid catalysts we have obtained measurements of H–D exchange between the catalyst and propylene that have some bearing on this general question. Of course the geometries and energies of species adsorbed on a catalyst surface are expected to differ from those of the same species in the gas phase but the results given below tend to confirm 2-Pr^+ as being the most stable ion with 1-Pr^+ possibly being sufficiently stable to make a significant contribution to the exchange.

Experimental Section

Materials. The catalyst was a NaY synthetic zeolite (Linde SK40, lot 51-31, composition corresponding to 0.93Na, 0.04Ca, 1.00Al, 2.33Si) that had previously been shown to have significant Brønsted acidity toward cyclopropane and propylene.[4-6] It was used as received after

---

(1) Contribution No. 584 from the Research Council of Alberta.

(2) L. Radom, J. A. Pople, V. Buss, and P. v. R. Schleyer, *J. Amer. Chem. Soc.*, **93**, 1813 (1971); **94**, 311 (1972).

(3) N. Bodor and M. J. S. Dewar, *J. Amer. Chem. Soc.*, **93**, 6685 (1971).

(4) B. H. Bartley, H. W. Habgood, and Z. M. George, *J. Phys. Chem.*, **72**, 1689 (1968).

(5) H. W. Habgood and Z. M. George, *Conf. Soc. Chem. Ind. (London)*, 130 (1968).

(6) Z. M. George and H. W. Habgood, *J. Phys. Chem.*, **74**, 1502 (1970).

being pelletized, crushed, and sieved to 20–40 mesh granules.

Propylene-d_0 was Phillips Research Grade with reported purity of 99.9 mol %; propylene-d_6 was from Merck Sharp and Dohme of Canada, Ltd., and had a reported purity of 98% *d*. Low-voltage mass spectrometry showed a d_5h content of 1.2%; cyclopropane-d_0 was from Matheson of Canada and had a reported purity of 99%.

Procedures. The microcatalytic reactor assembly with provision for equilibrating the catalyst with a low partial pressure of H_2O or D_2O was the same as described previously.[4,5] A 2-g sample of catalyst was used and activation was normally at 500° in flowing helium as previously described.[6]

Gas chromatographic separations were carried out either on a 20 ft by 0.25 in. column packed with 20% squalane on Chromosorb P and using a thermal conductivity detector or on a 12 ft by 0.25 in. column packed with 20% diisooctyl phthalate on Chromosorb P and using a flame ionization detector equipped with a Varian 747 electronic digital integrator. The ratio of sensitivities of cyclopropane and propylene using the thermal conductivity detector was determined as 0.98, and using the flame ionization detector as 1.08. No corrections were made for the effect of deuteration on sensitivity.

Mass spectra were determined on a Veeco GR 4 spectrometer using 14-V ionizing electrons for propylene after purification by gas chromatography (particularly to remove traces of carbon dioxide). There was no detectable fragmentation and correction was made for the small decrease in intensity caused by deuterium substitution.[6]

The nmr spectra were determined at 100 MHz using a Varian HA 100 spectrometer equipped with a 15-in. magnet. About 0.1 mmol of propylene was mixed with half its volume of cyclopropane-d_0 to act as an internal standard and the exact composition of the mixture was obtained by gas chromatographing the entire mixture. The sample was then dissolved in chloroform (80% deuterated to provide a "locking" signal without interfering with the CH hydrogens in propylene) and measurements were made at −55°. The integrated peak areas were determined as the average of five scans on the sample and in one experiment in which propylene-d_6 was the starting material the low concentration of H on the C2 carbon was measured by averaging 25 scans using a Varian C-1024 CAT apparatus.

Results

The catalyst was converted to the deuterium form by prolonged treatment with a low partial pressure of D_2O at 500°.[6] Twenty successive slugs of propylene-d_0 (10 ml, 10 Torr) were passed over the catalyst in the presence of D_2O, purified by gas chromatography and analyzed by mass and nmr spectrometry as described earlier. On the basis of experiments with NaX[5] the concentration of adsorbed water was estimated to be about 0.1 molecules per cavity and the maximum concentration of propylene to be about 0.04 molecules/cavity at 400°. The average concentration of adsorbed propylene is probably one quarter of this value so that there is a tenfold excess of adsorbed water. The catalyst was then converted to the hydrogen form by heating in oxygen at 500° followed by equilibration with H_2O at this temperature. The exchange experiment was then repeated using propylene-d_6 in the presence of H_2O.

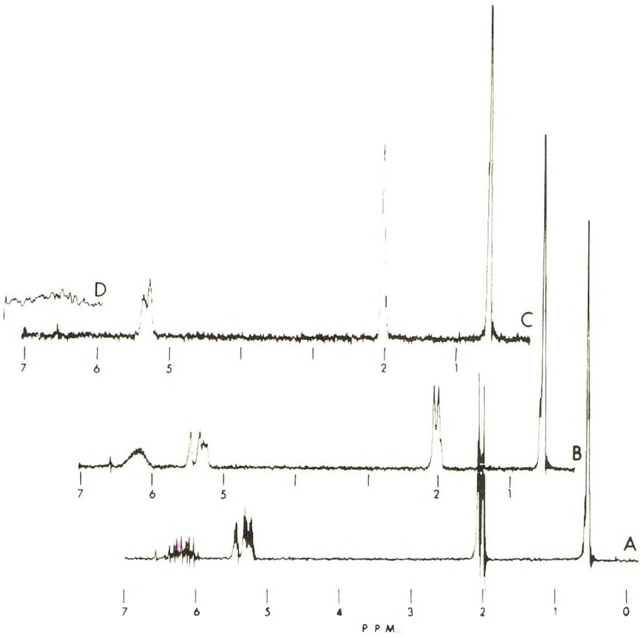

Figure 1. The 100-MHz nmr spectra of propylenes at −55° in chloroform (80% *d*) with cyclopropane as an internal standard: (A) propylene-d_0; (B) exchanged propylene-d_0; (C) exchanged propylene-d_6; (D) 25 × CH portion of exchanged propylene-d_6.

In the experiment in which propylene-d_0 was exchanged with the deuterated catalyst the extent of exchange of each of the hydrogen positions was determined from the decrease in the intensity of the integrated nmr peak area (relative to the measured fraction of cyclopropane present in the mixture). The uncertainties in position were estimated from the 2σ deviations observed among nine repeated scans of a sample of unexchanged propylene treated and measured by the same procedure to give the number of hydrogens per 100 molecules as 198 ± 2, 97 ± 3, and 298 ± 2 in the C1, C2, and C3 positions. The uncertainty in determining the ratio of propylene to cyclopropane in the sample for nmr analysis was assumed to be 1%. In the case of propylene-d_6 exchanged with the H catalyst, the extent of exchange in each position was determined directly from the proton peaks observed in the nmr spectrum. The greater uncertainty associated with experiments using propylene-d_6 is probably due to the difficulty of integrating weak signals especially in the CH region. The relevant nmr spectra are shown in Figure 1. The over-all extent of exchange was also calculated from the mass spectra.

The data are summarized in Table I. The total degree of exchange determined by the two methods agrees well and the exchange in each of the two systems is identical within experimental error. The data of Table I also show that exchange is primarily in the C1 and C3 positions as expected for a 2-propyl cation intermediate and in the expected 2:3 ratio. In addition, however, a significant degree of exchange also occurs in the C2 position. A completely random distribution of exchanged atoms among all positions would give 17% exchange on C2; the observed exchange is about one third of that.

Our previous studies had shown that this same catalyst was active for the isomerization of cyclopropane to propylene. Equilibration between propylene and cyclopropane over the catalyst could provide a mechanism for the H–D mixing that would explain the exchange on C2. The rate of the propylene → cyclopropane reaction can be estima-

TABLE I: Exchange of Propylene with Brønsted Acid Sites[a]

	Product composition (mass spectrometer)							D or H introduced per/100 molecules			% exchange		% distribution of D (or H)		
System	d_0	d_1	d_2	d_3	d_4	d_5	d_6	C1	C2	C3	Ms	Nmr	C1	C2	C3
C_3H_6 D catalyst	9.5	24.6	30.0	22.1	8.6	5.2	0	92 ± 3	14 ± 3	135 ± 4	36	40	38	6	56
C_3D_6 H catalyst	0	3.2	40.0	34.5	34.2	18.0	5.7	84 ± 3	11 ± 5	130 ± 3	36	37	37	5	58

[a] The weight of catalyst was 2.01 g; the flow rate was 0.75 ml/sec; the contact time (equal to retention time of propylene pulse) was 4.1 sec; the temperature was 400 ± 1°; and the partial pressures of D_2O (H_2O) over the catalyst were about 4 Torr.

ted from the rate of the cyclopropane → propylene reaction previously measured and the equilibrium constant. By way of confirmation of this predicted value an attempt was made to measure the degree to which equilibrium was achieved over the catalyst under the approximate conditions of the exchange experiment.

The catalyst was in the hydrogen form and experiments were carried out in the presence of H_2O vapor. Samples of 100 μl of cyclopropane or 300 μl of propylene at 20 Torr were injected, the products were collected in a liquid nitrogen trap and chromatographed using a flame ionization detector. The relative sensitivities of the detector to cyclopropane and propylene were assumed to remain constant over the 10^4 range in concentration of the two substances. Cyclopropane was observed as a small peak on the tail of the propylene peak and the detection limit was estimated to be 25 ppm. Interestingly, the propylene used in this work was found to be free of cyclopropane within this limit.

The material balance in these experiments was poor. The recovery of propylene plus cyclopropane ranged from 93 to about 50% of the injected reactant for contact times between 2 and 30 sec. Previous work had suggested extensive retention of propylene on the catalyst although in the present experiments trace amounts (25 ppm or less) of other C_2 to C_4 hydrocarbons were observed. It was assumed that the cyclopropane peak gave a true measure of the amount of cyclopropane and the propylene was estimated by difference based on the amount of sample injected. A separate experiment in which the catalyst was replaced by a 130-ml dispersion volume yielded direct measurements of the propylene and cyclopropane injected and showed the reproducibility of injection to be 2%.

The data thus obtained are summarized in Table II. The experiments with long contact times indicate that the equilibrium concentration of cyclopropane is about 100 ppm. At a contact time of 4.4 sec (which is similar to that used in the exchange experiments) the approach to equilibrium is about 99% on the basis of the experiment in which cyclopropane was the reactant.

TABLE II: Equilibration of Cyclopropane and Propylene over a Wet[a] **NaY Zeolite Catalyst at 384°**

			Fraction of cyclopropane in product, ppm	
Contact time, sec	Reactant	Sample vol, μl at 20 Torr	Cutting and weighing	Triangulation
1.8	Propylene	300	120	
1.8	Propylene	300	100	150
4.4	Propylene	300	100	120
4.4	Cyclopropane	100	12,000	10,000
29.8	Propylene	300	100	120
27.4	Cyclopropane	100	100	100

[a] Partial pressure H_2O was 4.6 Torr.

Discussion

It has been generally assumed that 2-Pr^+ is the most stable of the $C_3H_7{}^+$ ions and hence it is the most likely species to be found when propylene reacts with a Brønsted catalyst. Consequently H-D exchange between propylene and a deuterated catalyst would be expected to be confined to the C1 and C3 carbons. The experiments showed that a major proportion of the exchange did occur at carbons 1 and 3 but, in addition, there was exchange on carbon 2 to an extent of about 30% of what would be expected for a fully random exchange at all hydrogen positions.

The following possibilities may be considered to explain the observed deuteration at C2: (a) propylene-cyclopropane equilibration by way of a protonated cyclopropane intermediate which would lead to completely random exchange at all positions; (b) the direct formation of some 1-Pr^+ by reaction of propylene with the deuterated catalyst (The reversal of this reaction would lead to 50% probability of exchange of the C-2 hydrogen as compared with the 83% probability of an exchange in one of the five C1 or C3 hydrogens to be expected from the propylene ⇌ 2Pr^+ reaction.); (c) the 2-Pr^+ formed directly from propylene may undergo a shuffling of all of its hydrogens among the positions on the three carbons [This would be by some undefined process occurring in the adsorbed state which did not yield a clearly differentiated 1-Pr^+ cation (in such case the process would, effectively, be indistinguishable from b).]

In view of the demonstrated Brønsted acidity of our catalyst and of the relatively high partial pressure of water during the reaction, we consider highly unlikely the participation of either a dissociative mechanism involving a π complex as suggested by Hightower and Hall[7,8] for the H-D exchange of vinyl hydrogens of olefins over strongly dehydrated alumina or the radical mechanism proposed with metal catalysts to explain such diverse exchange patterns (including the C2 hydrogen) as those found by Hirota and Hironaka[9] for propylene on Ni and Pd.

Our results provide compelling evidence that propylene-cyclopropane isomerization is much too slow to make any significant contribution to H-D exchange in propylene. In the presence of a sufficient excess of water to provide an essentially constant H or D composition in the Brønsted

---

(7) J. W. Hightower and W. K. Hall, *J. Catal.*, **13,** 161 (1969).

(8) J. W. Hightower and W. K. Hall, *Trans. Faraday Soc.*, **66,** 477 (1970).

(9) K. Hirota and Y. Hironaka, *Tetrahedron Lett.*, **No. 25,** 1645 (1964).

acid sites, the exchange reaction can be considered as a succession of steps first order in propylene. It is also reasonable to assume that the isomerization of propylene to cyclopropane over the catalyst is first order (the reverse reaction has been demonstrated to be first order[10]). It was not possible to measure in the same experiment the relative rates of exchange and isomerization but we can obtain approximate estimates as follows. Treating the exchange as a simple first-order reaction and assuming all six hydrogens equivalent gives, for 40% exchange in 4.1 sec at 400°, a rate constant of 0.12 sec^{-1}. The isomerization equilibrium, approached from the cyclopropane side was 99% complete in 4.4 sec. This corresponds to a rate constant for cyclopropane–propylene isomerization of 1.05 sec^{-1}, a value close to that expected from direct kinetic measurements.[5] The observed equilibrium fraction of propylene of about 100 ppm is in reasonable agreement with the equilibrium constant calculated from the thermodynamic data of Stull, Westrum, and Sinke[11] as 92×10^{-6} at 400° and 63×10^{-6} at 384°. Consequently the rate constant for the isomerization of propylene to cyclopropane is about 10^{-4} sec^{-1}, smaller than the rate constant for exchange by a factor of 10^3. The use of the cyclopropane–propylene isomerization data is justified only if these rates are not limited by mass transfer resistances. Previous work in cyclopropane–zeolite systems had never given any indication of diffusional limitations; the Arrhenius plots are always linear over a wide range of temperatures (up to 450° ($k \simeq 1$ sec^{-1}) for dry NaX[5] and up to 320° ($k = 0.06$ sec^{-1}) for wet NaY[4]) and the chromatographic peak of unreacted cyclopropane from the reactor is always relatively sharp[10] as would be expected for the case of low mass transfer resistance.

Further evidence that propylene isomerization is slow relative to propylene exchange is provided from the results of Bartley, *et al.*,[4] using a sample of the same SK40 catalyst but which had been washed with NaCl solution to reduce the Ca^{2+} level and which, therefore, probably was somewhat less active. Their results extrapolated to 400° gave 0.32 sec^{-1} for the cyclopropane isomerization rate constant corresponding to a propylene isomerization rate constant of 3×10^{-5}. The propylene exchange rate constant extrapolated to 400° was 1.0 sec^{-1}, 3×10^4 greater than the rate of isomerization.

Thus we are able to eliminate the participation of protonated cyclopropane as a significant mechanism in the exchange reaction. Our results do not permit us to differentiate between possibilities b and c, the participation of significant amounts of $1\text{-}Pr^+$ cation or the presence of some hydrogen-mixing process in the $2\text{-}Pr^+$ cation. One might hope for guidance from theoretical calculations although it must be remembered that there may be significant differences in energy level differences between adsorbed and gaseous species.

Acknowledgments. The authors wish to acknowledge valuable discussions with Dr. A. T. Blades. Nmr spectra were measured in the laboratory of G. Bigam, Chemistry Department, University of Alberta. Technical assistance was provided by J. J. Mendiuk.

---

(10) D. W. Bassett and H. W. Habgood, *J. Phys. Chem.*, **64**, 769 (1960).

(11) D. R. Stull, E. F. Westrum, Jr., and G. C. Sinke, "The Thermodynamics of Organic Compounds," Wiley, New York, N. Y., 1969, Chapter 9.

Electron Spin Resonance Studies of Dialkoxydialkylbenzenes. Evidence for Some Unusual Rearrangements in Sulfuric Acid

Paul D. Sullivan

Department of Chemistry, Ohio University, Athens, Ohio 45701

(Received August 2, 1972)

Publication costs assisted by the Petroleum Research Fund

The esr spectra of a series of cation radicals derived from 1,4-dialkoxy-2,5- or 2,3-dialkylbenzenes in aluminum chloride–nitromethane are reported and compared in several cases with previously reported spectra in concentrated sulfuric acid. The 1,4-dialkoxy-2,5-di-*tert*-butylbenzenes are anomalous giving different spectra in the two systems. Reasons for the discrepancy are suggested and the nature of the radical species observed in sulfuric acid is discussed.

Introduction

Two recent papers have described the esr spectra of a series of 1,4-dialkoxy-2,5-dialkylbenzenes dissolved in concentrated H_2SO_4.[1,2] In particular it was reported that the esr spectrum of a concentrated solution ($>10^{-2}$ *M*) of 1,4-dimethoxy-2,5-di-*tert*-butylbenzene (I) in sulfuric acid consisted of nine equidistant lines of separation 2.87 G. This was interpreted as an accidental equivalence of the methoxyl and ring proton splitting constants, thereby giving a group of eight equivalent protons. This large value of

---

(1) A. Nishinaga, P. Ziemek, and T. Matsuura, *Tetrahedron Lett.*, 4905 (1969).

(2) A. Nishinaga, P. Ziemek, and T. Matsuura, *J. Chem. Soc. C*, 2613 (1970).

the ring proton splitting constant is, however, not observed in the other 1,4-dimethoxy-2,5-dialkylbenzenes which were investigated. In each case the ring proton splitting constant from these compounds was less than 1 G.

As part of our general interest in cation radicals we have observed the esr spectra of a number of the 1,4-dialkoxy-2,5-dialkylbenzene cation radicals generated in the $AlCl_3$–CH_3NO_2 system,[3,4] and in this paper we wish to report a number of inconsistencies with the previous reports.[1,2]

Results and Discussion

Our analysis of the cation radical from I in $AlCl_3$–CH_3NO_2 differs appreciably (see Table I) from the analysis proposed for I in H_2SO_4. Substantial agreement between the two systems is obtained for compounds II and IV but not for VI. It is noted that the spectrum of I in $AlCl_3$–CH_3NO_2 is analogous to the other 1,4-dialkoxy-2,5-dialkylbenzenes, particularly with regard to the magnitude of the ring proton splitting constant. Also the spectrum accounts for all the protons in the molecule including the *tert*-butyl protons. Because of these two factors it is proposed that the genuine cation radical is only formed in the $AlCl_3$–CH_3NO_2 solution and not in the concentrated H_2SO_4 system as previously reported. The question then arises as to the identity of the radical observed in sulfuric acid. In order to attack this problem, the work of Nishinaga was repeated with essentially the same results as was initially reported. It was observed, however, that the spectrum of I in H_2SO_4 which consisted of nine lines did show some evidence for some further hyperfine structure in each of the lines.[5] In order to obtain a better resolved spectrum a solution of I in H_2SO_4 was made in an evacuated system and an equal quantity of nitromethane was added to the solution.[6] Under these conditions somewhat better resolution was obtained and splittings of the nine major components were indeed observed. This spectrum was analyzed in terms of six protons with splitting 3.03 G, two protons with splitting 2.79 G, and two protons with splitting 0.27 G. A computer simulation indicated that this analysis was correct. The *g* factor of the radical was 2.00371 ± 0.00001. The identity of the radical species giving this signal is not known with certainty. However, by analogy with some of the results shown in Table I it is proposed that the species is a cation radical of a 2,3-dialkyl-1,4-dimethoxybenzene. This hypothesis is made due to the similarity between the splittings of the unknown radical species and those of the cation radicals derived from 2,3-dimethyl-1,4-dialkoxybenzenes (VIII and IX in Table I), *e.g.*, $a(OCH_3)H = 3.070$, $a(CH)H = 2.896$ G for 2,3-dimethyl-1,4-dimethoxybenzene. The nature of the alkyl substituents in the unknown species can only be hypothesized. Since a splitting of 0.27 G is observed from two equivalent protons it would seem unlikely that *tert*-butyl groups are involved. The results would be consistent with either 2,3-isopropyl or 2,3-*sec*-butyl substituents, each of which would have two methine protons.[7] The preferred conformation of these groups might be one in which the methine protons were close to the plane of the benzene ring in which case their splittings would be small. A consideration of *g* factors adds considerable weight to this hypothesis. It is indicated from the proposed theories of isotropic *g* factors[8] that in a group of similar molecules the *g* factor can be expressed as the sum of various contributions. This means that, for example, the effect of two methyl groups should be a constant contribution to the *g* shift. This is seen to be approximately the case from the results in Table II, where on going from 1,4-dialkoxybenzenes to 2,5-dimethyl-1,4-dialkoxybenzenes the *g* factor decreases by approximately 10×10^{-5}. The change in *g* between the dihydroxy and dimethoxy derivatives is $16 \pm 2 \times 10^{-5}$, which leads us to estimate that the *g* factor of 2,5-diisopropyl-1,4-dimethoxybenzene should be 2.00367 ± 0.00002. The available data also suggest that the difference in *g* factors between 2,3 and 2,5 isomers is $3\text{–}6 \times 10^{-5}$ which leads us to estimate that the *g* factor of 2,3-diisopropyl-1,4-dimethoxybenzene should be 2.00372 ± 0.00002. This is to be compared to the value of 2.00371 ± 0.00001 found for the radical derived from I in sulfuric acid.

TABLE I: Hyperfine Splitting Constants for the Cation Radicals of 1,4-Dialkoxy-2,5- or 2,3-Dialkylbenzenes

			Hyperfine splittings,[a] G			
Alkoxy group	Alkyl group	Compd no.	Alkoxy protons	Ring protons	Alkyl protons	Other
			2,5-Dialkyl Derivatives			
OH	Me	II	3.012	0.915	3.718[b]	
OMe	Me	III	3.153	0.572	4.210[b]	
OEt	Me	IV	3.582[b]	0.581	4.158	0.136[e]
OH	*t*-Bu	V	3.069	1.432	0.112[c]	
OMe	*t*-Bu	I	3.242	1.025	0.103[c]	
OEt	*t*-Bu	VI	4.050	1.057	0.099[c]	0.155[e]
O-*i*-Pr	*t*-Bu	VII	1.795	1.065	0.135[c]	0.045[d]
			2,3-Dialkyl Derivatives			
OMe	Me	VIII	3.070	2.896	1.480[b]	
OH	Me	IX	3.138	2.583	1.828[b]	

[a] Measured at −25° in $AlCl_3$–CH_3NO_2. [b] Methyl protons. [c] *tert*-Butyl protons. [d] Methyl protons of isopropoxy group. [e] γ-Methyl protons of ethoxy group.

TABLE II: *g* Factors of the Cation Radicals of Some 1,4-Dialkoxy-2,5- and 2,3-Dialkylbenzenes

	Alkoxy substituent			
Alkyl substituent	OH	OMe	OEt	O-*i*-Pr
	(i) 2,5-Substituents			
None	2.00350[b]	2.00368[b]	2.00371[b]	2.00369[a]
Me	2.00340[c]	2.00356[c]	2.00363[a]	
t-Bu	2.00345[c]	2.00359[a]	2.00366[a]	2.00369[a]
i-Pr	2.00351[a]	2.00367[d]		
	(ii) 2,3 Substituents			
Me	2.00343[a]	2.00362[a]		
i-Pr		2.00372[d]		

[a] Error ±0.00001. [b] Error ±0.00002. [c] Error ±0.00003. [d] Estimated.

---

(3) P. D. Sullivan and J. R. Bolton, *J. Amer. Chem. Soc.*, **90**, 5366 (1968).

(4) W. F. Forbes and P. D. Sullivan, *J. Chem. Phys.*, **48**, 1411 (1968).

(5) This splitting is hinted at in the published spectrum of ref 2.

(6) It is important that all the neutral compound is dissolved in the sulfuric acid before the addition of nitromethane, otherwise an esr spectrum of the genuine cation radical of I can be obtained.

(7) Unfortunately neither of these compounds is readily available to us otherwise our hypothesis could be easily tested.

(8) A. J. Stone, *Mol. Phys.*, **6**, 509 (1963).

The formation of 2,3-diisopropyl or 2,3-di-*sec*-butyl-1,4-dimethoxybenzene in concentrated solutions of I in concentrated sulfuric acid does not seem that unlikely when one considers the facile inter- and intramolecular alkyl group shifts and isomerizations which have been documented in acid solutions.[9,10]

It was also noted that the spectrum of VI is different in $AlCl_3$-CH_3NO_2 from that in sulfuric acid. A similar explanation may also be advanced (*i.e.*, the formation of a 2,3-dialkyl-1,4-diethoxybenzene cation radical) for this compound.

Acknowledgment. Acknowledgment is made to the donors of the Petroleum Research Fund administrated by the American Chemical Society for support of this research.

(9) D. A. McCauley, "Friedel-Crafts and Related Reactions," Vol. II, Part 2, G. A. Olah, Ed., Interscience, New York, N. Y., 1964, Chapter XXIV, p 1049.

(10) G. A. Olah, R. H. Schlosberg, R. D. Porter, Y. K. Mo, D. P. Kelly, and G. D. Mateescu, *J. Amer. Chem. Soc.*, **94**, 2034 (1972).

An Electron Spin Resonance Investigation of the Reactions in Irradiated Aqueous Solutions of Hydrogen Cyanide and the Cyanide Ion[1]

D. Behar and Richard W. Fessenden*

Radiation Research Laboratories, Center for Special Studies and Department of Chemistry, Mellon Institute of Science, Carnegie-Mellon University, Pittsburgh, Pennsylvania 15213

(Received June 7, 1972)

Publication costs assisted by Carnegie-Mellon University and the U. S. Atomic Energy Commission

Use of the *in situ* radiolysis–esr method has shown that the reactions of H and OH with HCN in acid solutions yield the radicals $H_2C{=}\dot{N}$ (a^H = 87.2, a^N = 10.2 G, g = 2.0028) and $HC(OH){=}\dot{N}$ (a^H = 54.40, $a_{OH}{}^H$ = 0.89, a^N = 10.14 G, g = 2.00322), respectively. The pK for the dissociation of the OH proton in the latter radical is estimated to be ~5. Scavenging of e_{aq}^- with HCN also yields $H_2C{=}\dot{N}$. The reaction of OH and O^- with CN^- in alkaline solutions was found to produce the radical $\cdot CONH_2$ as observed either directly at pH ~10 or by radical trapping with $CH_2{=}NO_2^-$ at higher pH. Exactly parallel behavior was found for CN^- and $HCONH_2$ in basic solutions. However, $HCONH_2$ yielded only $\cdot CONH_2$ in acid and neutral solutions and no rearrangement of this radical to $HC(OH){=}\dot{N}$ was found. The adduct to $CH_2{=}NO_2^-$ found in CN^- solutions and previously identified as $NCCH_2\dot{N}O_2^-$ must now be assigned the structure $H_2NCOCH_2\dot{N}O_2^-$.

Introduction

Ogura[2] has studied the products found in the radiolysis of aqueous solutions of HCN and has proposed that the intermediates HCN^-, H_2CN, and H(OH)CN are formed from the three primary radicals (e_{aq}^-, H, and OH). Existence of such intermediates is supported by the formation from nitriles of radicals of the type $RCH{=}\dot{N}$ by both e_{aq}^- and H as observed by esr.[3] Similar intermediates of the form XOH^- are proposed in irradiated solutions of SCN^- [4,5] and Br^- [6,7] to be in equilibrium with the more familiar X_2^-. By analogy the species $(CN)_2^-$ might be expected in cyanide solutions. Because the intermediates proposed for cyanide solutions should have characteristic esr spectra it is likely that the *in situ* radiolysis–esr method[8] can be used to advantage in demonstrating the formation of these species. Two previous papers by us reported esr investigations of the reactions in irradiated aqueous solutions of inorganic ions. The first of these,[9] dealing with direct observations of the intermediates, omitted the cyanide system while the second[10] discussed an intermediate in CN^- solutions as studied by radical trapping with $CH_2{=}NO_2^-$. Under conditions of O^- attack on CN^- it was found that this intermediate added to $CH_2{=}NO_2^-$ to give an adduct tentatively identified as $NCCH_2\dot{N}O_2^-$. The work described here shows that esr spectra of intermediates in cyanide solutions can be observed directly and that the identification of the above-mentioned adduct to $CH_2{=}NO_2^-$ must be revised.

Results and Discussion

Esr experiments with *in situ* radiolysis of the flowing sample solution by a 2.8-MeV electron beam were carried out as previously described.[8,10] Analytical grade KCN was used to make solutions of both CN^- and HCN. When HCN was desired the water was deoxygenated by bubbling with either N_2O or N_2 before addition of the KCN. After addition of the cyanide and the desired amount of

---

(1) Supported in part by the U. S. Atomic Energy Commission.

(2) H. Ogura, *Bull Chem. Soc. Jap.*, **41**, 2871 (1968).

(3) P. Neta and R. W. Fessenden, *J. Phys. Chem.*, **74**, 3362 (1970).

(4) D. Behar, P. L. T. Bevan, and G. Scholes, *J. Chem. Soc. D, Chem. Commum.*, 1486 (1971).

(5) D. Behar, P. L. T. Bevan, and G. Scholes, *J. Phys. Chem.*, **76**, 1537 (1972).

(6) D. Zehavi and J. Rabani, *J. Phys. Chem.*, **76**, 312 (1972).

(7) D. Behar, *J. Phys. Chem.*, **76**, 2517 (1972).

(8) K. Eiben and R. W. Fessenden, *J. Phys. Chem.*, **75**, 1186 (1971).

(9) D. Behar and R. W. Fessenden, *J. Phys. Chem.*, **76**, 1706 (1972).

(10) D. Behar and R. W. Fessenden, *J. Phys. Chem.*, **76**, 1710 (1972).

TABLE I: Esr Parameters of Intermediates in the Radiolysis of Aqueous Solutions of HCN, CN^-, and $HCONH_2$[a]

Source	pH	Radical	a^N	a^H	$a^{H'}$	g
CN^-	10.4	$\cdot C(=O)-NH_2$	21.62	30.49	1.34	2.00150
$HCONH_2$	10.2	$\cdot C(=O)-NH_2$	21.63	30.46	1.32	2.00148
$HCONH_2$[b]	Neutral	$\cdot C(=O)-NH_2$	21.62	30.47	1.31	2.00154
HCN	6.3	$HC(O^-)=\dot{N}$	10.76	54.45		2.00335
HCN	2.8-4	$HC(OH)=\dot{N}$	10.14	54.40	0.89	2.00322
HCN	2.5	$HC(H)=\dot{N}$	10.2[c]	87.2[c]		2.0028[c]

[a] Hyperfine constants in gauss, accurate to ±0.05 G; g factors accurate to ±0.00003. Second-order corrections have been made. [b] Results of Livingston and Zeldes.[11] [c] Because of the broad lines and weak signals the accuracy here is only ±0.1 G and ±0.0001 for the g-factor.

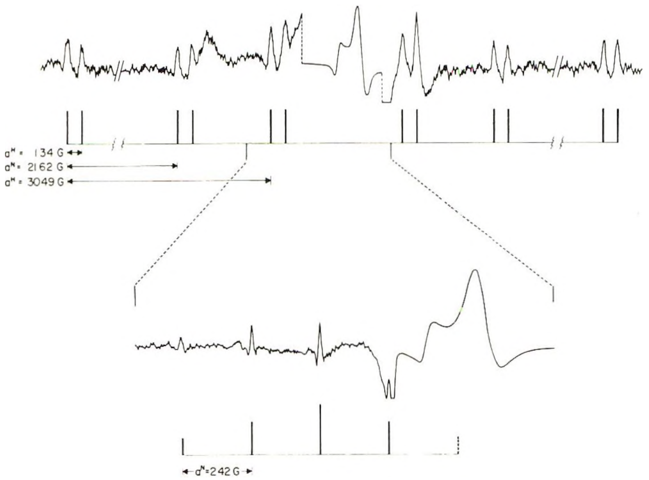

Figure 1. Second-derivative esr spectra obtained during radiolysis of N_2O saturated solutions of 0.01 M KCN at pH 10.4 (upper spectrum) and 13.5 (lower spectrum). The central portion is recorded at reduced gain and contains the signal from the silica cell. Magnetic field increases to the right. Note the expanded scale on the lower trace. The upper spectrum of 12 lines is the same as that obtained under conditions of OH attack on $HCONH_2$ and matches that attributed to $\cdot CONH_2$.[11] The radical responsible for the lower spectrum is a secondary reaction product and has not been identified.

$HClO_4$ the rate of gas flow was restricted to prevent removal of the HCN.

Reactions of OH. The reactions of OH were studied in N_2O saturated solution to increase the yield and to prevent possible complicating reactions of e_{aq}^-. In considering the results to follow and their relationship to possible pulse radiolysis experiments several points must be kept in mind. Most important is the fact that the steady-state esr experiments pertain to radicals with an average lifetime of ~500 μsec. Because of this fact, the radicals observed by esr do not necessarily represent those which would be found on the shorter time scale of pulse experiments. This situation is modified in the radical trapping experiments because rapid reaction of radicals with $CH_2=NO_2^-$ at a rate constant of $\sim 10^8$ M^{-1} sec^{-1} is likely. Thus the half-life for pseudo-first-order reaction with 5×10^{-3} M $CH_2=NO_2^-$ is <2 μsec and the time scale is similar to that of pulse experiments.

Radiolysis of a 0.01 M solution of KCN at pH 10.4 produced a weak 12-line spectrum with a greater line width (0.5 G) than is usual for most organic radicals. The spectrum (shown in Figure 1) is described by the parameters $a^N = 21.62$, $a^H = 30.49$, $a^{H'} = 1.34$ G, and $g = 2.00150$. Such a low value of the g factor is unusual and is often characteristic of a σ electron radical. In fact, this radical has already been identified as $O=\dot{C}NH_2$ by Livingston and Zeldes[11] who produced it photolytically in formamide solutions. (Further discussion of the identification and a reaction mechanism for forming this radical is given in a later section.) As further confirmation of this intermediate in the radiolytic studies an experiment was carried out with formamide (pH 10.2) and the same spectrum obtained. The intensity of the lines was the same with either source of the radical so that production of this radical must be a major reaction in the case of CN^-. The spectral parameters are given in Table I.

Because optical pulse radiolysis experiments[12] suggest a change in the nature of the species produced in CN^- solutions at pH ~12 an esr experiment was also carried out at pH ~13.5. Under those conditions two sets of weak lines were found: one set consists of several broad lines which cannot be characterized further; the other set of narrower lines is best described as a 1:2:3:2:1 quintet with the parameters $a^N = 2.42$ G for two equivalent ^{14}N nuclei and $g = 2.00362$. The radical responsible for the latter set of lines appears to be the result of secondary reactions because the intensity of its lines decreases with increased flow rate of the solution. The same set of narrow lines was obtained in experiments starting with formamide. No specific radical is proposed to account for this spectrum.

As mentioned in the Introduction, the esr spectrum of an adduct, $RCH_2NO_2^-$, was observed in experiments with nitromethane trapping agent[10] at pH 13. The spectrum was characterized by a 0.5-G hyperfine splitting for an ^{14}N nucleus in the group R. In the previous work[10] this adduct was identified as $NCCH_2\dot{N}O_2^-$ with the possibility acknowledged that the group R was more complex than just CN. A repetition here of the previous experiment gave the same spectrum. In addition, however, an identical spectrum (see Table II) was found when formamide was the solute at pH 13. The conclusion seems clear that the reaction of O^- with both CN^- and $HCONH_2$ yields the same radical in strongly basic solution. The spectrum obtained with formamide and nitromethane in strongly basic solution contains, in addition to the above-mentioned radical, the lines of the adduct of $\dot{C}O_2^-$ ($^-O_2CCH_2\dot{N}O_2^-$). The intensity of these lines was found to increase with aging of the formamide solution and must result from OH attack on HCO_2^- formed by the hydrolysis of the formamide.

The parallel between the products formed from CN^- and $HCONH_2$ is also evident in $CH_2=NO_2^-$ trapping experiments at lower pH. Under these conditions (pH 10.4) a different adduct spectrum is observed (the same for both solutes) which displays both a proton and a nitrogen

---

(11) R. Livingston and H. Zeldes, *J. Chem. Phys.*, **47**, 4173 (1967).
(12) D. Behar, to be submitted for publication.

TABLE II: Esr Parameters of Adducts to $CH_2{=}NO_2^-$ in Irradiated Solutions of CN^- and $HCONH_2$[a]

Source	pH	Radical	$a_{NO_2}{}^N$	$a_{CH_2}{}^H$	$a_{NH}{}^N$	$a_{NH}{}^H$	g
CN^-	13	$H_2NCOCH_2\dot{N}O_2^-$	25.27	8.04	0.51		2.00505
$HCONH_2$	13	$H_2NCOCH_2\dot{N}O_2^-$	25.26	8.07	0.50		2.00505
CN^-	10.4	$H_2NCOCH_2\dot{N}O_2^-$	25.24	8.06	0.50	0.35	2.00504
$HCONH_2$	10.4	$H_2NCOCH_2\dot{N}O_2^-$	25.25	8.03	0.50	0.36	2.00506

[a] Hyperfine constants in gauss accurate to ±0.05 G; g factors accurate to ±0.00003. Second-order corrections have been made.

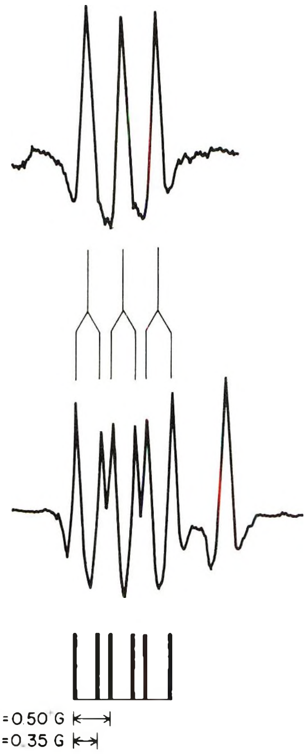

Figure 2. Structure of the lowest field "line" of the adduct to $CH_2{=}NO_2^-$ found in irradiated solutions of N_2O saturated 2 × 10^{-2} M CN^- containing 5 × 10^{-3} M nitromethane at pH 13 (upper) and 10.4 (lower). This adduct is identified as $H_2NCOCH_2NO_2^-$. The line on the right of the lower spectrum is one of those of the electron adduct to $CH_2{=}NO_2^-$. The stick spectrum at the bottom shows the decomposition to ^1H and ^{14}N hyperfine splittings and the connecting lines in the center show the collapse of the proton splitting by exchange under the highly basic conditions.

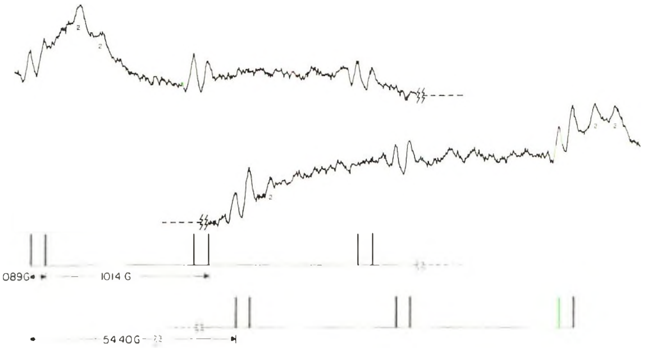

Figure 3. Outer portions of the esr spectrum obtained during radiolysis of an N_2O saturated 2.5 × 10^{-3} M solution of HCN at PH 2.8. The positions of the 12 lines assigned to $HC(OH){=}\dot{N}$ are indicated by the stick spectrum at the bottom. The lines marked by the number 2 are those of $\cdot CONH_2$.

splitting by nuclei in the group R. The structure of a line group for both pH conditions is shown in Figure 2; the corresponding parameters are given in Table II. From this table it is evident that the spectrum observed in strongly basic solution is the same as that at lower pH but with the absence of the 0.35-G proton splitting. Although it is possible that dissociation of a proton in the group R has occurred and that the parameters for both dissociated and undissociated forms happen to be the same, a much more probable explanation is that a base-catalyzed proton exchange occurs which averages the one proton splitting to zero.[13]

The reaction of OH with HCN (pK = 9.3) was studied at pH values of 6.3, 4.0, and 2.8. All solutions were 2.5 × 10^{-3} M in HCN and were saturated with N_2O and those at pH 4.0 and 6.3 were buffered with phosphate. Under these pH conditions some contribution to the spectrum from the radical $\cdot CONH_2$ was evident but in addition new lines appeared. At pH 4.0 and 2.8 the spectrum of Figure 3 was found. These lines are described by the parameters a^H = 54.41, $a^{H'}$ = 0.89, a^N = 10.14 G, and g = 2.00322. (These lines are ~0.5 G wide as was found with $\cdot CONH_2$.) From the large proton hyperfine constant it is evident that the radical must be $HC(OH){=}\dot{N}$ with the CH proton producing the large splitting. The radicals $RCH{=}\dot{N}$ derived from nitriles[3] have a^H ~ 80 G and $H_2C{=}N$ in the solid phase[14] has been found to have a^H ~ 90 G. The value of a^H and the g factor are consistent with those of the radicals from the nitriles. The reduction in a^H from 90 G for $H_2C{=}\dot{N}$ to 54 G for $HC(OH){=}\dot{N}$ is believed to be a specific effect of OH substitution as occurs for the methylene proton in cyclohexadienyl radical where a drop from 48 to 34 G is observed upon OH substitution.[8] The results of INDO calculations shown in Table III support this idea, especially for the first of the two structures for $HC(OH){=}\dot{N}$. A radical which appears in retrospect to have been $HC(OH){=}\dot{N}$ (or the dissociated form $HC(O^-){=}\dot{N}$, see below) was observed by Root, *et al.*,[15] in irradiated crystals of alkali halides doped with CN^-. Their assignment of the spectrum was, however, to HON^+.

At pH ~6 a spectrum similar to that attributed to $HC(OH){=}\dot{N}$ was found which did not show an OH proton splitting. Lines of $\cdot CONH_2$ were also evident under these conditions. The parameters for the new radical are shown in Table I and it is clear that the values of a^N and the g

---

[13] The mechanism of this base-catalyzed exchange is presumed to involve the rapid dissociation-protonation reactions, $\dot{R}OH + OH \rightleftharpoons \dot{R}O^- + HOH$, but with an equilibrium point such that the concentration of RO^- is very small. This type of behavior has been observed in these laboratories for several radicals the most notable of which is hydroxycyclohexadienyl. In this case the OH splitting of 0.42 G is observed only in neutral solution and is averaged to zero in both acid and basic solution. The other hyperfine constants are the same under all conditions (ref 8 and R. W. Fessenden, *J. Chem. Phys.*, submitted for publication.)

[14] F. J. Adrian, E. L. Cochran, and V. A. Bowers, *J. Chem. Phys.*, **36**, 1938 (1962); J. A. Brivati, K. D. J. Root, M. C. R. Symons, and J. A. Tinling, *J. Chem. Soc. A*, 1942 (1969).

[15] K. D. J. Root, M. C. R. Symons, and B. C. Weatherley, *Mol. Phys.*, **11**, 161 (1966).

TABLE III: Results of INDO Calculations on Imino Radicals[a]

Structure	a_{CH}^H	a^N	a^C	a_{OH}^H
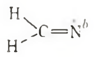	82.7	8.4	−28.7	
(Experimental values)	87.2	10.2	*c*	
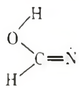	63.9	8.7	−24.4	−4.6
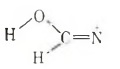	75.7	8.7	−25.8	−3.2
(Experimental values)	54.40	10.14	*c*	0.89

[a] After Pople, Beveridge, and Dobosh.[17] Hyperfine constants in gauss. The bond lengths were r_{CN} = 1.25, r_{CH} = 1.10, r_{CO} = 1.36, and r_{OH} = 0.96 (all in Å). The angles were ∠HCN = 125°, ∠OCH = 125°, and ∠HOC = 105° 56′. The structure for $H_2C{=}\dot{N}$ is that which Chiu, *et al.*,[19] found gave the minimum energy. [b] These values are essentially identical with those given by Chiu, *et al.*[19] [c] Not determined.

factor are significantly different than those of the form found in more acid solutions. This spectrum is assigned, therefore, to the dissociated form $HC(O^-){=}\dot{N}$. At pH ~6 another set of three lines is observed. These lines are not equally spaced and it is very likely that a fourth line in this spectrum is masked by the signal from the silica cell. Under this assumption the spectral parameters are a^H = 27.44, $a^{H'}$ = 19.78 G, and g = 2.00426. The intensity of these lines is not dependent upon sample flow rate so the associated radical does not seem to be a secondary reaction product. No identification of this species which lacks a ^{14}N hyperfine splitting can be suggested.

To clarify the origin of the $\cdot CONH_2$ observed in acid solutions a study of the signal heights as a function of flow rate was carried out. It was found that at pH 2.8 the signals of this radical as observed in Figure 3 were visible only at low flow rates. At higher pH the signals were also inversely dependent upon flow rate but were considerably stronger and could not be completely eliminated at the highest flow rate used. It is likely that some of this radical is produced in secondary reactions, particularly at low pH. An experiment was also carried out with formamide at pH 2.8 and 6.0 to determine if the radical $HC(OH){=}\dot{N}$ could be formed from this source. Only the spectrum of $\cdot CONH_2$ was observed.

Reactions of H and e_{aq}^-. The reaction of H atoms with HCN was studied at pH 2.5 with a 2.5 × 10^{-3} *M* solution. Because Ogura[2] has shown the rate constant for e_{aq}^- + HCN to be only moderately fast (2 × 10^8 M^{-1} sec^{-1}) HCN cannot compete with H^+ for e_{aq}^- and reaction of only H with HCN is assured. By analogy with the nitriles[3] the reaction should be

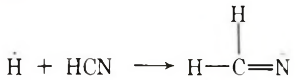

$$\dot{H} + HCN \longrightarrow H{-}\overset{\displaystyle H \atop |}{C}{=}\dot{N} \qquad (1)$$

A search for the lines of $H_2C{=}\dot{N}$ was carried out under modulation conditions appropriate for broad lines and lines attributable to this species were found; the two outer line groups are illustrated in Figure 4. The lines of this radical are nearly 1 G wide and, because of the large modulation amplitudes required, the central set of six lines could not be observed because of interference from the wings of the line from the silica cell. The parameters for $N_2C{=}\dot{N}$ found here are a^H = 87.2, a^N = 10.2 G, and g = 2.0028 and are in good agreement with those found in the solid phase.[14] We attribute the atypical line width for this species (as well as that for the others studied here which show this effect) to spin-rotation interactions as a result of the low moments of inertia.[16]

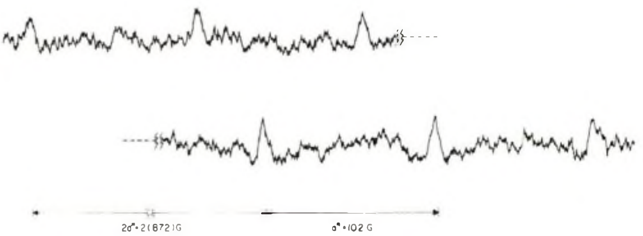

Figure 4. Outer portions of the esr spectrum attributed to $H_2C{=}\dot{N}$ as observed in 2.5 × 10^{-3} *M* HCN at pH 2.5 during irradiation. Shown are the three-line patterns representing the splitting by ^{14}N (10.2 G) of the outer lines of the triplet produced by the two equivalent protons.

The observation[3] of radicals of the type $RCH{=}\dot{N}$ produced by e_{aq}^- + $RC{\equiv}N$ suggested that $H_2C{=}\dot{N}$ could result also from

$$e_{aq}^- + HC{\equiv}N \rightarrow [HCN]^- \qquad (2)$$

$$[HC\dot{N}]^- + H_2O \rightarrow H_2C{=}\dot{N} + OH^- \qquad (3)$$

Experiments with 0.1 *M* HCN at several pH values between 7.0 and 11.1 showed the formation of this radical. The signal intensity at pH 11.1 was, however, reduced by about one-half. At pH 11.8 and above no signals were detectable. This result suggests that e_{aq}^- reacts with HCN but not with CN^- and that because of the high cyanide concentration sufficient HCN remained at pH 11.1 to partially react with e_{aq}^-. A search for the lines of $HC\dot{N}^-$ [15] at these various pH values was unsuccessful. Apparently, as found for $RCH{=}\dot{N}$ up to pH 13, the protonation step (reaction 3) is rapid and the radical exists in the undissociated form. (It is also possible that the lines of $HC\dot{N}^-$ were too broad to detect.)

Structure of the Radical $\cdot CONH_2$. The very large difference in the two proton hyperfine constants of the radical designated as $\cdot CONH_2$ (30.5 and 1.3 G) is peculiar, as has been noted before,[11] and other structures for the radical must be considered. The experiments with $HCOND_2$ reported by Livingston and Zeldes[11] clearly show that the aldehyde hydrogen is abstracted so that without a complex rearrangement the radical cannot be HCONH. Those authors also argued against the enol form $HO\dot{C}{=}NH$ because no proton exchange was evident in 1 *M* acid. (The OH protons of more conventional radicals are found to exchange under these conditions.) In all esr experiments a rearrangement from keto to enol form, if occurring, would have to be complete within the radical lifetime of ~500 μsec. Because this rate might be strongly influenced by water an experiment with pure formamide was undertaken. In fact, the spectrum and its intensity were very similar to that found in aqueous solution.

As an alternative approach it was hoped that molecular orbital calculations would allow the rejection of one of the two structures for the above radical. The results of INDO[17] calculations for two geometries of $\cdot CONH_2$ and one of $HO\dot{C}{=}NH$ are presented in Table IV. The results

---

(16) For some comments on this effect for hydrocarbon radicals see H. G. Benson, A. J. Bowles, A. Hudson, and R. A. Jackson, *Mol. Phys.*, **20**, 713 (1971).

(17) J. P. Pople, D. L. Beveridge, and P. A. Dobosh, *J. Amer. Chem. Soc.*, **90**, 4201 (1968).

TABLE IV: Results of INDO Calculations on $CONH_2$[a]

Structure	a^N	a^H	$a^{H'}$
1.[b] 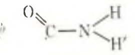 (planar)	15.1	35.9	−3.2
	18.1	39.8	−3.4
2.[b] 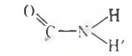 (nonplanar)	26.7	69.1	1.39
3.[c] 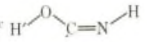			
4. (Experimental values)	21.6	30.5	1.3

[a] After Pople, Beveridge, and Dobosh.[17] Hyperfine constants in gauss. [b] In structures 1 and 2 the geometry is derived from that of $HCONH_2$ [C. C. Costain and J. M. Dowling, *J. Chem. Phys.*, **32**, 158 (1960)]. The parameters for structure 1 are $r_{CN} = 1.376$, $r_{CO} = 1.193$, $r_{NH} = 1.014$, $r_{NH'} = 1.002$ (all in Å) and $\angle OCN = 123°\ 48'$, $\angle CNH = \angle CNH' = 120°$. For structure 2 the parameters are the same except that H' is moved out of the plane of the other atoms by an amount corresponding to an azimuthal angle of 60°. [c] All atoms are in one plane with the parameters $r_{OH'} = 0.96$, $r_{OC} = 1.36$, $r_{CN} = 1.28$, $r_{NH} = 1.00$ and $\angle H'OC = 105°\ 56'$, $\angle OCN = 120°$, $\angle CNH = 128°\ 5'$. Standard values[17] are used except for r_{CN} [E. G. Cox and G. A. Jeffrey, *Proc. Roy. Soc., Ser. A*, **207**, 110 (1951)], $\angle H'OC$[methanol value, E. V. Ivash and D. M. Dennison, *J. Chem. Phys.*, **21**, 1804 (1953)], and $\angle CNH$ [as for OCNH, L. H. Jones, J. N. Schoolery, R. G. Shulman, and D. M. Yost, *ibid.*, **18**, 990 (1950)].

for all structures are of the correct magnitudes[18] and in particular a large difference between the two values of the hyperfine constants for the NH_2 protons of the keto form is found.[19] Further refinement of the calculations is possible but it seems unlikely that it will be possible to reject either structure. On the basis mainly of the chemical arguments the structure $\cdot CONH_2$ seems most appropriate although the other cannot completely be excluded.

With the assignment of this radical as $\cdot CONH_2$ it is evident that, barring a rearrangement following addition, the adduct to nitromethane must be assigned the structure $H_2NC({=}O)CH_2\dot{N}O_2^-$. The 0.50-G ^{14}N hyperfine constant is not unreasonable for nitrogen in this position. To explain only one proton splitting from the NH_2 protons one must argue that the NH_2 group is not free to rotate so that the protons are inequivalent and that one splitting is too small to resolve. This behavior is similar to that of the radical $\cdot CONH_2$ itself which has two very different proton splittings and so is not unexpected. The absence of the N–H proton splitting of the adduct under strongly basic conditions is most likely the result of an exchange with water by means of the dissociation

$$OH^- + H_2NCOCH_2\dot{N}O_2^- \rightleftharpoons H_2O + {}^-HNCOCH_2\dot{N}O_2^- \quad (4)$$

as is observed[8] for radicals such as $(CH_3)_2\dot{C}OH$. (It is most likely that this equilibrium lies to the left under the conditions used, however.)

Reaction Mechanism

From the results above it is clear that the reactions of H and e_{aq}^- with HCN are quite simple and yield $H_2C{=}\dot{N}$. The reaction of OH with HCN also seems to be a simple addition

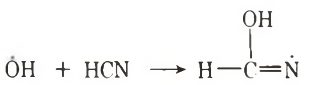

$$\dot{O}H + HCN \longrightarrow H{-}\overset{\displaystyle OH}{\overset{|}{C}}{=}\dot{N} \quad (5)$$

and in acid solutions splittings by all of the nuclei of this radical are observed. At pH 6 the splitting of the OH proton is absent and small changes in some of the other spectral parameters have occurred. It is clear that under these conditions the radical exists as the anion

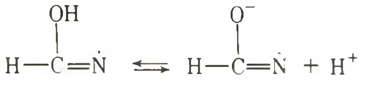

$$H{-}\overset{\displaystyle OH}{\overset{|}{C}}{=}\dot{N} \rightleftharpoons H{-}\overset{\displaystyle O^-}{\overset{|}{C}}{=}\dot{N} + H^+ \quad (6)$$

The pK for this reaction is estimated to be ~5.

The reaction of OH with CN^- is much more complex. The exact parallel in behavior of CN^- and $HCONH_2$ has been noted and the resultant radical identified as $\cdot CONH_2$. A reasonable sequence of reactions for forming this species is

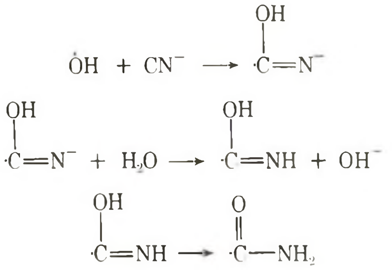

$$\dot{O}H + CN^- \longrightarrow \cdot\overset{\displaystyle OH}{\overset{|}{C}}{=}N^- \quad (7)$$

$$\cdot\overset{\displaystyle OH}{\overset{|}{C}}{=}N^- + H_2O \longrightarrow \cdot\overset{\displaystyle OH}{\overset{|}{C}}{=}NH + OH^- \quad (8)$$

$$\cdot\overset{\displaystyle OH}{\overset{|}{C}}{=}NH \longrightarrow \cdot\overset{\displaystyle O}{\overset{\|}{C}}{-}NH_2 \quad (9)$$

The protonation step 8 can be very rapid as can reaction 9 which probably proceeds by dissociation of the OH followed by a protonation on the nitrogen. If the identification of the final radical is incorrect and it exists as the enol form then reaction 9 is not needed for cyanide solutions but with $HCONH_2$ reaction 9 would then have to be reversed.

It is important to note that the reactions of OH with HCN and CN^- lead to different radicals on the time scale of the esr experiments. Off hand, the rearrangement of $HC(OH){=}\dot{N}$ to $\cdot CONH_2$ by a sequence of reactions similar to 7–9 does not seem unlikely. The esr results which show $\cdot CONH_2$ to be only a secondary product in the reaction of OH with HCN in the acid region indicate, that this rearrangement does not readily occur. The situation with $HC(O^-){=}\dot{N}$ is less clear as in neutral solutions a larger yield of $\cdot CONH_2$ is observed which cannot definitely be called a secondary product. It is possible therefore that this form can convert to $\cdot CONH_2$. The experiments with formamide at pH 2.8 and 6.0 which found only $\cdot CONH_2$ shows clearly that this radical does not rearrange to the form $HC(OH){=}\dot{N}$ or $HC(O^-){=}\dot{N}$. The factor determining the form of the radical seems most probably to be whether a hydrogen is bonded to the carbon. Once such a hydrogen is in place it apparently cannot be removed by ionization. The lack of ionization of the comparable radicals $RCH{=}\dot{N}$ has been noted. Related to this point is the representation of the structure of the first intermediate in reactions 7 and 8 by $\cdot C(OH){=}N^-$. If a large fraction of charge were on the carbon so the structure should be more correctly represented by $^-C(OH){=}\dot{N}$ then protonation should occur on the carbon leading to the radical $HC(OH){=}N$ contrary to the observations.

The reaction of O^- with CN^- in strong base can be identified from the result of the nitromethane trapping experiment and the parallel between CN^- and $HCONH_2$. Because the same adduct is formed as in less alkaline solutions where the intermediate is known to be $\cdot CONH_2$ it is clear that the reaction sequence starting with O^- is essentially the same as that with OH. The fact that the esr spectrum of $\cdot CONH_2$ itself is not observable in strong base means that some transformation is occurring. By far the most likely is an exchange of protons by the dissociation

---

[18] Better agreement with observed hyperfine parameters for the enol form would probably be obtained with a longer CN bond. The three other structures for this form with H and H' transposed cis to trans (with respect to the unpaired electron) or *vice versa* give much poorer agreement with experiment. In each case the trans proton has the larger hyperfine constant.

[19] Recent calculations by M. F. Chiu, B. C. Gilbert, and B. T. Sutcliffe, *J. Phys. Chem.*, **76**, 553 (1972), also show this difference and are otherwise in reasonable agreement with the observations.

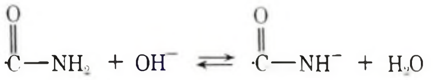

$$\cdot\overset{\overset{\displaystyle O}{\|}}{C}{-}NH_2 + OH^- \rightleftarrows \cdot\overset{\overset{\displaystyle O}{\|}}{C}{-}NH^- + H_2O \qquad (10)$$

which broadens the lines. Because a change in initial optical density of pulse irradiated CN^- solutions is evident[12] at about pH 12, a shift of this equilibrium toward the right probably also occurs. An experiment at 2 *M* KOH and 10^{-2} *M* CN^- was conducted in order to determine if the ionized keto radical, $\cdot C({=}O)NH^-$ can rearrange to the enol form $HC(O^-){=}\dot{N}$; the absence of the lines of this species showed that the rearrangement does not occur.

The observation of only one adduct to $CH_2{=}NO_2^-$ in basic solutions of CN^- tells several things. On the most trivial level the absence of the $\dot{C}O_2^-$ adduct shows that cyanide in these solutions does not hydrolyze significantly to $HCONH_2$ (it has been found that formamide solutions do give some of the CO_2 adduct). The $\cdot CONH_2$ found in CN^- solutions cannot, therefore, come from $HCONH_2$ produced by such hydrolysis. Furthermore, production of CN in addition to $\cdot CONH_2$ radical can probably be ruled out because only the one adduct to $CH_2{=}NO_2^-$ is found. Reaction of $\cdot SO_4^-$ with CN^-, on the other hand, leads to both the $\cdot CONH_2$ adduct and what is probably the $\dot{C}N$ adduct.[20]

The behavior of CN^- is, from this work, clearly different than that of the halides and pseudohalides such as SCN^-. The adduct of OH + CN^- is stable toward dissociation and does not undergo equilibria leading to $(CN)_2^-$. The factor which probably controls these reaction pathways is the stability of the X-O bond in XOH^-. In the case of CN^- there is a strong C-O bond in contrast to the rather weaker bond in the case of the halides.

Reexamination of Other Systems. The previous misassignment[10] of the $CH_2{=}NO_2^-$ adduct obtained with CN^- solutions, as detailed above, suggests that with some of the other systems studied previously[10] the radicals R in $RCH_2\dot{N}O_2$ may also have been incorrectly identified. The most likely cases are that of SCN^- and perhaps N_3^- and SH^-. The latter was studied at a number of pH values and results consistent with adducts of $\dot{S}^-$ and SH found. In the present work the SCN^- system was investigated at low pH where the CN^- system gave the new spectrum reported above. No change in the spectrum was found at pH 9.8 so no new structure for the adduct to $CH_2{=}NO_2^-$ seems necessary. The N_3^- system was not reexamined.

Conclusions

The primary radicals H and OH from the radiolysis of water clearly add to HCN to form $H_2C{=}\dot{N}$ and $HC(OH){=}\dot{N}$, respectively. The other intermediate, e_{aq}^-, also leads to $H_2C{=}\dot{N}$ by addition followed by protonation. No product resulting from the possible reaction of e_{aq}^- with CN^- was found but reaction of OH (or O^-) with CN^- yields a radical which is most probably $\cdot CONH_2$ (or $CONH^-$). This radical is the same as that obtained from reaction of OH with formamide. It is not clear whether the intermediate $HC(OH){=}\dot{N}$ can rearrange to $\cdot CONH_2$ but the reverse reaction is not found. Thus in experiments with $HCONH_2$ the radical $\cdot CONH_2$ is found under conditions where HCN yields $HC(OH){=}\dot{N}$.

[20] O. P. Chawla and R. W. Fessenden, to be submitted for publication.

Electron Paramagnetic Resonance Line Widths of Vanadyl(IV) α-Hydroxycarboxylates[1]

N. Dennis Chasteen and Melvin W. Hanna*

Department of Chemistry, University of Colorado, Boulder, Colorado 80302

(Received June 8, 1972)

Publication costs assisted by the National Science Foundation

Electron paramagnetic resonance line widths were measured at 24° on 2:1 ligand-metal vanadyl(IV). α-hydroxycarboxylate chelates of varying molecular size with the ligands benzilic, mandelic, α-hydroxyisobutyric, lactic, and glycolic acids in aqueous solution at pH 8.5. Measurements on vanadyl sulfate in 3 *N* HCl and vanadyl bis(α-hydroxyisobutyrate) in 9 mol % ethanol-water were also made. In general the theory of Kivelson and Wilson satisfactorily explains the observed line widths although the values of the rotational correlation time derived from different parameters in the theory are not exactly equal. A nearly linear relationship exists between the rotational correlation time, τ_R, and the molecular weights of the hydroxycarboxylates. The residual line widths are readily accounted for by a spin-rotational interaction. Hydrated vanadyl ion appears to be an exception to these results in two ways. First, the residual line width (2.80 G) is much larger than expected from the spin-rotation interaction and is most likely due to the isotropic coupling of the unpaired electron with the protons of the coordinated water molecules. Second, the τ_R values, and hence all of the line widths, are anomalously large relative to the hydroxycarboxylates. This lengthening of τ_R appears to be due to the presence of bound water molecules in the second coordination sphere of hydrated vanadyl ion.

Introduction

One of the most striking features of the epr spectrum of vanadyl ion, VO^{2+}, in liquids is the variation of the line width with nuclear hyperfine component (Figure 1). This dependence of electron relaxation on nuclear orientation was first explained semiquantitatively by McConnell in terms of motional modulation of anisotropic *g* and nuclear hyperfine tensors.[2a] A more detailed line width theory, which also included spin-rotational interactions, was later developed by Wilson, Atkins, and Kivelson[2b-4] and successfully applied to the temperature dependence study of the epr line widths of vanadyl bis(acetylacetonate) in toluene solution.[3,4] Subsequent investigations on two other vanadyl chelates[5,6] have raised a question about the theory, in that the rotational correlation time, τ_R, derived from different parameters in the theory is not exactly the same.

This study was undertaken to further examine the line width theory as applied to several other vanadyl chelates and to determine the sensitivity of rotational correlation times to differences in molecular structure and to metal ion-solvent interactions. Accordingly we have made careful line width measurements on aqueous solutions of vanadyl sulfate ($VOSO_4$) and of a series of α-hydroxycarboxylate chelates, I, with similar anisotropic magnetic properties but of varying molecular size, *viz*, where R_1, R_2 is H, H (glycolate); H, CH_3 (lactate); CH_3, CH_3 (hydroxyisobutyrate); H, C_6H_5 (*dl*-mandelate); and C_6H_5, C_6H_5 (benzilate). A few measurements in ethanol-water mixtures were also made. The results are compared with previous epr line width studies of vanadyl chelates in water,[5] dimethylformamide,[6] methanol,[7] and toluene.[3]

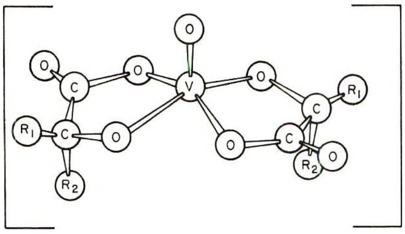

Experimental Section

Preparation of Compounds. The aqueous solutions of the hydroxycarboxylate chelates were prepared as described elsewhere[8-11] and titrated to pH 8.5 with ammonia carried over in a stream of nitrogen gas bubbling through the sample solution. The hydroxyisobutyrate chelate in 8.86 mol % ethanol-water was titrated with NaOH. The solutions were nominally 2×10^{-3} *M* VO^{2+} and 4×10^{-2} *M* ligand, a tenfold excess of ligand being used to establish equilibrium favorable to the parent species.[9-11] Identical line widths were obtained for solutions having a two- or tenfold excess of ligand, or for solutions titrated with NH_3 or NaOH. All solution transfers were made with a system of syringes and serum stoppers to avoid contact of the solutions with atmospheric oxygen.

---

(1) Supported by National Science Foundation Grants No. GP 11387 and GP 28215 and a National Institutes of Health Postdoctoral Fellowship awarded to N. D. C., 1969-1970.

(2) (a) H. M. McConnell, *J. Chem. Phys.*, **25**, 709 (1956); (b) D. Kivelson, *ibid.*, **33**, 1094 (1960).

(3) R. Wilson and D. Kivelson, *J. Chem. Phys.*, **44**, 154 (1966).

(4) P. W. Atkins and D. Kivelson, *J. Chem. Phys.*, **44**, 169 (1966).

(5) D. C. McCain and R. J. Myers, *J. Phys. Chem.*, **71**, 192 (1967).

(6) R. B. Jordan and N. S. Angerman, *J. Chem. Phys.*, **48**, 3983 (1967).

(7) N. S. Angerman and R. B. Jordan, *Inorg. Chem.*, **8**, 1824 (1969).

(8) R. E. Tapscott and R. L. Belford, *Inorg. Chem.*, **6**, 735 (1967).

(9) R. L. Belford, N. D. Chasteen, H. So, and R. E. Tapscott, *J. Amer. Chem. Soc.*, **91**, 4675 (1969).

(10) N. D. Chasteen, R. L. Belford, and I. C. Paul, *Inorg. Chem.*, **8**, 408 (1969).

(11) R. R. Reeder and P. H. Rieger, *Inorg. Chem.*, **10**, 1258 (1971).

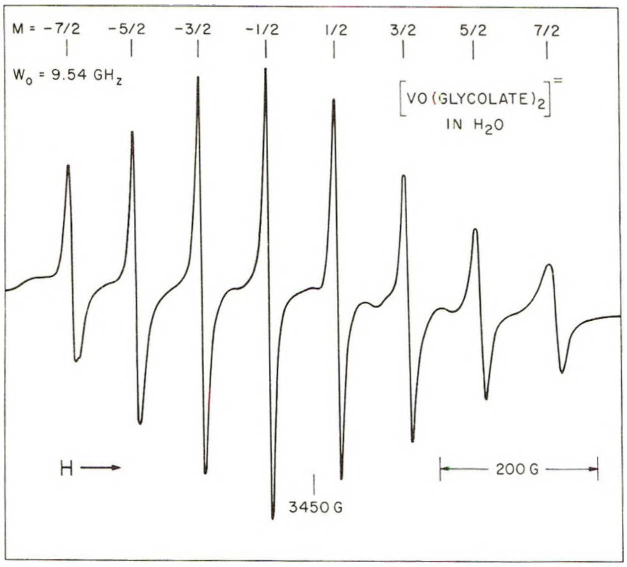

Figure 1. First-derivative X-band epr spectrum of ammonium vanadyl glycolate plus excess ligand, 2 × 10^{-3} *M* VO^{2+} in H_2O, pH 8.5, at 297°K.

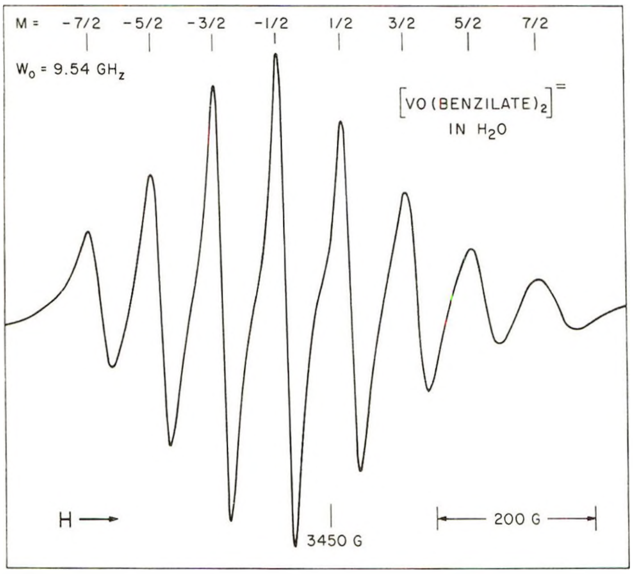

Figure 2. First-derivative X-band epr spectrum of ammonium vanadyl benzilate plus excess ligand, 2 × 10^{-3} *M* VO^{2+} in H_2O, pH 8.5, at 297°K.

Epr Spectra. All spectra were measured with a Varian V-4502 spectrometer, operating at X-band (~9.535 GHz) with 100 kHz field modulation. Generally, the field was measured with a proton probe and a Hewlett-Packard 5245M frequency counter. The *g* values were determined both directly by measuring the klystron frequency with a Micro-Now Model 101 frequency multiplier and the frequency counter or indirectly by comparison with the resonance of a speck of powdered DPPH (g = 2.0036). The spectra were recorded on a Honeywell x-t strip chart recorder equipped with a field marker.

Effects of overmodulation and saturation on the line widths were avoided. The temperature was maintained at 24.0 ± 0.3° as measured by a copper-constantan thermocouple taped to the aqueous solution flat cell.

Viscosity Measurements. The solution viscosities relative to that of water were determined with an Ostwald viscometer[12] immersed in a constant temperature bath at 24°.

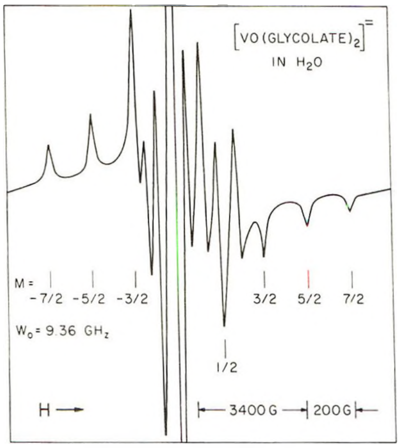

Figure 3. First derivative X-band epr spectrum of ammonium vanadyl glycolate plus excess ligand, 2 × 10^{-3} *M* VO^{2+} in H_2O, pH 8.5, at 77°K.

Results and Discussion

Determination of g and Hyperfine Splitting Parameters. Knowledge of the anisotropic epr parameters is needed for later treatment of the line width theory. Typical room temperature solution spectra of the vanadyl chelates are shown in Figures 1 and 2. These spectra are governed by the isotropic spin Hamiltonian

$$\mathcal{H} = g_0\beta_0\vec{H}\cdot\vec{S} + a\vec{S}\cdot\vec{I} \qquad (1)$$

with the transition energies, correct to second-order perturbation theory, given by

$$\omega_0 = g_0\beta_0 H/\hbar + aM + \frac{1}{2}a^2\left[\frac{I(I+1) - M^2}{g_0\beta_0 H/\hbar}\right] \qquad (2)$$

where $\vec{S}$ and $\vec{I}$ are the electron and nuclear spin operators respectively, $\vec{H}$ is the applied magnetic field (G), ω_0 is the microwave frequency (rads/sec), $I = 7/2$, and $M = \pm 7/2, \ldots \pm 1/2$.

Anisotropy in the epr parameters is seen in the spectra of frozen solution samples (Figure 3) where the averaging effect of molecular rotation is absent. These spectra are governed by the anisotropic spin Hamiltonian

$$\mathcal{H} = \beta_0(g_zH_zS + g_xH_xS_x + g_yH_yS_y) + A_xS_xI_x + A_yS_yI_y + A_zS_zI_z \qquad (3)$$

where *x*, *y*, and *z* refer to the molecular fixed axis system with principal axes of the **g** and **A** tensors assumed to be coincident. The *z* axis presumably corresponds to the vanadyl, VO, bond direction. Unfortunately, we were unable to assign the *x* and *y* components of these spectra (Figure 3) because of the width of the lines encountered in the frozen solutions. Therefore, we assumed an axially symmetric system with $g_z = g_\parallel$, $g_x = g_y = g_\perp$, $A_z = A_\parallel$, and $A_x = A_y = A_\perp$. We derived g and A from the frozen solution spectrum according to the equation[13]

$$\omega_0 = g\beta_0 H/\hbar + AM + \frac{A^2}{2}\left[\frac{I(I+1) - M^2}{g\beta_0 H/\hbar}\right] \qquad (4)$$

for the transition energies. Values for g and A were then

---

(12) F. Daniels, J. W. Williams, P. Bender, R. A. Alberty, and C. D. Cornwall, "Experimental Physical Chemistry," 6th ed, McGraw-Hill, New York, N. Y., 1962, p 147.

(13) B. Bleaney, *Phil. Mag.*, **42**, 441 (1951).

TABLE I: Epr Parameters Of Vanadyl Complexes

Complex	g_0 (±0.001)	$g_{\parallel}$ (±0.002)	$g_{\perp}$ (±0.003)	a (±0.006)[b]	$A_{\parallel}$ (±0.020)[b]	$A_{\perp}$ (±0.030)[b]
Glycolate	1.972	1.950	1.983	1.583	3.084	0.833
Lactate	1.973	1.956	1.982	1.561	2.928	0.877
Hydroxyisobutyrate	1.973	1.954	1.983	1.530	2.917	0.836
dl-Mandelate	1.974	1.954	1.984	1.553	2.925	0.867
Benzilate	1.974	1.955	1.984	1.466	2.856	0.772
VO^{2+} in 3 *N* HCl[a]	1.965	1.932	1.981	2.004	3.440	1.353
	±0.002	±0.002	±0.002	±0.010	±0.010	±0.010

[a] Reference 14. [b] Units of 10^9 rads sec^{-1}.

determined from the relations

$$g_0 = \frac{1}{3}g_{\parallel} + \frac{2}{3}g_{\perp} \tag{5}$$

and

$$a = \frac{1}{3}A_{\parallel} + \frac{2}{3}A_{\perp} \tag{6}$$

a and g_0 being available from the room temperature solution spectrum and eq 2. More details concerning the application of eq 2 and 4 are given in ref 3. The resultant parameters are given in Table I.

Within experimental error, the parameters for the hydroxycarboxylates are in agreement with those reported earlier.[9,11] The parameters for $VOSO_4$ in 3 *N* HCl were taken from the literature;[14] however, we did measure $g_0 = 1.966 \pm 0.001$ and $a = 2.008 \pm 0.006 \times 10^9$ rads/sec^{-1} in good agreement with the literature values[14] of 1.965 and 2.004×10^9 rads/sec^{-1}, respectively. The isotropic g and a values were the same for the hydroxyisobutyrate in both water and ethanol–water mixtures.

Measurement of Line Widths. The variation in the line width ΔH_M with nuclear spin state can be fitted to an equation of the form

$$\Delta H_M = \alpha' + \alpha'' + \beta M + \gamma M^2 + \delta M^3 \tag{7}$$

where $\alpha = \alpha' + \alpha''$, β, γ, and δ are constants.[2b,3]

The width of each line can be measured directly or alternately, indirectly from the relative peak-to-peak heights, h, and the relationship

$$\Delta H_M = \Delta H_{-1/2}\left(\frac{h_{-1/2}}{h_M}\right)^{1/2} \tag{8}$$

where $\Delta H_{-1/2}$ is the width of the sharpest line in the spectrum of the hydroxycarboxylates. The indirect method assumes that $h\Delta H^2$ is the same for all hyperfine lines, *i.e.*, all lines have the same line shape, and has worked well for other vanadyl complexes.[3,5,15]

To test the indirect method on the compounds reported here, the relative values of $h\Delta H^2$ for the lactate were measured and found to be 0.87, 0.92, 1.07, 1.00, 1.03, 1.02, 1.06, and 0.95 ($M = -7/2$ to $+7/2$). The deviation of the two lowest field lines from the expected value of unity probably arises from the presence of more than one species in solution.[9-11] Earlier workers have noted[9] substantial amounts of other species present in the glycolate solution, and this phenomenon is also evident in the weak extra lines and in the pronounced asymmetry of the low-field lines of our glycolate spectrum (Figure 1). Under high resolution, the $M = -7/2$ and $M = -5/2$ lines consist of two overlapping lines with similar widths. Some asymmetry, but less than that in the glycolate, was also observed in the low-field lines of the lactate. Further evidence for this interpretation of the breakdown of the indirect method for the low-field lines in the glycolate and lactate solutions is provided by the recent pH and temperature dependence epr study of vanadyl lactate and glycolate solutions by Reeder and Rieger. Their results suggest that the $M = -7/2$ line consists of two overlapping lines due to a mixture of cis and trans isomers in the ratio 0.23/1.0 at 25°.[11] We think that the predominant species has a trans configuration about the vanadyl group since the visible spectra of both the vanadyl glycolate and lactate solutions exhibit four bands characteristic of *trans*-vanadyl α-hydroxycarboxylate chelates.[10] Furthermore, the low-field lines of the larger molecules (hydroxyisobutyrate, mandelate, and benzilate) show little asymmetry or evidence of more than one predominant species. This can be explained by a reduction in the fraction of cis molecules due to a steric interaction between the large R groups of these ligands.

The lactate line widths measured indirectly give a far better least-squares fit to eq 7 than those measured directly (Table II). The indirectly measured values give an rms deviation from the regression line of ±0.04 G compared to ±0.27 G for the directly measured values. Omission of the $-7/2$ and $-5/2$ lines from the least-squares calculation of the directly measured values considerably improves the fit, with a reduction in the rms deviation from ±0.27 to ±0.12 G. This is consistent with the observed asymmetry of these two lines. Because the line width measurements are hampered to some degree by overlapping spectra of more than one species, there is no reason to assume that the direct or indirect method gives a better measure of the "true" line width. We chose to measure the line widths of the remaining compounds by the indirect method, since the method is faster and somewhat more precise, and gives a better least-squares fit to eq 7 than the direct method. We wish to emphasize that the difference in line widths obtained from these two methods is too small to invalidate any conclusions drawn later.

To test if overlap of adjacent lines seriously affects the line width measurements, the room-temperature spectrum of the lactate was computer simulated by summing eight first-derivative Lorentzian lines with the line widths listed in Table II. The experimental (and calculated) relative heights, h, of the eight lines were as follows: 0.404 (0.404), 0.646 (0.644), 0.903 (0.902), 1.00 (1.00), 0.831 (0.831), 0.543 (0.540), 0.328 (0.327), and 0.194 (0.194). Clearly overlap of lines is insignificant. This is true for all the compounds except the benzilate (Figure 2). To correct for overlap in this case, the benzilate spectrum was computer analyzed into eight first-derivative Lorentzian lines. The rms deviation of ΔH from eq 7 was increased after overlap correction, ±0.24 G without overlap correction *vs.* ±0.52 G with overlap correction. The very broad $M = 7/2$ line en-

---

(14) H. Kon and N. E. Sharpless, *J. Phys. Chem.*, **70**, 105 (1966).

(15) R. N. Rogers and G. E. Pake, *J. Chem. Phys.*, **33**, 1107 (1960).

TABLE II: Experimental and Calculated Line Widths and Calculated Line Width Parameters for a Series of Vanadyl Complexes

		Experimental and calculated[a] linewidths							
Complex and parameter values	M	−7/2	−5/2	−3/2	−1/2	+1/2	+3/2	+5/2	+7/2
Glycolate in H_2O									
$\alpha = 7.38$ G, $\beta = 0.540$ G,	Exptl	10.78 ± 0.08	8.88 ± 0.08	7.60 ± 0.07	7.14 ± 0.06	7.69 ± 0.09	9.26 ± 0.09	11.67 ± 0.13	14.87 ± 0.21
$\gamma = 0.449$ G, $\delta = 0.0036$ G	Calcd	10.83	8.78	7.57	7.22	7.76	9.21	11.59	14.92
	Δ	−0.05	+0.10	+0.03	−0.08	−0.07	+0.05	−0.08	−0.05
					rms dev = ±0.07				
Lactate in H_2O[b]	Exptl	12.29 ± 0.11	9.72 ± 0.10	8.22 ± 0.10	7.81 ± 0.06	8.57 ± 0.09	10.60 ± 0.09	13.63 ± 0.14	17.73 ± 0.15
$\alpha = 8.10$ G, $\beta = 0.790$ G,	Calcd	12.32	9.68	8.19	7.85	8.63	10.55	13.60	17.75
$\gamma = 0.566$ G, $\delta = 0.0010$ G	Δ	−0.03	+0.04	+0.03	−0.04	−0.06	+0.05	+0.03	+0.02
					rms dev = ±0.04				
Lactate in H_2O[c]	Exptl	11.44 ± 0.15	9.30 ± 0.11	8.49 ± 0.11	7.81 ± 0.06	8.43 ± 0.06	10.70 ± 0.11	14.07 ± 0.14	17.27 ± 0.17
$\alpha = 8.27$ G, $\beta = 0.864$ G,	Calcd	11.52	9.30	8.12	7.96	8.83	10.71	13.60	17.49
$\gamma = 0.509$ G, $\delta = 0.0009$ G	Δ	−0.08	0.00	+0.37	−0.15	−0.40	−0.01	+0.47	−0.22
					rms dev = ±0.27				
Hydroxyisobutyrate in H_2O	Exptl	14.03 ± 0.24	10.74 ± 0.12	9.03 ± 0.13	8.60 ± 0.10	9.46 ± 0.13	11.90 ± 0.15	15.57 ± 0.23	20.35 ± 0.21
$\alpha = 8.90$ G, $\beta = 0.987$ G,	Calcd	14.03	10.77	8.97	8.58	9.56	11.89	15.50	20.38
$\gamma = 0.678$ G, $\delta = 0.0065$ G	Δ	0.00	−0.03	+0.06	+0.02	−0.10	+0.01	+0.07	−0.03
					rms dev = ±0.05				
Mandelate in H_2O	Exptl	18.70 ± 0.27	13.96 ± 0.21	11.33 ± 0.13	10.72 ± 0.08	12.17 ± 0.14	15.77 ± 0.12	21.03 ± 0.17	28.41 ± 0.24
$\alpha = 11.23$ G, $\beta = 1.471$ G,	Calcd	18.71	13.95	11.31	10.75	12.22	15.68	21.09	28.40
$\gamma = 1.006$ G, $\delta = 0.0071$ G	Δ	−0.01	+0.01	+0.02	−0.03	−0.05	+0.09	−0.06	+0.01
					rms dev = ±0.04				
Benzilate[d] in H_2O	Exptl	36.99 ± 0.95	25.90 ± 0.33	20.45 ± 0.23	19.15 ± 0.16	22.55 ± 0.28	30.14 ± 0.37	42.91 ± 0.60	58.15 ± 0.14
$\alpha = 20.33$ G, $\beta = 3.511$ G,	Calcd	36.96	26.07	20.20	19.13	22.63	30.48	42.45	58.31
$\gamma = 2.229$ G, $\delta = 0.0038$ G	Δ	+0.03	−0.17	+0.25	+0.02	−0.08	−0.34	+0.46	−0.16
					rms dev = ±0.24				
Benzilate[e] in H_2O	Exptl	36.59 ± 0.95	26.12 ± 0.33	20.68 ± 0.23	19.37 ± 0.16	22.72 ± 0.28	29.87 ± 0.37	41.18 ± 0.60	51.56[f] ± 0.14
$\alpha = 20.51$ G, $\beta = 3.197$ G,	Calcd	36.56	26.21	20.57	19.44	22.63	29.94	41.16	56.07
$\gamma = 2.106$ G, $\delta = 0.0033$ G	Δ	+0.03	−0.09	+0.11	+0.08	−0.08	−0.07	−0.02	+4.51
					rms dev = ±0.07				
$VOSO_4$ in 3 N HCl	Exptl	16.37 ± 0.12	12.88 ± 0.12	11.48 ± 0.10	11.87 ± 0.12	13.92 ± 0.17	17.63 ± 0.13	23.14 ± 0.25	29.81 ± 0.24
$\alpha = 12.67$ G, $\beta = 2.125$ G,	Calcd	16.35	12.93	11.45	11.82	13.94	17.72	23.05	29.84
$\gamma = 0.851$ G, $\delta = 0.0162$ G	Δ	+0.02	−0.05	+0.03	+0.05	−0.02	−0.09	+0.09	−0.03
					rms dev = ±0.05				
Hydroxyisobutyrate in 8.86%									
ETOH–H_2O	Exptl	22.83 ± 0.72	16.77 ± 0.11	13.47 ± 0.07	12.47 ± 0.06	14.22 ± 0.07	18.39 ± 0.15	25.00 ± 0.33	33.39 ± 0.43
$\alpha = 13.12$ G, $\beta = 1.728$ G,	Calcd	22.86	16.75	13.35	12.57	14.29	18.42	24.84	33.46
$\gamma = 1.229$ G, $\delta = 0.0175$ G	Δ	−0.03	+0.02	+0.12	−0.10	−0.07	−0.03	+0.16	−0.07
					rms dev = ±0.09				

[a] ΔH_{calcd} is computed from eq 7 with α, β, γ, and δ determined from the least-squares method. [b] Experimental line widths measured by the method of relative heights. [c] Experimental line widths measured directly. [d] Experimental line widths uncorrected for overlap of lines. [e] Experimental line widths corrected for overlap of lines. [f] This line was omitted from the least-squares calculation.

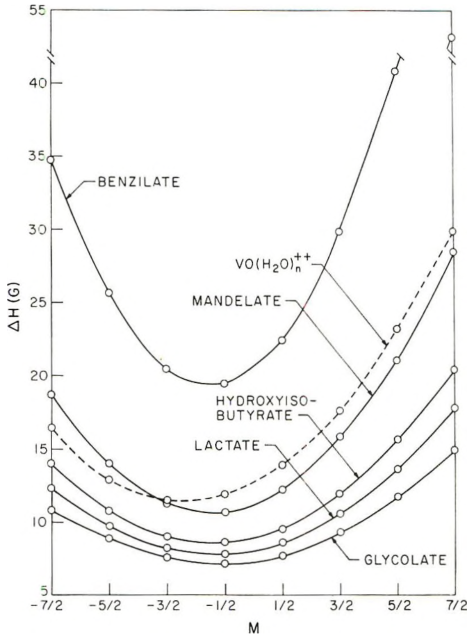

Figure 4. Dependence of the epr line widths on M for the various complexes.

countered with the benzilate was very difficult to measure precisely and is responsible for the poor fit to eq 7. Omission of this line from the least-squares fit to the line widths corrected for overlap significantly reduced the rms deviation from ±0.52 to ±0.07 G. Accordingly, the least-squares parameters α, β, γ, and δ obtained from only seven lines were used in all the calculations for the benzilate.

At the concentrations employed in these experiments, we found that oxygen and intermolecular spin-spin exchange had no effect on the line widths in agreement with earlier results.[5] As oxygen tends to oxidize vanadyl ion in alkaline solution, it was excluded from the hydroxycarboxylate solutions, however.

Sulfate ion has been found to broaden the epr lines of vanadyl[5] and manganous[16] ion in aqueous solutions. This effect is likely absent in our solution since at concentrations below 0.01 M $VOSO_4$ in 3 N HCl, no further narrowing of the resonance lines is observed. We estimate from the stability constant[17] of 2.5 M^{-1}, that only about 0.5% of SO_4^{2-} is directly bound to VO^{2+} at the concentration employed here. Furthermore, our results for $VOSO_4$ in 3 N HCl are in accord with those for $VO(ClO_4)_2$ in $HClO_4$.[5,18] It is noteworthy that in a recent crystal structure determination of $VOSO_4 . 5H_2O$, the SO_4^{2-} ion is coordinated to the VO^{2+} ion in an equatorial position.[19]

The line widths presented in Table II generally are the average of ten or more spectral scans on two or more sample preparations. The line widths as a function of M for the various complexes are shown in Figure 4. The $M = -3/2$ line is the sharpest of the $VO(H_2O)_n^{2+}$ complex whereas the $M = -1/2$ line is the sharpest of the hydroxycarboxylates. This is due to differences in the anisotropic epr parameters.

The sensitivity of the line widths of the hydroxycarboxylates to changes in molecular size is readily seen in Figure 5 in which the line widths are plotted against molecular weight. The width of the broadest line, $M = 7/2$, increases the most with increasing molecular weight; the width of the narrowest line, $M = -1/2$, increases the least. For example, the addition of one methyl group to the ligand in going from the glycolate to the lactate increases the width of the $M = 7/2$ line by 2.66 G compared to only 0.67 G for the $M = -1/2$ line. In Figure 6 the least-squares parameters α, β, and γ are plotted against molecular weight. In general the results for the largest complex, the benzilate, are anomalous with respect to the other hydroxycarboxylates. The reason for this is not clear.

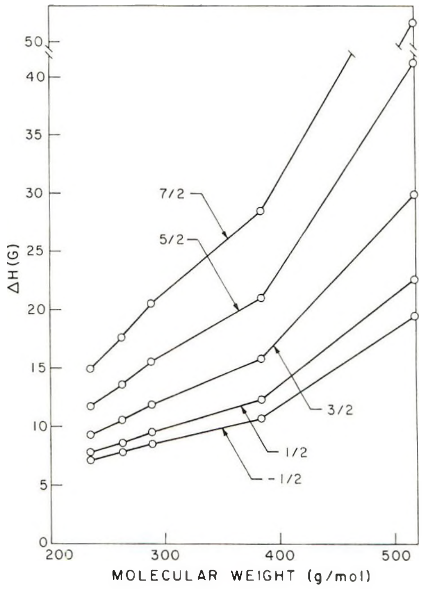

Figure 5. Dependence of the epr line widths on the molecular weights of the hydroxycarboxylates. The widths of only five of the eight lines are shown. One water coordinated in the sixth position was assumed in calculating the molecular weights for all the hydroxycarboxylates except the benzilate.

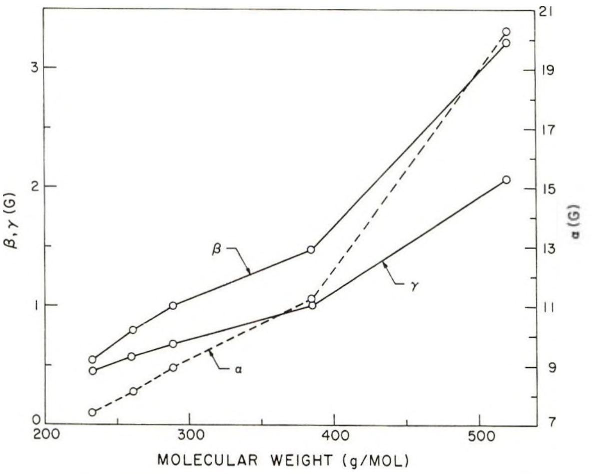

Figure 6. Dependence of the least-squares parameters α, β, and γ on the molecular weight of the hydroxycarboxylates. One water coordinated in the sixth position was assumed in calculating the molecular weights for all the hydroxycarboxylates except the benzilate.

Viscosities. The viscosities, η, of all the hydroxycarboxylates in water were not very different from one another, falling in the range 0.935–0.941 ± 0.005 cP at 24°. The viscosity of the hydroxyisobutyrate in ethanol-water was

---

(16) R. G. Hayes and R. J. Myers, *J. Chem. Phys.*, **40,** 877 (1964).

(17) H. Strehlow and H. Wendt, *Inorg. Chem.*, **2,** 6 (1963).

(18) J. C. Evans, *Inorg. Chem.*, **2,** 372 (1963).

(19) C. D. Balhausen, B. F. Djurinski, and K. J. Watson, *J. Amer. Chem. Soc.*, **90,** 3305 (1968).

found to be 1.83 ± 0.02 cP, compared to an interpolated literature value of 1.87 cP for a pure ethanol-water mixture.[20] We used $\eta = 1.19$ cP[21] for calculations involving 3 N HCl.

Calculations. The line widths of vanadyl complexes largely originate in motional modulation of anisotropic g and nuclear hyperfine tensors. For a Lorentzian line, the total line width parameter, T_2 (sec/rad), is related to the derivative peak-to-peak separation, ΔH, by the equation

$$\Delta H = \frac{2}{\sqrt{3}}\frac{\hbar}{T_2 g_0 \beta_0} \qquad (9)$$

Both spin-lattice relaxation, T_1, and transverse relaxation, T'_2, contribute significantly to the total line width $1/T_2{}^2$. Spin-lattice relaxation primarily arises from a coupling of the electron spin with molecular rotation through modulation of anisotropic g and hyperfine tensors. On the other hand, transverse relaxation arises from rotational modulation of spin energy levels; in effect, the rotational averaging of the anisotropic spectrum encountered in frozen solutions. The effect of molecular motion on line width can be readily seen by comparing Figures 1, 2, and 3.

The constant α' of eq 7 arises from modulation of both anisotropic g and hyperfine tensors, β from a cross correlation between these two, γ from modulation of anisotropic hyperfine tensor alone, and δ from electron-nuclear anisotropic dipolar and g tensor relaxation.[2b,3] α'' is attributed to all other unspecified mechanisms but primarily arises from the interaction of the electron spin magnetic moment with the magnetic moment generated by the rotating molecule (*i.e.*, spin-rotational interactions).[4]

If a single τ_R is assumed, the theory[2b-4] relates the experimental values of α, β, γ, and δ to τ_R and the experimental g and hyperfine parameters. The expressions are reproduced (eq 10-14) in a form more useful for obtaining τ_R than those given in the original papers.[3-5]

$$\alpha' = \frac{2}{\sqrt{3}}\frac{\hbar\tau_R}{g_0\beta_0}\left\{\frac{H_0{}^2}{45}[\Delta\gamma^2(4+3\mu) + \delta\gamma^2(4+9\mu)] + \frac{I(I+1)}{5}\left[\frac{b^2}{8}(3+7\mu-5\mu fa/\omega_0) + \frac{c^2}{3}(6+14\mu) - \Delta\gamma H_0\frac{ba}{\omega_0}(1+\mu)\right]\right\} \qquad (10)$$

$$\alpha = \frac{2\hbar}{9\sqrt{3}\,g_0\beta_0\tau_R}(\Delta g_\parallel{}^2 + 2\Delta g_\perp{}^2)$$

(spin-rotation contributions only)[4] (11)

$$\beta = \frac{2}{\sqrt{3}}\frac{\hbar\tau_R}{g_0\beta_0}\left\{\frac{H_0}{45}[(12+9\mu)b\Delta\gamma - (8+6\mu+6\mu f)\Delta\gamma^2 H_0 a/\omega + (48+36\mu)c\delta\gamma] - \frac{b^2}{40}\frac{a}{\omega}[2I(I+1)(1+\mu+7\mu f) + 2\mu + 3]\right\} \qquad (12)$$

$$\gamma = \frac{2}{\sqrt{3}}\frac{\hbar\tau_R}{g_0\beta_0}\left[\frac{b^2}{8} - (7+5\mu+12\mu f)\frac{\Delta\gamma b H_0 a}{30\omega_0} + (5fa/\omega_0 - 1)\frac{b^2\mu}{40} + \frac{c^2}{15}(10-2\mu)\right] \qquad (13)$$

$$\delta = \frac{\hbar b^2 a\tau_R}{10\sqrt{3}\,g_0\beta_0\omega_0}(1+\mu\omega_0+\mu f) \qquad (14)$$

where $H_0 = \hbar\omega_0/g_0\beta_0$, $\mu = [1 + \omega_0{}^2\tau_R{}^2]^{-1}$, $f = \omega_0{}^2\tau_R{}^2\mu$, $b = \frac{2}{3}[A_z - \frac{1}{2}(A_x + A_y)]$, $c = (A_x - A_y)/4$, $\Delta g = g_z - (g_x + g_y)/2$, $\delta g = (g_x - g_y)/2$, $g_\perp = (g_x + g_y)/2$, $\Delta\gamma = \beta_0\Delta g/h$, $\delta\gamma = \beta_0\delta g/h$, $\Delta g_\parallel = g_\parallel - 2.0023$, and $\Delta g_\perp = g_\perp - 2.0023$. The quantities α', β, γ, and δ are nearly directly proportional to τ_R.

The value of τ_R can be obtained most reliably by varying τ_R in eq 12 and 13 to match calculated with experimental values of β and γ. We find that τ_R values derived from matching β are not the same as those derived from matching γ. The two values of τ_R along with computed averages of α', α'', and δ based on these two values are summarized in Table III.

Comparison of Theory and Experiment. The line widths of the lactate, hydroxyisobutyrate, *dl*-mandelate, and $VOSO_4$ are the most reliable for purposes of comparing theory and experiment (see Line Width Measurements).

For all the complexes, except the benzilate corrected for overlap of lines, τ_R derived from β is less than the value from γ. Similar results have been found for $VO(ClO_4)_2$ in water[5] and N,N-dimethylformamide[6] and vanadyl bis(acetylacetonate) in toluene.[3,22] The difference is considerably less for the acetylacetonate than for the others. Jordan and Angerman have suggested that this discrepancy lies in the experimental error of the line widths and epr parameters which enter into the calculations.[6] Because this phenomenon now has been observed for a rather large number of compounds, we feel that it likely indicates a weakness in the theory, although not a serious one. Moreover, McCain and Myers have determined relative values of T_1 for each of the eight hyperfine lines of $VO(H_2O)_5{}^{2+}$ by means of dynamic nuclear polarization spectroscopy.[5] Their experimental T_1 contributions to α, γ, and δ agree well with the values calculated from the theory[3] for a given τ_R. But the calculated contribution to β is too high; this is consistent with the discrepancy in the epr results (*i.e.*, a lower value of τ_R is required for β than for γ to match experimental and theoretical contributions to these terms). Inclusion of reasonable values for the anisotropy in the x and y directions[23] has a negligible effect on τ_R.

Experimental δ values for all the compounds, except glycolate, is negative as predicted by the theory (Table III). The agreement between δ and δ_{calcd} is quite satisfactory in view of the large experimental uncertainty in δ (nearly 100%) and the incompleteness of the theory for this term.[3]

Likewise, the magnitude of residual line width α'' ($= \alpha - \alpha'_{calcd}$) for the hydroxycarboxylates is well accounted for by a spin-rotation interaction through eq 11. However, α'' for $VOSO_4$ is about a factor of 3 larger than predicted by eq 11. Furthermore, McCain and Myers find almost no temperature dependence in α'' for $VOSO_4$ in aqueous solution, which indicates little spin-rotation interaction.[5] Our value for α'' is in good agreement with theirs, 2.85 *vs.* 2.80 G.

The source of the residual line width in $VO(H_2O)_5{}^{2+}$ thus remains open to question. We expect electron-nuclear dipolar broadening involving the ten water protons in the first coordination sphere to be of the order $\tau_R(10\mu_H/d^3)^2$ where μ_H is the proton magnetic moment and d is the metal-proton distance. For $d = 3.0$ Å, we estimate a broadening of only 0.1 G which is too small to account for

---

[20] "International Critical Tables," Vol. V, McGraw-Hill, New York, N. Y., 1929, p 22.

[21] Reference 20, p 12.

[22] R. Wilson and D. Kivelson, *J. Chem. Phys.*, **44**, 4440 (1966).

[23] M. A. Hitchman, B. W. Moores, and R. L. Belford, *Inorg. Chem.*, **8**, 1817 (1969).

TABLE III: Experimental and Calculated[a] Line Width Parameters

Complex	τ_R, $\times 10^{11}$ sec rads^{-1}[b]	r, Å[c]	α'_{calcd}, G[d]	α''_{calcd}, G[e]	α''_{exptl}, G[f]	δ_{calcd}, $\times 10^{-3}$ G[g]	δ_{exptl}, $\times 10^{-3}$ G[h]
Glycolate in H_2O	1.07, 2.44	2.59	6.59 ± 1.58	1.74 ± 0.68	0.79 ± 1.63	−5.7 ± 1.7	3.6 ± 4.0
Lactate in H_2O	2.54, 3.64	3.17	7.14 ± 0.60	0.72 ± 0.13	0.96 ± 0.63	−7.0 ± 0.7	−1.0 ± 2.3
Hydroxyisobutyrate in H_2O	3.05, 4.20	3.35	8.01 ± 0.66	0.88 ± 0.14	0.90 ± 0.70	−7.8 ± 0.8	−6.5 ± 3.0
dl-Mandelate in H_2O	5.14, 6.29	3.90	10.40 ± 0.75	0.54 ± 0.05	0.83 ± 0.78	−10.6 ± 0.8	−7.1 ± 25
Benzilate in H_2O	12.7, 12.8	5.11	20.80 ± 1.17	0.17 ± 0.01	−0.29 ± 1.21	−20.7 ± 1.0	−33.3 ± 19.7
$VOSO_4$ in 3 *N* HCl	4.37, 4.96	3.39	9.86 ± 0.40	0.95 ± 0.06	2.80 ± 0.44	−12.5 ± 0.8	−16.2 ± 3.1
Hydroxyisobutyrate in 8.86 mol % ethanol–water	6.40, 7.50	3.33	12.28 ± 0.78	0.45 ± 0.04	0.83 ± 0.85	−12.6 ± 0.8	−17.5 ± 5.1

[a] Average of two values calculated from the two values for τ_R. [b] Obtained from eq 12 and 13, respectively. Errors are nominally ±15 and ±5% of the two values of τ_R, respectively. [c] Equation 15. [d] Equation 10. [e] Equation 11. [f] $\alpha''_{exptl} = \alpha - \alpha'_{calcd}$. [g] Equation 14. [h] Table II.

the observed 2.80 G residual line width. Recently Reuben and Fiat determined the isotropic proton hyperfine coupline constant of aquated vanadyl ion from deuterium nmr chemical shift measurements.[24] Their value of 1.1 G is more than enough to account for the residual epr line width. If the origin of the residual line width is due to an isotropic electron–proton coupling, this would explain the near lack of temperature dependence observed by McCain and Myers.[5] Lewis and Morgan have made a similar argument to explain the residual line width by considering the 2.6-G proton hyperfine splitting of $VO(H_2O)_5^{2+}$ units in vanadyl-doped zinc Tutton salt.[25]

Another interesting feature of these spectra is the rather large line widths of $VOSO_4$ relative to the hydroxycarboxylates (Figure 4). One possible explanation is a larger molecular size than is suggested by the formula $VO(H_2O)_5^{2+}$. Assuming that the average τ_R is a measure of molecular weight, through Figure 7 we estimated the molecular weight of $VOSO_4$ in 3 *N* HCl to be 292. This corresponds to the formula $VO(H_2O)_{12.5}^{2+}$, which suggests seven to eight water molecules in the outer coordination sphere, a reasonable result. Following the same procedure for $VO(ClO_4)_2$ in the coordinating solvents dimethylformamide (DMF),[6] methanol,[7] and water,[5] and for vanadyl bis(acetylacetonate) in the noncoordinating solvent toluene,[3] we obtain the formulas $VO(DMF)_{10}^{2+}$, $VO(CH_3OH)_{13}^{2+}$, $VO(H_2O)_{11}^{2+}$, and $VO(acac)_2$. These formulas are reasonable in view of the uncertainty in our procedure and perhaps indicate the sensitivity of line widths to the presence of second coordination sphere molecules. The formula $VO(DMF)_{10}^{2+}$ was obtained by extrapolating the dashed curve in Figure 7 to a molecular weight of ~800 g/mol.

For a sphere of radius r, rotating in a fluid medium of viscosity η, τ_R is given by the Debye relationship[26]

$$\tau_R = 4\pi r^3\eta/3kT \qquad (15)$$

To test if molecular motion in our solutions is governed by the macroscopic viscosity according to eq 15, we measured τ_R for the hydroxyisobutyrate in ~9 mol % ethanol–water mixture. Ethanol–water has several anomalous properties at this composition[27,28] and it was hoped that any effects due to a microviscosity would show up in τ_R. In fact, τ_R obeyed the Debye relationship reasonably well, with a measured τ_R of 6.9×10^{-11} compared to 7.2×10^{-11} sec/rad predicted from the relative macroscopic viscosities of pure water and the ethanol–water mixture. A rough check of the line widths in a 50 mol % mixture indicated that τ_R was following the viscosity–composition curve.

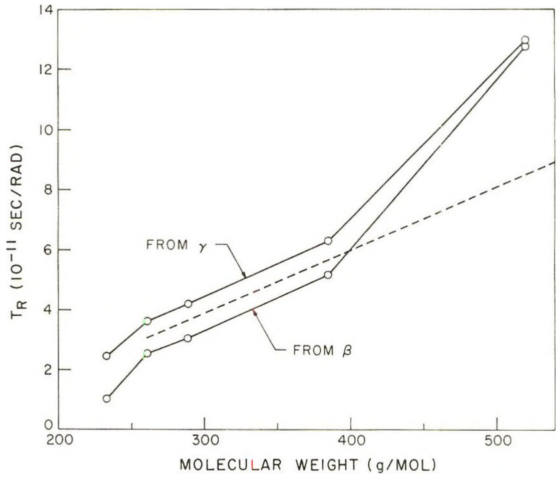

Figure 7. Dependence of the rotation correlation time τ, derived from the β and γ terms, on the molecular weight of the hydroxycarboxylates. One water coordinated in the sixth position was assumed in calculating the molecular weights of all the hydroxycarboxylates except the benzilate. The dashed curve was used for the determination of the molecular formulas of the other complexes in different solvents (see text).

The hydrodynamic radius r from eq 15 increases with molecular weight of the hydroxycarboxylates (Table III). The value of r which is a measure of the effective molecular size in solution can be compared with the crystal radius, R, calculated from a hexagonal closest packed or cubic closest packed model, *viz.*

$$\frac{4}{3}\pi R^3 = \frac{0.74\,W}{N\rho} \qquad (16)$$

where W is the molecular weight, N is Avogadro's number, and ρ is the density of the crystal. The factor 0.74 accounts for the 26% void volume. If we choose a common value of ρ for all the hydroxycarboxylates of 1.24 g/cc from the X-ray structure determination of the benzilate,[10] the values of R and r respectively are as follows: benzilate

---

(24) J. Reuben and D. Fiat, *Inorg. Chem.*, **8**, 1821 (1969).

(25) W. B. Lewis and L. O. Morgan, "Transition Metal Chemistry," Vol. 4, R. L. Carlin, Ed., Marcel Dekker, New York, N. Y., 1968, p 33.

(26) N. Bloembergen, E. M. Purcell, and R. V. Pound, *Phys. Rev.*, **73**, 679 (1948).

(27) R. L. Kay, G. P. Cunningham, and D. Fennell, "Hydrogen Bonded Solvent Systems," A. K. Covington and P. Jones, Ed., Taylor and Francis, London, 1968, p 255.

(28) F. Franks, "Physico-Chemical Processes in Mixed Aqueous Solvents," American Elsevier, New York, N. Y., 1962, p 51.

(5.0, 5.1 Å), mandelate (4.5, 3.9 Å), hydroxyisobutyrate (4.1, 3.4 Å), lactate (4.0, 3.2 Å), and glycolate (3.8, 2.6 Å). A similar calculation for vanadyl bis(acetylacetonate) with ρ = 1.49 g/cc from the reported crystal structure[29] yields R = 3.7 Å compared to r = 3.3 Å for toluene solutions. Except for the benzilate, in general, the closest packing crystal radii are larger than hydrodynamic radii. We discover an exception to this "general rule" with vanadyl sulfate, $VOSO_4 \cdot 5H_2O$, with R = 2.9 Å compared to r = 3.4 Å (R was calculated with ρ = 2.00 g/cc from the crystal structure[19] and W corresponding to $VO(H_2O)_5^{2+}$). Such a large value of r relative to R is a further indication that the vanadyl species in aqueous solution is larger than $VO(H_2O)_5^{2+}$ as discussed earlier. For vanadyl bis(acetylactonate) in seven different solvents Wilson and Kivelson have found variations in r from 3.01 to 3.56 Å which can be explained in terms of differences in solvent coordinating ability.[22]

Conclusion

Due to the similarities in g and hyperfine anisotropies for all the hydroxycarboxylate chelates, we expected variations in their line widths to primarily reflect differences in the viscosity of the medium and molecular size. Indeed, τ_R, which is a measure of molecular tumbling rates in solution, correlates quite well with the molecular weights. In general, the theory satisfactorily explains the principal features of the spectra although the same τ_R is still not obtained from different parameters. The rotational correlation time and residual line width for vanadyl sulfate in aqueous solution appear to be anomalous with respect to the hydroxycarboxylates, perhaps because of strong metal ion-solvent interactions in the former.

(29) R. P. Dodge, D. H. Templeton, and A. Zalkin, *J. Chem. Phys.*, **35**, 55 (1961).

An Electron Spin Resonance Study of the Geometry of 9-Phenylacridine

Ann Lomax, L. S. Marcoux, and A. J. Bard*

Department of Chemistry, University of Texas at Austin, Austin, Texas 78712 *(Received July 7, 1972)*

Publication costs assisted by the Robert A. Welch Foundation and the National Science Foundation

The electron spin resonance spectrum of the radical anion of 9-phenylacridine (9PAC) was obtained and the coupling constants were assigned. Correlation of the coupling constants with Hückel molecular orbital calculations indicated that the phenyl ring was twisted approximately 65° out of the plane of the acridine nucleus. The effect of the value of the Coulomb integral on the twist angle determination is discussed.

In a previous paper[1] we discussed the relative importance of resonance energy and steric interactions in determining the molecular geometry of a group of highly hindered molecules (the aryl-substituted polynuclear aromatic hydrocarbons) and concluded that the overriding influence was steric. The steric strain was assumed to be relieved by twisting of the aryl substituent out of the plane of the other ring system, the degree of twisting being related to the type and number of steric interactions present in the molecule. Molecules with steric repulsions like those in 9-phenylanthracene have been found to exhibit a twist angle lying between 60 and 72°;[2-8] to test further the direct relation of twist angle to steric strain, we have investigated the geometry of 9PAC, the N-heterocyclic analog of 9-phenylanthracene. The instability of the cation radical precluded its study; however, we have prepared the anion radical and have determined its twist angle to be approximately 65°.

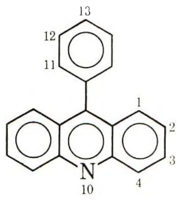

Experimental Section

The 9PAC was prepared according to Albert.[9] Hexamethylphosphoramide (HMPA) was triply distilled under vacuum from a solution of 9PAC and sodium; N,N-dimethylformamide (DMF) was dried over Linde 4A molecular sieves and vacuum distilled under nitrogen from a suspension of anhydrous copper sulfate; 1,2-dimethoxyethane (DME) was dried and distilled over lithium alumi-

(1) L. S. Marcoux, A. Lomax, and A. J. Bard, *J. Amer. Chem. Soc.*, **92**, 243 (1970).
(2) B. Tinland, *Theor. Chim. Acta*, **11**, 385 (1968).
(3) L. O. Wheeler, K. S. V. Santhanam, and A. J. Bard, *J. Phys. Chem.*, **71**, 2223 (1967).
(4) L. O. Wheeler, K. S. V. Santhanam, and A. J. Bard, *J. Phys. Chem.*, **70**, 404 (1966).
(5) L. O. Wheeler, Ph.D. Dissertation, The University of Texas, 1967.
(6) M. D. Sevilla and G. Vincow, *J. Phys. Chem.*, **72**, 3641 (1968).
(7) K. Maruyama, M. Yoshida, and K. Murakami, *Bull. Chem. Soc. Jap.*, **43**, 152 (1970).
(8) L. Lunazzi, A. Mangini, G. Placucci, C. Vincenzi, and I. Degani, *Mol. Phys.*, **19**, 543 (1970).
(9) A. Albert, "The Acridines," 2nd ed, St. Martin's Press, New York, N. Y., 1966, p 100.

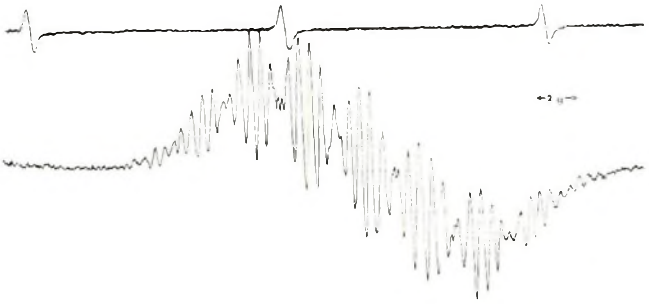

Figure 1. Poorly resolved esr spectrum of the 9PAC anion radical.

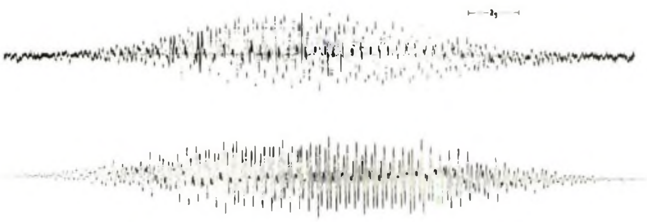

Figure 2. Esr spectrum (top) of the 9PAC anion radical and its computer simulation using the coupling constants of Table I, a 0.06-G line width, and a completely Lorentzian line shape.

TABLE I: Coupling Constants for the 9PAC Anion Radical

Position	Type	No. of nuclei	a, G
1	H	2	2.936
2	H	2	1.094
3	H	2	1.964
4	H	2	1.822
11	H	2	0.385
13	H	1	0.526
10	N	1	3.665

num hydride and stored under vacuum over pieces of sodium. Tetra-*n*-butylammonium perchlorate (TBAP) was obtained from Southwestern Analytical Chemical Co. (Austin, Tex.) and dried in a vacuum oven before use. The esr spectrometer used was a Varian V-4502 with standard accessories; both the spectrometer and the spectral simulation program have been previously described.[3,4]

Results and Discussion

The radical anion of 9PAC was prepared by alkali metal reduction of the parent in DME and by electrochemical reduction in DMF; in both cases the poorly resolved spectrum shown in Figure 1 was obtained. Alkali metal reduction in HMPA, however, yielded a highly resolved spectrum; this spectrum and its computer simulation, using the coupling constants in Table I, a 0.060-G line width, and a completely Lorentzian line shape, are shown in Figure 2. Though the noise level obscures the outer lines, the sensitivity of the central portion of the spectrum to small changes in the coupling constants allows a high degree of confidence in positing that the coupling constants of Table I are those giving rise to the experimental spectrum.

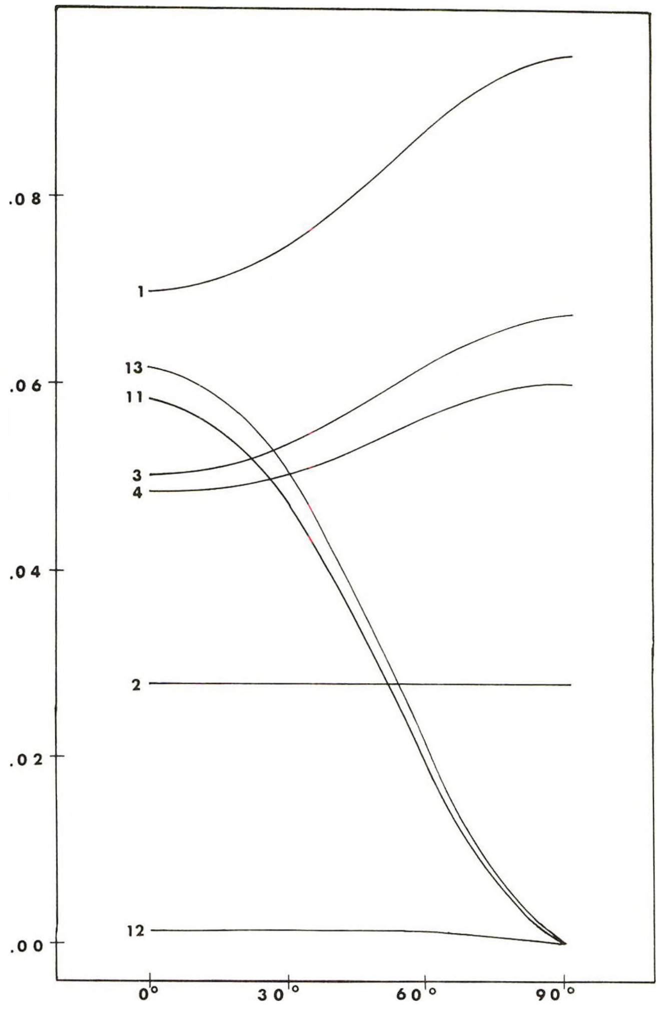

Figure 3. Ued's of the 9PAC anion radical as a function of the twist angle θ. The ued's were calculated using h_N = 0.7, k_{CN} = 1.0; similar curves were obtained using other values of h_N.

The assignment of the coupling constants to positions in the molecule was based on Hückel calculations. Assignment on this basis was straightforward with the exception of positions 3 and 4; for these positions the relative magnitude of the calculated spin densities was a function of the value chosen for the Coulomb integral of the nitrogen atom. Szwarc, *et al.*,[10] used nmr line broadening results to assign these positions in the acridine anion radical; we have assumed that the ordering would be unchanged by the presence of the phenyl substitutent and have followed their assignment.

A certain ambiguity also exists in the assignment of the splittings on the phenyl ring. The simulation in Figure 2 is based on a 0.526-G splitting from the single para proton and a 0.385-G splitting from the two equivalent ortho protons. A simulation based on a 0.526-G splitting from three equivalent protons (ortho and para) and a 0.385-G splitting from two equivalent protons (meta) is indistinguishable at the intensity of the experimental spectrum from that shown in Figure 2. On the basis of the Hückel calculations we decided that the meta proton splittings would be too small to be detected and thus made the assignment given in Table I.

The method and assumptions involved in determining the twist angle, θ, have been previously discussed.[1] The unpaired electron density (ued) at each atom was calculated using Hückel molecular orbital theory and is shown as a function of twist angle, θ, in Figure 3. To ensure that the value of θ_{9PAC} determined does in fact reflect the molecular geometry and not simply a particular HMO con-

---

[10] J. Chaudhuri, S. Kume, J. Jagur-Grodzinski, and M. Szwarc, *J. Amer. Chem. Soc.*, **90**, 6421 (1968).

TABLE II: Twist Angles Determined from the Ratios of the Ued's[a]

	1/11	2/11	3/11	4/11	Av
Case 1	67	70	65	68	67
Case 2	66	68	65	66	66
Case 3	66	66	65[b]	64[b]	65

[a] All values are in degrees. [b] These values were obtained by inverting the assignment of the two positions.

struct, we used three sets of values for the parameters and determined θ_{9PAC} for each set. From among the values cited in calculations on heteromolecules,[11] we chose three sets which would span the commonly used range of values: case 1,[12] $h_N = 0.84$, $k_{CN} = 1.0$; case 2,[13,14] $h_N = 0.7$, $k_{CN} = 1.0$; case 3,[10,15] $h_N = 0.5$, $k_{CN} = 1.0$.

The effect of the value of h_N on the twist angle is small; the average θ_{9PAC} value varies by only 2^c (Table II). With $h_N = 0.5$ the order of the ued's at positions 3 and 4 is inverted; however, if we also invert the assignment of the coupling constants at these positions, the value of θ_{9PAC} is in good agreement with that derived from the other sets of parameters. A similar inversion was noted by Pedersen and Muus[14] for the quinoxaline anion radical upon changing the value of h_N from 0.7 to 0.4.

Acknowledgment. The support of the National Science Foundation (Grant No. GP-31414X) and the Robert A. Welch Foundation is gratefully acknowledged. The esr spectrometer was purchased with funds provided by the National Science Foundation (Grant No. GP-2090).

(11) For example, C. L. Talcott and R. J. Myers, *Mol. Phys.*, **12**, 549 (1967); A. R. Buick, T. J. Kemp, G. T. Neal, and T. J. Stone, *J. Chem. Soc. A*, 1609 (1967); A. Carrington and J. dos Santos-Viega, *Mol. Phys.*, **5**, 21 (1962); D. R. Geske and G. R. Padmanabhan, *J. Amer. Chem. Soc.*, **87**, 1651 (1965).

(12) B. J. Tabner and J. R. Yandle, *J. Chem. Soc. A*, 381 (1968).

(13) J. C. M. Henning, *J. Chem. Phys.*, **44**, 2139 (1966).

(14) J. A. Pedersen and L. T. Muus, *Mol. Phys.*, **16**, 589 (1969).

(15) R. Zahradnik and J. Koutecky, *Advan. Heterocycl. Chem.*, **5**, 72 (1965).

Electronic and Electron Spin Resonance Spectra of the Anion Radicals of Phenyl- and Diphenylethylenes

A. Gamba, V. Malatesta, G. Morosi, and M. Simonetta*

C.N.R. Center for the Study of the Relationship between Structure and Chemical Reactivity and The Institute of Physical Chemistry, University of Milan, 20133 Milan, Italy

(Recieved June 27, 1972)

Publication costs assisted by the Physical Chemistry Institute of the University of Milan

A number of previously unknown esr and uv spectra have been observed for aryl- and diarylethylene anion radicals generated by IG (internal generation) and EG (external generation) electrolytical reductions in dimethyl sulfoxide and acetonitrile, respectively. Semiempirical self-consistent field calculations combined with limited configuration interaction (LCI–SCF), according to Longuet-Higgins and Pople and Roothaan methods, allow a satisfactory interpretation of the electronic spectra of the anion radicals. Also uv spectra of parent neutral molecules have been taken into consideration and discussed. Spin densities, obtained by the aforementioned and McLachlan's methods, have been translated into coupling constants through McConnell's relationship and compared with experimental data. These three methods allow an unequivocal assignment of proton hyperfine splitting (hfs) constants for all considered anion radicals.

Introduction

While the esr spectra of ion radicals have been the subject of extensive experimental and theoretical investigations[1] only scanty information about the ultraviolet spectra of the same compounds has been collected. Recent literature references in the field can be found in papers by Zahradnik and Cársky[2] and by Shida and Iwata.[3] In the present work we present the uv and esr spectra of a series of anion radicals as well as the uv spectra of the parent neutral molecules. An attempt is made to interpret all the experimental data by means of a single MO calculation. The latter has been performed according to different methods in order to confront the merits of the different semiempirical MO theories in predicting both energy and electron distribution in radical anions. The skeleton of *p*-nitrophenylethylene was present in all compounds under examination. The formulas together with twist angles are shown in Figure 1, where the twist angles are taken counterclockwise looking from the ethylenic carbon.

(1) See, for example, (a) E. T. Kaiser and L. Kevan, Ed., "Radical Ions," Interscience, New York, N. Y., 1968; (b) F. Gerson, "High Resolution E.S.R. Spectroscopy," Wiley, New York, N. Y., 1970.

(2) R. Zahradnik and P. Cársky, *J. Phys. Chem.*, **74**, (a) 1235, (b) 1240, (c) 1249 (1970).

(3) T. Shida and S. Iwata, *J. Phys. Chem.*, **75**, 2591 (1971).

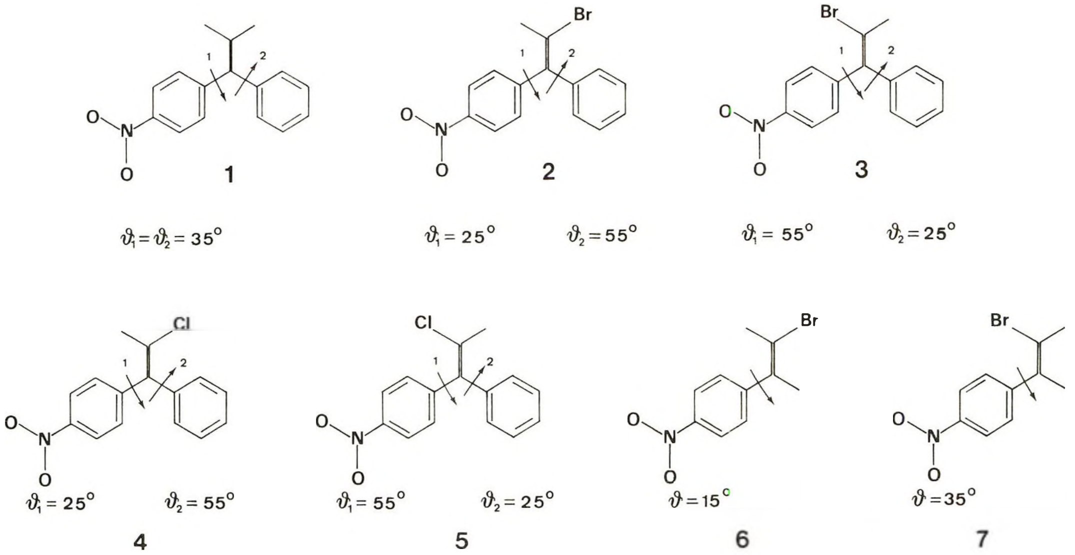
1
$\vartheta_1 = \vartheta_2 = 35°$
2
$\vartheta_1 = 25°$ $\vartheta_2 = 55°$
3
$\vartheta_1 = 55°$ $\vartheta_2 = 25°$
4
$\vartheta_1 = 25°$ $\vartheta_2 = 55°$
5
$\vartheta_1 = 55°$ $\vartheta_2 = 25°$
6
$\vartheta = 15°$
7
$\vartheta = 35°$
Br
Cl
O
N

Figure 1. Numbering of molecules.

Experimental Section

Materials. 1-*p*-nitrophenyl-1-phenylethylene, *trans*- and *cis*-2-bromo-1-*p*-nitrophenyl-1-phenylethylenes, *trans*- and *cis*-2-chloro-1-*p*-nitrophenyl-1-phenylethylenes, and *trans*- and *cis*-β-bromo-*p*-nitrostyrenes have been kindly supplied by P. L. Beltrame. For the synthesis of the compounds see ref 4 and 5. The high degree of purity did not require further purification. Acetonitrile (ACN) was Merck UVASOL 16/66. It was further purified following the method given in ref 6. Dimethyl sulfoxide (DMS) was Carlo Erba RS, further purified following the method given in ref 7–9. Isooctane (ISO) was a Rudipont product for spectrophotometry. Tetraethylammonium perchlorate (TEAP) was a Carlo Erba product for polarography.

Preparation of Anion Radicals and Measurements. Anion radicals of the considered molecules have been electrolytically generated. Two techniques have been used. The IG (internal generation)[6,10] technique places the mercury pool cathode within the microwave cavity. This technique has the advantage of simplicity and is particularly suitable for short lifetime radicals. The EG (external generation) technique[11-13] places the cell outside the microwave cavity. The arrangement necessitates transfer of the solution prior the esr observation, but allows rapid quantitative reduction of material because it permits the use of large electrode area. Complete reduction is desirable because many of the radicals undergo rapid electron exchange reaction with their precursor, with line broadening in the spectrum. Moreover, the last technique presents the advantage of measuring in parallel esr and uv spectra of radicals, which gives more confidence in the assignment of the observed electronic spectra to the respective anion radicals.

Dimethyl sulfoxide and acetonitrile have been used as solvents in EG and IG techniques, respectively. In both processes electrolytic reductions have been made in vacuum cells[14] at controlled potentials by using a multipurposes AMEL Model 436 polarograph. Reduction potentials for each compound have been evaluated from polarographic curves recorded at room temperature. A saturated calomel electrode (sce) was the external reference. About 0.1 *M* solution of tetra-*n*-ethylammonium perchlorate (TEAP) was used as supporting electrolyte, and the solution was *ca.* 10^{-3} *M*. Dissolved oxygen was removed by bubbling purified nitrogen gas through the sample solution. Polarographic data measured in DMS and ACN are collected in Table I.

TABLE I: Polarographic Data[a]

	Solvent			
	DMS		ACN	
Anion radical	$-E_{1/2}$ vs. sce	$E_{1/4}-E_{1/2}$	$-E_{1/2}$ vs. sce	$E_{1/4}-E_{1/2}$
1	1.00	0.058	1.13	0.060
2	0.96	0.058	1.13	0.063
3	0.97	0.066	1.06	0.062
4	1.28	0.062	1.05	0.065
5	1.05	0.070	1.12	0.060
6	0.95	0.061	1.07	0.058
7	0.96	0.061	1.07	0.065

[a] It appears from Tomes' relation, $E_{1/4}-E_{1/2}$ = 0.056/*n* (*n* is the electrons number), that the first wave is reversible and monoelectronic (J. Tomes, *Collect. Czech. Chem. Commun.*, **9**, 12, 81, 150 (1937)).

Electron spin resonance spectra were obtained with a Varian 4500-10 A X-band spectrometer with a 100-kHz magnetic field modulation. Electronic absorption spectra were taken with a Beckman DK-2A spectrophotometer.

Esr Experimental Data. 1-p-Nitrophenyl-1-phenylethylene. The electrolytic reduction at proper potential for the first reversible polarographic wave produces a blue-green

---

(4) P. Beltrame and P. L. Beltrame, *Gazz. Chim. Ital.*, **98**, 367 (1968).

(5) P. Beltrame, P. L. Beltrame, and L. Bellotti, *J. Chem. Soc. B*, 932 (1969).

(6) D. H. Geske and A. H. Maki, *J. Amer. Chem. Soc.*, **82**, 2671 (1960); **83**, 1852 (1961).

(7) E. R. Talaty and G. A. Russel, *J. Amer. Chem. Soc.*, **87**, 4867 (1965).

(8) S. F. Nelson, B. M. Trost, and D. H. Evans, *J. Amer. Chem. Soc.*, **89**, 3034 (1967).

(9) I. Bernal and G. K. Fraenkel, *J. Amer. Chem. Soc.*, **86**, 1671 (1964).

(10) A. H. Maki and D. H. Geske, *J. Chem. Phys.*, **30**, 1356 (1959); **33**, 825 (1960).

(11) P. H. Rieger, I. Bernal, W. H. Reinmuth, and G. K. Fraenkel, *J. Amer. Chem. Soc.*, **85**, 683 (1963).

(12) C. S. Johnson, Jr., and R. Chang, *J. Chem. Phys.*, **43**, 3183 (1965).

(13) J. R. Bolton and G. K. Fraenkel, *J. Chem. Phys.*, **40**, 3307 (1964).

(14) (a) C. Oliva, Thesis, University of Milano, 1969; (b) R. Mariano, Thesis, University of Milano, 1970.

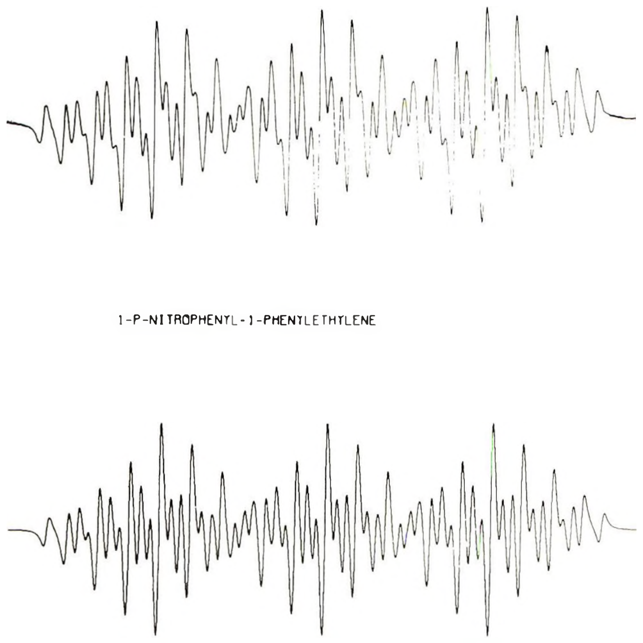

Figure 2. (a) Esr spectrum in ACN of 1-*p*-nitrophenyl-1-phenylethylene. (b) Simulated spectrum.[15]

TABLE II: Spin Densities for 1-*p*-Nitrophenyl-1-phenylethylene

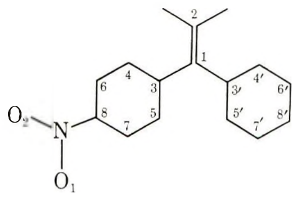

	ρ_i[a]		
	A	B	C
1	0.00221	−0.00509	−0.02126
2	0.09348	0.13169	0.10093
3	0.17580	0.17356	0.15515
4	−0.02111	−0.01409	−0.03740
5	−0.02109	−0.01453	−0.03740
6	0.14528	0.14188	0.12316
7	0.13599	0.13342	0.12316
8	0.09638	0.10878	0.01767
N	0.22173	0.17648	0.21151
O_1	0.08613	0.08455	0.18302
O_2	0.08598	0.08431	0.18302
3′	0.00727	0.00832	0.00113
4′	−0.00236	−0.00303	−0.00080
5′	−0.00181	−0.00215	−0.00080
6′	0.00164	0.00150	−0.00046
7′	0.00138	0.00117	−0.00046
8′	−0.00691	−0.00679	−0.00013

[a] A represents spin densities calculated according LCI-SCF (Roothaan method,[17b] B spin densities calculated according LCI-SCF (Longuet-Higgins and Pople) method,[17a] and C spin densities calculated according McLachlan method.[18]

solution in ACN and a grey-green solution in DMS, respectively. Well-resolved esr spectra of 53 lines in ACN and 64 lines in DMS have been recorded and interpreted on the basis of four triplets. On the basis of the spin densities obtained by MO calculations (see Table II), the four triplets were assigned to the nitrogen and three groups of two protons of equal coupling constants in ortho and meta positions to the nitro group and in the 2 position.

TABLE III: Calculated and Experimental Proton Hyperfine Splittings

		Theoretical[a]			Experimental[c]	
Anion radical	H position[b]	A	B	C	DMS	ACN
1	H_{ortho}	3.100	2.922	3.135	3.200	3.220
	H_{meta}	−0.837	−0.637	−1.008	−1.150	−1.058
	H_β	2.740	2.758	2.009	1.800	1.618
2	H_{ortho}	3.184	3.163	3.091	3.180	
	H_{meta}	−0.990	−0.816	−0.979	−1.070	
	H_β	1.890	1.814	2.196	2.124	
3	H_{ortho}	3.371	3.438	3.443	3.320	3.15
	H_{meta}	−1.131	−0.621	−1.202	−1.000	−1.10
	H_β	0.532	0.484	0.533	1.020	0.95
4	H_{ortho}	3.166	3.109	3.092	3.051	3.23
	H_{meta}	−0.918	−0.749	−0.979	−1.074	−1.05
	H_β	2.069	2.053	2.195	2.141	2.16
5	H_{ortho}	3.352	3.404	3.444	3.248	3.220
	H_{meta}	−1.074	−0.555	−1.203	−1.052	−1.073
	H_β	0.616	0.584	0.531	1.089	0.945
6	H_{ortho}	3.089	3.137	3.139	3.220	3.119
	H_{meta}	−1.151	−1.444	−1.017	−1.080	−1.058
	H_α	−0.297	−0.296	−0.544	−1.520	−1.496
	H_β	2.156	1.869	2.061	2.360	2.543
7	H_{ortho}	3.193	3.253	3.091	3.250	3.12
	H_{meta}	−1.219	−1.529	−0.999	−1.030	−1.04
	H_α	−0.217	−0.209	−0.398	0	0
	H_β	1.383	1.869	2.006	2.100	2.20

[a] A represents spin densities calculated according LCI-SCF (Roothaan) method,[17b] B spin densities calculated according LCI-SCF (Longuet-Higgins and Pople) method,[17a] and C spin densities calculated according McLachlan method.[18] [b] Ortho and meta position to the nitro group. [c] Hfs constants were optimized by least-squares fitting.[15]

TABLE IV: Calculated[a] and Experimental Nitrogen Hyperfine Splittings

		Experiment	
Anion radical	Theory[b]	DMS	ACN
1	7.835	8.80	8.77
2	7.671	8.06	
3	8.927	8.75	9.50
4	7.671	7.90	8.96
5	8.928	8.55	8.95
6	7.854	8.06	7.97
7	7.695	7.85	8.13

[a] $a^N = (S^N + Q_{NC}{}^N + 2Q_{NO}{}^N)\,\rho_N{}^\pi + Q_{CN}{}^N\rho_C{}^\pi + 2Q_{ON}{}^N\rho_O{}^\pi (S^N + Q_{NC}{}^N + 2Q_{NO}{}^N) = \pm(99.0 \pm 10.2)$ G; $Q_{NO}{}^N = \mp(35.8 \pm 5.9)$ G, $Q_{CN}{}^N = 0$.[19] [b] Nitrogen spin density evaluated by McLachlan method.[18]

The protons of the unsubstituted ring do not contribute to the hyperfine pattern. The spectra recorded in ACN and simulated with optimized hfs constants[15] are shown in Figure 2. Optimized hfs constants are shown in Tables III and IV.

trans- and cis-2-Bromo-1-p-nitrophenyl-1-phenylethylene. Electrolytical reduction in DMS produces a light-green solution in the case of trans isomer and a dark-green solution in the case of cis isomer. Both spectra are well

---

(15) J. Heinzer, "Least-Squares Fitting of Isotropic Multiline Esr Spectra," Program 197, Quantum Chemistry Program Exchange (QCPE), Indiana University.

TABLE V: Energy and Geometry Parameters Used Throughout the Calculations

Bond distances (Å) and bond angles (degrees)	C–N = 1.47; N–O = 1.22; $-NO_2$ group in the plane of phenyl $C\text{–}C_{phenyl}$ = 1.397; $C{=}C_{ethylene}$ = 1.334; C–C = 1.49 for small twist angles ($\theta < 35$); C–C = 1.51 for large twist angles ($\theta = 65$) C–Cl = 1.72;[a] C–Br = 1.87[b] All bond angles = 120°				
Twist angles (degrees)	$\theta_1 = \theta_2 = 35°$ for molecule **1** (see Figure 1) $\theta = 25°$ for *trans*-phenyl (respect to halogen) for molecul **2–5** $\theta = 65°$ for *cis*-phenyl $\theta = 25°$ for molecule **6**; $\theta = 65°$ for molecule **7**				
Resonance integrals (eV)	$\beta_{C=C(phenyl)} = \beta_{C-N} = \beta_{N-O} = -2.40$;[c] $\beta_{C=C(Ethylene)} = -2.665$ $\beta_{C-Cl} = -1.351$; $\beta_{C-Br} = -1.34$; $\beta_{C-C}(R, \theta) = -2.40\, S_{C-C}(R)/S_{C-C(1.397)} \cos\theta$				
		I_μ	A_μ	$\gamma_{\mu\mu}(I-A)$	δ_μ
Ionization potentials (I_μ), electron affinities (A_μ), monocentric electron repulsion integrals ($\gamma_{\mu\mu}$), and Slater exponents (δ_μ)	C	11.16[d]	0.03[d]	11.13	1.625
	N[i]	28.855[e]	12.26[e]	16.595	3.125
	O[i]	17.860[e]	3.87[e]	13.99	2.275
	Cl	26.380[f]	15.09[f]	11.29	2.150
	Br	21.430[g]		11.925[h]	2.271

[a] L. E. Sutton, *Chem. Soc., Spec. Publ.*, **No. 11** (1958). [b] Reference 21. [c] Reference 28. [d] G. Favini, I. Vandoni, and M. Simonetta, *Thero. Chim. Acta*, 3, 45 (1965). [e] G. Pilcher and H. A. Skinner, *J. Inorg. Nucl. Chem.*, **24**, 937 (1962). [f] G. Favini, S. Carra, and M. Simonetta, *Gazz. Chim. Ital.*, **90**, 247 (1960), and references therein. [g] (Br^{2+}) has been obtained from experimental value of ionization energy of the process $Br^+(s^2p^4, {}^3P) \rightarrow Br^{2+}(s^2p^3, {}^4S)$ −19.2 eV (Landolt-Bornstein, "*Atome und Ionen*," I. Band – I. Tail, p 212 Springer-Verlag, West Berlin, 1950, and from the energy difference between these and valence states Br^+ (s^2x^2yz, V_2) and Br^{2+} ($s^2x^2y^2$, V_1) the energies of which are 0.49 and 2.72 eV, respectively (H. A. Skinner and H. O. Pritchard, *Trans. Faraday Soc.*, **49**, 1254 (1953)). [h] Evaluated according to the relationship $\gamma_{BrBr} = \gamma_{ClCl}(\delta_{Br}/\delta_{Cl})$. [i] For anion radicals the parameters have been corrected according to ref 3.

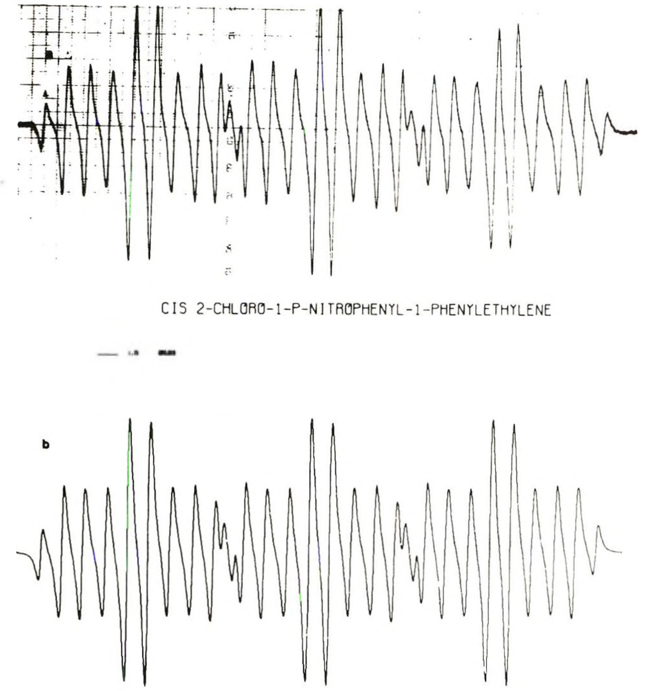

Figure 3. (a) Esr spectrum in ACN of *cis*-2-chloro-1-*p*-nitrophenyl-1-phenylethylene. (b) Simulated spectrum.

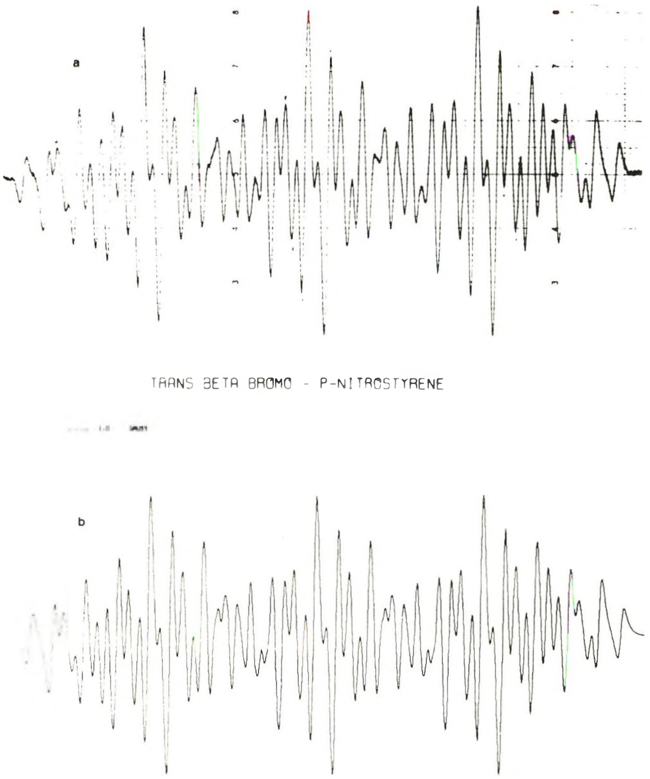

Figure 4. (a) Esr spectrum of *trans*-β-bromo-*p*-nitrostyrene in ACN. (b) Simulated spectrum.

resolved and have been interpreted on the basis of three triplets due to nitrogen and protons in ortho and meta positions to the nitro group, and a doublet due to the proton in 2 position. Optimized hfs constants are shown in Tables III and IV. The radicals are moderately stable and after about 0.5 hr significant changes appear in the spectrum. When ACN is used as the solvent the spectrum changes rapidly with different rates for trans and cis isomers. The radical for the cis isomer is stable enough to record the esr spectrum, which has been completely resolved and interpreted. The optimized hfs constants are reported in Tables III and IV. In the case of the trans isomer the spectrum is rapidly evolving to a final spectrum which is identical with that of 1-*p*-nitrophenyl-1-phenylethylene. The same spectrum can be recorded for the cis isomer 1 hr after the start of electrolysis. This spectral evidence suggests bromine exchange with solvent protons.[16] To substantiate

[16] Particular care has been devoted to avoid the presence of traces of water in the vacuum electrolytic cell.

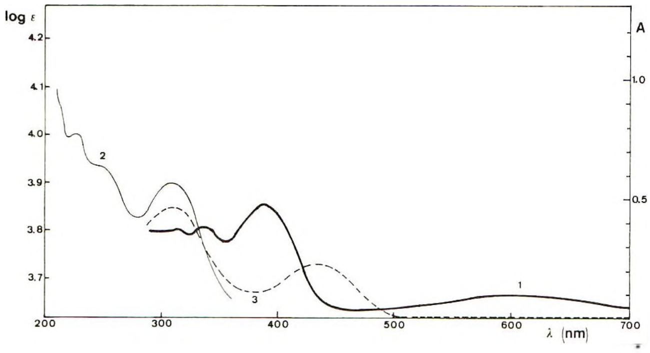

Figure 5. Uv spectra of 1-*p*-nitrophenyl-1-phenylethylene: (1) radical anion (scale on the right, absorbance *vs.* wavelength); (2) neutral molecule (scale on the left, log ε *vs.* wavelength); (3) radical after air exposure.

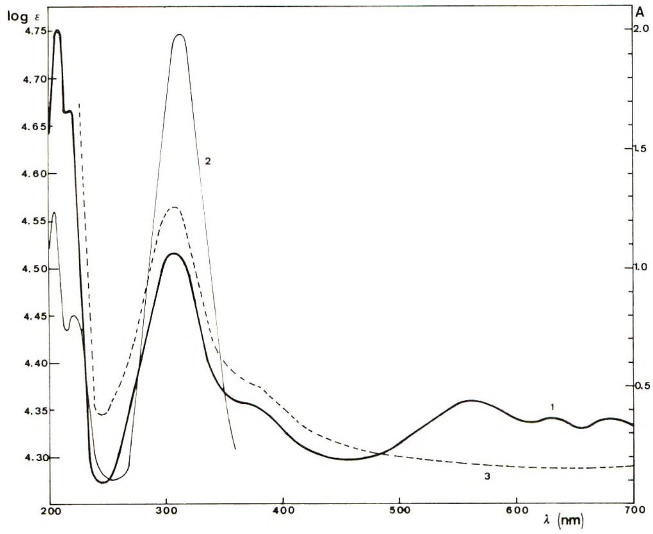

Figure 6. Uv spectra of *cis*-β-bromo-*p*-nitrostyrene: (1) radical anion (scale on the right, absorbance *vs.* wavelength); (2) neutral molecule (scale on the left, log ε *vs.* wavelength); (3) radical after air exposure.

this reaction mechanism and to verify if bromine–proton exchange occurs with configuration retention, experiments with CD_3CN solvent are in progress.

trans- and cis-2-Chloro-1-p-nitrophenyl-1-phenylethylene. In both solvents radical anions undergo a fast decay. However, well-resolved spectra have been recorded and the hfs constants fitting experimental data are shown in Tables III and IV. The magnetic nuclei that contribute to hyperfine patterns are the same as for bromo-substituted compounds. The spectra of cis isomer recorded in ACN and simulated with optimized hfs constants are shown in Figure 3.

trans- and cis-β-Bromo-p-nitrostyrene. Stable radicals and well-resolved spectra have been obtained in both solvents. In DMS the trans isomer radical anion exhibits a mint green solution and a spectrum of 53 lines. In the case of the cis isomer a violet solution is observed and the spectrum shows 37 lines. In ACN the solution is dark green and indigo for the trans and cis anion radicals, respectively. The spectra are very similar to those recorded in DMS and bromine elimination has not been observed. The same spectra have been recorded when CD_3CN has been used as solvent. The spectrum of the trans isomer has been interpreted by means of five hfs constants, that is, three triplets due to nitrogen and protons in ortho and meta position to the nitro group and two doublets due to α and β protons, respectively. For the cis isomer the doublet of α proton is not observable in the spectrum. Hfs constants fitting experimental spectra are reported in Table III and IV. Esr spectra of the trans isomer measured in ACN and simulated are shown in Figure 4.

TABLE VI: Energy and Oscillator Strength of Doublet–Doublet Absorption Bands for Anion Radicals

	Theory				Experiment[c]	
	A_{calcd}[a]		B_{calcd}[b]			
	ΔE, eV	f	ΔE, eV	f	ΔE, eV	
1	1.783	0.124	1.614	0.177	1.878	
	1.819	0.069	1.805	0.004	2.032	
	2.957	0.019	2.840	0.000		
	2.996	0.004	3.116	0.017	3.203	
	4.072	0.204	4.161	0.152	3.646	
	4.411	0.039	4.492	0.077		
	4.673	0.055	4.683	0.039		
2	1.776	0.005	1.745	0.005	1.922	(1.893)[d]
	2.138	0.201	2.026	0.151	2.119	(2.025)[d]
	2.833	0.003	2.696	0.000		
	2.853	0.014	2.857	0.029		
	4.312	0.290	4.261	0.290	4.427	
	4.494	0.039	4.744	0.043		
3	1.695	0.005	1.603	0.005	(1.823)	
	2.204	0.104	1.932	0.036	2.214	
	2.935	0.067	2.826	0.000	2.951	
	3.060	0.003	3.483	0.008		
4	1.765	0.004	1.749	0.005	(1.968)	
	2.114	0.200	2.009	0.161	2.101	
	2.904	0.009	2.780	0.000	3.178	
	2.913	0.004	2.912	0.022		
	4.324	0.257	4.338	0.045	3.646	
	4.470	0.042	4.425	0.223		
5	1.693	0.005	1.610	0.005	(1.907)	
	2.109	0.100	1.819	0.042	2.097	
	2.925	0.059	2.736	0.000		
	2.979	0.018	3.477	0.022	3.237	
	4.332	0.024	4.210	0.012		
	4.583	0.034	4.572	0.040		
	4.635	0.110	4.748	0.102	3.935	
6	1.720	0.004	1.702	0.005	1.812	
	1.954	0.223	1.899	0.221	1.999	
	3.293	0.032	3.269	0.036	2.194	
	4.032	0.323	4.132	0.236	4.786	
	4.321	0.052	4.360	0.142		
	4.369	0.093	4.484	0.050		
7	1.746	0.057	1.718	0.018	1.961	
	1.882	0.207	1.751	0.183	2.137	
	2.977	0.023	2.946	0.035	2.817	
	3.819	0.235	4.094	0.253	3.350	
	4.226	0.148	4.243	0.034	4.132	
	4.370	0.028	4.534	0.030		
	4.523	0.128	4.681	0.201		

[a] A_{calcd} derived by the LCI–SCF (Roothaan) method[17b] [b] B_{calcd} derived by the LCI–SCF (Longuet–Higgins and Pople) method.[17a] [c] Solvent acetonitrile. [d] Solvent dimethyl sulfoxide.

Uv Experimental Data. Visible and uv spectra for the anion radical and the neutral molecule of 1-*p*-nitrophenyl-1-phenylethylene and *cis*-β-bromo-*p*-nitrostyrene are shown in Figures 5 and 6.

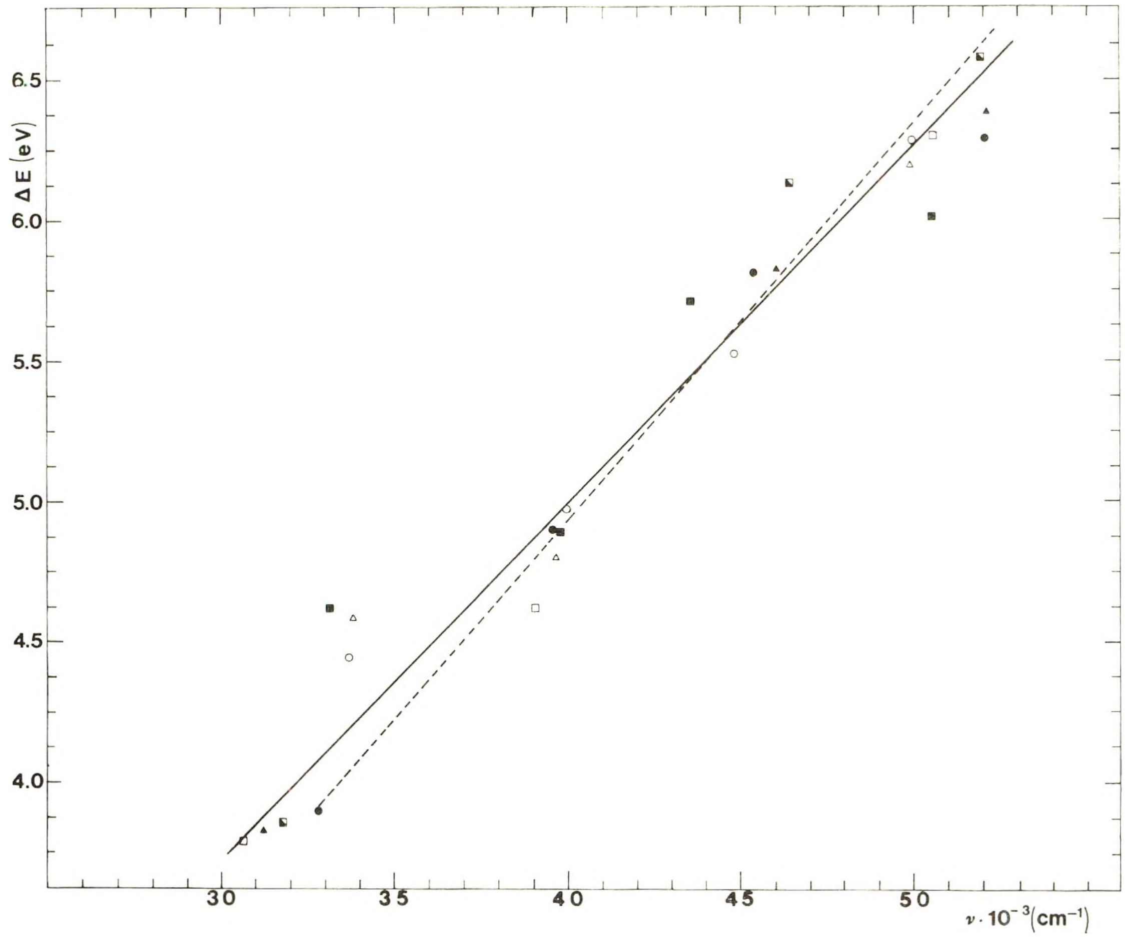

Figure 7. Regression of theoretical excitation energies of the first, second, third, and fourth bands of neutral molecules on observed frequencies (solid line: correlation coefficients $r = 0.983$, $n = 24$; 1, ○; 2, ●; 3, □; 4, ■; 5, △; 6, ▲; 7, ◩. (For numbering of molecules see Figure 1).

Calculations

Calculations of spin densities and excitation energies were carried out by means of semiempirical methods based on the σ/π approximation, due to the large dimensions of the considered molecules. Namely, restricted LCI-SCF methods, in the versions given by Pople and Longuet-Higgins[17a] and by Roothaan,[17b] and the McLachlan method,[18] have been used.

The starting H MO's have been evaluated adopting the parametrization suggested by Rieger and Fraenkel[19] for carbon, nitrogen, and oxygen, and the parameters reported in ref 20 for bromine and chlorine atoms.

Careful examination of X-ray data for related compounds[21-24] allowed the assumption of idealized geometries for neutral molecules. The geometries for the ions were assumed equal to those of parent neutral molecules. These geometrics are described in Table V. In the same table the energy parameters adopted through the calculations and the corresponding references are reported. The nonplanarity of the molecules was introduced by reducing the appropriate resonance integrals through the relation

$$\beta_{C-C}(R,\theta) = -2.40\,\frac{S_{C-C}(R)}{S_{C-C}(1.397)}\cos\theta \quad (\text{eV})$$

Two-center Coulomb repulsion integrals were estimated using the Pariser-Parr approximations.[25] At distances greater than 2.80 Å, two-center integrals were calculated theoretically with formulas given by Roothaan.[26] In the case of interatomic distances less than 2.80 Å, interpolation formulas have been obtained for each pair of atoms following the criteria indicated by Hoffman, *et al.*[27]

In the CI calculations we considered the interaction of the ground state with the singly excited configurations of types A, B, C_α, and C_β according to the definition reported in ref 2a. The 41 configurations, namely, four configurations of type A, four of type B, sixteen of type C_α, and sixteen of type C_β, represent all the configurations arising from one-electron transitions between the four highest doubly occupied MO's, the singly occupied MO, and the four lowest unoccupied MO's.

Energy and oscillator strength matrix elements for doublets based on Longuet-Higgins and Pople SCF-MO's

---

(17) (a) H. C. Longuet-Higgins and J. A. Pople, *Proc. Phys. Soc. A*, **68**, 591 (1955); (b) C. C. J. Roothaan, *Rev. Mod. Phys.*, **32**, 179 (1960).

(18) A. D. McLachlan, *Mol. Phys.*, **3**, 233 (1960).

(19) P. H. Rieger and G. K. Fraenkel, *J. Chem. Phys.*, **39**, 609 (1963).

(20) A. Streitwieser, Jr., "Molecular Orbital Theory for Organic Chemists," Wiley, New York, N. Y., 1962, p 135.

(21) G. Casalone, C. Mariani, A. Mugnoli, and M. Simonetta, *Acta Crystallogr.*, **22**, 228 (1967).

(22) G. Casalone, C. Mariani, A. Mugnoli, and M. Simonetta, *Theor. Chim. Acta*, **8**, 228 (1967).

(23) G. Casalone, A. Gavezzotti, C. Mariani, A. Mugnoli, and M. Simonetta, *Acta Crystallogr., Sect. B*, **26**, 1 (1970).

(24) G. Casalone and M. Simonetta, *J. Chem. Soc. B*, 1180 (1971).

(25) R. Pariser and R. G. Parr, *J. Chem. Phys.*, **21**, 466, 767 (1953).

(26) C. C. J. Roothaan, *J. Chem. Phys.*, **19**, 1445 (1951).

(27) R. Hoffmann, A. Imamura, and G. D. Zeiss, *J. Amer. Chem. Soc.*, **89**, 5215 (1967).

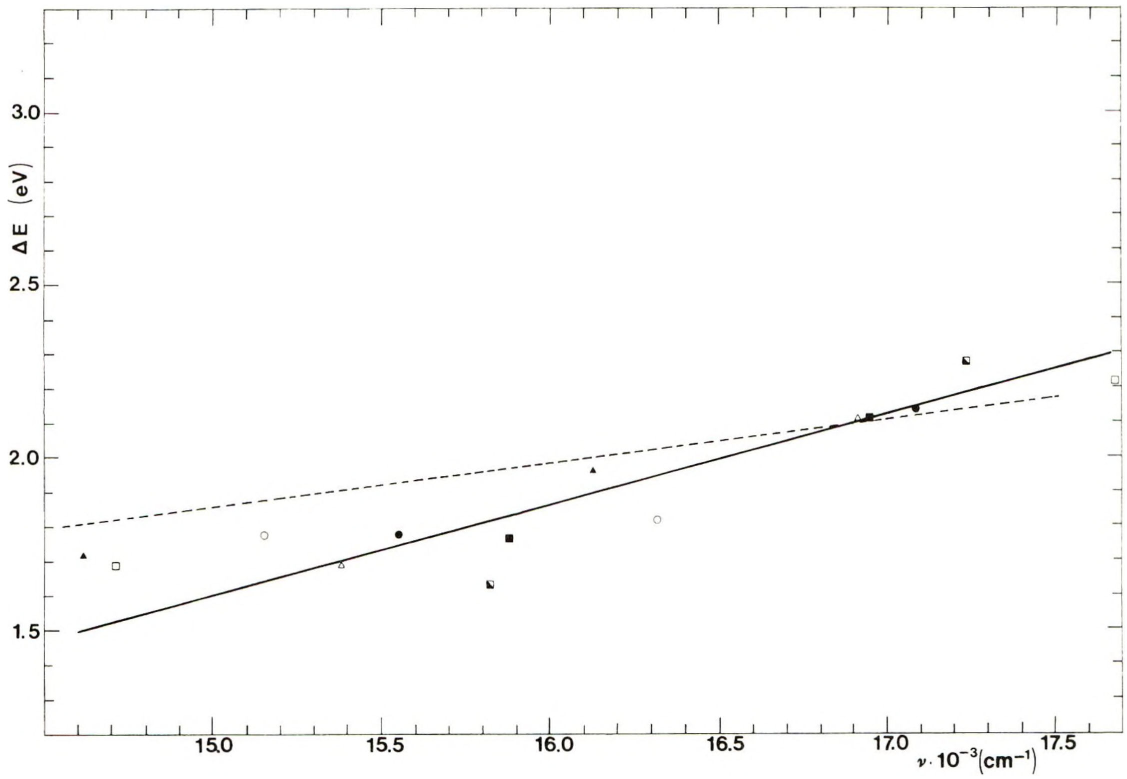

Figure 8. Regression of theoretical excitation energies of the first and second bands of radical anions on observed frequencies (solid line): correlation coefficient $r = 0.885$, $n = 14$.

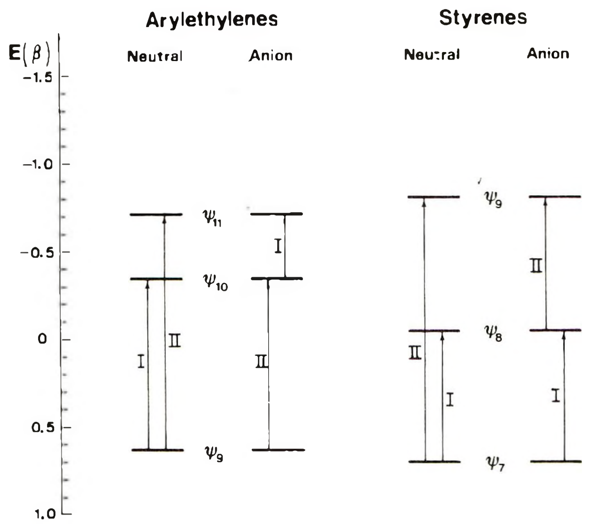

Figure 9. Huckel's MO diagram for 1-*p*-nitrophenyl-1-phenylethylene and *trans*-β-bromo-*p*-nitrostyrene. The general features of the diagram are common to all studied diarylethylenes and styrenes.

were taken from Ishitani and Nagakura.[28] Matrix elements in Roothaan's method have been recently published by Záhradník and Čársky.[2] Upon rederivation of formulas we found one minor misprint. The correct expression for the matrix element $\langle {}^2\Psi_{C(\alpha)}\ (i \rightarrow k)|H|{}^2\Psi_{C(\alpha)}\ (h \rightarrow l)\rangle$ is $2(hk|G|li) - (hk|G|il) + \delta_{hi}(mk|G|lm) + \delta_{kl}(mh|G|im)$ with $k \neq l$ or $i \neq h$.

Both SCF-CI procedures have been programmed and the programs checked against published data for some aromatic hydrocarbon ions.[2,28,29]

Singlet-singlet excitation energies and probabilities for neutral molecules have been evaluated according to standard PPP method adopting the parametrization used for ions (see Table V). Forty-nine singly excited configurations have been considered for diarylethylenes and full configuration interaction for *trans*- and *cis*-nitrostyrenes, respectively. Calculated excitation energies together with experimental results are collected in Table VI for radical ions and in Table VII for neutral molecules. Proton hyperfine coupling constants obtained from calculated spin densities are shown in Table III together with the values obtained by esr data. Calculated spin densities have been translated into coupling constants by means of the usual

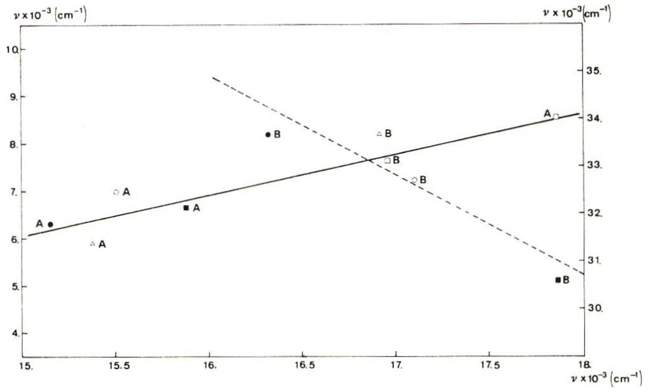

Figure 10. (A) Plot (solid line) of the first absorption band of radical anions against the energy difference between the second and first absorption bands of neutral molecules for diarylethylenes (left *y* axis): $r = 0.935$, $n = 5$. (B) Plot (----) of the second absorption band of radical anions against the first absorption band of neutral molecules for diarylethylenes (right *y* axis): $r = 0.908$, $n = 5$.

---

(28) A. Ishitani and S. Nagakura, *Theor. Chim. Acta*, **4**, 236 (1966).
(29) Y. A. Kruglyak and E. V. Mozdor, *Theor. Cnim. Acta*, **15**, 365 (1969).

TABLE VII: Energy and Oscillator Strength of Singlet-Singlet Absorption Bands

	Theory[a]		Experiment			
			ISO		ACN	
Molecule	ΔE, eV	f	ΔE, eV	f	ΔE, eV	f
1	4.451	0.189	4.174	0.21	4.025	0.25
	4.456	0.302				
	4.784	0.004	4.958	0.18	4.958	0.24
	4.967	0.218				
	5.553	0.023	5.559	0.27	5.584	0.34
	6.020	0.220				
	6.076	0.313	~6.2		6.198	0.62
	6.240	0.189				
	6.293	0.883				
2	3.904	0.675	4.051	0.27	3.937	0.37
	4.444	0.030				
	4.885	0.017	4.919	0.34	4.861	0.20
	4.905	0.065				
	5.316	0.008				
	5.530	0.032	5.635	0.64	5.509	0.26
	5.826	0.074				
	6.050	0.035				
	6.106	0.041				
	6.155	0.090			6.276	0.85
	6.321	0.770				
	6.333	0.631				
3	3.791	0.113	(3.791)	~0.10	(3.850)	
	4.494	0.037	(4.188)	~0.18		
	4.642	0.523	4.842	0.49	4.823	0.76
	4.785	0.001				
	5.032	0.184				
	5.240	0.022				
	5.370	0.053				
	5.871	0.016				
	6.184	0.052			6.198	0.80
	6.301	1.182			6.456	1.36
4	4.460	0.040	(3.850)			
	4.515	0.527	4.105	0.42	3.986	0.42
	4.903	0.001	4.927	0.34	(4.79)	
	5.320	0.019			(4.88)	
	5.726	0.134	5.401	0.36	5.461	0.76
	6.075	0.015				
	6.225	0.672			6.198	
	6.334	0.089				
	6.536	0.890				
5	4.509	0.048	4.188	0.16	4.216	0.13
	4.800	0.112				
	4.805	0.152	4.919	0.35	4.900	0.59
	5.031	0.235				
	5.081	0.007				
	6.026	0.618				
	6.148	0.037			6.261	1.26
	6.352	1.243				
6	3.809	0.792	3.862			
			4.064	0.33	4.011	0.49
	4.413	0.028	4.160			
	4.933	0.010				
	5.719	0.010	5.712		5.485	0.31
	5.849	0.090				
	6.133	0.525			6.198	0.40
	6.306	0.225				
	6.396	0.450	6.439		6.473	0.69
	6.804	0.042				
7	3.849	0.688	3.935			
			4.132	0.37	4.091	0.35
	4.424	0.030	4.245			
	4.880	0.091				
	5.365	0.596			5.596	0.29
	5.832	0.333	5.766			
	6.044	1.028			6.439	0.50
	6.211	0.076				
	6.600	0.521				
	6.696	0.621				

[a] Interaction among 49 singly excited configurations has been considered for **1**–**5** systems. For smaller systems (**6** and **7**) full configuration interaction has been performed.

McConnel relationship. For each method of calculation different Q constants for each proton position have been optimized through a least-squares fitting of experimental hfs constants *vs.* the corresponding spin densities. Nitrogen hyperfine coupling constants have been obtained only by means of McLachlan spin densities. The calculated values together with the relationship between spin densities and coupling constants, the numerical values of the Q constants, and the corresponding experimental values are reported in Table IV.

Discussion

Uv Spectra. From Tables VI and VII it is clear which assignment of absorption bands to electronic transitions is suggested from calculated transition energies and oscillator strengths. If such assignments are accepted experimental and theoretical transition energies can be correlated. The results are shown in Figures 7 and 8, from which it is evident that the correlation is satisfactory in general. A better correlation is shown in the case of neutral molecules, where up to four bands are available and the energy spread amounts to about 2.6 eV.

In the scope of the Hückel approximation a relationship between the first two bands of each arylethylene or styrene molecule and the corresponding anion is present, as shown in Figure 9. Such a relationship is not supported by experimental findings on an absolute scale, but in the case of arylethylenes, where a series of at least five examples is available, a correlation between the pairs of spectra does exist (see Figure 10). As usual the Hückel approximation is meaningful if data concerning a series of similar compounds are considered.

Esr Spectra. Data reported in Tables III and IV are the results of a number of well-resolved esr spectra, which have allowed the unequivocal assignment of all the proton and nitrogen coupling constants for a series of unknown radical anions. The spectra do not show a significant dependence on the solvents used.

The three theoretical methods that we have used always agree as to relative magnitude and sign of the calculated spin densities. On this basis we gave a sign also to experimental coupling constants. When the three different methods are compared, the McLachlan procedure seems to give a general better agreement with experimental data. For this reason spin densities obtained by this method have been used to derive nitrogen coupling constants. From Table IV it appears that the order of magnitude of such constants is calculated correctly, but the relative order for the seven anions is not reproduced. That is due to the extremely small range of experimental and theoretical values.

Conclusions

From the discussion of uv and esr spectra it appears that our approximate wave functions allow reasonable predictions of state energies and electron distributions for the considered molecules and anions. This fact is particularly gratifying since all the compounds are considerably distorted from planarity so that the validity of the $\sigma-\pi$ approximation was not assured in advance. The important influence of the absence of planarity is substantiated by the fact that in diarylethylenes the spin densities in the unsubstituted phenyl ring are practically zero. This also agrees with the fact that calculated coupling constants of the β protons in anions **3** and **5**, where the twist angle of the substituted phenyl was assumed as high as 65°, are too low, about 50% of the experimental value.

Acknowledgment. One of us (G. M.) thanks Professor C. Moser for hospitality at CECAM laboratories in Orsay; programs have been written during this stay.

Infrared Spectra of S_4

B. Meyer* and T. Stroyer-Hansen

Department of Chemistry, University of Washington, Seattle, Washington 98195

(Received May 26, 1972)

In matrices containing S_2 at an M/R ratio of 100 to 500 at 20°K, uv absorption at 530 nm characteristic for S_4 appears, and ir bands at 668, 483, 320, and 270 cm^{-1} are found. Both the uv and ir spectra gain intensity during annealing and irradiation with visible light. Fine structure of the 668-cm^{-1} absorption, in Kr at 688, 681, 668, 660, 654, 647, 640, and 636 cm^{-1}, is due to different normal vibrations, and to lattice sites and to a transient species which absorbs at 647 cm^{-1}. A very weak absorption around 625 nm, apparently related to the 647-cm^{-1} peak, belongs to a transient species, probably S_6 chains or S_4 rings.

Recently S_3 and S_4 were produced in low-temperature solution,[1] and their uv spectrum was determined.[2] Furthermore, it was discovered that S_4 forms when S_2 in a krypton matrix is illuminated with visible light. This led us to restudy the ir absorption around 668 cm^{-1} which is found in matrices containing trapped S_2 [3,4] and in pure trapped sulfur vapor.[5]

The present study followed earlier experimental methods[3,4] except that ir spectra were recorded with a PE 225 instrument, and samples were trapped on a CsI target instead of a sapphire window. We used M/R ratios between 100 and 500 and studied samples in various rare gases of varying thickness. The sulfur vapor was always at 1000°K and 0.1 Torr to optimize S_2 and eliminate all other sulfur species.[6] For each sample, spectra were recorded four times: (a) immediately after deposit at 20°K; (b) after 1-hr exposure to a tungsten-iodine lamp; (c) after evaporation of the matrix, annealing at 76°K, and quenching to 20°K; and (d) at room temperature. As observed earlier,[4] the spectra always showed the strong uv system of S_2 and the ir absorption around 668 cm.$^{-1}$

In earlier work,[3-5] the relation between the uv spectrum of S_2 and the 668-cm^{-1} absorption was described. The ir band was tentatively assigned to matrix-induced absorption of S_2. The present work confirmed that the ir band increases with S_2, but it was noted that the intensity of the ir band increases more than linearly with the concentration of S_2 and that at the onset of diffusion of S_2 the ir band intensity increases further. In addition, in experiments with $M/R \leq 200$ the matrix is red and a strong visible absorption at 530 nm appears during deposition simultaneously with the 668-cm^{-1} bands. This visible absorption is characteristic for S_4.[2] This suggests that the 668-cm^{-1} bands belong to S_4, rather than S_2.[3-5] This interpretation is in accord with fluorescence work[7] and a recent Raman spectrum,[8] both of which show a vibrational frequency of about 710 cm^{-1} for matrix-isolated S_2.

In the present work, new ir bands were observed in ad-

(1) B. Meyer, T. V. Oommen, and D. Jensen, *J. Phys. Chem.*, 75, 912 (1971).

(2) B. Meyer, T. Stroyer-Hansen, and T. V. Oommen, *J. Mol. Spectrosc.*, **42**, 335 (1972).

(3) B. Meyer, *J. Chem. Phys.*, **37**, 1577 (1962).

(4) L. Brewer, G. D. Brabson, and B. Meyer, *J. Chem. Phys.*, **42**, 1385 (1965).

(5) B. Meyer, *Helv. Chim. Acta*, **43**, 1333 (1960).

(6) J. Berkowitz and J. R. Marquart, *J. Chem. Phys.*, **39**, 275 (1963).

(7) L. Brewer and G. D. Brabson, *J. Chem. Phys.*, **44**, 3274 (1966).

TABLE I: Positions and Vibrational Spacings of the 625-nm Band System

No.	Position nm	Position cm^{-1}	Spacing, cm^{-1}
0	642.50	15,560	275
1	631.25	15,835	265
2	621.00	16,100	295
3	609.75	16,395	290
4	599.25	16,685	275
5	586.00	17,060	

dition to the very strong bands around 668 cm^{-1}: a strong band at 320 cm^{-1}, and medium-strong, broad bands at 483 and 270 cm^{-1}. They all seem to belong to S_4.

As reported earlier,[4] the absorption at 668 cm^{-1} depends on the matrix. In neon and in pure sulfur, a broad band is observed at 675 and 668 cm^{-1}, respectively. In argon and xenon, the band is split into two components at 660 and 680 cm^{-1}. The krypton matrix yields sharp and complex fine structure, as is shown in Figure 1a. The peaks and their intensities are 688 (m), 681 (s), 668 (m), 660 (s), 654 (w), 640 (w), and 636 cm^{-1} (s). All values are believed to be accurate to ±2 cm^{-1}. A further peak at 647 cm^{-1} distinguishes itself in that it gains intensity at a different rate than all others. Furthermore, it is accompanied by a very weak uv absorption at 625 nm. Six well-resolved visible absorption bands could be measured and are listed in Table I. Weak absorption has been reported in the same region previously[2] in sulfur vapor and in matrices containing S_4 and photolysis products of S_4Cl_2.[9] This absorption was tentatively assigned to S_6 or S_8 chains, on the basis of Wolfsberg–Helmholz-type extended Hückel calculations on various sulfur rings and chains.[10] The 647-cm^{-1} peak and the 625-nm absorption fade upon illumination at 20°K. This suggests that they belong to an unstable species, possibly S_6 chains, which convert upon illumination to S_6 rings which absorb in the uv. It is also possible that this band belongs to a metastable S_4 isomer.

As mentioned before, upon vaporization of the matrix and annealing at 76°K, all samples show the spectrum in Figure 1c. As is seen, a fraction of the intensity at 668 cm^{-1} remains, and the uv absorption at 550 nm weakens. This indicates that S_4 disappears partly during the matrix loss, probably by reaction with residual S_2. It was recently suggested[11] that the recombination might produce a branched chain which could yield a similar ir absorption and could contribute to the observed spectrum. At −102° the 668-cm^{-1} band decays with a lifetime of 57.7 hr and a heat of recombination of about 14.1 kcal/mol.[12] It is likely that other thermal effects observed during heating of a colored sulfur sample[13] are at least partly also connected with S_4. However, the bulk of these pure sulfur samples consists certainly of recombination products. Thus, it is to be expected that the Raman spectrum of the colored solids is essentially that of room temperature allotropes, as has been found,[14] and not that of the species responsible for the ir absorption in the matrix and the color in the visible.

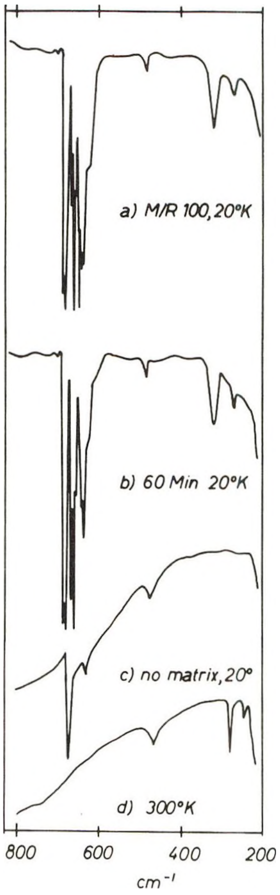

Figure 1. Infrared absorption spectra of different sulfur species: (a) deep red deposit at 20°K in Kr (M/R = 200); (b) orange deposit at 20°K after annealing at 33°K; (c) yellow deposit at 20°K; (d) yellow deposit at room temperature.

The question arises what the structure of S_4 is. The above-mentioned Wolfsberg–Helmholz calculations[10] indicate that S_4 can exist in several almost equally stable isomers and conformers. Among them are chains, rings, and a branched SO_3-type structure. The most likely form seems the chain. It yields six frequencies which fit the observed ir spectrum well, and leads to the tentative assignment of fundamental vibrations to 681, 660, 636, 483, 320, and 270 cm^{-1}. One of these observed frequencies could be a combination with a low torsion frequency. In pure sulfur, neon, argon, and xenon, the first three peaks overlap. In krypton, where an extremely sharp spectrum is observed ir spectrum well and leads to the tentative assigntioned above, the frequency at 647 cm^{-1}, however, exhibits independent behavior and must be due to a different species. Calculations[10] indicate that a SO_3-type S_4 structure should be quite stable, but the formation of such a molecule would probably consume a substantial activation energy. However, it seems to us more likely that S_4 rings form. A puckered ring would yield two ir active vibrations, a planar ring only one. Both types of rings would have a degenerate stretching vibration fitting the 647-cm^{-1} band. Conclusive interpretation of the fine structure at 668 cm^{-1} must wait for synthesis of S_4 and S_6 isomers and conformers.

Acknowledgment. This work was partly supported by the National Science Foundation research Grant No. GP 25310. T. S.-H. was partly supported by the Danish Statens Naturvidenskabelige Forskningsrad.

---

(8) R. E. Barletta, H. H. Claassen, and R. L. McBeth, *J. Chem. Phys.*, **55**, 5409 (1971).

(9) B. Meyer, M. Gouterman, D. Jensen, T. V. Oommen, K. Spitzer, and T. Stroyer-Hansen, *Advan. Chem. Ser.*, **No. 110**, 53 (1972).

(10) B. Meyer and K. Spitzer, *J. Phys. Chem.*, **76**, 2274 (1972).

(11) R. Steudel, *Z. Naturforsch. B*, **27**, 469 (1972).

(12) B. Meyer, Ph.D. Thesis, University of Zurich, 1960.

(13) A. K. Maltsev and A. F. Kapustinskii, *Tr. Mosk. Khim.-Tekhnol. Inst.*, **35**, 73 (1961).

(14) R. E. Barletta and C. W. Brown, *J. Phys. Chem.*, **75**, 4058 (1971).

Hypochromism and Exciton Interaction in Halofluorescein Dyes

K. K. Rohatgi* and A. K. Mukhopadhyay

Departments of Chemistry (Physical) and Physics, Jadavpur University, Calcutta-32, India

(Received June 5, 1972)

The dimer spectra of fluorescein and some of its halogen derivatives in aqueous solution at pH 12 are reported. From the splitting observed in the spectra the inclination of the component molecules in a dimer has been obtained on application of the theory of exciton interaction. The value of the twist angle θ has been found to decrease in the series Fl > $FlCl_2$ > FlI_2 > $FlBr_4$ > FlI_4 > $FlCl_4Br_4$ > $FlCl_4I_4$. The interaction energy ΔE is linearly related to the square of the transition moment $|M|^2$ of the series of dyes. The distance R between the two component molecules in the dimer has been calculated for various geometries. Hypochromism has been observed in each case and it has been found to change systematically with the twist angle. From these studies a possible geometry of the dimer and higher n-mers has been suggested.

A systematic study of the aggregation characteristics of dyes from spectrophotometric data has become a useful field of research because of its possible application in understanding such phenomena as energy transfer in biological systems,[1] metachromasia,[2] hypochromism and conformation of polypeptides,[3] and staining properties of dyes for biological specimens,[4] etc. The force responsible for holding the component molecules in the dimer or a polymer is not yet well understood.[5-10] Nevertheless, it is clear that for ionic dyes aggregation will be possible if there exists some very strong attractive interaction which first of all overcomes the coulombic repulsion and then brings the component molecules to a reasonable distance to form dimers and subsequently higher polymers.

Most of the highly aggregating dyes are planar and cationic in nature and exhibit blue shift on dimerization. Red shift has been observed for some cyanine dyes.[11] The fluorescein dyes are anionic and the dimerization constant can be systematically varied from 5 for fluorescein to 250 for rose bengal on gradual halo substitution. Therefore they provide a good system for such studies. The absorption spectra of fluorescein (Fl) and some of its halo-substituted derivatives, namely dichlorofluorescein ($FlCl_2$), diiodofluorescein (FlI_2), eosin ($FlBr_4$), erythrosin (FlI_4), phloxin ($FlCl_4Br_4$), and rose bengal ($FlCl_4I_4$), have been studied in the present work and their dimer spectra obtained by the method described in a previous communication.[12] The study has been confined to the dimer stage only.

Nature of Dimer Spectra. The dimer spectra of the series of halofluoresceins investigated are given in Figure 1. All the spectra are observed to give two peaks whose wavelengths are above and below the monomer peak wavelength, that is, the monomer peaks for all the compounds are split on dimerization, but the intensities of the two peaks show variations. The short-wave peak is normally of higher intensity and the peak intensity of this band gradually decreases as the number of halogen substitution increases.

In Table I are given the difference in wave number between the monomer M and the high-frequency dimer peak D_2 (column 4) and the wave number difference between the $0 \rightarrow 0$ and the $0 \rightarrow 1$ vibrational bands in the monomer (column 5). The former is seen to increase with halo substitution whereas the latter decreases. This definitely establishes that the enhancement of the high-frequency shoulder on aggregation is not due to vibronic coupling. Other forces are operative in producing the dimer spectra.

There have been different approaches to the problem,[13,14] the simplest of which is the theory of exciton coupling.[13] The splitting of the energy levels has been nicely explained by the theory of exciton interaction. For a perfectly parallel dimer, only the high-frequency or the short-wave peak is expected to appear, whereas for the head-to-tail dimer only the red-shifted peak is allowed. But for any intermediate geometry, both the peaks may appear. The ratio of the peak heights may be correlated with the angle θ between the main oscillators of the two molecules. The values of θ calculated with the help of the relationship

$$f_1/f_2 = \tan^2(\theta/2)$$

where f_1 and f_2 are the oscillator strengths of the long-wave and the short-wave peaks, respectively, are given in Table II, column 5.

The second point of variation between these dyes is the difference in the extent of splitting (ΔE). The ΔE values in terms of wave number are given in Table II, column 3.

---

(1) M. Kasha, M. A. El-Bayoumi, and W. Rhodes, *J. Chim. Phys., Physicochim. Biol.*, **58**, 916 (1961); M. Kasha and M. A. El-Bayoumi, *J. Chem. Phys.*, **34**, 2181 (1961).

(2) M. K. Pal and M. Schubert, *J. Phys. Chem.*, **67**, 1821 (1963); M. K. Pal, *Histochemie*, **5**, 24 (1965).

(3) I. Tinoco, Jr., *J. Amer. Chem. Soc.*, **82**, 4786 (1960).

(4) B. L. Van Durren, "Fluorescence and Phosphorescence Analysis," M. Hercules, Ed., Interscience, New York, N. Y., 1966, p 195.

(5) E. Rabinowitch and L. Epstein, *J. Amer. Chem. Soc.*, **63**, 69 (1941).

(6) S. E. Sheppard and A. L. Geddes, *J. Amer. Cnem. Scc.*, **66**, 2003 (1944).

(7) V. I. Levschin and L. V. Krotova, *Opt. Spektrosk.*, **13**, 457 (1962).

(8) P. Mukherjee and A. K. Ghose, *J. Amer. Chem. Soc.*, **92**, 6403 (1970).

(9) K. Suzuki and M. Tsuchiya, *Bull. Chem. Soc. Jap.*, **44**, 967 (1971).

(10) K. K. Rohatgi and A. K. Mukhopadhyay, *Chem. Phys. Lett.*, **12**, 259 (1971).

(11) C. H. Gibs, S. M. K. Rahman, and D. Smith, *J. Chem. Soc.*, 1209 (1961).

(12) K. K. Rohatgi and A. K. Mukhopadhyay, *Photochem. Photobiol.*, **14**, 551 (1971).

(13) E. G. McRae and M. Kasha, "Physical Processes in Radiation Biology," L. Augenstein, B. Rosenberg, and R. Mason, Ec., Academic Press, New York, N. Y., 1964, p 23.

(14) V. Czikelley, G. Dreizler, H. D. Forsterling, H. Kuhn, J. Sondermann, P. Tillman, and J. Wiegand, *Z. Naturforsch. A*, **24**, 1821 (1969); V. Czikelley, H. D. Forsterling, and H. Kuhn, *Chem. Phys. Lett.*, **6**, 11 (1970).

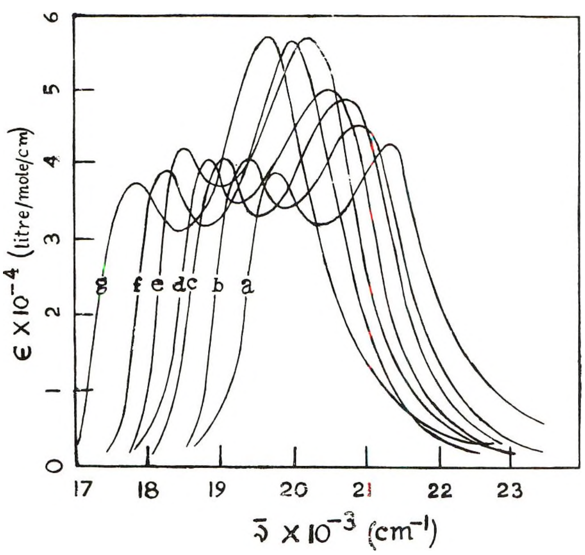

Figure 1. Absorption spectra of the dimers of halofluoresceins at pH 12: (a) fluorescein, (b) dichlorofluorescein, (c) diiodofluorescein, (d) eosin, (e) erythrosin, (f) phloxin, (g) rose bengal.

TABLE I: Spectral Data for the Dilute and Concentrated Solutions of the Halofluorescein Dyes[a]

Dye	ν(M), cm^{-1}	$\bar{\nu}(D_2)$, cm^{-1}	$\bar{\nu}(D_2) - \bar{\nu}$(M), cm^{-1}	$\bar{\nu}(M_v) - \bar{\nu}$(M), cm^{-1}
Fl	20,370	21,370	1000	910
$FlCl_2$	19,880	20,920	1040	870
FlI_2	19,610	20,660	1050	850
$FlBr_4$	19,310	20,410	1100	840
FlI_4	19,010	20,160	1150	830
$FlCl_4Br_4$	18,730	19,880	1150	810
$FlCl_4I_4$	18,480	19,650	1170	830

[a] $\bar{\nu}(M_v)$ is the monomer vibrational shoulder, $\bar{\nu}$(M) is the monomer frequency, $\bar{\nu}(D_2)$ is the enhanced shoulder for concentrated solutions.

TABLE II: Square of the Transition Moment Integrals $|M|^2$ of the Monomer and the Observed Interaction Energy (ΔE), Dimerization Constant, (K), Twist Angle (θ), and Calculated Values of the Intermolecular Distance (R) for Different Assumed Geometries for the Dimer

Dye	$\|M\|^2 \times 10^{36}$, esu	ΔE, cm^{-1}	K, M^{-1}	θ, deg	R, Å a	 b	 c
Fl	55.6	1610	5	71	−1.68	7.73	4.81
$FlCl_2$	58.9	1650	60	68	2.89	7.76	5.11
FlI_2	60.0	1660	83	67	3.24	7.78	5.21
$FlBr_4$	60.7	1680	110	66	3.25	7.81	5.25
FlI_4	68.1	1720	140	63	4.12	7.97	5.65
$FlCl_4Br_4$	73.0	1800	190	62	4.34	8.04	5.75
$FlCl_4I_4$	76.1	1830	250	60	4.70	8.04	5.92

[a] Brick-work model. [b] In-plane model. [c] Parallel-plane model.

The extent of splitting will depend on the strength of interaction between the two oscillating dipoles in the two molecules. The interaction is coulombic in nature and from the considerations of dipole–dipole terms only, the expectation value of the interaction energy is correlated with the square of transition moment integral $|M|^2$ and the reciprocal of R^3, where R is the separation distance between the centers of gravity of the two component molecules in the dimer. The relative geometry of the transition dipoles is also important, and in general the appropriate expression for ΔE is

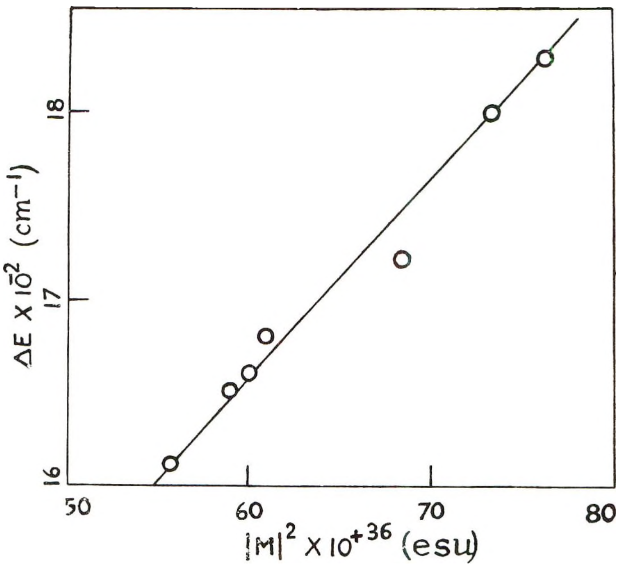

Figure 2. Plot of ΔE, the interaction energy of the dimer, *vs.* $|M|^2$, the square of the transition moment integral.

$$\Delta E = (2|M|^2/R^3)\,G$$

where G is the geometry factor.[15] For the simple case of one-dimensional transition dipoles, it is possible to assume various geometries and to calculate R from the experimental value of interaction energy ΔE. In the series of halo-substituted fluoresceins, the interaction energy ΔE is found to increase with increased halo substitution or by substitution of heavier halogens. The variation follows the same sequence as the increase in oscillator strength which is proportional to the square of the transition moment integral $|M|^2$. A linear correlation has been established in Figure 2 and the data are given in Table II.

Hypochromism. From the law of conservation of oscillator strength it is expected that the oscillator strength of the dimer should be twice that of the monomer. The oscillator strength f was calculated from the relationship

$$f = 4.39 \times 10^{-9}[9n^2/(4n^2 + 2)^2]\int \epsilon_{\bar{\nu}}\,d\bar{\nu}$$

where $9n^2/(4n^2 + 2)^2$ is the Lorentz factor to correct for the medium effect. The areas of the monomer and the dimer bands were measured by means of a planimeter. If a quantity called hypochromicity factor H is defined[3,16] as the ratio $f_{\text{dimer}}/2f_{\text{monomer}}$ then H is found to decrease in the series as the aggregation constant K increases on halo substitution as shown in Table III.

Discussion

In their studies on halofluorescein dyes, Sheppard and Geddes[6] had observed a decrease in the aggregation tendency in aqueous solutions on halo substitution as judged from conformity to Beer's law. The argument was forwarded that the large sizes of the halogen atoms cause steric hindrance to optical coupling of the dye molecules due to increase in the distance between the two component molecules. In the present study the opposite effect has been observed. The dimerization constant K has been

---

(15) M. Kasha, H. R. Rawls, and M. A. El-bayoumi, *Pure Appl. Chem.*, **11**, 371 (1965).

(16) W. Rhodes, *J. Amer. Chem. Soc.*, **83**, 3609 (1961).

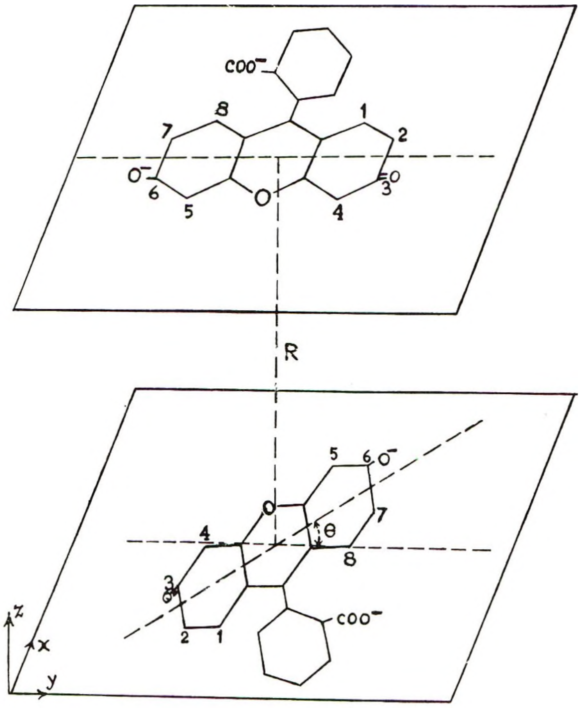

Figure 3. Structure of the fluorescein dimer.

TABLE III: Observed and Calculated Values of the Hypochromicity Factor, *H*, for the Halofluoresceins[a]

			H	
Dye	λ_1, nm	λ_2, nm	Obsd	Calcd
Fl	491	320	0.85	0.86
$FlCl_2$	502	335	0.84	0.83
FlI_2	510	330	0.83	0.83
$FlBr_4$	518	340	0.82	0.80
FlI_4	526	353	0.79	0.74
$FlCl_4Br_4$	534	355	0.75	0.62
$FlCl_4I_4$	541	356	0.74	0.61

[a] λ_1 are the longest wavelength monomer peaks and λ_2 that of the corresponding neighboring *y*-polarized transition bands.

found to increase systematically on substitution of more halogens, as also halogens of higher atomic number. The interaction energy ΔE increases with concomitant increases in the transition moment integrals. Although exciton theory is an oversimplification for the problem of dye aggregation, the interdipole distance R computed therefrom appears to be quite reasonable, if proper geometry of the aggregate is taken into consideration. In earlier studies[17] the high values of R reported for fluorescein and rhodamine were due to the fact that the values were not multiplied by the geometry factor.

Monahan, Germano, and Blossey[18] have shown a definite effect of steric hindrance on the dimerization of arylazonaphthols. The free energy of dimerization became less negative in the order of substitution of $CH_3 > C_2H_5 > i\text{-}C_3H_7$ in the chlorosulfonic acid moiety. At the same time, the twist angle θ increased in the same order with not much variation in the oscillator strength of the monomer. The angle θ is independent of any model assumed for the geometry but the values of R are severely model dependent.[18] Monahan, *et al.*, have discussed two possible models, (i) in-plane oblique angle model and (ii) parallel-plane twist angle model. From the trend in R, they arrived at certain conclusions regarding the dimer geometry for the singly charged and doubly charged dye ions. A third type of geometry for dye aggregate has been proposed by Czikelley, Forsterling, and Kuhn.[14] A brick-work structure has been preferred by them.

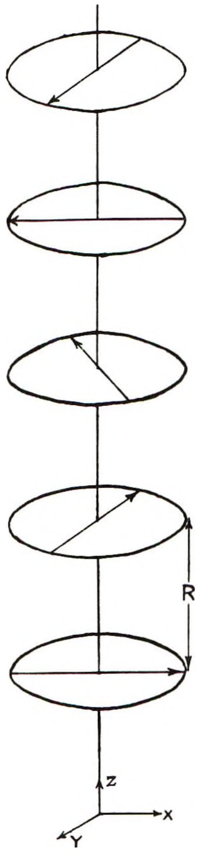

Figure 4. Helical arrangement or "sis-kababi" model for dye aggregates.

The relationship between interaction energy, strength of transition dipole, and the geometry of the dimer is given by the general expression[15]

$$\Delta E = [2|M|^2/R^3](\cos\theta + 3\cos^2\phi)$$

where θ is the angle between the polarization direction of the dipoles in the composite molecules and ϕ is the angle between the polarization direction and the line joining the centers of the two component molecules. We can consider various geometries and see how they fit our observations.

Model I ($\theta = \theta$ and $\phi = 90°$; Sandwich Dimer with a Twist Angle θ)

$$\Delta E = [2|M|^2/R^3]\cos\theta$$

The linear relationship between ΔE and $|M|^2$ obtained for the halofluorescein series (Figure 2) means that the term $\cos\theta/R^3$, as given by the slope, is constant. The cosines of the twist angle θ should vary as the inverse cube of the interdipole distance. The values of R, calculated from the derived values of the twist angle θ, are given in Table II, column 8. The phase relationship is such as to give rise to a blue-shifted dimer in which in-phase transition dipoles are favored over the out-of-phase transitions. From Figure 1, it is observed that the high-frequency in-phase

---

(17) K. K. Rohatgi, *J. Mol. Spectrosc.*, **27**, 545 (1968).

(18) A. R. Monahan, N. J. Germano, and D. F. Blossey, *J. Chem. Phys.*, **75**, 1227 (1971).

transition probability increases in the series Fl < $FlCl_2$ < FlI_2 < $FlBr_4$ = FlI_4 = $FlCl_4Br_4$ = $FlCl_4I_4$.

Model II ($\theta = 0°$ *and* $\phi = 0°$; *Head-to-Tail Dimer*). This model represents the in-line dimers and phenomenologically corresponds to a red-shifted dimer spectrum. Therefore this model is not applicable.

Model III ($\theta = \theta$ *and* $\phi = \phi$; *Coplanar Inclined Angle Dimer*)

$$\Delta E = [2|M|^2/R^3](\cos\theta + 3\cos^2\phi) = [2|M|^2/R^3](\cos\theta + 3\sin^2\theta/2)$$

The values of R calculated for this model are fairly high and range from 7.7 to 8 Å (Table II, column 7).

Model IV ($\theta = 0°$ *and* $\phi = \phi$; *Sandwich Dimer with Displaced Origin*)

$$\Delta E = [2|M|^2/R^3](1 - 3\cos^2\phi)$$

when $\phi = 90°$, it is the same as the model I with $\theta = 0°$; when $\phi = 0°$, it is the same as the model II with $\theta = 0°$. For a higher aggregate than the dimer, this may correspond to the brick-work structure of Czikelley, *et al.*[14] Kasha[15] has shown that for such a geometry, the exciton splitting will be smaller for $\phi = 90°$ than for $\phi = 60°$. When $\phi = 54.7°$, there will be no splitting. R values calculated using this expression are low and even negative. Hence this geometry need not be considered.

It is obvious from the table that the values of R, calculated for the sandwich dimer with twist angle θ, are very close to those obtained from crystal studies. Therefore it may be considered to be the most probable geometry for the fluorescein and the halofluorescein dyes, as represented by Figure 3. It appears that in the dimer the three rings of the component molecules are trans to each other. No steric effect is apparent since the dimerization constant increases in the series. The interplanar distances increase for halo-substituted fluoresceins systematically and the angle θ between the transition dipoles decrease correspondingly. Apparently the increased dipole strength due to substitution of more polarizable halogens creates a stronger field such that the dipoles tend toward parallel alignment. Better overlap due to more parallel geometry enhances the aggregation tendency, overriding the steric effect. This causes a slight increase in R value.

A further confirmation of this geometry can be obtained from the hypochromic effects observed for these series of dyes. An increased tendency toward parallel orientation is expected to cause greater loss of oscillator strength on dimerization. This is reflected in the values of hypochromicity factor H given in Table III. In the same table are also given the values of H calculated using the neighboring y-axis-polarized transition frequency as the interacting level in Rhodes'[16] expression for hypochromism. The two values are surprisingly close for most of the dyes.

An interesting extension of this geometry is that for a trimer, the next molecule will again be twisted by an angle θ and so on for higher aggregates. If θ is near about 60°, as observed for these dyes, the trimer will be more stable than the dimer. This actually has been observed by Mukherjee and Ghose[8] for methylene blue, using the isoextraction technique. The value of K_3, the trimerization constant, has been reported to be greater than the dimerization constant K_2. Thus the higher aggregates are likely to have a screw or helical arrangement of the dye molecules as represented in Figure 4. This kind of configuration has been called as "sis-kababi" model by Daudel as referred to by Förster[19] for covalently bonded polymeric systems.

(19) Th. Förster, "Modern Quantum Chemistry," Part 3, Section III, O. Sinanoğlu, Ed., Academic Press, New York, N. Y., 1965, p 101.

Tetracyanomethane. X-Ray Diffraction and Differential Scanning Calorimetry Study from −150 to +160° [1]

Kerry Rubin[2] and Reuben Rudman*

Department of Chemistry, Adelphi University, Garden City, New York 11530

(Received July 3, 1972)

Publication costs assisted by the National Science Foundation

$C(CN)_4$ is monoclinic and crystallizes in space group *Cc* or *C2/c* in which $a = 9.361(6)$Å, $b = 8.881(5)$Å, $c = 6.241(8)$Å, and $\beta = 91.30(6)°$ with four molecules per unit cell. No crystallographic phase transitions were observed at standard pressure between −150° and the decomposition temperature of +160°. An analysis of the data available for several methylcyanomethane compounds indicates that, in these compounds, dipole–dipole interactions are more important than hydrogen-bond formation.

Introduction

Many compounds composed of tetrahedral, approximately spherical, molecules (*e.g.*, the carbon tetrahalides) undergo solid–solid phase transitions. Crystals of the highly disordered phase stable just below the melting point are generally referred to as *plastic crystals.*[3] A re-

---

[1] This research was supported by the National Science Foundation.

[2] Undergraduate Senior Research Student.

TABLE I: Crystal Data for Tetracyanomethane

Name: tetracyanomethane
Compound: $C(CN)_4$
Formula weight: 116.34 (based on C-12)
Crystal system: monoclinic
$a = 9.361(6)$[a] Å
$b = 8.881(5)$ Å
$c = 6.241(8)$ Å
$\beta = 91.30(6)°$
Systematic absences: hkl, $h + k$ odd
$h0l$, l odd
Space group: Cc (#9) or $C2/c$ (#15)
$Z = 4$
Density (experimental) = 1.42_2 g/ml[b]
Density (X-ray) = 1.49_0

[a] The numbers in parentheses are the estimated standard deviations in the last figure. [b] By flotation in a solution of CCl_4 and CH_3CCl_3.

TABLE II: Powder Pattern for $C(CN)_4$

I	d_{obsd}, Å	d_{calcd}, Å	hkl
S	4.69	4.68	200
S	4.55	4.52	$11\bar{1}$
S	2.95	2.94	310
S	2.88	2.88	$22\bar{1}$
S	2.64	2.64	311
M	2.341	2.340	400
M	2.143	2.147	330
M	1.831	1.831	510
VW	1.783	1.782	$33\bar{2}$
M	1.715	1.716	$31\bar{3}$
VW	1.452	1.453	423
		1.451	$24\bar{3}$
VW	1.4004	1.4002	532
VW	1.3373	1.3373	062
VW	1.2839	1.2845	404
		1.2831	$44\bar{3}$
		1.2825	262

[a] Based on data in Table I.

cent electron diffraction investigation[4] of tetracyanomethane, $C(CN)_4$, as well as previous studies of the synthesis[5] and properties[6] of this compound have shown that the molecule is tetrahedral and that some of its chemical properties are similar to those of the carbon tetrahalides. As part of our attempts to define the sphericity of the molecular envelope that is required in order for the plastic-crystal phase to form, it was decided to test for the presence of any solid-solid phase transitions in tetracyanomethane, over a wide temperature range.

Experimental Section

Synthesis. Tetracyanomethane was prepared according to the following scheme.

$CH_2(CN)_2 \rightarrow KBr\cdot[Br_2C(CN)_2]_4$[7] $\rightarrow KC(CN)_3$[8] $\rightarrow AgC(CN)_3$[9] $\rightarrow C(CN)_4$[5]

The infrared spectra of $KC(CN)_3$ and $AgC(CN)_3$, and the physical properties of $C(CN)_4$, agreed with previously reported data.[5,8]

X-Ray Diffraction Study. Powder patterns were obtained with a Norelco 114.6-mm diameter Debye-Scherrer powder camera; single-crystal data were measured on a precession camera at room temperature. Ni-filtered Cu K radiation was used throughout. A high-temperature (150–155°) study of $C(CN)_4$ was carried out using a commercially available wound-filament quartz tube gas heater[10] with compressed air.

Differential Scanning Calorimetry (DSC) Study. $C(CN)_4$ was studied from −150° to the decomposition temperature of approximately +160° on a Perkin-Elmer DSC-1B calorimeter, using techniques described elsewhere.[11]

Computing. The powder patterns were indexed and the unit cell constants refined using a modified version of the program PIRUM[12] on a CDC 3300 computer.

Results and Discussion

Room-temperature single-crystal data for $C(CN)_4$, based on precession photographs and least-squares refinement of the powder data, are found in Table I. The powder pattern is listed in Table II. The crystal structures of $KC(CN)_3$[13] and $AgC(CN)_3$[14] have been reported previously, but the powder patterns were not listed. Indexed powder patterns for these substances have been submitted to the Joint Committee on Powder Diffraction Standards.

Several studies of similar compounds have been reported in the literature. Evidence for the formation of plastic crystals was found for trimethylacetonitrile[15,16] ($(CN_3)_3CCN$) and dimethylmalononitrile[17] ($(CH_3)_2C(CN)_2$) but not for malononitrile[17,18] ($H_2C(CN)_2$). In the discussion of their results, Ribner and Westrum[17] state that cyano groups on aliphatic molecules do not form sufficiently strong intermolecular bonds to hinder molecular rotation. The increasing difficulty in forming a plastic-crystal phase as the number of cyano groups increases is explained as being due to one of two factors: (a) the formation of a weak hydrogen bond (between a methyl hydrogen and the nitrogen of the cyano group) resulting from an increase in the acid strength of the methyl hydrogen as the number of cyano groups increases, or (b) dipole–dipole interaction of the cyano groups.

Ribner and Westrum prefer the first explanation and present a table showing a correlation between the strength of the hydrogen bond and the existence of a rotational transition in the solid for several cyano-containing compounds. According to this reasoning, tetracyanomethane,

---

(3) J. Timmermans, *J. Phys. Chem. Solids*, **18**, 1 (1961).
(4) H. Oberhammer, *Z. Naturforsch. A*, **26**, 2043 (1971).
(5) E. Mayer, *Monatsh. Chem.*, **100**, 462 (1969); **101**, 846 (1970).
(6) R. E. Hester, K. M. Lee, and E. Mayer, *J. Phys. Chem.*, **74**, 3373 (1970).
(7) R. A. Carboni, *Org. Syn.*, **39**, 64 (1960).
(8) S. Trofimenko, E. L. Little, Jr., and H. F. Mower, *J. Org. Chem.*, **27**, 433 (1962).
(9) E. Cox and A. Fontaine, *Bull. Soc. Chim. Fr.*, 948 (1954).
(10) Gas heater, Model SGH 114680, Sylvania Special Products Division, Exeter, N. H. 03833.
(11) L. Silver and R. Rudman, *J. Pnys. Chem.*, **74**, 3134 (1970).
(12) P. Werner, *Ark. Kemi*, **31**, 513 (1970).
(13) J. R. Witt and D. Britton, *Acta Crystallogr., Sect. B*, **27**, 1835 (1971).
(14) J. Konnert and D. Britton, *Inorg. Chem.*, **5**, 1193 (1966).
(15) E. F. Westrum, Jr., and A. Ribner, *J. Phys. Chem.*, **71**, 1216 (1967).
(16) Z. M. El Safaar, P. Schultz, and E. F. Meyer, *J. Chem. Phys.*, **56**, 1477 (1972).
(17) A. Ribner and E. F. Westrum, Jr., *J. Phys. Chem.*, **71**, 1208 (1967).
(18) J. G. Powles, A. Begum, and M. O. Norris, *Mol. Phys.*, **17**, 489 (1969).

TABLE III: Fusion and Transition Temperatures for the Methylcyanomethane Compounds $(CH_3)_{4-n}C(CN)_n$

n	Mol wt	T_f, °K	T_{tr}, °K	Ref
0	72	256.5	140.0	11
1	83	292.13	213,232.74	15
2	94	307.47	302.60	17
3	105	367	?	*a*
4	116	dec ~433	...	5

[a] M. B. Frankel, A. B. Amster, E. R. Wilson, M. McCormick, and M. McEachern, Jr., *Advan. Chem. Ser.*, **No. 54**, 108 (1965); J. R. Witt, D. Britton, and C. Mahon, *Acta Crystallogr., Sect. B*, **28**, 950 (1972).

in which no hydrogen bonds are possible, should undergo a phase transition to a plastic crystal. However, in the present study, neither the DSC nor the high-temperature X-ray diffraction investigations revealed any phase transitions in tetracyanomethane from −150° to the decomposition temperature.

It has already been shown,[19] in the case of the methylchloromethane compounds, that methyl groups increase the sphericity of tetrahedral molecules to a greater extent than do chlorine atoms. This same statement can also be made for the methylcyanomethane compounds. The data in Table III indicate that for the series of compounds $(CH_3)_{4-n}C(CN)_n$), where n varies from 0 to 4, the melting point rises with increasing numbers of cyano groups at a faster rate than does the transition temperature. If the melting point and the transition temperature are each plotted as a function of the molecular weight, it will be seen that the two curves intersect between $n = 2$ and $n = 3$. The prediction could be made that no solid–solid phase transition would occur for $n = 3$ or 4. This has now been verified for $n = 4$. Reexamination of Table VIII of Ribner and Westrum[17] also permits the interpretation that the transitions occur at lower temperatures as the spherical character of the molecules increases.

Although it might be claimed that tetracyanomethane does not form a plastic crystal simply because it is not sufficiently spherical, it would still be expected to have a low melting point (similar to that of a carbon tetrahalide of comparable molecular weight[6]). Several other cyano-containing compounds[20] in which significant hydrogen bonds would not occur[21] are known to have melting points higher than expected when the molecular weights alone are considered. The physical properties of these compounds agree with the results of the present work, as well as with Clementi's analysis,[22] that dipole–dipole interactions are significant in cyano-containing compounds. We therefore conclude that dipole–dipole interactions are of considerably greater importance in determining the physical properties of the methylcyanomethane compounds than are hydrogen bonds. An investigation of 1,1,1-tricyanomethane would be of interest.

---

(19) R. Rudman and B. Post, *Mol. Cryst.*, **5**, 95 (1968).

(20) *E.g.*, tricyanocyclopropane (F. Hirshfeld, *Acta Crystallogr.*, **20**, 80 (1966)) and tetracyanocyclobutane (B. Greenberg and B. Post, *Acta Crystallogr. B*, **24**, 918 (1968)).

(21) W. C. Hamilton and J. A. Ibers, "Hydrogen Bonding In Solids," W. A. Benjamin, New York, N. Y., 1968, pp 182–183.

(22) E. Clementi and D. Klint, *J. Chem. Phys.*, **50**, 4899 (1969).

High-Resolution X-Ray Emission Study of Central Atom–Ligand Bonding in Phosphorus Oxy Anions[1]

K. Myers and G. Andermann*

Department of Chemistry and Hawaii Institute of Geophysics, University of Hawaii, Honolulu, Hawaii 96822

(Received June 12, 1972)

Publication costs assisted by the University of Hawaii

The molecular bonding environment of PO_4^{3-} and of the substituted phosphorus oxy anions HPO_3^{2-}, $H_2PO_2^-$, HPO_4^{2-}, $H_2PO_4^-$, and H_3PO_4 has been investigated by X-ray photon emission spectroscopy. The effect upon the electronic structure of introducing a second ligand type into the molecule has been evaluated through the interpretation of both the Kβ and $L_{2,3}$ emission spectra. The spectral assignments have been based upon molecular orbital CNDO/2 calculations utilizing a combined intensity parameter–energy level model. Through the use of the calculated atomic orbital composition of the molecular orbitals, the origins and nature of the Kβ spectral bands have been shown to be due to specific central atom orbital–ligand orbital bonding.

Introduction

X-Ray photon emission, resulting from valence electron transitions, has been investigated experimentally for over 50 years.[2a] The possibility of probing electronic structure by this technique has received particular impetus with the development of high-resolution double-crystal spectrome-

---

(1) Hawaii Institute of Geophysics Contribution No. 485.

(2) (a) A. H. Compton and S. K. Allison, "X-Rays in Theory and Experiment," 2nd ed, Van Nostrand, New York, N. Y., 1935; (b) R. D. Deslattes, *Phys. Rev. A*, **133**, 390 (1964).

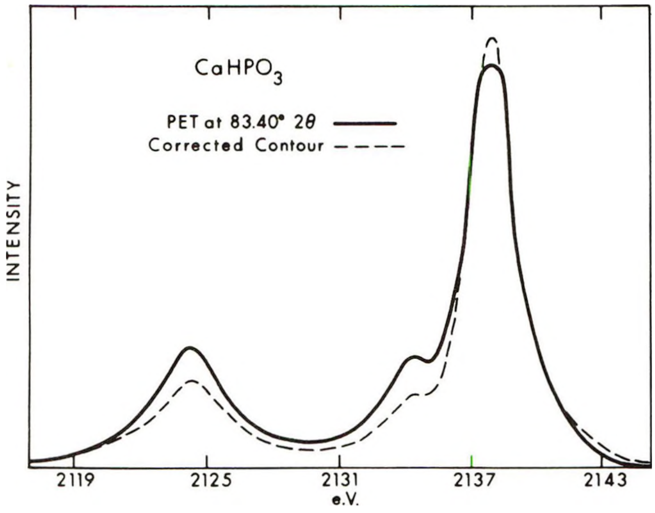

Figure 1. Intensity contour correction for Kβ spectrum of $CaHPO_3$.

ters.[2b-5] However, rigorous theoretical interpretation of chemical interest is more recent. The application of molecular orbital concepts to high-resolution X-ray photon emission spectra has provided interpretation for the bonding in various ionic crystals[5-10] for which other theories proved inadequate. Particular interest has centered upon compounds of the second periodic row elements. These studies have dealt only with the relatively simple bonding of one type of ligand, under various symmetries, to a central atom. It has been our intention to evaluate multiple-type ligand effects upon the electronic structure by studying a series of phosphorus salts with oxygen, hydroxy, and hydrogen ligands.[9,11] While Fichter[12] has investigated the Kβ spectrum of a large series of phosphorus oxy anions, Fichter's spectra are not well resolved and the interpretation is not on a molecular model.

The evaluation, to be discussed below, deals with the interpretation of Kβ and $L_{2,3}$ spectral series in terms of molecular orbital CNDO/2 calculations. In particular, the possibility of assigning certain spectral transitions to specific central atom orbital-ligand orbital bonding is proposed.

Experimental Section

The phosphorus Kβ spectra were obtained in this laboratory on a high-resolution double-crystal spectrometer[10] modified for phosphorus analysis into a novel "hybrid spectrometer."[11] This hybrid arrangement employed a stationary PET (002) crystal in the first position and a rotating calcite crystal (100) in the second position. While a satisfactory resolving power of about 1400 for phosphorus Kβ radiation was obtained, the scan was limited to a 6.5-eV range for proper intensity contour at any one PET position. To cover the full range of the 20-eV Kβ spectrum for each compound, therefore, three separate scans at three different settings of the PET crystal had to be obtained, normalized, and joined together. A rigorous evaluation of the intensity contour and energy scale fidelity with this approach is currently under study in this laboratory. Preliminary results are shown in Figure 1. As shown, the spectrum obtained at a PET setting of 83.40° 2θ constitutes a good approximation to the "true" intensity contour. Therefore, the spectra presented here are the uncorrected spectra obtained with the PET crystal set at 83.40° 2θ. Although some distortion of the intensity distribution exists, the spectra are still useful for the assignment of valence electron transitions.

The salts studied were all reagent grade chemicals and no further purification was made. All samples were ground manually to a powder from which a briquette of "infinite thickness" was prepared.

All of the compounds were investigated for effects of decomposition. The calcium salts were used due to the rapid decomposition of the sodium salts. In order to evaluate decomposition each sample was irradiated for a total of 3 hr, spectral data being recorded each hour. Decomposition of all the calcium salts appeared negligible. Spectra were run in a helium atmosphere at 45 kV and 60 mA with a 3-kW chromium X-ray tube; a gas flow proportional counter served as a detector. The use of a pulse height analyzer increased the peak-to-background ratio by a factor of 2. One hundred second counts were taken for each point, each spectrum requiring about 85 points. A Fe(III) $K\alpha_{1,2}$ standard was run after each phosphorus compound as a constant check on wavelength stability, and to provide a reference for energy and intensity calibration. The reproducibility of spectral positions was determined to be within 0.06 eV.

The original copies of the published[13] $L_{2,3}$ spectra were furnished by Henke. The PO_4^{3-} $L_{2,3}$ spectrum was furnished by Wiech.[14]

Theoretical

The molecular orbital approach to the interpretation of X-ray photon emission spectra has been discussed in various articles.[15,16] For molecules of second periodic row elements two spectral series are of interest: Kβ and $L_{2,3}$.

In evaluating molecular bonding the following aspects will be considered: (1) the relative intensity of a formally allowed transition, (2) the correlation, wherever possible, of the Kβ spectra with the $L_{2,3}$ spectra, and (3) correlation of all experimental energy levels with theoretically calculated levels. These factors will be briefly presented to provide an understanding of the framework of interpretation.

The activity of a molecular orbital in a spectral series may be determined from the usual electric dipole selection rules. According to Manne,[17] the intensity, I, of a transition depends upon the contribution of a specific central atom orbital to the ith molecular orbital; *i.e.*

$$I_i \sim \Sigma C_{ji}^2 \qquad (1)$$

where C_{ji} is the central atom's 3p coefficient for a Kβ transition, or the 3s or 3d coefficient in a $L_{2,3}$ transition. Few molecular orbitals are active in both Kβ and $L_{2,3}$ for

(3) Y. Gohshi, unpublished results.
(4) L. V. Azaroff, *Advan. X-Ray Anal.*, **9**, 242 (1966).
(5) P. E. Best, *J. Chem. Phys.*, **44**, 3248 (1966); **49**, 2797 (1968).
(6) G. Karlsson and R. Manne, Preliminary Research Report No. 257, Quantum Chemistry Group, Uppsala, Sweden (1970); *Phys. Scr.*, **4**, 119 (1971).
(7) V. I. Nefedov, *J. Struct. Chem.*, **8**, 612 (1967); **8**, 919 (1967).
(8) D. W. Fischer, *Advan. X-Ray Anal.*, **13**, 159 (1970).
(9) K. Myers and G. Andermann, *J. Chem. Soc., Chem. Commun.*, in press.
(10) H. C. Whitehead, J. D. Layfield, and G. Andermann, *Rev. Sci. Instrum.*, **43**, 50 (1972).
(11) K. Myers, M.S. Thesis, University of Hawaii, 1972.
(12) M. Fichter, Ph.D. Dissertation, University of Munich, 1966.
(13) B. L. Henke and E. N. Smith, *J. Appl. Phys.*, **37**, 922 (1966).
(14) G. Wiech, *Z. Phys.*, **216**, 472 (1968).
(15) D. S. Urch, *Quart. Rev., Chem. Soc.*, **25**, 343 (1971).
(16) D. S. Urch, *Advan. X-Ray Anal.*, **14**, 250 (1971).
(17) R. Manne, *J. Chem. Phys.*, **52**, 5733 (1970).

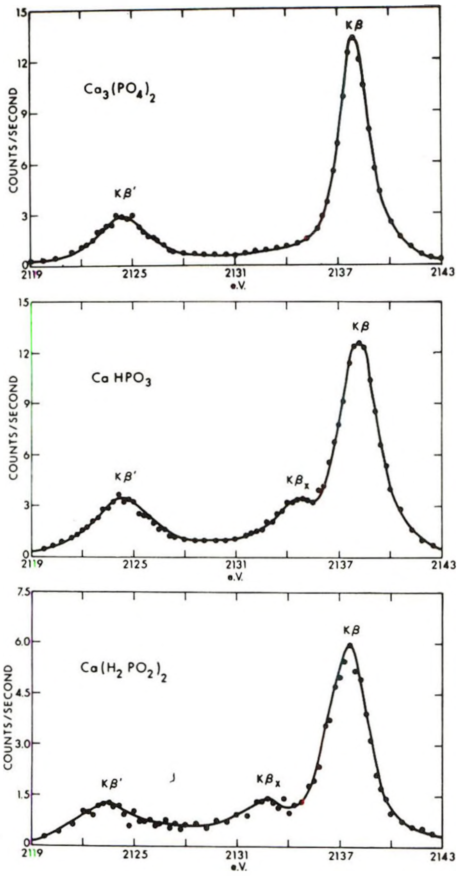

Figure 2. P Kβ emission spectra of (a) $Ca_3(PO_4)_2$, (b) $CaHPO_3$, and (c) $Ca(H_2PO_2)_2$.

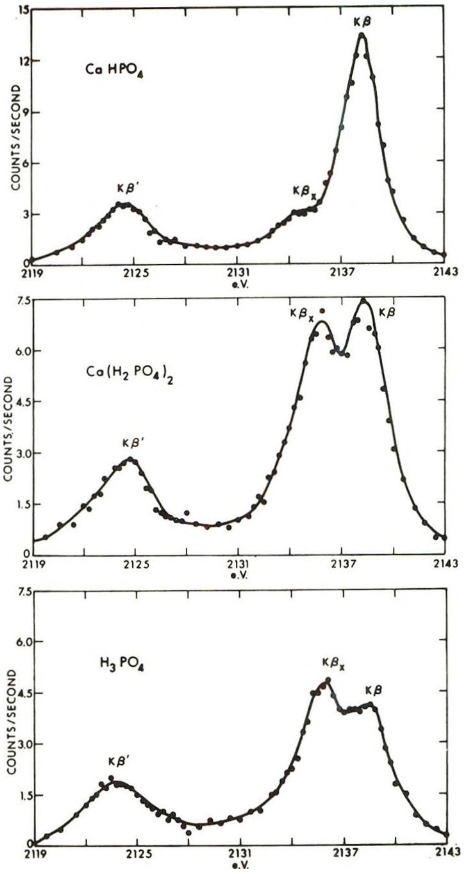

Figure 3. P Kβ emission spectra of (a) $CaHPO_4$, (b) $Ca(H_2PO_4)_2$, and (c) H_3PO_4.

molecules of high symmetry. But as the symmetry is reduced, the resultant greater orbital mixing may allow mutual activity. We can define an experimentally determined valence energy level, E_i, as

$$E_i = h\nu_{if} - \bar{V}_f \tag{2}$$

where, with f = K or L, $h\nu_{if}$ is the transition energy for Kβ and $L_{2,3}$ transitions, respectively, and $\bar{V}_f$ is the 1s or 2p core binding energies usually obtained from photoelectron (ESCA) measurements. If both E_i(K) and E_i(L) are allowed under dipole selection rules[18]

$$h\nu_{iK} - \bar{V}_K = h\nu_{iL} - \bar{V}_L \tag{3}$$

i.e.

$$E_i(\mathrm{K}) = E_i(\mathrm{L}) \tag{4}$$

Equation 4 provides a useful method for the assignment of bands. Equation 2 provides a method for calculating, to a good approximation, the energy levels of the occupied molecular orbitals producing these bands. Simultaneous evaluation of the Kβ and $L_{2,3}$ spectra also provides a comprehensive construct of the total electronic structure.

The interpretation of observed bands in this study is based upon a combined intensity-energy level evaluation model. Selection rules and Manne's intensity arguments have been used to determine the activity of a particular molecular orbital and then the experimental E_i(K), E_i(L) values correlate the Kβ and $L_{2,3}$ spectra with one another and with the theoretically calculated energy level structure.[11]

For molecules with multiple-type ligand bonding the above approach was considered to be especially pertinent. The introduction of a second type of ligand necessarily reduces the overall molecular symmetry, and we hoped to observe the resultant alteration of the electronic distribution. To determine if a particular photon emission line corresponds to simple lowering of symmetry or to a specific ligand effect, an eigenvector analysis was performed. We made use of the fact that the eigenvectors represent the contribution of individual atomic orbitals to the total molecular orbital and that they further indicate whether the contribution is bonding or antibonding.[19]

It should be noted that the CNDO/2 calculations performed were based on the use of significant 3d orbital participation from the central atom. This is in contrast with Manne's work which does not include 3d orbitals. Interpretation of the $L_{2,3}$ spectra, on the basis of Manne's intensity arguments (eq 1), however, would be quite difficult without 3d occupation.[20] Recent theoretical and experimental evidence seems to support the need for invoking 3d orbital participation.[20,21]

Results and Discussion

Starting with the highly symmetrical phosphate ion, $PO_4^{3-}(T_d)$, we have investigated the electronic environment resulting from the substitution of oxygen ligands by hydrogen atoms to give the phosphite and hypophosphite

---

(18) G. Andermann and H. C. Whitehead, *Advan. X-Ray Anal.*, **14**, 453 (1971).

(19) J. A. Pople and D. Beveridge, "Approximate Molecular Orbital Theory," McGraw-Hill, New York, N. Y., 1970.

(20) J. A. Connor, I. H. Hillier, V. Saunders, and M. Barker, *Mol. Phys.*, **23**, 81 (1972).

(21) A. Meisel, R. Szargan, G. Leonhardt, and H. J. Kohler, *J. Phys. (Paris), Colloq. C-4*, **32**, 301 (1971).

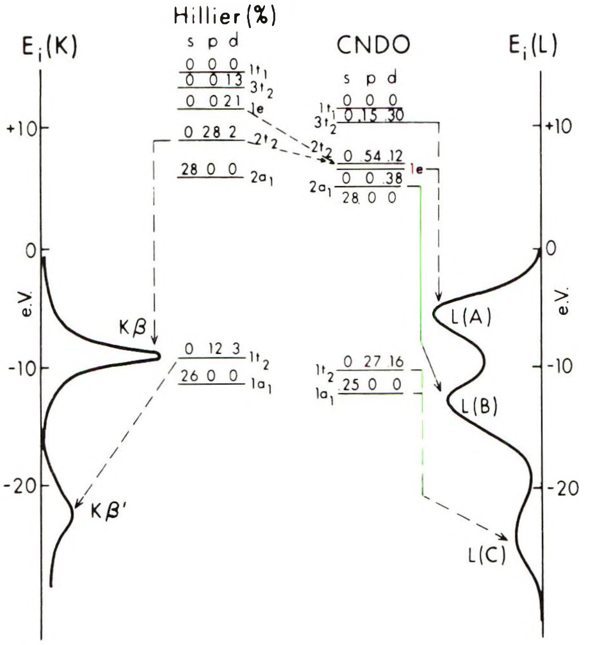

Figure 4. Correlation diagram for PO_4^{3-}

TABLE I: Transition Energies and Experimental Energy Levels

Line	$h\nu$, eV	$-E$(K), eV	Compound	Line	$h\nu$, eV	$-E$(L), eV
Kβ	2137.70	8.50	PO_4^{3-}	L_A	126.4	5.7
Kβ′	2124.50	21.70		L_B	119.6	12.5
				L_C	107.8	24.3
Kβ	2138.23	8.56	HPO_4^{2-}	L_A		
$K\beta_x$	2134.86	11.93		L_B		
Kβ′	2124.21	22.58		L_C		
Kβ	2138.50	9.46	$H_2PO_4^-$	L_A	125.5	8.4
$K\beta_x$	2135.78	12.18		L_B	121.2	12.7
Kβ′	2124.60	23.36		L_C	108	26
Kβ	2138.54		H_3PO_4	L_A		
$K\beta_x$	2135.93			L_B		
Kβ′	2123.30			L_C		
Kβ	2137.70	9.20	HPO_3^{2-}	L_A	125.0	7.9
$K\beta_x$	2133.30	13.60		L_B	121.0	11.9
Kβ′	2124.20	22.70		L_C	108	25
Kβ	2137.75	8.49	$H_2PO_2^-$	L_A	126.0	6.4
$K\beta_x$	2133.03	13.21		L_B	119.4	13.0
Kβ′	2124.20	22.04		L_C	108	24

ions and by the less distinct hydroxy ligands to give phosphoric acid and its mono- and dibasic salts. These two series are shown below.

PO_4^{3-}
(T_d)

$H_2PO_2^-$ (C_{2v}) HPO_3^{2-} (C_{3v}) HPO_4^{2-} (C_{3v}) $H_2PO_4^-$ (C_{2v}) H_3PO_4 (C_{3v})

The full Kβ spectrum for each of these ions is given in Figures 2 and 3. Transition energies for each spectral band and its corresponding valence energy levels, E_i(K) and E_i(L) values, are compiled in Table I. The binding energies, $\bar{V}_f$, necessary to calculate E_i are from the ESCA data furnished by Jolly, *et al.*[22]

A graphical correlation of the Kβ and $L_{2,3}$ spectra is demonstrated in Figures 4-8. In these diagrams the two spectral series are correlated with one another *via* their E_i values and with the CNDO/2 calculated levels, ϵ_i, through the s, p, and d intensity parameters. These parameters were obtained according to eq 1. The activity of a formally allowed transition is deduced on the basis of these parameters.

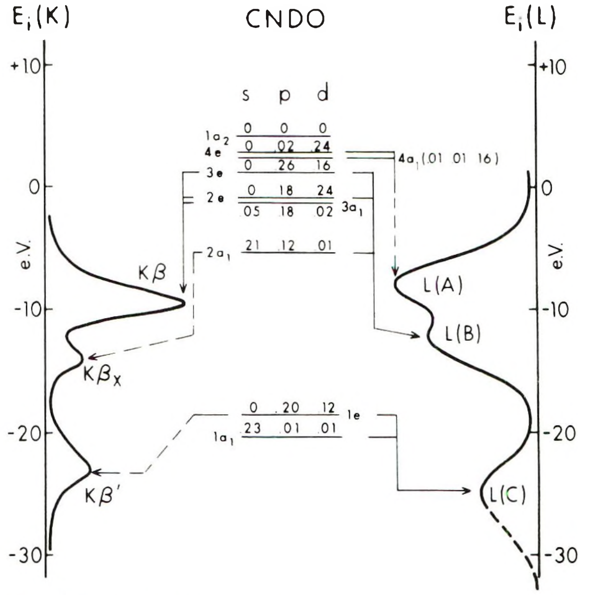

Figure 5. Correlation diagram for HPO_3^{2-}.

The Kβ spectral feature most significantly distinguishing the substituted oxy anions from PO_4^{3-} is the third band, $K\beta_x$; the origin of the band concerns us here. Two possibilities exist; the transition may reflect a symmetry reduction effect, or, as we propose here, it may be attributable to transitions from molecular orbitals defining specific central atom orbital-ligand orbital (CAO-LO) interactions.

The $L_{2,3}$ spectra, however, do not appear to correlate well with such specific ligand bonding.

Each of the molecules is discussed individually, below.

Ligand Characterization. $PO_4^{3-}(T_d)$. Since the 1s level has a_1 symmetry, Kβ transitions are allowed under electric dipole selection rules only from states of t_2 symmetry. The two observed lines are, therefore, assigned as

$$K\beta \quad 2t_2 \longrightarrow 1s$$
$$K\beta' \quad 1t_2 \longrightarrow 1s$$

The electronic structure calculated by CNDO/2, as shown in Figure 4, predicts a third transition from $3t_2$ on the high-energy side of Kβ. However, such a line is not observed here or for other similar oxy anions of T_d symmetry.[6,20] Moreover, this is in agreement with *ab initio* calculations which give a zero 3p coefficient for $3t_2$.[20]

An analysis of the atomic orbital eigenvector contribution to the valence molecular orbitals has helped to establish the assignment of the experimentally observed bands.[11] The $2t_2$ molecular orbital appears to consist primarily of phosphorus 3p and oxygen 2p atomic coefficients with a very small contribution from phosphorus 3d and oxygen 2s. The atomic components of the $1t_2$ level are almost exclusively of phosphorus 3p and oxygen 2s character. Each Kβ band thus appears to be associated with a specific ligand orbital. We, therefore, designate the Kβ and Kβ′ bands as resulting from P_{3p}-O_{2p} and P_{3p}-O_{2s} bonding, respectively.

A more complex spectrum than Kβ may be anticipated for $L_{2,3}$, since transitions are formally allowed from va-

---

[22] M. Pelavin, D. N. Hendrickson, J. M. Hollander, and W. L. Jolly, *J. Phys. Chem.*, **74**, 1164 (1970).

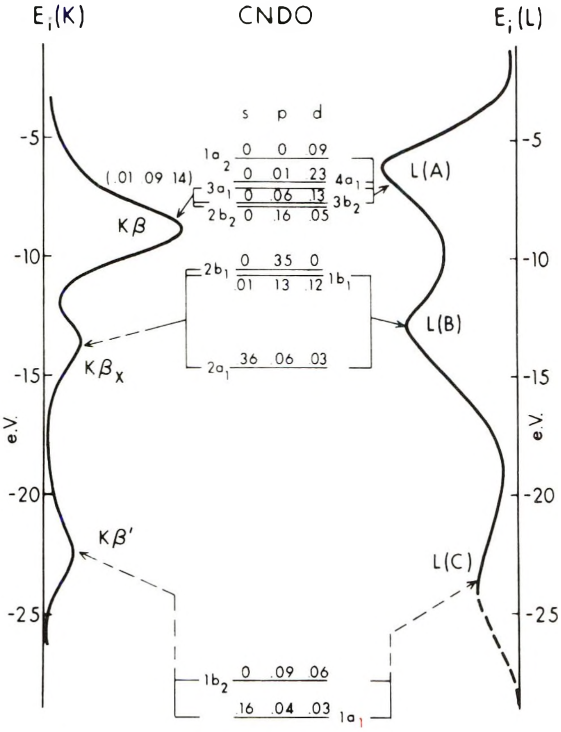
E_i(K)
CNDO
E_i(L)
s p d
Kβ
Kβ_X
Kβ'
L(A)
L(B)
L(C)
e.V.
-5
-10
-15
-20
-25
(.01 09 14)
1a_2 0 0 .09
3a_1 0 .01 .23 4a_1
.0 .06 .13 3b_2
2b_2 0 .16 .05
2b_1 0 .35 0
.01 .13 .12 1b_1
2a_1 .36 .06 .03
1b_2 0 .09 .06
.16 .04 .03 1a_1

Figure 6. Correlation diagram for $H_2PO_2^-$.

TABLE II: Comparison of Calculated Eigenvalues (ϵ_i) with Experimental Energy Levels (E_i) for PO_4^{3-}

	ΔE_i, eV	$\Delta\epsilon_i$ (Hillier), eV	$\Delta\epsilon_i$ (CNDO), eV
$K\beta - L_B$	3.6	2.9	1.40
$L_A - L_B$	6.8	6.6	3.17 (4.96)
$L_A - K\beta$	3.2	3.7	1.77 (3.56)
$L_A - L_C$	18.6	24.3	20.89 (22.68)
$K\beta - K\beta'$	13.20	17.9	16.99

lence orbitals of a_1, e, t_2, and t_1 symmetry, with the major component of the transition moment involving both the 3s and 3d atomic orbitals. As seen in Table I and Figure 4, $E(K\beta)$ occurs between $E(L_A)$ and $E(L_B)$ indicating distinct orbital origins for these three bands. Assuming that the band L_A includes orbitals lying above $2t_2$, then L_B must originate in orbitals lying below $2t_2$. The occurrence of $E(L_C)$ about 2 eV below $E(K\beta')$ suggests the activity of the lower $1a_1$ orbital ($3s^2$, 0.25) with $1t_2$ ($\Sigma\ 3d^2$, 0.16).

A reasonable assignment of the $L_{2,3}$ spectrum for PO_4^{3-} is, thus, the following

$$L_A\ 1e + 3t_2 \longrightarrow 2p$$
$$L_B\ 2a_1 \longrightarrow 2p$$
$$L_C\ 1a_1 + 1t_2 \longrightarrow 2p$$

The $1t_1$ orbital has not been included, since it does not have any central atom contribution and would, therefore, be extremely weak.

The $K\beta$ and $L_{2,3}$ assignments are further supported by a comparison of the experimentally and theoretically calculated energy levels. Since the latter values are consistently higher than the former, there is no direct, absolute correlation possible. However, the experimental and theoretical values may be correlated on a relative basis. For example, although $E_i(K) \neq \epsilon_i$ and $E_j(L) \neq \epsilon_j$, $E_i(K) - E_j(L)$ may be compared with $\epsilon_i - \epsilon_j$ for two bands in different, or in the same, spectra. Such a correlation for PO_4^{3-} is shown in Table II. Also shown is the same comparison for an *ab initio* calculated structure by Hillier, *et al.*[20] Although our assignment is the same as Hillier's, the agreement between experimental and theoretical values is considerably better for the *ab initio* calculation. In parentheses under the CNDO/2 column is also given the correlation when only the $3t_2$ level is used to calculate ϵ_i for L_A, as the 1e level has been misordered in this calculation. The agreement with Hillier's calculations and with

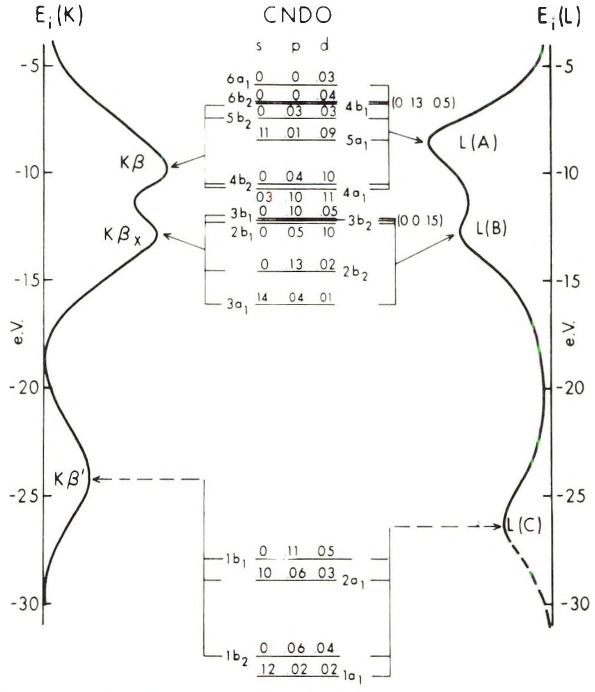
E_i(K)
CNDO
E_i(L)
s p d
Kβ
Kβ_X
Kβ'
L(A)
L(B)
L(C)
e.V.
-5
-10
-15
-20
-25
-30
6a_1 0 0 .03
6b_2 0 0 .04 4b_1
5b_2 0 .03 .03
.11 .01 .09 5a_1
(0 13 05)
4b_2 0 .04 .10
.03 .10 .11 4a_1
3b_1 0 .10 .05 3b_2
(0 0 15)
2b_1 0 .05 .10
0 .13 .02 2b_2
3a_1 .14 .04 .01
1b_1 0 .11 .05
.10 .06 .03 2a_1
1b_2 0 .06 .04
.12 .02 .02 1a_1

Figure 7. Correlation diagram for $H_2PO_4^-$.

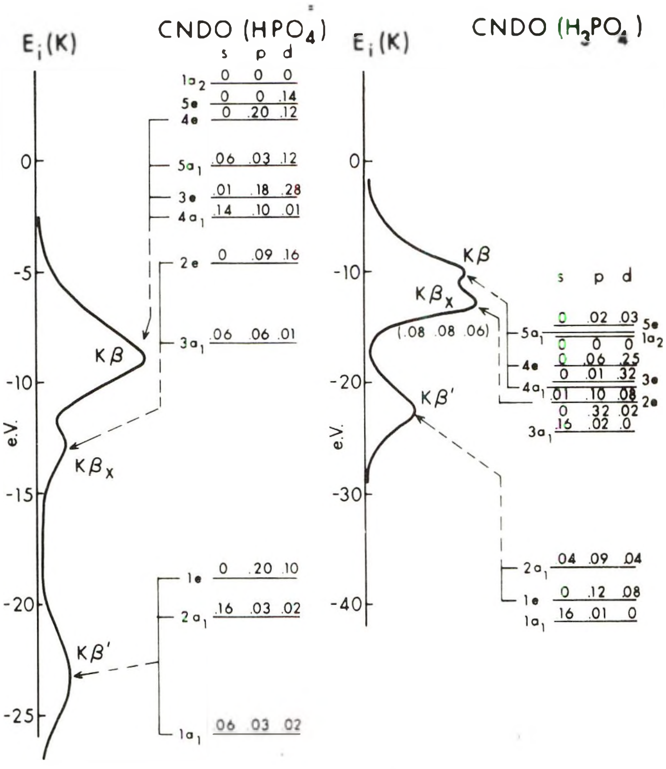
E_i(K)
CNDO (HPO_4)
CNDO (H_3PO_4)
s p d
Kβ
Kβ_X
Kβ'
e.V.
0
-5
-10
-15
-20
-25
-30
-40
1a_2 0 0 0
5e 0 0 .14
4e 0 .20 .12
5a_1 .06 .03 .12
3e .01 .18 .28
4a_1 .14 .10 .01
2e 0 .09 .16
3a_1 .06 .06 .01
1e 0 .20 .10
2a_1 .16 .03 .02
1a_1 .06 .03 .02
(.08 .08 .06)
5a_1 0 .02 .03 5e
0 0 0 1a_2
4e 0 .06 .25
4a_1 0 .01 .32 3e
.01 .10 .08 2e
0 .32 .02
3a_1 .16 .02 0
2a_1 .04 .09 .04
1e 0 .12 .08
1a_1 .16 .01 0

Figure 8. Correlation diagram for HPO_4^{2-} and H_3PO_4.

experiment improves greatly. Apparently, the 1e level is most significantly affected by the approximations made in the CNDO/2 method, or in the initial choice of parameters.

Eigenvector analysis shows band L_A to represent P_{3d}–O_{2p} bonding as the $3t_2$ and 1e levels are compared predominantly of phosphorus 3d and oxygen 2p atomic coefficients. Band L_B, however, contains significant bonding contributions from both the oxygen 2s and 2p atomic orbitals with phosphorus 3s. Similarly, L_C mixes phosphorus 3s and 3d in the bonding with oxygen 2s orbitals. These two bands, and thus the $L_{2,3}$ spectrum, cannot be associated with central atom orbital–ligand orbital (CAO–LO) bonding.

Although no significant mutual activity is noted for the two spectra, simultaneous evaluation of $L_{2,3}$ with Kβ did allow a more complete description of the valence electronic structure.

Oxygen Atom Ligand Replacement by Hydrogen Atom Ligand. HPO_3^{2-} (C_{3v}). Under C_{3v} symmetry electric dipole selection rules allow Kβ emission transitions from a_1 and e molecular orbitals.

The main Kβ band is assignable to the close lying $3a_1$ and 2e levels. Also included is the 3e orbital due to its large phosphorus 3p coefficient (Figure 5). Similarly, Kβ′ originates from the 1e molecular orbital.

Unlike for other C_{3v} molecules of second periodic row atoms,[5,6] no high-energy Kβ″ band is discernible for HPO_3^{2-}. Rather a lower energy $K\beta_x$ transition is noted. The assignment of $K\beta_x$ follows immediately as only one orbital, $2a_1$, falls between those assigned to Kβ and Kβ′.

Analysis of the $3a_1$, 2e, and 3e molecular orbital levels shows the phosphorus 3p atomic orbital to be bonding almost exclusively with the oxygen 2p orbitals. The main Kβ band may, then, still be described as representing P_{3p}–O_{2p} bonding. Analogously, Kβ′ is again associated with P_{3p}–O_{2s} bonding. In the $2a_1$ molecular orbital, however, the ligand contributions are most significantly from the single hydrogen 1s orbital and to a lesser extent from the three oxygen 2s orbitals. This is the only level containing significant hydrogen bonding. We, therefore, denote the $K\beta_x$ band as reflecting primarily P_{3p}–H_{1s} bonding.

Thus, as shown in Figure 5, the Kβ spectral assignment is

$$\begin{array}{lll} K\beta & 3a_1 + 2e + 3e \longrightarrow 1s & P_{3p}\text{–}O_{2p} \\ K\beta_x & 2a_1 \longrightarrow 1s & P_{3p}\text{–}H_{1s} \\ K\beta' & 1e \longrightarrow 1s & P_{3p}\text{–}O_{2s} \end{array}$$

$L_{2,3}$ transitions under C_{3v} symmetry are allowed from a_1, a_2, and e levels with significant phosphorus 3s or 3d orbital coefficients. As seen in Table I and Figure 5, none of the E(L) values coincide exactly with any E(K), suggesting the possibility of distinct bonding features for each spectral band. A reasonable $L_{2,3}$ assignment[11] is

$$\begin{array}{ll} L_A & 3b_2 + 3a_1 + 4a_1 + 1a_2 \longrightarrow 2p \\ L_B & 2a_1 + 1b_1 \longrightarrow 2p \\ L_C & 1a_1 + 1b_2 \longrightarrow 2p \end{array}$$

Eigenvector analysis indicates no basis for designating these L bands to specific CAO–LO bonding.[11] Evaluation of the $L_{2,3}$ spectrum has, however, provided for observation of transitions from the $4a_1$, 4e, and $1a_1$ orbitals and further justifies the assumption of significant 3d orbital participation in bonding.[11]

The relative internal consistency of our assignments is given in Table III. The good correlation between the experimental and theoretical energy levels lends further support to our assignments.

TABLE III: Comparison of Calculated Eigenvalues (ϵ_i) with Experimental Energy Levels (E_i) for HPO_3^{2-}

	ΔE_i, eV	$\Delta\epsilon_i$ (CNDO), eV
$K\beta - K\beta_x$	4.40	4.89
$K\beta - L_B$	2.30	2.25
$L_A - L_B$	4.0	5.3
$L_A - K\beta$	1.7	3.1
$K\beta - K\beta'$	13.50	17.78

$H_2PO_2^-$ (C_{2v}). Under C_{2v} symmetry transitions from a_1, b_1, and b_2 molecular orbitals to the 1s level are formally allowed.

The Kβ spectrum's similarity to that observed for HPO_3^{2-} substantiates the spectral distinction between P–O and P–H bonding. The interpretation is basically the same as for HPO_3^{2-} but with greater complexity due to the further lowering of symmetry.

The CNDO/2 calculated electronic structure of $H_2PO_2^-$ is indicated in Figure 6. The Kβ assignment, as shown graphically in Figure 6, is

$$\begin{array}{lll} K\beta & 2b_2 + 3b_2 + 3a_1 \longrightarrow 1s & P_{3p}\text{–}O_{2p} \\ K\beta_x & 2a_1 + 2b_1 + 1b_1 \longrightarrow 1s & P_{3p}\text{–}H_{1s} \\ K\beta' & 1a_1 + 1b_1 \longrightarrow 1s & P_{3p}\text{–}O_{2s} \end{array}$$

The $L_{2,3}$ spectrum resembles those for PO_4^{3-} and HPO_3^{2-} and the assignment follows analogously. As shown in Table I and Figure 6, $E(L_B)$ approximately equals $E(K\beta_x)$ indicating mutual spectral origins. Only the $2b_1$ orbital will not contribute to L_B. The L_A band includes most of the orbitals active in Kβ and several higher lying levels, $E(L_A) > E(K\beta)$. The transition L_C results from $1a_1$ and $1b_2$ activity as does Kβ′.

The $L_{2,3}$ assignment then is

$$\begin{array}{ll} L_A & 4a_1 + 4e \longrightarrow 2p \\ L_B & 2a_1 + 2e + 3e \longrightarrow 2p \\ L_C & 1a_1 + 1e \longrightarrow 2p \end{array}$$

Again there is no CAO–LO bonding designation possible for $L_{2,3}$. Note that the decreased C_{2v} symmetry results in greater activity in both spectra. Whereas the Kβ and $L_{2,3}$ spectra represent almost mutually exclusive levels for PO_4^{3-} (T_d), the Kβ and $L_{2,3}$ transitions contain most of the same orbital activity for $H_2PO_2^-$.

Table IV, comparing the experimentally and theoretically determined electronic structures, lends further support to the assignments made for $H_2PO_2^-$.

Oxygen Atom Ligand Replacement by Hydroxy Ligand. In the phosphite and hypophosphite ions there appears to be experimental and theoretical basis for associating the various Kβ bands with specific bonding within the molecule. For the hydroxy compounds the bonding structure may be considerably more complex. There is a larger basis set to consider producing a larger series of molecular levels. Furthermore, the oxygen and hydroxy ligands are similar, thus yielding similar eigenvalues. Despite these complications, the Kβ spectra do appear to distinguish between the two bonding ligands. As hydroxy ligands are substituted for oxygen, the $K\beta_x$ band increases in intensity (Figure 3) at the expense of Kβ. Theoretical justification for such an assignment is, however, desirable.

$H_2PO_4^-$ (C_{2v}). The calculated electronic structure of $H_2PO_4^-$ (Figure 7) does not constitute two distinct sets of levels assignable to Kβ and $K\beta_x$. Rather, there results a successive group of molecular orbitals with varying ligand orbital components. The atomic coefficients are larger for

TABLE IV: Comparison of Calculated Eigenvalues (ϵ_i) with Experimental Energy Levels (E_i) for $H_2PO_2^-$

	ΔE_i, eV	$\Delta\epsilon_i$ (CNDO), eV
$K\beta - K\beta_x$	4.72	4.42
$K\beta - L_B$	4.13	5.11
$L_A - L_B$	6.6	5.7
$L_A - K\beta$	2.47	0.62
$K\beta - K\beta'$	13.53	20.94

TABLE V: Comparison of Calculated Eigenvalues (ϵ_i) with Experimental Energy Levels (E_i) for $H_2PO_4^-$

	ΔE_i, eV	$\Delta\epsilon_i$ (CNDO), eV
$K\beta - K\beta_x$	2.72	4.94
$K\beta - L_B$	2.86	4.31
$L_A - L_B$	4.3	5.1
$L_A - K\beta$	1.44	0.80
$K\beta - K\beta'$	13.86	20.90

TABLE VI: Half-Widths for $K\beta$ Spectral Bands

Spectrum	Line	Half-Width, eV	No. of transitions
PO_4^{3-}	$K\beta$	2.15	(1)
	$K\beta'$	4.09	(1)
HPO_4^{2-}	$K\beta$	2.76	(4)
	$K\beta_x$	3.98	(2)
	$K\beta'$	4.24	(3)
$H_2PO_4^-$	$K\beta$	2.92	(4)
	$K\beta_x$	3.21	(4)
	$K\beta'$	4.24	(3)
H_3PO_4	$K\beta$	3.07	(3)
	$K\beta_x$	3.36	(1)
	$K\beta'$	4.54	(2)
HPO_3^{2-}	$K\beta$	2.91	(3)
	$K\beta_x$	3.05	(1)
	$K\beta'$	4.39	(1)
$H_2PO_2^-$	$K\beta$	2.91	(3)
	$K\beta_x$	2.29	(3)
	$K\beta'$	4.39	(2)

the hydroxy-oxygen 2p orbitals in the lower lying levels but become progressively less hydroxy and more oxygen in character in the higher levels. A complete assignment is not immediately evident, however.

The two active $3a_1$ and $2b_2$ molecular orbitals are strongly bonding with the hydroxy-oxygen 2p orbitals, but only weakly bonding with the oxygen atom 2p orbitals. These levels are assignable to $K\beta_x$. For the higher lying levels, $4a_1$, $4b_2$, $4b_1$, and $5b_2$, the converse bonding scheme holds. We attribute these orbitals to be responsible for the $K\beta$ band. However, between these two definitive groups of orbitals lie the $2b_1$ and $3b_1$ molecular orbitals, also active in $K\beta$. The hydroxy-oxygen 2p coefficients are large in these molecular orbitals, but are antibonding. The pure oxygen atom 2p orbitals, conversely, are bonding but small. Association with neither $K\beta$ not $K\beta_x$ is obvious. We have arbitrarily assigned the $2b_1$ and $3b_1$ levels to be contributing to the $K\beta_x$ band.

$K\beta'$ is again accredited to participation by the molecular orbitals with large oxygen 2s components. However, the $1b_2$ orbital's oxygen 2s coefficient is from the hydroxy-oxygen ligand. $K\beta'$ then represents P_{3p}-O_{2s} and P_{3p}-$O_{2s}H_{1s}$ bonding which is not resolved here.

$$K\beta \quad 4a_1 + 4b_2 + 5b_2 + 4b_1 \longrightarrow 1s \quad P_{3p}{-}O_{2p}$$
$$K\beta_x \quad 3a_1 + 2b_2 + 2b_1 + 3b_1 \longrightarrow 1s \quad P_{3p}{-}O_{2p}H_{1s}$$
$$K\beta' \quad 1b_2 + 2a_1 + 1b_1 \longrightarrow 1s \quad P_{3p}{-}O_{2s}H_{1s} \text{ and } P_{3p}{-}O_{2s}$$

The $L_{2,3}$ spectrum resembles that for the other oxy anions. The interpretation basically follows the discussion given for $H_2PO_2^-$, also of C_{2v} symmetry. Specifically note that the $E(K\beta_x)$ and $E(L_B)$ levels are approximately the same suggesting extensive mutual spectral activity, as for $H_2PO_2^-$.

$$L_A \quad 4a_1 + 4b_2 + 5a_1 + 5b_2 + 4b_1 + 6b_2 + 6a_1 \longrightarrow 2p$$
$$L_B \quad 3a_1 + 2b_1 + 3b_2 + 3b_1 \longrightarrow 2p$$
$$L_C \quad 1a_1 + 1b_2 + 2a_1 + 1b_1 \longrightarrow 2p$$

Here again, the low symmetry allows for many common features in $K\beta$ and $L_{2,3}$ transitions. Table V compares the experimental and theoretical electronic structures for internal consistency.

HPO_4^{2-} and $H_3PO_4(C_{3v})$. No $L_{2,3}$ spectra are available for these two molecules, but this does not appear to hinder the $K\beta$ spectral interpretation.

The $K\beta$ spectra for both molecules show the two high-energy bands now recognized as characteristic of two different bonding interactions. The calculated electronic structures, Figure 8, confirm this. Two groups of molecular orbitals, one with large phosphorus 3p-oxygen 2p bonding coefficients and the other with phosphorus 3p and hydroxy-oxygen 2p coefficients, are formed which are associated with the $K\beta$ and $K\beta_x$ bands, respectively.

Considerably more mixing of ligand orbitals is observed for HPO_4^{2-} and H_3PO_4 than for the simpler HPO_3^{2-} molecule, also of C_{3v} symmetry. But the mixing is not as extensive as for the $H_2PO_4^-(C_{2v})$ hydroxy compound. The assignments here appear to be more obvious. As for $H_2PO_4^-$, however, $K\beta'$ represents the unresolved P_{3p}-O_{2s} and P_{3p}-$O_{2s}H_{1s}$ bonding.

The $K\beta$ assignments then are

HPO_4^{2-}

$$K\beta \quad 4a_1 + 3e + 5a_1 + 4e \longrightarrow 1s \quad P_{3p}{-}O_{2p}$$
$$K\beta_x \quad 3a_1 + 2e \longrightarrow 1s \quad P_{3p}{-}O_{2p}H_{1s}$$
$$K\beta' \quad 1a_1 + 2a_1 + 1e \longrightarrow 1s \quad P_{3p}{-}O_{2s} \text{ and } P_{3p}{-}O_{2s}H_{1s}$$

H_3PO_4

$$K\beta \quad 4a_1 + 5a_1 + 4e \longrightarrow 1s \quad P_{3p}{-}O_{2p}$$
$$K\beta_x \quad 2e \longrightarrow 1s \quad P_{3p}{-}O_{2p}H_{1s}$$
$$K\beta' \quad 2a_1 + 1e \longrightarrow 1s \quad P_{3p}{-}O_{2s} \text{ and } P_{3p}{-}O_{2s}H_{1s}$$

Evaluation of Half-Widths. The effects of electronic structural modification by ligand substitution are clearly manifested in the $K\beta$ spectrum. The $L_{2,3}$ spectrum, probably because of the poor resolution, is less descriptive in this respect. While the $K\beta$ bands are associated with specific CAO–LO bonding, further information may be obtainable from the half-widths of these bands. Table VI lists the full-widths-at-half maximum for each band in each $K\beta$ spectrum.

Two pertinent factors may affect the widths of spectral bands; unresolved transitions and solid state broadening. Both factors have special significance in bonding studies. Of possible interest is the broadening due to unresolved transitions. The $K\beta$ band depicts an increase in bandwidth with an increase in the number of transitions assigned to this band. In the series $PO_4^{3-} \rightarrow HPO_3^{2-} \rightarrow H_2PO_2^-$ the $K\beta$ bandwidth has increased by 50% for $HPO_3^{2-}(C_{3v})$ and $H_2PO_2^-(C_{2v})$ correlating nicely with the two additional transitions assigned to these latter two ions' Kβ band. Furthermore, note that the half-width values are the same (2.9 eV) for HPO_3^{2-} and $H_2PO_2^-$ in agreement with the same number of assigned transitions. A similar trend for Kβ may be seen in comparing PO_4^{3-}-(T_d) with HPO_4^{2-}(C_{3v}) and $H_2PO_4^-$(C_{2v}). Both of these latter two ions have four transitions assigned to their Kβ bands, and the half-widths are considerably greater than that for PO_4^{3-}. Kβ half-width for $H_2PO_4^-$ is somewhat greater than for HPO_4^{2-}, although both are associated with the same number of transitions. Only for H_3PO_4, the Kβ half-width does not appear to fit this trend, the half-width being considerably larger than those for HPO_4^{2-} and $H_2PO_4^-$ with fewer transitions assigned to the band. However, H_3PO_4 was a "syrupy liquid," not a solid like the salts. Different states of matter may exhibit different broadening effects so that a correlation for H_3PO_4 with the other compounds is not pertinent.

The Kβ' band exhibits a similar trend becoming broader with a reduction of symmetry and the subsequent greater number of active transitions. Comparison of the Kβ_x bands is more difficult as no Kβ_x band is observed for PO_4^{3-}. There does, then, appear to be a definite correlation between spectral bandwidths and molecular symmetry. Thus, while the spectral bands have been designated as reflecting specific ligand bonding, the bandwidths may be associated with symmetry effects. The CNDO/2 calculations indicate that some of these transitions are over 1 eV apart and thus should be resolvable with higher quality instrumentation.

Some General Comments. Evaluation of the hydroxy compounds indicates the ability of X-ray photon emission spectroscopy to distinguish even among similar ligands. In addition, the spectral positions of these distinct bands appear significant. The occurrence of the transitions due to hydroxy-oxygen ligand bonding at lower energies than those arising from oxygen bonding indicates the capability to detect the environment generated by nonadjacent atoms. Thus, not only different ligand atoms, but even the same ligand atoms in modified environments may be distinguished. In the case of the hydroxy ligand, bond formation between the oxygen and hydrogen atoms results in an initially higher ionization potential for the hydroxy ligand with respect to the oxygen ligand. Thus, the Kβ band corresponding to P_{3p}-$O_{2p}H_{1s}$ bonding occurs at lower energy than that describing P_{3p}-O_{2p} bonding.

Another interesting trend may be noted for the phosphite and hypophosphite ions. The Kβ_x band defining P_{3p}-H_{1s} bonding lies at considerably higher energy than the Kβ' band describing P_{3p}-O_{2s} bonding. Such an order may be anticipated from perturbation effects alone, the more electronegative ligand producing a lower molecular energy state. A correlation between electronegativity and spectral position necessarily suggests practical applications for ligand characterization.

A comprehensive comparison of our interpretations with previous work is not possible as only unsubstituted oxy anions have been studied to any appreciable degree. As mentioned previously, Fichter has investigated the Kβ spectrum for the same phosphorus oxy anions that we studied here, but his spectra do not resolve the Kβ and Kβ_x bands as well.[12] Furthermore, Fichter's interpretation is not on a molecular model. The $L_{2,3}$ spectrum of $H_2PO_4^-$ has been discussed by several people.[7,16,20] However, all assumed a T_d symmetry for the ion, whereas we have found it necessary to consider C_{2v} symmetry. Nevertheless, one appropriate point of comparison is their assignment of the L_A band to transitions from molecular orbitals with significant 3d orbital occupation, in agreement with our assignment. Hillier further supplements a similar assignment[20] with photoelectron data and *ab initio* calculations.

Only one example of nonidentical ligand bonding evaluation is available for discussion. Karlsson and Manne[6] has studied the SO_3F^- ion predicting three additional molecular orbital levels at lower energies to those calculated for SO_3^{2-}. This is analogous to the structures we observed here for the substituted phosphorus oxy anions. However, the experimental spectrum as reported does not split out these additional levels for SO_3F^- and Karlsson and Manne attach no particular significance to them.

Conclusions

Investigation of these simple phosphorus oxy anions has provided considerable insight into bonding processes *vis a vis* ligand effects. Several general conclusions may be appropriate.

First, and most importantly, X-ray photon emission spectroscopy appears to provide direct spectroscopic capability as a central atom probe within a molecule.

Second, the capability to act as a central atom probe allows differentiation between nonidentical ligands. This spectral distinction between ligands offers X-ray photon emission spectroscopy as a pratical tool for ligand characterization.

Third, while with lower molecular symmetry the Kβ and $L_{2,3}$ spectra may represent much of the same information, a comprehensive construct of the electronic structure appears to necessitate evaluation of both of these spectral series. This is especially important for molecules of high symmetry for which the spectral series may be mutually exclusive.

Acknowledgments. We gratefully acknowledge support from the National Science Foundation. We are indebted to Dr. R. Cramer for helpful discussions.

Fluorescence and Absorption Spectra of Polyphenyls. Theoretical Study on the Band Shape

Fabio Momicchioli,* Maria C. Bruni, and Ivan Baraldi

Istituto di Chimica Fisica, Universita di Modena, 41100 Modena, Italy (Received July 7, 1972)

Publication costs assisted by Consiglio Nazionale delle Ricerche (Roma)

Intramolecular reasons were sought for the deviation of absorption and emission spectra of polyphenyls from the mirror image relation. As a working hypothesis it was supposed that the differences between absorption and fluorescence spectra originate in the excitation of the twisting mode of interannular bonds. Curves of the potential energy as a function of the dihedral angle between phenyl rings were obtained for the ground state and the lowest singlet excited states by using semiempirical calculation procedures. A polynomial approximation was adopted for the potential functions so that vibrational energies and wave functions could be calculated simply by expanding the wave functions in a harmonic oscillator basis set. By this technique, Franck–Condon distributions were obtained for both absorption and emission. The contours of the distributions enabled us to explain both the fine structure of fluorescence spectra and the structureless long-wavelength uv bands in polyphenyls.

I. Introduction

The comparison between absorption and fluorescence spectra and their departure from the mirror image relation provides important information about the relative locations of the lowest excited states of a molecule and the shape of the potential energy surfaces, thus helping the theoretician to elucidate the energy decay mechanisms.

If aromatic molecules are considered[1] it is found that the mirror image relation between absorption and emission curves is better retained by single aromatic systems (*e.g.*, benzene, anthracene, naphthacene, etc.), while molecules where a few aromatic systems are connected to one another essentially by single bonds generally show fluorescence spectra which are quite different from absorption spectra. Polyphenyls are typical examples of the latter type of molecule. In Figure 1 we have reported absorption and fluorescence spectra of the first two terms of the polyphenyl series, *i.e.*, biphenyl and *p*-terphenyl, together with those of 4-vinylbiphenyl. The most evident difference between absorption and emission spectra is that the former appear to be completely diffuse, while the latter show a well-resolved vibrational structure.

In the present work we attempt a theoretical interpretation of this experimental fact. The paper consists of two parts. In the first part, the correlation between the lowest singlet excited states of the molecules in Figure 1 is stated so as to single out the electronic state from which the emission originates and the vibrational mode to which the spacing of the fine structure has to be assigned in each case. In the second part, energy potential curves corresponding to a low-frequency vibrational mode, namely, the twisting of the interannular bonds, are obtained for the ground state and the lowest excited states, and finally distributions of transition probability are calculated for both emission and absorption. It is on this basis that the difference between the shape of the absorption bands and that of fluorescence bands in polyphenyls will be discussed.

II. Origin of the Emission

As the first step in explaining the spectra reported in Figure 1, we must state, in each case, whether the emission originates from the same singlet excited state that is chiefly responsible for the absorption intensity or not. To this end we carried out a correlation between the lowest singlet excited states of the molecules in question using a PPP calculation procedure for the treatment of π electrons. Alternant hydrocarbon simplifications[2] were adopted, and the configuration mixing was extended to include all the singly excited configurations. Two-electron repulsion integrals (γ_{pq}) were calculated according to Pariser–Parr procedure,[3] and molecular geometries were chosen as follows: R_{CC} = 1.397 Å in the rings, R_{CC} = 1.507 Å between the rings,[4,5] and R_{CC} = 1.46 and 1.34 Å for the essential single and essential double bond, respectively, in the vinyl group. The corresponding elements of the core matrix hold −2.30, −1.44, −1.76, and −2.95 eV, the first being arbitrarily fixed and the others derived according to the relationship $H_{pq}{}^{c} = KR_{pq}{}^{-6}$, previously used by one of us.[6] Bond angles were assumed equal to 120° and, in this model calculation, the dihedral angle between the planes of the phenyl rings was equal to zero.

The results are reported in Figure 2 where the excited states are labeled according to their symmetry properties (D_{2h} point group). Figure 2 suggests that in biphenyl the emission originates from the $^1B_{3u}$ state, while in *p*-terphenyl the fluorescence (*F*) is due to the $^1B_{2u} \rightarrow {}^1A_g$ transition. On the other hand, the $^1B_{3u} \leftarrow {}^1A_g$ transitions (short-axis polarized) are very weak and they are hidden by the $^1B_{2u} \leftarrow {}^1A_g$ transitions (long-axis polarized), which provide almost all the intensity of the absorption band in both biphenyl and *p*-terphenyl. In 4-vinylbiphenyl, where the excited states can be easily correlated with those of the other molecules by analyzing the CI coefficients,[6,7] the situation is similar to that of *p*-terphenyl, except for the energy difference between the two lowest excited states, which is very small. In conclusion, a direct com-

---

(1) I. B. Berlman, "Handbook of Fluorescence Spectra of Aromatic Molecules," Academic Press, New York, N. Y., 1965.
(2) R. Pariser, *J. Chem. Phys.*, **24**, 250 (1956).
(3) R. Pariser and R. G. Parr, *J. Chem. Phys.*, **21**, 767 (1953).
(4) J. Trotter, *Acta Crystallogr.*, **14**, 1135 (1961).
(5) A. Hargreaves and S. H. Rizvi, *Acta Crystallogr.*, **15**, 365 (1962).
(6) F. Momicchioli and A. Rastelli, *J. Mol. Spectrosc.*, **23**, 310 (1967).
(7) F. Momicchioli and A. Rastelli, *J. Chem. Soc. B*, 1353 (1970).

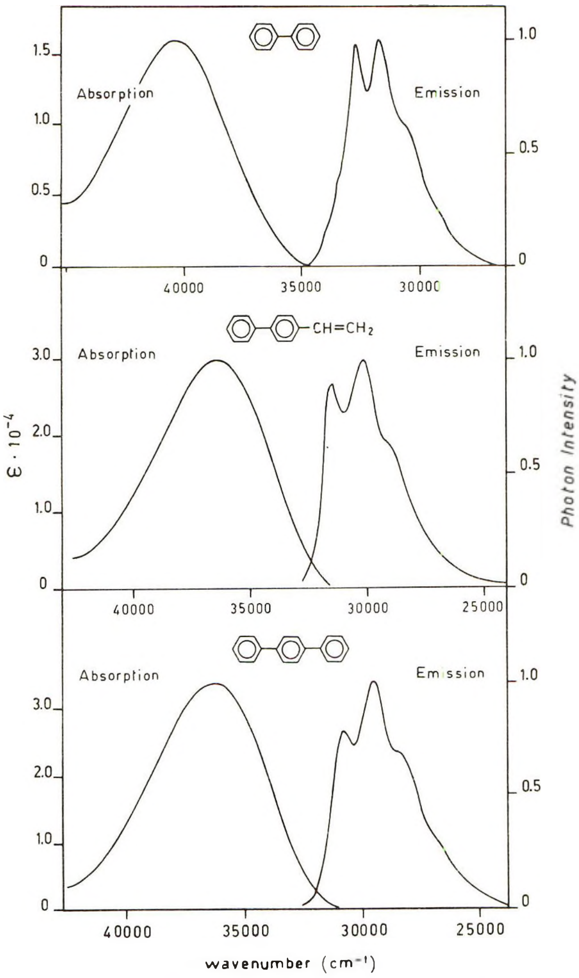

Figure 1. Solution uv and fluorescence spectra of biphenyl, 4-vinylbiphenyl, and *p*-terphenyl (from the top downward) reported from ref 1. Cyclohexane was the solvent and the spectra were recorded at room temperature. The wave numbers of the exciting radiations for the emission spectra were ~39,410 cm^{-1} for biphenyl and 33,000 cm^{-1} for 4-vinylbiphenyl and *p*-terphenyl.

parison between the absorption and emission curves reported in Figure 1 can only be made for *p*-terphenyl and 4-vinylbiphenyl, while in biphenyl the two transitions involve different excited states. This interpretation is supported by some experimental facts. First of all, we refer to the comparison[1,8] between the natural fluorescence lifetime (τ_{0c}) derived from the integrated intensity of the absorption band (*e.g.*, by using Forster's formula[9]) and that obtained by the relationship $\tau_{0m} = \tau/Q$, where τ is the measured decay time and Q is the quantum yield. In Table I, where the values of τ_{0m} and τ_{0c} are reported from ref 1 and 8, it is evident that a good agreement between measured and "calculated" natural lifetime is found only for *p*-terphenyl. The strong discordance between τ_{0m} and τ_{0c} in biphenyl clearly indicates that the emission does not originate from the same excited level that is responsible for the absorption band.[8] In the case of 4-vinylbiphenyl the fairly short decay time agrees with our prediction (Figure 2) concerning the level responsible for emission, and the relatively low quantum yield might be due to internal quenching caused by the closely lying excited level. Further evidence for the results of Figure 2 is forthcoming from the spacings of the vibrational peaks in the emission spectra. These spacings are ~1000 cm^{-1} in biphenyl and ~1300 cm^{-1} in 4-vinylbiphenyl and *p*-terphenyl, and they most likely correspond to the ring breathing vibration and to the central bond stretching vibration,[10-12] respectively. As a consequence, if our predictions are right (Figure 2), the $^1B_{3u} \rightarrow {}^1A_g$ transition must be coupled with the ring breathing vibration and the $^1B_{2u} \rightarrow {}^1A_g$ transition with the central bond stretching vibration. This condition can be qualitatively checked within our calculation scheme; if a π bond order–bond length relationship[13] is used to estimate the length of the interannular bond in ^1A_g, $^1B_{3u}$, and $^1B_{2u}$ states of biphenyl it is found (see Table II[14]) that in $^1B_{3u}$ state the bond in question is nearly unchanged with respect to ^1A_g state, while in $^1B_{2u}$ state it is much shorter (a similar trend also occurs in 4-vinylbiphenyl and *p*-terphenyl). Thus, in ^1A_g and $^1B_{2u}$ states, the minima of the potential energy curves corresponding to the stretching mode of the interannular bond are far apart, and hence the vertical transition $^1B_{2u} \rightarrow {}^1A_g$, which originates from the zero point of the upper state, involves excitation of the stretching mode, which explains the observed progressions in the emission spectra of 4-vinylbiphenyl and *p*-terphenyl.

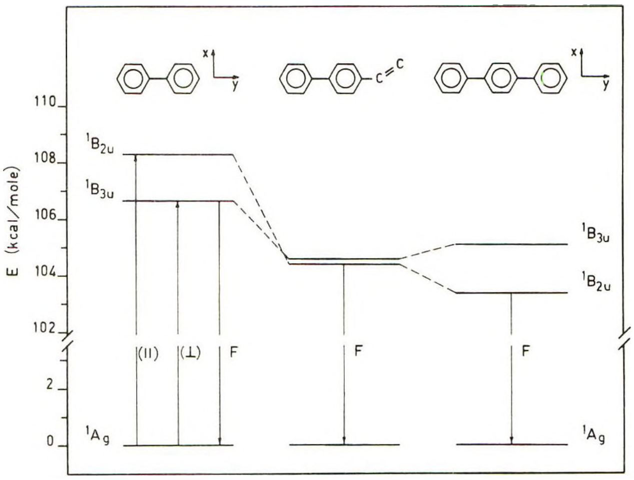

Figure 2. Correlation among the lowest singlet excited states of biphenyl, 4-vinylbiphenyl, and *p*-terphenyl in their planar configurations. Energies are given relative to the ground state. The excited states involved in the emission (*F*) are indicated and they can be directly correlated with those corresponding to the short-axis (⊥) and long-axis (∥) polarized uv transitions.

III. Shape of the Emission and Absorption Bands

Since the electronic states responsible for the emission and absorption bands of Figure 1 have been identified, it remains to be seen why the $^1B_{2u} \leftarrow {}^1A_g$ transitions lead to completely diffuse uv bands in contrast with the corresponding fluorescence bands ($^1B_{2u} \rightarrow {}^1A_g$), which exhibit a marked progression in the inter-rings bond stretching mode. Here we will attempt a completely intramolecular interpretation. The working hypothesis is that the difference between the distribution of transition probability of absorption ($^1B_{2u} \leftarrow {}^1A_g$) and that of emission ($^1B_{2u} \rightarrow {}^1A_g$) can be caused by the excitation of a low-frequency

(8) I. B. Berlman and O. J. Steingraber, *J. Chem. Phys.*, **43**, 2140 (1965).

(9) Th. Forster, "Fluoreszenz Organischer Verbindungen," Vandenhoeck und Ruprecht, Gottingen, 1951, p 158.

(10) D. Steele and E. R. Lippincott, *J. Mol. Spectrosc.*, **6**, 238 (1961).

(11) G. Zerbi and S. Sandroni, *Spectrochim. Acta*, **24**, 483 (1968).

(12) A. L. Len and C. H. Ting, *J. Chin. Chem. Soc. (Taipei)*, **17**, 14 (1970).

(13) K. Nishimoto and L. S. Forster, *Theor. Chim. Acta*, **4**, 155 (1966).

(14) E. F. McCoy and I. G. Ross, *Aust. J. Chem.*, **15**, 573 (1962).

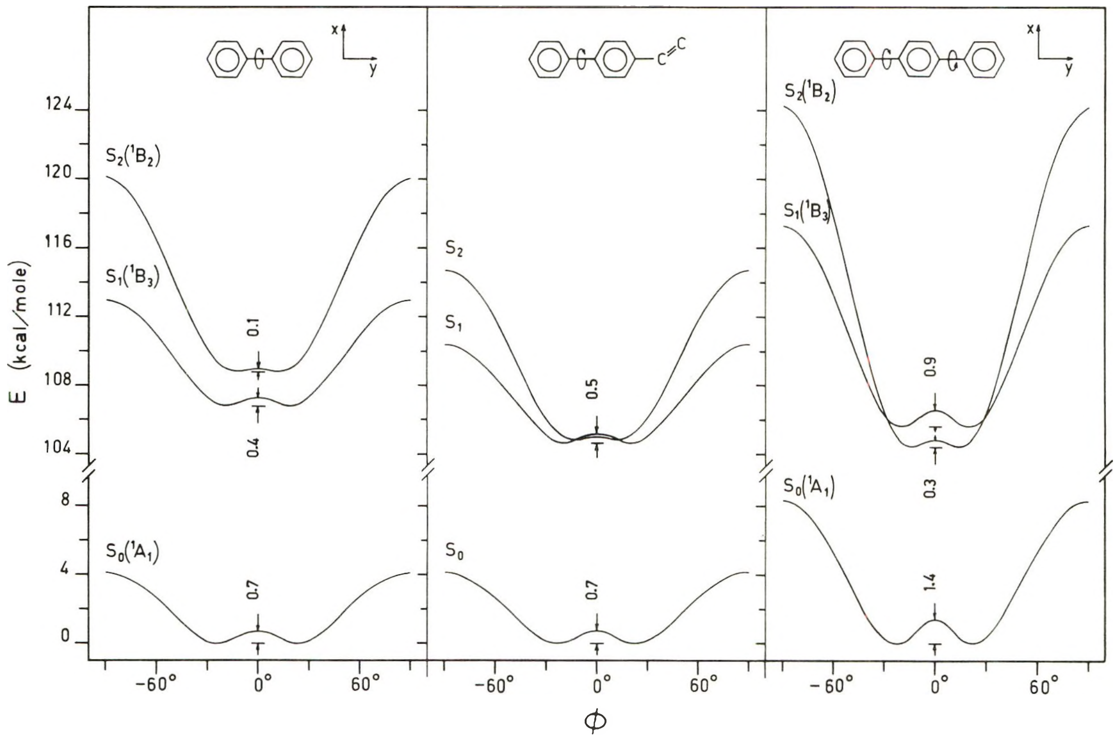

Figure 3. Potential energy curves for the twisting mode of the interannular bonds of biphenyl, 4-vinylbiphenyl, and *p*-terphenyl. In the latter molecule only the symmetrical rotation of the outside phenyls is considered. The ground state (S_0) and the two lowest singlet excited states (S_1 and S_2) are analyzed. The energy zero is arbitrarily assigned to the minimum of the ground state curve.

TABLE I: Measured (τ_{0m}) and "Calculated" (τ_{0c}) Fluorescence Natural Lifetimes Reported in Ref 1 and 8

Molecules	τ, nsec[a]	Q[b]	τ_{0m}, nsec[c]	τ_{0c}, nsec[d]
Biphenyl	16.0	0.18	88.9	2.87
4-Vinylbiphenyl	2.6	0.61	4.3	1.51
p-Terphenyl	0.95	0.93	1.02	1.43

[a] Decay time. [b] Quantum yield. [c] $\tau_{0m} = \tau/Q$. [d] Computed from the integrated intensity of the absorption band by using Forster's formula.[9]

TABLE II: π Bond Orders and Length Changes of the Interannular Bond of Biphenyl in the Lowest Electronic States

Electronic state	π bond order[a]	ΔR, Å[b]
^1A_g	0.1921	
$^1B_{3u}$	0.2445	−0.009
$^1B_{2u}$	0.3775	−0.033

[a] Corrections on bond orders due to configuration interaction have been included (see Appendix III of ref 14). [b] Bond lengths are calculated by the relationship $R_{pq} = 1.517 - 0.18 l_{pq}$[13] (where l_{pq} is the π bond order) and ΔR values are referred to the ground state ^1A_g.

vibrational mode, namely, the twisting of the interannular bonds. To test this hypothesis, curves of the potential energy as a function of the dihedral angle (ϕ) between the planes of the phenyl rings will be obtained first. Then the potential curves of both the ground and the excited states will be used to calculate Franck-Condon factors for emission and absorption, and, on this basis, an interpretation of the difference between near-uv and fluorescence spectra will be proposed.

Potential Energy Diagrams for the Twisting Mode of Interannular Bonds. The calculation procedure used here was first proposed by Fischer-Hjalmars[15] and recently adopted by us to study the internal rotations of α,ω-diphenylpolyenes.[16] Briefly, the potential energy is evaluated, for each value of the angle of twist, as a sum of three terms, the π electron energy (E_π), the core repulsion energy ($E_C{}^c$), and the nonbonded interaction energy (E_v). The calculation procedure of the first term (E_π) is that outlined in the previous section (for the core integrals of the interannular bonds a cosine dependence on the angle of twist was assumed, *i.e.*, $H\phi^c = H_0{}^c \cos\phi$). The ($E_C{}^c$) term was calculated according to a formula proposed by Dewar and Klopman[17] in the PNDO procedure. The theoretical reasons, as well as the practical convenience for the use of this recipe in π calculations,[18] have been discussed elsewhere.[16,19] All the interactions between nonbonded atoms (HH, HC, and CC) were included in the steric interaction energy (E_v) and were evaluated using both the formula and the parameters suggested by Allinger, *et al.*[20]

The potential energy diagrams thus obtained are reported in Figure 3. In *p*-terphenyl we limited ourselves to analyzing a vibrational mode where the outside phenyls

---

(15) I. Fischer-Hjalmars, *Tetrahedron*, **19**, 1805 (1963).

(16) F. Momicchioli, I. Baraldi, and M. C. Bruni (part 1); I. Baraldi, F. Momicchioli and M. C. Bruni (part 2), *J. Chem. Soc., Faraday Trans.* 2, **68**, 1556, 1571 (1972).

(17) M. J. S. Dewar and G. Klopman, *J. Amer. Chem. Soc.*, **89**, 3089 (1967).

(18) Let it be remembered that the quoted formula used for the core repulsion energy is

$$E_C{}^c = \frac{1}{2}\sum_{\substack{p,q\\p\neq q}} n_p n_q \left\{\gamma_{pq} + \left[\frac{1}{R_{pq}} - \gamma_{pq}\right] e^{-K_{pq}R_{pq}}\right\}$$

where the symbols have the usual meaning and for the parameter K_{pq} the value 0.4Å^{-1} has been chosen.[16]

(19) G. Del Re, F. Momicchioli, and A. Rastelli, *Theor. Chim. Acta*, **23**, 316 (1972).

(20) E. L. Eliel, N. L. Allinger, S. J. Angyal, and G. A. Morrison, "Conformational Analysis," Wiley, New York, N. Y., 1965, pp 451 and 452.

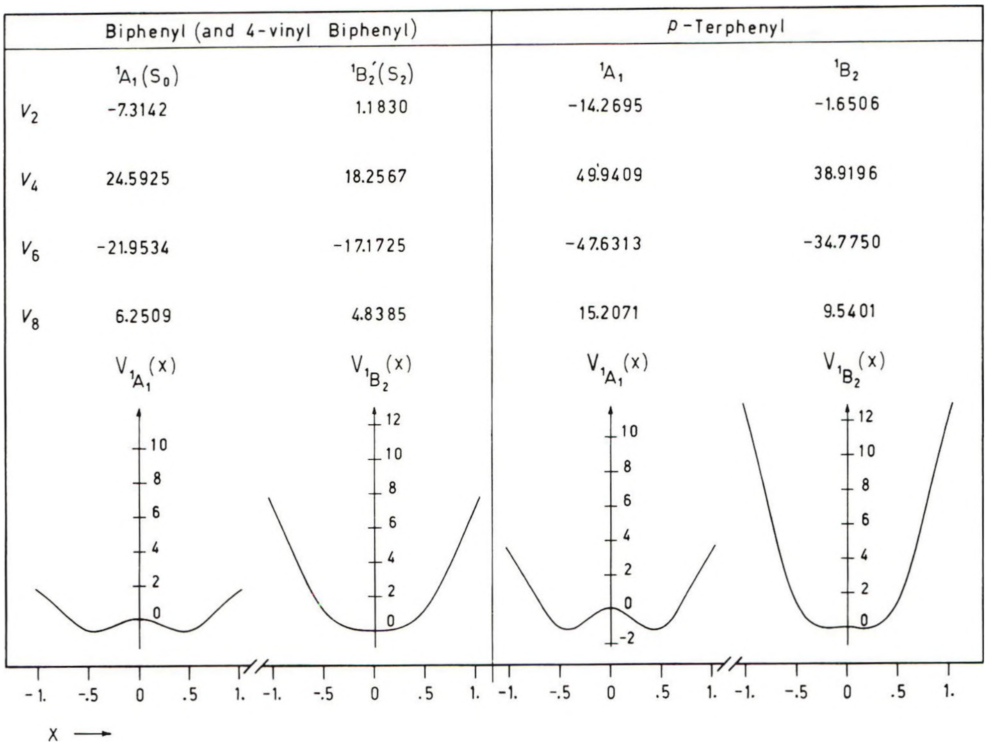

Figure 4. Polynomial approximations for the potential energy curves corresponding to S_0 and S_2 electronic states (see Figure 3). Potential curves for biphenyl and 4-vinylbiphenyl are assumed to be identical. In the upper part of the figure are reported the best values for the coefficients (v_l) of the power series $V(x) = \Sigma_l v_l x^l$. V and x are given in kcal/mol and radians, respectively.

TABLE III: Energies of the Twisting Vibration (in $^1A_1$ and $^1B_3$ States of Biphenyl) and Franck-Condon Factors Corresponding to the Principal Progressions in $^1B_3 \rightarrow {}^1A_1$ and $^1B_3 \leftarrow {}^1A_1$ Transitions

		Emission ($^1B_3 \rightarrow {}^1A_1$)[b]				Absorption ($^1B_3 \leftarrow {}^1A_1$)[b]	
$v(2)''$	$E_{v(2)''}$, kcal/mol[a]	$q_{0'v(2)''}$	$q_{1'v(2)''}$	$v(2)'$	$E_{v(2)'}$, kcal/mol[a]	$q_{v(2)'0''}$	$q_{v(2)'1''}$
0	0.1015	0.5310	0.0000	0	0.0745	0.5310	0.0000
1	0.1015	0.0000	0.5575	1	0.0764	0.0000	0.5575
2	0.2976	0.3391	0.0000	2	0.1905	0.2259	0.0000
3	0.2976	0.0000	0.3382	3	0.2238	0.0000	0.3018
4	0.4752	0.1123	0.0000	4	0.3048	0.1783	0.0000
5	0.4777	0.0000	0.0936	5	0.3851	0.0000	0.1151
6	0.6150	0.0176	0.0000	6	0.4773	0.0561	0.0000
7	0.6433	0.0000	0.0104	7	0.5762	0.0000	0.0231

[a] Twofold degeneracy of the lowest levels is due to the presence of two equivalent minima in the potential curve (see Figure 3); in the excited state ($^1B_3$) this degeneracy is almost completely removed because of the decrease of the central barrier. [b] Selection rules $\Delta v(2) = 0, \pm 2, \pm 4, \ldots$ hold according to the fact that vibrational wave functions are alternately symmetric and antisymmetric with respect to $\phi = 0$.

rotate symmetrically with respect to the central phenyl, and so the electronic states of both biphenyl and p-terphenyl can be assigned according to the irreducible representations of the D_2 point group. Regarding the ground-state potential curves, our calculations suggest that a very low barrier hinders the planarity of the molecules in question, and the most probable configurations fall at $\phi \cong 25°$. The potential energy curves of the S_1 excited states ($^1B_3$ in biphenyl and p-terphenyl) are similar to those of the ground states, while the curves of the S_2 states ($^1B_2$ in biphenyl and p-terphenyl) are very different. In fact, on account of a marked increase in the double-bond character of the interannular links the conjugation energy markedly increases on passing from S_0 to S_2 states, and, consequently, the molecules appear to be quasiplanar in S_2 states (similar conclusions hold for the corresponding triplet states; for the sake of brevity their potential curves are not reported here).

The reliability of these predictions cannot be easily checked because the experimental reports, all devoted to biphenyl, are scanty and often interpreted in a contradictory fashion. For example, Kurland and Wise,[21] assuming for biphenyl a potential curve of the form $V(\phi) = V_0 + (V_2/2)(1 + \cos 2\phi) + (V_4/2)(1 + \cos 4\phi)$, and by fitting the parameters V_2 and V_4 to the observed temperature variation of the chemical shift between ortho and meta protons, found a small barrier (0.44-1.10 kcal/mol) at $\phi = 0°$ and the energy minimum at $\phi = 90°$. The latter result conflicts with those of electron diffraction on biphenyl in the vapor phase[22] and of electron spin resonance on the biphenyl radical anion in solution,[23] which indicate 45 ± 10 and 38 ± 2°, respectively, as the preferred value of the

(21) R. J. Kurland and W. B. Wise, *J. Amer. Chem. Soc.*, **86**, 1877 (1964).
(22) O. Bastiansen, *Acta Chem. Scand.*, **3**, 408 (1949).
(23) K. Moebius, *Z. Naturforsch. A*, **20**, 1117 (1965).

dihedral angle ϕ. On the other hand, the various theoretical approaches based on π electron[24,25a] as well as on all-valence-electron calculations (EHT, CNDO/2)[26-28] also gave different answers to the puzzle of the internal rotation of biphenyl. In particular, the latter types of calculation place the most probable configuration of biphenyl at very high values of the dihedral angle (~70° for EHT[27] and 90° for CNDO/2[26,28]), while the planar configurations are hindered by rather high barriers (~12 kcal/mol for EHT[27] and ~5 kcal/mol for CNDO/2[26,28]). These results are unrealistic, and they demonstrate the inefficiency of the current all-valence-electron approximations in conformational problems of conjugated molecules,[28] for the orthogonality of the aromatic rings in biphenyl not only disagrees with electron diffraction and epr data,[22,23] but also leaves unexplained the differences between the uv spectrum of biphenyl and that of benzene, especially regarding the "conjugation" band (p band).[29,30] In π calculations, where realistic results concerning the preferred value of the dihedral angle of biphenyl in the ground state are generally obtained,[15,24,25] the use of different formulas for the nonbonded interactions and for "core repulsions," as well as the adoption of different sets of parameters for the evaluation of electronic energy, can cause the barrier at $\phi = 0°$[25a] or that at $\phi = 90°$[24] to assume the greater importance. In this respect, our calculations agree with those of Imamura and Hoffmann on biphenyl,[24,31] and suggest that the barrier at $\phi = 0°$ is lower than that at $\phi = 90°$. This result, on which the conclusions reached in the next section strictly depend, seems to be most reasonable in that it is the only one that is coherent with the asserted "planarity" of the lowest triplet state ($^3B_2$).[32]

In conclusion, considering the general outline of the previous experimental and theoretical reports on conformation and internal rotation of biphenyl, the potential curves reported in Figure 3 probably represent a good compromise and add weight to all the previsions of the previous section. In particular, Figure 3 clearly shows that in 4-vinylbiphenyl the S_1 state can cause a deactivation of the S_2 state, *via* an internal conversion process, and this explains the different value of τ_{0m} with respect to *p*-terphenyl (see Table I).

Franck-Condon Distributions. In this section the torsional potential curves corresponding to the electronic states involved in the emission and absorption processes (Figure 3) are used to set up distributions of transition probability. To this end vibrational energies and wave functions must be first obtained, and then overlap integrals between vibrational wave functions of the initial and final states must be calculated. The method of calculation adopted here is the same as recently used by us to study the shape of the "conjugation" band of the α,ω-diphenylpolyenes[16] (see also ref 33). The basic approximation of this method is that it expresses the potential function as a power series (*i.e.*, $V(x) = \Sigma_l v_l x^l$). The matrix elements of this type of potential for a harmonic oscillator basis set are known (up to $l \leq 8$[16,34]), and hence the vibrational wave functions were expressed as linear combinations of eigenfunctions of an arbitrary HO. The problem thus consists in the setting up and the diagonalization of a Hamiltonian matrix whose elements are

$$H_{nm} = H_{nm}{}^{\mathrm{K}} + H_{nm}{}^{\mathrm{V}}$$

where

$$H_{nm}{}^{\mathrm{K}} = \left\langle \phi_n \middle| -\frac{1}{2}\frac{\mathrm{d}^2}{\mathrm{d}\xi^2} \middle| \phi_m \right\rangle$$

and

$$H_{nm}{}^{\mathrm{V}} = \Sigma_l v_l \langle \phi_n | \xi^l | \phi_m \rangle$$

are the matrix elements of the kinetic energy[34] and of the potential energy, respectively, in units of $\epsilon = h\nu_0 = (k\hbar^2/I)^{1/2}$ (the energy of the arbitrary chosen HO, where k is the force constant and I is the reduced moment of inertia of the internal rotor[35]). In these formulas $\phi_n(\xi)$ and $\phi_m(\xi)$ are the HO eigenfunctions corresponding to n and m quantum numbers, $\xi = x\alpha^{1/2}$, with $\alpha = (Ik/\hbar^2)^{1/2}$, and $v_l' = v_l/(\epsilon\alpha^{l/2})$. If the vibrational wave functions of both the initial and the final electronic states are expanded in the same HO basis set the Franck-Condon factors are very simply expressed as follows

$$q_{v'v''} = \left|\sum_{n=0}^{N} C_{nv'} C_{nv''}\right|^2$$

where v'' and v' are the quantum numbers of the vibrational mode in the ground and the excited states, respectively, $C_{n''}$ and $C_{n'}$ are the corresponding mixing coefficients of the HO eigenfunctions, and $N + 1$ is the chosen number of basis functions (in this work $N + 1 = 80$ was fixed; with this basis set a very good convergence was obtained for the first 30 or 40 levels in all cases treated here). With this procedure we calculated the distributions of transition probability corresponding to excitation of the twisting mode of the interannular bonds in $S_2 \leftarrow S_0$ and $S_2 \rightarrow S_0$ transitions (Figure 3). The "best" values of the parameters v_l for the potential functions were obtained by means of a least-squares procedure. The results are reported in Figure 4. The same potential functions were adopted for both biphenyl and 4-vinylbiphenyl on account of the great similarity between the corresponding potential curves (see Figure 3) and according to the qualitative character of our calculation. The comparison of the curves in Figure 4 with the corresponding curves in Figure 3 shows that the polynomial approximations fit the bottom and the walls of the potential functions fairly well, especially as regards the S_0 states (in the S_2 state of biphenyl and 4-vinylbiphenyl the very low barrier at $\phi = 0°$ is not reproduced, and hence this excited state is considered to be planar in our calculation). The use of the polynomial approximation is certainly convenient in that it makes easy the calculation of Franck-Condon factors, but there is the objection that it may affect the results unless the potential well is very deep. This objection seems to apply particularly in the case of the ground state curves of biphenyl and 4-vinylbiphenyl, where the barrier at $\phi = 90°$ is rather low (4.2 kcal/mol). On the other hand, the fre-

---

(24) A. Imamura and R. Hoffmann, *J. Amer. Chem. Soc.*, **90,** 5379 (1968).

(25) (a) M. J. S. Dewar and A. J. Harget, *Proc. Roy. Soc., Ser. A*, **315,** 443 (1970); (b) present work.

(26) B. Tinland, *Theor. Chim. Acta*, **11,** 452 (1968).

(27) B. Tinland, *J. Mol. Struct.*, **3,** 161 (1969).

(28) O. Gropen and H. M. Seip, *Chem. Phys. Lett.*, **11,** 445 (1971).

(29) A. Rastelli and F. Momicchioli, *Boll. Sci. Fac. Chim. Ind. Bologna*, **24,** 189 (1966).

(30) R. Grinter, *Mol. Phys.*, **11,** 7 (1966).

(31) In the quoted paper the relative positions of $^1B_2$ and $^1B_3$ states are inverted with respect to those found by us (see Figure 3 of ref 24 and Figure 3 of the present work). This is probably due to the use of a shorter inter-rings bond distance (1.48 Å instead of 1.51 Å) that enhances the conjugation between the benzene rings and causes a decrease of the $^1B_2 \leftarrow {}^1A_1$ transition energy. Such a result does not explain the value of τ_{0m} in biphenyl (see Table I), and it should be rejected accordingly.

(32) P. J. Wagner, *J. Amer. Chem. Soc.*, **89,** 2820 (1967).

(33) L. L. Lohr, Jr., *J. Amer. Chem. Soc.*, **92,** 2210 (1970).

(34) E. Heilbronner, Hs. H. Gunthard, and R. Gerdil, *Helv. Chim. Acta*, **39,** 1171 (1956).

(35) The values of the reduced moments of inertia are 0.075×10^{-37} and 0.200×10^{-37} g cm^2 for the twisting mode of biphenyl (and 4-vinylbiphenyl) and of *p*-terphenyl, respectively.

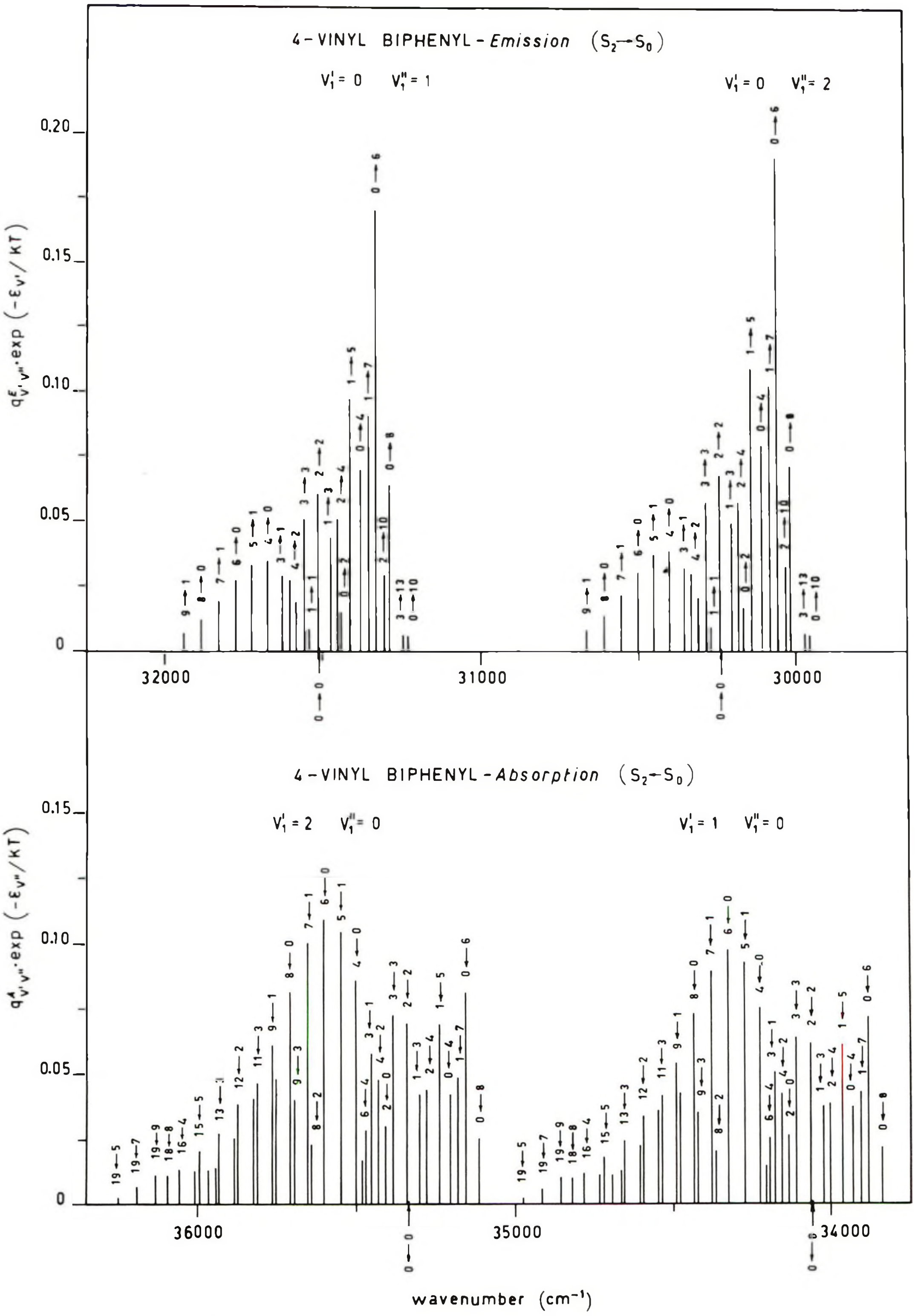

Figure 5. Franck-Condon distributions for the absorption ($S_2 \leftarrow S_0$) and the emission ($S_2 \rightarrow S_0$) in 4-vinylbiphenyl. Two vibrational modes, namely, the stretching and the twisting of the interannular bond, are considered to be excited. $v(1)''$ and $v(1)'$ are the quantum numbers of the stretching mode in the ground and the excited state, respectively. On each vertical line we have reported the quantum numbers relative to the transition in the twisting mode.

quency of the twisting mode in biphenyl is extremely low (the value reported in the literature for the crystalline state is 70 cm^{-1},[36] but it is probably lower for the vapor phase[37]), and hence the first 15 or 20 levels, as many as are important in our problem, should be well accounted for within the approximation adopted here.

The Franck-Condon distributions thus obtained were further elaborated in order to emphasize the effect

---

(36) K. Krebs, S. Sandroni, and G. Zerbi, *J. Chem. Phys.*, **40**, 3502 (1964).

(37) T. Sekiya, K. Sakamoto, and Y. Watari, *Nippon Genshiryoku Kenkyusho Kenkyu Hokoku, JAERI*, No. 1181, 75 (1969).

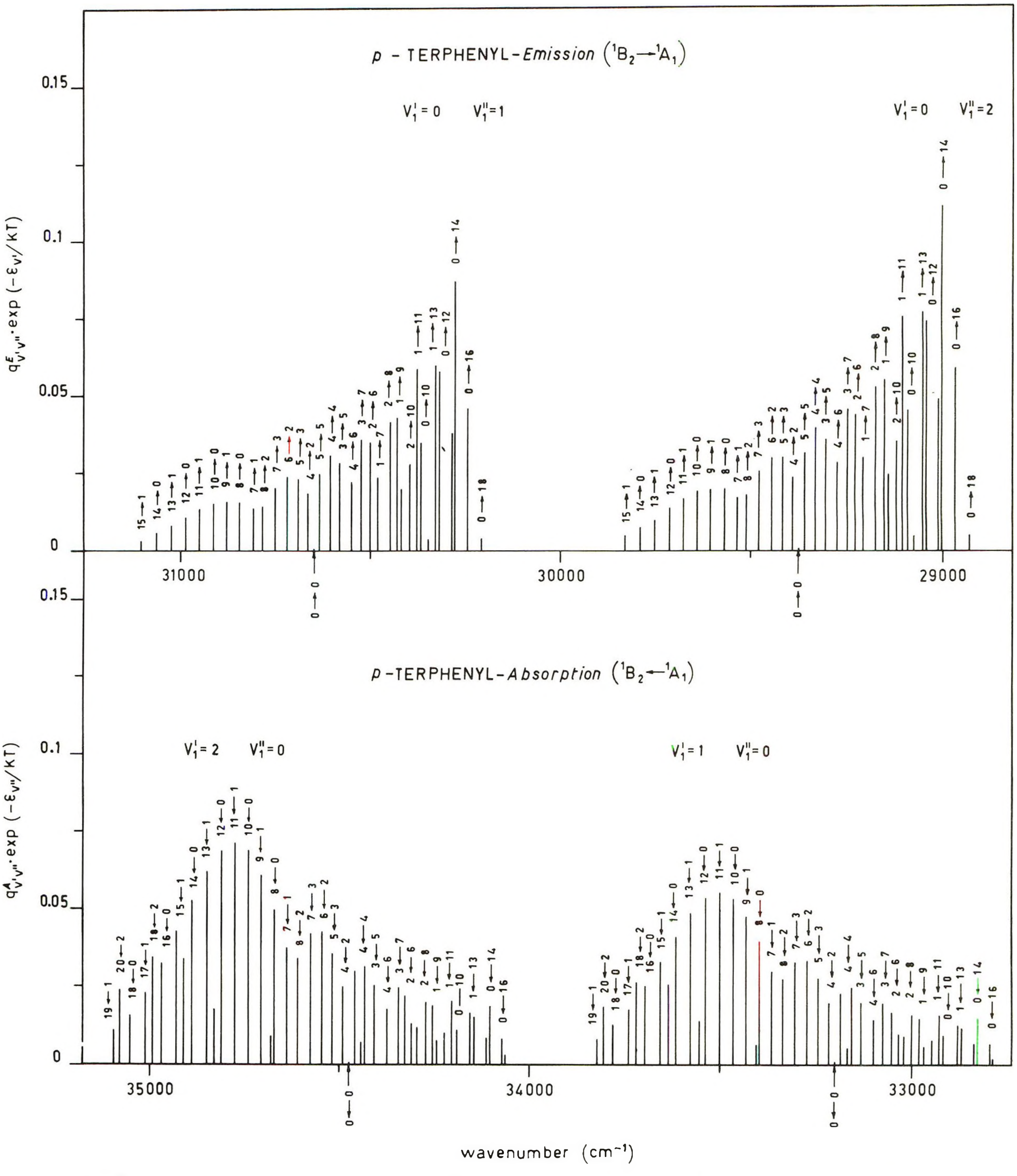

Figure 6. Franck-Condon distributions for the absorption ($^1B_2 \leftarrow {}^1A_1$) and the emission ($^1B_2 \rightarrow {}^1A_1$) in p-terphenyl. For further details see the caption of Figure 5.

brought about by excitation of the twisting mode on each member of the principal progression in the stretching mode of the interannular bonds (to which the fine structure observed in fluorescence spectra of 4-vinylbiphenyl and p-terphenyl has to be assigned). Briefly, we calculated distributions of transition probability, the individual terms of which are

$$q_{v'v''}^{A} = q_{v(1)'0''} q_{v(2)'v(2)''} \quad \text{absorption}$$

$$q_{v'v''}^{E} = q_{0'v(1)''} q_{v(2)'v(2)''} \quad \text{emission}$$

where $q_{v(1)'0''}$ and $q_{0'v(1)''}$ are probabilities of individual transitions due to excitation of the stretching mode in absorption and emission, respectively, and where $q_{v(2)'v(2)''}$ are Franck-Condon factors corresponding to excitation of the twisting mode. The latter were calculated as described above, while the former were derived from the emission spectra (Figure 1). The frequency of the stretching mode was assumed equal to 1275 cm^{-1} in both the ground (S_0) and the excited (S_2) states. The resulting distributions of transition probability for absorption and emission of 4-vinylbiphenyl and p-terphenyl are reported in Figures 5 and 6, where the probability of each thermally-induced transition has been multiplied by the Boltzmann factor calculated at room temperature. In Figures 5 and 6 only the two principal members of the stretching progression are considered, and for each of them some progressions in the twisting mode are reported.

From Figures 5 and 6 it is clear that the contours of Franck-Condon distributions corresponding to emission are very different from those corresponding to absorption. More precisely, the distributions appear to be quite smooth in absorption, while sharp peaks are found in emission. In particular, it can be observed that the maximum transition probability value in emission is almost twice that calculated for absorption. The distributions of transition probability therefore qualitatively justify the different shape of the absorption and fluorescence bands in 4-vinylbiphenyl and *p*-terphenyl, and they suggest that this difference originates in the excitation of the twisting mode of the interannular bonds. This result depends partly on the general features of the potential curves, but above all on the molecules being twisted in the ground state while being quasiplanar in the excited state.

The Franck-Condon distribution reported in the bottom half of Figure 5 can also be used to explain the blurring of the vibrational structure in the absorption spectrum of biphenyl (Figure 1), which is due to the $^1B_2 \leftarrow {}^1A_1$ transition. On the other hand, in biphenyl the emission originates from $^1B_3$ state, and hence the properties of the fluorescence spectrum are related to the shape of the corresponding potential curve (Figure 3). In view of the great similarity between $^1A_1$ and $^1B_3$ curves, the twisting vibration should be weakly coupled with $^1B_3 \leftarrow {}^1A_1$ and $^1B_3 \rightarrow {}^1A_1$ transitions, and, in consequence, it should not cause any appreciable blurring of the vibrational structure neither in the absorption nor in the fluorescence spectrum. In order to carry out a quantitative check of this prediction, we extended the calculation of Franck-Condon factors to the $^1B_3 \leftarrow {}^1A_1$ and $^1B_3 \rightarrow {}^1A_1$ transitions of biphenyl. For the sake of brevity we limit ourselves to reporting in Table III the values of the transition probabilities corresponding to the principal progressions in the twisting mode both in absorption and in emission (in Table III the calculated energies for the twisting vibration in the $^1A_1$ and $^1B_3$ states are also reported). The probability appears to be greatly concentrated on the $0' \leftrightarrow 0''$ and $1' \leftrightarrow 1''$ transitions (which are almost degenerate), and hence the twisting vibration of the interannular bond should not affect the vibrational structure due to excitation of the ring-breathing mode in $^1B_3 \leftarrow {}^1A_1$ and $^1B_3 \rightarrow {}^1A_1$ transitions of biphenyl. These conclusions provide an explanation for the shape of the fluorescence spectrum of biphenyl (Figure 1), while, regarding the corresponding absorption band which is hidden by the much more intense $^1B_2 \leftarrow {}^1A_1$ transition, they cannot be directly checked.

IV. Conclusions

In the present work we looked for a simple theoretical scheme to explain why the near-uv spectrum of polyphenyls is completely diffuse in contrast with the fluorescence spectrum where a sharp fine structure is observed (Figure 1). First of all, our SCF-CI calculation, in accordance with the experimental values of the fluorescence natural lifetimes and with the spacings of vibrational peaks in the emission spectra, shows that in the first, biphenyl, term of the polyphenyl series near-uv and fluorescence spectra cannot be directly compared because absorption and emission involve different excited states, the long-wavelength uv band being chiefly due to the long-axis polarized transition ($^1B_2 \leftarrow {}^1A_1$), while the fluorescence band is ascribable to the short-axis polarized transition ($^1B_3 \rightarrow {}^1A_1$) (section II). In *p*-terphenyl, as in the 4-vinyl derivative of biphenyl, both absorption and emission are related to the long-axis polarized transition. In these cases we supposed that the peculiar differences between absorption and fluorescence spectra originate in the excitation of the twisting mode of the interannular bonds. This hypothesis was "quantitatively" checked by setting up diagrams of the potential energy as a function of the dihedral angle between phenyl rings and by calculating distributions of transition probability for both absorption and emission. Regarding the potential curves our calculation suggests that in the ground state the molecules in question are twisted ($\phi \cong 25°$), while in the lowest singlet excited state they are quasiplanar. The order of magnitude of the barrier that hinders planarity in the ground state is of 1 kcal/mol (quite low with respect to the barrier found at $\phi = 90°$). Using these potential curves, Franck-Condon distributions were calculated that show sharp peaks in emission while exhibiting smooth contours in absorption. These results support our working hypothesis, for they show that the well-resolved vibrational structure observed in the fluorescence spectrum of 4-vinylbiphenyl and *p*-terphenyl, whose spacing ($\sim$1300 cm^{-1}) is ascribable to the interannular bond stretching mode, may be blurred in the absorption spectrum by excitation of the twisting vibration of the interannular bonds. This interpretation also holds for the near-uv spectrum of biphenyl. On the other hand, on account of the great similarity between the potential curves of $^1A_1$ and $^1B_3$ states, the twisting vibration is not appreciably coupled with $^1B_3 \rightarrow {}^1A_1$ transition, and this explains why the vibrational structure, ascribable to excitation of the ring-breathing mode ($\nu \cong 1000$ cm^{-1}), is retained in the fluorescence spectrum of biphenyl.

Acknowledgment. This work was supported by a fund of Consiglio Nazionale delle Ricerche (Roma).

Charge-Transfer Properties of the Hydrogen Bond. II. Charge-Transfer Theory and the Relation Between the Enhancement of Dipole Moment and the Ionization Potential of Hydrogen-Bonded Systems[1]

Henryk Ratajczak

Institute of Chemistry, University of Wroclaw, Wroclaw, Poland *(Received May 17, 1972)*

An extension of Mulliken's charge-transfer theory leads to a relation between the enhancement of dipole moment and the ionization potential of donors of structurally similar hydrogen-bonded complexes. Experimental data of hydrogen-bonded systems formed between 3,5-dinitrophenol and amines are in agreement with theoretical prediction. It is shown that the observed polarity of the hydrogen bond in the systems studied is connected with the electron delocalization effect.

One of the more important experimental properties of hydrogen-bonded complexes is the electric dipole moment. This quantity can give valuable information on the bonding character of the complex. However, so far the origin of the observed enhancement of dipole moment of hydrogen-bonded complexes has not been completely elucidated; whether it is connected with the existence of tautomeric equilibrium between molecular and ion-pair species as a consequence of the proton-transfer effect,[2] or with the electron delocalization (charge-transfer) effect is still a matter of much debate.[2,3]

The purpose of the present work is to give some strong support in favor of charge-transfer theory of the hydrogen bond.[2-5] This aim will be pursued by the discussion, using Mulliken's charge transfer theory,[6] of correlation found between the enhancement of dipole moment and ionization potential of the donor for some hydrogen-bonded complexes formed between 3,5-dinitrophenol and several amines.[7-10]

The analysis developed here leads to the evaluation of some important structural parameters ($\beta_0 = H_{01} - SW_0$; $E_A{}^v + C$) of hydrogen-bonded complexes and throws new light on the nature of this type interaction.

Theoretical Consideration

According to charge-transfer theory in its simplest form, the ground state of the hydrogen bond, X-H···Y, can be described by the following wave function

$$\Psi_N = a\Psi_0 + b\Psi_1 \qquad (1)$$

where Ψ_0 and Ψ_1 are the wave functions for nonbond (X-H···Y) and dative (X-H$^-$···Y$^+$) states, respectively.

The dipole moment of the hydrogen bond,[1] X-H···Y, is

$$\mu_N = \langle \Psi_N | \hat{\mu} | \Psi_N \rangle \qquad (2)$$

The change of dipole moment when the complex is formed is given by the equation

$$\overrightarrow{\Delta\mu} = \overrightarrow{\mu}_{\text{complex}} - \sum \overrightarrow{\mu}_{\text{component}} \qquad (3)$$

It is to be expected that the observed enhancement of the dipole moment of hydrogen bonded complexes might be due to two contributions; one coming from the induced dipole moment and one due to the presence of charge-transfer (electron delocalization) in the ground state. Therefore, we can write

$$\overrightarrow{\Delta\mu} = \overrightarrow{\Delta\mu_{\text{ind}}} + \overrightarrow{\Delta\mu_{\text{CT}}} \qquad (4)$$

According to Mulliken's charge-transfer theory[6] for weak complexes, $\overrightarrow{\Delta\mu_{\text{CT}}}$ is given approximately by

$$\overrightarrow{\Delta\mu_{\text{CT}}} = \overrightarrow{\mu_1}(b^2 + abS) \cong b^2\overrightarrow{\mu_1} \qquad (5)$$

where $\mu_1 = \langle \Psi_1 | \hat{\mu} | \Psi_1 \rangle$ is the dipole moment of the dative structure.

Applying the variation method to eq 1 one can get the following relation

$$aW_0 + bH_{01} = W_N(a + bS) \qquad (6)$$

where $W_0 = \langle \Psi_0 | \hat{H} | \Psi_0 \rangle$, $H_{01} = \langle \Psi_0 | \hat{H} | \Psi^1 \rangle$, $S = \langle \Psi_0 | \Psi_1 \rangle$, and $W_N = \langle \Psi_N | \hat{H} | \Psi_N \rangle \cong -\Delta H$ if Ψ_N is a normalized function and the reference energy of two separated solvated molecules is equal to zero.[3,4]

For weak complexes, $a \cong 1$, $bS \ll a$. Therefore, eq 6 reduces to

$$W_0 + b\beta_{01} = -\Delta H \qquad (7)$$

where H_{01} is replaced by β_{01}.

Thus combining eq 5 and 7, one finds that

$$-\Delta H = W_0 + \frac{\beta_{01}}{\sqrt{\mu_1}} \left(\overrightarrow{\Delta\mu_{\text{CT}}} \right)^{1/2} \qquad (8)$$

This relation has recently been discussed by Ratajczak and Orville-Thomas with the connection with the hydrogen-bonded[3] and charge-transfer complexes.[11]

From the other side, by applying second-order perturbation theory to eq 1 one can get the following relation

$$W_N = W_0 - \frac{(H_{01} - SW_0)^2}{W_1 - W_0} \qquad (9)$$

---

(1) Part I. H. Ratajczak, *J. Phys. Chem.*, **76**, 3000 (1972).
(2) H. Ratajczak and L. Sobczyk, *J. Chem. Phys.*, **50**, 556 (1969).
(3) H. Ratajczak and W. J. Orville-Thomas, *J. Chem. Phys.*, in press.
(4) S. Bratož, *Advan. Quantum Chem.*, **3**, 209 (1967).
(5) R. S. Mulliken and W. B. Person, "Molecular Complexes," Wiley-Interscience, New York, N. Y., 1969.
(6) R. S. Mulliken, *J. Amer. Chem. Soc.*, **74**, 811 (1952).
(7) H. Ratajczak and L. Sobczyk, *Zh. Strukt. Khim.*, **6**, 262 (1965).
(8) H. Ratajczak, unpublished data.
(9) L. Sobczyk, A. Koll, and H. Ratajczak, *Bull. Acad. Pol. Sci., Ser. Sci. Chim.*, **11**, 85 (1963).
(10) H. Ratajczak and L. Sobczyk, *Bull. Acad. Pol. Sci., Ser. Sci. Chim.*, **18**, 93 (1970).
(11) H. Ratajczak and W. J. Orville-Thomas, *J. Mol. Struct.*, in press.

TABLE I. Dipole Moment Data for Some Amine–3,5-Dinitrophenol Complexes in Benzene at 25°

No.	Complex of 3,5-dinitrophenol with	μ_{amine}, D	μ_{complex}, D	$\overrightarrow{\Delta\mu}$, D	$(\overrightarrow{\Delta\mu_{\text{CT}}})^{-1/2}$, $\text{D}^{-1/2}$	I_{D}^{v}, eV
1	Pyridine	2.20	6.97[a]	0.96	1.150	10.54
2	*n*-Butylamine	1.42	7.18[b]	1.98	0.752	8.72
3	Piperidine	1.13	7.56[c]	2.72	0.633	~8.0
4	Di-*n*-butylamine	1.03	7.93[b]	3.23	0.575	7.69
5	Triethylamine	0.83	7.86[d]	3.35	0.565	7.50

[a] Reference 7. [b] Reference 8. [c] Reference 9. [d] Reference 10.

and further

$$-\Delta H = W_0 - \frac{\beta_0^2}{I_{\text{D}}^{v} - E_{\text{A}}^{v} - C}$$

where $\beta_0 = H_{01} - SW_0$, $W_1 = \langle\Psi_1|\hat{H}|\Psi_1\rangle$, and I_{D}^{v} and E_{A}^{v} are the vertical ionization potential of the electron donor and vertical electron affinity of the acceptor, respectively. C is the difference in stabilization energies between the excited state and the ground state (further approximated by the Coulomb energy term of the ion pair).

Thus combining eq 8 and 9, one finds that

$$I_{\text{D}}^{v} = -\frac{\beta_0^2\sqrt{\mu_1}}{\beta_{01}}\left(\overrightarrow{\Delta\mu_{\text{CT}}}\right)^{-1/2} + \left(E_{\text{A}}^{v} + C\right) \qquad (10)$$

This equation predicts that a linear relation exists between I_{D}^{v} and $(\Delta\vec{\mu}_{\text{CT}})^{-1/2}$ if $\beta_0^2\sqrt{\mu_1}/\beta_{01}$ and $(E_{\text{A}}^{v} + C)$ are constants.

In order to use eq 10, it is necessary to obtain a value for $\Delta\vec{\mu}_{\text{CT}}$. This can be obtained from eq 4, provided that $\Delta\vec{\mu}_{\text{ind}}$ can be calculated. $\Delta\vec{\mu}_{\text{ind}}$ has been evaluated according to Frank's method which gives the value of the order of 0.20 D.[12]

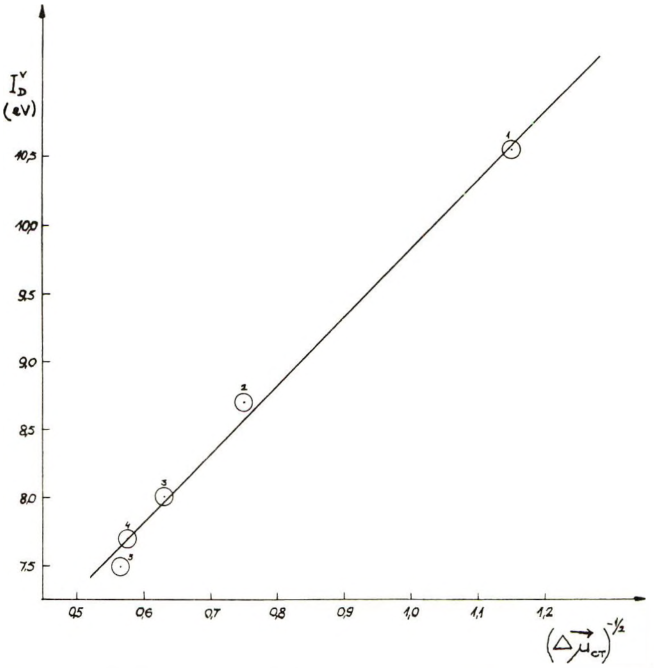

Figure 1. Relation between the ionization potential of donor I_{D}^{v} vs. $(\Delta\mu_{\text{CT}})^{-1/2}$.

Analysis of Experimental Data

The experimental data for some hydrogen-bonded complexes are given in Table I and presented in Figure 1 as a relation between I_{D}^{v} and $(\Delta\vec{\mu}_{\text{CT}})^{-1/2}$. As predicted by eq 10 a straight line relation is found; the slope of this line is $\beta_0^2\sqrt{\mu_1}\beta_{01}^{-1} = 5.10$ eV $\text{D}^{1/2}$ and the intercept is $(E_{\text{A}}^{v} + C) = 5.3$ eV. Assuming the reasonable value of -0.43 eV $\text{D}^{1/2}$ for $\beta_{01}/\sqrt{\mu_1}$, one can estimate $\beta_0 = 1.5$ eV. This value is in excellent agreement with that obtained recently by Ratajczak and Orville-Thomas[3] from an analysis of the relation between the enthalpy and the enhancement of dipole moment of the hydrogen-bonded systems. On the other hand, good agreement has been reached as far as the $(E_{\text{A}}^{v} + C)$ value is concerned with that obtained by Szczepaniak,[13] *et al.*, on the basis of spectroscopic consideration.

Obtained agreement lends further support to the assignment of the lowest ionization potential value of pyridine due to ionization from the π orbital.[14,15] Naturally this argument implies that β_0 and C have the same values as those found for the 3,5-dinitrophenol aliphatic amine complexes.

---

(12) F. C. Frank, *Proc. Roy. Soc., Ser. A*, **152**, 171 (1936).
(13) K. Szczepanijak, M. Golinska, and J. Mikołajczyk, *Acta Phys. Pol.*, **24**, 421 (1968).
(14) D. W. Turner, *Advan. Phys. Org. Chem.*, **4**, 31 (1966).
(15) J. D. Bene and H. H. Jaffe, *J. Chem. Phys.*, **50**, 563 (1969).

First-Order Perturbation Theory in the LCAO Approximation. The Case of an Ionic Crystal in a Magnetic Field[1]

T. Vladimiroff

Feltman Research Laboratory, Propellants Division, Picatinny Arsenal, Dover, New Jersey 07801

(Received June 13, 1972)

Publication costs assisted by Picatinny Arsenal

The Löwdin theory of ionic crystals is extended to include the effects of a small, one-electron perturbation. First Löwdin's approach is discussed in terms of the Roothaan expansion technique. Then the effects of the perturbation are taken into account by considering the polarization of the basis functions and the change in the expansion coefficients. The method is shown to be equivalent to a minimum basis set, self-consistent perturbation theory but no two-electron integrals have to be evaluated. The case of a homogeneous magnetic field is considered in detail.

Introduction

Quantum mechanics, in conjunction with approximate methods[2a] and high-speed electronic computers, has made it possible to perform *ab initio* calculations on atoms and small molecules. Some progress[2b,3] has also been made on the difficult problem of calculating the so-called second-order physical properties such as nmr chemical shifts, electric polarizabilities, and magnetic susceptibilities. In principle these techniques are also applicable to ionic crystals but practical applications of these methods are somewhat inhibited by the large size of the crystal. Löwdin[4] proposed that a good approximation to the crystal orbitals could be obtained by symmetrically orthogonalizing the free ion orbitals. This contribution is particularly valuable since calculations using this simple approach are surprisingly accurate. It would therefore be interesting to calculate second-order properties using this model. For example, some attempts have been reported for chemical shifts. However, Kondo and Yamashita[5] were forced to use the "average energy" approximation to obtain a formula in closed form. Since there is no rigorous method by which the average energy can be estimated, this is an unsatisfactory aspect of their theory. The purpose of this paper is to remedy the situation by generalizing Löwdin's formulation[4] to include the effects of a small perturbation. First the method will be discussed in the context of the Roothaan expansion technique,[2a] then the effects of the perturbation will be included somewhat along the lines recently proposed[3] for self-consistent field (SCF) perturbation theory.

Löwdin Procedure

The electronic Hamiltonian for a crystal, with $2n$ electrons using the Born–Oppenheimer approximation, is (in atomic units)

$$\mathcal{H} = -\frac{1}{2}\sum_{i}\nabla^2(i) - \sum_{N,i} Z_N/r_{Ni} + \sum_{i<j} 1/r_{ij} \qquad (1)$$

where Z_N is the charge of the Nth nucleus, r_{Ni} is the distance between particles N and i, the sum on N is over all the nuclei, and the sums on i and j are over the $2n$ electrons. Since the eigen problem for $\mathcal{H}_c$ is too difficult to solve, Löwdin made several approximations. First the electrons were restricted to move in one-electron orbitals and the wave function was assumed to take the form of a Slater determinant

$$\Psi = |\psi_1(1)\alpha(1)\psi_1(2)\beta(2)\cdots\psi_n(2n)\beta(2n)| \qquad (2)$$

in order to satisfy the Pauli exclusion principle. Minimizing the total energy of $\mathcal{H}_C$ with respect to Ψ resulted in the familiar Hartree–Fock equations for the desired ψ_m's

$$\left\{-\frac{1}{2}\nabla^2(1) - \sum_{N} 1/r_{N1} + \sum_{k}(2J_k - K_k)\right\}\psi_m(1) = \epsilon_m\psi_m(1) \qquad (3)$$

with J_k and K_k being the usual Coulomb and exchange operators, respectively.[6] The large size of the ionic crystal inhibits the solution of eq 3 so that a further approximation has to be introduced.

A popular approach[2a] is to expand ψ_m using a suitable set of basis functions. The free ion orbitals, ϕ_l, constitute a reasonable choice for this basis set. We seek a solution of eq 3 of the form

$$\psi_m = \sum_{l} a_{lm}\phi_l, \qquad (4)$$

It has been pointed out by Fock[7] that the wave function as expressed in eq 2 is invariant with respect to unitary transformations among the ψ_m's. It is completely determined by the finite-dimensional function space spanned by these orbitals and does not depend on the basis chosen within this space. In eq 4 we construct n doubly occupied ψ_m's using n doubly occupied ϕ_l's. Thus a transformation such as eq 4 does not affect the value of Ψ and the free ion orbitals are completely equivalent to the ψ_m's. Since the ϕ_l's and the ψ_m's both span the same space, they form an equivalent basis for expanding ψ; however, the former is not an orthogonal basis. Löwdin[4] found this inconvenient and proposed to orthogonalize them in a symmetrical way. This can be accomplished by the transformation

---

(1) Part of the work on this paper was performed at the State University of New York at Stony Brook with support from the National Science Foundation, Grant No. GP-5780.

(2) (a) C. C. J. Roothaan, *Rev. Mod. Phys.*, **23**, 69 (1951); (b) R. McWeeny, *Phys. Rev.*, **126**, 1028 (1962); R. M. Stevens, R. M. Pitzer, and W. N. Lipscomb, *J. Chem. Phys.*, **38**, 550 (1963); A. T. Amos and G. G. Hall, *Theor. Chim. Acta*, **5**, 148 (1966).

(3) T. Vladimiroff, *J. Phys. Chem.*, **74**, 2415 (1970).

(4) P. O. Lowdin, Thesis, Uppsala University, Sweden, 1948; *Advan. Phys.*, **5**, 1 (1956).

(5) J. Kondo and J. Yamashita, *J. Phys. Chem. Solids*, **10**, 245 (1959).

(6) R. Daudel, R. Lefebver, and C. Moser, "Quantum Chemistry Methods and Applications," Interscience, New York, N. Y., 1959, p 462.

(7) V. Fock, *Z. Phys.*, **61**, 126 (1930).

$$\varphi = \mathbf{S}^{-1/2}\phi \qquad (5)$$

where φ is a column matrix of orthogonal free ion orbitals φ_l and $\mathbf{S}$ is the overlap matrix with $S_{kl} = \int \phi_k{}^*\phi_l d\tau$.

At first glance it might appear that since the Roothaan expansion[2a] using a minimum basis set yields no improvement, such a basis set entails a total loss of flexibility and is therefore inadequate for an ionic crystal. On the other hand, it must be remembered that in an ionic crystal the binding is mostly electrostatic and is not due to the distortion of the atomic orbitals as in a covalent bond. Thus the flexibility to produce such distortions may not be necessary. Extensive Hartree-Fock (HF) calculations on ionic crystals are presently out of the question; however, interactions of closed-shell systems have been studied in He_2, Ne_2, and Ar_2 by Gilbert and Wahl.[8] Kestner[9] performed extended basis set calculations on He_2. Interpretation[10] of these data reveals that the contribution of distortion is small for small overlaps. The results of Löwdin's own crystal calculations[4] also agree well with experiment. Thus the wave function proposed by Löwdin is attractive because it is a good first approximation and can be obtained with a minimum amount of labor.

These considerations are not particularly significant if it is desirable to evaluate the total energy of the crystal, since all the multicenter, two-electron integrals would still have to be computed to determine this expectation value. A saving is realized if one-electron properties are required since only one-electron, two-center integrals will occur. The second-order properties are of this type except that they are more difficult to evaluate because it is necessary to obtain the first-order distortion the crystal wave function undergoes in an external field. This problem has been most successfully handled by the perturbed SCF methods.[2b,3] The ease with which the minimum basis set HF solution is obtained for the crystal using the Löwdin technique[4] suggests that it should be possible to perform something similar for the perturbed problem.

The conventional method[2b] is not applicable because the same basis set is used to expand both the zero-order and the first-order orbitals. For the ionic crystal all the zero-order orbitals are occupied so that none are available for expanding the first-order crystal orbitals. The addition of supplementary, one-center orbitals to the minimum basis set would require the zero-order HF problem to be resolved which is exactly what we are trying to avoid. A possible way out of this dilemma has recently been suggested by Vladimiroff.[3] In this approach, expansion orbitals are utilized which are already eigenfunctions of a local Hamiltonian[3] which includes the perturbation.

Perturbed Löwdin Procedure

Let us add to the Hamiltonian of eq 1 a one-electron perturbation, $\lambda h(i)$ so that

$$\mathcal{H}_c(\lambda) = -\frac{1}{2}\sum_i \nabla^2(i) - \sum_{N,i}\frac{Z_N}{r_{Ni}} + \sum_{i<j} 1/r_{ij} + \lambda\sum h(i) \qquad (6)$$

Since a one-electron perturbation introduces no new correlation effects let us again seek a solution in the form of a Slater determinant in order to satisfy the Pauli exclusion principle

$$\Psi(\lambda) = |\psi_1{}^\lambda(1)\alpha(1)\psi_1{}^\lambda(2)\beta(2)\cdots\psi_n{}^\lambda(2n)\beta(2n)| \qquad (7)$$

where the $\psi_m{}^\lambda$ satisfy the equation

$$\{-\tfrac{1}{2}\nabla^2(1) - \Sigma 1/r_{N1} + \Sigma(2J_k - K_k) + \lambda h(1)\}\psi_m{}^\lambda(1) = \epsilon_m(\lambda)\psi_m{}^\lambda(1) \qquad (8)$$

To solve eq 8 we resort to the expansion technique.[2a] It has recently been suggested[3] that a reasonable basis set for this task is to employ one-center orbitals $\phi_1{}^\lambda$, which are already eigenfunctions of a local Hamiltonian[3] $H_0{}^1$ including the perturbation

$$(H_0{}^1 + \lambda h)\phi_l{}^\lambda = E_l\phi_l{}^\lambda$$

$H_0{}^1$ can always be constructed[11] using the known function ϕ_l, $H_0{}^1 = T + E_l - T\phi_l/\phi_l$, where T is the one-electron kinetic energy operator. We again seek a solution of the expansion type

$$\psi_m{}^\lambda = \Sigma a_{lm}(\lambda)\phi_l{}^\lambda \qquad (9)$$

Since $\Psi(\lambda)$ must satisfy the Pauli exclusion principle a transformation of the type 9 is again of no consequence and the set $\psi_m{}^\lambda$ is equivalent to the set $\phi_l{}^\lambda$. Thus it is not necessary to solve a perturbed HF problem to obtain $a_{lm}(\lambda)$. Since it is convenient to work with a set of orthogonal orbitals, we use the symmetric orthogonalization procedure suggested by Löwdin[4] to calculate these coefficients

$$\varphi^\lambda = \mathbf{S}^{-1/2}(\lambda)\phi^\lambda \qquad (10)$$

where $\mathbf{S}(\lambda)$ is a matrix with $S_{kl}(\lambda) = \int \phi_k{}^{\lambda *}\phi_l{}^\lambda d\tau$.

In this paper we are only concerned with the first-order distortions the wave functions undergo in the presence of the perturbation, so that both $a_{lm}(\lambda)$ and $\phi_{lm}{}^\lambda$ can be expanded to yield

$$a_{lm}(\lambda) = a_{lm}{}^0 + \lambda a_{lm}{}^1 + \cdots \qquad (11)$$

$$\phi_l{}^\lambda = \phi_l{}^0 + \lambda\phi_l{}^1 + \cdots$$

where $\phi_l{}^1$ is the first-order correction to $\phi_l{}^0$ due to the perturbation λh. Formally $\phi_l{}^1$ can be obtained by solving eq 5a or 5b of ref 3. Sometimes these functions can be deduced by other methods. For the case of a magnetic field, the property of gauge invariance can be used[12] as will be indicated later in this paper. Substituting eq 11 into 9, we obtain

$$\psi_m(\lambda) = \Sigma a_{lm}{}^0\phi_l{}^0 + \lambda\Sigma(a_{lm}{}^1\phi_l{}^0 + a_{lm}{}^0\phi_l{}^1) + \ldots \qquad (12)$$

In other words, we expand the first-order distortion that $\psi_m(\lambda)$ undergoes using the set $\phi_l{}^0$ and the set $\phi_l{}^1$. As has already been indicated, the Löwdin procedure is equivalent to the determination of the $a_{lm}{}^1$ using the SCF perturbation theory so that for the case of closed shells, it is only necessary to obtain $a_{lm}{}^1$ by finding $\mathbf{S}^{-1/2}(\lambda)$ to first order in λ.

Case of a Magnetic Field

If the perturbation is a magnetic field, H, finding $\phi_l{}^H$ correct to first order in H can easily be done since the ions are spherically symmetric. Following Aleksandrov[12] we take the origin at the center of the ion in question and the magnetic field in the z direction, the first-order perturbation due to the magnetic field becomes $e/(2mc)HL_z(1)$ where $L_z(1)$ is the z component of angular momentum operator acting on electron 1. If ϕ_l^0 is taken to be a product of a radial part and a spherical harmonic then ϕ_l^0 is already an eigenfunction of L_z, *i.e.*, it is already correct to first order in the magnetic field. Other ions will not be at the center of the coordinate system. However, this problem can be resolved by observing that once a *solution* is obtained in a one-coordinate system the *solution* in any other coordinate system can be obtained by gauge transformation. Thus, the solution can be found in a coordinate system centered on the nucleus of an individual ion and then expressed in terms of a coordinate system centered on some other ion. This can be achieved as follows. By a well-known theorem, if the vector potential $\mathbf{A}$ is replaced by $\mathbf{A}' = \mathbf{A} + \quad f$, the new solution ψ' is related to the old solution ψ by the transformation $\psi' = \psi\ \exp(-ife/hc)$ where f is an arbitrary scalar function of position. The vector potential with the lth orbital at position $\mathbf{R}_l$ becomes

---

[8] T. L. Gilbert and A. C. Wahl, *J. Chem Phys.*, **47**, 3425 (1967).

[9] N. R. Kestner, *J. Chem. Phys.*, **48**, 252 (1968).

[10] D. Butler and N. R. Kestner, *J. Chem. Phys.*, **53**, 1704 (1970).

[11] R. M. Sternheimer, *Phys. Rev.*, **96**, 951 (1954).

[12] I. V. Aleksandrov, *Sov. Phys.-Dokl.*, **3**, 325, 799 (1958).

$$\tfrac{1}{2}\mathbf{H} \times (\mathbf{r}_l(1) + \mathbf{R}_l) = \tfrac{1}{2}\mathbf{H} \times \mathbf{r}_l(1) + \tfrac{1}{2}\mathbf{H} \times \mathbf{R}_l \qquad (13)$$

where $\mathbf{r}_l(1)$ is the position of electron 1 relative to the coordinate system centered at $\mathbf{R}_l$. The first term on the right-hand side of eq 13 is the vector potential for which $\phi_l^0(1)$ is already a solution. Since gradient $\mathbf{H}\cdot(\mathbf{r}_l(1) \times \mathbf{R}_l) = -\mathbf{H} \times \mathbf{R}_l$, the second term can be identified as the gradient of a scalar function. The general solution for $\phi_l^H(1)$ is therefore

$$\phi_l^H(1) = \phi_l^0(1)\exp\{ie\mathbf{H}\cdot(\mathbf{r}_l(1) \times \mathbf{R}_l)/2\hbar c\}$$

Only the linear term in H is required so that the exponential can be expanded to yield

$$\phi_l^H(1) = \phi_l^0(1)(1 + ie\mathbf{H}\cdot(\mathbf{r}_l(1) \times \mathbf{R}_l)/2hc + \cdots)$$

These new orbitals, which are correct to first-order in the magnetic field, must now be orthogonalized.

The Löwdin theory requires that the matrix $\mathbf{S}^{-1/2}$ be evaluated. This can easily be done if $\mathbf{S}$ is first diagonalized, *i.e.*, we find the transformation $\mathbf{U}$ such that $\mathbf{S} = \mathbf{UDU}^+$. $\mathbf{U}$ is a matrix whose columns are eigenvectors of $\mathbf{S}$ and $\mathbf{D}$ is a diagonal matrix which contains the eigenvalues d_i of $\mathbf{S}$ on the diagonal. It can then be shown that $\mathbf{S}^{-1/2} = \mathbf{UD}^{-1/2}\mathbf{U}^+$. In the case of a magnetic field we have $\mathbf{S} = \mathbf{S}_0 + H\mathbf{S}_1$ where the elements of $\mathbf{S}_1$ are given by

$$S_{kl}^1 = ie/2hc(\textstyle\int \phi_k^*\phi_l\mathbf{H}\cdot(\mathbf{r}_l \times \mathbf{R}_l)\mathrm{d}\tau - \int \phi_k^*\phi_l(\mathbf{H}\cdot(\mathbf{r}_k \times \mathbf{R}_k)\mathrm{d}\tau) \qquad (14)$$

To obtain $(\mathbf{S}_0 + H\mathbf{S}_1)^{-1/2}$ we employ the same technique, being careful to keep terms first order in H

$$\begin{aligned}(\mathbf{S}_0 + H\mathbf{S}_1)^{-1/2} &= (\mathbf{U}_0 + H\mathbf{U}_1 + \cdots) \times \\ &\qquad (\mathbf{D}_0 + H\mathbf{D}_1 + \cdots)^{-1/2}(\mathbf{U}_0 + H\mathbf{U}_1 + \cdots)^+ \\ &= \mathbf{S}_0^{-1/2} + H\mathbf{P} + \cdots\end{aligned}$$

$\mathbf{U}_0$ and $\mathbf{D}_0$ are eigenvector and eigenvalue matrices of $\mathbf{S}_0$, respectively. $\mathbf{U}_1$ is the matrix which must be added to $\mathbf{U}_0$ so that $\mathbf{S}_0 + H\mathbf{S}_1$ can be diagonalized to first order in H. Since $\mathbf{U}_1$ contains the first-order corrections to the eigenvectors of $\mathbf{S}_0$ due to the addition of the perturbation matrix $\mathbf{S}_1$ it can be found by matrix perturbation theory. The matrix $\mathbf{D}_1$ is diagonal and is composed of the first-order corrections d_i^1 to the eigenvalues d_i^0 of $\mathbf{S}_0$. The $\mathbf{P}$ matrix contains the desired first-order coefficients and is given by $\mathbf{U}_0\mathbf{D}_0^{-1/2}\mathbf{U}_1^+ + \mathbf{U}_1\mathbf{D}_0^{-1/2}\mathbf{U}_0^+ - \mathbf{U}_0\mathbf{D}\mathbf{U}_0^+$. $\mathbf{D}$ is a diagonal matrix with $d_i^1/2(d_i^0)^{3/2}$ along the diagonal. The only other complication in evaluating the wave function correct to first order in H for a crystal is that the two-center, one-electron integrals of the form of eq 14 must be computed.

Although this approach does not seem to have been applied to ionic crystals, a chemical shift calculation[12] has been reported for the mathematically similar Heitler–London[13] treatment of the hydrogen molecule. (Although this case does not involve the interactions of closed shells, the molecular orbitals are determined by symmetry.) On the basis of this model the paramagnetic contribution to the shift is -0.43×10^{-5} if $z = 1.0$ and -0.54×10^{-5} if the more appropriate Wang[14] value of $z = 1.166$ is used. Both calculations are reported for the internuclear distance of 1.4 au. These values are in good agreement with experimental result of -0.56×10^{-5} determined by Ramsey.[15] The Wang[14] value of z represents a certain shrinkage of the atomic orbitals. It is reasonable to suspect that this effect will not be as important for ionic systems as it is for covalent hydrogen.

Acknowledgment. Thanks are due to Professor Paul C. Lauterbur for suggesting the problem of calculating chemical shifts in ionic crystals. The author would also like to express his gratitude to Miss Terry Jacobsen for help with the preparation of the manuscript and to Dr. Yvon P. Carignan for his interest and encouragement.

---

(13) W. Heitler and F. London, *Z. Phys.*, **44**, 455 (1927).

(14) S. C. Wang, *Phys. Rev.*, **31**, 579 (1928).

(15) N. F. Ramsey, *Phys. Rev.*, **78**, 699 (1950).

Ion Transport through Layered Ion Exchange Membranes

Ain A. Sonin* and Gershon Grossman

Department of Mechanical Engineering, Massachusetts Institute of Technology, Cambridge, Massachusetts 02139

(Received May 30, 1972)

Publication costs assisted by the Office of Saline Water, U. S. Department of the Interior

The steady-state transport characteristics of a family of ion exchange membranes composed of contiguous layers of anion and cation exchange materials are described in terms of a simple physical model. Membranes consisting of up to four layers are considered. Explicit analytic expressions are derived which relate the current-voltage characteristics and transport numbers to the membrane structure and to the concentrations of the bounding solutions. The current-voltage characteristics are shown to be anisotropic with respect to current direction, showing current saturation in one or both directions, depending on membrane structure. The results are compared with available data on bipolar membranes. An analysis is also given for the general performance characteristics, including the effects of concentration polarization in the bounding solutions, of a three-layered membrane consisting of a thick central ion exchange layer sandwiched between two extremely thin ion exchange layers of opposite sign. This combination may serve as a model for the effects of certain types of membrane fouling in practical applications such as electrodialysis. It is shown that even very thin surface layers can reduce the limiting current to a value significantly below the diffusion-controlled one which is expected in the absence of the surface films.

1. Introduction

This paper is concerned with ionic transport in membranes composed of contiguous layers of anion exchange and cation exchange materials. Such laminar membranes have attracted interest for several reasons. Many biological membranes are thought to be composed of, or at least contain, one or more layers of ion exchange type materials, and explanations for several aspects of their behavior have been proposed in terms of models based on such a structure.[1-6] Synthetic layered membranes have been prepared in the laboratory,[7-11] and have been found to have peculiar performance characteristics with possible industrial applications.[8] There is also reason to believe that in many applications where supposedly homogeneous membranes are used, the membranes have in fact thin surface layers, caused by fouling, which give the membrane as a whole a laminar character. The occurrence of such fouling layers has been found, for example, in electrodialysis systems, where the presence of minute quantities of certain impurities in the feed water can build up a thin ion exchange surface layer with fixed charge of opposite sign to that of the membrane itself.[12-14] Even extremely thin films of this nature can cause a serious degradation in the performance of electrodialysis systems.

An interesting property of laminar ion exchange membranes is that, depending on their structure, their steady-state current-voltage characteristics can be anisotropic with respect to current direction and can show current saturation in one or both directions, even when only one ionic species is involved and when there is no polarization in the solution outside the membrane. These features were demonstrated experimentally by Frilette[7] and Ishibashi and Hirano[8-10] with bipolar membranes consisting of an anion and a cation exchange layer joined together. They showed that the current rose linearly with voltage when the current vector entered the membrane on the side of the anion layer, while in the other direction it tended to level off at a saturation value which was, however, exceeded at sufficiently high voltages where the dissociation of the water began to play a dominant role. The bipolar ion exchange membrane was proposed by Mauro[4] as a model for the biological cell membrane. Mauro noted the anisotropic nature of the current-voltage characteristic, but was more directly concerned with the high capacitance that such a membrane would exhibit. Using a quasi-equilibrium analysis, he derived an expression for the capacitance of a bipolar membrane for small departures from the resting state of zero current. Following Mauro, the bipolar membrane was taken up by Coster[5-6] who suggested it as a model for the membranes of *Chara australis*. Coster carried out an approximate analysis of the steady-state response of the membrane, and showed that when the membrane is not too thick compared with the Debye length, there is a punch-through effect where the current suddenly increases over its saturation value as the voltage is increased, much as had been observed for the biological membrane. This punch-through results from a breakdown of charge neutrality and is not to be confused with the similar effect which occurs even with thick synthetic membranes as a result of water dissociation, as

---

(1) T. Teorell, *Progr. Biophys. Biophys. Chem.*, **3**, 305 (1953).
(2) G. Eisenman and F. Conti, *J. Gen. Physiol.*, **48**, 65 (1965).
(3) K. S. Cole, "Membranes, Ions and Impulses," University of California Press, Berkeley, Calif., 1968.
(4) A. Mauro, *Biophys. J.*, **2**, 179 (1962).
(5) H. G. L. Coster, *Biophys. J.*, **5**, 669 (1965).
(6) H. G. L. Coster, *Aust. J. Biol. Sci.*, **22**, 365 (1969).
(7) V. Frilette, *J. Phys. Chem.*, **60**, 435 (1956).
(8) N. Ishibashi and K. Hirano, *J. Electrochem. Soc. Jap.*, **26**, E 8 (1958).
(9) N. Ishibashi, *J. Electrochem. Soc. Jap.*, **26**, E 58 (1958).
(10) N. Ishibashi and K. Hirano, *J. Electrochem. Soc. Jap.*, **27**, E 193 (1959).
(11) N. Lakshminarayanaiah, "Transport Phenomena in Membranes," Academic Press, New York, N. Y., 1969, pp 42–47.
(12) T. R. E. Kressman and F. L. Tye, *J. Electrochem. Scc. Electrochem. Sci.*, **116**, 25 (1969).
(13) E. Korngold, F. deKorosy, R. Rahav, and M. F. Taboch, *Desalination*, **8**, 195 (1970).
(14) G. Grossman and A. A. Sonin, *Desalination*, **10**, 157 (1972).

mentioned above. Some exact numerical calculations for bipolar membranes of biological dimensions have also been given by George and Simons,[15] and the results have been compared with Coster's approximate analysis.[16]

A different analysis of composite laminar membranes has been presented by Kedem and Katchalsky.[17] Their analysis is a phenomenological one based on nonequilibrium thermodynamics, and assumes that fluxes can be related linearly to the differences in driving potential across each homogeneous layer within the membrane. Such an analysis, although quite general within its intended scope, is not well suited for describing saturation effects where large changes in concentrations occur within and across each homogeneous phase. Also of interest, although not central to our present purpose, is the theory of Conti and Eisenman[18] for the performance of an ion exchange membrane with an arbitrary distribution of fixed charge of the same sign. This theory assumes a negligible coion concentration and cannot be applied to cases where the fixed charge changes sign within the membrane, as in bipolar or more complex laminar membranes.

The present paper gives a theoretical analysis for the ionic transport characteristics of laminar membranes consisting of alternating layers of cation and anion exchange materials. The performance characteristics are linked directly to the membrane structure and the solution properties (section 3). Various combinations of up to four layers are considered. In order to keep the analysis simple and physically transparent, yet mathematically rigorous, it is based on certain simplifying assumptions (section 2), the main ones being that the only mobile species is a dilute, fully dissociated salt with positive and negative ions which have equal diffusion coefficients and charge numbers in each homogeneous phase, and that the fixed ion concentrations in the ion exchange layers are large (but not infinite) compared with the concentration of the salt outside the membrane. The membrane layers are furthermore assumed to be very thick compared with the Debye length, a restriction which must be kept in mind when biological applications are contemplated. The analysis is extended in section 4 to illustrate how the influence of concentration polarization in the exterior solutions on the current-voltage characteristics can be taken into account as well. A separate paper describes an application of the theory to model the effects of certain types of membrane fouling in electrodialysis systems.[19]

2. Model and Basic Equations

We consider the isothermal, steady-state ion transport in a membrane consisting of a series of plane, paralled ion exchange layers of homogeneous composition, one next to the other, as shown in Figure 1. The only mobile species are assumed to be the ions of a single, fully dissociated salt. Thus, ions resulting from the possible dissociation of the solvent (for example, water) are not accounted for. The positive and negative ionic species are taken to have equal charge numbers of magnitude Z and equal diffusion coefficients D, the latter having a given constant value in each phase. The motion of the ions is assumed to be governed by the well-known transport laws for dilute solutions. Each membrane phase is modelled as being either neutral or having a uniform distribution of fixed charge of concentration c_m and charge number Z_m per mole, where c_m is assumed to be large compared with the salt concentration outside the membrane and hence, large compared with the coion concentration in the membrane. Each layer is thick compared with the Debye length, so that Poisson's equation for the electric field is replaced by the simple requirement of local charge neutrality. The boundaries between salt solution and membrane, or between adjacent layers of the membrane, are assumed to be sharp and to offer no interfacial resistance to diffusion, so that the ionic species are in Donnan equilibrium across them.

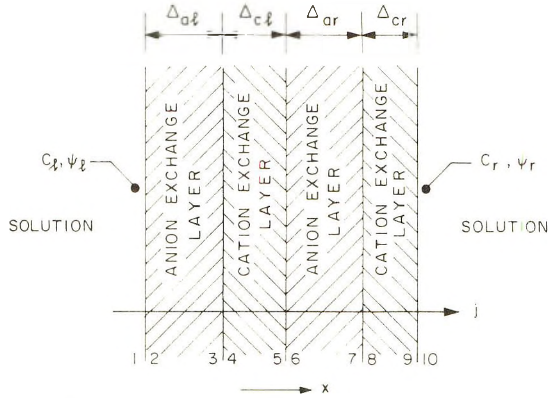

Figure 1. Four-layered membrane.

The motion of the ions within a given phase is given by the flux equations

$$\Gamma_{\pm} = -D\frac{dc_{\pm}}{dx} \mp Dc_{\pm}\frac{d\psi}{dx} \qquad (1a,b)$$

where Γ_+ and Γ_- represent the (constant) molar flux densities of the positive and negative ions, c_+ and c_- their molar concentrations, and

$$\psi \equiv ZF\phi/RT \qquad (2)$$

is a dimensionless potential, ϕ being the actual potential, F the Faraday constant, R the universal gas constant, and T the temperature. In addition, we have the quasi-neutrality condition which couples the concentrations of the positive and negative ions

$$c_+ + \frac{Z_m c_m}{Z} = c_- \qquad (3)$$

Here, c_m is the molar concentration of the fixed charges in the membrane and Z_m their charge number per molecule.

Solutions are given below for the ion concentration and potential distributions in anion and cation exchange layers as well as in neutral layers. In the ion exchange layers, the solutions are obtained by expanding the equations in terms of the ratio of the coion concentration to the fixed ion concentration, and keeping only terms of lowest order, consistent with the assumption that the coion concentration is small compared with the fixed ion concentration in the membrane.

It is convenient to express the solution in terms of dimensionless ion fluxes, for which we choose the transport numbers

$$t_{\pm} = \pm\Gamma_{\pm}(ZF/j) \qquad (4a,b)$$

---

(15) E. P. George and R. Simons, *Aust. J. Biol. Sci.*, **19**, 459 (1956).

(16) H. G. L. Coster, E. P. George, and R. Simons, *Biophys. J.*, **9**, 666 (1969).

(17) O. Kedem and A. Katchalsky, *Trans. Faraday Soc.*, **59**, 1941 (1963).

(18) F. Conti and G. Eisenman, *Biophys. J.*, **5**, 511 (1965).

(19) G. Grossman and A. A. Sonin, Fluid Mechanics Laboratory Report No. 72-6, Department of Mechanical Engineering, Massachusetts Institute of Technology, Cambridge, Mass., 1972. Also submitted for publication in *Desalination*.

where

$$j = ZF(\Gamma_+ - \Gamma_-) \tag{5}$$

is the (constant) current density. From eq 4 and 5, we have as usual $t_+ + t_- = 1$. Note that these transport numbers are defined for the general case where the ion fluxes are caused by diffusion in concentration gradients as well as by migration in an electric field. They are dependent variables whose values are governed by boundary and operating conditions (see section 3).

Cation Exchange Layer. Within the cation exchange layer, we set

$$-Z_m c_m/Z \equiv c_c \tag{6}$$

where $c_c \gg c_-$. From eq 1, 3, and 4, we obtain to lowest order in c_-/c_c

$$c_+ = c_c \tag{7}$$

$$c_- = (c_-)_0 + t_-(jx/ZFD_c) \tag{8}$$

$$\psi = \psi_0 - jx/ZFD_c c_c \tag{9}$$

where $(c_-)_0$ and ψ_0 are the salt anion concentration and electric potential, respectively, at $x = 0$, and D_c is the ion diffusion coefficient in the cation exchange layer. Equation 7 is obtained simply from eq 3, neglecting c_-/c_c compared with unity. Equation 8 is obtained from eq 1 by first substituting eq 3 to eliminate c_+, then eliminating $d\psi/dx$, and integrating the resulting equation for dc_-/dx. The equation is then linearized to the form given in eq 8 by assuming that $|jt_+x|/ZFD_c c_c$ is small compared with unity (see the discussion in section 3.2), and keeping only terms to lowest order in c_-/c_c. Equation 9 can then be obtained from either of eq 1, again to lowest order in c_-/c_c.

Anion Exchange Layer. Within the anion exchange layer we set

$$Z_m c_m/Z \equiv c_a \tag{10}$$

where $c_a \gg c_+$. Proceeding as for the cation exchange layer, but now expanding in terms of c_+/c_a and keeping only terms of lowest order, we get

$$c_+ = (c_+)_0 - t_+(jx/ZFD_a) \tag{11}$$

$$c_- = c_a \tag{12}$$

$$\psi = \psi_0 - jx/ZFD_a c_a \tag{13}$$

where $(c_+)_0$ and ψ_0 are the cation concentration and the potential at $x = 0$, and D_a is the ion diffusion coefficient in the anion exchange layer. In deriving eq 11 we assume that $|jt_-x|/ZFD_a c_a$ is small compared with unity.

Neutral Layer. In a phase without fixed charge, $c_m = 0$, and we have from eq 3

$$c_+ = c_- \equiv c \tag{14}$$

Eliminating $d\psi/dx$ between eq 1 and integrating, we obtain the well-known result

$$c = c_0 - \left(t_+ - \frac{1}{2}\right)\frac{jx}{ZFD_n} \tag{15}$$

where c_0 is the salt concentration at $x = 0$ and D_n is the ion diffusion coefficient in the neutral layer. Using this in either of eq 1, we obtain

$$\psi = \psi_0 + \frac{1}{2\left(t_+ - \frac{1}{2}\right)} \ln\left[1 - \left(t_+ - \frac{1}{2}\right)\frac{jx}{ZFD_n c_0}\right] \tag{16}$$

Again, ψ_0 is the potential at $x = 0$.

Condition Across Phase Boundaries. If a sharp phase transition occurs between point 1 and point 2 which are infinitely close together, and if the interface offers no barrier to diffusion, then, regardless of the magnitude of the ion fluxes across the boundary, the positive and negative ion species must be in Boltzmann equilibrium across the transition. That is

$$\psi_1 - \psi_2 = -\ln[(c_+)_1/(c_+)_2] \tag{17a}$$

$$= \ln[(c_-)_1/(c_-)_2] \tag{17b}$$

From these equations it follows that

$$(c_+)_2(c_-)_2 = (c_+)_1(c_-)_1 \tag{18}$$

Equation 17 is the familiar Donnan boundary condition. It follows directly from eq 1 once one makes use of the fact that because of the sharp transition region, each of the two gradient terms on the right is very large in magnitude compared with the flux term on the left.

3. Performance Characteristics of Layered Ion Exchange Membranes

We are concerned with membranes consisting of two or three layers of ion exchange material, with anion and cation exchange materials alternating in order. The various possible two or three membrane combinations can all be viewed as subcases of a four-layer membrane, shown in Figure 1, which consists of two anion and two cation exchange membranes in alternating order. Once the performance of the four-layer system is described in analytic form, the characteristics of membranes consisting of all the various combinations of one to three layers can be derived by letting one or more of the four membrane thicknesses go to zero.

The four-layer membrane shown in Figure 1 is in contact on its left side with a salt solution whose concentration and potential at the membrane surface are c_l and ψ_l, respectively, and on its right side with a solution whose concentration and potential at the surface are c_r and ψ_r. The layers have different thicknesses, but for simplicity the two anion exchange layers are assumed to have the same fixed ion concentration c_a and ion diffusion coefficient D_a, and the two cation exchange layers are also assumed to have the same properties. Points 1 to 10 represent stations at the interfaces between the phases.

The performance of the composite membrane is described by expressing the transport numbers t_+ and t_- and the total dimensionless potential drop across the membrane

$$\Psi \equiv \psi_1 - \psi_{10} = \psi_l - \psi_r \tag{19}$$

as a function of the current density, the exterior salt concentrations, and the properties of the membrane. The potential drop is given by

$$\Psi = \ln\frac{c_l}{c_a} + \frac{j\Delta_{al}}{ZFD_a c_a} - \ln\frac{(c_+)_3}{c_c} + \frac{j\Delta_{cl}}{ZFD_c c_c} - \ln\frac{c_c}{(c_+)_6} + \frac{j\Delta_{ar}}{ZFD_a c_a} - \ln\frac{(c_+)_7}{c_c} + \frac{j\Delta_{cr}}{ZFD_c c_c} - \ln\frac{c_c}{c_r} \tag{20}$$

Here, the first term on the right represents the potential drop across the interface 1–2 (eq 17b, with $(c_-)_1 = c_l$ and $(c_-)_2 = c_a$), the second the ohmic potential drop across the interior of the left-hand anion exchange membrane (eq 13), the third the drop across the interface 3–4 (eq 17a, with $(c_+)_4 = c_c$), the fourth the ohmic drop across the interior of the left-hand cation exchange membrane (eq 9), and so on. Equation 20 can be more succinctly written as

$$\Psi = \frac{j}{ZF}\left[\frac{\Delta_a}{D_a c_a} + \frac{\Delta_c}{D_c c_c}\right] + \ln\left[\frac{(c_+)_6 c_r c_l}{(c_+)_3 (c_+)_7 c_a}\right] \quad (21)$$

where

$$\Delta_a \equiv \Delta_{al} + \Delta_{ar} \quad (22)$$

$$\Delta_c \equiv \Delta_{cl} + \Delta_{cr}$$

represent the total thicknesses of the anion and cation exchange layers in the system, respectively.

The concentrations which appear in eq 21 can readily be obtained from the equations derived in section 2. Carrying the solution from point 1 to point 10 in Figure 1, we obtain

$$(c_+)_1 = (c_-)_l \equiv c_l \quad (23)$$

$$(c_-)_2 = (c_-)_3 = c_a \quad (24)$$

$$(c_+)_2 = c_l^2/c_a \quad (25)$$

$$(c_+)_3 = \frac{c_l^2}{c_a} - \frac{t_+ j \Delta_{al}}{ZFD_a} \quad (26)$$

$$(c_+)_4 = (c_+)_5 = c_c \quad (27)$$

$$(c_-)_4 = \frac{c_l^2}{c_c} - t_+ \frac{j\Delta_{al}}{ZFD_a}\frac{c_a}{c_c} \quad (28)$$

$$(c_-)_5 = \frac{c_l^2}{c_c} - t_+ \frac{j\Delta_{al} c_a}{ZFD_a c_c} + t_- \frac{j\Delta_{cl}}{ZFD_c} \quad (29)$$

$$(c_-)_6 = (c_-)_7 = c_a \quad (30)$$

$$(c_+)_6 = \frac{c_l^2}{c_a} - \frac{t_+ j\Delta_{al}}{ZFD_a} + \frac{t_- j\Delta_{cl} c_c}{ZFD_c c_a} \quad (31)$$

$$(c_+)_7 = \frac{c_l^2}{c_a} - \frac{t_+ j(\Delta_{al} + \Delta_{ar})}{ZFD_a} + \frac{t_- j\Delta_{cl} c_c}{ZFD_c c_a} \quad (32)$$

$$(c_+)_8 = (c_+)_9 = c_c \quad (33)$$

$$(c_-)_8 = \frac{c_l^2}{c_c} - \frac{t_+ j(\Delta_{al} + \Delta_{ar})c_a}{ZFD_a c_c} + \frac{t_- j\Delta_{cl}}{ZFD_c} \quad (34)$$

$$(c_-)_9 = \frac{c_l^2}{c_c} - \frac{t_+ j(\Delta_{al} + \Delta_{ar})c_a}{ZFD_a c_c} + \frac{t_- j(\Delta_{cl} + \Delta_{cr})}{ZFD_c} \quad (35)$$

$$c_r^2/c_c = (c_-)_9 \quad (36)$$

Here, eq 24 follows from eq 12, eq 25 is obtained by applying eq 18 to the transition 1–2, eq 26 then follows from eq 11, and so on. The results are obtained in a straightforward manner, using eq 18 for the transitions across phase boundaries, eq 7–8 for the concentration distributions within the cation exchange membranes, and eq 11–12 for the distributions within the anion exchange membranes.

The requirement expressed by eq 36 determines the transport numbers. Solving eq 36 and 35 with $t_+ + t_- = 1$, we get

$$t_+ = \frac{\dfrac{\Delta_c c_c}{D_c}}{\dfrac{\Delta_a c_a}{D_a} + \dfrac{\Delta_c c_c}{D_c}} + \frac{(c_l^2 - c_r^2)}{\dfrac{j}{ZF}\left(\dfrac{\Delta_a c_a}{D_a} + \dfrac{\Delta_c c_c}{D_c}\right)} \quad (37)$$

$$t_- = \frac{\dfrac{\Delta_a c_a}{D_a}}{\dfrac{\Delta_a c_a}{D_a} + \dfrac{\Delta_c c_c}{D_c}} - \frac{(c_l^2 - c_r^2)}{\dfrac{j}{ZF}\left(\dfrac{\Delta_a c_a}{D_a} + \dfrac{\Delta_c c_c}{D_c}\right)} \quad (38)$$

We note that although the transport numbers are usually positive and less than unity (as they invariably are when the only transport mechanism is migration in an electric field), they may in the general case have magnitudes larger than unity, in which case one of them is negative. This happens for example in the limit $j \rightarrow 0$, where (except when $c_l = c_r$) one transport number tends to $+\infty$ and the other to $-\infty$. A transport number larger than unity simply means that the flux of the ion species involved is larger than the current density divided by ZF [see eq 4], and a negative transport number signifies that due to diffusion in a concentration gradient, the net ion flux is opposite to the expected direction of migration in the applied electric field. The infinite transport numbers in the limit $j \rightarrow 0$ result simply because in that limit, the fluxes Γ_+ and Γ_- remain finite (and equal, so that $j = 0$), and therefore the ratios of the fluxes to the current density go to infinity. The finite ion fluxes at $j = 0$ imply that even if no current passes across the membrane, there will be net transport of salt from one side to the other unless $c_l = c_r$.

The solution for the current-voltage characteristic can now be obtained by substituting eq 26, 31, and 32 into eq 21, with t_+ and t_- taken from eq 37 and 38. The result can be expressed most succinctly in terms of a reduced current density which has the dimensions of concentration squared

$$\hat{j} \equiv \frac{j}{ZF}\left(\frac{\Delta_a c_a}{D_a} + \frac{\Delta_c c_c}{D_c}\right) \quad (39)$$

and dimensionless parameters characterizing the relative effective thicknesses of the various membrane layers

$$\beta_{al} \equiv \frac{\dfrac{\Delta_{al} c_a}{D_a}}{\dfrac{\Delta_a c_a}{D_a} + \dfrac{\Delta_c c_c}{D_c}}, \quad \beta_{ar} \equiv \frac{\dfrac{\Delta_{ar} c_a}{D_a}}{\dfrac{\Delta_a c_a}{D_a} + \dfrac{\Delta_c c_c}{D_c}} \quad (40)$$

$$\beta_{cl} \equiv \frac{\dfrac{\Delta_{cl} c_c}{D_c}}{\dfrac{\Delta_a c_a}{D_a} + \dfrac{\Delta_c c_c}{D_c}}, \quad \beta_{cr} \equiv \frac{\dfrac{\Delta_{cr} c_c}{D_c}}{\dfrac{\Delta_a c_a}{D_c} + \dfrac{\Delta_c c_c}{D_c}}$$

$$\beta_a \equiv \beta_{al} + \beta_{ar}, \quad \beta_c \equiv \beta_{cl} + \beta_{cr}$$

In terms of these quantities one obtains, for the current-voltage relation

$$\Psi = \left(\frac{\beta_a}{c_a^2} + \frac{\beta_c}{c_c^2}\right)\hat{j} + \ln \frac{c_l c_r[c_r^2(\beta_{al} + \beta_{cl}) + c_l^2(\beta_{ar} + \beta_{cr}) + (\beta_a\beta_{cl} - \beta_c\beta_{al})\hat{j}]}{[c_r^2\beta_{al} + c_l^2(1 - \beta_{al}) - \beta_c\beta_{al}\hat{j}][c_l^2\beta_{cr} + c_r^2(1 - \beta_{cr}) - \beta_a\beta_{cr}\hat{j}]} \quad (41)$$

Again, the first term represents the ohmic potential drop across the interiors of the membrane layers, and the second term the net contribution from the potential drops across the interfaces. This result will be discussed below in connection with specific membrane combinations.

3.1 Anion–Cation–Anion Membrane. Consider a cation exchange membrane sandwiched between two anion exchange membranes with different thicknesses (Figure 2). The current–voltage characteristic of this combination can be obtained from eq 41 by setting $\beta_{cr} = 0$ (that is, $\Delta_{cr} = 0$) and $\beta_{cl} = \beta_c$

$$\Psi = \left(\frac{\beta_a}{c_a^2} + \frac{\beta_c}{c_c^2}\right)\hat{j} + \ln \frac{c_l[c_r^2(1 - \beta_{ar}) + c_l^2\beta_{ar} + \beta_c\beta_{ar}\hat{j}]}{c_r[c_l^2(1 - \beta_{al}) + c_r^2\beta_{al} - \beta_c\beta_{al}\hat{j}]} \quad (42)$$

Here, the first term is the ohmic drop and the second term arises from the interfacial potentials. In the absence of the anion exchange layers ($\beta_{ar} = \beta_{al} = 0$), the second term yields the usual Donnan potential across the cation membrane, $\ln(c_r/c_l)$.

The second term in eq 42 shows that when the anion layers exist, the current reaches finite limiting values at

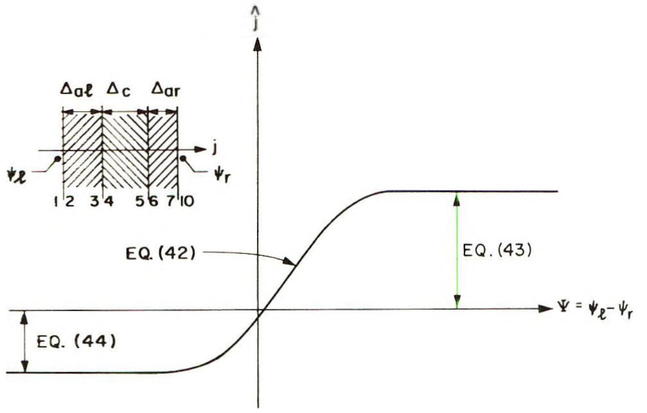

Figure 2. Current–voltage characteristic of anion–cation–anion composite membrane (sketch).

both high positive and high negative potential drops, as illustrated in Figure 2. In terms of the reduced current defined in eq 39

$$\hat{j} \rightarrow \frac{c_r^2\beta_{al} + c_l^2(1-\beta_{al})}{\beta_c\beta_{al}} \text{ for } \Psi \rightarrow +\infty \tag{43}$$

$$\hat{j} \rightarrow -\frac{c_l^2\beta_{ar} + c_r^2(1-\beta_{ar})}{\beta_c\beta_{ar}} \text{ for } \Psi \rightarrow -\infty \tag{44}$$

The positive limiting current is controlled primarily by the left-hand anion exchange layer, and the negative limiting current by the right-hand anion exchange layer. In other words, the anion exchange layer on the side where the current enters controls the limiting current.

The saturation of the current occurs because the Donnan potential drop across the interface between the anion and cation layers, on the side where the current enters, becomes infinite at a finite value of current density. The reason for this is illustrated in Figure 3. Figure 3a is a sketch of the ion concentration distributions within the membrane for a positive current density (see eq 23–32, with eq 37 and 38). In this as in the similar sketches which follow, the coion concentrations are exaggerated for purposes of illustration. Within a phase the distributions are linear, as shown in section 2. The concentrations $(c_+)_2$ and $(c_+)_7$ just inside the anion exchange layers are determined by c_a and the exterior salt concentrations, and are independent of current density. However, as j is increased, $(c_+)_3$ decreases in proportion (eq 26), and the potential drop across the 3–4 interface (Figure 3b) which is proportional to the log of $(c_+)_3$ increases. At some finite value of j, the concentration $(c_+)_3$ and at the same time $(c_-)_4$ go to zero, and the potential drop across 3–4 goes to infinity. In other words, the current saturates. For negative currents, the slopes of the concentration distributions are reversed, and the critical point becomes the 5–6 interface.

It is to be noted from eq 42 that the resting potential, or the potential across the membrane at zero current, depends on the membrane structure as well as on c_l and c_r. Depending on β_{al}, β_{ar}, and β_c, it varies from the limit ln (c_r/c_l) when the anion layers are absent, to the limit − ln (c_r/c_l) when the central cation layer is absent and we have a simple anion exchange membrane of thickness $\Delta_a = \Delta_{al} + \Delta_{ar}$ (see also eq 40 and 22). These limits represent of course the Donnan potentials for a simple cation and anion exchange membrane, respectively.

3.2 Cation Membrane with Thin Anion Exchange Surface Films. A particularly interesting special case of the anion–cation–anion membrane combination is the one where the anion exchange layers are extremely thin compared with the cation exchange layer in the center (but still thick compared with the Debye length). Such a case might occur, for example, when the surfaces of a cation exchange membrane are fouled by deposits of colloidal anion–exchange type material from the exterior solutions.

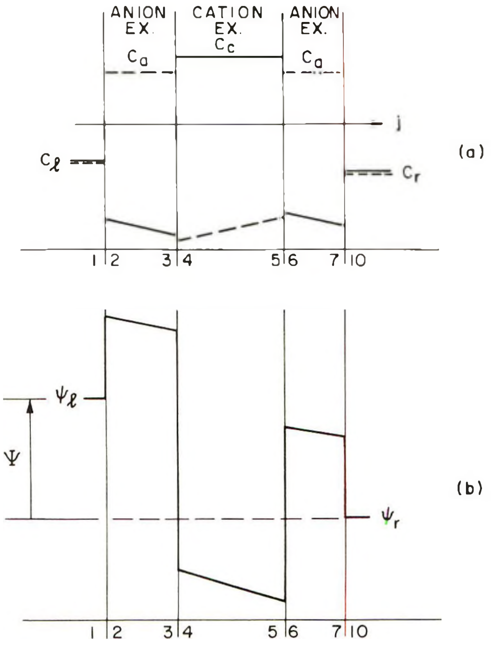

Figure 3. (a) Sketch of concentration distributions of positive mobile ions (solid line) and negative mobile ions (broken line) within anion–cation–anion membrane, for $j > 0$. (b) Potential distribution corresponding to (a).

For very thin anion exchange films on a cation exchange membrane, one considers the asymptotic limit where β_{ar}, $\beta_{al} \rightarrow 0$. In this limit eq 42 yields

$$\frac{ZF\Phi}{RT} = \frac{j\Delta_c}{ZFD_cc_c} + \ln\frac{c_r}{c_l} + \ln\frac{\left(1 + \dfrac{j}{ZF}\dfrac{\Delta_{ar}c_a}{D_ac_r^2}\right)}{\left(1 - \dfrac{j}{ZF}\dfrac{\Delta_{al}c_a}{D_ac_l^2}\right)} \tag{45}$$

where $\Phi = \phi_l - \phi_r$ is the actual potential drop across the membrane. Here, the first term represents the ohmic drop (to which the anion exchange films contribute negligibly). the second term is the Donnan potential which would arise for the cation membrane alone, and the third term arises from the interfacial potentials associated with the anion exchange films. The latter give rise to the saturation of the current at both positive and negative potentials

$$j \rightarrow \frac{ZFD_ac_l^2}{\Delta_{al}c_a} \text{ for } \Psi \rightarrow +\infty \tag{46}$$

$$j \rightarrow -\frac{ZFD_ac_r^2}{\Delta_{ar}c_a} \text{ for } \Psi \rightarrow -\infty \tag{47}$$

The positive limiting current is controlled by the left-hand anion exchange film and by the salt concentration in the left-hand compartment, and the negative limiting current is controlled by the right-hand anion exchange film and the salt concentration in the right-hand compartment. If either film is absent, the current will not saturate in the corresponding direction.

In summary, then, the current saturates if the cation membrane has an anion exchange film on the side where the current vector *enters* the membrane (this is also the side where concentration polarization would tend to occur in the solution, if allowed). Current saturation occurs because the coion (cation) concentration in the anion film goes to zero at the film-membrane interface, giving rise to an infinite junction potential at a finite current. The point to note is that when the fixed ion concentration in the anion exchange films is large compared with the salt concentrations outside the membrane, a *very thin* anion exchange film can have a dominant effect on the current-voltage characteristic of the membrane as a whole. Consider, for example, a very conservative situation where the applied potentials are onlv of the order of the thermal energy, *i.e.*, $\Psi \sim 1$. Without anion films, the current through the cation membrane would then be of order $ZFD_c c_c/\Delta_c$. However, if c_r and c_l are of order $10^{-2}c_a$, say, then an anion exchange film with a thickness of only 10^{-4} times that of the cation exchange membrane would cause a saturation of the current at a value less than the expected ohmic value (assuming $c_a \sim c_c$ and $D_a \sim D_c$ for purposes of illustration).

The current-voltage characteristic of a cation exchange membrane with thin films of anion exchange material is similar to the one sketched in Figure 2, except that the complete curve is given by eq 45 and the positive and negative saturation currents are given by eq 46 and 47, respectively. We are assuming, of course, that the exterior salt concentrations c_r and c_l at the membrane surfaces are independent of current density, that is, the left- and right-hand compartments are infinitely well stirred.

The transport numbers for this case are given by eq 37 and 38 with $\Delta_a c_a/D_a \ll \Delta_c c_c/D_c$. It is easy to show that except for very small potentials (where $\Psi \ll |c_l^2 - c_r^2|/c_c^2$), we have $t_+ \simeq 1$ and $t_- \ll 1$. In other words, the central cation membrane controls the transport numbers, with very little influence from the thin anion surface films.

Finally, a comment is required on one of our simplifying assumptions. As discussed in section 2, the linear expressions for the coion concentration in a cation and an anion exchange layer are based on the assumptions

$$\frac{|jt_+|\Delta_c}{ZFD_c c_c} \ll 1 \tag{48}$$

and

$$\frac{|jt_-|\Delta_a}{ZFD_a c_a} \ll 1 \tag{49}$$

respectively. If we substitute for the current density and the transport numbers from the expressions derived previously, we find that as long as the total thicknesses of the cation and anion exchange layers of the membrane are not too different (more precisely, as long as neither β_a nor β_c is very small), both of the above assumptions are always satisfied if the fixed charge concentrations within the layers are large compared with the exterior salt concentrations. However, as the total thickness of one kind of layer is made smaller and smaller, the assumption for the other, thicker layer eventually breaks down. For example, in our present case of a cation exchange layer bounded by two very thin anion exchange films, we substitute for j, t_+, and t_- and find that eq 49 always holds, but that eq 48 will eventually break down as the anion film thickness is made smaller and smaller. In other words, our model always correctly describes the coion concentration in the thin anion exchange surface films, but for sufficiently small Δ_a it may be in error regarding the coion concentration within the central cation exchange layer. We wish to emphasize, however, that eq 46 and 47 for the saturation currents will always remain correct, since for the case of thin anion exchange surface layers (where $t_+ \simeq 1$) these expressions can be derived without considering the central cation exchange layer. The positive saturation current, for example, is reached when the coion concentration approaches zero at station 3 in Figure 3, and an expression for it can be obtained simply by applying the equilibrium condition (eq 18) across the 1–2 interface in Figure 3 and using eq 11 for the coion concentration in the anion exchange film. The latter remains valid no matter how small the film thickness. The only restriction on eq 46 and 47, therefore, is our basic premise that the film thicknesses must be large compared with the Debye length.

3.3 Cation–Anion–Cation Membrane. The solution for an anion exchange membrane sandwiched between two cation exchange membranes is obtained from that for the four-layer membrane by setting $\beta_{al} = 0$ and $\beta_{ar} = \beta_a$ (Figure 1). For the current-voltage characteristic one obtains from eq 41 a result which has the same form as eq 42, except that the roles of subscripts "a" and "c," as well as "r" and "l," are interchanged. The system thus exhibits limiting currents which have the same form as eq 43 and 44, but with the above interchange of subscripts.

The behavior of this membrane combination is thus analogous to that of the anion-cation-anion combination discussed above. One must simply read "anion" for "cation," and "right" for "left." The critical point in polarization is now the anion-cation layer interface on the side where the current vector *exits* from the membrane system. At this interface (c_-) goes to zero within the cation exchange layer and (c_+) goes to zero within the anion exchange layer at a certain finite value of j. As a result $\Psi \rightarrow \infty$, and current saturation occurs.

3.4 Anion Membrane with Thin Cation Exchange Surface Films. This case is obtained from the solution for the four-layer membrane in Figure 1 by setting $\beta_{al} = 0$ $(\Delta_{al} = 0)$ and $\beta_{ar} = \beta_a(\Delta_{ar} = \Delta_a)$, and considering the asymptotic limit β_{cl}, $\beta_{cr} \rightarrow 0$. Again, the results are similar to those for a cation membrane with anion films, except that the roles of the subscripts "c" and "a," as well as "r" and "l," are interchanged. For the current-voltage characteristic one obtains

$$\frac{ZF\Phi}{RT} = \frac{j\Delta_a}{ZFD_a c_a} - \ln\frac{c_r}{c_l} + \ln\frac{\left(1 + \dfrac{j}{ZF}\,\dfrac{\Delta_{cl}c_c}{D_c c_l^2}\right)}{\left(1 - \dfrac{j}{ZF}\,\dfrac{\Delta_{cr}c_c}{D_c c_r^2}\right)} \tag{50}$$

where Φ is the potential drop across the membrane system. The first term on the right is the ohmic drop in the central anion exchange membrane, the second is the Donnan potential which would exist for the anion exchange membrane alone, and the third represents the influence of the thin cation exchange surface films. The system has limiting currents

$$j \rightarrow \frac{ZFD_c c_r^2}{\Delta_{cr}c_c} \text{ for } \Phi \rightarrow +\infty \tag{51}$$

$$j \rightarrow -\frac{ZFD_c c_l^2}{\Delta_{cl}c_c} \text{ for } \Phi \rightarrow -\infty \tag{52}$$

Thus, the positive limiting current is controlled by the right-hand cation exchange film and the right-hand salt concentration, and the negative limiting current is controlled by the left-hand film and left-hand salt concentration. In other words, the saturation current is controlled by the cation film and the salt concentration on the side

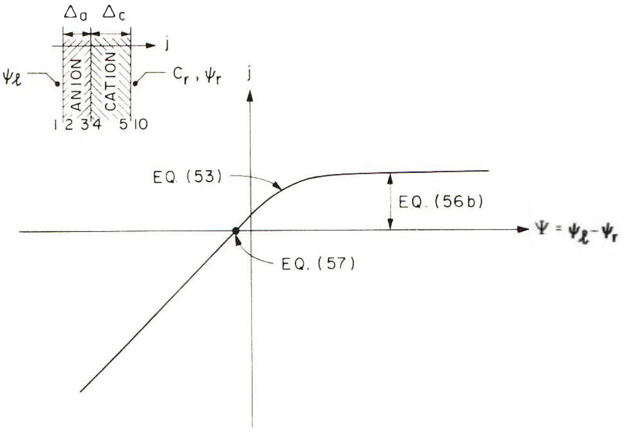

Figure 4. Current-voltage characteristic of bipolar membrane.

where the current vector exits from the system. Again, this is the same side where concentration polarization would tend to occur in the solution, if allowed.

3.5 Bipolar Membrane. The bipolar membrane is an anion exchange layer and a cation exchange layer joined together. Suppose the anion exchange layer has a thickness Δ_a and is on the left of the cation exchange layer, which has a thickness Δ_c (Figure 4). The current voltage characteristic of such a membrane is obtained from eq 41 if we let $\beta_{ar} = \beta_{cr} = 0(\Delta_{ar} = \Delta_{cr} = 0)$ and $\beta_{al} = \beta_a$, $\beta_{cl} = \beta_c$

$$\Psi = \left(\frac{\beta_a}{c_a^2} + \frac{\beta_c}{c_c^2}\right)\hat{j} + \ln\left[\frac{c_l c_r}{c_l^2\beta_c + c_r^2\beta_a - \beta_c\beta_a\hat{j}}\right] \tag{53}$$

where

$$\beta_a = \frac{\dfrac{\Delta_a c_a}{D_a}}{\dfrac{\Delta_a c_a}{D_a} + \dfrac{\Delta_c c_c}{D_c}} \tag{54}$$

$$\beta_c = 1 - \beta_a \tag{55}$$

The current-voltage characteristic given by eq 53 is shown in Figure 4. For sufficiently high negative potentials, the predominant behavior is ohmic (the first term on the right), whereas at high positive potentials the current tends to saturate at a level indicated by the second term

$$\hat{j}_{\lim} = \left[\frac{c_l^2}{\beta_a} + \frac{c_r^2}{(1 - \beta_a)}\right] \text{ for } \Psi \rightarrow +\infty \tag{56a}$$

where we have used eq 55. As discussed earlier, this saturation occurs because as the positive current is increased, the coion concentrations within both layers decrease, and eventually go to zero, at the interface where the two layers are joined (see Figure 2). Equation 56a can be rewritten in terms of the actual current density j as

$$j_{\lim} = ZF\left(\frac{c_l^2}{c_a}\frac{D_a}{\Delta_a} + \frac{c_r^2}{c_c}\frac{D_c}{\Delta_c}\right) \tag{56b}$$

The transport numbers of the positive and negative ions are given by eq 37 and 38. Note that the denominator of the second terms on the right-hand sides of these equations represents the reduced current $\hat{j}$.

The dimensionless potential across the membrane at zero current (the resting potential) is obtained from eq 53 as

$$\Psi_0 = -\ln\left[\frac{c_l}{c_r}(1 - \beta_a) + \frac{c_r}{c_l}\beta_a\right] \tag{57}$$

Ψ_0 is the potential of the solution on the anion exchange layer side relative to that on the cation exchange layer side. Its value depends on the membrane properties through β_a, and on the ratio of the salt concentrations in the bounding solutions, c_l/c_r. When $j = 0$, the potential is constant within each ion exchange layer, and the membrane potential is simply the algebraic sum of the potentials across the phase boundaries. The potential across the interface between the two layers depends on the local coion concentration, which in turn is a function of membrane properties and solution concentrations (see eq 8 and 11 together with eq 37 and 38). Hence the appearance of β_a in eq 57.

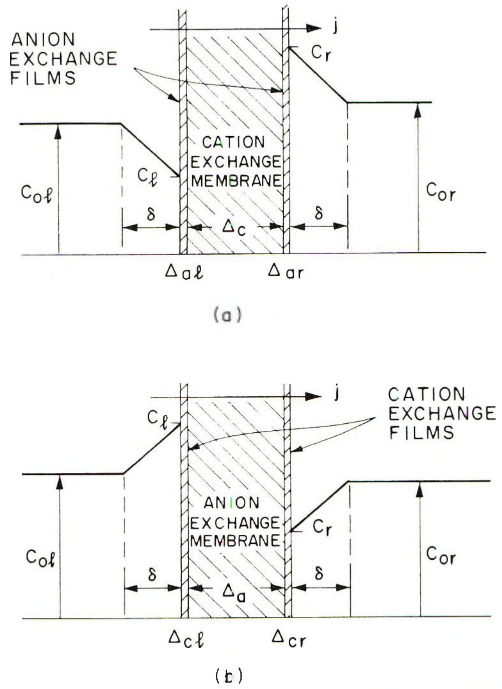

Figure 5. Concentration distributions in bouncing solutions according to Nerst layer model, for $j > 0$. (a) Cation exchange membrane with thin anion exchange surface films, (b) anion exchange membrane with thin cation exchange surface films.

Equation 53 and 57 are discussed further in section 5, and compared with some available experimental data as well as with the earlier theory of Coster.

4. Effect of Concentration Polarization in the Solution Outside the Membrane

In the general case concentration polarization occurs in the solutions outside the membrane whenever current is passed, and the salt concentrations c_l and c_r just outside the membrane then depend on current density and cannot be arbitrarily specified. The performance characteristics of the composite membrane are therefore linked with the diffusion-convection processes in the exterior solutions. In this section we describe how a layered membrane performs when concentration polarization occurs in the solutions outside it.

For illustration we deal only with the case of a cation exchange membrane with a thin anion exchange layer on each side (Figure 5a). Results are also given for an anion exchange membrane with cation surface films (Figure 5b). The analysis can readily be extended to other specific membrane combinations, like the ones discussed in section 3. The present combination was chosen mainly with a view of applying the results to analyze how certain types of membrane fouling affect the limiting current in electrodialysis systems. This is done in a separate paper.[19]

Diffusion polarization in the solutions on each side of the membrane will be characterized in terms of the familiar Nernst model, where ions are assumed to arrive at the membrane boundary by diffusion across a hypothetical stagnant film of thickness δ, outside which the ion concentrations are taken to be uniform. An analysis in terms of a Nernst layer is quite general, since one can insert into it whatever value of δ is appropriate for the particular convective process and geometry at hand. Expressions for δ can be obtained for various types of free and forced convection from several empirical as well as theoretical studies of related mass transfer processes.[20,21] One must keep in mind, however, that in general δ varies with distance along the membrane, and an analysis for a given δ therefore applies *locally*.

Figure 5a shows the effects of concentration polarization in the Nernst layers outside a cation exchange membrane with thin anion exchange surface film. For this combination we have $t_+ \simeq 1$ and $t_- \ll 1$. (See section 3.2. We are concerned here with currents of the order of the limiting values, where the second terms in eq 37 and 38 can be shown to be small.) The salt concentration profile in the Nernst layers is linear, as given by eq 15. With $t_+ = 1$, eq 15 yields

$$c_l = c_{ol} - \frac{1}{2}\frac{j\delta}{ZFD} \tag{58}$$

$$c_r = c_{or}\frac{1}{2}\frac{j\delta}{ZFD} \tag{59}$$

where c_{ol} and c_{or} are salt concentrations in the undisturbed solutions on the left- and right-hand sides, and D is the salt diffusion coefficient in the solution.

Let us consider first how saturation occurs at positive currents. It was shown in section 3 that a cation membrane with thin anion surface films has a positive limiting current given by

$$j_{\mathrm{lim}} = \frac{ZFD_a c_l^2}{\Delta_{al} c_a} \tag{60}$$

This limiting current is the result of polarization within the layered membrane. Substituting for c_l from eq 58, eq 60 yields the following equation for j_{lim}

$$\frac{j_{\mathrm{lim}}}{j_{al}} = \left(1 - \frac{j_{\mathrm{lim}}}{j_{ol}}\right)^2 \tag{61}$$

Here

$$j_{ol} \equiv \frac{2ZFDc_{ol}}{\delta} \tag{62}$$

is the diffusion-controlled limiting current which one would obtain in the absence of an anion film on the membrane, and

$$j_{al} \equiv \frac{ZFD_a c_{ol}^2}{\Delta_{al} c_a} \tag{63}$$

is the membrane-controlled limiting current one would have with infinitely effective stirring of the left-hand solution ($c_l = c_{ol}$ in eq 60).

From eq 61 we obtain the positive limiting current density as

$$j_{\mathrm{lim}} = j_{ol}\left[1 + \frac{\alpha}{2} - \alpha^{1/2}\left(1 + \frac{\alpha}{4}\right)^{1/2}\right] \tag{64}$$

where

$$\alpha \equiv \frac{j_{ol}}{j_{al}} = \frac{2\Delta_{al} c_a}{D_a}\frac{D}{\delta c_{ol}} \tag{65}$$

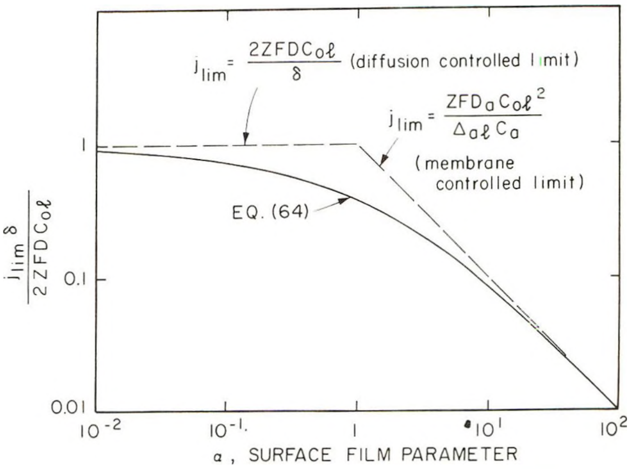

Figure 6. Limiting current density as a function of the surface film parameter α, for a cation exchange membrane with thin anion exchange surface films.

is the ratio of the diffusion-controlled and the membrane-controlled values of the limiting current.

Equation 64 establishes that the ratio of the limiting current to the value it would have if the anion exchange surface layers were absent is a function of the single parameter α. It is clear that the magnitude of the actual limiting current is controlled by the *smaller* of the quantities j_{ol} and j_{al}. If one expands eq 64 for small and large α, keeping only terms to first order, one obtains

$$\alpha \ll 1{:}\ j_{\mathrm{lim}} = j_{ol}(1 - \alpha^{1/2}) \tag{65a}$$

$$\alpha \gg 1{:}\quad j_{\mathrm{lim}} = j_{al}(1 - 2/\alpha) \tag{65b}$$

Thus, when $\alpha^{1/2}$ is small, the limiting current is controlled by concentration polarization in the diffusion layer, and is somewhat less than j_{ol}. When α is large, on the other hand, the anion film controls the limiting current, and polarization outside the membrane is negligible. The limiting current is then somewhat smaller than j_{al}.

Figure 6 shows the ratio of the positive limiting current to the diffusion-controlled value it would have in the absence of the anion surface films, as a function of the "surface film parameter" α defined in eq 65. The transition from the diffusion-controlled limit (at $\alpha \ll 1$) to the film-controlled limit (at $\alpha \gg 1$) is actually quite gradual.

The above discussion applies to the positive limiting current. The negative limiting current follows in a similar fashion. The complete current-voltage characteristic for the system shown in Figure 5a can be obtained from the equations derived in section 3.2. Let $\Delta\psi$ be the dimensionless potential drop from the outer edge of the left-hand diffusion layer to the outer edge of the right-hand diffusion layer. $\Delta\psi$ is thus the sum of the potential drop Ψ across the layered membrane, which for the case at hand is given by eq 45 with c_l and c_r from eq 58 and 59, and the total drop across the two diffusion layers. The latter can be obtained from eq 16. The result is

$$\Delta\psi = \frac{j}{j_c} + \ln\frac{\left(1 + \frac{j}{j_{or}}\right)^2 + \frac{j}{j_{ar}}}{\left(1 - \frac{j}{j_{ol}}\right)^2 - \frac{j}{j_{al}}} + \ln\frac{c_{or}}{c_{ol}} \tag{66}$$

[20] V. G. Levich, "Physicochemical Hydrodynamics," Prentice-Hall, Englewood Cliffs, N. J., 1962.

[21] A. J. Arviva and S. L. Marchiano, "Modern Aspects of Electrochemistry," No. 6, J. O'M. Bockris and B. E. Conway, Ed., Plenum Press, New York, N. Y., 1971, pp 159-241.

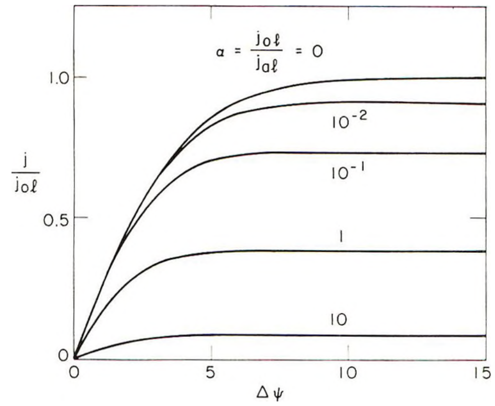

Figure 7. Current–voltage characteristics for a cation exchange membrane with thin anion exchange surface films, showing the effect of the surface film parameter α.

Here

$$j_c = \frac{ZFD_cc_c}{\Delta_c} \tag{67}$$

is a quantity with the dimensions of current density which measures the conductance of the cation exchange membrane. The quantities

$$j_{or} = \frac{2ZFDc_{or}}{\delta} \tag{68}$$

and

$$j_{ar} = \frac{ZFD_ac_{or}^2}{\Delta_{ar}c_a} \tag{69}$$

are the magnitudes of the diffusion-controlled and membrane-controlled limiting currents, respectively, for negative current density. These are similar to j_{ol} and j_{al}, except that they are based on the right-hand salt concentration and the properties of the right-hand anion exchange film. We recall that the limiting current for the anion-cation-anion membrane is governed by the conditions where the current vector enters the membrane.

Figure 7 shows j as a function of $\Delta\psi$ for $j > 0$, as given by eq 66. These particular results are for the case of a symmetrical membrane with the same salt solution on both sides ($j_{ar} = j_{al}$, $j_{or} = j_{ol}$), and for simplicity we have also assumed that the ohmic resistance of the cation membrane itself is negligible ($j_c \gg j_{ol}, j_{al}$) so that only the logarithmic term contributes to the potential. The curves then depend only on the parameter α defined in eq 65.

For an anion exchange layer with thin cation exchange surface films (Figure 5b), the results are quite similar in form to the ones we have developed above for the cation layer with anion films. All the equations can be transformed to this case by exchanging the subscript l with r, and a with c. For positive current, polarization is now controlled by conditions on the *right*-hand side in this case, that is, on the side where the current vector exits from the membrane.

5. Discussion and Comparison with Available Data

In section 3 we have derived the steady-state performance characteristics of a family of ion exchange membranes composed of contiguous layers of anion and cation exchange materials. The current–voltage characteristics and ion transport numbers are given in explicit analytic form.

Previous work in this area has been essentially confined to the bipolar membrane, which consists of an anion exchange layer and a cation exchange layer joined together. Coster[5] has presented an approximate analysis for the current–voltage characteristic of a bipolar membrane. If one takes his result (eq 20. ref 5) to our limit where the Debye length is infinitely thin compared with the thickness of the layers, one obtains in our notation

$$\Psi - \Psi_0 = -\ln\left[1 - \frac{j}{ZF\left(\frac{c_l^2}{c_a}\frac{D_a}{\Delta_a} + \frac{c_r^2 D_c}{c_c\Delta_c}\right)}\right] \tag{70}$$

where Ψ_0 is the potential at zero current (not explicitly specified in ref 5). Equation 70 is equal to our eq 53 with the first (ohmic) term on the right-hand side deleted, and with Ψ_0 expressed by eq 57. Coster's result gives the same saturation current as ours, and is also in agreement with ours for currents in the opposite direction provided the negative applied voltage is sufficiently small. However, for larger negative voltages the ohmic term is the governing influence on the current–voltage relation, and Coster's result is in error.

We note that the diffusion coefficients which appear in Coster's result are those of the *co-ions* in the layers of the membrane. Our own eq 53 might be generalized in an *ad hoc* fashion to the case where the positive and negative ions have unequal diffusion coefficients by interpreting the diffusion coefficients which appear in the first (ohmic) term as those of the counterions, and the diffusion coefficients which appear in the second (logarithmic) term as those of the coions.

Some numerical computations for bipolar membranes have also been given by George and Simons,[15,16] but these are for cases where the Debye length is not small, and cannot be compared with our present theory.

Experimental data on the steady-state characteristics of bipolar membranes have been published by Frilette[7] and Ishibashi and Hirano.[8,9] They showed that the current–voltage relation was essentially ohmic in one direction (current vector entering from the cation exchange layer side), while in the reverse direction the current tended to saturate. This is in qualitative agreement with our theory. In the experiments, however, the current was found to increase again as sufficiently high voltages were applied in the reverse direction (Figure 5, ref 8). This was due to the ionization of water, and the current in this "polarized" region was carried predominantly by H^+ and OH^- ions rather than by the salt ions (Figure 2, ref 8). Our theory is not applicable in this region of the current–voltage characteristic. Most of Frilette's quantitative data fall outside the scope of our analysis for this reason. Ishibashi and Hirano, however, have published a current–voltage characteristic showing clearly the initial current saturation prior to the onset of water splitting (Figure 5, ref 8). Although they do not specify sufficient parameters to allow a rigorous comparison, our eq 56b gives a saturation current which is of the same order as their measurement of 80 A/m^2, if one assumes reasonable values[8-10] for the missing parameters.

Ishibashi[9] has also measured the potential across a bipolar membrane at zero current. His published data are somewhat ambiguous, at least in the English language version of his paper,[9] since the sense of the quoted potential is not explicitly defined. It appears, however, that the potentials quoted must refer to the potential of the more dilute solution with respect to that of the more concentrated solution (this can be inferred by analyzing the data

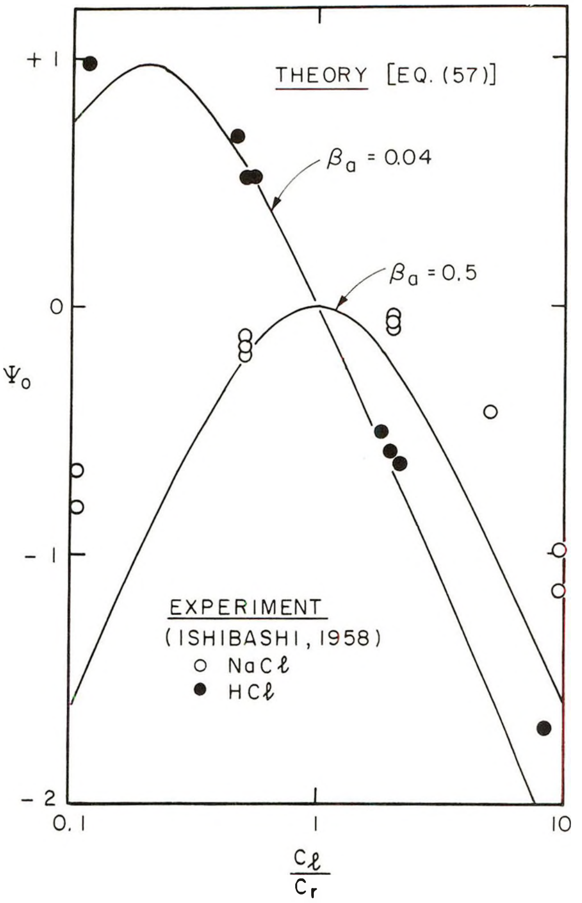

Figure 8. Potential across a bipolar membrane at zero current as a function of the concentration ratio across the membrane.

on Figure 2 of ref 9).[21a] In Figure 8 we plot Ishibashi's data, interpreted in this way, against the ratio of the left-hand concentration to the right-hand concentration. The membrane is oriented as in Figure 4, with the anion exchange layer on the left, and Ψ represents the dimensionless potential on the left side with respect to that on the right, as in section 3. The temperature in the experiments was assumed to be 20°.

Also shown on Figure 8 are theoretical curves (eq 57) for $\beta_a = 0.5$ and 0.04. The precise values of β_a appropriate to the data are not known, since Ishibashi does not give sufficient information on the structure of his membrane. However, assuming that the thickness and fixed charge concentrations of the anion and cation exchange layers are roughly the same, the value of β_a (see eq 54) for NaCl should be in the neighborhood of 0.5, since the effective diffusion coefficient in the anion layer was only somewhat smaller than in the cation layer.[9] For HCl, the diffusion coefficient in the anion layer was very large compared with that in the cation layer, and β_a should be small compared with unity. The value of 0.04 gives a good fit with the data. The theory seems to correctly predict the trend of the measurements. The quantitative agreement obtained with a reasonable choice for the value of a single unknown parameter is also quite good, particularly if one considers that some of the theoretical assumptions (dilute salt solutions, salt concentrations very small compared with fixed charge concentrations, equal diffusion coefficients for positive and negative ions) were violated to a greater or lesser degree in experiments.

The theory of section 3 can be applied directly to practical cases only if the salt concentrations on both sides of the membrane are independently known. In other words, the degree of concentration polarization in the bounding solutions must be either known or negligible. An analysis for the effects of concentration polarization is given in section 4 for the particular case of a membrane consisting of a thick central ion exchange layer of one sign with very thin surface layers of ion exchange material of the opposite sign. The local current is expressed in terms of the membrane structure and the local Nernst layer thickness. To apply the analysis to practical cases, the Nernst layer thickness must be known from external considerations (either empirical or theoretical). In many cases an average value can be used, but in others it is important to take into account the spatial variation of the layer thickness. In a separate paper[19] we have applied this analysis to an electrodialysis system with laminar flow, where the effective Nernst layer thickness is accurately known from theory.[22] The analysis is intended to model the effects of certain types of fouling, where the membranes acquire thin surface layers with ion exchange properties of opposite sign. Experiments show that such layers cause the reduction of the limiting current below the value expected on the basis of concentration polarization alone, and the theory[19] is shown to correctly predict the trend of the experimental results.

Acknowledgment. This research was sponsored by the Office of Saline Water, U. S. Department of the Interior, under Grant No. 14-30-2749.

Symbols

$c_\pm$	concentration of positive/negative (mobile) ions, gm mol/m^3.
c_a, c_c	reduced fixed charge concentrations in anion and cation exchange layers, respectively (eq 10 and 6).
c_l, c_r	concentrations (gm mol/m^3) on left and right sides of membrane, respectively.
c_m	fixed charge concentration in ion exchange membrane, gm mol/m^3.
c_{0l}, c_{0r}	undisturbed concentrations (gm mol/m^3) in compartments on left and right side of membrane, respectively.
D	diffusion coefficient; in section 4, diffusion coefficient in solution bounding membrane, m^2/sec.
D_a, D_c, D_n	diffusion coefficients in anion exchange, cation exchange, and neutral layers, m^2/sec.
F	Faraday's constant, 96,500 coulombs/gm-equivalent weight.
j	current density, A/m^2.
$\grave{j}$	reduced current density defined in eq 39.
j_{lim}	limiting current density, A/m^2.
j_{0l}, j_{0r}	diffusion-controlled limiting current densities for left- and right-hand sides of membrane (eq 62 and 68) A/m^2.
j_{al}, j_{ar}	membrane-controlled limiting current densities for left- and right-hand sides of cation membrane with anion surface films (eq 63 and 69), A/m^2.

(21a) Note Added in Proof. This interpretation is confirmed by N. Ishibashi, private communication.

(22) A. A. Sonin and R. F. Probstein, *Desalination*, **5**, 293 (1968); **6**, 270 (1969).

R	universal gas constant, 8.31 J/°K g mol.
$t_\pm$	transport numbers for positive/negative ions, eq 4.
T	absolute temperature, °K.
x	distance, measured in direction of positive current.
Z	charge number of salt ions.
Z_m	charge number of fixed ions in membrane layer.
α	dimensionless surface film parameter, eq 65.
β_a, β_c, β_{al}, β_{ar}, β_{cl}, β_{cr}	dimensionless parameters characterizing membrane structure, eq 40.
$\Gamma_\pm$	positive/negative ion flux density, gm mol/m^2 sec.
δ	Nernst layer thickness, m.
Δ_{al}, Δ_{ar}	thickness of left- and right-hand anion exchange layers, respectively, m.
Δ_{cl}, Δ_{cr}	thickness of left- and right-hand cation exchange layers, respectively, m.
Δ_a, Δ_c	total thicknesses of anion and cation exchange materials in membrane, m.
ϕ	potential, V.
Φ	potential drop from left- to right-hand side of membrane, $\phi_l - \phi_r$.
ψ	dimensionless potential, $ZF\phi/RT$.
ψ_l, ψ_r	dimensionless potentials on left- and right-hand sides of membrane.
Ψ	dimensionless potential drop from left- to right-hand side of membrane, $\Psi = \psi_l - \psi_r = ZF\Phi/RT$.
$\Delta\psi$	dimensionless potential drop from the outer edge of the Nernst diffusion layer on the left side of the membrane to the outer edge of the Nernst diffusion layer on the right side of the membrane.

Factors Influencing Reverse Osmosis Rejection of Organic Solutes from Aqueous Solution

J. E. Anderson,* S. J. Hoffman, and C. R. Peters

Scientific Research Staff, Ford Motor Company, Dearborn, Michigan 48121

(Received May 15, 1972)

Publication costs assisted by the Ford Motor Company

Factors governing the reverse osmosis rejection of organic solutes from aqueous solutions have been examined. The partition coefficients, diffusion constants, and RO rejection of 12 organic solutes were studied relative to "tight" cellulose acetate and cellulose acetate butyrate membranes. The solute partition coefficients between water and membrane parallel partition coefficients between water and organic liquids. Un-ionized and hydrophobic solutes are strongly sorbed by the membranes; these solutes exhibit poor RO rejection. Ionized and hydrophilic solutes have low solubility in the membranes and experience good rejection. Significant changes in sorption and rejection accompany solute ionization through pH adjustment. For example, *p*-nitrophenol exhibits −0.4 negative rejection in its un-ionized form, but +0.84 positive rejection when it is ionized. An inverse proportionality between diffusion constants and partition coefficients is observed; this can be interpreted in terms of "bound" and "free" solute molecules within the membranes.

Introduction

The reverse osmosis (RO) rejection of organic solutes from aqueous solutions has received much less attention than the rejection of inorganic solutes. With a few notable exceptions,[1-5] scant RO data on aqueous-organic systems have been published. It has been established, however, that organic solutes show much larger variations in rejection characteristics for a given membrane than do inorganic solutes. For example, Lonsdale, *et al.*,[1,2] studied rejection of organic solutes with RO membranes whose rejection of inorganic solutes was uniformly greater than 95%. Organic rejection varied from +99%, in the case of sugars, to −20%, in the case of phenol.

Owing to the limited amount of experimental data, it is difficult to assess the potential of RO in separating aqueous-organic systems. This motivated the present study; we have examined factors that influence RO rejection of organic solutes from aqueous solutions.

It is well established that the RO rejection characteristics of a membrane toward a given solute/solvent system is determined by the relative permeabilities of solute and solvent. The permeability, in turn, is the product of two factors: (a) the concentration of the species in the membrane, characterized by its solubility or partition coeffi-

---

(1) H. K. Lonsdale, B. P. Cross, F. M. Graber, and C. E. Milstead, *J. Macromol. Sci.-Phys.* **5B**, 167 (1971).

(2) H. K. Lonsdale, U. Merten, and M. Tagami, *J. Appl. Poly. Sci.*, **11**, 1807 (1967).

(3) F. M. Graber, H. K. Lonsdale, C. E. Milstead, and B. P. Cross, *Desalination*, **7**, 249 (1970).

(4) S. Sourirajan, *Ind. Eng. Chem., Prod. Res. Develop.*, **4**, 201 (1965).

(5) H. K. Lonsdale, R. L. Riley, C. E. Milstead, L. D. LaGrange, A. S. Douglas, and S. B. Sachs, *OSW (Off. Saline Water) Res. Develop. Progr. Rep.*, **No. 577** (1970).

cient; and (b) the rate at which the species is transported across the membrane, characterized by its diffusion coefficient.[6] The solubility and diffusion coefficients of water in RO membranes has been determined by Lonsdale, Merten, and Riley.[7] Consequently, we studied the partition coefficients, diffusion constants, and RO characteristics of organic solutes alone. "Tight" cellulose acetate (CA) and cellulose acetate butyrate (CAB) membranes were used. Solutes were chosen to represent a wide variety of water-soluble organic compounds. The solutes were chosen to have strong uv absorption, since uv spectroscopy is a convenient method for determining low solute concentrations in water. Much of the present study augments work recently published by Lonsdale, Cross, Graber, and Milstead.[1] Their paper is designated LCGM throughout the present article.

Experimental Section

The CA membranes used in this study were cast on glass plates from solutions containing 20% 39.8 CA (Eastman 4644), 30% formamide, and 50% acetone (by weight). The CAB membranes were prepared from casting solutions containing 22% CAB (Eastman 4623), 2% glycerol, 6% 1-propanol, 25% triethyl phosphate, and 45% acetone.[8] The solvents were removed by prolonged soaking in distilled water. Before use in diffusion or partition coefficient studies, the washed CA and CAB membranes were *fully dried* by heating in air at 85 ± 5° for at least 2 hr. The dried membranes were found to be uniform and nonporous by electron microscopy; microvoids were not observed. The electron microscopy observations were made at 22,400× magnification. Asymmetric CA membranes, prepared by the casting technique of Loeb and McCutchan,[9] were used in the RO studies. They typically gave 97% NaCl rejection and a water throughput (68 atm) of 6.3×10^{-4} cm/sec.

Partition coefficients were determined by the sorption method. Weighed amounts of the dried membrane were added to aqueous solutions of the various solutes. Changes in solute concentration in the solution upon addition of membrane were determined by uv spectroscopy. Sorption of urea was monitored with a differential refractometer. The starting solute concentrations varied somewhat, depending on uv extinction coefficients and expected solubility in the membrane. We generally worked with 10^{-4} gm/l. solutions; in no case was the solute concentration in the membrane allowed to exceed 5%. Duplicate samples were run. The resulting partition coefficients usually agreed to ±10%. The scatter was somewhat larger with weakly sorbed solutes, where in some cases partition coefficients were obtained by desorption. The experiments were performed at 23 ± 1°. Unless otherwise stated, the solutions were prepared with distilled water, pH 5.6.

All solutes were reagent grade chemicals. They were obtained from commercial sources and used without further purification. 3,5-Di(carbethoxy)phenol was donated by our colleague, L. R. Mahoney. Ultraviolet spectra were run on a two-beam Jasco Model ORD/UV-5 spectrometer. Distilled water was placed in the reference beam for most of the measurements. In studies of pH dependence, aqueous phosphate buffers served as reference solutions. We encountered several samples containing both the ionized and un-ionized forms of a given solute. These solutions have composite uv spectra, corresponding to uv absorption by both species. In order to minimize errors in these cases, the sample pH was lowered (bringing the solute completely into the un-ionized form) before uv analyses were carried out.

Diffusion coefficients were obtained by following the sorption, or desorption, of solute from plane sheets of membrane having a known thickness that ranged between 20 and 50 μ. The solutes were generally eluted into a known volume of distilled water; in the pH studies, this was replaced by an aqueous buffer solution. A Waters Associates Model 403 differential refractometer was used to monitor changes of solute concentration in the solution. This is the same method employed by LCGM.[1] With our system, we found that the refractometer sampling arm took some 30–50 sec to respond to concentration changes in the sorption vessel. A convolution correction was introduced into our data analysis to account for this time lag. This correction is important only for solutes with large diffusion constants ($\geq 10^{-8}$ cm^2/sec). Experimental data were matched to curves generated by the expression[10]

$$M(t)/M(\infty) = 1 - \sum_{n=1}^{\infty} \frac{2\alpha(1+\alpha)}{(1+\alpha+\alpha^2 q_n^2)} \exp[-Dq_n^2 t/l^2] \quad (1)$$

where α is the ratio of the volumes of solution and sheet, divided by the partition coefficient of solute between water and membrane. The q_n are roots of the equation $\tan q_n = -\alpha q_n$. Values of q_n for various values of α have been tabulated by Crank.[10] In some cases, notably when the membrane contained both the ionized and un-ionized forms of a solute, experimental data gave a poor fit to eq 1. In these situations, diffusion coefficients were determined from the long-time behavior of M(t). The possibility of non-Fickian diffusion was not investigated. All measurements were made at 23 ± 1°.

The design of our reverse osmosis unit followed that of Loeb and McCutchan.[9] The RO cell has an effective area of 13.2 cm^2. Pressure was generated by a Sprague Model S216-CS air-driven pump. The RO unit experiences pressure fluctuations of order 20% in the course of each pumping cycle.

Results and Discussion

Our experimental partition coefficients, K, diffusion coefficients, D, and RO solute rejections, R, are presented in Table I. Our definitions of R and K are

$$R = 1 - \frac{\text{(concn of solute in product water)}}{\text{(concn of solute in feed water)}} \quad (2)$$

$$K = \frac{\text{(final wt of solute in membrane)}}{\text{(wt of membrane)}} \Big/ \frac{\text{(final wt of solute in solution)}}{\text{(wt of solution)}} \quad (3)$$

This definition of K differs slightly from that used by LCGM,[1] and by Lonsdale, Merten, and Tagami.[2] If the density of the water-swollen tight membranes is 1.25 gm/

---

[6] See, for example, J. Crank and G. S. Park in "Diffusion in Polymers," J. Crank, Ed., Academic Press, London, 1968, p 5.

[7] H. K. Lonsdale, U. Merten, and R. L. Riley, *J. Appl. Poly. Sci.*, **9**, 1341 (1965).

[8] This recipe for CAB is given by S. Mankikian and M. I. Foley, *OSW (Off. Saline Water) Res. Develop. Progr. Rep.*, **No. 612** (1970), p 15.

[9] S. Loeb and J. W. McCutchan, *Ind. Eng. Chem., Prod. Res. Develop.*, **4**, 114 (1965).

[10] See, for example, J. Crank, "Mathematics of Diffusion," Clarendon Press, Oxford, 1956, p 53.

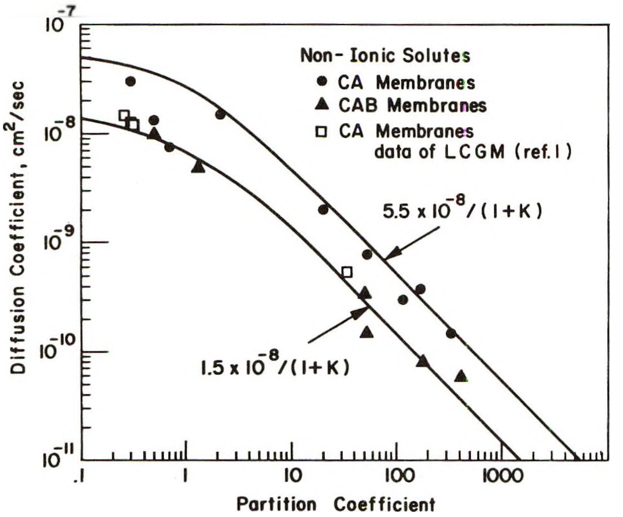

Figure 1. Solute diffusion coefficients *vs.* solute partition coefficients. Solid lines conform to the indicated mathematical expressions, with constants obtained by curve fitting.

TABLE I: Diffusion Coefficients, Partition Coefficients, and RO Rejection of Organic Solutes by CA and CAB Membranes

Solute	Membrane	$D \times 10^{10}$ cm²/sec	K	R (68 atm)
Phenol	CA	10	37 ± 1	−0.09
	CAB	1.5	51 ± 1	
2,4-Dichlorophenol	CA	1.5	332 ± 7	(−0.33)[a]
	CAB	0.7	405 ± 5	
p-Bromophenol	CA	3.8	165 ± 2	
	CAB	0.84	175 ± 2	
Acetone	CA	300	0.3 ± 0.1	(+0.17)[b]
	CAB	100	0.49 ± 0.05	
Hydroquinone	CA		3.5 ± 0.2	
	CAB		5.4 ± 1.5	
Nitromethane	CA	150	2.1 ± 0.5	−0.06
	CAB	100	4.0 ± 0.6	
Nitrobenzene	CA	8.0	54 ± 4	
	CAB	3.5	105 ± 5	
Pyridine	CA	75	0.7	
	CAB	50	1.33 ± 0.03	
Urea	CA	130	0.49 ± 0.03	(+0.45)[a]
Aniline	CA	20	20 ± 2	+0.04
	CAB	3.5	52 ± 3	
3,5-Di(carbethoxy)phenol	CA	1.8	129 ± 12	
	CAB		110 ± 10	

[a] Data of LCGM (ref 1), 102 atm. [b] Data of Sourirajan (ref 4), 102 atm.

cm³, the values in Table I should be 20% lower than those reported by the other authors. There is fairly good agreement between the present results and data reported in the literature. The exception is 2,4-dichlorophenol, where our K values are roughly ten times larger than that reported by LCGM,[1] and our diffusion coefficients are some five times smaller.

It can be seen that the partition coefficients obtained using CAB membranes are consistently larger than those found with CA membranes. In contrast, solute diffusion in CAB is slower than diffusion in CA.

It is clear that factors other than molecular size influence solute partition coefficients; pyridine, aniline, and phenol have roughly the same molecular dimensions, yet exhibit substantially different K values. A crucial test of solubility arguments based on molecular size and membrane "pore dimensions" is afforded by 3,5-di(carbethoxy)-phenol, a bulky molecule whose dimensions approximate the 8–10 Å pore diameter determined experimentally for "tight" CA membranes.[11] Rather than being rejected, this compound is strongly sorbed! This finding could be taken to indicate the complete inadequacy of the "pore model" of solute rejection, at least for compounds of this type. Alternatively, one might view experimental pore dimensions as average values of a time-dependent quantity, whose fluctuations produce larger pores for short intervals of time. This would allow for the sorption of solutes whose dimensions exceed the nominal pore diameter.

We found good correlation between solute partition coefficients and the hydrophilic/hydrophobic nature of the solute. The experimental K values for water/CA and water/CAB parallel partition coefficients of organic solutes between water and organic solvents, *e.g.*, hexane, benzene, etc.[12,13] It would appear that the partition coefficients of organic solutes in these membranes can be understood simply by viewing the membrane as an immiscible organic phase. This implies that any factors that increase or decrease the relative solubility in water will influence partition coefficients, and consequently RO rejection. We confirmed this hypothesis through studies of diffusion coefficients, partition coefficients, and RO rejection as a function of pH. This work is described in the next section.

When $K > 10$, the observed KD product is constant within experimental error. The amount of solute taken up by a membrane can be understood on the basis of hydrophobicity. However, there is no *a priori* reason for a hydrophobic solute to diffuse slower than a hydrophilic solute once both are within the membrane. One might question the possible influence of surface sorption on these diffusion measurements. We studied desorption of several solutes out of membranes of varying thickness. The results were consistent with the thickness dependence predicted by eq 1; on this basis, we conclude that surface effects are unimportant.

It seems likely that the polymer–solute interactions that produce strong solute sorption by the membrane (large partition coefficients) also impede the translational mobility of the solute molecules. The exact nature of these polymer–solute interactions is unknown, but it is useful to think of them in terms of an exchange reaction within the membrane between "free" (or mobile) solute molecules, S_f, and "bound" (or immobile) solute molecules, S_b[14]

$$[S_b] \rightleftharpoons [S_f] \tag{4}$$

If we define an equilibrium constant, $H = [S_b]/[S_f]$, the observed diffusion constant is $D_{obsd} = D_f/(1 + H)$, where D_f is the diffusion constant of the free solute molecules; this is the diffusion rate of the free molecules multiplied by the fraction of time they are free. We can go further and assume that the partition coefficient is determined by this mobile/immobile equilibrium. This equates H and K and yields the relation $D_{obsd} = D_f/(1 + K)$. The rationale for using this expression to link diffusion and partition coefficients is admittedly crude. It requires several as-

---

(11) G. Thau, R. Bloch, and O. Kedem, *Desalination*, **1**, 129 (1966).

(12) C. Golumbic, M. Orchin, and S. Weller, *J. Amer. Chem. Soc.*, **71**, 2624, 2627 (1949); **72**, 4145 (1950).

(13) C. Hansch, K. Kiehs, and G. L. Lawrence, *J. Amer. Chem. Soc.*, **87**, 5770 (1965), and earlier papers in this series.

(14) Reference 10, p 121.

TABLE II: Reverse Osmosis Results (Asymmetric CA Membranes)

Solute	Feed pH	ΔP, atm	Product flux, $\times 10^4$ cm/sec	Product pH	Rejection
Phenylacetic acid,	2.6	34	2.02	3.5	+0.29
10^{-4} g/l.	2.6	68	4.7	3.5	+0.25
[pK_a = 4.31 (25°)][a]	7.8	34	2.5	7.2	+0.93
	7.8	68	5.8	7.3	+0.92
Aniline,	3.3	34	3.3	6.4	+0.88
10^{-4} g/l.	3.3	68	7.3	6.4	+0.78
[pK_b = 4.58 (25°)][a]	9.1	34	3.3	7.3	+0.09
	9.1	68	6.8	7.5	+0.04
Phenol,	4.4	34	1.4	6.1	−0.09
5×10^{-4} g/l.	4.4	68	3.0	6.3	−0.12
[pK_a = 9.89 (25°)][a]	11.2[b]	34	5.4	9.5	+0.88
	11.2[b]	68	10.8	9.6	+0.83
Nitromethane	7.2	34	5.8	7.3	−0.06
	7.2	68	11.5	6.6	−0.09
Boric acid	7.0	34	4.7	6.6	+0.43
[pKa = 9.1 (25°)][a]	7.0	68	9.0	6.5	+0.67
	11.0[b]	34	3.1	9.6	+0.97
	11.0[b]	68	8.8	9.7	+0.97

[a] pK values taken from "Handbook of Chemistry and Physics," Chemical Rubber Publishing Co., Cleveland, Ohio. [b] Possible membrane hydrolysis is indicated by the high product flux.

sumptions and ignores many factors, such as, the variation of D with molecular size. However, as illustrated in Figure 1, it represents our experimental data very well.

As indicated in Table I, we did not carry out RO studies on all solutes whose partition and diffusion coefficients were determined. The analysis of LCGM[1] (see eq 6 of the present paper) indicates poor or negative RO rejection whenever the DK product of the solute is comparable to $(D_w C_w \bar{V}_w \Delta P)/RT \simeq 2 \times 10^{-8}$ gm/cm sec (for $\Delta P = 100$ atm); where D_w, C_w, and $\bar{V}_w$ are the diffusion constant, solubility, and partial molal volume of water in the membrane, and ΔP is the applied pressure difference across the membrane. On the basis of the large KD products of the various solutes, it was evident that none would be strongly rejected. We note that LCGM[1] found the partition and diffusion coefficients of NaCl to be 0.038 and 3.2×10^{-9} cm²/sec in CA membranes. Other ionic solutes, all showing strong RO rejection, have similar coefficients. Comparing these values with those in Table I, it seems clear that the great solubility of un-ionized and hydrophobic solutes in the membranes is primarily responsible for their poor rejection.

Effects of pH on Permselectivity. It is well known that pH variations change the partition coefficient of a solute between immiscible organic and aqueous layers. These effects are particularly dramatic near the pK_a of a weak acid or weak base, where the solute changes from a predominantly ionized state to a predominantly un-ionized form. Since the ionized solute is more soluble in the water layer and insoluble in the organic layer than the un-ionized solute, large changes in partition coefficients are not unusual.

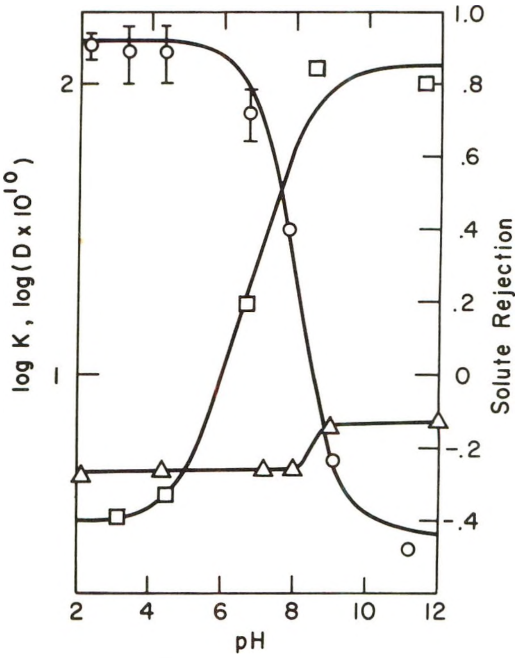

Figure 2. Partition coefficients, ○; diffusion coefficients, △, and RO rejection, □, of p-nitrophenol as a function of pH. The curve through the partition coefficient data was obtained from eq 5a–d of the text.

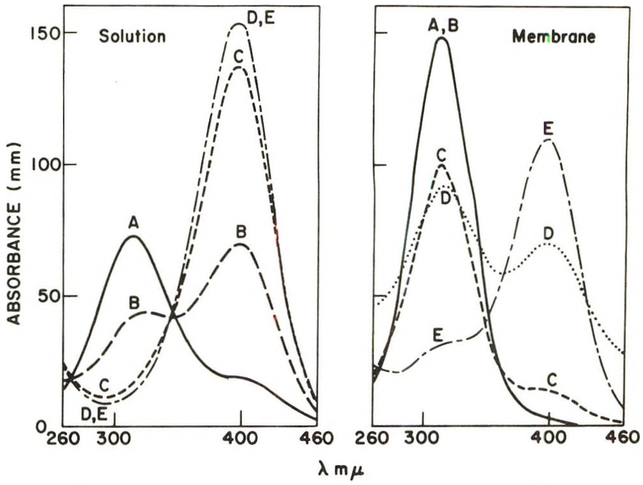

Figure 3. Uv absorption of p-nitrophenol in CA membranes and in solution. The solutions contained 0.2 g/l. of p-nitrophenol in each case. Letters designate the various pH values of the solutions with which the membranes were equilibrated. One should compare the relative intensities of the 314- and 398-mμ maxima in the membrane and the solution as a function of pH. The absolute intensities in the membrane mean very little, as the total solute sorbed by the membrane varies strongly with pH.

With this in mind, we studied the partition coefficients, diffusion coefficients, and RO rejection of p-nitrophenol as a function of pH. Phosphate buffers were used. Other solutes, notably phenol, aniline, and phenylacetic acid, were examined above and below their respective pK_a's (Table II). These results conform to those obtained on p-nitrophenol.

Figures 2–4 show results on p-nitrophenol. The RO rejection (68 atm) increases from −0.4 to +0.84 going from pH 3 to pH 11. There is a concomitant increase in D, from 4×10^{-10} to 1.2×10^{-9} cm²/sec. The partition coefficient drops from 132 ± 5 to 3 ± 1 over this pH range. The variation of K with pH can be computed from the expressions

$$[H^+]_{sol}[NP^-]_{sol}/[NPH]_{sol} = 6.3 \times 10^{-8} \quad (5a)$$

$$[NP^-]_{mem}/[NP^-]_{sol} = 3; \ [NPH]_{mem}/[NPH]_{sol} = 132 \quad (5b)$$

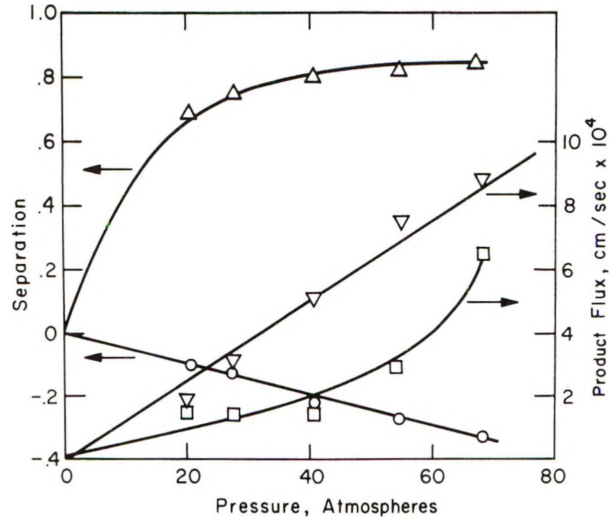

Figure 4. The RO rejection and product flux of *p*-nitrophenol as a function of pressure gradient across the membrane: △, rejection, pH 8.5; ▽, product flux, pH 8.5; ○, rejection, pH 3.0; □, product flux, pH 3.0.

$$[C] = [\mathrm{NP}^-]_{\mathrm{mem}} + [\mathrm{NP}^-]_{\mathrm{sol}} + [\mathrm{NPH}]_{\mathrm{mem}} + [\mathrm{NPH}]_{\mathrm{sol}} \quad (5c)$$

$$K_{\mathrm{obsd}} = ([\mathrm{NP}^-]_{\mathrm{mem}} + [\mathrm{NPH}]_{\mathrm{mem}})/([\mathrm{NP}^-]_{\mathrm{sol}} + [\mathrm{NPH}]_{\mathrm{sol}} \quad (5d)$$

The abbreviations NPH and NP^- denote $O_2NC_6H_4OH$ and $O_2NC_6H_4O^-$; while the subscripts mem and sol refer to the membrane and the bulk solution, respectively. $[C]$ is the total concentration of *p*-nitrophenol added. Equation 5a is obtained from the pK_a; eq 5b, by fitting data at low and high pH; eq 5c is the mass balance requirement. The curve resulting from this treatment is shown in Figure 2.

This analysis implies that $[\mathrm{NP}^-]_{\mathrm{mem}}/[\mathrm{NPH}]_{\mathrm{mem}}$ is smaller than $[\mathrm{NP}^-]_{\mathrm{sol}}/[\mathrm{NPH}]_{\mathrm{sol}}$. This is a consequence of the preferential sorption of uncharged NPH by the membrane relative to NP^-. We confirmed this prediction by comparing the uv absorption of *p*-nitrophenol in the membrane with that in the bulk solution. Ionized *p*-nitrophenol has an absorption maximum at 398 mμ, the un-ionized species at 314 mμ. As shown in Figure 3, the relative intensity of these maxima in the mgmbrane differs from their relative intensity in solution. The variation of $[\mathrm{NP}^-]_{\mathrm{mem}}/[\mathrm{NPH}]_{\mathrm{mem}}$ with the pH of the bulk solution is consistent with preferential sorption of NPH by the membrane. The analysis also suggests that the pH within the membrane is somewhat less than the pH of the solution. This is consistent with our observations that the pH of the RO product waters is slightly less than the pH of the feed solutions.

The RO rejection of *p*-nitrophenol was studied as a function of pressure at pH 3 and 8.5 (Figure 4). At pH 8.5, solute rejection improved with increasing pressure; this result is commonly observed in RO studies of inorganic solutes. At pH 3, negative rejection (solute enrichment in the product water) increased with pressure. Pressure hysteresis effects were not apparent. We could obtain a sample at 34 atm; increase the pressure to 68 atm, take a second sample, then return to 34 atm, and collect a third sample. The solute concentrations of the first and third samples are reproducible.

Similar effects of pressure variation upon negative rejection were reported by Lonsdale, Merten, and Tagami,[2] who studied phenol solutions. These results are consistent with the trend predicted by the expression[15]

$$R = (D_1C_1\bar{V}_1(\Delta P - \Delta\pi) - D_2K_2\bar{V}_2\Delta P)/ \\ (D_1C_1\bar{V}_1(\Delta P - \Delta\pi) + D_2k_2RT) \quad (6)$$

provided that $D_2K_2\bar{V}_2 > D_1C_1\bar{V}_1$. This is simply the requirement for negative rejection. It is noteworthy (Figure 4) that the variation of water flux with pressure is different for positive and negative rejection; the throughput is much more pressure sensitive in the former case. Similar effects were observed by Lonsdale, Merten, and Tagami.[2] It is not clear whether this results from flow coupling, or from plasticization of the membrane by the solute.

Having encountered negative rejection experimentally, one naturally questions its potential application to liquid separation. Different solution/membrane combinations are expected to produce a variety of enrichment factors, owing to diverse interactions among solvent, solute, and membrane. However, enrichment can never exceed the equilibrium value for a membrane completely permeable to *solute* and completely impermeable to *solvent*. (Note that this is the opposite of the optimum situation for solvent separation.) Under these conditions, the chemical potential of the solute on both sides of the membrane can be expressed

$$\mu_A = \mu_0 + RT \ln C_A + \bar{V}P_A$$

$$\mu_B = \mu_0 + RT \ln C_B + \bar{V}P_B$$

where the subscripts A and B denote the two sides of the membrane. Equating these expressions, we find

$$(C_A/C_B) = \exp[\bar{V}(P_B - P_A)/RT]$$

If $\bar{V}$, the partial molar volume of the solute, is 0.1 l. and RT = 24 l.-atm, a pressure difference of some 98 atm is necessary for 50% enrichment of the product; for 200% enrichment, a 168 atm pressure difference is required. Practical applications probably would require concentration enhancements of 10 to 1000 times. Under optimum conditions, pressure differences of some 500–2000 atm would be required to attain such enhancements. Such pressures are, of course, far above the operating range of conventional RO systems at present.

Summary

When the results of the present study are compared with earlier data, a number of conclusions can be drawn.

(1) The partition coefficients of *solutes*, organic and inorganic, ionized and un-ionized, in water/CA and water/CAB parallel solute partition coefficients between water and organic solvents. Ionic and hydrophilic solutes show little tendency to enter the membrane, while uncharged and hydrophobic solutes are strongly sorbed.

(2) Uncharged and hydrophobic solutes, strongly sorbed by the membrane, exhibit poor or negative RO rejection with CA and CAB. The more hydrophobic the solute, the poorer its rejection is likely to be. Our experiments indicate that the great solubility of organic solutes (relative to inorganic solutes) in the membranes is responsible for their poor RO rejection.

(3) Significant changes in sorption (partition coefficients) and RO rejection accompany solute ionization

---

(15) This equation results from combining eq 7 of LCGM (ref 1) with the definition of solute rejection.

through pH adjustment. The strong positive rejections of phenol and substituted phenols at high pH are significantly better than RO rejections reported previously. It must be noted, however, that RO with pH adjustment cannot be used with CA or CAB membranes as a practical means of rejecting phenol. This is a consequence of the hydrolysis and deterioration of CA and CAB membranes under basic conditions.

(4) Molecular size is less important than electrical charge and hydrophilicity in determining RO rejection of a solute. It should be noted, however, that all solutes used in the present study had roughly the same size. It is perfectly reasonable to expect RO differences among a monomer, its oligomers, and its higher polymers.

(5) At least for the uncharged organic solutes examined in the present study, there seems to be an inverse proportionality between diffusion constants and (large) partition coefficients.

A number of puzzling RO results can be understood on the basis of these observations. The poor RO rejection of urea, boric acid, and aromatic amines is explicable from knowledge of their pK_a values. Each of these solutes exists, either partially or wholly, as an uncharged species in water at pH 6. For this reason, one would anticipate their observed RO behavior, *viz.*, water/membrane partition coefficients that are larger than those of ionized solutes, and RO rejection that is poorer. In contrast, primary and secondary aliphatic amines have higher pK_b values than aromatic amines, and exist as charged ions near pH 6. Since they are charged, their good RO rejection[5] might have been predicted. The same argument explains the poor RO rejection of NH_4OH and good rejection of NH_4Cl.[1]

Acknowledgments. We are grateful to H. K. Plummer for electron micrographs, to R. Ullman for useful discussions, and to L. R. Mahoney for access to his unparalleled supply of substituted phenols.

Specific Interactions of Anilines with Water

A. Gomez,[1a] J. Mullens, and P. Huyskens*

University of Louvain, Department of Chemistry, 3030 Heverlee, Belgium *(Received August 9, 1971)*

Publication costs assisted by F. K. F. O. Belgium and the University of Louvain (K. U. L.) Belgium

The extrapolated distribution coefficients P_1 at infinite dilution of several methyl- and chloro-substituted anilines between cyclohexane and water were determined at 15, 25, and 35° using an interferometric method. From these values the transfer heats $\Delta H_1°$ of the monomeric molecules from water to cyclohexane were deduced. Taking into account the effects of the various specific interactions on the change of free energy that occurs when an aniline monomolecule passes from the former to the latter solvent, the following equation is deduced: $\log P_1 = \log P_1^0 + 0.03(\phi - \phi^0) - 0.28(pK_a - pK_a^0) + 0.60(2 - n_{N-H})$, where ϕ is the molar volume of the aniline, n_{N-H} the number of N-H links in the molecule and the superscript ^{0} refers to the unsubstituted molecules. A similar expression is derived for $\Delta H_1°$: $\Delta H_1° = \Delta H_1°^0 - 0.030(\phi - \phi^0) + 0.38(pK_a - pK_a^0) - 0.82(2 - n_{N-H})$, where $\Delta H_1°^0$ refers to unsubstituted anilines. The experimental values of P_1 fit by better than 20% with the calculated values and ΔH does not differ by more than 0.2 kcal from the experimental values. This demonstrates the intervention of N–H···O hydrogen bonds that stabilize the anilines with N–H groups in the water phase. The equilibrium constant for the formation of such bonds is of the order of magnitude of 0.1 M^{-1}. On the other hand Cl···H–O hydrogen bonds do not play an important role in the stabilization of chloroanilines in water and the effects of varying the global dipole moments of the molecules seem to cancel out in the two solvents.

The solubility of anilines in water depends largely on the nature and position of the substituents. For instance, 2,6-dimethylaniline is over five times as soluble in water as *N,N*-dimethylaniline at 25°.

The solubility of anilines in water is determined on one hand by the specific interactions which occur in the aqueous solvent and on the other hand by the stabilization of the aniline molecules in their own phase by the specific links that bring about their association. The two effects can be separated by diluting the anilines in an inert solvent and thus suppressing the specific interactions in the organic phase.

The limiting value of the partition coefficient at infinite dilution of the anilines between this inert solvent and water will be determined only by the specific interactions in the aqueous phase. In this work, we have determined this limiting value of the distribution coefficient, P_1, of several anilines between cyclohexane and water at 15, 25, and 35°.[1b]

The enthalpy charge ΔH_1 associated with the transfer of the monomolecule from water to cyclohexane is deduced

---

(1) (a) Holder of a scholarship from the Belgian Ministry of National Education. (b) Ph. Mahillon assisted with the measurements at 15 and 35°.

TABLE I: Polynomial Coefficients of Eq 1

Aniline substituent	P_1[a]	β	γ	δ
H	1.13 ± 0.02	0.784	1.161	−0.300
2-Methyl	4.45 ± 0.18	5.288	0.986	−0.127
3-Methyl	3.53 ± 0.13	6.262	1.435	−0.215
4-Methyl	3.13 ± 0.07	2.915	2.238	0.000
2,6-Dimethyl	14.34 ± 1.13	18.423	−0.285	0.000
2-Chloro	12.15 ± 0.36	13.344	2.048	−0.274
3-Chloro	4.91 ± 0.11	8.132	4.777	−1.100
4-Chloro	3.94 ± 0.05	8.884	−11.840	0.000
2,6-Dichloro	109.6 ± 6.20	139.920	−17.210	0.000
N-Methyl	15.50 ± 0.36	16.653	0.931	−0.118
N,*N*-Dimethyl	147.6 ± 7.58	113.830	−5.810	0.000

[a] P_1 values given with standard deviation.

from the variation of P_1 with the temperature. Equations relating P_1 and ΔH_1 with the molar volume of the aniline, its pK_a, and the numbers of N–H links are deduced from theoretical considerations. The calculated values are compared with the experimental ones.

I. Determination of the Limiting Value P_1 of the Partition Coefficient. The formalities F_o and F_w of the aniline in both phases are determined by an interferometric method.[2] This method allows for accuracy of better than 0.001 *M* in these measurements. The P_1 values are obtained by the extrapolation of some 30 experimental values whose concentrations in the organic phase, F_o, lie between 0.05 and 4 *M* depending on the solubility of the compound. The experimental values are thus represented by a polynomial of the type

$$P \equiv F_o/F_w = P_1 + \beta F_o + \gamma F_o^2 + \delta F_o^3 \qquad (1)$$

The coefficients of the polynomials are given in Table I.

Table II gives the pK_a values, the molar volume, and the P_1 values found using the polynomial form described above. At the same time we give the P_1 values reported by Columbic and Goldbach[3] and by Kemula, Buchowski, and Pawtowski,[4] and the P_1 values calculated with the equation that will be derived later.

The agreement between our data and those in the publications remains good until P_1 reaches very high values where, at high dilution in the organic phase, the concentration in the water phase is too low to be detected with sufficient precision. We think that in these cases the values of Columbic and Goldbach are very high, because even at higher concentrations in the organic phase we do not observe such high values for *P*.

II. Experiments at Other Temperatures. Heat of Transfer. Similar experiments were also performed at 15 and at 35°. From the values of P_1 at different temperatures it is possible to derive the molar heat of transfer $\Delta H_1°$ of the monomers from water to the organic phase. The values of $\Delta H_1°$ can be compared to those obtained from the difference between the heats of solution of the anilines at infinite dilution in cyclohexane and in water determined by direct calorimetry.[5,6] From the comparison of $\Delta H_1°$ and $\Delta G_1°$ the molar entropy change $\Delta S_1°$ when the monomolecules of aniline pass from water to cyclohexane can be deduced. These results are given in Table III. It must be emphasized that the computed values of ΔS_1 are heavily dependent on those of ΔH_1. However, it appears from the data in Table III that ΔS_1 increases when the molar volume increases. As a crude approximation we can write

$$\Delta S_1° = \Delta S_1°^0 + 0.037(\phi - \phi^0) \qquad (2)$$

III. Deduction of an Equation Relating P_1 to Characteristics of the Substituted Anilines. The transfer of a monomolecule of aniline from the organic phase to water involves the following transformations.

(1) Formation of an Adequate Cavity in Water and Suppression of an Corresponding Cavity in the Organic Phase. This step involves the destruction of some hydrogen bonds between water molecules. The number of hydrogen bonds that must be destroyed is proportional to the volume of the cavity; consequently the corresponding free energy change will be proportional to the molar volume ϕ of the aniline

$$\Delta g_{cav} \equiv a\phi \qquad (3)$$

An alternative method to evaluate g_{cav} could be derived from the scaled particle theory[7,8] which expresses this free energy charge as a polynomial of the third degree of the radius of the sphere which excludes the centers of the solvent molecules. However, approximations must be made owing to the lack of sphericity of the cavities considered here.

(2) Formation of Hydrogen Bonds of the Type O–H···N between Water and the Aniline Molecules. Owing to the basicity of the anilines, these bonds may be expected to constitute the major specific interactions between the anilines and water.

In a great variety of cases, Zeegers-Huyskens[9] showed that for a given proton donor, the logarithm of the complexation constants for such bonds varies in linear fashion with the pK_a of the proton acceptor. It may therefore be expected that the free energy variation corresponding to the formation of these O–H···N bonds between the anilines and water will obey a relation of the form

$$\Delta g_{O\text{-}H\cdots N} = -b - \rho pK_a \qquad (4)$$

where *b* and ρ are appropriate constants.

(3) Formation of N–H···O links between the Anilines in Water. These bonds are expected to be weaker than the previous ones. It may therefore be assumed that, in an initial approximation, the free energy change corresponding to the formation of one bond is the same for all the anilines. Under these circumstances the molar free energy change is proportional to the number of N–H links ($n_{N\text{-}H}$) that the aniline molecule bears

$$\Delta g_{N\text{-}H\cdots O} = -c(n_{N\text{-}H}) \qquad (5)$$

In principle the coefficient *c* also depends on the pK_a of the aniline owing to the expected dependence of the acidi-

---

(2) E. Meeussen and P. Huyskens, *J. Chim. Phys.*, **63**, 845 (1966).

(3) C. Columbic and G. Goldbach, *J. Amer. Chem. Soc.*, **73**, 3966 (1951).

(4) (a) W. Kemula, H. Buchowski, and W. Pawtowski, *Rocz. Chem.*, 42, 1951 (1968); (b) *ibid.*, 43, 1555 (1969).

(5) A. Gomez, L. Lamberts, anc P. Huyskens, *Bull. Soc. Chim. Fr.*, 1734 (1972).

(6) J. Mullens and P. Huyskens, *Annu. Soc. Scient. Bruxell.*, submitted for publication.

(7) H. Reiss, H. L. Fiesch, and L. Lebowitz, *J. Chem. Phys.*, **31**, 369 (1959).

(8) R. A. Pierotti, *J. Phys. Chem.*, **67**, 1840 (1963); **69**, 281 (1965).

(9) (a) A. M. Dierckx, P. Huyskens, and Th. Zeegers-Huyskens, *J. Chim. Phys.*, **62**, 336 (1965); (b) P. Lutgen, M. P. Van Damme, and Th. Zeegers-Huyskens, *Bull. Soc. Chim. Belg.*, **75**, 824 (1966); (c) D. Clotman, J. P. Muller and Th. Zeegers-Huyskens, *ibid.*, **79**, 689 (1970); (d) G. Lichtfus, F. Lemaire, and Th. Zeegers-Huyskens, *Spectrochim. Acta*, in press.

TABLE II: pK_a Values, Molar Volume, and Limiting Partition Coefficients of the Anilines between Cyclohexane and Water at 25°

Aniline substituent	pK_a (25°)	ml/mol	$P_{1(\text{exptl})}$, this work	$P_{1(\text{lit.})}$	$P_{1(\text{calcd})}$
H	4.60[a]	91.56	1.13	1.04,[g] 1.19[i]	
2-Methyl	4.44[a]	107.80	4.45	4.68,[g] 4.04[h]	3.84
3-Methyl	4.70[a]	108.82	3.53	4.32,[g] 3.80[h]	3.49
4-Methyl	5.08[a]	110.94[d]	3.13	3.76,[g] 3.53[h]	3.17
2,6-Dimethyl	3.95[a]	124.17	14.34	22.2[g]	16.27
2,5-Dimethyl	4.53[a]	124.75[e]		16.7[g]	11.70
3,5-Dimethyl	4.91[a]	125.23[e]		15.1[g]	9.49
2,4-Dimethyl	4.89[a]	124.73[e]		16.8[g]	9.29
2-Chloro	2.65[a]	105.79	12.15	17.75[h]	10.47
3-Chloro	3.52[a]	105.33	4.91	7.80[h]	5.83
4-Chloro	4.00[a]	101.60[e]	3.94	4.90[h]	3.32
2,6-Dichloro	0.42[b]	120.23[f]	109.6		117.8
N-Methyl	4.68[c]	109.13	15.50	16.9[g]	14.39
N,*N*-Dimethyl	5.15[a]	127.28	147.6	295[g]	148.7
N,*N*-Dimethyl-2-methyl	5.85[c]	146.38	380	890[g]	356

[a] D. D. Perrin, "Dissociation Constants of Organic Bases in Aqueous Solutions," Butterworths, London, 1965. [b] R. A. Robinson, *J. Res. Nat. Bur. Stand., Sect. A*, **68** (2), 159 (1964). [c] F. Aufauvre, Thèse de Doctorat, Clermont-Ferrand, France, 1969. [d] Calculated value with the density at the melting point (mp 43.5°, $d_4{}^{45}$ = 0.9659; Handbook of Chemistry and Physics, 59th ed, The Chemical Rubber Publishing Co., Cleveland, Ohio, 1968–1969). [e] G. Debecker, Thèse de Doctorat, Louvain, Belgium, 1970. [f] Calculated value with the measured density at melting point (mp ~36.5°, d = 1.34758). [g] Reference 3. [h] Reference 4a. [i] Reference 4b.

ty of the N–H protons on this factor. However, as a first approximation, the variation of c in the case of the anilines studied here can be disregarded, for the p values become low for weak complexation constants.[9]

(4) Formation of Specific Bonds of the Type O–H$\cdots\pi$ and Possibly of the Type O$\cdots\pi$ between the OH Group or the Lone Pairs of Electrons of the Water Molecules and the π Electrons of the Aromatic Ring of the Aniline. It may be assumed as a first approximation that the corresponding variation of free energy remains constant for all the anilines.

$$\Delta g_{\pi\ldots} = -d \qquad (6)$$

(5) Changes in the Nonspecific Interactions. These changes, which must be of minor importance, are proportional to the surface of the aniline molecules and so, in a rough approximation, to their molar volume

$$\Delta g_{\text{ns}} = a'\phi \qquad (7)$$

(Here also an alternative way to compute this term could be derived from the scaled particle theory.)

Assembling these various contributions to the free energy change, one can write

$$RT \ln P_1 = \Delta g_{\text{cav}} + \Delta g_{\text{O-H}\ldots\text{H}} + \Delta g_{\text{N-H}\ldots\text{O}} + \Delta g_{\pi\ldots} + \Delta g_{\text{ns}} = (a + a')\phi - \rho \text{p}K_a - c(n_{\text{N-H}}) - (b + d) \qquad (8)$$

Comparing the limiting partition coefficient P_1 of an aniline with that of the unsubstituted aniline $P_1{}^0$ and owing to the presence of two N–H links in unsubstituted aniline, we can expect a relation of the form

$$\log(P_1/P_1{}^0) = A(\phi - \phi^0) - B(\text{p}K_a - \text{p}K_a{}^0) + C[2 - (n_{\text{N-H}})] \qquad (9)$$

IV. Comparison with the Experimental Values and Deductions. The coefficients A, B, and C of eq 9 were computed from our experimental values of P_1 using a least-squares method; with these values eq 9 becomes

$$\log(P_1/P_1{}^0) = 0.030(\phi - \phi^0) - 0.28(\text{p}K_a - \text{p}K_a{}^0) + 0.60[2 - (n_{\text{N-H}})] \qquad (10)$$

TABLE III: Enthalpy and Entropy Changes with the Transfer of the Monomolecules from Water to Cyclohexane

Aniline substituent	T, °C	P_1	$\Delta H_1°$, kcal mol^{-1}	$\Delta H_1°$, (exptl), kcal mol^{-1}	$\Delta S_1°$, cal °K mol^{-1}	$\Delta H_1°$ (calcd), kcal mol^{-1}
None	15	0.90			12.2	
None	25	1.13	3.57	3.48	12.2	
None	35	1.35			12.2	
2-Methyl	15	3.83			12.6	
2-Methyl	25	4.45	2.86	3.07	12.6	3.02
2-Methyl	35	5.30			12.6	
4-Methyl	15	2.60			13.2	
4-Methyl	25	3.13	3.26		13.2	3.17
4-Methyl	35	3.74			13.2	
N-Methyl	15	13.90			12.8	
N-Methyl	25	15.50	2.17		12.7	2.25
N-Methyl	35	17.80			12.8	

By means of this equation, we recalculated the various P_1 values. The results are given in Table I. The calculated values do not differ by more than 20% from our observations.

The transfer heat $\Delta H_1°$ is related to P_1 by the equation

$$\Delta H_1° = -RT \ln P_1 + T\Delta S_1° \qquad (11)$$

Using eq 2 for evaluating $\Delta S_1°$, $\Delta H_1°$ can be deduced from expression 9 and this gives

$$\Delta H_1° = \Delta H_1{}^{\circ 0} - 0.030(\phi - \phi^0) + 0.38(\text{p}K_a - \text{p}K_a{}^0) - 0.82(2 - n_{\text{N-H}}) \qquad (12)$$

where $\Delta H_1{}^{\circ 0}$ refers to the unsubstituted anilines.

The values of $\Delta H_1°$ calculated by means of this equation are shown in Table III. The calculated values and the experimental ones are again in fairly good agreement, thus justifying the approximations made in deriving eq 9.

It can also be noted here that the value of $\Delta H_1°$ given by calorimetric readings[5] for 2-chloroaniline is 2.60 kcal mol^{-1}, while the calculated value from eq 12 is 2.44 kcal mol^{-1}.

On the other hand, an expression for ΔH_1° can also be found by differentiating eq 9 with respect to $1/T$. From the Van't Hoff law

$$\Delta H_1^\circ = -2.3R(\mathrm{d}\log P_1/\mathrm{d}1/T) \qquad (13)$$

it follows that

$$\begin{aligned}\Delta H_1^\circ = \Delta H_1^{\circ 0} - 2.3R(\phi - \phi^0)(\mathrm{d}A/\mathrm{d}\,1/T) - \\ 2.3RA(\mathrm{d}(\phi - \phi^0)/\mathrm{d}\,1/T) - \\ 2.3(\mathrm{p}K_a - \mathrm{p}K_A^0)(\mathrm{d}B/\mathrm{d}\,1/T) - \\ 2.3RB[\mathrm{d}(\mathrm{p}K_a - \mathrm{p}K_a^0)/\mathrm{d}\,1/T] - \\ 2.3R(2 - n_{\text{N-H}})(\mathrm{d}C/\mathrm{d}\,1/T) \qquad (14)\end{aligned}$$

It can be assumed, as a first approximation, that the derivatives $\mathrm{d}(\phi - \phi^0)/(\mathrm{d}\,1/T)$ and $\mathrm{d}(\mathrm{p}K_a - \mathrm{p}K_a^0)/(\mathrm{d}\,1/T)$ are proportional respectively to the differences $(\phi - \phi^0)$ and $(\mathrm{p}K_a - \mathrm{p}K_a^0)$. This leads to an expression of the form of eq 12.

If, as a crude approximation, the two terms of eq 14 arising from the variation of $(\phi - \phi^0)$ and $(\mathrm{p}K_a - \mathrm{p}K_a^0)$ with the temperature are neglected, and if the values of A, B, and C at 35 and 15° are used for estimating their derivatives with respect to $1/T$, one obtains the following expression

$$\begin{aligned}\Delta H_1^\circ = \Delta H_1^{\circ 0} - 0.04(\phi - \phi^0) + \\ 0.7(\mathrm{p}K_a - \mathrm{p}K_a^0) - 0.8(2 - n_{\text{N-H}}) \qquad (15)\end{aligned}$$

whose coefficients remain of the same order of magnitude as those obtained using eq 2.

For most of the anilines studied here that are not N substituted, the differences between the P_1 and ΔH_1 values are chiefly due to the changes in molar volume. This result is in agreement with the observations of Przyborowska and Soczewinski,[10] who studied the chromatography parameters of methyl derivatives of aniline and concluded that their chromatographic behavior was mainly determined by the molecular volume of the solute while basicity plays only a minor part in the neutral systems. On the other hand, we can compare the coefficient A with the effect of increasing the molar volume of the alcohols upon their P_1 coefficient in the same solvents. From propanol to heptanol we determined in a previous work[11] an increment of 0.68 in log P_1 for each addition of a CH_2 group. This addition corresponds roughly to an increase of 18 ml in the molar volume, giving an increase of 0.038 per ml, of the same order of magnitude as the A constant found for the anilines.

The last term of eq 9 and the corresponding term of eq 12 are very important. When these terms are disregarded, the calculated values of P_1 are four times too low for N-methylaniline (and fifteen times too low for the N,N-disubstituted anilines), and the transfer enthalpies are 0.8 kcal too high.

These terms were introduced to take into account the formation of the N-H···O bonds between the anilines and water. It is difficult to interpret as a result of steric hindrance of the H substituents, for such effect will also appear in the pK_a values of the anilines. The importance of the last terms in eq 9 and 12 may therefore be considered as a strong indication of the formation of the N-H···O bonds. The equilibrium constant $K_{\text{N-H}\cdots\text{O}}$ of the complexation of water molecules by these bonds can be estimated. Taking into account the concentration of the water in the dilute aqueous solutions, this constant is related to the variation of free energy, and consequently to the C parameter by the expression

$$\log(55.5K_{\text{N-H}\cdots\text{O}}) = C \qquad (16)$$

This gives for $K_{\text{N-H}\cdots\text{O}}$ an order of magnitude of 0.1 M^{-1}.

The P_1 value of the Cl derivatives fits well with the proposed equation. This equation, however, does not take into account the formation of O-H···Cl bonds between water and these derivatives. This shows that these bonds do not play an important role in the stabilization of the Cl derivatives of aniline in water.

Another factor that was not taken into account is the influence of the varying dipole moments of the compounds. That this influence can be disregarded may be due to the fact that it is cancelled out in the two phases.

Experimental Section

The partition experiments were performed using a method described by Brown and Burry.[12] The Hilger Rayleigh M 75 interference refractometer with the cell M 160 for liquids was used for the determination of the concentrations. Cell thicknesses were 1, 3, and 10 cm depending on the concentration range. About 60 standard solutions, covering the whole range of concentrations investigated, were used for the calibration of the interferometer. These solutions were saturated with the other solvent in order to take into account the mutual solubility of the phases.

The reagents used were cyclohexane (Merck pro analysi) and distilled water. All the anilines were Fluka purissimum except 2,6-dimethylaniline which was purified by distillation *in vacuo*.

Acknowledgments. The authors wish to express their thanks to the Belgian Ministry of National Education and to the Katholieke Universiteit te Leuven, which gave a scholarship to A. G.

---

(10) M. Przyborowska and E. Soczewinski, *J. Chromatogr. Sci.*, **42**, 516 (1969).

(11) I. Hanssens, J. Mullens, Ch. Deneuter, and P. Huyskens, *Bull. Soc. Chim. Fr.*, 1342 (1968).

(12) F. S. Brown and C. B. Burry, *J. Chem. Soc.*, **123**, 2430 (1923).

Electrokinetic Salt Rejection in Hyperfiltration through Porous Materials. Theory and Experiment

G. Jacazio,[1] R. F. Probstein,* A. A. Sonin, and D. Yung

Department of Mechanical Engineering, Massachusetts Institute of Technology, Cambridge, Massachusetts 02139

(Received May 30, 1972)

Publication costs assisted by the Office of Saline Water, U. S. Department of the Interior

A theory is presented for the salt rejecting characteristics of porous membranes, whose pore size is large compared with molecular dimensions, under reverse osmosis conditions where the saline solution is moved through the membrane pores by an applied pressure gradient. The salt rejection mechanism is assumed to be an electrokinetic one resulting from charge built up on the interior surfaces of the material when in contact with the salt solution. The performance of the porous material is shown to depend on three parameters: the ratio of Debye length to effective pore radius; a dimensionless wall potential related to the ζ potential; and a Peclet number based on the filtration velocity through the pore, the membrane thickness, and the diffusion coefficient of the salt in the water. A universal correlation is given for the fractional salt rejection in terms of the three membrane parameters. Experiments were carried out on the salt rejecting properties of compacted clay, through which saline solutions were forced under high pressures. Absolute comparisons between the experimentally determined and theoretically predicted rejection characteristics are shown to be excellent. A comparison of the theory with experimental data of Michelsen and Harriott on cellophane also shows very good agreement.

Introduction

It has long been known that clays[2,3] and other porous solids have the property of partially rejecting salt when a saline solution filters through them. The same phenomenon has been evidenced by many relatively porous materials including cellophane membranes[4] and porous glass,[5] as well as by finely porous materials like ion exchange resins.[6,7] Porous dynamically formed membranes developed by the Oak Ridge National Laboratory group,[8,9] as, for example, those formed from colloidal dispersions of hydrous oxides, solutions of hydrolyzable salts, and solutions containing small concentrations of organic polyelectrolytes, have been proposed for and successfully used in brackish water desalting applications. In many such macroporous materials, where the pore size is large compared with molecular dimensions, the rejection mechanism has been assumed to be an electrokinetic one, resulting from charge built up on the interior surfaces of the porous material when in contact with the salt solution.

The salt-rejection phenomenon in reverse osmosis (hyperfiltration) through macroporous media can be analyzed in terms of a relatively simple physical model, where the fluid is assumed to flow through the porous material *via* a series of uniformly distributed, straight, cylindrical pores. The problem can first be solved for a single capillary and then transformed back to apply to an actual porous medium by expressing the effective pore radius and pore length in terms of physically measurable bulk quantities like the permeability, porosity, and thickness of the porous bed.[10]

The physical mechanism of salt rejection in a flow through a capillary with a charged interior wall is qualitatively clear. The surface charge gives rise to a potential field which extends a distance approximately equal to the Debye length into the liquid within the pore. Within this region, there is an excess of ions (counterions) having a charge opposite to that of the wall. If a pressure gradient is applied to make the salt solution flow through the pore, then because of an excess of charge of one sign within the pore liquid there results a net transport of charge and the buildup of the streaming potential. The effect of the potential is to set up an electric field parallel to the surface which will increase the transport of the coions and reduce that of the counterions until there is an equal steady-state transport of positive and negative ions, the feed and effluent solutions being insulated from each other so that there is no current flow. In this steady-state salt and water are transported through the capillary, but not charge. However, the net effect of the coion exclusion and the axial field is such as to cause the ratio of the molar salt flux to the volume flux of water to be less than the molar salt concentration on the upstream side of the membrane. In other words, the membrane tends to reject salt.

Related electrokinetic phenomena in a simple capillary tube have been analyzed in a large number of works.[11] In

---

(1) Present address: Politecnico di Torino, Torino, Italy.
(2) A. S. Michaels and C. S. Lin, *Ind. Eng. Chem.*, **47**, 1249 (1955).
(3) J. G. McKelvey and I. H. Milne, "Clays and Clay Minerals," Vol. 9, Pergamon Press, New York, N. Y., 1962, p 248.
(4) D. L. Michelsen and P. Harriott, "Membranes from Cellulose and Cellulose Derivatives," A. F. Turbak, Ed., Wiley, New York, N. Y., 1970, p 27.
(5) K. A. Kraus, A. E. Marcinkowsky, J. S. Johnson, and A. J. Shor, *Science*, **151**, 194 (1966).
(6) J. C. McKelvey, K. S. Spiegler, and M. R. J. Wyllie, *Chem. Eng. Progr. Symp. Ser.*, **55**, No. 24, 199 (1959).
(7) S. B. Sachs, E. Hoffer, and O. Kedem, *OSW (Off. Saline Water) Res. Develop. Progr. Rep.*, **No. 324** (1968).
(8) A. E. Marcinkowsky, K. A. Kraus, H. O. Phillips, J. S. Johnson, Jr., and A. J. Shor, *J. Amer. Chem. Soc.*, **88**, 5744 (1966).
(9) K. A. Kraus, A. J. Shor, and J. S. Johnson, Jr., *Desalination*, **2**, 243 (1967).
(10) A. E. Scheidegger, "The Physics of Flow through Porous Media," University of Toronto Press, Toronto, 1963.
(11) J. T. Davies and E. K. Rideal, "Interfacial Phenomena," Academic Press, New York, N. Y., 1963.

general the earlier treatments were approximate and applied to the case where the Debye length was small compared with the tube radius and/or the surface charge was sufficiently small that the Poisson equation could be linearized. Dresner[12] solved the capillary model without either of these assumptions, but he considered only the special case of electro osmosis where the flow of the electrolyte is associated with gradients in pressure and electric potential across the membrane but with no concentration gradient. He showed the dependence of various electrokinetic quantities such as the streaming potential on both the surface charge and Debye length to radius ratio. However, because no calculations were carried out with an axial concentration difference the corresponding information on the salt rejection characteristics of the capillary was not obtained.

A paper on the capillary membrane problem was published in 1968 by Gross and Osterle[13] for the general case, assuming only that the Debye sheath can be described by the Chapman-Gouy model. However, as will be noted in connection with the model to be adopted, an approximate form for the axial ion concentration distribution was implicitly introduced. Their formulation was the usual phenomenological one in which the transport of ions and water molecules results from the effects of gradients across the membrane in pressure, concentration, and electrical potential. The authors applied their model to some fundamental electrokinetic problems, but restricted themselves to small concentration gradients and did not work out explicit solutions for the problem of interest here.

In the present paper we apply the capillary membrane model to derive explicit solutions for salt rejection for a viscous flow driven by a pressure gradient through a macroporous medium with charged interior surfaces. The analysis is carried out for the case of a dilute fully dissociated salt solution, and we assume the potential of the pore wall to have a fixed value independent of salt concentration. In order to check out the theoretical results derived for the salt rejection characteristics, hyperfiltration experiments were carried out on the salt rejecting properties of compacted clay. Measurements were made of the wall potential and all of the bulk properties which determine the parameters appearing in the theoretical solution. In what follows we shall describe the general experimental setup along with the results and comparisons with the theoretical predictions. Comparison of the theory with experimental data of Michelsen and Harriott[4] on cellophane will also be presented.

Model and Equations

For the capillary membrane model described in the Introduction the performance of a single cylindrical capillary pore characterizes the membrane performance as a whole. This is a consequence of relating the membrane permeability, porosity, and thickness to an equivalent uniform distribution of cylindrical pores having the same radius and length. The interior wall of the capillary is assumed to become charged when in contact with a saline solution, as a result, for example, of ion adsorption, surface chemical reaction, or other reasons.[14] This surface charge leads to the formation of a Debye screening layer of opposite charge in the liquid adjacent to the wall. The ratio of this thickness (λ_D) to the pore radius (a) will be one measure of the salt rejection, with the salt rejection being greater the larger is this ratio.

In the analysis to follow we adopt a cylindrical coordinate system (x,r) with x positive in the direction of flow and r the radial coordinate with origin at the axis of symmetry. Following Gross and Osterle[13] we split the electric potential Φ into two parts

$$\Phi = \phi(x) + \psi(x,r) \tag{1}$$

where the total potential Φ is connected with the ion concentration distribution $c_\pm(x,r)$ through the Poisson equation, the subscript + referring to cations and the subscript − to anions. Because of the cylindrical symmetry of the problem, within the pore there is no net ion flux or bulk flow in the radial direction. The integration of the radial ion flux equations leads to the radial ion concentration distribution being in Boltzmann equilibrium with respect to the radial component of the field, ψ

$$c_\pm(x,r) = f_\pm(x)\exp[\mp\bar{\psi}(x,r)] \tag{2a}$$

$$\approx c(x)\exp[\mp\bar{\psi}(x,r)] \tag{2b}$$

Here $\bar{\psi} = ZF\psi/\mathcal{R}T$ is the dimensionless radial potential, Z is the absolute value of the charge number which we shall take equal for the positive and negative ions, F and $\mathcal{R}$ the Faraday and gas constants, respectively, T the absolute temperature.

With $f_\pm(x)$ undetermined functions, eq 2a applies at any station *within* the pore. For the case when the Debye length is very small compared with the capillary radius, the potential in the central core of the capillary depends essentially on x alone, and the positive and negative ion concentrations are equal except within the thin Debye sheaths next to the wall. For this case we have $c_+ = c_-$ in the core of the capillary where we set $\bar{\psi} \approx 0$. Equation 2a then takes the approximate form given by eq 2b, with $c(x)$ the salt concentration in the core where the total potential is defined by $\phi(x)$.

Although eq 2b was derived only for conditions within the pore it can also be taken outside the pore, since it contains the conditions of equilibrium for the ionized species at the pore entrance and exit. We emphasize again that it is generally applicable only in the limit when the Debye length is small. However, when the Debye length is comparable with the pore radius or larger, eq 2b still describes accurately the situation within the pore near either end of it, but inside the rest of the pore it implies a certain axial distribution of charge either on the pore wall or in the solid wall material.

Throughout their formulation for arbitrary Debye lengths, Gross and Osterle[13] used eq 2b rather than eq 2a. We shall adopt this approach, since the use of eq 2b greatly simplifies the analysis and the calculations for arbitrary Debye length. The results obtained for integrated quantities, such as, salt rejection and streaming potential, are rigorous for small Debye lengths, and in the general case they satisfy all the boundary conditions and represent a good approximation to the exact solution.

With a denoting the radius of the cylindrical pore, the potential $\psi(x,a) = \psi_w$ is termed the wall potential. In the present development we shall assume the wall potential ψ_w to be constant, largely because it is a reasonable assumption for a number of materials in typical aqueous solutions. However, the salt concentration varies along the pore and in general the wall potential may not remain constant. Depending on the particular solid–liquid interface[14] instead of a constant wall potential a constant charge density might be more appropriate, although most interfaces are expected to behave in a manner intermediate between these two limits.

---

[12] L. Dresner, *J. Phys. Chem.*, **67**, 1635 (1963).

[13] R. J. Gross and J. F. Osterle, *J. Chem. Phys.*, **49**, 228 (1968).

[14] P. Sennit and J. P. Olivier, "Chemistry and Physics of Interfaces," American Chemical Society, Washington, D. C., 1965, p 73.

With the pore length large in comparison with the radius a, the Poisson equation governing the potential distribution can be shown to be expressible in the dimensionless form[13]

$$\lambda^2 \frac{1}{\bar{r}} \frac{\partial}{\partial \bar{r}} \left(\bar{r} \frac{\partial \bar{\psi}}{\partial \bar{r}} \right) = \sinh \bar{\psi} \tag{3}$$

Here $\bar{r} = r/a$ and $\lambda = \lambda_D/a$ where the Debye length is given by

$$\lambda_D = (\epsilon \Re T / 2cZ^2F^2)^{1/2} \tag{4}$$

with ϵ the permittivity. We note that λ is a local value which depends on x through the dependence of λ_D on the salt concentration $c(x)$. Equation 3 is solved subject to the constant wall potential condition $\bar{\psi} = \bar{\psi}_w$ at $\bar{r} = 1$ and to the symmetry condition on the pore axis $\partial\bar{\psi}/\partial\bar{r} = 0$ at $\bar{r} = 0$. Although we shall discuss later analytic solutions of this equation which are available for large and small values of the Debye ratio λ, we would only note here that in general eq 4 can be solved numerically when coupled appropriately to the equations for the concentration distribution. To illustrate the behavior of $\bar{\psi}$ we have shown in Figure 1 the potential distribution across the pore calculated for a wall potential $\bar{\psi}(1) = 2.79$ for different constant values of λ. It can be seen that the influence of the potential, and hence the salt rejecting characteristic, increases markedly with λ, and for a Debye ratio greater than about 2 the potential distribution is closely characterized by the constant value it assumes when $\lambda \rightarrow \infty$.

To complete the statement of the problem we must write the Nernst–Planck equations for the ion fluxes which couple the ion concentration distribution to that of the potential. Employing eq 1 and 2 the flux equations may be written

$$j_{\pm} = uc_{\pm} - D\exp(\mp\bar{\psi})(\mathrm{d}c/\mathrm{d}x) \mp Dc_{\pm}(\mathrm{d}\bar{\phi}/\mathrm{d}x) \tag{5}$$

where j denotes the ion flux per unit area, $\bar{\phi} = ZF\phi/\Re T$, and D is the diffusion coefficient which we have taken equal for the positive and negative ions.

For hyperfiltration conditions, where the flow velocity resulting from the applied pressure gradient is large in comparison with that resulting from either the concentration or potential gradients across the membrane, the velocity distribution in the cylindrical pore is given by the Poiseuille relation

$$u = 2V(1 - \bar{r}^2) \tag{6}$$

Here, the mean flow velocity $V = Q/A$ with Q the total volume flow rate and A the pore cross-sectional area. When the pressure gradient across the pore is not sufficiently large it is necessary to take into account the modifications to the Poiseuille flow resulting from the concentration gradient and, in particular, the potential gradient[2] as, for example, in the treatment of Gross and Osterle.[13]

Of interest is the total flux J which may be obtained by integrating eq 5 over the pore cross-sectional area. The total flux of dissociated salt molecules is given by $J_s = J_+ + J_-$, while the total current is $I = ZF(J_+ - J_-)$. In the present problem there is no net current through the pore so that from eq 2b, 5, and 6

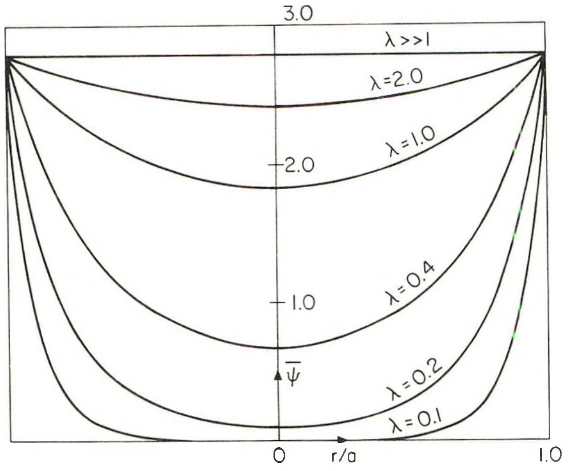

Figure 1. Dimensionless radial potential distribution across a cylindrical pore for different Debye ratios and a fixed wall potential ($\bar{\psi}_w = 2.79$).

$$J_s = +2cQK_1 - 2ADK_3(\mathrm{d}c/\mathrm{d}x) + 2ADcK_4(\mathrm{d}\bar{\phi}/\mathrm{d}x) \tag{7a}$$

$$0 = -2cQK_2 + 2ADK_4(\mathrm{d}c/\mathrm{d}x) - 2ADcK_3(\mathrm{d}\bar{\phi}/\mathrm{d}x) \tag{7b}$$

The K's are definite integrals of functions of $\bar{\psi}$ over the cross section defined by

$$\begin{gathered} K_1 = 4\int_0^1 \cosh\bar{\psi}(1-\bar{r}^2)\bar{r}\,\mathrm{d}\bar{r},\ K_3 = 2\int_0^1 \cosh\bar{\psi}\,\bar{r}\,\mathrm{d}\bar{r} \\ K_2 = 4\int_0^1 \sinh\bar{\psi}(1-\bar{r}^2)\bar{r}\,\mathrm{d}\bar{r},\ K_4 = 2\int_0^1 \sinh\bar{\psi}\,\bar{r}\,\mathrm{d}\bar{r} \end{gathered} \tag{8}$$

Since $\bar{\psi}$ is determined from the solution of eq 3 it follows that the K's are functions of $\bar{\psi}_w$ and $\lambda(c)$ or alternatively $\bar{\psi}_w$ and $\lambda(x)$, thereby coupling any solution of the ion flux equations to that of the Poisson equation.

Elimination of $\mathrm{d}\bar{\phi}/\mathrm{d}x$ in eq 7 leads to the following equation for the salt concentration

$$(\kappa_1/Pe)(\mathrm{d}\bar{c}/\mathrm{d}\bar{x}) - \bar{c} = -\bar{c}_{II}\kappa_2 \tag{9}$$

Here, the axial coordinate x is made dimensionless with respect to the pore length L and Pe is the Peclet number based on the average pore velocity

$$\bar{x} = x/L,\ Pe = VL/D = QL/AD \tag{10}$$

We have chosen for the reference concentration the known feed concentration c_I at $x = 0$. With the product concentration at $x = L$ denoted by $c_{II}(= J_s/2Q)$

$$\bar{c} = c/c_I,\ \bar{c}_{II} = 1 - R = c_{II}/c_I = J_s/2Qc_I \tag{11}$$

The salt rejection coefficient R defined above is equal to 1 for complete salt exclusion by the membrane and 0 for no exclusion.

The functions κ_1 and κ_2 appearing in eq 9 depend on the K's and are defined by

$$\begin{gathered} \kappa_1 = (K_3^2 - K_4^2)/(K_1K_3 - K_2K_4) \\ \kappa_2 = K_3/(K_1K_3 - K_2K_4) \end{gathered} \tag{12}$$

Since κ_1 and κ_2 depend on $\bar{\psi}_w$ and $\lambda(c)$ through the K's it follows that eq 9 is coupled with the Poisson eq 3. These equations can be solved numerically, as, for example, by

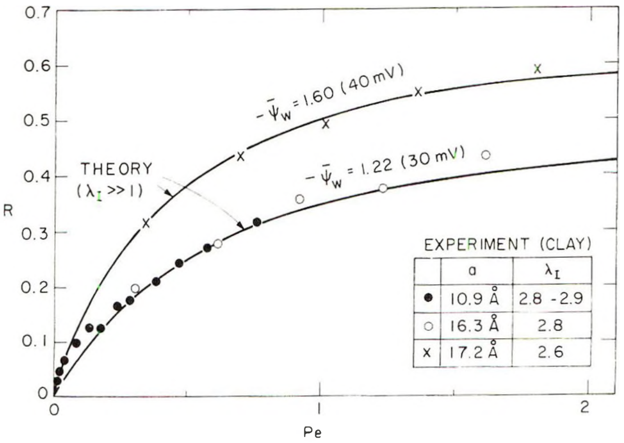

Figure 2. Salt rejection coefficient of a cylindrical pore with a constant surface potential for large Debye ratio as a function of Peclet number, and comparison with experiments on compacted clay.

treating κ_1 and κ_2 as functions of c and solving the system by a direct step-by-step forward marching procedure in x. Alternatively an iterative procedure could be used in which κ_1 and κ_2 are treated as functions of x with initial values, say, taken constant. Equation 9 is then a first-order linear equation in c with constant coefficients from which a first approximation for $c(x)$ and $\lambda(x)$ are readily found. The Poisson equation can then be integrated for $\bar{\psi}$ and new values of κ_1 and κ_2 obtained, with the procedure repeated until convergence is achieved. Other numerical procedures are also possible.

Parameters and Solutions

From the system of equations and boundary conditions defining the pore problem it is easily shown that the rejection coefficient $R = -\Delta c/c_I$ will depend on three dimensionless parameters. These parameters are the dimensionless wall potential $\bar{\psi}_w$, the Peclet number Pe, and the Debye ratio λ_I which is the ratio of the Debye length evaluated at the feed concentration to the pore radius. That the Debye ratio parameter is based on the feed concentration is a result of having chosen this concentration as the reference value. This same general result can be shown to hold for the streaming potential $\Delta\bar{\phi}$. To determine the explicit solution behavior in its dependence on the parameters $\bar{\psi}_w$, Pe, and λ_I can only be done in general numerically. However, before presenting the numerical solutions we shall investigate a number of analytic asymptotic solutions for limiting values of the dimensionless similarity parameters. Such analytic solutions, apart from their own value, can serve as a guide to how the numerical solutions scale with changes in the parameters.

Two limiting cases of particular interest are for large and small values of the Debye ratio. For values of λ large $\bar{\psi}$ becomes independent of λ, while for values which are sufficiently small λ may be taken constant and set equal, for example, to λ_I so that $\bar{\psi} = \bar{\psi}(\bar{r}; \bar{\psi}_w, \lambda_I)$. It follows that in either case the K's of eq 8, and hence κ_1 and κ_2 of eq 12, are constants dependent at most on $\bar{\psi}_w$ and λ_I. Equation 9 is then easily integrated subject to the conditions that $\bar{c} = 1$ at $\bar{x} = 0$ and $\bar{c} = \bar{c}_{II}$ at $\bar{x} = 1$. This leads to the following general expression, valid in either the small or large Debye ratio limits, for the concentration ratio across the pore

$$\bar{c}_{II} = 1 - R = \frac{e^{Pe/\kappa_1}}{(1 + \kappa_2) + \kappa_2 e^{Pe/\kappa_1}} \tag{13}$$

Eliminating dc/dx in eq 7b by means of eq 9 and $c(x)$ by means of the solution of eq 9 just described, yields a simple quadrature for $\phi(x)$. In this manner one can determine the corresponding streaming potential across the capillary. With some manipulation this result may be expressed in the form

$$\Delta\bar{\phi} = -\kappa_4 \ln\left[\frac{(1 - \kappa_2)e^{-Pe/\kappa_1} + \kappa_2}{e^{-Pe/\kappa_1}}\right] \tag{14}$$

where $\Delta\bar{\phi} = \bar{\phi}_{II} - \bar{\phi}_I$ is the dimensionless potential difference between the solutions at the pore ends (with the potential made dimensionless with respect to $\mathcal{R}T/ZF$). The parameters κ_3 and κ_4 are here defined by

$$\kappa_3 = K_4/K_2, \quad \kappa_4 = K_4/K_3 \tag{15}$$

We next consider the specific solution for λ everywhere sufficiently large compared to one. Physically this situation corresponds to a problem which is one-dimensional in x, with the salt rejection taking place entirely in the "thick" sheaths which are formed outside the pore at the feed entrance and product exit. It was shown in the last section that the large Debye ratio behavior is already manifested at values of $\lambda \gtrsim 2$. This is principally a consequence, as may be seen from eq 3, of the fact that the requirement for the limit is $\lambda^2 \gg 1$ which is a weaker one than $\lambda \gg 1$. For this limit it is readily apparent from Figure 1 and eq 3 that $\bar{\psi}(r)$ is constant across the capillary and the solution of eq 3 satisfying the boundary conditions is simply $\bar{\psi} = \bar{\psi}_w$. It follows that

$$K_1 = K_3 = \cosh \bar{\psi}_w, \quad K_2 = K_4 = \sinh \bar{\psi}_w \tag{16}$$

from which

$$\kappa_1 = 1, \kappa_2 = \cosh \bar{\psi}_w \tag{17}$$
$$\kappa_3 = 1, \kappa_4 = \tanh \bar{\psi}_w$$

From eq 13 and 14 we find for $\lambda \gg 1$ the following limiting forms for the rejection coefficient and streaming potential

$$1 - R = \frac{e^{Pe}}{(1 - \cosh \bar{\psi}_w) + e^{Pe} \cosh \bar{\psi}_w} \tag{18}$$

$$\Delta\bar{\phi} = -\tanh \bar{\psi}_w \ln\left[(1 - \cosh \bar{\psi}_w) + e^{Pe} \cosh \bar{\psi}_w\right] \tag{19}$$

Figures 2 and 3 are plots of the rejection coefficient R as a function of Peclet number for different values of the wall potential. The theoretical curves were calculated using eq 18. The data points shown in the figures will be discussed later in connection with the experimental results. For a fixed wall potential the rejection is seen to increase with the Peclet number, as it should, since the Peclet number is a measure of the ratio of the convective to diffusive effects. At small Pe diffusion is dominant with the result that there is a lower rejection, while at large values of Pe convection is dominant and the rejection is increased (see, *e.g.*, eq 7a). The maximum possible rejection for a fixed wall potential is given by the asymptotic limit

$$R_{\max} = 1 - (1/\cosh \bar{\psi}_w) \tag{20}$$

obtained from eq 18 for $Pe \gg 1$. The approach to this limit is characterized by a typical relaxation behavior so that the rejection is already an appreciable fraction of the asymptotic value for Peclet numbers as low as 2. That the

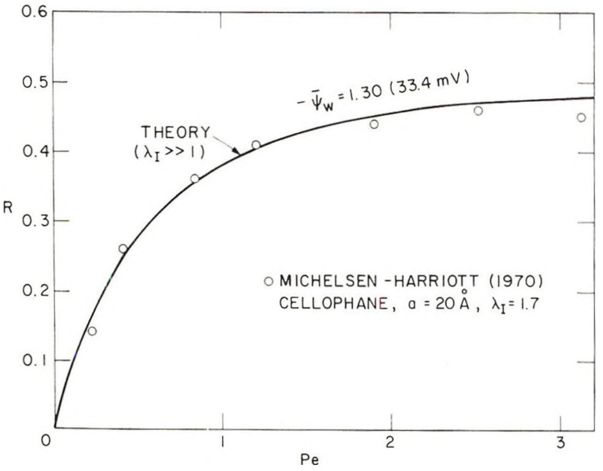

Figure 3. Salt rejection coefficient of a cylindrical pore with a constant surface potential for large Debye ratio as a function of Peclet number, and comparison with experiments of Michelsen and Harriott[4] on cellophane membranes.

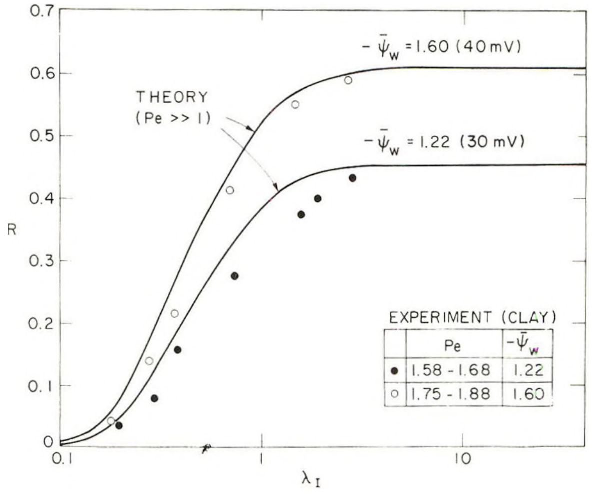

Figure 4. Salt rejection coefficient of a cylindrical pore with a constant surface potential for large Peclet number as a function of Debye ratio, and comparison with experiments on compacted clay.

rejection increases with increasing wall potential for all *Pe* is a direct consequence of the increased effect of the wall region on the charge distribution across the pore and hence on the rejection, as described earlier.

The opposite limit of $\lambda \ll 1$ (or really $\lambda^2 \ll 1$) although amenable to analytic description is somewhat more difficult to evaluate. This limit is characterized by the thinness of the Debye sheath and hence relatively low rejection. Because of the thin sheath the transverse curvature term in the Poisson equation $\bar{r}^{-1}\,(\partial\bar{\psi}/\partial\bar{r})$ may be neglected in comparison with $\partial^2\bar{\psi}/\partial\bar{r}^2$ and with λ set equal to λ_I eq 3 reduces to

$$d^2\bar{\psi}/d\bar{r}^2 = \sinh \bar{\psi}/\lambda_I^2 \tag{21}$$

This equation has a first integral given by

$$\lambda_I^2(d\bar{\psi}/d\bar{r})^2 = 2(\cosh \bar{\psi} - \cosh \bar{\psi}_0) \tag{22}$$

where $\bar{\psi}_0$ is the radial potential on the pore axis. Equation 22 can in turn be integrated, though not in terms of elementary functions, and $\bar{r}(\bar{\psi}; \bar{\psi}_0)$ is expressible as an elliptic integral of the first kind.[15]

For the limits of large and small $\bar{\psi}$ eq 22 can be solved explicitly in terms of elementary functions. In the case where $\bar{\psi}$ is everywhere sufficiently small that we may replace $\cosh \bar{\psi}$ by $1 + (1/2)\bar{\psi}^2$ (a condition which will be met, say, for $\bar{\psi}_w^2 \ll 1$) eq 22 integrates explicitly to give $\bar{\psi} = \bar{\psi}_0 \cosh (\bar{r}/\lambda_I)$, where $\bar{\psi}_0 = \bar{\psi}_w/\cosh (1/\lambda_I)$. It may be recognized that we can to good approximation neglect the terms of order $\exp(-1/\lambda_I)$ in which case the potential is given by

$$\bar{\psi} = \bar{\psi}_w e^{-(1-\bar{r})/\lambda_I} \tag{23}$$

This result is essentially the familiar one-dimensional relation for a Debye sheath and in conjunction with eq 13 could serve to characterize the analytic behavior of the solution for small λ. However, because of the analytical complexity and limited use of the results we shall restrict our discussion to the general behaviors already noted, these characterizations being useful for the scaling arguments which are given below. We would also note here that eq 23 can serve as the basis of an approximate treatment for all λ.

One other limit which we have already discussed for the case of λ large but which is of interest over the whole range of Debye ratios and $\bar{\psi}_w$ is the case of $Pe \gg 1$. We may observe from eq 13 that the rejection ratio has a relaxation behavior as a function of *Pe* of the same type for both small and large Debye ratios. As we have already shown, for the case $\lambda \gg 1$ and $Pe \sim 2$ the rejection is an appreciable fraction of its asymptotic, Peclet number independent value. Therefore from eq 13 we may expect the same Peclet number independence for the small Debye ratio case. It is reasonable therefore that if this condition holds for the small and large Debye ratio limits that the intermediate regime is also likely to manifest the large Peclet number independent behavior at relatively low *Pe* values. That this is indeed the case is seen in Figure 4 which is a plot of the rejection as a function of the Debye ratio λ_I for two different values of the wall potential. The theoretical curves were obtained from a complete numerical step by step solution with $Pe \gg 1(\approx 10)$. Although not shown, comparison with other exact numerical calculations for $Pe = 2$ shows the results to be almost the same, with the $Pe = 2$ results only slightly below those for large Peclet number. The curves of Figure 4 clearly indicate the increasing rejection with larger Debye ratio λ_I, which follows from the arguments given earlier. Furthermore, the rapid increase in rejection with λ_I is seen to take place at $\lambda_I \sim 1$, which is also consistent with the expected exponential increase around this value (*cf.* eq 23). The data shown in Figure 4 will be discussed in connection with the presentation of the experimental results.

The similarity of the family of theoretical rejection curves as a function of Peclet number for different values of $\bar{\psi}_w$ with $\lambda_I \gg 1$ (Figures 2 and 3) and the similarity of the family of rejection curves as a function of the Debye ratio for different values of $\bar{\psi}_w$ with $Pe \gg 1$ (Figure 4) suggest that it might be possible to empirically correlate these solutions in the general case with a single universal correlation for the rejection coefficient *R* in terms of the three parameters λ_I, $\bar{\psi}_w$, and *Pe*. To carry out this correlation we use as a guide the limiting asymptotic solutions which have been derived.

Equation 13, which is valid for both small and large

---

(15) E. J. W. Verwey and J. Th. G. Overbeek, "Theory of the Stability of Lyophobic Colloids," Elsevier, New York, N. Y., 1948, p 67.

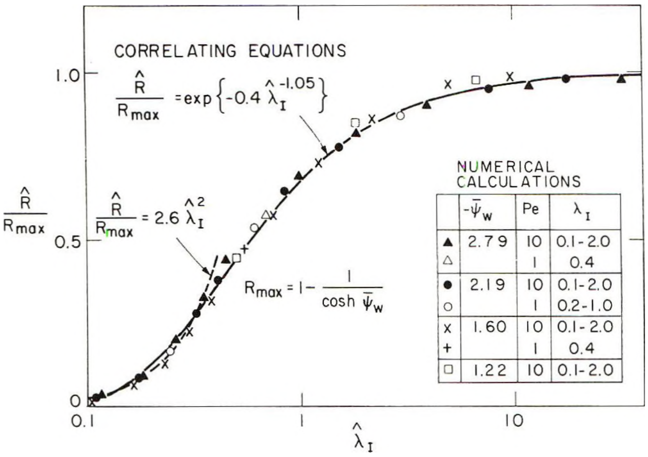

Figure 5. Empirical universal correlation of salt rejection coefficient. R and λ are defined in eq 33–35. Points represent exact numerical solutions.

Debye ratios, serves as a guide for the scaling of the family of solutions of R as a function of λ_I for different values of Pe with $\bar{\psi}_w$ constant. The parameters κ_1 and κ_2 of λ_I and $\bar{\psi}_w$ appearing in eq 13 were evaluated only in the large Debye ratio limit, where they become $\kappa_1 = 1$ and $\kappa_2 = \cosh \bar{\psi}_w$. We recognize, however, from eq 9 for the axial salt concentration distribution that Pe/κ_1 should represent the ratio of the time for the salt to diffuse across the length of the capillary in the sheath region compared to the time for it to be convected across (or alternatively the ratio of the axially convected to the axially diffused flux within the sheath). If we observe that the average streamwise velocity along the capillary in the sheath is given approximately by $V(\delta_D/a)$, where δ_D is the "sheath thickness," then in order of magnitude

$$(Pe/\kappa_1) \sim (VL/D)(\delta_D/a) \tag{24}$$

with $\kappa_1 \sim a/\delta_D$. It follows that for large Debye ratios, when the sheath region fills the capillary, $\kappa_1 = 1$ consistent with the previously obtained result.

From numerical solutions of the Poisson equation the qualitative behavior of δ_D/a is of the form

$$\delta_D/a \sim 1 - \exp(-\alpha\lambda_I/\bar{\psi}_w) \tag{25}$$

where α is a constant. It is to be noted that the calculations were carried out over a wide range of $\lambda_I (\approx 0.1 \text{ to } 2)$ but for only the relatively narrow range of $\bar{\psi}_w$ of interest (≈ 1.2 to 2.8). The linear function of $\bar{\psi}_w$ should be interpreted in this context. In any case, the empirical form of eq 25 is physically reasonable, approaches the proper limits for small and large λ_I, and is consistent with all the derived asymptotic limits such as eq 23.

From eq 13 with $\kappa_2 = \cosh \bar{\psi}_w$ and eq 24 and 25 the Peclet number dependence can be shown to be scaled out of the rejection R, referenced with respect to the maximum value of eq 20 by the relations

$$\frac{\hat{R}}{R_{max}} = R\left[\frac{\cosh\bar{\psi}_w\,(e^{Pe/\kappa_1} - 1) + 1}{\cosh\bar{\psi}_w(e^{Pe/\kappa_1} - 1)}\right]\left[\frac{\cosh\bar{\psi}_w}{\cosh\bar{\psi}_w - 1}\right] \tag{26}$$

with

$$Pe/\kappa_1 = Pe[1 - \exp(-5\lambda_I/\bar{\psi}_w)] \tag{27}$$

Here we note that the scaled rejection coefficient is denoted by $\hat{R}$ and that the value of $\alpha = 5$ was determined empirically.

To scale out the dependence on $\bar{\psi}_w$ of the family of solutions of $\hat{R}/R_{max}$ as a function of λ_I it is necessary to determine what is the "proper" scale measuring the sheath thickness. As in all nonconstant density boundary layer-sheath type problems, the appropriate normal scale is a length which is measured by the integral of the density over the normal coordinate, and not the value of the coordinate itself, in this case λ_I when measured in pore radii. For the present problem the appropriate "density" is the counter ion charge distribution in the sheath, which is proportional to exp $\bar{\psi}$. Consistent with the derived asymptotic relations we may estimate a mean charge strength over the sheath as $\exp(\bar{\psi}_w\lambda_I/2)$ and conclude that a proper normal scale, denoted by $\hat{\lambda}_I$, is

$$\hat{\lambda}_I = \lambda_I \exp(\lambda_I\bar{\psi}_w/2) \tag{28}$$

Figure 5 presents numerical calculations for the rejection coefficient for various ranges of the parameters $\bar{\psi}_w$, Pe, and λ_I. These results are plotted using the scalings of eq 26–28. It can be seen that all of the solutions collapse onto a single curve which to good approximation is given by

$$\hat{R}/R_{max} = \exp(-0.4\,\hat{\lambda}_I^{-1.05}) \tag{29}$$

A slightly more accurate representation for small $\hat{\lambda}_I$ is given by

$$\hat{R}/R_{max} = 2.6\hat{\lambda}_I^2 \qquad (\hat{\lambda}_I^2 \ll 1) \tag{30}$$

We present the above result to indicate that the empirically correlated behavior has the correct asymptotic form in the small as well as in the large Debye ratio limit. That the three parameter family of theoretical solutions for the rejection can be scaled to a single universal curve is clearly of significance for the characterization of membranes described by the present model. In the sections which follow we shall show that experimental membrane data compares well with the universal correlation.

Transformation to Porous Membrane

The architecture of a real membrane or porous bed is of course much more complex than that of our simple model. The flow takes place not in continuous pores of specified radius and length, but rather *via* the random interstices in a fibrous or granular structure which an experimenter can often characterize only by a bulk permeability k, a porosity γ, and a thickness h. It is nevertheless possible to make a rational definition of an effective pore radius and an effective pore length, the quantities which must be specified in our model, in terms of the measurable bulk properties of a membrane or porous bed. We choose for this purpose those values of pore radius and pore length which give a simple capillary bed the experimentally measured permeability and porosity, and at the same time yield a permeability coefficient which is in agreement with the widely applicable Kozeny-Carman relation.

The permeability coefficient k is defined in terms of Darcy's law

$$q = -(k/\mu)(\Delta p/h) \tag{31}$$

Here q is the volume flow rate per unit cross sectional area of the bed, Δp the pressure difference across the bed, h the thickness of the bed, and μ the viscosity of the permeating fluid. The Kozeny-Carman relation gives the permeability as[10]

$$k = K[\gamma^3/S_0^2(1-\gamma)^2] \qquad (32)$$

where γ is the porosity of the bed, S_0 the specific surface exposed to the fluid (surface exposed to the fluid per unit volume of solid), and K the Kozeny constant. Carman[16] showed that with $K = 1/5$, eq 32 applies to a wide class of materials.

If one assumes that the porous bed or membrane is traversed by capillaries of radius a and length L, through which fluid is transported by Poiseuille flow, one obtains for the permeability the expression

$$k = \tfrac{1}{2}(h/L)^2[3/S_0^2(1-\gamma)^2] \qquad (33)$$

where the specific surface S_0 is related to the porosity and the capillary radius by

$$S_0 = (2/a)[\gamma/(1-\gamma)] \qquad (34)$$

The mean flow speed in a pore is found in this model to be

$$V = (q/\gamma)(L/h) \qquad (35)$$

The capillary model is consistent with the Kozeny-Carman equation and can be made to match it by setting the effective length $L = h/\sqrt{2K}$. The effective pore radius and mean flow speed are then given respectively by

$$a = 2(k/\gamma K)^{1/2}, \qquad V = q/\gamma\sqrt{2K} \qquad (36)$$

With these relations we can express the two dimensionless parameters Pe and λ_{I} in our theory in terms of the measurable bulk properties of the porous medium

$$Pe = VL/D = (1/2K\gamma)(qh/D) = -k\Delta p/2K\gamma\mu D \qquad (37)$$

$$\lambda_{\mathrm{I}} = [(\lambda_{\mathrm{D}})_{\mathrm{I}}/a] = (\epsilon\mathcal{R}TK\gamma/8Z^2F^2kc_{\mathrm{I}})^{1/2} \qquad (38)$$

where eq 4 was used for λ_{D}. In all the work reported here, the Kozeny constant was given the value determined empirically by Carman[16] of $K = 1/5$.

We note that the above matching procedure ignores the fact that the electrostatic effects associated with the salt rejection process actually influence the permeability somewhat.[2,3] The resulting permeability change was, however, computed to be quite small in our experiments, and it can in fact be shown that even though the effect is sometimes measurable[2] it is never a dominant one.

Experimental Section

Experiments were performed on salt rejection in potassium chloride (KCl) solutions filtered through thin beds or "membranes" of clay (Wyoming bentonite, 325 and 625 mesh). The clay was chosen mainly because it is a substance where electrostatic effects are known to be significant, and where salt rejection has previously been observed by other investigators.[3] Clay beds are also relatively easy to prepare in a wide range of thicknesses and porosities.

The apparatus is shown schematically in Figure 6. The clay sample, 10 cm in diameter and typically 0.15 to 0.4 cm thick, was held between two porous disks which were compressed by pistons. The compaction stress exerted by the pistons was always larger than the applied fluid pressure drop across the membrane. The side walls of the chamber were lined with Teflon and the feed and the product solutions were in electrical contact only through the clay membrane itself. The feed was pressurized *via* an inflatable balloon in the supply reservoir and circulated (by convection: one of the connecting tubes was heated slightly, the other cooled) over the feed side of the clay membrane so as to prevent concentration polarization. Silver-silver chloride reversible electrodes were fitted on either side of the sample for the measurement of streaming potential. All metal parts of the system, including the porous disks which supported the clay, were made of stainless steel.

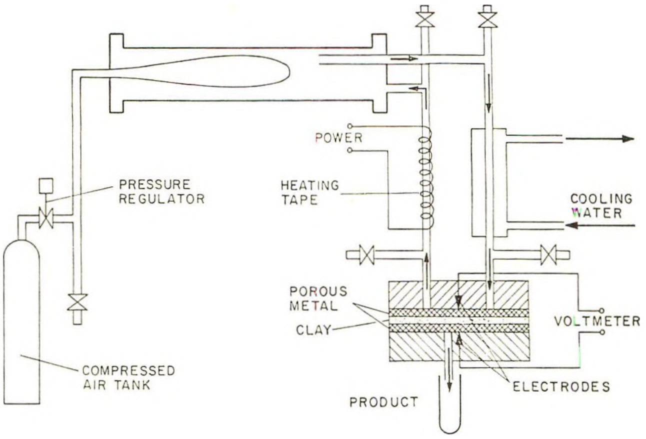

Figure 6. Experimental setup for measurement of salt rejection by compacted clay.

The KCl feed concentration in these tests was in the relatively narrow range between 0.005 and 0.012 *N*. The pressure drop applied across the membrane ranged up to 2000 psi, and the porosity γ was usually between 0.45 and 0.75. Typical product flow rates were measured in cm³/hr.

For any given applied pressure difference Δp, steady-state measurements were made of the volume flow rate q per unit bed area, and the feed and product concentrations c_{I} and c_{II}. The latter were determined by the standard titration method. The permeability was calculated from Δp, q, and the bed thickness h. The porosity of the bed was derived from the dry weight of clay and the final wet volume of the porous bed, which could be controlled by the stress exerted by the compressing pistons. This stress was always larger than Δp, so that the clay filled the compartment available to it. A clay grain density of 2.80 gm/cm³, quoted from pycnometer measurements by the clay supplier (Nispel, Inc.), was used in the calculation of porosity.

The aim of the experiments was to map out the dependence of the salt rejection coefficient $R = (c_{\mathrm{I}} - c_{\mathrm{II}})/c_{\mathrm{I}}$ (eq 11) on the three dimensionless parameters which characterize the problem theoretically. These are the Peclet number Pe, the Debye ratio λ_{I}, and the dimensionless wall potential $\bar{\psi}_{\mathrm{w}}$. For the clay membrane the Peclet number is given by eq 37. Its value can easily be varied by means of the applied pressure difference Δp, and to a certain extent through γ which also controls k. The Debye ration is expressed in terms of the bed properties by eq 38. Experimental control of this quantity is through c_{I} and γ.

The remaining parameter which must be determined in the experiments is the wall potential $\bar{\psi}_{\mathrm{w}}$. The wall potential ψ_{w} is defined in the same way as the classical ζ potential, in the sense that it represents the potential at the radius where the flow velocity goes to zero (this is the wall in our macroscopic, continuum formulation). Although this potential cannot be measured directly, it can be in-

---

(16) P. C. Carman, *Trans. Inst. Chem. Eng.* **15**, 150 (1937); **16**, 168 (1938); *J. Soc. Chem. Ind.*, **57**, 225 (1938).

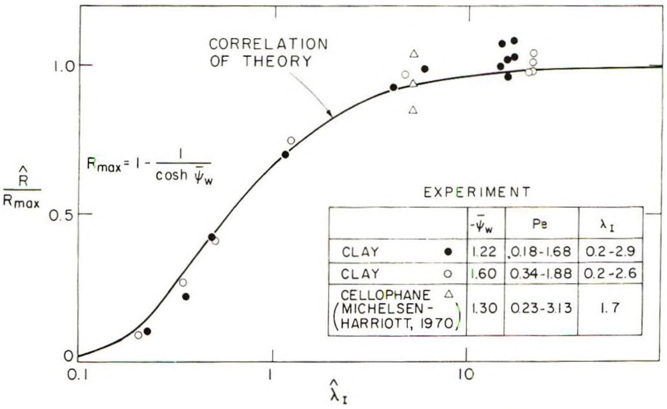

Figure 7. Comparison with experiment of theoretical universal correlating function for salt rejection coefficient.

ferred from measurements of classical electrokinetic quantities like the streaming potential. For flow through a capillary there is a classical relation between the wall potential (here termed the ζ potential) and the streaming potential $\Delta\phi$

$$\zeta = \frac{\Delta\phi}{\Delta p}\frac{\mu}{\epsilon}\left(\sigma + \frac{2\sigma_w}{a}\right) \tag{39}$$

Here σ is the conductivity of the solution in the capillary and σ_w is the surface conductance of the capillary material. The classical relation given by eq 39 correctly represents the wall potential only when the Debye length is negligible compared with the capillary radius, that is $\lambda_I \rightarrow 0$. However, Oldham, Young, and Osterle[17] have derived a correction which enables one to calculate a value of ψ_w from ζ in the more general case where λ_I is finite. There are, however, several implicit assumptions in ref 16, not noted by the authors, which still restrict the correction to small (but finite) values of λ_I.

In the present experiments ψ_w was obtained from measurements of streaming potential, with λ_I in the range 0.1–0.2. The correction of ref 16 was applied to the ζ potential given by eq 39 to account for the finite value of λ_I. The value of ψ_w obtained in this way was quite sensitive to the magnitude of the surface conductance term in eq 39 which dominated. Street[18] has shown that in the concentration range 0.005–0.12 N of our experiments, the surface conductance of bentonite in a KBr solution is about 4×10^{-9} ohm^{-1}, with the data scattering about ±10 to 15%. Since for bentonite the current associated with the surface conductance is carried by the cations,[19] we assumed that Street's value held also for our KCl solution. In any case, this value is quite consistent with other estimates.[19] The effective capillary radius appearing in eq 39 was evaluated from eq 36.

The value of ψ_w was found to be somewhat dependent on the pH of the feed solution. At a feed concentration of 0.0051 N KCl, ψ_w was 30 mV at the normal pH value of 5 ± 0.3 found in the feed, while at a pH of 4 it rose to 40 mV. These values are based on the assumption that $\sigma_w = 4 \times 10^{-9}$ ohm^{-1}, and are subject to an absolute error equal at least to the scatter in Street's data for σ_w, as mentioned above, that is ±10 to 15%. Whether ψ_w was in fact constant, as assumed in our theory, or depended on salt concentration could not be conclusively established from the present limited data, mainly because the uncertainty in the surface conductance was large enough to mask a possible variation with salt concentration. In any case, the feed concentration was varied only by about a factor of 2 in these preliminary experiments (indeed, most data are for a fixed feed concentration of 0.0051 N KCl) and it seems likely that we would not incur a gross error by approximating the wall potential as being independent of concentration.

Figure 2 shows data for the rejection coefficient as a function of the Peclet number. We note that the Peclet number is proportional to Δp, as expressed in eq 37, and hence this figure can be read as showing the rejection *vs.* Δp, as is commonly done when characterizing hyperfiltration membranes. In these data the Debye ratio was kept relatively fixed about a sufficiently large value, for which the theory indicates the dependence of R on Pe should be essentially independent of λ_I. For a = 10.9 and 16.3 Å, the experimental wall potential was 30 mV, while for the a = 17.2 Å data the wall potential was increased to 40 mV by decreasing the feed pH from 5 to 4, as mentioned previously. The data for the two larger pore radii are for c_I = 0.0051 N, while for a = 10.9 Å the feed concentration is 0.01 N.

The agreement with theory is excellent. The theoretical trend with both Pe and $\bar{\psi}_w$ is well confirmed. This agreement is all the more remarkable because the effective pore radius, as defined by eq 36, was only between 10 and 20 Å, which is not very large compared with molecular dimensions. Our macroscopic theory, which is based entirely on continuum concepts, nevertheless seems to predict the results very accurately.

Figure 3 shows a similar plot of data for cellophane obtained by Michelsen and Harriott.[4] These authors did not measure the streaming potential so that the value of $\bar{\psi}_w$ for their data is unknown. However, with an assumed value of $\bar{\psi}_w$ = 1.30 our theory provides an excellent match with these experimental results. This corresponds to a wall potential of 33.4 mV, a quite reasonable value for cellophane.

In Figure 4 we plot our data for clay to show the rejection coefficient as a function of the Debye ratio λ_I. Here, the value of Pe is maintained high enough in all the data points so that its precise magnitude should not influence R critically, as discussed earlier in connection with the theoretical analysis (*cf.* Figures 2 and 3 for $Pe \gg 1$). Again, two experimental values of ψ_w were obtained by changing the feed pH. For ψ_w = 30 mV all the points except two, and for ψ_w = 40 mV all except one, were taken with c_I = 0.0051 N. Again, the results are in quite good agreement with theory, with what differences that exist ascribable to the fact that the Peclet number of the experiments was somewhat lower than required to compare with the large Pe theory. The results clearly show the increase in R with λ_I predicted by theory and the tendency of R to level off at higher values of λ_I. The dependence on $\bar{\psi}_w$, with R increasing with $\bar{\psi}_w$, is also verified quantitatively.

The final Figure 7 shows all of the previous data, including that of Michelsen and Harriott[4] for cellophane, plotted as the reduced rejection $\hat{R}$ *vs.* the reduced Debye ratio $\hat{\lambda}_I$ (see eq 26–28). In terms of these variables, the

---

(17) I. B. Oldham, F. J. Young, and J. F. Osterle, *J. Colloid Sci.*, **18**, 328 (1963).

(18) N. Street, *Aust. J. Chem.*, **10**, 207 (1957).

(19) H. van Olphen and M. H. Waxman, "Clays and Clay Minerals," A. Swineford, Ed., Publication No. 566, National Academy of Sciences-National Research Council, Washington, D. C., 1958, p 61.

theoretical curves for all $\bar{\psi}_w$ and Pe collapse into the single curve shown, as discussed earlier. Again, the agreement is very good. We would note that the apparent larger scatter of the data is misleading in the sense that it is due to the fact that the rejection coordinate has been stretched by referencing it with respect to the maximum rejection R_{max}.

Concluding Remarks

A theory of salt rejection by hyperfiltration through macroporous membranes has been presented. The theory is based on a relatively simple capillary model, wherein the membrane is assumed to consist of a uniform distribution of cylindrical pores whose interior surfaces acquire a constant potential when in contact with the saline solution. Although the flow phenomena in actual porous membranes is undoubtedly more complex, the simple model appears to provide a theory in excellent agreement with salt rejection data from experiments on bentonite clay and cellophane. Furthermore, the theoretical characterization of the rejection in terms of a dimensionless wall potential, the ratio of the Debye length to an effective pore radius, and a Peclet number based on the filtration velocity and an effective membrane thickness seems appropriate for the materials and operating conditions tested so far.

Our present macroscopic, continuum model requires that both the Debye length and the effective pore size be large in comparison with the molecular dimensions. Although the Debye length always satisfied this requirement in the present tests, the same was not true of the effective pore radius, which was in the range 10–20 Å. An explanation is required as to why the theory holds so well down to geometrical dimensions of the order of molecular size. In addition, although the assumption of a constant wall potential independent of salt concentration was made in the present work this is known not always to be true, depending on the solid–solution interface, so that the effect of relaxing this assumption should be determined. Another assumption in the present work is that the axial distribution of charge on the pore wall is such that the ion distributions in the pore follow the functional relationship (eq 2b) suggested by Gross and Osterle.[13] Although the effect of this assumption is not expected to be large on such integrated characteristics as fractional salt rejection and streaming potential, nevertheless a detailed study should be made of the rejection characteristics corresponding to various physically realistic wall charge or potential specifications.

If the theory is to be useful for characterizing porous membranes for desalination or demineralization of water by reverse osmosis it should be extended to the case where the fluid contains several ionic solutes of the same sign having different valences and diffusion coefficients. It would also be of interest to extend the analysis to model geometries more complicated than a straight cylindrical pore. Finally, it is evident that a much wider range of membrane materials and operating conditions must be investigated experimentally before the full utility of the theory can be properly assessed.

Acknowledgment. This research was sponsored by the Office of Saline Water, U. S. Department of the Interior, under Grant No. 14-30-2575.

Kinetics of Acid Dissociation–Ion Recombination of Aqueous Methyl Orange

Richard G. Sandberg, Gary H. Henderson, Robert D. White, and Edward M. Eyring*

Department of Chemistry, University of Utah, Salt Lake City, Utah 84112

(Received May 25, 1972)

Publication costs assisted by the Air Force Office of Scientific Research

In ~10^{-5} M acidic aqueous solutions of Methyl Orange the rate constant at 25° for the recombination of a proton with the monoanion of the indicator is $2.9 \pm 0.4 \times 10^9$ M^{-1} sec^{-1}. This specific rate, determined by a spectrophotometric electric field jump relaxation technique, is significantly smaller than that expected for a diffusion-controlled ion recombination. An explanation for this result follows from a comparison with similar kinetic data for aqueous Methyl Red.

Introduction

Methyl Orange (I) is one of the most frequently used acid–base indicators at acidic pH values near its reported[1] pK_a = 3.47 in water at 25°. In general, when Methyl Orange is used as the indicator in temperature jump or other relaxation experiments exact numerical values for the dissociation and ion recombination specific rates are unnecessary if the relaxation time (τ) of the coupled system is long compared to that of Methyl Orange. However, in studying very fast reactions (*e.g.*, metal hydrolysis) characterized by relaxation times of the order of microseconds, values for the recombination and dissociation specific rates of the indicator should be known in order to reliably interpret the observed relaxation data.

The dissociation kinetics of Methyl Red (II) in dilute aqueous solution were reported[2] in terms of a one-step

---

(1) R. L. Reeves, *J. Amer. Chem. Soc.*, **88**, 2240 (1966).

(2) L. P. Holmes, A. Silzars, D. L. Cole, L. D. Rich, and E. M. Eyring, *J. Phys. Chem.*, **73**, 737 (1969).

mechanism (eq 1) with the values of k_D and k_R given as 4.8×10^5 sec^{-1} and 3.5×10^{10} M^{-1} sec^{-1}, respectively. Using these data and the normal relaxation expression (eq 2 and 3) for the one-step process,[3] one would predict relaxation times as short as 20 nsec for Methyl Orange at concentrations near 10^{-5} M in the pH range of 3.2 to 4.4 where this indicator is customarily used. It is known that the pK_a of the β-azo nitrogen is quite different in Methyl Red and in Methyl Orange.[4-7] Since the resonance contribution in both systems should be approximately the same, the pK_a difference seems anomalous. It was, therefore, our purpose to determine by means of the dissociation kinetics in what way the acid-base behavior is affected by variations in structure in azo dyes.

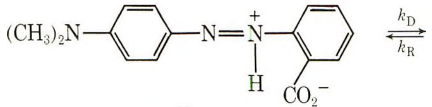

II

$$H^+ + \text{Methyl Red anion} \tag{1}$$

$$\tau^{-1} = k_R([H^+] + [In^-]) + k_D \tag{2}$$

$$= k_R([H^+] + [In^-] + K_a) \tag{3}$$

Experimental Section

Methyl Orange (I), p-[(p-dimethylamino)phenyl]azobenzenesulfonic acid, was obtained from J. T. Baker Co. The indicator was twice recrystallized from hot water, and the precipitate was washed with ethanol and ether and dried at low temperature for several hours.

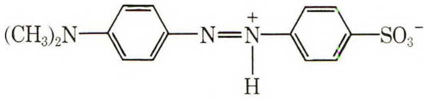

I

All solutions used in the study were freshly prepared using doubly distilled deionized water (specific conductivity 0.9×10^{-6} ohm^{-1} cm^{-1}). The dilute sample solutions were prepared from a 2.14×10^{-4} M stock solution. Adjustments of pH were made using either dilute hydrochloric acid or dilute sodium hydroxide. (This correction caused less than 0.1% error in the final indicator concentration.) The pH measurements were made using a Beckman Model 1019 pH meter equipped with a combination glass electrode (Beckman 40498). Sample solutions evidenced a pH constant to within ±0.03 pH units when tested prior to and immediately succeeding the E-jump experiment (a time interval of up to 30 min). The electric field jump (E-jump) relaxation method apparatus used was basically identical with that described by Olsen, *et al.*[8] The major modification involved the use of a digital delay trigger generator having a time base referenced to a 10-MHz quartz crystal. This allows for more accurate control of the square, high-voltage pulse width. It also becomes possible by accurately varying pulse width to enhance the relative amplitude of a given relaxation time compared to others in a relaxation spectrum.

All kinetic measurements were made spectrophotometrically in the absence of an applied electric field (*i.e.*, immediately following the termination of the square, high-voltage pulse). The electrical resistance of the sample cell in all cases exceeded 10^4 ohms, so that the rise in sample temperature incident to the E-jump was negligible.

Results

Presented in Table I are the values of τ, the pH, and associated statistical parameters obtained in the Methyl Orange experiments. Additionally, the Methyl Red ionization kinetics were reevaluated using the modified E-jump and the results obtained were in good agreement with those reported by Holmes, *et al.*[2] The calculated Methyl Red recombination and dissociation specific rates are $4.02 \pm 0.4 \times 10^{10}$ M^{-1} sec^{-1} and $5.0 \pm 0.4 \times 10^5$ sec^{-1}, respectively, yielding a kinetic pK_a = 4.91. This value is in good agreement with both the previously reported[2] kinetic pK_a of 4.88 and the literature thermodynamic value[6,7] of 5.00.

If the single-step ionization mechanism (eq 1) identical with that for Methyl Red is followed, a plot of the reciprocal relaxation time (τ^{-1}) *vs.* the sum of the concentrations of the Methyl Orange anion and hydrogen ion ($[A^-] + [H^+]$) (eq 2) should yield a straight line (see Figure 1). The slope of the line gives the recombination rate constant $k_R = 2.9 \pm 0.4 \times 10^9$ M^{-1} sec^{-1} and the intercept the dissociation rate constant $k_D = 7.9 \pm 1.0 \times 10^5$ sec^{-1} at 25°. These constants yield a kinetic pK_A = 3.57 in reasonable agreement with the spectrophotometrically determined[4] β-azo nitrogen pK_a = 3.37 of Methyl Orange.

Discussion

From the experimental work of Eigen and coworkers[3,9,10] we have come to expect that unless intramolecular hydrogen bonding, intramolecular electronic rearrangement as in pseudo acids, or steric factors are present, the specific rate of an ion recombination should closely approach the limiting value predicted by Debye's phenomenological equation[11] for a diffusion-controlled reaction. On this basis, for a proton reacting with a monoanion as in the case of Methyl Orange we would expect a k_R of about 5×10^{10} M^{-1} sec^{-1}. Thus, the $k_R = 2.4 \times 10^9$ M^{-1} sec^{-1} reported above is somehwat surprising since none of the above-mentioned factors appear to be operative in the case of Methyl Orange we would expect a k_R of about 5 × Methyl Red anion does have a $k_R = 4.02 \times 10^{10}$ M^{-1} sec^{-1}.

A possible explanation for the Methyl Orange observed ion recombination rate may be found in the coupled ionization mechanism proposed by Sawicki[4] (eq 4). The relaxation times, τ, for this coupled equilibrium system are given by expression 5, where the specific rates are identified in eq 4. It is obvious from eq 5 that a plot of $1/\tau$ *vs.* ($[A^-] + [H^+]$) will not, in general, be linear. Agreement is obtained, however, between the expression 5 for $1/\tau$ and the experimental data if the recombination rate constant, k_{3R}, for the amine group is near its diffusion-controlled limit (*e.g.*, $k_R = 1.5 \times 10^{10}$ M^{-1} sec^{-1} for imidazole[12]) and the value of K_T, the ratio of the protonated β-azo to

---

(3) M. Eigen and L. De Maeyer, "Technique of Organic Chemistry," Vol. VIII, Part II, S. L. Friess, E. S. Lewis, and A. Weissberger, Ed., Interscience, New York, N. Y., 1963, Chapter 18.

(4) E. Sawicki, *J. Org. Chem.*, **21**, 605 (1956).

(5) G. E. Lewis, *Tetrahedron*, **10**, 129 (1960).

(6) I. M. Kolthoff, *J. Phys. Chem.*, **34**, 1466 (1930).

(7) S. W. Tobey, *J. Chem. Educ.*, **35**, 514 (1958).

(8) S. L. Olsen, R. L. Silver, L. P. Holmes, J. J. Auborn, P. Warrick, Jr., and E. M. Eyring, *Rev. Sci. Instrum.*, **42**, 1247 (1971).

(9) M. Eigen, *Angew. Chem.*, **75**, 489 (1963); *Angew. Chem., Int. Ed. Engl.*, **3**, 1 (1964).

(10) M. Eigen, W. Kruse, G. Maass, and L. De Maeyer, *Progr. React. Kinet.*, **2**, 287 (1964).

(11) P. Debye, *Trans. Electrochem. Soc.*, **82**, 265 (1942).

(12) M. Eigen, G. G. Hammes, and K. Kustin, *J. Amer. Chem. Soc.*, **82**, 3482 (1960).

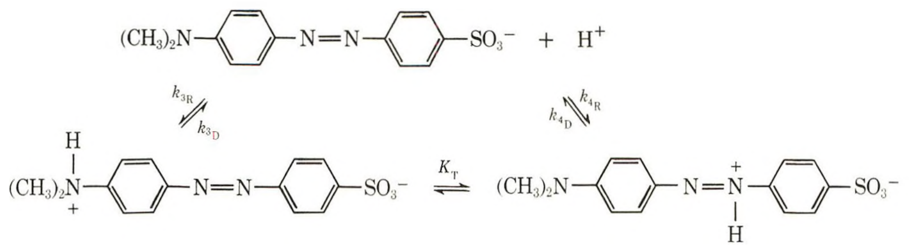

(4)

$$1/\tau = \tfrac{1}{2}[(k_{3R} + k_{4R})([A^-] + [H^+])] = \tfrac{1}{2}(k_{3D} + k_{4D}) + \tfrac{1}{2}X \qquad (5)$$

$$X \equiv \{[(k_{3R} - k_{4R})([A^-] + [H^+]) + k_{3D} - k_{4D}]^2 + 4k_{3R}k_{4R}[(A^-) + (H^+)]^2\}^{1/2}$$

amine forms of Methyl Orange, is as large as the maximum value of 4.7 estimated by Reeves.[1] Under these conditions the large τ's observed experimentally are entirely consistent with the coupled mechanism. Additionally, it is evident that over the limited concentration range of this study the effect of the amine protonation is minimal (see Figure 1). Finally, the value obtained for the kinetic pK_a of Methyl Orange is in good agreement with that of the β-azo nitrogen determined spectrophotometrically.[1] The conclusion then must be that the ionization kinetics observed are those of the β-azo nitrogen.

TABLE I: Electric Field Jump Relaxation Data for Aqueous Methyl Orange and Methyl Red at 25°

C_0,[a] 10^{-5} *M*	pH[b]	τ,[c] 10^{-6} sec	σ[d]	*n*[e]	μ,[f] 10^{-5} *M*	([H$^+$] + [A$^-$]),[g] 10^{-5} *M*
			Methyl Orange			
2.19	3.36	0.46	0.05	4	44.1	45.2
2.19	3.39	0.50	0.03	2	41.2	42.2
2.19	3.48	0.54	0.08	4	33.7	34.9
2.19	3.55	0.64	0.02	4	28.8	29.9
2.19	3.57	0.60	0.09	4	28.1	28.7
2.19	3.63	0.67	0.07	4	25.2	25.2
2.19	3.73	0.71	0.01	2	20.4	20.4
2.19	3.92	0.813	0.04	3	18.9	13.8
			Methyl Red			
3.41	4.60	0.51	0.07	3	2.51	3.48
3.41	4.72	0.59	0.05	6	1.9	3.06
3.41	4.92	0.62	0.07	6	1.6	2.75
2.17	5.16	0.71	0.03	6	1.3	1.97
1.66	5.16	0.85	0.05	7	0.99	1.67
1.26	5.13	0.94	0.06	5	0.74	1.46

[a] Total molar concentration of sample acid. [b] Average glass electrode pH measured before and after kinetic experiments. [c] Average relaxation time for *n* independent measurements. [d] Standard deviation of τ calculated for *n* experiments. [e] Number of independent determinations of τ. [f] Ionic strength of the sample solution. [g] Total concentration of hydrogen ion and sample acid anion calculated from pK_a = 3.47 in the case of Methyl Orange and pK_a = 5.00 for Methyl Red.

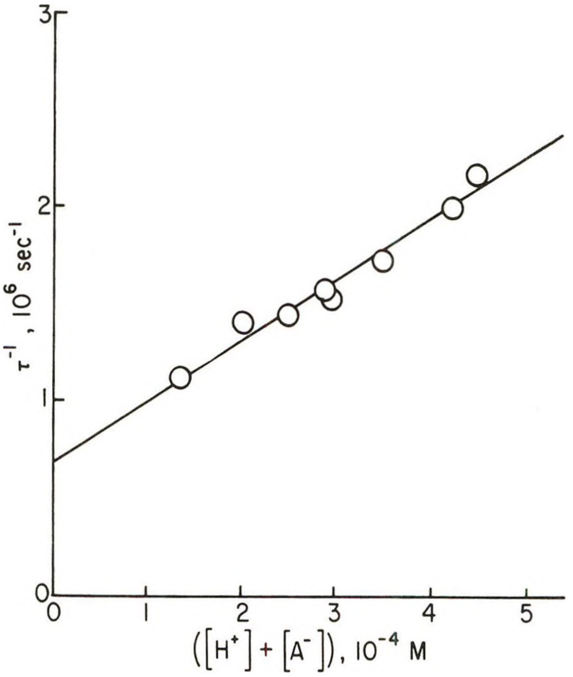

Figure 1. Plot of E-jump reciprocal relaxation times, τ^{-1}, *vs.* the sum of the concentrations of hydrogen ion and Methyl Orange anion at 25°.

The question remains then why the recombination rates of the β-azo group of Methyl Red and Methyl Orange differ by more than a factor of 10. Although it appears that the β-azo group of Methyl Red behaves kinetically as a "normal acid,"[10] there is no obvious reason[3,9,10] why the analogous process in Methyl Orange should not approximate the diffusion limit (4×10^{10} M^{-1} sec^{-1}). The most reasonable explanation would seem to be that, in Methyl Red, the barrier to proton binding to the azo group from the solvent is lowered by the presence of the negatively charged carboxyl group adjacent to the site of binding. The fact that the dissociation constant for the carboxy acid group of Methyl Red is much smaller (by a factor of ~10) than for benzoic acid[13] as well as the fact that the dissociation constant of the β-azo group for Methyl Orange is 34 times that for Methyl Red tends to indicate that a significant interaction between the β-azo proton and the ortho carboxy group of Methyl Red exists. Further study is necessary to clarify this point, but at this time one is led to suspect that the rate of recombination at the β-azo nitrogen is not in general diffusion controlled and that the recombination rate is strongly influenced by ortho substituents.

Acknowledgment. This work was supported by the Directorate of Chemical Sciences, Air Force Office of Scientific Research, under Grant No. AFOSR 69-1717.

(13) I. M. Kolthoff and W. Bosch, *J. Phys. Chem.*, **36**, 1695 (1932).

Equilibrium Sedimentation Studies of the Aggregation of Methylene Blue

Emory H. Braswell

Biochemistry and Biophysics Section, Biological Sciences Group, University of Connecticut, Storrs, Connecticut 06268

(Received January 24, 1972)

Publication costs assisted by the University of Connecticut Research Foundation

The aggregation of Methylene Blue in aqueous solutions at 30° was studied by means of sedimentation equilibrium techniques. These studies were carried out over a dye concentration range of from *ca.* 10^{-5} to *ca.* 10^{-3} M in the presence of NaCl concentrations which were from 77- to 200-fold higher than that of the dye. In the absence of NaCl it was possible to make measurements over a concentration range of from 2×10^{-5} to *ca.* 6×10^{-2} M. The results indicate that (1) at the lowest concentration studied the dye is 60% ionized; (2) in the presence of a high concentration ratio of NaCl to dye, the dye is not ionized and aggregates by means of a simple "condensation" type polymerization with an equilibrium constant of 600 M^{-1} (which corresponds to a dimerization constant of 2400 M^{-1}); (3) in the absence of NaCl the aggregates formed are charged; (4) the reaction goes far beyond pentamer formation; and (5) the β absorption band is at a maximum when the quantity of dimer is maximal.

Introduction

Upon the addition of certain high molecular weight anionic polymers such as heparin (a chromotrope) to a dilute aqueous solution of certain cationic dyes such as Methylene Blue, there occurs a shift in the wavelength of maximum absorption toward shorter wavelengths. This "metachromatic effect" is easily observed as a change in the color of the solution from blue to purple or red. A similar effect can be observed as the dye concentration is increased in a solution of the dye alone and is believed to be due to aggregation ("stacking") of the dye molecule (see, for example, ref 1-8) which presumably is brought about by dispersion forces operating in a direction perpendicular to the plane of the delocalized π electrons.[1-3] Metachromasia, therefore, is thought to be due to the facilitated aggregation of the dye molecules which are bound to the chromotrope.[7,9-11] Bradley and his associates[12-15] were able to develop a semiquantitative description of the metachromatic phenomenon by using a statistical approach and by assuming that bound dye molecules only associate with each other to the extent of forming dimers. However he acknowledged that higher stages of aggregation probably exist. In this manner however he was able to clearly delineate the factors involved which contribute to the degree of metachromasia obtained. First, is the innate ability of the dye molecule to "stack" or aggregate with itself. This is a function of the organic and hence electronic structure of the dye. The second factor involves the spacing of the sites on the chromotrope.

This study is limited to the investigation of the mechanism of the dye-dye association. It must be pointed out that many different types of dye associate, and some show shifts in wavelength of maximum absorption upon association. Of this latter group only some dyes aggregate principally through π electron interaction and show the peculiar metachromatic type of absorption maximum shift (see, for example, ref 16). That is, as the dye concentration is increased there appears a second absorption band (β band) at shorter wavelengths than that associated with the monomeric dye (α band), while this latter band decreases in height. Then as the concentration is further increased the β band shifts slowly to shorter wavelengths simultaneously decreasing in height while the α band diminishes until it becomes undetectable.

Very little is known about the mechanism of aggregation or the number of dye molecules in a metachromatic aggregate. Most attempts to study the effect quantitatively have been limited to considering only dimerization[2,4,6,17] even though many authors note that higher aggregates probably also form.[2,4,6,8,17] The role of water in the formation of the aggregates, either as a dielectric sandwiching between the dye molecules[5,6] or as a former of hydrogen bonds,[17,18] has been found to be of great importance. In a series of articles[19-25] Hillson and McKay presented evidence to back their belief that the metachromasia of dyes observed in solvents of low dielectric strength was due to strong interactions between dye ions and counterions to produce an undissociated dye in which the ions are in intimate contact and are not separated by solvent molecules.[21] In one article they suggest that aggregation probably does not occur at all in solvents of very low dielectric strength[22] even though metachromasia is evident. In a later article, they imply that even when the dye is in the presence of a chromotrope in water metachromasia occurs largely as a result of the interaction of the dye cation with the polyanion, resulting in a perturbation of the charge distribution of the dye cation.[20] Still later, however, they concede that dimerization of the dye is an important cause of metachromasia in water and that this is due to the tendency of water molecules to self-associate, giving rise to strong hydrophilic bonding between dye molecules.[25] Because salt is known to increase dye aggregation, Haugen and Hardwick[18] have suggested that the dye dimerization may take place in the following manner

---

(1) G. Scheibe, *Angew. Chem.*, **50**, 212 (1937).
(2) G. Scheibe, *Kolloid Z.*, **82**, 1 (1938).
(3) G. Scheibe, *Angew. Chem.*, **52**, 631 (1939).
(4) E. Rabinowitch and L. F. Epstein, *J. Amer. Chem. Soc.*, **63**, 69 (1941).
(5) S. E. Sheppard and A. L. Geddes, *J. Amer. Chem. Soc.*, **66**, 1995 (1944).
(6) S. E. Sheppard and A. L. Geddes, *J. Amer. Chem. Soc.*, **66**, 2003 (1944).
(7) L. Michaelis and S. Granick, *J. Amer. Chem. Soc.*, **67**, 1212 (1945).
(8) T. Vickerstaff and D. R. Lemin, *Nature (London)*, **157**, 373 (1946).
(9) J. M. Wiame, *J. Amer. Chem. Soc.*, **69**, 3146 (1947).
(10) B. Sylven, *Quart. J. Microscop. Sci.*, **95**, 327 (1954).
(11) M. Schubert and A. Levine, *J. Amer. Chem. Soc.*, **77**, 4197 (1955).
(12) D. F. Bradley and M. K. Wolf, *Proc. Nat. Acad. Sci. U. S.*, **45**, 944 (1959).
(13) D. F. Bradley and F. Felsenfeld, *Nature (London)*, **185**, 1920 (1959).
(14) A. L. Stone and D. F. Bradley, *J. Amer. Chem. Soc.*, **83**, 3627 (1961).
(15) A. L. Stone, L. G. Childers, and D. F. Bradley, *Biopolymers*, **1**, 111 (1963).
(16) E. Braswell, *J. Phys. Chem.*, **72**, 2477 (1968).
(17) M. E. Lamm and D. M. Neville, Jr., *J. Phys. Chem.*, **69**, 3872 (1965).
(18) G. R. Haugen and E. R. Hardwick, *J. Phys. Chem.*, **67**, 725 (1963).
(19) P. J. Hillson and R. B. McKay, *Trans. Faraday Soc.*, **61**, 374 (1965).
(20) P. J. Hillson and R. B. McKay, *Nature (London)*, **210**, 297 (1966).
(21) R. B. McKay and P. J. Hillson, *Trans. Faraday Soc.*, **61**, 1800 (1965).
(22) R. B. McKay and P. J. Hillson, *Trans. Faraday Soc.*, **62**, 1439 (1966).
(23) R. B. McKay, *Trans. Faraday Soc.*, **61**, 1787 (1965).
(24) R. B. McKay, *Nature (London)*, **210**, 296 (1966).
(25) R. B. McKay and P. J. Hillson, *Trans. Faraday Soc.*, **63**, 777 (1967).

$$2D^+ + A^- \rightleftharpoons (D_2A)^+$$

Lamm and Neville,[17] however, have found for Acridine Orange that it is impossible to distinguish between this model and the simple dimerization one.

Some progress has been made on determining the degree of polymerization attainable by the dye. Hillson and McKay[19] found, using polarographic methods, that the degree of aggregation of Methylene Blue at high concentrations was about 3. Braswell[16] using spectral techniques and studying dye concentrations far higher than those studied previously found that a limiting aggregation number of 3 described the data qualitatively at moderately high concentrations but poorly at the highest concentrations. Vapor pressure osmometry data presented in the same paper indicated a limiting aggregation number of 3. In addition Braswell[16] obtained an equilibrium constant for both the dimerization and trimerization steps of the reaction. The latter value was 1.5 times the former (3000 *vs.* 2000 M^{-1}). The third unit is therefore easier to add than the second, indicating a second nearest neighbor effect.

Recently a series of papers[26-30] by Mukerjee and Ghosh cast new light on the problem. They pointed out that most methods of studying the dye reaction involved the determination of an additional parameter, *e.g.*, for absorption spectrophotometry the molar extinction coefficient for each species, as well as the equilibrium constant for each association step. Therefore they developed an equilibrium method which they called the "isoextraction technique." This technique is essentially a sensitive way of determining the monomer concentration as a function of the total dye concentration by means of the extractability of the monomeric dye-salt into an organic phase. By means of it they were able to show that the aggregation of Methylene Blue goes at least as far as the pentamer stage and in agreement with Braswell[16] have found that the equilibrium constant associated with the addition of the third dye unit is about 1.5 times greater than that for the dimerization step. They further show that as the association proceeds beyond trimerization the equilibrium constants gradually decrease. The well-known increase of dye aggregation caused by the presence of salt was felt by these authors to be in "rough accord with that expected from changes in activity coefficients" and that there is "negligible counterion participation in association equilibria at low ionic strengths."

An equilibrium technique that seems to be especially suited for the study of such aggregating systems is that of equilibrium sedimentation. It has been used extensively for the study of multistep equilibria in protein aggregation and other substances (see for representative bibliography ref 31-41). A system which bears resemblance to the aggregation of metachromatic dyes which was studied by van Holde[36,39] involves the association of cytidine and purine. Since these substances have similar molecular weights but lower association constants than Methylene Blue, the feasibility of using sedimentation techniques for the study of the aggregation of Methylene Blue seemed firmly based.

Experimental Methods and Results

The dye was purified by the method of Bonneau, Faure, and Jousset-Dubien.[42] This method gave a product which was found to be somewhat purer by chromatographic analysis on Eastman thin layer silica gel chromagram sheets (using 9:1 methanol:acetic acid) than that purified in the manner used for our previous study.[16] That is, the faint leading spot previously observed was missing or extremely faint in the purified dye samples used for this study.

The sedimentation studies were performed at 30° in a Spinco, Model E, analytical ultracentrifuge using a Spinco photoelectric scanner (with monochromator) to detect dye concentration changes across the cell due to absorption. The wavelength of light chosen depended largely on the cell thickness-dye concentration combination studied. It was found that observation near 406 mμ obeyed Beer's Law over the widest concentration range and, since this was near the wavelength of least absorption, was the wavelength chosen most often at high dye concentration. At low dye concentration, however, there was not enough absorption for accurate concentration measurement hence other wavelengths (principally 366 and 436 mμ) were used. Corrections for deviation from Beer's Law were made from data gathered from spectral studies performed with a Cary 14 spectrophotometer. Ultracentrifuge cells varying in thickness from 3 to 0.004 cm were used. Although double sector cell operation of the scanner was possible for the larger cell sizes, for the smaller single sec-

(26) P. Mukerjee and A. K. Ghosh, *J. Amer. Chem. Soc.*, **92**, 6403 (1970).
(27) A. K. Ghosh and P. Mukerjee, *J. Amer. Chem. Soc.*, **92**, 6408 (1970).
(28) A. K. Ghosh and P. Mukerjee, *J. Amer. Chem. Soc.*, **92**, 6413 (1970).
(29) A. K. Ghosh, *J. Amer. Chem. Soc.*, **92**, 6415 (1970).
(30) P. Mukerjee and A. K. Ghosh, *J. Amer. Chem. Soc.*, **92**, 6419 (1970).
(31) E. T. Adams, Jr., and H. Fujita, "Ultracentrifugal Analysis in Theory and Experiment," Academic Press, New York, N. Y., 1963, p 119.
(32) E. T. Adams, Jr., *Proc. Nat. Acad. Sci. U. S.*, **51** (3), 509 (1964).
(33) E. T. Adams, Jr., and J. W. Williams, *J. Amer. Chem. Soc.*, **86**, 3454 (1964).
(34) E. T. Adams, Jr., and D. L. Filmer, *Biochemistry*, **5**, 2971 (1966).
(35) E. T. Adams, Jr., *Biochemistry*, **6**, 1864 (1967).
(36) K. E. van Holde and G. P. Rossetti, *Biochemistry*, **6**, 2189 (1967).
(37) M. Derechin, *Biochemistry*, **7**, 3253 (1968).
(38) D. E. Roark and D. A. Yphantis, *Ann. N. Y. Acad. Sci.*, **164**, 245 (1969).
(39) K. E. van Holde, G. P. Rossetti, and R. D. Dyson, *Ann. N. Y. Acad. Sci.*, **164**, 279 (1969).
(40) N. R. Langerman and I. M. Klotz, *Biochemistry*, **8**, 4746 (1969).
(41) P. J. Trotter and D. A. Yphantis, *J. Phys. Chem.*, **74**, 1399 (1970).
(42) R. Bonneau, J. Faure, and J. Joussot-Dubien, *Talanta*, **14**, 121 (1967).

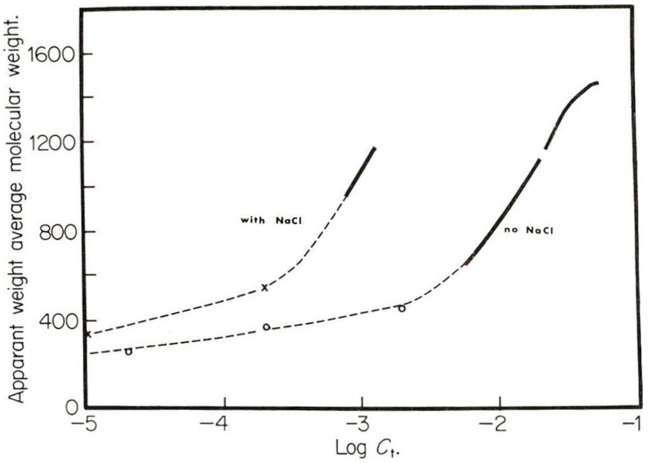

Figure 1. Apparent weight average molecular weight of Methylene Blue as a function of concentration. Thickened lines represent continuous data over a range of concentration; points represent discrete data. Upper line represents data obtained in the presence of NaCl (NaCl:dye ratio = 200/1 to 77/1); lower line represents data obtained in the absence of NaCl.

tor cells, solvent balancing was performed by centrifuging the solution cell with an identical cell containing solvent. The smallest cell (*ca.* 0.004 cm) was formed by simply placing a red polythene gasket between two sapphire windows and tightening the cell to an average torque of 140 in. lb. The sample or solvent was measured out with a microsyringe on the window before assembling the cell. Since the thickness of the cell was amazingly reproducible (10%) the solution column which formed as soon as the centrifuge was rotating at a few thousand rpm was approximately the desired height. With solution columns of 3-mm centrifugation at 48 or 56 krpm for 6 hr was enough to obtain practical equilibrium. For solution columns of 6 mm 24 hr of sedimentation was required. At low dye concentration the concentration gradient formed was small (1.2-2.0) and generally a plot of ln concentration *vs.* X^2 yielded a line with little or no curvature. It was found necessary to include 0.5% sucrose in solutions of low dye-plus-salt concentration (<0.01 *M*) in order to provide a density gradient large enough to stabilize the system and eliminate turbulance. Spectral studies indicated that this concentration of sucrose had no effect on the aggregation of the dye at low concentration.

At high dye concentration or in the presence of NaCl considerably larger gradients were formed, the largest having a concentration ratio of almost fourfold. The results obtained from these studies are shown in Figure 1. The data from each single experiment at low dye concentration or short column height or both are shown as single points. At high dye concentration with long columns the data are shown as a thickened line over the concentration range of the experiment. The graph of the effect of NaCl on the molecular weight of the dye ends at a dye concentration of about 1.3 × 10^{-3} *M* due to the insolubility of the dye at a NaCl concentration of 0.1 *M*. Since the molecular weights obtained were found to be approximately at a maximum when the salt concentration is about 100 times the dye concentration, the concentration of salt included in an experiment is from 77 to 200 times that of the dye concentration used.

The effect of pressure was determined by making equilibrium runs at different speeds. Since the same values for the molecular weight were obtained at a given dye concentration regardless of speed, it was felt that the effect of pressure on aggregation, due to a change in the partial molar volume of the dye upon aggregation, could be ignored.

Specific volumes were determined picnometrically on aqueous Methylene Blue solutions ranging from 5 × 10^{-3} *M* to approximate saturation (*ca.* 0.06 *M*). The values of $\bar{V}$ over this concentration range were found to be from 0.762 to 0.745. Unfortunately it was not possible with this technique to measure specific volumes at lower concentrations.

Discussion

Although it is not yet possible to assign a unique model to the aggregation of Methylene Blue, the data presented in the figure considerably reduce the number of possibilities. At low dye concentration it can be seen that the weight average molecular weight of the dye in the absence of salt is *ca.* 260 at a dye concentration of 10^{-5} *M*. If every dye molecule had one charge on it under these conditions it would yield an apparent molecular weight of $320/(Z + 1)$ or 160. An apparent molecular weight of 260 indicates that the dye is only ionized *ca.* 60% under these conditions. In the presence of salt the molecular weight at this concentration rises to *ca.* 330, using $\bar{V}$ = 0.75. It is known by spectrophotometry studies that there is no significant aggregation at this dye concentration.[16] Since there is no detectable change in spectrum upon addition of 0.002 *M* NaCl (NaCl to dye concentration ratio 200:1)[43] indicating that this level of salt does not cause aggregation, it seems reasonable to conclude that the addition of this quantity of NaCl suppresses the ionization of the dye.

If the dye is assumed to be at low concentration (monomeric, concentration-dependent terms omitted, and ρ = 1) and to be singly charged, the following relation should hold.[44]

$$(RT/\omega^2 r C_{\mathrm{DCl}})(\mathrm{d}C_{\mathrm{DCl}}/\mathrm{d}r) = M_{\mathrm{DCl}}(1 - \bar{V}_{\mathrm{DCl}}) - 1/2 M_{\mathrm{NaCl}}(1 - \bar{V}_{\mathrm{NaCl}})$$

where M_{DCl} and M_{NaCl} are the formula weights and $\bar{V}_{\mathrm{DCl}}$ and $\bar{V}_{\mathrm{NaCl}}$ are the specific volumes of the dye chloride and salt, respectively. The left-hand term is experimentally determined and the symbols have the usual meanings. According to the definition of components used, the left-hand side of the equation is identical with $M_{\mathrm{A}}(1 - \bar{V}_{\mathrm{A}})$, where M_{A} is the apparent molecular weight, $\bar{V}_{\mathrm{A}} = (U_{\mathrm{DCl}} - {}^1/_2 U_{\mathrm{NaCl}})/M_{\mathrm{A}}$, and U represents the respective molar volumes. Performing this calculation yields predicted values of 291 for M_{A} and 0.79 for $\bar{V}_{\mathrm{A}}$. The data at 10^{-5} *M* yielded respective values of 314 and 0.74. Since the observed molecular weight is close to that expected when no charge is present (320) it is reasonable to treat data at higher concentrations as un-ionized also, therefore $\bar{V}_{\mathrm{DCl}}$ (0.75) was used for all calculations. This results, at a dye concentration of 10^{-5} *M*, in the value for M_{A} of 330 (instead of 314) which was mentioned previously. The fact that the dye is not charged at high salt to dye concentration ratios simplifies the theoretical treatment considerably since one does not have to apply polyelectrolyte theory to the results.

If one assumes that the dye in the presence of a high salt to dye concentration ratio is un-ionized throughout the dye concentration range and that the dye can undergo

---

(43) Data to be published in the future.

(44) C. Tanford, "Physical Chemistry of Macromolecules," Wiley, New York, N. Y., 1961, pp 267-269.

a condensation type of infinite polymerization wherein each dye molecule contributes two aggregation sites, one can write the following relations

$$n(\text{dye}) \rightleftharpoons (\text{dye})_n$$

or

$$2(\text{sites}) \rightleftharpoons \text{bond}$$

$$K = [\text{bonds}]/[\text{sites}]^2$$

and

$$P = \text{reacted sites}/\text{total sites} = [\text{bonds}]/C_t$$

where P is the probability of a site having reacted (the degree of reaction) and C_t is the original dye concentration in moles/liter of dye monomer units. It then follows that

$$K = P/4C_t(1 - P)^2 \qquad (1)$$

and

$$M_w = M_1[(1 + P)/(1 - P)] \qquad (2)$$

where M_w is the observed weight average molecular weight and M_1 is the molecular weight of the un-ionized monomer (320). It was found that eq 1 and 2 fitted the experimental data obtained from experiments performed in the presence of high salt to dye concentration ratios when K was approximately equal to 600 M^{-1}. This value is equivalent to a dimerization constant of 2400 M^{-1}. In an earlier publication,[16] by assuming a stepwise aggregation, an equilibrium constant of dimerization of 2000 M^{-1} and that of the next step (dimer to trimer) of 3000 M^{-1} were found in the absence of salt. The equivalent value of 2400 found in the current study may be partially reflecting the value of the equilibrium constant of the dimer–trimer step, or it may be higher than the dimerization constant because of the small reaction-promoting effect of salt at the higher dye and salt concentrations (see below).

An observation of interest is that the weight average molecular weight obtained in the presence of salt attains a value of 640 at a dye concentration of *ca.* 3.4×10^{-3} M. This should correspond to a number average molecular weight of 480 and a degree of polymerization of 0.333 for the assumed aggregation model and equilibrium constants. It can be shown that, for an infinite condensation type of aggregation, at a degree of polymerization of 0.333 the concentration of dimer is at a maximum. We have previously shown that in this region of dye concentration, the β absorption peak is at its maximum.[16] Since this peak has traditionally been associated with the absorption of the dimer it is felt that this is further indicative evidence that the foregoing conclusions regarding aggregation mechanism are not in great error. In fact this observation provides support for the identification of the β band with dye dimers.

In the situation where salt was absent, the apparent molecular weights are lower than those determined in the presence of salt at all dye concentrations where comparison was possible. The increasing divergence of the data taken in the presence of salt from that in the absence of salt may be due to either or both of two factors. Either the NaCl strongly increases the degree of polymerization, or an increasingly larger charge per molecule developing on the aggregated dye in the absence of salt, reduces the observed molecular weight. Since 0.1 M salt was the highest concentration used in this study, and since the effect of this amount of salt on the polymerization as observed by spectrophotometry (as will be shown in a future publication[43]) is equivalent to increasing the dye concentration by at most 30% it is clear that the latter cause is more important. Therefore it is clearly the effect of charge on the dye molecules which suppresses the observed molecular weights. That this effect is not enormous though can be seen in the only 60% ionization observed in 10^{-5} M dye solutions in the absence of salt. It might be expected that this degree of dissociation would decrease as the molecule grows, so that at high degrees of polymerization one would expect on the average there to be *less* than one charge for every two subunits in the chain. The maximum weight average molecular weight found in the absence of salt is approximately 1450. This is lower than the true uncharged molecular weight by a factor which could be estimated from the following equation.

$$MA = nM_1/(Z + 1) = nM_1/(n\alpha + 1)$$

where Z is the charge per chain, n is the number of monomers in the aggregate, M_1 the molecurar weight of the uncharged monomer, α the degree of ionization, and MA the apparent molecular weight. It can be shown from the equation that the maximum value that α can have for $MA = 1450$ when the molecules are of infinite size ($n = \infty$) is 0.22. If we assume that the value of α is 0, then the maximum value of the true molecular weight would be 1450 (or $n \simeq 4.5$). More insight can be achieved if one felt confident that the equilibrium constant obtained at high salt and low dye concentration applied also at high dye and low salt concentrations. The limited justification for this has already been presented as resting on the fact that the highest concentrations of NaCl used for these studies increase metachromasia by an amount equivalent to that which would occur if the dye concentration had been increased by a maximum of only 30%. Further the fair agreement between the K found in salt *via* sedimentation techniques (2400 M^{-1} for dimerization) with that found earlier[16] by means of spectrophotometry (2000 M^{-1}) lends stronger credence to this belief. Use of the value (600 M^{-1}) found here for K (for a condensation-type polymerization) leads to a value of 0.913 for P. This means that at this concentration the dye has a weight average molecular weight of 7037. Since the apparent weight average molecular weight is 1450, one can conclude that there is, on the average, about 3.85 charges ((7037/1450) − 1) for every 22 dye units (7037/320) or an average ionization of about 0.18. Because of the small reaction-promoting effect of the salt one must regard these calculated values of the molecular weight and the extent of ionization as a bit high. Two conclusions can therefore be arrived at from the data taken without the presence of salt. First, is that the degree of ionization decreases from 60% at low dye concentrations to a value close to 18% at high concentration. The second conclusion is that there are aggregates present at high dye concentrations that are most certainly far larger than pentamer in size. This then provides some justification for applying an infinite polymerization mechanism at low dye concentration, and does not rule out the possibility of some larger limiting aggregation number such as might be expected in the case of micelle formation. This cannot be determined until studies can be made in the presence of high concentrations of a salt which does not cause precipitation and preferably does not affect the degree of polymerization of the dye. Such studies are now in progress.

No treatment of nonideality effects at high dye and low salt concentration has been attempted in this study, for not enough is known about the charged nature of the dye. Our current investigations at high salt concentration should help elucidate this situation. However, it was felt that nonideality could be ignored in the case of dye concentrations below 1×10^{-3} *M* in the presence of salt. The excellent agreement of the simple aggregation model with the data bears out this contention.

Acknowledgments. The author is indebted to Professor Geoffrey A. Gilbert of The University, Birmingham, U. K., for his hospitality and help while the author was there on sabbatical, and also for his interesting suggestion that this charged aggregating system has striking similarities with that of the starch-$(I_3^-)_n$ complex. Credit is also due to Jeffrey Lary for his expert technical work in obtaining the data at the University of Connecticut.

Influence of a Hard-Sphere Solute on Water Structure

Michel Lucas

Département de Génie Radioactif, 92260 Fontenay-aux-Roses, France *(Received April 10, 1972)*

Publication costs assisted by the Commissariat à l'Energie Atomique

Equations were derived by Pierotti yielding the thermodynamic properties of solutions of a hard-sphere solute in water at infinite dilution. A possible interpretation of these equations is that a hard-sphere solute enhances the bonds between water molecules at temperatures below 4° and lessens these bonds at higher temperatures. Such a solute also increases the water temperature of maximum density. Calculated thermodynamic properties of hard-sphere solutes in water are very similar to those of real nonpolar gases with the same size. It follows then that the experimental entropies of solution, increase in the water temperature of maximum density by a solute, heat capacity changes, and solute molal volume in water, cannot be taken as evidences for water structure promotion by nonpolar solutes at temperatures higher than 4°. Finally some measurements of the enthalpies of transfer of tetraalkylammonium bromides from H_2O to D_2O at 51° suggest that these cations also enhance the water structure at low temperature and lessen it at higher temperatures.

The solubility of nonpolar gases in water is the subject of considerable interest since a difference exists between the solubility of gases in water and in organic solvents.[1] This difference is manifest in the large negative heats, negative entropies, and positive molal heat capacities of solution of gases into water.[2] Frank and Evans[3] ascribed this difference to the formation of an ordered, more hydrogen bonded than pure water, structure around the solute. In order to account for this effect, Nemethyl and Scheraga[4] developed a statistical thermodynamic theory of water. However this model has been criticized, since the difference in density between the water cluster molecules and other water molecules assumed in the model is not in agreement with results of small angle X-ray scattering.[5] On the other hand, the solubility of gases in water was treated with very good success by Pierotti.[2] He has divided the process of solution of nonpolar gas in water into two steps. First a cavity has to be made in the solvent to accomodate the solute particle. Its diameter is exactly the hard-sphere diameter of the gas particle. The scaled particle theory allows the computation of the free energy involved in this step. The second step is to consider the interactions of the solute with the solvent molecules through dispersion forces. The first step only needs to be considered if the solute is a hard sphere not interacting with the solvent. From the thermodynamic equations computed by Pierotti, the possible influence of a hard-sphere solute on the water structure may be derived. The comparison between the thermodynamic properties of real nonpolar solutes and of hard-sphere solutes of the same size may help to determine which thermodynamic properties yield evidence for water structure promotion by the real solute.

First let us consider some equations of interest for the discussion. From ref 2, the internal energy change on dissolving 1 mol of a hard-sphere solute at infinite dilution is

$$\Delta U = \alpha RT^2[f(y) + 1] \qquad (1)$$

where α is the thermal expansion coefficient of water at constant pressure and $f(y)$ a function of the solvent and solute molecular dimensions, and the solvent molal volume. $f(y)$ is positive and increases with the solute size. At 4° the molal heat capacity change ΔCp for the solution process is

---

(1) (a) D. D. Eley, *Trans. Faraday Soc.*, **35**, 1281 (1939); (b) *ibid.*, **35**, 1242 (1939).

(2) R. A. Pierotti, *J. Phys. Chem.*, **69**, 281 (1965).

(3) H. S. Frank and M. W. Evans, *J. Chem. Phys.*, **13**, 507 (1945).

(4) G. Nemethy and H. A. Scheraga, *J. Chem. Phys.*, **36**, 3382, 3401 (1962).

(5) A. H. Narten and H. A. Levy, *Science*, **165**, 447 (1969).

$$\Delta Cp = \frac{\partial \alpha}{\partial T} RT^2[f(y) + 1] - R \qquad (2)$$

derived from relation 1, since at 4° α is equal to zero. The molal volume of the solute $\bar{V}_2$ is

$$\bar{V}_2 = \beta RT[f(y) + 1] + (\pi/6)a^3N \qquad (3)$$

where β is the solvent coefficient of isothermal compressibility and a the hard-sphere solute diameter. Finally y is given by the equation $y = \pi N a^3/6v$ where a and v are respectively the water hard-sphere diameter and its molar volume.

The effect of the hard-sphere solute on the water temperature of maximum density (TMD) may be derived from relation 3. $\partial\bar{V}_2/\partial T$ is given by

$$\partial\bar{V}_2/\partial T = R[(\beta + T\partial\beta/\partial T)(f(y) + 1) - \beta T\alpha y\partial f(y)/\partial y]$$

Here $\partial f(y)/\partial y$ is a positive function. From the literature data,[6] it may be calculated that $T\partial\beta/\partial T + \beta$ is negative for water at 4°, so that at this temperature $\partial\bar{V}_2/\partial T$ is also negative. Then a hard-sphere solute must raise the TMD of water.[7]

Now let us examine the influence of a hard-sphere solute on water structure. From relation 1 it follows that the internal energy of solution of a hard-sphere solute in water is equal to zero at 4°, negative at lower temperature, and positive at higher temperature, following the variation of α. The influence of the solute on water structure may be pictured as follows: at a temperature lower than 4°, the solution of a hard-sphere in water results in an increase of the bonds between water molecules, and the bigger the solute, the more important the effect, since $f(y)$ increases with the solute size. At a higher temperature, the solution results in a decrease of the bonds between water molecules and the influence of the temperature appears to be especially important and this influence increases with the solute size.

A deeper insight on the way in which the solute influence is manifested may be gained if the isothermal expansion coefficient of water (α) is split into a configurational contribution α_c and a vibrational contribution (α_v).[6] The first is associated with changes in the average configuration of molecules in the liquid as water is heated. This arises from the fact that the open structure of water arising from the four coordination of molecules weakens or breaks down thus reducing the volume. α_c is negative. The vibrational contribution α_v is positive and arises from the fact that the amplitude of anharmonic intermolecular vibration increases with the temperature, thus enlarging the volume.[6] In the same vein ΔU may be split into a configurational contribution ΔU_c which is negative and may be interpreted as showing an increase in the water structure caused by the introduction of the solute. This may be interpreted as follows: since there is more room in the open more hydrogen-bonded structure of water than in the broken down structure, the solute is more easily soluble in the former than in the latter. The solute shifts the equilibrium between the open and the broken down structure toward the more open one since the solute chemical potential is lower in the former than in the latter. This is what is sometimes called hydrophobic hydration. The vibrational contribution ΔU_v which is positive may be interpreted as showing the influence of the solute kinetic energy which weakens the bonds between water molecules. In an organic solvent this later effect is prevailing. In water there is a balance between the two effects. The former is more important at temperatures below 4° and the latter is more important above this temperature. In our opinion the difficulties in dealing with the influence of a nonpolar solute on the water structure comes from the fact that the first effect is often considered, but the second is underestimated as is its growing influence with an increase in the temperature.

In a different approach, Frank and Franks have considered water as two species of dense and bulky (more open) constituents.[8] An hydrocarbon is represented as dissolving separately in these constituents as if were distributed between two phases. The mole fraction of the bulky specie is f and the fraction of the hydrocarbon in the bulky specie is g. The authors state that the equilibrium between bulky and dense water is shifted toward the production of the bulky water if g is greater than f. This is equivalent to our assumption that the force driving the equilibrium between the open structure and the weakened more dense structure is the greater solubility of the hydrocarbon in the former. Frank and Franks ascribe somewhat arbitrarily to f and g the values 0.75 and 0.78 at 25°, so that in their opinion at 25° methane is a structure promoter. The influence of the temperature on f and g may be deduced from the eq 13 and 14 of their paper: $\partial f/\partial T = (1 - f)f\Delta H_1°/RT^2$ and $\partial g/\partial T = g(1 - g)(\Delta H_1° + \Delta H_2°)/RT^2$. According to the values they give to the two quantities $\Delta H_1°$ and $\Delta H_2°$, which are both negative, g becomes very quickly smaller than f as the temperature is raised. From their data at temperatures above 15°, butane is a structure breaker and methane behaves as such at temperatures higher than 28.7°. The calculations show also that the bigger the solute the more it acts as a structure breaker at high temperatures.

The molal heat capacity charge for the solution process of a hard-sphere solute in water at 4°, given by eq 2, is fairly important and very similar for a hard-sphere solute and a real nonpolar solute with the same size as shown by Pierotti.[2] To explain the difference between the low heat capacity of ice and the higher heat capacity of the less hydrogen-bonded liquid water, Eisenberg and Kauzmann[6] have hypothetized the existence of a configurational heat capacity arising from the change in the solvent structure with the temperature. In the same vein a configurational heat capacity for a solute may arise from the fact that its influence on the water structure changes with the temperature, whatever this influence may be at a given temperature. Therefore the configurational heat capacity for a hard-sphere solute at 4° may possibly be equated to $(\partial\alpha/\partial T)RT^2[f(y) + 1]$ since this term arises from the internal energy change with temperature. Then the high heat capacity found for real nonpolar solutes is probably mainly configurational in origin and then should not be taken as an evidence for water structure promotion by the solute.

Pierotti has also shown that the entropy of solution is similar for a real nonpolar solute and a hard-sphere solute.[2] Further. at 4° the entropy of solution of gaseous water itself is very similar to that of solutes with a similar

---

(6) D. Eisenberg and W. Kauzmann, "The Structure and Properties of Water," Oxford University Press, London, 1969.

(7) F. Franks and D. G. Ives, *Quart. Rev., Chem. Soc.*, **20**, 1, (1966).

(8) H. S. Frank and F. Franks, *J. Chem. Phys.*, **48**, 4746 (1968).

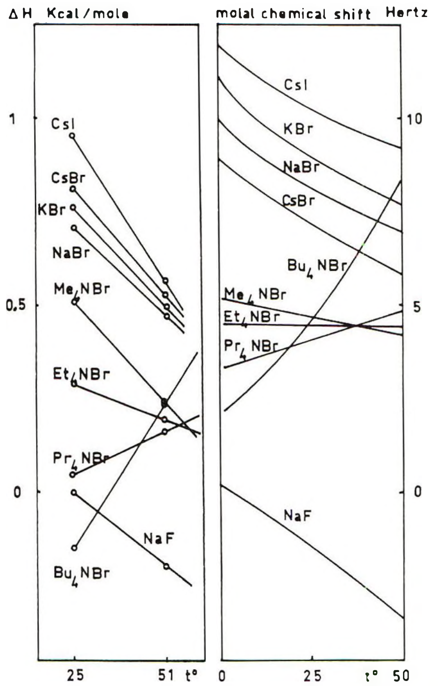

Figure 1. Plots of the enthalpy of transfer from H_2O to D_2O at 25 and 51° for the various salts and of the molal chemical shifts for the same salts.

size and as He or Ne.[9] These values should as well be taken as evidences that water is a structured medium rather than the solute add more structure to it. The latter interpretation is also questioned in ref 8.

In the same vein the decrease of the partial molal value $\bar{V}_2$ of a solute when it is transfered from an organic solvent to water has been sometimes taken as an evidence for water structure promotion since it has been more or less assumed that this decrease occurred since the solid was accomodated in voids in the water structure surrounded by a more hydrogen-bonded water cage.[4] Here again the calculations of Pierotti show that the molal volume $\bar{V}_2$ calculated for a hard-sphere particle in water[2] and CCl_4[10] is very similar to that of the real solutes with the same sizes in the two solvents. Furthermore, the volume $\bar{V}_2$ of H_2O at high dilution in CCl_4 is nearly twice that of H_2O in water.[11] Should this be interpreted as an evidence that the water molecules dissolves in cavities in water? From relation 3, the smaller volume for a solute in water compared to its volume in CCl_4 arises mainly from the fact that the compressibility β of the water is nearly twice as small as the compressibility of a nonpolar solvent such as benzene or CCl_4. This may be related to the force fields between either water molecules or CCl_4 molecules. The force field may be more important in water than in CCl_4 and water gains less added volume than CCl_4 on the impact of the solute kinetic energy.

The consideration of the properties of aqueous solutions of hard-sphere solutes suggests that the experimental entropies of solution, heat capacity changes, molal volume, and raising of the water TMD by a solute are not in themselves evidence for water–structure promotion by a nonpolar solute above 4°. This structure promotion may well exist above this temperature, but, in our opinion, it has to be proved by different arguments than usually found in the literature. On the other hand, Frank's ideas appear to be substantiated when the solution process takes place in water at temperatures lower than 4°.

Finally, recent nmr measurements on tetraalkylammonium halide solutions in water, when extrapolated to infinite dilution, suggest that at temperatures lower than 20° the structure forming character increases in order $Me_4N^+ < Pr_4N^+ < Bu_4N^+$. At higher temperatures the trend is reversed.[12] Kay has taken the ratio $\lambda\eta$ in H_2O to $\lambda\eta$ in D_2O, where η is the solvent viscosity and λ the limiting ionic conductance, as an evidence for water structure promotion by Bu_4N^+ and Pr_4N^+ at 25°.[13] Since the ratio for Br is of the opposite sign and larger in absolute magnitude than the ratio for Bu_4N^+, Kay findings are not inconsistent with our interpretation that Bu_4NBr is wholly a structure breaker at 25°. On the other hand, from the measurements of the enthalpies of transfer of the tetraalkylammonium salts from H_2O to D_2O at 25°, Friedman has drawn similar conclusions as Kay.[14] The enthalpy of transfer is positive for Me_4NBr and negative for Bu_4NBr. Negative values were taken as evidences for water structure promotion. We have measured the enthalpy of transfer from H_2O to D_2O at 51° for the salts KBr, NaBr, CsBr, NaF, CsI, Me_4NBr, Et_4NBr, Pr_4NBr, and Bu_4NBr at high dilution. They are plotted on Figure 1 together with the results of Friedman at 25°. At 51°, the trend at 25° for the quarternary ammonium bromides is reversed. The enthalpies are all positive and should increase with the cation size at higher temperatures. Then, according to Friedman's interpretation, at temperatures higher than 51°, the bigger cation should act as the stronger structure breaker. On the same figure are plotted the chemical shift of the water proton induced by 1 mol of salt extrapolated from the data at high dilution from ref 12 and 15. Positive shifts are upfield. Both types of measurements are qualitatively in agreement. However, the temperature at which the influence of the tetraalkylammonium bromides on the water structure is the same is different when deduced from nmr and enthalpies measurements. The influence of the tetraalkylammonium ions on the water structure is not so peculiar if it is compared with what is expected for a hard-sphere solute. At temperatures lower than 4°, the bigger the solute, the more it acts as a structure former, at higher temperatures, this trend is reversed. For the real solutes such as tetraalkylammonium ions, the temperature of reversal is not 4°, but higher. This may be possibly ascribed to the influence of the cation charge.

---

(9) M. Lucas, *Bull. Soc. Chim. Fr.*, 2902 (1970).
(10) R. A. Pierotti, *J. Phys. Chem.*, **67**, 1840 (1963).
(11) W. L. Masterton, *J. Phys. Chem.*, **72**, 4257 (1968).
(12) M.-M. Marciacq-Rousselot, A. de Trobriand, and M. Lucas, *J. Phys. Chem.*, **76**, 1455 (1972).
(13) R. L. Kay and D. F. Evans, *J. Phys. Chem.*, **69**, 4216 (1965).
(14) C. V. Krishnan and H. L. Friedman, *J. Phys. Chem.*, **74**, 2356 (1970).
(15) J. Davies, S. Ormondroyd, and M. C. R. Symons, *Trans. Faraday Soc.*, **67**, 3465 (1971).

Solutions of N-Substituted Amino Acids. IV. Tautomerism in *N,N*-Di-*n*-butyl-α-, -β-, and -γ-amino Acids

Joseph W.-O. Tam and Charles P. Nash*

Department of Chemistry, University of California, Davis, California 95616

(Received May 8, 1972)

The equilibrium constants for the intramolecular proton transfer process (classical form) $\rightleftharpoons$ (zwitterion) for *N,N*-di-*n*-butyl-α-, -β-, and -γ-amino acids in nonhydroxylic solvents increase in the order $K_\beta < K_\gamma < K_\alpha$. This order, which is not the one which would be predicted from the relative basicities of the amino groups in these molecules, is rationalized on the basis of continuum electrostatic theory.

Introduction

In a previous study[1] it was shown that dielectric constant measurements on solutions of *N,N*-di-*n*-butyl-β-alanine (NDBBA) in a variety of nonaqueous solvents could be interpreted on the basis of shifts in the equilibrium between an intramolecularly hydrogen bonded classical structure and its dipolar ion tautomer. Furthermore, a simple electrostatic model based on the free energy change attending the increase in dipole moment upon proton transfer accounted for the magnitudes of the equilibrium constants found in inert media.

The present work is a study of *N,N*-di-*n*-butylglycine (NDBAA) and *N,N*-di-*n*-butyl-γ-aminobutyric acid (NDBGA) undertaken to explore the extent to which the earlier conclusions have general applicability.

Experimental Section

Syntheses. The ethyl ester of NDBAA was prepared by refluxing ethyl chloroacetate with a twofold excess by volume of di-*n*-butylamine for 20 hr. The ester, after its recovery by fractional distillation at 3 Torr, was converted to the free acid by the method previously employed for the β homolog (mp 137°; *Anal:* Calcd for $C_{10}H_{21}O_2N$: C, 64.1; H, 11.3; N, 7.5. Found: C, 64.4; H, 11.5; N, 7.5).

N,N-Di-*n*-butyl-γ-aminobutyronitrile was prepared by refluxing γ-chlorobutyronitrile and a twofold excess by volume of di-*n*-butylamine for 10 hr, after which it was recovered by fractional distillation at 4 Torr. The nitrile (10 ml) was refluxed with 20 ml of concentrated hydrochloric acid for 5 hr, 1 l. of water was added, and the reflux continued for another 5 hr. The solution was concentrated to 300 ml, neutralized to pH 7 with 6 *M* sodium hydroxide, and the remaining nitrile was extracted with ether. The aqueous solution was evaporated to dryness and the crude NDBGA was extracted by reflux with 1:1 chloroform–ethanol. The product was purified by repeated recrystallizations, first from ether and finally from cyclohexane (mp 59°; *Anal.* Calcd for $C_{12}H_{25}O_2N$: C, 66.9; H, 11.7; N, 6.5. Found: C, 66.9; H, 11.7; N, 6.4).

Solvents. The solvents used, acetonitrile, benzene, chloroform, ethylene chloride, methylene chloride, methanol, and nitromethane, were all purified by accepted procedures under moisture-free conditions to yield materials whose physical properties agreed with values cited in standard compendia to within ± 0.0007 g/cm^3 for the density and ± 0.0004 for the refractive index.

Dielectric Constant Determinations. As in the previous study, solutions in benzene were examined by the heterodyne beat method at 1 MHz using a triple-concentric-cylinder cell having air capacitance 46.79 pF, while all other solutions necessitated the use of bridge methods. Impedances were measured with a General Radio Type 1606-A rf bridge at 12 frequencies between 1 and 30 MHz. Water at 30 ±0.2° was circulated through the outer jacket of concentric cylinder cells constructed from gold-plated copper tubing. Inductance corrections and lead capacitances for the two cells used were determined by making measurements on the cells filled with purified carbon tetrachloride, benzene, ethylene chloride, and nitrobenzene, the dielectric constants of which have been well characterized.[2] The air capacitances of the two cells were 3.45 and 8.60 pF.

Miscellaneous. Specific gravities were determined by using a Christian Becker Model SG-1 specific gravity balance. Molecular weights in solution were estimated by using a Mechrolab Model 301-A vapor-phase osmometer operated at 37° and employing biphenyl as a calibration solute. Infrared spectra were taken with a Beckman IR-12 infrared spectrophotometer using either sodium chloride or Irtran-2 cells. Potentiometric titrations were followed with a Beckman research pH meter equipped with a Corning No. 476024 glass electrode and a silver–silver chloride electrode constructed in our laboratory.

Results

The experimental result of most immediate interest is a quantity δ, the dielectric increment at infinite dilution. It is defined as the limiting slope of a plot of the solution dielectric constant *vs.* molar concentration.

Given the precision of the heterodyne beat method, ±0.1%, measurements on benzene solutions of NDBAA and NDBGA could be made down to 1×10^{-3} *M* concentrations. The limiting values of δ found were 1.71 M^{-1} for the α-amino acid and 3.58 M^{-1} for the γ-amino acid, while our earlier result was 4.27 M^{-1} for the β-amino acid.

Molecular weight determinations showed that NDBGA remained monomeric to the extent of 90% or greater in chloroform, methylene chloride, ethylene chloride, and

---

(1) D. A. Horsma and C. P. Nash, *J. Phys. Chem.*, **72**, 2351 (1968).

(2) A. A. Maryott and E. R. Smith, *Nat. Bur. Stand. (U. S.), Circ.* **No. 514** (1951).

TABLE I: Dielectric Increments, Dipole Moments, and Tautomeric Equilibrium Constants for *N,N*-Di-*n*-butyl-β- and -γ-amino Acids at 30°

Solvent	ϵ	δ, M^{-1}		μ, D		K	
		β	γ	β	γ	β	γ
Benzene	2.26	4.27	3.58	6.06	5.61	. . .	. . .
Chloroform	4.8	9.38 ± 0.04	15.6 ± 0.1	7.80	9.99	0.33	0.65
Methylene chloride	8.6	9.1 ± 0.1	17.3 ± 0.1	7.79	10.45	0.33	0.81
Ethylene chloride	10.1	8.3 ± 0.2	12.5 ± 0.1	7.58	9.10	0.27	0.42
Acetonitrile	35.1	5.1 ± 0.1	17.3 ± 0.2	9.16	12.47	0.96	2.53
Nitromethane	36.4	4.7 ± 0.2	8.7 ± 0.1[a]	8.72	10.30[a]	0.69	*a*
Methanol	32.2	20.8 ± 0.5	33.6 ± 0.2	11.53	14.30	. . .	. . .

[a] See text.

acetonitrile up to 0.13 M concentration, and reasonably accurate rf bridge measurements could be made in these solvents on solutions as dilute as 0.05 M. At this concentration these solutions all contain at least 98% monomer. Thus the limiting values of δ determined in these solvents could differ from the monomer values by −2% at most, since association leads to apparent δ values which decrease with increasing concentration.[1] In nitromethane, however, dielectric constant measurements on solutions more dilute than 0.1 M could not be made with sufficient accuracy to yield reliable concentration derivatives. Since a 0.1 M solution of NDBGA in nitromethane contains less than 65% monomer, based on its molecular weight in solution, the δ value we find for the γ acid in this solvent is undoubtedly significantly low.

With this single reservation, the rf bridge data were treated as in our previous work to yield values of δ for NDBGA which are listed in Table I, together with those previously found for NDBBA.

Molecular weight studies on NDBAA revealed that in no polar solvent save methanol was a sufficiently low degree of association present to admit δ values appropriate to monomeric species to be obtained with reliability. In methanol we find $\delta = 30.9 \pm 0.2$ for NDBAA. The qualitative indications are that the most stable dimeric entity of NDBAA is a "double zwitterion" which has no dipole moment. Thus, for example, we obtain an apparent value of δ for the α acid in chloroform of 3.0, which may be compared to the values 9.4 and 15.6 found for the β and γ homologs, respectively. Also, the infrared spectrum of a 0.05 M solution of NDBAA in chloroform shows only a single sharp peak at 1642 cm^{-1}, a carboxylate frequency, with no trace of absorption at frequencies between 1700 and 1800 cm^{-1} which would be indicative of carbonyl groups present in the solution. This dimer structure has previously been postulated by Barrow[3] in order to account for infrared spectroscopic results on diethyl-substituted amino acids which were, in general, similar to the present ones.

Discussion

It is a straightforward matter to proceed from δ values to an estimate of the dipole moment of a species in solution. The model employed is the Böttcher modification of the Onsager equation for a spherical dipolar molecule imbedded in a dielectric continuum.[4] When δ values are substituted in eq 9 of ref 1, together with vapor-phase values of the dipole moments of the solvent molecules,[5] there result dipole moments for the β- and γ-amino acids which are also listed in Table I. If the δ values in the various polar solvents (excluding nitromethane) were systematically low by as much as 2% owing to association phenomena, in no case would the derived dipole moment be low by more than 0.06 D. The values reported here for NDBBA are a few per cent smaller than those given previously, since we now choose to include the atomic polarization of the solute in the calculations, estimating it as 10% of the electronic contribution determined from the molar refraction.[6]

We now assume that the square of the observed dipole moment is a mole fraction average of the squares of the moments found in benzene and methanol, *i.e.*, the solvents in which the infrared spectra show the molecule to be "entirely" in either the classical or zwitterion forms. By this procedure we calculate the tautomeric equilibrium constants ($K \equiv$ zwitterion/classical form) given in Table I.

The critical assumption on which this method of estimating K rests is that the dipole moment of the dipolar ion species measured in methanol is truly that of the isolated solute molecule. There can be little doubt that one or more methanol molecules hydrogen bond to an amino acid. If the measured moment was perhaps that of a 1:1 complex in which a methanol molecule having dipole moment 1.7 D[5] was H bonded linearly to either of the sets of lone pair electrons in sp^2 hybrid orbitals on the oxygen atom in the carboxyl group which is not involved in the proton transfer reaction, and if the attached methanol molecule could rotate freely about the O–H–O axis, then vector addition shows that for NDBBA the resultant moment of 11.5 D would imply a zwitterion moment of 11.0 D, while for NDBGA the measured resultant of 14.3 D would imply a zwitterion moment of 13.4 D. When these smaller values of μ_d are used to calculate K values from the average moments measured in acetonitrile, one finds $K_\beta = 1.3$, $K_\gamma = 5.3$, and $K_\gamma/K_\beta = 4$.

This ratio of equilibrium constants is in qualitative disagreement with conclusions based on the infrared spectra of these acids as monomers in solution. The carbonyl absorption maxima of the classical tautomers of the β- and γ-amino acids in acetonitrile occur at 1722 and 1710 cm^{-1}, respectively. The carboxylate maximum shown by the dipolar ion tautomer occurs at 1640 cm^{-1} for both acids. To the extent that one may neglect the overlap of

---

(3) G. M. Barrow, *J. Amer. Chem. Soc.*, **80**, 86 (1958).

(4) C. J. F. Böttcher, "Theory of Electric Polarization," Elsevier, New York, N. Y., 1952. See also J. R. Weaver and R. W. Parry, *Inorg. Chem.*, **5**, 703 (1966).

(5) A. L. Mc Clellan, "Tables of Experimental Dipole Moments," W. H. Freeman, San Francisco, Calif., 1963.

(6) C. P. Smyth, "Dielectric Behavior and Structure," McGraw-Hill, New York, N. Y., 1955.

the peaks of the two tautomers, Beer's law yields, for each acid

$$K = A_d a_n / A_n a_d \tag{1}$$

where A is the measured absorbance of a peak, a is an absorptivity, and the n and d subscripts denote the values appropriate to the classical and zwitterionic tautomers, respectively. If the value of the ratio (a_n/a_d) is approximately the same for the β- and γ-amino acids, then

$$K_\gamma/K_\beta \approx (A_d/A_n)_\gamma/(A_d/A_n)_\beta = (1.5)/(0.8) = 1.9 \tag{2}$$

Here we have introduced experimental values of the absorbance ratios determined from the infrared spectra of 0.056 M solutions of the two acids in acetonitrile. This spectroscopic estimate of the ratio of K's agrees much better with the value of 2.6 obtained by using the moments measured in methanol directly than it does with the value of 4, which would be obtained by assuming 1:1 complexing with methanol. The results found for solutions in chloroform, methylene chloride, and ethylene chloride lead to similar conclusions. Apparently even a hydrogen bonding interaction does not appreciably alter the spherical symmetry of the nearest neighbor shell of methanol molecules, and the dipole moment found for the zwitterion in this solvent closely approximates its actual value.

Since the dipole moments of the β- and γ-amino acids in benzene, 6.06 and 5.61 D, respectively, are significantly larger than the 4.5 and 4.3 D which would result if the group moments[6] were simply added vectorially, and since the carbonyl absorption frequencies of both these molecules occur at 1740 ± 5 cm^{-1} in benzene or carbon tetrachloride, whereas a typical monomeric carboxylic acid molecule in CCl_4 absorbs at about 1760 cm^{-1},[7] we conclude that for both molecules the nondipolar classical form is strongly hydrogen bonded intramolecularly. Also, since the dipole moment of the zwitterionic tautomer of the γ molecule in nonaqueous media is only 14.3 D *vs.* about 20 D found for γ-amino acids in water,[8] where free rotation around bonds evidently occurs, we infer that even in the proton-transferred form both amino acids remain in a cyclic configuration in nonaqueous solvents. Both the amount by which the dipole moment of the β acid is augmented in benzene and the amount by which its moment in methanol is reduced by comparison with the behavior of the γ acid in these solvents suggest that cyclization is more facile sterically for the β acid, which forms a six-membered ring. An inspection of molecular models reveals that the O-H-N configuration is essentially linear with a β-amino acid, whereas a slight nonlinearity occurs with a γ amino acid.

The similarities found between the β and γ acids in solution suggest that the same theoretical model might be used to treat the intramolecular proton transfer reaction of both of these molecules. We have earlier suggested[1] that on a continuum electrostatic model the equilibrium constant for tautomerization in solution, K_s, is related to the gas-phase value, K_g, by the equation

$$RT \ln (K_s/K_g) = [(\epsilon - 1)/(2\epsilon + 1)](1 + B)[(\mu_d{}^2 - \mu_n{}^2)/b^3] \tag{3}$$

Here ϵ is the dielectric constant of the solvent, μ_d and μ_n are the dipole moments of the two tautomers in methanol and benzene, respectively, b is the effective radius of the sphere bearing the dipole, and B is a function of ϵ and of the position and orientation of the dipole within the sphere. When one wishes to compare two molecules in the same solvent which are qualitatively as similar as our β- and γ-amino acids, it is perfectly realistic to assume identical values of B. In a qualitative way, eq 3 predicts that if neither the K_g values nor the sphere sizes for the β and γ acids are radically different, then the tautomerization constant for the γ acid in solution will exceed that for the β acid. This prediction is in agreement with the several K values shown in Table I.

The two solvents which are most likely to conform to a continuum model are ethylene chloride and nitromethane. For the reasons we have noted, no experimental value of K for the γ acid in nitromethane was obtained. We may, however, use the ethylene chloride results and the continuum model to estimate K_γ in nitromethane, from it a dipole moment, and thus a predicted δ value which turns out to be completely reasonable by comparison with the other values listed in Table I.

When one forms the ratio of a pair of equations like eq 3 for the β- and γ-amino acids in the same solvent, there results

$$\frac{\ln (K_{s(\beta)}/K_{g(\beta)})}{\ln (K_{s(\gamma)}/K_{g(\gamma)})} = \frac{\mu_{d(\beta)}{}^2 - \mu_{n(\beta)}{}^2}{\mu_{d(\gamma)}{}^2 - \mu_{n(\gamma)}{}^2} \left(\frac{b_{(\gamma)}}{b_{(\beta)}}\right)^3 = 0.55 \left(\frac{b_{(\gamma)}}{b_{(\beta)}}\right)^3 \tag{4}$$

where the dipole moments from Table I have been substituted into the μ-dependent factor. To estimate the ratio of sphere volumes we elect to use the apparent molecular volumes of the two molecules in solution, determined from density measurements to be 212 ml for NDBBA and 246 ml for NDBGA. With this estimate eq 4 may be rearranged to read

$$K_{s(\beta)}/K_{s(\gamma)}{}^{0.64} = K_{g(\beta)}/K_{g(\gamma)}{}^{0.64} = \text{constant} \tag{5}$$

If we now substitute the equilibrium constants for the two acids in ethylene chloride into eq 5, together with the nitromethane value for NDBBA, we find a predicted value for the tautomerization constant of NDBGA in nitromethane of 1.8. When $K = 1.8$ the average dipole moment must be 11.9 D, and this moment in nitromethane would follow from a dielectric increment of 14.5 M^{-1}, clearly a reasonable value. We therefore conclude that tautomerization of the β- and γ-amino acids may be described satisfactorily by the same model.

Spectroscopically, the behavior of the α-amino acid is different from that of the two higher homologs. Whereas NDBBA and NDBGA display carbonyl absorptions in the range 1710–1740 cm^{-1} in all the solvents used here, NDBAA absorbs at 1775–1785 cm^{-1}. A similar behavior was also noted by Barrow.[3] Barrow assumed that the α-amino acid was unusual, and postulated the existence of a strained, intramolecularly hydrogen-bonded ring to explain, by analogy with the small ring lactones, the high-frequency carbonyl absorption. Hall and Zbinden,[9] however, rejected the notion that any significant strain could be present in a ring held closed simply by a hydrogen bond.

Our results show that the α-amino acid in its classical form is indeed intramolecularly hydrogen bonded. The measured dipole moment of 3.96 D in benzene solution is, within experimental error, exactly the sum of the group

---

(7) M.-L. Josien, J. Lascombe, and C. Vignalou, *C. R. Acad. Sci.*, **250**, 4146 (1960).

(8) J. P. Greenstein and M. Winitz, "Chemistry of the Amino Acids," Wiley, New York, N. Y., 1961, pp 456–464.

(9) H. K. Hall, Jr., and R. Zbinden, *J. Amer. Chem. Soc.*, **80**, 6428 (1958).

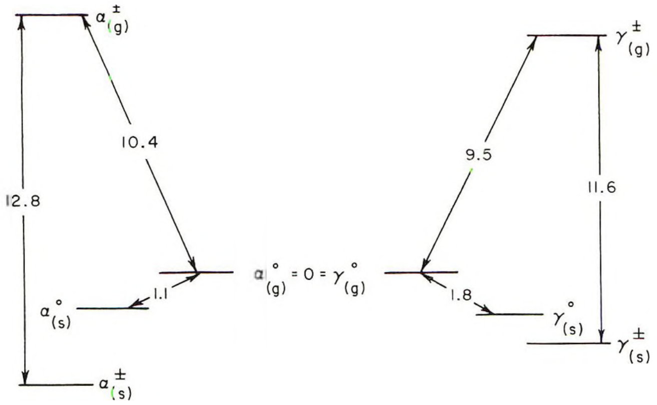

Figure 1. Free energy changes for the tautomerism of NDBAA and NDBGA in the gas phase, and free energies of transfer of all the species to nitromethane solution.

moments for a cyclic geometry in which the O-H and C=O functions are trans. If they adopted the cis configuration which is customary for monomeric carboxylic acids,[6] a moment between 1.3 and 2.1 D would result, depending upon the dispositions of the other groups in the molecule.

In a recent critical review Bellamy[10] has discussed the accumulating evidence for a significant increase in carbonyl frequency occurring when the hydroxyl group of a carboxylic acid adopts the trans configuration. From a spectroscopic viewpoint it is evidently the β- and γ-amino acids, rather than the α, which are exceptional. Their behavior may be rationalized by recalling the significant augmentation in the dipole moment of these molecules which accompanies formation of the intramolecular hydrogen bond. Thus, even though proton transfer does not occur, electron density seemingly accumulates in the C-O bond at the expense of the C=O bond, whose vibration frequency is thereby decreased by some 40-50 cm^{-1}.

The tautomerization behavior of NDBAA in solution is also, at first sight, unusual. Owing to its extensive aggregation in solution, we were unable to obtain the dipole moment of monomeric NDBAA in any polar solvent except methanol, in which it remains a monomer having dipole moment 13.7 D. A consideration of the intensity of the sharp carbonyl absorption maximum, together with osmometric measurements, does permit us to estimate, albeit crudely, the extent of proton transfer in the monomer in acetonitrile and nitromethane, in which association is relatively slight up to ~0.05 *M*.

By analyzing osmometric measurements according to a model which considers dimers separately from higher aggregates, all the rest of which are assumed to have the same stepwise formation constant,[11] we conclude that in a 4.8×10^{-3} *M* solution of NDBAA in benzene the monomer concentration is 4.0×10^{-3} *M*. This solution has the same carbonyl absorbance as a 3.0×10^{-2} *M* solution of NDBAA in acetonitrile, which is not significantly associated on the basis of a comparison with a biphenyl calibration curve. If no proton transfer has occurred in the monomer in benzene, the apparent tautomerization constant in acetonitrile is ~6.5. Carbonyl intensity comparisons show that in nitromethane the constant is even larger, on the order of 10.

From the standpoint of one's chemical intuition, it is surprising that the *K* value of NDBAA is appreciably larger than the values found for the longer chain amino acids. It is well known that, at least in water, the basicity of the nitrogen of naturally occurring α-amino acids is much less than that of either β- or γ-amino acids, whereas the acidities of the carboxylic acid functions differ very little within the series.[12] This significant basicity difference also persists to alkyl-substituted amino acids in aprotic solvents, as shown by potentiometric titrations we have conducted on the ethyl esters of NDBAA and NDBBA in acetonitrile. When 0.05 *M* acetonitrile solutions of the bases triethylamine, benzylamine, NDBBA ethyl ester, and NDBAA ethyl ester were titrated with 0.15 *M* *p*-toluenesulfonic acid monohydrate in acetonitrile, half-neutralization emf's of −437, −353, −356, and −257 mV, respectively, were measured with a glass electrode *vs.* a Ag-AgCl external reference electrode immersed in a dilute solution of tetraethylammonium chloride in acetonitrile which was connected to the titration vessel through a fine-frit disk. The emf difference we find between triethylamine and benzylamine is in the same direction as that found by Hall[13] in a similar experiment, in which he titrated 0.003-0.01 *M* bases in acetonitrile with a 1.1 *M* solution of *p*-toluenesulfonic acid monohydrate in dioxane, but his difference of 119 mV is somewhat larger than our value of 84 mV. Our results nevertheless show that the substituted β-amino acid ester has a basicity similar to that of benzylamine, while the ester of the α-amino acid is an even weaker base.

The present electrostatic model of the intramolecular proton transfer process in inert solvents provides a satisfactory resolution of the apparent dilemma. The factor $(\mu_d{}^2 - \mu_n{}^2)$ in eq 3 has the same numerical value for both the α- and the γ-amino acids. From density measurements the molar volume of the γ acid exceeds that of the α acid by a factor of 1.2. Thus, if $K_{s(\alpha)} > K_{s(\gamma)}$, $K_{g(\alpha)} < K_{g(\gamma)}$. If in eq 3 we choose $B = 0.6$,[1] $b_{(\gamma)} = 5.8$ Å,[1] and $\epsilon = 36$ (nitromethane) we find, from the solution values of $K_{s(\gamma)} \simeq 1.8$, $K_{s(\alpha)} \simeq 10$, gas-phase values of $K_{g(\alpha)} \cong 2.5 \times 10^{-8}$, $K_{g(\gamma)} \cong 1{,}2 \times 10^{-7}$, $\Delta G^{\circ}{}_{g(\alpha)} \sim +10.4$ kcal/mol, $\Delta G^{\circ}{}_{g(\gamma)} \sim +9.5$ kcal/mol. Thus, the expected effect of basicity differences is manifest in the gas phase. The various free energy relationships are summarized in Figure 1. Here the common zero of energy for the two molecules has been chosen as the gaseous, intramolecularly hydrogen-bonded classical tautomeric form.

If we were to locate the common zero of energy at the gaseous, open-chain classical structure of the two amino acids, the free energy of the gaseous α dipolar ion would be greater than that of the gaseous γ dipolar ion by even more than the 0.9 kcal shown in Figure 1, since the hydrogen bond in NDBAA is undoubtedly weaker than that in NDBGA. Not only is the nitrogen of NDBAA inherently a weaker acceptor site,[14] but also the internal hydrogen bond in this molecule is severely bent. The HON angle is about 45°, which is near the upper limit of distortion from linearity of OH-N hydrogen bonds cited in Donohue's sur-

(10) L. J. Bellamy, "Advances in Infrared Group Frequencies," Methuen, London, 1968, p 175.

(11) A statistical treatment showing the necessity for using at least two constants for successive association equilibria has been given by L. Sarolea-Mathot, *Trans. Faraday Soc.*, **49**, 8 (1953).

(12) E. J. Cohn and J. T. Edsall, "Proteins, Amino Acids, and Peptides," Reinhold, New York, N. Y., 1943, p 99.

(13) H. K. Hall, *J. Phys. Chem.*, **60**, 63 (1956).

(14) R. W. Taft, D. Gurka, L. Joris, P. v. R. Schleyer, and J. W. Rakshys, *J. Amer. Chem. Soc.*, **91**, 4801 (1969), have shown that if acceptors with the same kind of functional group are compared, a good correlation exists between hydrogen bond acceptor ability and basicity toward the proton. The correlation with pK_a breaks down when different functional groups are compared.

vey.[15] Moreover, the recent calculations of van Duijneveldt-van de Rijdt and van Duijneveldt[16] clearly show that a significant increase in energy ($\sim$3 kcal/mol) results when an OH–N hydrogen bond is bent to this extent.

We have estimated from solution data that in the gas phase the free energy of the zwitterion in a cyclic conformation exceeds that of the same conformation of the classical tautomer by $\sim$10 kcal/mol. Thermochemical and electrostatic considerations show that this is a plausible result. By combining thermochemical data[17-20] for the elementary gas-phase processes

$$\mathrm{CH_3COOH \rightarrow CH_3COO\cdot + \cdot H} \qquad \Delta H = +111\ \mathrm{kcal} \tag{6}$$

$$\mathrm{CH_3COO\cdot + e^- \rightarrow CH_3COO^-} \qquad \Delta H = -78\ \mathrm{kcal} \tag{7}$$

$$\mathrm{R_3N \rightarrow R_3N\cdot^+ + e^-} \qquad \Delta H \sim +180\ \mathrm{kcal} \tag{8}$$

$$\mathrm{R_3N\cdot^+ \cdot H \rightarrow R_3NH^+} \qquad \Delta H \sim -93\ \mathrm{kcal} \tag{9}$$

we estimate, for a typical bimolecular gaseous acid–base reaction

$$\mathrm{CH_3COOH + R_3N \rightarrow CH_3COO^- + R_3NH^+} \qquad \Delta H \sim +120\ \mathrm{kcal} \tag{10}$$

When the cation and anion products are permitted to attract each other, Coulomb's law shows that when the charges are separated by 3.0 Å the free energy of the system is lowered by 110 kcal, so that $\Delta H_{\mathrm{net}} \sim +10$ kcal. This charge separation is slightly larger than the 2.9 Å O–N distance typical of OHN hydrogen bonded systems, and therefore our estimates of the gas-phase equilibrium constants appear to be justified. Presumably this kind of agreement also supports the qualitative validity of the electrostatic model of the proton transfer process from which the gas-phase values of the equilibrium constants were deduced.

(15) J. Donohue, "Structural Chemistry and Molecular Biology," A. Rich and N. Davidson, Ed., W. H. Freeman, San Francisco, Calif., 1968.
(16) J. G. C. M. van Duijneveldt-van de Rijdt and F. B. van Duijneveldt, *J. Amer. Chem. Soc.*, **93**, 5644 (1971).
(17) L. Jaffe, E. J. Prosen, and M. Szwarc, *J. Chem. Phys.*, **27**, 416 (1957).
(18) (a) W. E. Wentworth, E. Chen, and J. C. Steelhammer, *J. Phys. Chem.*, **72**, 2671 (1968); (b) S. Tsuda and W. H. Hamill, "Advances in Mass Spectrometry," Vol. III, W. L. Mead, Ed., The Institute of Petroleum, London, 1966.
(19) Based on an ionization potential $\sim$7.8 eV for gaseous alkyl amines. See K. Watanabe and J. R. Mottl, *J. Chem. Phys.*, **26**, 1773 (1957).
(20) Based on the N–H single bond energy given by L. Pauling, "The Nature of the Chemical Bond," 3rd ed, Cornell University Press, Ithaca, N. Y., 1960, p 85.

Molecular Movements and Phase Transitions in Solids. Tetrakis(trimethylsilyl) methane

J. M. Dereppe

Laboratorie de Chimie-Physique, Universite de Louvain, Louvain, Belgique

and J. H. Magill*

Department of Metallurgical and Materials Engineering, University of Pittsburgh, Pittsburgh, Pennsylvania 15213

(Received December 29, 1971)

Broad line nmr measurements on crystalline tetrakis(trimethylsilyl)methane show that this material undergoes a transitional change when its temperature is slowly raised stepwide through 213°K. The onset of the λ transition determined by differential scanning calorimetry (DSC) is in accord with this result. The entropy change associated with the transition is about 7.68 cal (mol °K)$^{-1}$. On heating and cooling cycles covering rates from 0.625 to 40° min^{-1}, considerable hysteresis is found by the DSC method. The displacement of the λ peak on heating relative to cooling diminishes as the rate is lowered, in conformity with the time effects involved in the transition process.

Introduction

Since tetrakis(trimethylsilyl)methane was shown[1] to behave as an Einstein sphere in dilute solution, it was immediately suspected that it would exhibit interesting transitional behavior in the solid state. Other spherical molecules[2-5] display changes in specific heat, nmr second moment, and X-ray spacings. Such changes in physical properties are associated with the onset of rotation of the molecules in the solid state and attest to Simon's original suggestion[6] many years ago. A study of molecular freedom and transformations in the solid state has been presented by Westrum.[7]

(1) R. L. Merker and M. J. Scott, *J. Colloid Sci.*, **19**, 245 (1964).
(2) D. W. McCall and D. C. Douglas, *J. Chem. Phys.*, **33**, 777 (1960).
(3) A. R. Ubbelolde, "Melting and Crystal Structure," Oxford University Press, London, 1965, Chapter 4.
(4) E. F. Westrum, Jr., and J. P. McCullough, "Physics and Chemistry of the Organic Solid State," Vol. 1, Wiley-Interscience, New York, N. Y., 1963, Chapter 1.
(5) E. R. Andrew and P. Allen, *J. Chim. Phys.*, **1**, 85 (1966).
(6) F. Simon and C. Von Simson, *Z. Phys.*, **21**, 168 (1924).
(7) E. F. Westrum, Jr., *J. Chim. Phys.*, **1**, 46 (1966).

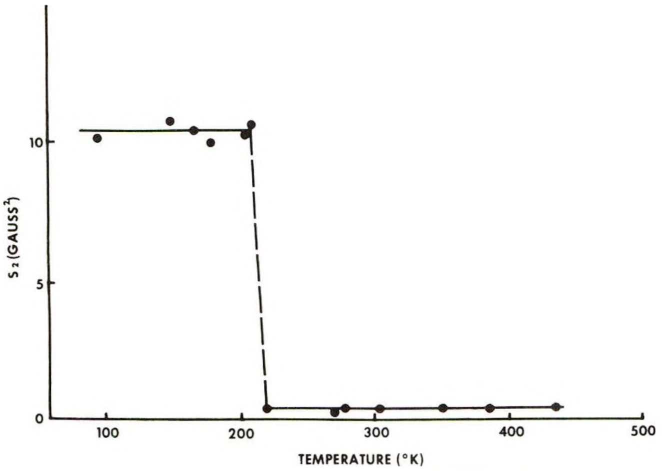

Figure 1. Plot of the experimental second moment S_2 (G^2) as a function of temperature, °K.

The tetrakis(trimethylsilyl)methane is a large spherically symmetrical molecule having 12 geometrically equivalent methyl groups. This crystalline material[8] appears to undergo a phase transition in the solid state at about 200°, but under atmospheric pressure sublimation occurs without melting. This behavior is typical of spherically symmetrical molecules which rotate freely in the crystal lattice in accord with Westrum's classification.[7] The present nmr and calorimetric studies were undertaken in order to investigate the onset of molecular motions in the solid. X-Ray diffraction studies have shown that the tetrakis(trimethylsilyl)methane crystallizes in a face-centered cubic lattice with the space group *Fm*3*m*.

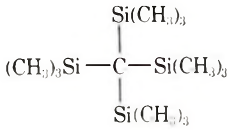

$$(CH_3)_3Si-\overset{\displaystyle Si(CH_3)_3}{\underset{\displaystyle Si(CH_3)_3}{C}}-Si(CH_3)_3$$

Experimental Results

Nmr Second Moment. Nmr spectrum of powdered tetrakis(trimethylsilyl)methane was investigated between liquid nitrogen temperature and 450°K. Measurements were made with a Varian DP 60 spectrometer, equipped with a variable temperature accessory. The following experimental conditions were used: rf amplitude of 2.65 mG at temperatures below 213°K and 0.83 mG above this value; the modulation amplitude was 0.5 G at temperatures below 213°K and 0.25 G above it. The measurements were made on cooling down the sample stepwise. At each temperature the sample was allowed to reach its equilibrium temperature for at least 15 min before performing any measurement. In this way, time effects were eliminated (or minimized). The experimental second moments are shown in Figure 1.

An X-ray diffraction study[9] on the same compound provides the following data: space group *Fm*3*m*, $a = 12.90 \pm 0.01$ Å, $Z = 4$. The symmetry of the molecule is only 23 and the threefold axis does not coincide with the threefold axis of the unit cell. The molecules are statistically distributed in order to maintain the *m*3*m* symmetry for the crystal. According to this study the C–Si bonds are located in the (100), (010), and (001) planes and one of the CH_3 groups is out of plane by an angle $\phi = 34.5°$.

The contribution of a static methyl group to the second moment was calculated by the Van Vleck formula[10] to be 21.7 G^2. The experimental values indicate that even at low temperatures the methyl groups cannot be considered static,[11] so the following calculations were made assuming fast rotation of the methyl groups about their threefold axis. In this case, it is well known that the group contribution is only ¼ of the static value, *i.e.*, 5.43 G^2. The interactions between protons belonging to different rotating methyl groups were estimated, assuming that the three protons for each group lie at the center of the circle described during their motion. The intermolecular interactions were calculated by the same process. These interactions were calculated to be 4.70 G^2. The calculated total S_2 value of 10.13 G^2 is in good agreement with the experimental one especially if we consider that the experimental value must be corrected for modulation effects. This correction can be estimated to 0.12 G^2 which gives an experimental S_2 of 10.38 G^2.

At temperatures above 213°K, the low value of the second moment suggests that the molecular reorientations are very important. Such a low S_2 value combined with the fact that the line remains practically Gaussian in shape, can only be explained by fast reorientation of the molecule as a whole. In this case, the intramolecular contribution to S_2 is equal to zero and the intermolecular contribution is calculated by assuming that the 36 protons of the molecule are concentrated at the center of gravity of the molecule. Under these circumstances, the calculated S_2 value, 0.3 G^2, is very close to the experimental one (see Figure 1).

Differential Scanning Calorimetry. The solid-solid transition in tetrakis(trimethylsilyl)methane was also examined using a Perkin-Elmer differential scanning calorimeter, Model DSC-1B. Heating runs were made at rates ranging from 0.625 to 40° min^{-1}. Cooling runs were only possible from 0.625 to 20° min^{-1}. Time effects are clearly observable in the results of this "dynamic" calorimetric technique. The difference between the peak positions in the heating and cooling cycles decreases as the rate is lowered to 0.625° min^{-1} where the hysteresis displacement is approximately 8.5°. Some typical results of these measurements are shown in Figure 2. The heating curve, A, indicates that the onset of the molecular transition occurs just above −60° and peaks at −34.8°. The cooling curve, B, shows considerable hysteresis about the transition point of A, the peaks being displaced relative to each other by 17.7°. Only one peak is obtained on heating from −90 to 200° where the material sublimes in the sample holder. The heat of transition associated with curves A and B is 1838 cal mol^{-1} at −33.8° and 1700 cal mol^{-1} at −52.5°. The corresponding entropy changes are 7.68 and 7.69 cal (mol °K)$^{-1}$, respectively.

Discussion

The onset of the calorimetric transition corresponds fairly closely to the nmr value depicted in Figure 1. The onset of this premonitory change is a few degrees higher than that arrowed in Figure 2, but this is understandable in view of the fact that the scanning rate in the illustrated calorimetric determination was 10° min^{-1} However, the agreement between both techniques is acceptable when based on the onset of the molecular rotation. The discrep-

---

(8) R. L. Merker and M. J. Scott, *Acta Crystallogr.*, **17**, 315 (1964).
(9) P. Piret, private communication.
(10) J. H. Van Vleck, *Phys. Rev.*, **74**, 1168 (1948).
(11) E. R. Andrew and P. S. Allen, *J. Chim. Phys.*, **1**, 85 (1966).

ancy between the actual calorimetric peak position and the nmr transition (an equilibrium measurement by the procedure used here, Figure 1) is more apparent although not serious in view of other work of a related nature.[12a] The abrupt drop in the second moment at 213°K corresponds to the onset of the calorimetric transition which involves molecular rotation that peaks at a higher temperature. The proton magnetic resonance studies of McCall and Douglas[2] exhibit a sharp fall in the second moment at a lower temperature than the calorimetric transition. The nmr method is a very sensitive probe for the detection of the onset of molecular motion.

In classical calorimetric studies, sufficient time is permitted (after a temperature increment) for the sample to reach equilibrium before each measurement is made. In differential scanning calorimetry which is a continuous process, rate effects are "built into" the measurement in accord with the hysteresis displayed in Figure 2. The fact that the peak displacements between A and B diminish as the rate is lowered and move apart as it is raised supports this point. At zero heating rate they will overlap. Hysteresis has also been reported for infrared spectroscopic measurements on adamantane in general accord with the pattern followed in our work. A comprehensive review of most aspects of adamantane are given by Fort and Schleyer.[12b]

It is worth noting that the magnitude of this enthalpy and entropy change associated with transition is comparable with the value found for adamantane; ΔH = 1679 cal mol^{-1}, ΔS = 8.02 eu. Presumably only van der Waals forces are involved in these "rotator" molecules.

The idea that the methyl groups in tetrakis(trimethylsilyl)methane are in a state of motion down to very low temperatures is also well documented in the literature for other materials.[11] In this regard, our analysis based on fast rotating methyl groups is acceptable. Still, it must be remembered that self-diffusion of the molecule in the lattice may further reduce the value of the second moment reported here and that the lack of very accurate crystallographic information could leave some aspects of our analysis subject to further interpretation. From calorimetric studies of small spherical molecules Staveley and Gupta[13] claim that in methane and its tetrahalide derivatives completely free rotation is not attained prior to fusion. Furthermore, one should not ignore the influence of impurities which are manifest to varying degrees in different methods of measurement.[3,7]

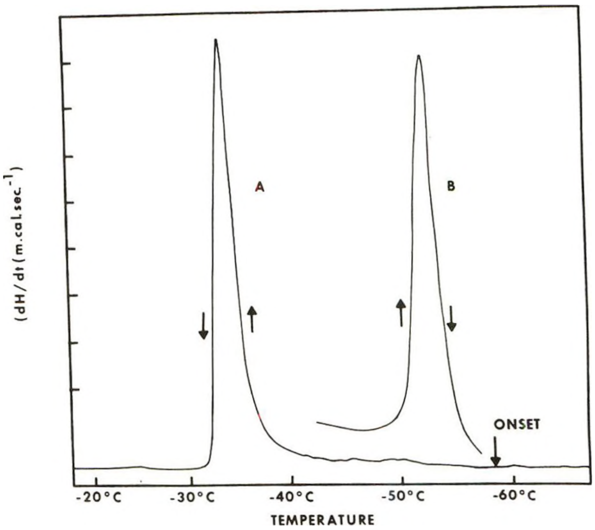

Figure 2. Differential scanning calorimetry curves (A heating, B cooling) at 10 min^{-1}. Ordinate is dH/dt in mcal sec^{-1} (arbitrary scale) and the abscissa is °C.

It is clear, however, that the behavior of the comparatively large tetrakis(trimethylsilyl)methane molecule is in general accord with that of other smaller spherical[11] and with globular molecules[7,11] such as camphor[14,15] and adamantane.[2,16]

Acknowledgment. The authors wish to thank R. L. Merker for kindly providing the sample used in these investigations.

---

(12) (a) H. S. Gutowsky and G. E. Pake, *J. Chem. Phys.*, **18**, 162 (1950); (b) R. C. Fort and P. v. R. Schleyer, *Chem. Rev.*, **64**, 277 (1965).

(13) L. A. K. Staveley and A. K. Gupta, *Trans. Faraday Soc.*, **45**, 50 (1949).

(14) J. E. Anderson and W. P. Slichter, *J. Chem. Phys.*, **41**, 1922 (1964).

(15) V. V. Moskalew and M. P. Petrov, *Fiz. Tverd. Tela*, **5**, 1400 (1963).

(16) G. W. Smith, *J. Chem. Phys.*, **35**, 1134 (1961).

ADDITIONS AND CORRECTIONS

1961, Volume 65

Michael Ardon and Amos Linenberg: Cryoscopic Determination of Molecular Weights in Aqueous Perchloric Acid.

Page 1444. All K_f values reported in this paper are the calculated values of the freezing point depression in 1 *M* rather than 1 *m* solution. The correct K_f values are obtained by multiplying the reported values by the density of the solvent (1.3). *E.g.*, the corrected value for Mg (Table I) is 4.24 × 1.3 = 5.51.—Michael Ardon.

1968, Volume 72

Joseph Blanc and Daniel L. Ross: A procedure for Determining the Absorption Spectra of Mixed Photochromic Isomers Not Requiring Their Separation.

Page 2824. Equations A5 and A6 of the Appendix should read

$$\alpha_2 = \frac{D^{\lambda_2}\epsilon_c^{\lambda_1} - D^{\lambda_1}\epsilon_c^{\lambda_2}}{D^{\lambda_2}\epsilon_c^{\lambda_1} - RD^{\lambda_1}\epsilon_c^{\lambda_2}} \qquad \text{(A5)}$$

$$R(1-\beta)(\alpha_2)^2 + \left[(R-1)(1-\beta) + \frac{\epsilon_c^{\lambda_1}[\mathrm{A}]}{D^{\lambda_1}} - \frac{R\epsilon_c^{\lambda_2}[\mathrm{A}]}{D^{\lambda_2}}\right]\alpha_2 + \frac{\epsilon_c^{\lambda_2}[\mathrm{A}]}{D^{\lambda_2}} - \frac{\beta\epsilon_c^{\lambda_1}[\mathrm{A}]}{D^{\lambda_1}} + \beta - 1 = 0 \qquad \text{(A6)}$$

Our analysis for the absorption spectra of trans isomers of several indigoids reported here and elsewhere [D. L. Ross, J. Blanc, and F. J. Matticoli, *J. Amer. Chem. Soc.*, **92**, 5750 (1970); D. L. Ross, *Appl. Opt.*, **10**, 571 (1971)] was based on the correct equations and is therefore not altered.—Joseph Blanc.

1970, Volume 74

Masaaki Ogasawara, Keiichi Ohno, Koichiro Hayashi, and Junkichi Sohma: A Study of Thermal Decay of Trapped Electrons and Other Species in an Organic Glass by Rapid-Scan Electron Spin Resonance.

Page 3221. All the temperatures except for 77°K in the text as well as in the figures should be increased by 2.5°K according to the more precise calibration curve of the thermocouple.

Page 3223. The numbers upward along the ordinate axis in Figure 4 should be corrected to be −2.0, −3.0 and −4.0 instead of −1.0, −2.0 and −3.0 in the printed figure. No conclusion is modified by these minor corrections.—J. Sohma.

1971, Volume 75

R. D. Kern, Jr., and G. G. Nika: A Complementary Shock Tube Technique Study of the Exchange of Hydrogen Chloride and Deuterium.

Page 179. Several errors resulted in the transposition of data from copy to Table I. The correct values were used to calculate the Arrhenius parameters which remain as reported.

TABLE I

Mixture	T_5, °K	$P_5 \times 10^6$, mol cm^{-3}	$k \times 10^{-11}$, cm^3 mol^{-1} sec^{-2}
	Argon Diluent		
A. 2%HCl–2%D_2 P_1 = 5 Torr	1849	1.76	13.7
	2099	1.86	37.4
	2157	1.88	62.8
	2251	1.91	181
	2277	1.92	57.3
	2312	1.93	94.7
	2436	1.97	184
	2535	2.00	218
	2806	2.07	355
B. 1%HCl–1%D_2 P_1 = 5 Torr	1932	1.76	36.0
	2014	1.79	33.5
	2322	1.89	49.1
	2437	1.93	571
	2485	1.94	247
C. 2%HCl–2%D_2 P_1 = 10 Torr	1994	3.64	25.0
	2099	3.72	48.1
	2149	3.76	97.2
	2149	3.76	35.4
	2181	3.78	43.7
	2230	3.81	50.4
	2260	3.83	44.9
	2290	3.85	120
	2298	3.86	78.6
	2384	3.91	144
	Ne–1%Ar Diluent		
D. 2%HCl–2%D_2 P_1 = 5 Torr	1714	1.70	7.08
	2066	1.92	21.2
	2082	1.93	12.5
	2098	1.93	44.6
	2141	1.88	46.6
	2159	1.92	34.2
	2273	1.99	36.5
	2273	1.96	92.4
	2294	1.93	41.2
	2369	1.91	164
	2388	1.96	77.1
	2481	2.07	176
	2516	2.00	125
	2523	1.92	88.2
	2670	2.08	115
	2780	2.07	353
E. 1%HCl–1%D_2 P_1 = 5 Torr	1797	1.70	8.59
	1831	1.71	10.3
	2028	1.79	15.1
	2073	1.85	19.1
	2121	1.90	23.6
	2208	1.89	17.5
	2291	1.88	40.7
	2548	1.96	95.0
	2713	2.08	96.7

Ralph D. Kern, Jr.

John A. Tallmadge: On the Liquid Film Which Occurs in a Draining Vessel.

Page 583. This note on draining films appeared in February and is based in part on two earlier studies. Because the earlier studies appeared in print at later dates, they are referenced here. The first earlier study appeared in March as P. Groenveld, *A.I.Ch.E. J.*, 17, 489 (1971), and the second appeared in May as J. A. Tallmadge, *ibid.*, 17, 760 (1971).—John A. Tallmadge.

Ashoka Ray and George Némethy: Micelle Formation by Nonionic Detergents in Water-Ethylene Glycol Mixtures.

Page 810. In Table I, the third group of entries, containing the data for OPE_{30}, should read as follows to account for water content of the sample. The other entries in the table are unchanged.

Temp, °C	Cmc, mol/l. × 10⁴	$\Delta G°$, kcal/mol	$\Delta H°$, kcal/mol	$\Delta S°$ cal/deg mol
		OPE_{30}		
25	5.33	−6.84	+4.3	+37
35	4.48	−7.18	+2.1	+30
45	4.25	−7.44	−0.0	+23

Page 813. In the right-hand column, the sentence in lines 8 to 10 should read as follows: "The latter value is comparable to the value, 0.024 kcal/mol, obtained by us from the difference in $\Delta G°$'s for $OPE_{9\text{-}10}$ and OPE_{30}.—George Némethy.

Kenneth D. Philipson, S. Cheng Tsai, and Kenneth Sauer: Circular Dichroism of Chlorophyll and Related Molecules Calculated Using a Point Monopole Model for the Electronic Transitions.

Page 1445. Three values are incorrect in Table IV in the first column of numerical data, headed "Point dipole model, $R_A \times 10^{40}$ cgs." These should read BChl, Q_y, +1.8; BChl, Q_x, −1.0; and pyroChl a, Q_y, −0.4. The authors wish to thank Dr. Claude Houssier of the University of Liege for bringing these errors to their attention.—Kenneth Sauer.

E. M. Dantzler-Siebert and C. M. Knobler: Interaction Virial Coefficients in Hydrocarbon-Fluorocarbon Mixtures.

Page 3870. The Acknowledgment should read: "We gratefully acknowledge that this work was supported in part by the National Science Foundation under Grant No. GP-7814."—C. M. Knobler.

R. Reisfeld, R. A. Velapoldi, L. Boehm, and M. Ish-Shalom: Transition Probabilities of Europium in Phosphate Glasses.

Page 3981. In Table I, the values for the first three oscillator strengths under the column entitled "This work" should read

$^7F_2 \rightarrow {}^5D_0$	1.544
$^7F_1 \rightarrow {}^5D_0$	0.350
$^7F_0 \rightarrow {}^5D_0$	0.0064

R. Velapoldi.

1972, Volume 76

R. D. Koob: Methylene Produced by Vacuum-Ultraviolet Photolysis. IV. Energy Distribution for the Reaction $C_3H_8 + h\nu$ (123.6 nm) = $CH_2 + C_2H_6$.

Page 9. The name J. H. Vorachek was omitted in the byline. The coauthors of the article are J. H. Vorachek and R. D. Koob.—R. D. Koob.

Jean Dayantis: A Derivation of the Thermodynamics of Polymer Solutions through Use of the Free Volume Concept. A. The Entropy of Mixing.

Page 402. In section IIa, line 22, the expression should read: $\Phi_1^m = \Phi_1^0(1 - v_1^0)/(1 - v_1^m)$. In line 25, the expression should read: $\Phi_2^m = \Phi_2^0(1 - v_2^0)/(1 - v_2^m)$. Equation 4 and all following equations remain unchanged.—Jean Dayantis.

N. E. Bibler and R. F. Firestone: Exchange Mechanism and Arrhenius Parameters of Elementary Steps in the Reactions of Hydrogen Atoms with Water Vapor in Irradiated Mixtures of Hydrogen and Water Vapor.

Page 629. The sentence beginning in the 12th line of the second column should read: These conditions require that $\Delta E_{max} = 3.0$ kcal/mol, whence $E_{30,min} = 17.2 \pm 0.5$ kcal/mol and $E_{32,max} = 20.2 \pm 0.5$ kcal/mol are prescribed values consistent with all conditions imposed by our observations. Table III contains the corrected values.

TABLE III: Probable Values of the Arrhenius Parameters of Various Reactions of Hydrogen Atoms with Water Vapor (218–381°)

Reaction i	E_i, kcal/mol	(A_i/A_{30})
(28) $D + D_2O \rightarrow D_2 + OD$	20.2 ± 0.5	18
(30) $H + D_2O \rightarrow HOD + D$	17.2 ± 0.5	(1.0)
(31) $H + D_2O \rightarrow D_2 + OH$	21 ± 1	1.6
(32) $H + D_2O \rightarrow HD + OD$	20.2 ± 0.5	25
$D + H_2O \rightarrow HOD + H$	19 ± 1	
$D + H_2O \rightarrow HD + OH$	19 ± 1	

The sense of the last sentence of the text, beginning as the last paragraph on p 629, should be reversed to conclude:[11] "it is apparent that the requirement that two hydrogen-oxygen bonds be broken in reaction 31 is reflected *entirely* in the activation energy difference rather than in the frequency factor ratio."—Richard F. Firestone.

Gregory E. Gardiner and Norman O. Smith: Solubility and Partial Molar Properties of Helium in Water and Aqueous Sodium Chloride from 25 to 100° and 100 to 600 Atmospheres.

Page 1197. The parameters of Table II do not reproduce the results satisfactorily. We thank Professor C. A. Eckert for bringing this to our attention. Table II should be replaced by the new Table II. These parameters reproduce the experimental mole fractions with a mean deviation of 0.002×10^{-3} at 25° and 50°, and 0.011×10^{-3} at 100°. The above changes have no effect on the subsequent data since the experimental mole fractions were used in fitting the results to eq 4.

TABLE II: Coefficients of $X_2 = aP + bP^2 + cP^3$ [a]

Temp, °C	Solvent	$a \times 10^6$	$-b \times 10^9$	$c \times 10^{12}$
25.0	1.003 *m* NaCl	5.576	0.622	−0.418
	4.067 *m* NaCl	3.227	1.20	0.834
50.0	H_2O	7.403	3.79	3.95
	1.003 *m* NaCl	5.837	2.34	2.42
	4.067 *m* NaCl	3.371	1.38	0.788
100.0	H_2O	7.972	5.98	5.55
	1.003 *m* NaCl	6.707	5.56	5.10
	4.067 *m* NaCl	4.110	2.98	2.31

[a] *P* in atmospheres.

A listing of the experimental mole fractions will appear following these pages in the microfilm edition of this volume of the journal. Single copies may be obtained from the Business Operations Office, Books and Journals Division, American Chemical Society, 1155 Sixteenth St., N.W., Washington, D. C. 20036. Remit check or money order for \$3.00 for photocopy or \$2.00 for microfiche referring to code number JPC-72-4041.—Norman O. Smith.

D. L. Cocke and K. A. Gingerich: Mass Spectrometric Determination of the Bond Dissociation Energies of the Molecules CePd and CeC_2.

Page 2333. Equation 1 should read

$$k_{Ag} = \frac{\sigma_{Ag}\gamma_{Ag}}{\sigma_{Ag_2}\gamma_{Ag_2}} \times \frac{I_{Ag_2}E_{Ag_2}n_{Ag}^{2}}{(I_{Ag}E_{Ag})^2 n_{Ag_2}T} \times \text{antilog}\left\{\frac{-D^\circ_0 - T\Delta[(G^\circ_T - H^\circ_0)/T]}{2.303\,RT}\right\} \quad (1)$$

D. L. Cocke.

AUTHOR INDEX *to Volume 76, 1972*

Note: In this Author Index, titles of papers are listed after the name of each author of the paper. Multiple authorship is not indicated. Complete authorship may be ascertained by consulting the original paper.

Abbott, P. C. Quasi-equilibrium analysis of the reaction of atomic and molecular fluorine with tungsten. [Comments]. 2930

Abendroth, R. P. Surface charge development of porous silica in aqueous solution 2547

Abrahamson, E. W. Path of triplet excitation energy in simple carbonyl-monoolefins system in the liquid phase. 478

Abramowitz, S. Infrared spectrum of matrix isolated UO_2(g) and its thermodynamic properties. 648

Abu-Eittah, R. Intermolecular charge-transfer studies. Thioamide-iodine system. 2405

Ache, H. J. Reactions of energetic positronium atoms in solutions. 1124

Acquista, N. Infrared spectrum of matrix isolated UO_2(g) and its thermodynamic properties. 648

Adamic, K. J. Electron spin resonance study of γ-irradiated single crystal of ammonium oxalate monohydrate. 3274

Adamson, A. W. Photosensitized decomposition of hexaamminecobalt(III) by biacetyl and by quinoline. 1105

Ahluwalia, J. C. Thermodynamics of transfer of tetrabutylammonium bromide from water to aqueous urea solutions and the effects on the water structure. 1366

Ahluwalia, J. C. Excess partial molal heat capacities of n-tetraamylammonium bromide in water from 10 to 80° and in aqueous tert-butyl alcohol solvent system at 30° and the effects on the water structure. 2577

Ahluwalia, J. C. Thermodynamics of tetrabutylammonium bromide in aqueous sodium chloride and the effects on the water structure 2582

Al-Ani, Kh. Photochemistry of the fluorotoluenes. II. Quenching of the excited states. 2967

Albright, J. G. Mutual-diffusion coefficients at 25° in the system silver nitrate-water. 1853

Albright, J. G. Tracer diffusion and viscosity study at 25° in binary and ternary liquid systems. 2572

Alchalal, A. Biphotonic ionization processes in nonpolar solutions of N,N,N′,N′-tetramethyl-p-phenylenediamine. 2229

Al-Daher, I. M. Interaction of arsine ith evaporated metal films. 2851

Alfassi, Z. B. Bond dissociation energy of the carbon-hydrogen bond in ethanol. Kinetic study of the reaction iodine + ethanol. 3314

Alger, T. D. Carbon-13 nuclear magnetic resonance relaxation in hemimellitene and isodurene. 281

Alger, T. D. Nuclear magnetic resonance rate studies of hindered rotation in methyl N-acetylsarcosinate. 853

Allara, G. Electron spin resonance study of transient radicals in γ-irradiated organic inclusion compounds. II. Palmitic acid urea clathrate. 801

Allendoerfer, R. D. Ion pairing in alkali metal durosemiquinone solutions. 1012

Allendoerfer, R. D. Electron spin resonance and electron nuclear double resonance study of the α-phenylbenzylidene malononitrile anion radical. 3384

Alverez, V. L. Triplet ← triplet absorption and intersystem crossing in phthalazine. 3937

Ambrus, J. H. Conductivity relaxation in a concentrated aqueous electrolyte solution 3287

Ambrus, J. H. Ultrasonic and Brillouin scattering study of viscoelastic relaxation in a concentrated aqueous calcium nitrate solution. 3495

Andermann, G. High-resolution x-ray emission study of central atom-ligand bonding in phosphorus oxyanions. 3975

Andersen, T. N. Electrode reduction kinetics of carbon dioxide in aqueous solution. 3278

Anderson, J. E. Factors influencing reverse osmosis rejection of organic solutes from aqueous solution. 4006

Anderson, J. L. Non-Poisson distributions observed during counting of certain carbon-14-labeled organic (sub)monolayers. 3603

Andreassen, A. L. Reduction of diffraction data for molecules with large amplitude motions. Approximate, general analysis. 3099

Andrews, L. Matrix infrared spectra and bonding in the di- and triiodomethyl radicals. 2718

Andrews, L. Argon matrix Raman and infrared spectra and vibrational analysis of ozone and the oxygen-18 substituted ozone molecules. 3208

Angell, C. A. Fluidity and conductance in aqueous electrolyte solutions. Approach from the glassy state and high-concentration limit. I. Calcium nitrate solutions. 3244

Aoyagi, K. Tracer diffusion and viscosity study at 25° in binary and ternary liquid systems. 2572

Arai, S. Pulse radiolysis study of dimer cation formation of aromatic hydrocarbons in benzonitrile solution. 1119

Aratani, K. Experimental study of the relation between contact angle and surface roughness. 3267

Arbouw-van der Veen, H. M. R. Irreversible potentiometric behavior of isotactic poly(methacrylic acid). 2559

Arce-Quintero, R. Elementary processes in the photochlorination of 3-methylpentane glass at 77-97°K. 1800

Arezzo, B. Electronegativity effects in T-for-CH_2X substitutions for recoil tritium reactions with propyl fluoride. 187

Arin, L. M. Reaction of ozone with carbon monoxide. 1514

Arin, M. L. Photochemistry of azoisopropane in the 2000-Ang region. 1685

Arnett, E. M. Solvent effects in organic chemistry. XIV. Solvation of sodium salts in glycerol acetate binaries by sodium-23 nuclear magnetic resonance spectroscopy and thermodynamics. 2474

Aronson, S. Thermodynamic stability of perylene-iodine charge-transfer complexes from measurements of iodine vapor absorption. 921

Asmus, K. D. Ion yields and ion neutralization processes in pulse-irradiated acetone. 26

Atkinson, G. Ultrasonic absorption in aqueous solutions of low-molecular-weight polyamines. 334

Auborn, J. J. Viscosity effects on ion-recombination kinetics. Bromocresol green in water-glycerol mixtures. 1184

Auborn, J. J. Comproportionation kinetics of stable violene radical ions. 701

Autard, P. Photochemistry of phenylcyclobutane. 3355

Bahe, L. W. Structure in concentrated solutions of electrolytes. Field-dielectric-gradient forces and energies. 1062

Bahe, L. W. Relative partial molar enthalpies and heats of dilution of electrolytes in water. 1608

Bailar, J. C. Jr. Reactions of coordination compounds in the solid state. Racemization of (+)-[Co(en)$_3$] $X_3 \cdot nH_2O$. 119

Baker, E. B. Nitrogen-14 nuclear magnetic resonance study of 1,5-disubstituted tetrazoles. 2403

Baker, R. W. Low-pressure ultrafiltration of sucrose and raffinose solutions with anisotropic membranes. 238

Balakrishnan, I. Effect of temperature on the γ radiolysis of aqueous solutions. 1273

Ballan, D. G. Vacuum ultraviolet photolysis of cyclohexanone. 615

Balzani, V. Sensitization and quenching of the cis → trans isomerization of bis(glycinato)platinum(II). 3934

Banewicz, J. J. Spectroscopic study of the propionitrile-iodine molecular complex. 2098

Bangert, F. K. Apparent molal volumes of sodium chloride and magnesium chloride in aqueous solution. 3488

Bangert, F. K. Volume changes on mixing solutions of magnesium chloride and sodium chloride 3491

Bansal, K. M. Pulse radiolysis studies of 5-halouracils in aqueous solutions. 2392

Bansal, K. M. Radiolysis of liquid 2,2,4-trimethylpentane. Kinetics of scavenging processes. 2374

Bansal, K. M. Radiolysis of liquid 2,2,4-trimethylpentane. Effect of charge scavengers on product formation. 2381

Bansal, K. M. Production of halide ion in the radiolysis of aqueous solutions of the 5-halouracils. 2386

Baraldi, I. Fluorescence and absorption spectra of polyphenyls. Theoretical study on the band shape. 3983

Barat, F. Pulsed radiolysis and flash photolysis of iodates in aqueous solution. 302

Barchet, W. R. Water vapor adsorption by pure silver iodide above ice saturation. 2280

Bard, A. J. Electron spin resonance study of the geometry of 9-phenylacridine. 3958

Bard, A. J. Resistive effects in thin electrochemical cells. Digital simulations of electrochemistry in electron spin resonance cells. 2550

Bare, J. P. Electrolyte viscosities in associated solvents. 434

Barkatt, A. Pulse radiolysis of sodium metaphosphate glasses. 203

Barnes, H. L. Ion-product constant of water to 350°. 90

Barnett, R. E. Viscosity dependence of a putative diffusion-limited reaction. 1192

Bartal, L. J. Reactions of energetic positronium atoms in solutions. 1124

Bascom, W. D. Polywater. Comments. 456

Bascom, W. D. Infrared spectroscopy study of water adsorption at the silica-carbon tetrachloride interface. 3188

Bascom, W. D. Hydrolysis of triethylethoxysilane at the silica-carbon tetrachloride interface. 3192

Bastian, E. J. Jr. Conformations of isocitrate in solution. 3073

Bates, J. B. Raman spectra of molten alkali metal carbonates. 1565

Bates, J. B. Raman spectra of tetrafluoroberyllate ion in molten sodium fluoride and lithium fluoride to 686°. 78

Bauer, S. H. Reduction of diffraction data for molecules with large amplitude motions. Approximate, general analysis. 3099

Bauer, S. H. Vibrational relaxation in carbon dioxide with selected collision partners. I. Water and heavy water. 3108

Baugh, P. J. Polyanions and their complexes. VII. Interaction of methylene blue with cellulosic polyanions in heterogeneous systems. 688

Baum, G. Influence of hydrophobic interactions on the electrochemical selectivity ratios of liquid membranes responsive to organic ions. 1872

Baumgartner, E. Ultrasonic absorption in aqueous solutions of low-molecular-weight polyamines. 334

Beachell, H. C. Detection of species resulting from condensed phase decomposition of ammonium perchlorate. 3545

Beck, G. Picosecond observations of some ionic and excited state processes in liquids. 3856
Becker, C. A. L. Strong crystalline field perturbation calculations for d^3,d^7 pentacoordinate complexes. I. Trigonal bipyramid. 2907
Becker, E. D. Restricted rotation about the exocyclic carbon-nitrogen bond in cytosine derivatives. 64
Becker, E. D. Evaluation of the nuclear magnetic resonance total line shape analysis of uncoupled, exchanging two-site systems. 71
Begala, A. J. Dilatometric studies of counterion binding by polycarboxylates. 254
Behar, D. Photolysis of hydroxylamine in aqueous solution. 180
Behar, D. Pulse radiolysis of aqueous thiocyanate solutions. Nature of the intermediate transient species. 1537
Behar, D. Electron spin resonance studies of inorganic radicals in irradiated aqueous solutions. I. Direct observation. 1706
Behar, D. Electron spin resonance studies of inorganic radicals in irradiated aqueous solutions. II. Radical trapping with nitromethane. 1710
Behar, D. Pulse radiolysis studies on Br^- in aqueous solution. Mechanism of Br_2 formation. 1815
Behar, D. Lifetime of trifluoromethyl radical in aqueous solution. 2517
Behar, D. Electron spin resonance investigation of the reactions in irradiated aqueous solutions of hydrogen cyanide and the cyanide ion. 3945
Bell, L. C. Radioisotope determination of the surface concentrations of calcium and phosphorus on hydroxylapatite in aqueous solution. 900
Benedetti, E. X-ray study of the conformation of the molecule of 1,2-trans-cyclopentanedicarboxylic acid. 790
Bennett, S. L. Ion-molecule reactions in ethane. 3919
Bennion, B. C. Comproportionation kinetics of stable violene radical ions. 701
Bennoson, M. Ultraviolet adsorption spectra of polyphosphate solutions. 3673
Bentley, F. F. Torsional frequencies and enthalpies of intramolecular hydrogen bonds of o-halophenols. 1553
Bernas, A. Photoionization of aromatics in solid solutions. Ionization potential determinations. 2236
Bernas, A. Negative species formed in γ- or ultraviolet-irradiated nonpolar glasses 3894
Bernheim, R. A. Phase diagrams of liquid crystal solvents used in nuclear magnetic resonance studies. 925
Bernstein, H. J. Raman spectra and an assignment of the vibrational stretching region of water. 1147
Bevan, P. L. T. Pulse radiolysis of aqueous thiocyanate solutions. Nature of the intermediate transient species. 1537
Bibler, N. E. Exchange mechanism and Arrhenius parameters of elementary steps in the reaction of hydrogen atoms with water vapor in irradiated mixtures of hydrogen and water vapor. 621
Billingsley, F. P. II. Mixed basis scheme for the rapid computation of molecular electronic energy in the SCF-LCAO-(STO [Slater-type orbitals])-MO formalism, and its application to the lithium superoxide molecule. 2995
Bird, G. R. Circular dichroism of sensitizing dye aggregates. 2982
Biros, J. Pressure effects in polymer solution phase equilibriums. I. Lower critical solution temperature of poly(isobutylene) and poly(dimethylsiloxane) in lower alkanes. 1206
Birrell, G. B. Electron spin resonance of x-irradiated heptanal trapped in a single crystal of perhydrotriphenylene. 1008
Birrell, G. B. Electron spin resonance study of x-irradiated heptanal oxime trapped in a urea inclusion crystal. Evidence of a bimolecular reaction product. 1819
Blake, T. D. Adsorption on flat surfaces. III. Adsorption of branched-chain alcohols. 675
Blakeley, R. A. Efficiency of the electrochemiluminescent process. 1868
Blyholder, G. Isotope effect in the decomposition of ammonia on tungsten surfaces. 970
Blyholder, G. Infrared spectra of carbon monoxide chemisorbed on iron at low temperature. 3180
Blyholder, G. Photocatalytic reactions on zinc oxide. III. Hydrogenation of ethylene. 1394
Blyholder, G. Photocatalytic reaction on zinc oxide. II. Oxidation of carbon monoxide with nitrous oxide and oxygen. 1807
Blyholder, G. Adsorbed oxygen species on zinc oxide in the dark and under illumination. 3184
Bock, C. M. Crystal structure of 2,4,6-trinitroaniline. 3597
Bockris, J. O'M. Ionic solvation numbers from compressibilities and ionic vibration potentials measurements. 2140
Bockris, J. O'M. Approximate calculations of the heats and entropies of hydration according to various models. 2298
Bode, D. D. Jr. Calculated free energies of absorption of halide and hydroxide ions by mercury, silver, and gold electrodes. 2915
Boehm, L. Quantum efficiencies and radiationless transitions of europium(III) in phosphate glasses. 1293
Bolletta, F. Sensitization and quenching of the cis → trans isomerization of bis(glycinato)platinum(II). 3934
Bolton, G. L. Temperature shifts in the optical spectra of solvated electrons in methanol and ethanol. 3876
Bonner, O. D. Resolution of an infrared band of water-d into hydrogen-bonded and nonbonded components. 1228
Bookless, J. S. Use of F centers for the investigation of alloy thermodynamics. Potassium-lead system. 1202
Boone, D. Magnetic circular dichroism of ferrocene and substituted ferrocenes. d-d Transitions. 511
Booth, R. J. Electron spin resonance detection of Sn^{3+} and Pb^{3+} complexes in γ-irradiated stannous, plumbous, and plumbic salts. 141
Bosmans, H. J. Location of univalent cations in synthetic zeolites of the Y and X type with varying silicon to aluminum ratio. II. Dehydrated potassium exchanged forms. 650
Bourderon, C. Low-temperature infrared study of sterically hindered associated alcohols. 864
Bourderon, C. Vibrational overtone study of association in liquid methanol. 869
Bowers, P. G. Kinetic oscillations in the oxidation of 2,4-pentanedione by bromate ion, catalyzed by manganese(II). 2185
Bowman, M. K. Concentrated electron scavenger effects on the yields of trapped species in γ-irradiated alkaline glass. 1962
Boyd, G. E. Raman spectra of molten alkali metal carbonates. 1565
Boyd, G. E. Raman spectra of tetrafluoroberyllate ion in molten sodium fluoride and lithium fluoride to 686°. 78
Brado, J. A. Dimerization of a copper(II)-phthalocyanine dye in carbon tetrachloride and benzene. 446
Brado, J. A. Association of copper(II), vanadyl, and zinc(II) 4,4′,4′,4‴-tetraalkylphthalocyanine dyes in benzene. 1994
Bradspies, J. I. Polywater, an organic contaminant. Reply to comments. 457
Braswell, E. H. Equilibrium sedimentation studies of the aggregation of methylene blue. 4026
Braustein, J. New electrochemical measurements of the liquidus in the lithium fluoride-beryllium fluoride system. Congruency of lithium beryllium fluoride (Li_2BeF_4). 1154
Breheret, E. Solvent effects on acetophenone photoreduction studied by laser photolysis. 821
Breiland, W. G. Kinetic study of the reaction of methylene radicals with dimethylsilane. Decomposition of chemically activated trimethylsilane and methylethylsilane. 459
Breitling, S. M. Application of significant structures theory to some hydrocarbon liquids. 731
Brennan, M. Ultrasonic attenuation in basic purine solutions. 2838
Bressel, R. D. Fluidity and conductance in aqueous electrolyte solutions. Approach from the glassy state and high-concentration limit. I. Calcium nitrate solutions. 3244
Bridges, L. Photochemistry of ethanethiol at 254 and 214 nm. 2668
Bridgman, W. B. Columns of liquid bearing a constrained chemical activity gradient. 1637
Brinen, J. S. Electron spectroscopy for chemical analysis (ESCA) studies on catalysts. Rhodium on charcoal. 2525
Brinn, I. Excited state dissociation rate constants in naphthols. 3558
Brocklehurst, B. Emission from aromatic radicals in ion recombination luminescence. 3710
Brodale, G. E. Relation of crystalline forms I, III, IV, and V of anhydrous sodium sulfate as determined by the third law of thermodynamics. 737
Brooker, M. H. Raman spectra of molten alkali metal carbonates. 1565
Brown, C. W. Sodium and magnesium sulfate ion pairing. Evidence from Raman spectroscopy. 3664
Brown, G. H. Thermodynamic study of solutions with liquid crystal solvents by gas-liquid partition chromatography. 99
Brown, G. H. Ultrasonic shear wave study of the mechanical properties of a nematic liquid crystal. 2409
Brown, S. Coordination of fluoride and chloride anions with alcohol and phenol. 1775
Bruice, T. C. Effect of transfer from water to 1.0 M water in dimethyl sulfoxide on the reaction of nucleophiles with phenyl esters. 432
Brummer, S. B. Polywater, an organic contaminant. Reply to comments. 457
Bruni, M. C. Fluorescence and absorption spectra of polyphenyls. Theoretical study on the band shape. 3983
Bruno, G. V. Estimating slow-motional rotational correlation times for nitroxides by electron spin resonance. 1858
Bruno, P. Conductometric behavior of tetraamylammonium bromide and potassium picrate in some nonaqueous solvents. 1049
Bruno, P. Density, viscosity, and electrical conductance of sodium salts in formamide solutions at 25°. 3034
Brupbacher, J. M. Reaction of hydrogen cyanide and deuterium behind reflected shock waves. 285
Brus, L. E. Chemical lasers produced from $O(^1D)$ atom reactions. V. Carbon monoxide stimulated emission from flash-initiated O_3 + XCN systems. 1429
Bucher, J. Anion exchange in aqueous-organic solvent mixtures. II. 1040
Bucher, J. Selectivity in heterovalent anion exchange. Ion pairing vs. ion hydration. 2459
Buchheit, M. Detection of the triphenylmethyl radical by electron spin resonance in the thermal decomposition of sodium triphenylacetate. 937
Buchwald, M. I. Vibrational relaxation in carbon dioxide with selected collision partners. I. Water and heavy water. 3108
Buechler, E. Laser Raman spectroscopy of surfaces. 2325
Buehler, R. E. Correlation of spectral data for halogen atom complexes with the electron donors involved. 3220
Bufo, A. Redox mechanisms in an ionic matrix. Kinetics of the reaction $2O_2^- + H_2O = 2OH^- + 1.5O_2$ in molten alkali nitrates. 422
Bullock, G. E. Reaction of cyanogen radicals with ammonia. 1931
Bulusu, S. Photolysis of solid dimethylnitramine. Nitrogen-15 study and evidence for nitrosamide rearrangement. 496
Bumgardner, C. L. Pyrolysis of 1,1-difluoroethane. 1680
Bunker, D. L. Two familiar gas reactions at suprahigh pressure. 2614
Burneau, A. Near-infrared spectroscopic study of the interactions between water and acetone. Comments. 449
Burns, W. G. Modified prescribed diffusion in radical diffusion kinetics. 3008
Burr, J. G. Viscosity effects on the photohydration of pyrimidines. 3137
Burrows, B. Solubility study of silver halides in molten calcium nitrate tetrahydrate. 2759
Burrows, H. D. Solute radical cation yields in the pulse radiolysis of solutions of aromatic amines in chlorinated hydrocarbons. 20

Butler, J. N. Solvation and self-association of water in propylene carbonate. 855

Cabani, S. Volumetric properties of aqueous solutions of organic compounds. I. Cyclic ethers and cyclic amines. 1338

Cabani, S. Volumetric properties of aqueous solutions of organic compounds. II. Chloride salts of cyclic amines. 1343

Cabani, S. Kinetic study of the hydration reaction of 2-, 3-, and 4-pyridinecarboxaldehyde. 2959

Caja, J. Catalytic polarographic current of a metal complex. VIII. Effect of weakly complexing supporting electrolytes. 1170

Calder, G. V. Anomalous isotope shifts in the vibrational spectrum of hydrogen cyanide in argon matrixes. 454

Caldwell, K. E. Kinetic oscillations in the oxidation of 2,4-pentanedione by bromate ion, catalyzed by manganese(II). 2185

Capellos, C. Yields and reactions of lowest excited singlet and triplet states in the radiolysis of naphthalene and 1-methylnaphthalene. 2485

Carlson, G. L. Torsional frequencies and enthalpies of intramolecular hydrogen bonds of o-halophenols. 1553

Carman, C. J. Steric interactions in tert-butylethylenes observed through proton carbon-13 satellite spectra. 2877

Carmichael, H. Pyrolysis of 1,1-difluoroethane. 1680

Carr, R. W. Jr. Predictions of the rates of hydrogen abstraction by $CH_2(^3B_1)$ by the bond-energy bond-order method. 1581

Carstensen, E. L. Dielectric properties of quaternary ammonium salt hydrates. 1999

Carter, R. E. Barriers to rotation around the amide bond and the central carbon-carbon bond in tetrabenzyloxamide and its monothio and dithio analogs. 642

Caruso, J. A. Theoretical models for acid-base equilibrium data in nonaqueous solvents. 3618

Cassel, R. B. Thermodynamics of transfer of three tetraalkylammonium bromides from water to aqueous urea solutions at 25°. 1369

Cerjan, C. Viscosity dependence of a putative diffusion-limited reaction. 1192

Cerruti, L. Infrared study of surface properties of α-chromia. IV. Pyridine and heavy water adsorption on oxygen-covered surface. 571

Chan, L. L. Reactivities of ion pairs and free ions in proton abstraction reactions. Reaction between polystyryl carbanion salts and triphenylmethane. 695

Chang, H. W. Nonequilibrium unimolecular reactions and collisional deactivation of chemically activated fluoroethane and 1,1,1-trifluoroethane. 954

Chang, R. Electron spin resonance and electron nuclear double resonance study of the α-phenylbenzylidene malononitrile anion radical. 3384

Chang, W. S. Dissolution lifetime of a hydrated solute sphere. 2017

Chantooni, M. K. Jr. Critical study involving water, methanol, acetonitrile, N,N-dimethylformamide, and dimethyl sulfoxide of medium ion activity coefficients, γ, on the basis of the $\gamma_{AsPh_4^+} = \gamma_{BPh_4^-}$ assumption. 2024

Chao, C. C. Electron paramagnetic resonances study of the Cu^+-NO complex in a Y-type zeolite. 1546

Chasteen, N. D. Electron paramagnetic resonance line widths of vanadyl(IV) α-hydroxycarboxylates. 3951

Chatterjee, A. Adsorption isotherms and equations of state of insoluble vapors at the water-gas interface as studied by gas chromatography. 2769

Chaudhri, S. A. Ion yields and ion neutralization processes in pulse-irradiated acetone. 26

Chaudhri, S. A. Pulse radiolysis of dioxane and dioxane + water mixtures. Yield of free solvated electrons and kinetics of the radical reactions. 1279

Chawla, B. Thermodynamics of tetrabutylammonium bromide in aqueous sodium chloride and the effects on the water structure. 2582

Chen, H-Y. High molecular weight boron sulfides. VIII. Vapor pressures of $B_2S_3(g)$ and $B_4S_6(g)$ over stoichiometric B_2S_3. 2035

Chen, T-M. Nitrogen-14 magnetic relaxation of dimethylformamide solutions containing nickel(II), cobalt(II), and manganese(II) ions. 1968

Chen, T-M. Proton magnetic relaxation in N-methyl-γ-butyrolactam and hexamethylphosphoric triamide solutions containing manganese(II) ions. 1973

Chen, W. W. Investigation of micelle structure by fluorine magnetic resonance. VI. Quaternary ammonium salts. 3012

Chen, Y-J. Temperature dependence of the Kerr constant of water. 216

Cheng, T. M. H. Ionic reactions in monosilane. Radiation chemistry implications. 3321

Chester, A. W. Kinetics of the cobalt-catalyzed autoxidation of toluene in acetic acid. Role of cobalt. 1520

Cheung, M. W. Equilibrium and kinetic properties of 9,10-phenanthrenequinone-3-sulfonate in aqueous solutions. 1875

Chiu, M. F. Theoretical study of hyperfine coupling constants of some σ radicals based on the INDO [intermediate neglect of differential overlap] method. 553

Chohan, R. K. Oxidation kinetics of 2-dimethylaminoethanethiol hydrochloride by ferricyanide ion in acid medium. 3641

Choppin, G. R. Thermochemistry of halide exchange in an anion-exchange resin. 680

Christensen, H. Transient electrons in pulse-irradiated crystalline water and deuterium oxide ice. 1000

Christian, S. D. Association of trifluoroacetic acid in vapor and in organic solvents. 2039

Christophorou, L. G. Intermediate phase studies for understanding radiation interaction with condensed media. Electron attachment process. 3730

Chrysochoos, J. Fluorescence spectra and lifetimes of Sm^{3+} in phosphoryl chloride-tin tetrachloride. 3397

Chu, B. Selectivity in heterovalent anion exchange. Ion pairing vs. ion hydration. 2459

Chu, P. Osmotic properties of polystyrenesulfonates. II. Donnan equilibrium. 1881

Chua, P. T. Identity scrambling and isomerization networks in systems of excited alkyl radicals. 2507

Chung, Y. J. Reversible line broadening in the electron spin resonance spectra of tert-butyl radicals in γ-irradiated crystalline tert-butyl isothiocyanate. 1792

Ciecierska-Tworek, Z. Electron spin resonance of x-irradiated heptanal trapped in a single crystal of perhydrotriphenylene. 1008

Ciecierska-Tworek, Z. Electron spin resonance study of x-irradiated heptanal oxime trapped in a urea inclusion crystal. Evidence of a bimolecular reaction product. 1819

Clark, M. E. Thermochemistry of halide exchange in an anion-exchange resin. 680

Clark, W. G. Rate constants for quenching of molecular nitrogen ($A^3\Sigma_u^+$) in active nitrogen. 1

Clarke, G. A. Molecular orbital theory of the diatomic molecules of the first row transition metals. 2268

Clarke, J. H. R. Raman spectra and structure of molten cadmium chloride, molten cadmium bromide, and their molten mixtures with alkali metal halides. 1831

Clarke, R. M. Radiolysis of aqueous methane solutions. 3863

Claverie, P. Calculation of the interaction energy of one molecule with its whole surrounding. I. Method and application to pure nonpolar compounds. 2123

Cocke, D. L. Mass spectrometric determination of the bond dissociation energies of the molecules cerium-palladium and cerium dicarbide. 2332

Coffman, R. E. Electron spin resonance spectroscopy of the bisdithiooxalatonitrosyl iron anion. 49

Cogley, D. R. Solvation and self-association of water in propylene carbonate. 855

Cohen de Lara, E. Infrared spectra of nitrous oxide adsorbed on sodium type A synthetic zeolite. 945

Collin, C. H. Recoil and chargin contributions to organic incorporation of radiobromine atoms following neutron activation. 3331

Collins, K. E. Recoil and charging contributions to organic incorporation of radiobromine atoms following neutron activation. 3331

Coltharp, R. N. Rates of interaction of vibrationally excited hydroxyl (v = 9) with diatomic and small polyatomic molecules. 1511

Coluccia, S. Infrared study of surface properties of α-chromia. IV. Pyridine and heavy water adsorption on oxygen-covered surface. 571

Concepcion, J. G. Thermodynamic parameters for the cyclooctatetraene anion radical disproportionation as a function of ion pairing in hexamethylphosphoramide. 2176

Connor, H. D. Electron spin resonance studies of the electron-transfer equilibrium β-ethylnaphthalenide + α-ethylnaphthalene ⇌ β-ethylnaphthalene + α-ethylnaphthalenide. 1734

Conrad, R. E. Hydrogen-oxygen reaction on lanthanide oxides. II. Stoichiometric hydrogen-oxygen reaction on neodymium oxide, dysprosium oxide, and erbium oxide. 2199

Conti, G. Volumetric properties of aqueous solutions of organic compounds. I. Cyclic ethers and cyclic amines. 1338

Conti, G. Volumetric properties of aqueous solutions of organic compounds. II. Chloride salts of cyclic amines. 1343

Cooke, N. H. C. Fluorescence quenching by benzoic acid. 3563

Cooper, G. D. Photochemistry of the monoxalatoiron(III) ion. 2618

Cooper, R. Reaction of cyanogen radicals with ammonia. 1931

Cooper, W. F. Molecular orbital theory of the diatomic molecules of the first row transition metals. 2268

Copeland, J. L. Effects of high-pressure hydrogen chloride on transport properties of the molten 46 mole % potassium chloride-54 mole % zinc chloride eutectic system. 904

Copeland, V. C. Preparation and structure of bromobis(2-(2-aminoethyl)pyridine)copper(II) bromide. 2887

Corcione, M. Dissipative structures and diffusion in ternary systems. 2050

Corradini, P. X-ray study of the conformation of the molecule of 1,2-trans-cyclopentanedicarboxylic acid. 790

Corrin, M. L. Water vapor adsorption by pure silver iodide above ice saturation. 2280

Corset, J. Near-infrared spectroscopic study of the interactions between water and acetone. Comments. 449

Cox, R. A. Quantum yields for the photooxidation of sulfur dioxide in the first allowed absorption region. 814

Craig, N. L. Nonequilibrium unimolecular reactions and collisional deactivation of chemically activated fluoroethane and 1,1,1-trifluoroethane. 954

Cribley, K. Additivity in the carbon-13 chemical shifts of 1,2-disubstituted ethanes. 1466

Crossley, R. W. Solid state reaction kinetics. III. Calculation of rate constants of decomposition for a melting system undergoing volume and surface changes. 2253

Cruz, M. I. Methanol-silica gel system. II. Molecular diffusion and proton exchange from pulse proton magnetic resonance data. 3078

Csillag, K. Transfer diffusion. III. Kinetics and mechanism of the triiodide-iodide exchange reaction. 162

Cukor, P. M. Solubilities of gases in liquids at elevated temperatures. Henry's constants for hydrogen, methane, and ethane in hexadecane, bicyclohexyl, and diphenylmethane. 598

Cukor, P. M. Gas solubilities from a perturbed hard-sphere equation of state. 601

Cumper, C. W. N. Dielectric relaxation of p-benzoquinones and $Me_{4-n}C(OMe)_n$ and $Me_{4-n}Si(OMe)_n$ (n = 1-4) in benzene solution. 525

Cunningham, J. Reactions involving electron transfer at semiconductor surfaces. III. Dissociation of methyl iodide over zinc oxide. 2353

Cunningham, J. Reactions involving electron transfer at semiconductor surfaces. IV. Zinc oxide promoted photoreductions in aqueous solutions at neutral pH. 2362

Curtis, A. R. Modified prescribed diffusion in radical diffusion kinetics. 3008

Cvetanovic, R. J. Reaction of the excited oxygen atoms $O(^1D_2)$ with cyclopentane. 1375

Czapski, G. Concentration effects on primary processes in the radiation chemistry of aqueous solutions. 3677

Dahlberg, D. B. Aqueous solution structure as determined from thermodynamic paramters of transfer from water to heavy water. 2045

Dahlqvist, K. I. Barrier to internal rotation in amides. IV. N,N-Dimethylamides. Substituent and solvent effects. 2178

Dainton, F. Pulse radiolysis of solutions of stilbene. I. Evidence for triplet and singlet excited state formation. 3897

Daisey, J. M. Thermodynamic and spectral properties of molecular complexes of iodine with several aminopyridines. 1895

Daly, F. P. Sodium and magnesium sulfate ion pairing. Evidence from Raman spectroscopy. 3664

Damle, P. S. γ-Ray irradiated sodium chloride as a source of hydrated electrons. 3694

Danby, C. J. Existence of spin-forbidden predissociation in the mass spectrum of isocyanic acid. 2636

Daniel, S. H. Recoil tritium reactions with hexamethyldisilane in the gas phase. 1249

Daniel, S. H. Reactions of recoil chlorine atoms with cis and trans olefins. 2711

Danner, J. C. Solvent effect on metal hyperfine constants in alkali metal radical anion ion pairs. 2866

Danoczy, E. Sequence studies in liquid-phase hydrocarbon oxidation. I. Alcohol-ketone transition in the oxidation of ethylbenzene. 2785

D'Aprano, A. Ionic association of potassium perchlorate in sulfolane-water mixtures from conductance measurements at 25°. 2923

D'Aprano, A. Association of alkali perchlorates in anhydrous methanol at 25°. 2920

Darbari, G. S. Ultrasonic relaxation in calcium nitrate hydrated melts. 1507

Dardy, H. Ultrasonic and Brillouin scattering study of viscoelastic relaxation in a concentrated aqueous calcium nitrate solution. 3495

Das Gupta, A. Transport properties of polar gases. Collision integrals for the Kihara spherical core plus dipole-dipole potential. 1470

Das Gupta, G. Quenching of the excited states of benzene and substituted benzenes by olefins. 3668

David, C. W. CNDO [complete neglect of differential overlap]/2 calculation on the helical conformations of a tetrapeptide of glycine. III. phi-psi. Energy surface. 670

David, C. W. Extended Hueckel calculations on polypeptide chains. IV. ϕ-ψ Energy surface for a tetrapeptide of poly-L-alanine. 2793

Davidson, J. A. Path of triplet excitation energy in simple carbonyl-monoolefins system in the liquid phase. 478

Davis, D. D. Absolute rate constants for the reaction $O + O_2 + M \rightarrow O_3 + M$ over the temperature range 200-346°K. 2653

Davis, D. D. Absolute rate constants for the addition and abstraction reactions of atomic oxygen with 1-butene over the temperature range 190-491°K. 3311

Davis, H. T. Mobility of excess electrons in liquid hydrocarbon mixtures. 442

Davis, H. T. Theory of heats of mixing of certain charge-unsymmetrical molten salts. 1629

Day, C. L. Proton magnetic resonance investigation of the environment of aromatic compounds in aqueous zwitterionic micellar solutions. 1460

Day, M. C. Ion-solvent interactions. Effect on ionic aggregation in the system sodium tetra-n-butylaluminate-cyclohexane-tetrahydrofuran. 3472

Dayantis, J. Derivation of the thermodynamics of polymer solutions through use of the free volume concept. A. Entropy of mixing. 400

DeBacker, M. G. Pulse radiolysis study of the kinetics of formation of Na^- in ethylenediamine by the reaction of solvated electrons with sodium ions. 839

DeCorpo, J. J. Intermediates in the reactions of alkane and cycloalkane molecular ions with water vapor. 1517

Dedinas, J. Kinetics and mechanism of decafluorobenzophenone photochemical reactions in cyclohexane, benzene, and alkyl aromatics. 3926

DeGraff, B. A. Photochemistry of the copper(II)-malonate system. Sensitized reaction. 1387

DeGraff, B. A. Photochemistry of the monoxalatoiron(III) ion. 2618

DeHaas, N. Steady-state intermediate concentrations and rate constants. HO_2 results. 1586

DeHaas, N. Measurement of the rate constant for $H + H_2CO \rightarrow H_2 + HCO$ at 297-652°K. 2213

DeHaas, N. Relative rate constants for $O + HCO \rightarrow OH + CO$ and $O + HCO \rightarrow H + CO_2$. 2215

Della Monica, M. Conductometric behavior of tetraamylammonium bromide and potassium picrate in some nonaqueous solvents. 1049

Della Monica, M. Density, viscosity, and electrical conductance of sodium salts in formamide solutions at 25°. 3034

Delmas, G. Pressure effects in polymer solution phase equilibriums. I. Lower critical solution temperature of poly(isobutylene) and poly(dimethylsiloxane) in lower alkanes. 1206

DeLuca, A. F. Dimerization of a copper(II)-phthalocyanine dye in carbon tetrachloride and benzene. 446

DeLuca, A. F. Association of copper(II), vanadyl, and zinc(II) 4,4',4'',4'''-tetraalkylphthalocyanine dyes in benzene. 1994

De Montgolfier, Ph. Laser-induced gas breakdown. Spectroscopic and chemical studies. 31

DeMore, W. B. Pressure dependence and mechanism of the reaction of atomic oxygen and carbon monoxide. 3527

Den Engelsen, D. Transmission ellipsometry and polarization spectrometry of thin layers. 3390

Dereppe, J. M. Molecular movements and phase transitions in solids. Tetrakis(trimethylsilyl)methane. 4037

Deshpande, D. D. Use of exponential six potential in the statistical theory of solutions. 3005

De Sorgo, M. Aggregation of salts of thianthrene radical cations. 3468

De Trobriand, A. Nuclear magnetic resonance chemical shift of the water proton in aqueous tetraalkylammonium halide solutions at various temperatures. 1455

Devlin, J. P. Solid state spectra and conductivities of the potassium salts of anthracene. 1026

Devlin, J. P. Infrared and Raman spectra of group I nitrate aggregates in carbon dioxide matrixes and glassy thin films. 1826

Devlin, J. P. Alkali metal nitrate glass transition temperatures from vapor deposited films. 3093

Diamond, R. M. Anion exchange in aqueous-organic solvent mixtures. II. 1040

Diamond, R. M. Coordination of fluoride and chloride anions with alcohol and phenol. 1775

Diamond, R. M. Hydration of perchlorate, tetraphenylboride, and nitrate ions in some organic solvents. 2454

Diamond, R. M. Selectivity in heterovalent anion exchange. Ion pairing vs. ion hydration. 2459

Dickinson, C. Crystal structure of 2,4,6-trinitroaniline. 3597

Diehn, B. Hot-atom reactions of iodine in the liquid phase induced by x-ray resonance absorption. 2639

Dietrich, B. K. Ranges of photoinjected electrons in dielectric liquids. 3794

Doepker, R. D. Vacuum-ultraviolet photolysis of the C_4H_6 isomers. IV. 1-Butyne 1112

Doepker, R. D. Vacuum-ultraviolet photolysis of the C_4H_6 isomers. V. Methylenecyclopropane. 3153

Donato, I. D. Ionic association of potassium perchlorate in sulfolane-water mixtures from conductance measurements at 25°. 2923

Dorfman, L. M. Pulse radiolysis study of the kinetics of formation of Na^- in ethylenediamine by the reaction of solvated electrons with sodium ions. 839

Dorko, E. A. Solid state reaction kinetics. III. Calculation of rate constants of decomposition for a melting system undergoing volume and surface changes. 2253

Dorn, H. C. Carbon-13-carbon-13 coupling constants. VI. Homonuclear double resonance experiments for carbon-13 nuclear magnetic resonance assignments. 2972

Draganic, I. G. Formation of primary hydrogen atom yield (G■) in the γ radiolysis of water. 2733

Draganic, Z. D. Formation of primary hydrogen atom yield (G■) in the γ radiolysis of water. 2733

Drakenberg, T. Barrier to internal rotation in amides. IV. N,N-Dimethylamides. Substituent and solvent effects. 2178

Drakenberg, T. The ester bond. II. Nuclear magnetic-resonance studies of tert-butyl formate. 3582

Dresner, L. Stability of the extended Nernst-Planck equations in the description of hyperfiltration through ion-exchange membranes. 2256

Dubois, J. E. Structure effect on the fading rate of photochromic 3-substituted benzothiazolinic spiropyrans. 3554

Dubrin, J. Average value of the cross section for $H + HBr \rightarrow H_2 + Br$ over the 0.35-1.7-eV collision energy range. 1321

Duffy, J. A. Ionic-covalent interactions and glass formation in molten acetates. Cobalt(II) as a spectroscopic probe. 1035

Dullien, F. A. L. Diffusion of acetic acid dimers and their homomorphs. 2463

Dumont, P. Laser-induced gas breakdown. Spectroscopic and chemical studies. 31

Dunbar, R. C. Ion-molecule reactions of diborane and oxygen-containing compounds. 2467

Dunn, F. Ultrasonic absorption mechanisms in aqueous solutions of bovine hemoglobin. 528

Dunn, L. A. Electrical conductances and ionization behavior of sodium chloride in dioxane-water mixtures at 50°. 2294

Dunn, M. R. Mass spectrometric observations on the reaction of hydrogen atoms with iodine cyanide. 1392

Durig, J. R. Vibrational spectra and structure of organogermanes. XII. Normal vibrations and free rotation in p-chlorophenylgermane and p-fluorophenylgermane. 1558

Durig, J. R. Vibration analyses and barrier to internal rotation of 1,1-dichloroethane and 1,1-dichloroethane-d_4. 3591

Dutton, M. L. Two familiar gas reactions at suprahigh pressure. 2614

Duval, M. C. Solvent effects on acetophenone photoreduction studied by laser photolysis. 821

Dworkin, A. Transition phenomena of some organic solids by electrical conductivity measurement at low temperatures. Comment. 2798

Dye, J. L. Pulse radiolysis study of the kinetics of formation of Na^- in ethylenediamine by the reaction of solvated electrons with sodium ions. 839

Dye, J. L. Spectra of Na^-, K^-, and e^-_{solv} in amines and ethers. 2975

Eagland, D. Viscosity of concentrated aqueous solutions of tetraalkylammonium bromides. 1902

Echegoyen, L. Equilibrium studies by electron spin resonance. I. Free nitrobenzene anion radical. 1439

Echegoyen, L. Equilibrium studies by electron spin resonance. II. Nitrobenzene free ion-ion pair equilibrium. 2058

Edwards, J. O. Reactions of acetone and hydrogen peroxide. II. Higher adducts. 1283

Egan, J. J. Use of F centers for the investigation of alloy thermodynamics. Potassium-lead system. 1202

Eicher, L. D. Molecular structure and shear viscosity. Isomeric hexanes. 3295

Eirich, F. R. Low-pressure ultrafiltration of sucrose and raffinose solutions with anisotropic membranes. 238

Eisele, I. Temperature dependence of the drift mobility of electrons in glassy 10 M sodium hydroxide ice. 1509

Eland, J. H. D. Existence of spin-forbidden predissociation in the mass spectrum of isocyanic acid. 2636

Eliason, R. Isotope effects in proton transfer from general acids to carbon bases. 2951

Elkomoss, S. G. Excitons bound to ionized impurities in inorganic crystals. 3771

El-Kourashy, A. Intermolecular charge-transfer studies. Thioamide-iodine system. 2405
Eller, P. M. P. Theoretical models for acid-base equilibrium data in nonaqueous solvents. 3618
Elliott, R. L. Additivity in the carbon-13 chemical shifts of 1,2-disubstituted ethanes. 1466
Elworthy, P. H. Conductivity of sodium chloride and potassium chloride in polymer solutions and the obstruction effect. 1763
Emara, M. M. Ultrasonic absorption in aqueous solutions of low-molecular-weight polyamines. 334
Endicott, J. F. Ligand field photochemistry of halopentaamminerhodium(III) complexes. 1937
Endicott, J. F. Photochemical behavior of cobalt complexes containing macrocyclic (N_4) ligands. Oxidation-reduction chemistry of dihalogen radical anions. 2223
Entine, G. Polywater, an organic contaminant. Reply to comments. 457
Erwin, W. Hot-atom chemistry of carbon-14 in solid benzene at kinetic energies at or below 5 electron volts. 2521
Ethridge, D. R. Precise measurements of W, the average energy required for ion pair formation. II. Alcohols and water. 3842
Evans, D. H. Theory for a homogeneous reaction following a quasireversible electrode reaction. 1160
Evans, M. J. B. Kinetics of adsorption of carbon monoxide on alumina. 2349
Ewald, A. H. Effect of pressure on charge-transfer complexes in solution. II. Complexes formed between ions and between ions and neutral molecules. 249
Ewing, G. J. Interaction of leghemoglobin with nitrogen and with xenon. 591
Eyre, J. A. Pulse radiolysis study of the kinetics of formation of Na^- in ethylenediamine by the reaction of solvated electrons with sodium ions. 839
Eyring, E. M. Comproportionation kinetics of stable violene radical ions. 701
Eyring, E. M. Viscosity effects on ion-recombination kinetics. Bromocresol green in water-glycerol mixtures. 1184
Eyring, E. M. Kinetics of acid dissociation-ion recombination of aqueous methyl orange. 4023
Eyring, H. Application of significant structures theory to some hydrocarbon liquids. 731
Eyring, H. Magnetic circular dichroism of molecules in dense media. I. Theory. 1844
Eyring, H. Electrode reduction kinetics of carbon dioxide in aqueous solution. 3278
Eyring, H. Magnetic circular dichroism of ferrocene and substituted ferrocenes. d-d Transitions. 511
Eyring, H. Significant structure liquid theory of the alkali metals over the normal melting to boiling range. 1612
Faerber, G. L. Application of significant structures theory to some hydrocarbon liquids. 731
Falk, M. Solvation and self-association of water in propylene carbonate. 855
Farina, R. D. Kinetic study of the monomer-dimer equilibrium in aqueous vanadium(IV) tetrasulfophthalocyanine solutions. 2343
Fass, R. A. Photochemical production of hot hydrogen and deuterium atoms. Reactions with hydrogen halides and halogens. 2801
Fateley, W. G. Torsional frequencies and enthalpies of intramolecular hydrogen bonds of o-halophenols. 1553
Faucitano, A. Electron spin resonance study of transient radicals in γ-irradiated organic inclusion compounds. II. Palmitic acid urea clathrate. 801
Faucitano Martinotti, F. Electron spin resonance study of transient radicals in γ-irradiated organic inclusion compounds. II. Palmitic acid urea clathrate 801
Fehlner, T. P. Reactions of borane (BH_3). VII. Reactions with ketene. 3532
Feillolay, A. Solubility of helium and methane in aqueous tetrabutylammonium bromide solutions at 25 and 35°. 3068
Feldberg, S. W. Nuances of the ECE mechanism. IV. Theory of cyclic voltammetry and chronoamperometry and the electrochemical reduction of hexacyanochromate(III). 2439
Feldberg, S. W. Resistive effects in thin electrochemical cells. Digital simulations of electrochemistry in electron spin resonance cells. 2550
Fellner-Feldegg, H. Thin-sample method for the measurement of permeability, permittivity, and conductivity in the frequency and time domain. 2116
Fendler, E. J. Proton magnetic resonance investigation of the environment of aromatic compounds in aqueous zwitterionic micellar solutions. 1460
Fendler, J. H. Proton magnetic resonance investigation of the environment of aromatic compounds in aqueous zwitterionic micellar solutions. 1460
Ferradini, C. Radiolysis of water by tritium β-rays. Scavenging of hydrogen peroxide precursors. 1542
Ferradini, C. Direct effect in the radiolysis of 0.4 M sulfuric acid. 3676
Ferrer, I. J. Synergistic catalysis of ammonium nitrate decomposition. Visible spectra of ammine, chloro, and nitrato complexes of copper, nickel, and cobalt in fused ammonium nitrate. 2844
Fessenden, R. W. Electron spin resonance studies of inorganic radicals in irradiated aqueous solutions. I. Direct observation 1706
Fessenden, R. W. Electron spin resonance studies of inorganic radicals in irradiated aqueous solutions. II. Radical trapping with nitromethane. 1710
Fessenden, R. W. Electron spin resonance study of radicals produced by the reactions of hydrated electrons with unsaturated acids. 1957
Fessenden, R. W. Electron spin resonance spectra of di- and trimethylaminium radicals. 2857
Fessenden, R. W. Electron spin resonance investigation of the reactions in irradiated aqueous solutions of hydrogen cyanide and the cyanide ion. 3945
Field, F. H. Chemical ionization mass spectrometry. XVII. Effect of pressure on the decomposition of protonated tert-amyl acetate. 3917
Field, F. H. Ion-molecule reactions in ethane. 3919
Firestone, R. F. Exchange mechanism and Arrhenius parameters of elementary steps in the reaction of hydrogen atoms with water vapor in irradiated mixtures of hydrogen and water vapor. 621
Fisher, F. H. Ultrasonic absorption in dioxane-water solutions of magnesium sulfate. 1571
Fisher, H. F. Near-infrared spectral studies on the effects of perchlorate and tetrafluoroborate ions on water structure. 84
Fisher, H. J. Near-infrared spectroscopic study of the interactions between water and acetone. Reply to comments. 452
Fisher, J. R. Ion-product constant of water to 350°. 90
Fletcher, A. N. Molecular structure of ethanol-d_1 solutions. Near-infrared study of hydrogen bonding. 2562
Flinn, D. R. Alkali ion mobility and exchange equilibriums in silica glass. 1072
Florence, A. T. Conductivity of sodium chloride and potassium chloride in polymer solutions and the obstruction effect. 1763
Florence, A. T. Aureole profile in bursting soap films. Surface tension and surface relaxation in rapidly compressed monolayers. 3024
Flygare, W. H. Nitrogen-14 nuclear quadrupole coupling and the nitrogen localized electron distribution in diazirine. 2249
Follmer, D. W. Reaction of trifluoromethyl radicals with hexafluoroacetone imine. 487
Foresti, M. L. Influence of specific adsorption of reactant and product upon charge-transfer processes in voltammetry. Tl^{3+}/Tl^{+} couple in 1 M perchloric acid on smooth and platinized platinum. 976
Forsen, S. Barrier to internal rotation in amides. IV. N,N-Dimethylamides. Substituent and solvent effects. 2178
Forsen, S. Ester group. I. Ab initio calculations on methyl formate. 2430
Forsen, S. The ester bond. II. Nuclear magnetic-resonance studies of tert-butyl formate. 3582
Forst, W. Unimolecular rate theory test in thermal reactions. 342
Fox, M. F. Far-ultraviolet solvent spectroscopy. 2703
Frank, H. S. Liquid junction potentials and single-ion activities by computer simulation. I. Concentration cell with transference. 1758
Freed, J. H. Estimating slow-motional rotational correlation times for nitroxides by electron spin resonance. 1858
Freeman, C. G. Mass spectrometric observations on the reaction of hydrogen atoms with iodine cyanide. 1392
Freeman, G. R. Temperature shifts in the optical spectra of solvated electrons in methanol and ethanol. 3876
Freeman, G. R. Free ion yields in γ-irradiated mixed solvents. 944
Frens, G. Aureole profile in bursting soap films. Surface tension and surface relaxation in rapidly compressed monolayers. 3024
Friedman, H. L. Theories of the primitive model of ionic solutions. Comments. 1229
Friedrich, H. B. Infrared spectra and dielectric properties of crystalline hydrogen cyanide. 1140
Friedrich, V. J. Transfer diffusion. III. Kinetics and mechanism of the triiodide-iodide exchange reaction. 162
Friedrich, V. J. Transfer diffusion. IV. Numerical test of the correlation between prototrope mobility and proton exchange rate of H_3O^+ and OH^- ions with water. 2954
Friedrich, V. J. Transfer diffusion. V. Kinetics and mechansim of the exchange reaction between bromide and tribromide ions. 2957
Fripiat, J. J. Proton mobility in solids. IV. Study of proton motion in the decationated Y zeolite by nuclear magnetic resonance. 1220
Fripiat, J. J. Methanol-silica gel system. II. Molecular diffusion and proton exchange from pulse proton magnetic resonance data. 3078
Froehlich, P. M. Alkylbenzene luminescence. 3566
Frost, D. C. Photoelectron spectra of methyl mercaptan, dimethyl sulfide, thiophenol, and α-toluenethiol. Bonding between sulfur and carbon. 1030
Frost, J. J. Chemistry of recoiling silicon atoms. V. Product-forming reactions in phosphine-silane mixtures. 1352
Fu, Y. C. Mass spectrometry study of microwave discharges in hydrogen-carbon monoxide-argon mixtures. 2941
Fuchs, C. Formation of excited singlet states in irradiated aromatic liquids. 3867
Fujimoto, H. Molecular orbital calculation of chemically interacting systems. Bimolecular nucleophilic substitution. 232
Fujimoto, I. Role of added olefins and oxygen in the gas-phase radiolysis of butane. 1260
Fujimoto, T. Energy transfer in thermal methyl isocyanide isomerization. Relative efficiency of mercury atoms. 1935
Fujisaki, N. Role of added olefins and oxygen in the gas-phase radiolysis of butane. 1260
Fujita, Y. Electron spin resonance evidence for the photosensitized dissociation of hydrogen molecules on vanadium oxide. 2637
Fukui, K. Molecular orbital calculation of chemically interacting systems. Bimolecular nucleophilic substitution. 232
Fuller, E. L. Jr. Heats of immersion in the zirconium oxide-water system. 1497
Funabashi, K. Role of low-energy resonances in some elementary processes of radiation chemistry. 2726
Futrell, J. H. Ion-molecule reactions in gaseous acetone. 409
Gabelnick, S. D. Comparison of isotope shifts in the vibrational spectrum of gas-phase and matrix-isolated hydrogen cyanide. 2483
Gafney, H. D. Photosensitized decomposition of hexaamminecobalt(III) by biacetyl and by quinoline. 1105
Gajnos, G. E. Helix-coil transition of poly-γ-benzyl-L-glutamate in the solvent system, 1,3-dichlorotetrafluoroacetone-water. 3464
Gal, D. Sequence studies in liquid-phase hydrocarbon oxidation. I. Alcohol-ke

tone transition in the oxidation of ethylbenzene. 2785

Galanti, A. V. Thermal transitions and phase relations for binary mixtures of cholesteryl esters. 3089

Gale, D. M. Gas-phase thermolysis kinetics of small ring nitriles. 2817

Gallagher, P. K. Comparison of dynamic with isothermal techniques for the study of solid state decomposition kinetics. 1474

Gamba, A. Electronic and electron spin resonance spectra of the anion radicals of phenyl-and diphenylethylenes. 3960

Gambale, F. Formation of dynamic patterns in a fluid layer. 783

Gamer, G. Hydrogen bonding and complex formation of dimethylamine. Infrared investigations on the NH stretching vibration bands. 871

Gammage, R. B. Heats of immersion in the zirconium oxide-water system. 1497

Gann, R. G. Average value of the cross section for $H + HBr \rightarrow H_2 + Br$ over the 0.35-1.7-eV collision energy range. 1321

Gardiner, G. E. Solubility and partial molar properties of helium in water and aqueous sodium chloride from 25 to 100° and 100 to 600 atmospheres. 1195

Garnier, F. Structure effect on the fading rate of photochromic 3-substituted benzothiazolinic spiropyrans. 3554

Gaspar, P. P. Chemistry of recoiling silicon atoms. V. Product-forming reactions in phosphine-silane mixtures. 1352

Gaumann, T. Effect of temperature in the radiolysis of paraffins. 3851

Gaus, H. Ion and isotopic exchange among solids. 1317

Gauthier, M. Photoionization of aromatics in solid solutions. Ionization potential determinations. 2236

Gennaro, G. P. Recoil tritium reactions with hexamethyldisilane in the gas phase. 1249

George, Z. M. Mechanism of hydrogen-deuterium exchange of propylene over a Bronested zeolite catalyst. 3940

Gerace, M. J. Measurement of longitudinal relaxation times for spin-decoupled protons. 1152

Gershfeld, N. L. Physical chemistry of lipid films at the air-water interface. I. Intermolecular energies in single-component lipid films. 1231

Gershfeld, N. L. Physical chemistry of lipid films at the air-water interface. II. Binary lipid mixtures. Principles governing miscibility of lipids in surfaces. 1238

Gershfeld, N. L. Physical chemistry of lipid films at the air-water interface. III. Condensing effect of cholesterol. Critical examination of mixed-film studies. 1244

Gerstmayr, J. W. Photodissociation of nitrogen dioxide by pulsed laser light at 6943 Ang. 474

Gianni, P. Kinetic study of the hydration reaction of 2-, 3-, and 4-pyridinecarboxaldehyde. 2959

Giauque, W. F. Relation of crystalline forms I, III, IV, and V of anhydrous sodium sulfate as determined by the third law of thermodynamics. 737

Gibb, T. R. P. Jr. X-ray diffraction investigation of the vanadium-deuterium system. 927

Gibbons, R. M. Approximate equation of state. II. Simplified form for the Barker-Henderson theory. 1479

Giguere, P. A. Alleged resolution of an infrared bank of HDO. 3675

Gilbert, B. C. Theoretical study of hyperfine coupling constants of some σ radicals based on the INDO [intermediate neglect of differential overlap] method. 553

Gill, S. J. Calorimetric study of association of diketopiperazine in water. 3065

Gilles, L. Pulsed radiolysis and flash photolysis of iodates in aqueous solution. 302

Gilles, P. W. High molecular weight boron sulfides. VIII. Vapor pressures of $B_2S_3(g)$ and $B_4S_6(g)$ over stoichiometric B_2S_3. 2035

Gillis, H. A. Spectral shifts of trapped electrons in alkane glasses at 76°K. 3847

Gingerich, K. A. Mass spectrometric determination of the bond dissociation energies of the molecules cerium-palladium and cerium dicarbide. 2332

Gingerich, K. A. Gaseous phosphorus compounds. VIII. Thermodynamic study of antimony monophosphide with a mass spectrometer. 2336

Giomini, C. Adsorption behavior of tetraphenylborate anions at a mercury electrode. 707

Glasgow, L. C. Ethylene as an actinometer in the wavelength region 147-185 nanometers. 138

Gleria, M. Sensitization and quenching of the cis → trans isomerization of bis(glycinato)platinum(II). 3934

Gliozzi, A. Formation of dynamic patterns in a fluid layer. 783

Gloss, R. A. Structural investigations of calcium binding molecules. I. Crystal and molecular structures of ethane-1-hydroxy-1,1-diphosphonic acid monohydrate, $C(CH_3)(OH)(PO_3H_2)_2 \cdot H_2O$. 1298

Goitein, R. Effect of transfer from water to 1.0 M water in dimethyl sulfoxide on the reaction of nucleophiles with phenyl esters. 432

Goldberg, I. B. Resistive effects in thin electrochemical cells. Digital simulations of electrochemistry in electron spin resonance cells. 2550

Goldberg, M. Kinetics of defect and radiolytic product formation in single crystal sodium bromate determined from color-center measurements. 3751

Goldberg, R. N. Liquid junction potentials and single-ion activities by computer simulation. I. Concentration cell with transference. 1758

Golden, D. M. Bond dissociation energy of the carbon-hydrogen bond in ethanol. Kinetic study of the reaction iodine + ethanol. 3314

Goldman, S. A. Estimating slow-motional rotational correlation times for nitroxides by electron spin resonance. 1858

Goldstein, J. H. High-resolution carbon-13 nuclear magnetic resonance spectra and substituent effects for monohalobenzenes. 515

Goldstein, J. H. Steric interactions in tert-butylethylenes observed through proton carbon-13 satellite spectra. 2877

Goldstein, J. R. Kinetics of oxygen reduction on graphite/cobalt-iron oxide electrodes with coupled heterogeneous chemical decomposition of hydrogen peroxide. 3646

Golub, S. L. Ultrasonic shear wave study of the mechanical properties of a nematic liquid crystal. 2409

Gomez, A. Specific interactions of anilines with water. 4011

Goodman, R. Thermodynamic stability of perylene-iodine charge-transfer complexes from measurements of iodine vapor absorption. 921

Gopinathan, C. γ-Ray irradiated sodium chloride as a source of hydrated electrons. 3694

Gopinathan, C. Fluorescence of the uranyl ion in electron-irradiated sulfuric acid solutions. 3698

Gordon, S. Reaction of cyanogen radicals with ammonia. 1931

Gorse, R. A. Rate constant for the reaction of HO_2 with carbon monoxide. 3301

Goyal, R. D. Magnetochemical studies on diphenyldialkoxysilanes. 1579

Graceffa, P. Solvent effect on metal hyperfine constants in alkali metal radical anion ion pairs. 2866

Grand, D. Photoionization of aromatics in solid solutions. Ionization potential determinations. 2236

Grant, D. M. Carbon-13 nuclear magnetic resonance relaxation in hemimellitene and isodurene. 281

Grant, D. M. Influence of internal motion on the carbon-13 relaxation times of methyl carbons. 3213

Gray, D. Photochemistry of trifluoromethylbenzenes. III. 1,4-Bis(trifluoromethyl)benzene. 823

Gray, D. Reaction of hydrogen peroxide with nitrogen dioxide and nitric oxide. 1919

Greatorex, D. Solute radical cation yields in the pulse radiolysis of solutions of aromatic amines in chlorinated hydrocarbons. 20

Greenler, R. G. Infrared spectra of the oxides and carbonates of silver. 940

Gregory, N. W. Vapor-phase absorbance and thermodynamic properties of cuprous chloride and cuprous bromide. 1632

Gregory, N. W. Mass spectrometric study of the vaporization of cuprous bromide. 3271

Grellmann, K. H. Electron-transfer mechanism of fluorescence quenching in polar solvents. I. Dicyanobenzene as quencher. 469

Grellmann, K. H. Electron transfer mechanism of fluorescence quenching in polar solvents. II. Tetracyanoethylene and tetracyanobenzene as quenchers. 3132

Griffith, O. H. Electron spin resonance of x-irradiated heptanal trapped in a single crystal of perhydrotriphenylene. 1008

Griffith, O. H. Electron spin resonance study of x-irradiated heptanal oxime trapped in a urea inclusion crystal. Evidence of a bimolecular reaction product. 1819

Grimley, R. T. Study of ionization processes by the angular distribution technique. Silver cloride system. 2819

Grossman, G. Ion transport through layered ion exchange membranes. 3996

Growcock, F. B. Kinetics of vibrationally hot propane produced by methylene insertion into ethane. 607

Grunwald, E. Solvation and self-association of water in propylene carbonate. 855

Grushka, E. Chromatographic peak shapes. Their origin and dependence on the experimental parameters. 2586

Gubbins, K. E. Partial molal volumes of gases dissolved in electrolyte solutions. 3044

Guesten, H. Conductance of an intermolecular charge-transfer complex within an ion pair. 2452

Guglielmetti, R. Structure effect on the fading rate of photochromic 3-substituted benzothiazolinic spiropyrans. 3554

Guglielminotti, E. Infrared study of surface properties of α-chromia. IV. Pyridine and heavy water adsorption on oxygen-covered surface. 571

Guidelli, R. Influence of specific adsorption of reactant and product upon charge-transfer processes in voltammetry. Tl^{3+}/Tl^{+} couple in 1 M perchloric acid on smooth and platinized platinum. 976

Gunning, H. E. Rate constants for the reactions of deuterium atoms with silanes. 3911

Gupta, R. R. Magnetochemical studies on diphenyldialkoxysilanes. 1579

Haas, Y. Radiative and nonradiative pathways in solutions. Excited states of the europium(III) ion. 1093

Haas, Y. Nuclear magnetic resonance study of the solvation of europium(III) ions in water-acetonitrile mixtures. 1449

Habgood, H. W. Mechanism of hydrogen-deuterium exchange of propylene over a Bronested zeolite catalyst. 3940

Hackman, E. E. III. Detection of species resulting from condensed phase decomposition of ammonium perchlorate. 3545

Hadley, S. G. Triplet ← triplet absorption and intersystem crossing in phthalazine. 3937

Hagler, A. T. Structure of liquid water. Statistical thermodynamic theory. 3229

Haissinsky, M. γ Radiolysis of xenon trioxide in aqueous solution. 3909

Hale, C. F. Thermodynamics of the association of aqueous europium(III) and sulfate ions. 1887

Hale, C. F. Effect of high pressure on the formation of aqueous $EuSO_4^{+}$ at 25°. 2925

Halko, D. J. Kinetic study of the monomer-dimer equilibrium in aqueous vanadium(IV) tetrasulfophthalocyanine solutions. 2343

Hall, C. Ultrasonic relaxation in calcium nitrate tetrahydrate melts. 1506

Hall, H. K. Jr. Gas-phase thermolysis kinetics of small ring nitriles. 2817

Haller, G. L. Catalytic hydrogenation of propylene. Verification of maximum rate. 943

Hamill, W. H. Chemical effects due to low-energy electron impact on thin films of cyclohexane and n-hexane at 77°K. 1255

Hamlet, P. Paramagnetic relaxation study of spatial distribution of trapped radicals in γ-irradiated alkaline ice and organic glasses at 4.2°K. 1226

Hanazaki, I. Vapor-phase electron donor-acceptor complexes of tetracyanoethylene and of sulfur dioxide. 1982

Hand, C. W. Mass spectrometric study of the reaction of dicyanoacetylene with oxygen atoms. 269

Hand, C. W. Mass spectrometric study of the reaction of dicyanoacetylene with active nitrogen. 2643
Hanley, H. J. M. Application of the m-6-8 potential to simple gases. 1743
Hanna, M. W. Electron paramagnetic resonance line widths of vanadyl(IV) α-hydroxycarboxylates. 3951
Hanrahan, R. J. Radiation chemistry of carbon tetrafluoride-carbon tetrachloride mixtures in the gas phase. 3734
Hansen, R. S. Promoted adsorption of pyridine on nickel. 972
Hardcastle, K. I. X-ray diffraction investigation of the vanadium-deuterium system. 927
Hare, C. R. Molecular orbital theory of the diatomic molecules of the first row transition metals. 2268
Harriman, J. E. Electron spin resonance spectra of zwitterion radicals and isoelectronic anion radicals. 2479
Harris, H. H. Two familiar gas reactions at suprahigh pressure. 2614
Harris, R. K. Carbon-13 nuclear magnetic resonance relaxation in hemimellitene and isodurene. 281
Hart, E. J. γ-Ray irradiated sodium chloride as a source of hydrated electrons. 3694
Hart, E. J. Fluorescence of the uranyl ion in electron-irradiated sulfuric acid solutions. 3698
Hart, E. J. Radiolysis of aqueous methane solutions. 3863
Harteck, P. Photodissociation of nitrogen dioxide by pulsed laser light at 6943 Ang. 474
Hartley, P. J. Raman spectra and structure of molten cadmium chloride, molten cadmium bromide, and their molten mixtures with alkali metal halides. 1831
Harvey, D. J. Chemical ionization mass spectrometry using tetramethylsilane. 3217
Harvey, S. C. Dielectric relaxation spectra of water adsorbed on lysozyme. 2987
Hase, H. Electronic spectra of trapped electrons in organic glasses at 4°K. III. Effect of an electron scavenger in ethanol. 3744
Hase, W. L. Kinetic study of the reaction of methylene radicals with dimethylsilane. Decomposition of chemically activated trimethylsilane and methylethylsilane. 459
Hase, W. L. Kinetics of vibrationally hot propane produced by methylene insertion into ethane. 607
Haslam, J. L. Calculation of rate constants from relaxation spectra of enzyme reactions. 366
Hatano, H. Free-radical intermediates in the reaction of the hydroxyl radical with dialkyl sulfoxides. 135
Hatano, Y. Role of added olefins and oxygen in the gas-phase radiolysis of butane. 1260
Hatfield, W. E. Magnetic properties of three copper(II) complexes of 2-(2-aminoethyl)pyridine. 2707
Hatfield, W. E. Preparation and structure of bromobis(2-(2-aminoethyl)pyridine)copper(II) bromide. 2887
Hathaway, E. J. Structural studies of stannous chloride-potassium chloride melts by Raman spectroscopy. 2796
Hato, M. Physicochemical properties of aqueous solutions of fluorinated surfactants. 909
Hautojarvi, P. Effect of charge-transfer complex formation on the positronium-iodine reaction. 1951
Hawranek, J. P. Infrared spectra and dipole moments of hydrogen-bonded complexes. III. Adducts of 2,6-dichloro-4-nitrophenol with pyridine bases. 2112
Hayashi, K. Photoinduced ionic dissociation of tetracyanobenzene-α-methylstyrene complex. 1419
Hayashi, K. Dissociative electron attachment to dimethyl ether in irradiated 3-methylpentane glass. 3747
Hayashi, T. Physicochemical properties of aqueous solutions of fluorinated surfactants. 909
Hayes, D. M. Potential energy surface for the addition of benzyne to ethylene. 656
Hayes, D. M. Potential surfaces for the addition of methylene and difluoromethylene to ethylene and isobutene. 664
Hayon, E. Electron and hydrogen atom attachment to aromatic carbonyl compounds in aqueous solution. Absorption spectra and dissociation constants of ketyl radicals. 2072
Hayon, E. Far-ultraviolet solvent spectroscopy. 2703
Hayon, E. Ketyl radicals of benzoylpyridines. 3200
Hayon, E. pK_a of the $^+H_3NCHCOOH$ radical. 3507
Hegazi, M. Spontaneous and general base-catalyzed iodination of pyruvic acid and alkyl pyruvates. Activation parameters and solvent deuterium isotope effects. 3121
Heicklen, J. Bromine atom catalyzed oxidation of carbon monoxide. 1416
Heicklen, J. Reaction of hydrogen peroxide with nitrogen dioxide and nitric oxide. 1919
Heicklen, J. Vapor-phase thermal decomposition of some simple ozonides. 2659
Heisel, F. Formation of excited singlet states in irradiated aromatic liquids. 3867
Heitz, C. γ Radiolysis of xenon trioxide in aqueous solution. 3909
Held, E. Coordination of fluoride and chloride anions with alcohol and phenol. 1775
Heller, W. Determination of the partial specific volume of macromolecular solutes from light scattering. 2437
Hemmaplardh, B. Solubility of methanol in compressed nitrogen, argon, methane, ethylene, ethane, carbon dioxide, and nitrous oxide. Evidence for association of carbon dioxide with methanol in the gas phase. 2170
Hemmes, P. Volume changes of ionic association reactions. 895
Hemphill, G. L. Photochemistry of ethanethiol at 254 and 214 nm. 2668
Henderson, G. H. Kinetics of acid dissociation-ion recombination of aqueous methyl orange. 4023
Henglein, A. Reactive and elastic scattering of ions on molecules. 3883
Hennessy, J. Photochemistry of phenylimidazoles. 3362
Hentz, R. R. Optical absorption of solvated electrons in alcohols an their mixtures with alkanes. 2931
Hentz, R. R. Dealkylation of isopropylbenzene on γ-irradiated silica-alumina. Effect of various reagents on the active centers and on their yield. 3741
Hepfinger, N. F. Nuclear magnetic resonance study of acid-base interactions for the chloranil electrode system in acetonitrile. 246
Hepler, L. G. Molecular association of hydrogen bonding solutes. Phenol in cyclohexane and benzene. 3058
Herak, J. N. Electron spin resonance study of γ-irradiated single crystal of ammonium oxalate monohydrate. 3274
Herley, P. J. Kinetics of defect and radiolytic product formation in single crystal sodium bromate determined from color-center measurements. 3751
Hermann, R. B. Theory of hydrophobic bonding. II. Correlation of hydrocarbon solubility in water with solvent cavity surface area. 2754
Herring, F. G. Photoelectron spectra of methyl mercaptan, dimethyl sulfide, thiophenol, and α-toluenethiol. Bonding between sulfur and carbon. 1030
Herron, J. T. Absolute rate constants for the reaction $O + O_2 + M \rightarrow O_3 + M$ over the temperature range 200-346°K. 2653
Herron, J. T. Absolute rate constants for the addition and abstraction reactions of atomic oxygen with 1-butene over the temperature range 190-491°K. 3311
Hersh, L. S. Bronsted acid sites on porous glass from membrane potentials. 3633
Hertzberg, M. Bisdifluoraminoalkanes. Mass spectral decomposition of isomeric propanes. 60
Hesser, H. H. Detection of species resulting from condensed phase decomposition of ammonium perchlorate. 3545
Hickel, B. Pulsed radiolysis and flash photolysis of iodates in aqueous solution. 302
Higashimura, T. Electronic spectra of trapped electrons in organic glasses at 4°K. III. Effect of an electron scavenger in ethanol. 3744
Hilden, D. L. Vapor-phase absorbance and thermodynamic properties of cuprous chloride and cuprous bromide. 1632
Hill, K. L. Vacuum-ultraviolet photolysis of the C_4H_6 isomers. IV. 1-Butyne. 1112
Hill, K. L. Vacuum-ultraviolet photolysis of the C_4H_6 isomers. V. Methylenecyclopropane. 3153
Hisatsune, I. C. Vapor-phase thermal decomposition of some simple ozonides. 2659
Hodgson, D. J. Magnetic properties of three copper(II) complexes of 2-(2-aminoethyl)pyridine. 2707
Hodgson, D. J. Preparation and structure of bromobis(2-(2-aminoethyl)pyridine)copper(II) bromide. 2887
Hoekstra, P. Dielectric relaxation spectra of water adsorbed on lysozyme. 2987
Hoffer, E. Hyperfiltration in charged membranes. Prediction of salt rejection from equilibrium measurements. 3638
Hoffman, B. M. Paramagnetism and semiconductivity in doped charge-transfer complexes. 1849
Hoffman, M. Z. Electron spin resonance and pulse radiolysis studies of the reactions of OH and O^- radicals with aromatic and olefinic compounds. 847
Hoffman, M. Z. Acid-base properties of the radicals produced in the pulse radiolysis of aqueous solutions of benzoic acid. 1398
Hoffman, M. Z. Ultraviolet photochemistry of formatopentaamminecobalt(III) ion in aqueous solution. Hydrogen atom formation and oxygen → carbon linkage isomerization. 2492
Hoffman, S. J. Factors influencing reverse osmosis rejection of organic solutes from aqueous solution. 4006
Hoffmann, R. Potential energy surface for the addition of benzyne to ethylene. 656
Hoffmann, R. Potential surfaces for the addition of methylene and difluoromethylene to ethylene and isobutene. 664
Hogen Esch, T. E. Ion-pair aggregation in solutions of complexes of carbanion salts and macrocyclic polyethers. 2152
Holden, J. R. Crystal structure of 2,4,6-trinitroaniline. 3597
Holmes, H. F. Heats of immersion in the zirconium oxide-water system. 1497
Holroyd, R. A. Yields and reactions of lowest excited singlet and triplet states in the radiolysis of naphthalene and 1-methylnaphthalene. 2485
Holroyd, R. A. Ranges of photoinjected electrons in dielectric liquids. 3794
Holten, J. D. III. Chemistry of recoiling silicon atoms. V. Product-forming reactions in phosphine-silane mixtures. 1352
Honda, K. Electric conduction of the aluminum-auramine-stannic oxide system. 1655
Hong, K-Y. Reactions of photochemically produced hydrogen atoms at energies below 1.8 electron volts. 3337
Honig, D. S. Relaxation spectra of molybdate polymers in aqueous solution. Ultrasonic attenuation. 1575
Hoover, J. W. Photochemical production of hot hydrogen and deuterium atoms. Reactions with hydrogen halides and halogens. 2801
Hopkins, H. P. Jr. Thermodynamics of acid-base equilibriums. II. Ionization of m- and p-hydroxybenzotrifluoride and the concept of fluorine double bond-no bond resonance. 1909
Horgan, G. P. Mass spectrometric observations on the reaction of hydrogen atoms with iodine cyanide. 1392
Hove, M. J. Paramagnetism and semiconductivity in doped charge-transfer complexes. 1849
Howat, G. Stabilized cluster. Molecular model for the solvated electron. 3714
Howery, D. G. Proton magnetic resonance studies of the structure of water in Dowex 50W. 578
Howlett, G. J. Effects of pressure and thermodynamic nonideality on the sedimentation equilibrium of chemically reacting systems. Results with lysozyme at pH 6.7 and 8.0. 777
Howlett, G. J. Overspeeding technique in relation to sedimentation equilibrium. 2740
Howlett, G. J. Effect of charge in the sedimentation equilibrium of polymerizing protein systems. 3429

Hsu, C. C. Significant structure liquid theory of the alkali metals over the normal melting to boiling range. 1612

Huang, C. Resolution of components of the optical rotation tensor of collagen. 2935

Huang, J-T. J. Triplet formation in ion recombination in spurs. 3801

Huang, T. Temperature dependence of the drift mobility of electrons in glassy 10 M sodium hydroxide ice. 1509

Hubble, B. R. Effects of high-pressure hydrogen chloride on transport properties of the molten 46 mole % potassium chloride-54 mole % zinc chloride eutectic system. 904

Huber, J. R. Temperature effects in the intersystem crossing process of anthracene. 1524

Hudson, R. A. Hydrogen-bonded complex-ion-pair equilibriums in 3,4-dinitrophenol-amine-aprotic solvent systems. 1989

Huie, R. E. Absolute rate constants for the reaction $O + O_2 + M \rightarrow O_3 + M$ over the temperature range 200-346°K. 2653

Huie, R. E. Absolute rate constants for the addition and abstraction reactions of atomic oxygen with 1-butene over the temperature range 190-491°K. 3311

Hull, L. A. Vapor-phase thermal decomposition of some simple ozonides. 2659

Huron, M. J. Calculation of the interaction energy of one molecule with its whole surrounding. I. Method and application to pure nonpolar compounds. 2123

Huyskens, P. Specific interactions of anilines with water. 4011

Hyde, J. S. Powder ENDOR [electron nuclear double resonance] line shapes. Nuclear relaxation induced by motion of nearby electron spins. 2079

Hyde, J. S. Proton ENDOR [electron nuclear double resonance] of γ-irradiated Y-type zeolites. 2087

Ibata, T. Electron and hydrogen atom attachment to aromatic carbonyl compounds in aqueous solution. Absorption spectra and dissociation constants of ketyl radicals. 2072

Ichikawa, M. Identification of reaction intermediates by microwave spectroscopy. Catalytic reactions between propylene and deuterium over zinc oxide. 2184

Imamura, M. Pulse radiolysis study of dimer cation formation of aromatic hydrocarbons in benzonitrile solution. 1119

Inada, K. Electron spin resonance study of the far-ultraviolet photolysis of some inorganic and organic compounds. 2061

Infelta, P. P. Competitive electron-scavenging experiments in the radiolysis of hydrocarbons. Kinetics of the reactions of secondary ions. 987

Infelta, P. P. Lifetime distribution function for geminate ion pairs and its importance to the kinetics of ionic reactions in the radiolysis of hydrocarbon solutions. 3812

Ingham, K. C. Role of nonbonded intramolecular forces in barriers to internal rotation in molecules with two equivalent methyl groups. 551

Ingold, K. U. Alkylperoxy radical stabilization by cobalt ions. 1385

Ingram, M. D. Ionic-covalent interactions and glass formation in molten acetates. Cobalt(II) as a spectroscopic probe. 1035

Ionescu, L. G. Interaction of leghemoglobin with nitrogen and with xenon. 591

Irie, M. Photoinduced ionic dissociation of tetracyanobenzene-α-methylstyrene complex. 1419

Irie, M. Dissociative electron attachment to dimethyl ether in irradiated 3-methylpentane glass. 3747

Isa, S. A. Oxidation of metal films by nitrous oxide. 2530

Ishida, N. Effective fixed charge density governing membrane phenomena. IV. Further study of activity coefficients and mobilities of small ions in charged membranes. 2447

Ivanoff, N. Mercury sensitization of the isomerization of diazines. 2245

Iwasaki, M. Electron spin resonance evidence for the carbon-fluorine bond rupture by dissociative electron attachment. 1824

Iwata, S. Electronic absorption spectra of excess electrons in molecular aggregates. I. Trapped electrons in γ-irradiated amorphous solids at 77°K. 3683

Iwata, S. Electronic absorption spectra of excess electrons in molecular aggregates. II. Solvated electrons. 3691

Jacazio, G. Electrokinetic salt rejection in hyperfiltration through porous materials. Theory and experiment. 4015

Jacimovic, Lj. Kinetics of adsorption of mineral acids on alumina. 3625

Jacobs, P. A. Identification of the A-type hydroxyls on silica surfaces. 1434

Jacobs, P. W. M. Gas-phase reaction of perchloric acid with methane. 1795

Jakli, G. Vapor pressure isotope effect in aqueous systems. I. Water-water-d_2 (-64° to 100°) and water-water^{18}-0 (-17° to 16°). Ice and liquid. II. Alkali metal chloride solution in water and water-d^2 (-5° to 100°). 743

Jamieson, R. A. Electroanalytical measurements of flash-photolyzed ferrioxalate. 830

Janata, J. Oxidation pathways of 2 2′-benzothiazolinone azines. I. Electrochemistry. 1178

Jancso, G. Vapor pressure isotope effect in aqueous systems. I. Water-water-d_2 (-64° to 100°) and water-water^{18}-0 (-17° to 16°). Ice and liquid. II. Alkali metal chloride solution in water and water-d^2 (-5° to 100°). 743

Janzen, E. G. ESR studies of thermal decomposition mechanisms. II. Electron spin resonance study of the SO_2^- formation in the thermal decomposition of sodium dithionite, sodium and potassium metabisulfite, and sodium hydrogen sulfite. 157

Janzen, E. G. Detection of the triphenylmethyl radical by electron spin resonance in the thermal decomposition of sodium triphenylacetate. 937

Janzen, E. G. Detection and identification of gas phase free radicals by electron spin resonance spin trapping. 2056

Jao, L. Nuclear magnetic resonance studies of methanol-boron trifuloride complexes. 329

Japar, S. M. Path of triplet excitation energy in simple carbonyl-monoolefins system in the liquid phase. 478

Jeffers, P. M. Shock tube cis-trans isomerization studies. II. 2829

Jeffrey, P. D. Effects of pressure and thermodynamic nonideality on the sedimentation equilibrium of chemically reacting systems. Results with lysozyme at pH 6.7 and 8.0. 777

Jeffrey, P. D. Effect of charge in the sedimentation equilibrium of polymerizing protein systems. 3429

Jeftic, L. Nuances of the ECE mechanism. IV. Theory of cyclic voltammetry and chronoamperometry and the electrochemical reduction of hexacyanochromate(III) 2439

Jensen, C. H. Anion exchange in aqueous-organic solvent mixtures. II. 1040

Jensen, R. J. Hydrogen chloride chemical laser from hydrogen atom-chlorine azide reaction. 805

Jeter, D. Y. Magnetic properties of three copper(II) complexes of 2-(2-aminoethyl)pyridine. 2707

Jha, K. N. Temperature shifts in the optical spectra of solvated electrons in methanol and ethanol. 3876

Johns, H. E. Photoreactions in aqueous solutions of thymine, pH 12. 489

Johnson, C. S. Jr. Quasi-elastic light scattering from two-component mixtures 2744

Johnson, D. W. Jr. Comparison of dynamic with isothermal techniques for the study of solid state decomposition kinetics. 1474

Joppien, G. R. Chemical reactions on γ-irradiated silica gel and porous Vycor glass. 3158

Jortner, J. Thermodynamic properties of hydrated and ammoniated electrons. 683

Joyce, T. E. Mass spectrometric study of the vaporization of cuprous iodide. 2310

Kadoi, H. Studies of transition phenomena of some organic solids by electrical conductivity measurement at low temperature. 115

Kadoi, H. Transition phenomena of some organic solids by electrical conductivity measurement at low temperature. Reply to the comment. 2799

Kainz, C. Thermodynamics of the acetic acid-triethylamine system. 2764

Kajiwara, T. Role of low-energy resonances in some elementary processes of radiation chemistry. 2726

Kajiwara, T. Reactions of electrons in glycerol. 1700

Kamo, N. Effective fixed charge density governing membrane phenomena. IV. Further study of activity coefficients and mobilities of small ions in charged membranes. 2447

Kantrowitz, E. R. Ultraviolet photochemistry of formatopentaamminecobalt(III) ion in aqueous solution. Hydrogen atom formation and oxygen → carbon linkage isomerization. 2492

Kapoor, R. C. Oxidation kinetics of 2-dimethylaminoethanethiol hydrochloride by ferricyanide ion in acid medium. 3641

Karasz, F. E. Helix-coil transition of poly-γ-benzyl-L-glutamate in the solvent system, 1,3-dichlorotetrafluoroacetone-water. 3464

Karger, B. L. Adsorption isotherms and equations of state of insoluble vapors at the water-gas interface as studied by gas chromatography. 2769

Katrib, A. Photoelectron spectra of methyl mercaptan, dimethyl sulfide, thiophenol, and α-toluenethiol. Bonding between sulfur and carbon. 1030

Katsu, T. Electron spin resonance evidence for the photosensitized dissociation of hydrogen molecules on vanadium oxide. 2637

Katsumata, S. Visible-light effects on electronic absorption bands of some cation radicals produced by photoionization at 77°K. 639

Katz, S. Medium effects of urea and guanidine hydrochloride on the volume changes produced by protonation of carboxylate groups. 2778

Kaufman, B. Additivity in the carbon-13 chemical shifts of 1,2-disubstituted ethanes. 1466

Kaufman, M. J. Chemiluminescence excited by atomic fluorine. 3586

Kaufman, M. J. Molecular beam analysis investigation of the reaction between atomic fluorine and carbon tetrachloride. 947

Kedem, O. Hyperfiltration in charged membranes. Prediction of salt rejection from equilibrium measurements. 3638

Keenan, A. G. Synergistic catalysis of ammonium nitrate decomposition. Visible spectra of ammine, chloro, and nitrato complexes of copper, nickel, and cobalt in fused ammonium nitrate. 2844

Kelly, T. L. Ligand field photochemistry of halopentaamminerhodium(III) complexes. 1937

Kemp, T. J. Solute radical cation yields in the pulse radiolysis of solutions of aromatic amines in chlorinated hydrocarbons. 20

Kempter, V. Ionic reactions in monosilane. Radiation chemistry implications. 3321

Kenjo, T. Anion exchange in aqueous-organic solvent mixtures. II. 1040

Kenjo, T. Coordination of fluoride and chloride anions with alcohol and phenol. 1775

Kenjo, T. Hydration of perchlorate, tetraphenylboride, and nitrate ions in some organic solvents. 2454

Kennedy, R. C. Bistrifluoromethyl peroxide. II. Kinetics of the decomposition to carbonyl fluoride and trifluoromethyl hypofluorite. 3480

Kenney-Wallace, G. Optical absorption of solvated electrons in alcohols an their mixtures with alkanes. 2931

Kern, R. D. Reaction of hydrogen cyanide and deuterium behind reflected shock waves. 285

Kern, R. D. Exchange reaction of methane-d_4 with hydrogen chloride. 2809

Kerr, C. M. L. Electron spin resonance evidence for dissociative electron capture in γ-irradiated phosphate esters. 2848

Kerr, C. M. L. Investigation of the structure of the hydrated electron based on unpaired electron densities calculated by the INDO [intermediated neglect of differential overlap] method. 3838

Kester, D. R. Sodium and magnesium sulfate ion pairing. Evidence from Raman spectroscopy. 3664

Kestner, N. R. Higher excited states in metal-ammonia solutions. I. The 2s state. 2738

Kevan, L. Optical bleaching effects on the paramagnetic relaxation of trapped electrons in methyltetrahydrofuran at 77°K. 636
Kevan, L. Paramagnetic relaxation study of spatial distribution of trapped radicals in γ-irradiated alkaline ice and organic glasses at 4.2°K. 1226
Kevan, L. Temperature dependence of the drift mobility of electrons in glassy 10 M sodium hydroxide ice. 1509
Kevan, L. Thermally stimulated conductivity of γ-irradiated triethylamine and 3-methylpentane glasses. 2781
Kevan, L. Energy level structure and mobilities of excess electrons in aqueous and organic glasses. 3830
Kim, K. C. Rate constants, threshold energies, and energy partitioning for three and four centered hydrogen chloride elimination reactions of 1,1,2-trichloroethane-1-d_1. 283
Kimura, K. Visible-light effects on electronic absorption bands of some cation radicals produced by photoionization at 77°K. 639
Kimura, K. Electronic absorption studies of the radical complex between perylene and tetracene cations. 1549
Kinell, P. O. Electron spin resonance studies on irradiated heterogeneous systems. VIII. Radical cation formation from toluene. 1721
King, A. D. Jr. Solubility of methanol in compressed nitrogen, argon, methane, ethylene, ethane, carbon dioxide, and nitrous oxide. Evidence for association of carbon dioxide with methanol in the gas phase. 2170
King, J. W. Adsorption isotherms and equations of state of insoluble vapors at the water-gas interface as studied by gas chromatography. 2769
Kira, A. Pulse radiolysis study of dimer cation formation of aromatic hydrocarbons in benzonitrile solution. 1119
Kirowa-Eisner, E. Catalytic polarographic current of a metal complex. VIII. Effect of weakly complexing supporting electrolytes. 1170
Kishimoto, S. Catalytic activity of cold-worked and quenched gold for the decomposition of hydrogen peroxide. 1907
Kispert, L. D. Irradiated single crystal clathrate of Dianin's compound and 1,2-dibromo-1,1-difluoroethane. Electron spin resonance observation of the Br_2^- radical. 133
Kitajima, S. Diffusion in mixed solvents. III. Iodine in nonpolar solutions. Evidence for charge-transfer interaction. 2470
Klasinc, L. Conductance of an intermolecular charge-transfer complex within an ion pair. 2452
Klassen, N. V. Spectral shifts of trapped electrons in alkane glasses at 76°K. 3847
Klein, M. Application of the m-6-8 potential to simple gases. 1743
Kludt, J. R. Far-infrared spectra of tertiary ammonium salts. 339
Ko, H. C. Solvent effects in organic chemistry. XIV. Solvation of sodium salts in glycerol acetate binaries by sodium-23 nuclear magnetic resonance spectroscopy and thermodynamics. 2474
Kobatake, Y. Effective fixed charge density governing membrane phenomena. IV. Further study of activity coefficients and mobilities of small ions in charged membranes. 2447
Kobrinsky, P. C. Half-quenching pressures in the association of methyl radicals-d_0 and -d_3. 2196
Koehler, W. H. Raman scattering in sodium-liquid ammonia solutions. 2481
Kohler, F. Thermodynamics of the acetic acid-triethylamine system. 2764
Kohn, B. H. Proton magnetic resonance studies of the structure of water in Dowex 50W. 578
Koide, G. T. Dielectric properties of quaternary ammonium salt hydrates. 1999
Kolb, C. E. Molecular beam analysis investigation of the reaction between atomic fluorine and carbon tetrachloride. 947
Kolthoff, I. M. Critical study involving water, methanol, acetonitrile, N,N-dimethylformamide, and dimethyl sulfoxide of medium ion activity coefficients, γ, on the basis of the $\gamma_{AsPh_4^+} = \gamma_{BPh_4^-}$ assumption. 2024
Komatsu, T. Electron spin resonance studies on irradiated heterogeneous systems. VIII. Radical cation formation from toluene. 1721
Komatsu, T. Electron spin resonance studies on irradiated heterogeneous systems. IX. Anisotropy of the g factor and the hyperfine coupling constant of the benzene cation in the adsorbed state. 1727
Kominami, S. Radical cation produced in a γ-irradiated single crystal of DL-methionine as studied by electron spin resonance and optical absorption spectroscopy. 1729
Kondo, T. Identification of reaction intermediates by microwave spectroscopy. Catalytic reactions between propylene and deuterium over zinc oxide. 2184
Kongshaug, M. Reactivities of solvated electrons in ethylene glycol-water glass. 2217
Koob, R. D. Methylene produced by vacuum-ultraviolet photolysis. IV. Energy distribution for the reaction $C_3H_8+h\nu$ (123.6 nm) = $CH_2+C_2H_6$. 9
Kordis, J. Gaseous phosphorus compounds. VIII. Thermodynamic study of antimony monophosphide with a mass spectrometer. 2336
Koren, R. Kinetics of the hydrolysis of the dichromate ion. VI. Environmental influences on the acid-catalyzed reaction 582
Kotake, Y. Electron spin resonance study of the far-ultraviolet photolysis of some inorganic and organic compounds. 2061
Kouvarellis, G. K. Dielectric evidence of two-dimensional condensation of halides adsorbed on nonporous sodium chloride. 2535
Krause, P. F. Infrared spectra and dielectric properties of crystalline hydrogen cyanide. 1140
Kreevoy, M. M. Isotope effects in proton transfer from general acids to carbon bases. 2951
Ku, J. S. Rice-Allnatt transport theory. 2133
Kubin, R. F. Second virial coefficients for the polar species in steam. 2901
Kuck, V. J. Electron spin resonance of triplet nitrenes from aryl isocyanates. 3570
Kuder, J. E. Electronic structure of furanquinones. II. Emission spectra of dinaphtho[2,1:2′,3′]furan-8,13-dione and dinaphtho[1,2:2′,3′]furan-7,12-dione. 2240
Kuhlmann, K. F. Measurement of longitudinal relaxation times for spin-decoupled protons. 1152
Kuitu, L. Comparison of stabilization energy and resonance energy as a measure of the delocalization energy in free radicals. 918
Kukura, M. Radioisotope determination of the surface concentrations of calcium and phosphorus on hydroxylapatite in aqueous solution. 900
Kulevsky, N. Thermodynamics of hydrogen bond formation between phenol and some diazine N-oxides. 3502
Kuroda, Y. Raman spectra and structure of molten cadmium chloride, molten cadmium bromide, and their molten mixtures with alkali metal halides. 1831
Kurylo, M. J. Absolute rate constants for the reaction $H + O_2 + M \rightarrow HO_2 + M$ over the temperature range 203-404°K. 3518
Kushner, R. Temperature dependence of the reaction yields from recoil tritium reactions. II. Tritium atom addition to 1-butene and cis-2-butene. 190
Kustin, K. Relaxation spectra of molybdate polymers in aqueous solution. Ultrasonic attenuation. 1575
Kustin, K. Ultrasonic attenuation in basic purine solutions. 2838
Kutal, C. Reactions of coordination compounds in the solid state. Racemization of (+)-[Co(en)$_3$] $X_3 \cdot nH_2O$. 119
Kuwata, K. Electron spin resonance study of the far-ultraviolet photolysis of some inorganic and organic compounds. 2061
Kwong, G. Y. W. Far-infrared spectra of tertiary ammonium salts. 339
Lahmani, F. Mercury sensitization of the isomerization of diazines. 2245
Lampe, F. W. Reaction of ethyl radicals with nitric oxide. Nitrosoethane and triethylhydroxylamine formation. 3303
Lampe, F. W. Ionic reactions in monosilane. Radiation chemistry implications. 3321
Land, E. J. Excited states in the nanosecond pulse radiolysis and laser flash photolysis of N,N-dimethylaniline. 3805
Landholm, R. A. Isotope effects in proton transfer from general acids to carbon bases. 2951
Langer, S. H. Gas-chromatographic reactor study of the kinetics of dicyclopentadiene dissociation. 2159
Larsen, D. W. Nuclear magnetic resonance studies of quadrupolar and dipolar relaxation effects. Complexes of lithium halides with pyridine in aqueous solution 53
Larson, C. W. Identity scrambling and isomerization networks in systems of excited alkyl radicals. 2507
Lassiter, W. S. Interaction of sulfur dioxide and carbon dioxide with clean silver in ultrahigh vacuum. 1289
Laufer, A. H. Determination of the heat of formation of diazirine by photon impact. 3504
Laughlin, W. T. Viscous flow in simple organic liquids. 2317
Laurie, W. A. Chemical ionization mass spectrometry. XVII. Effect of pressure on the decomposition of protonated tert-amyl acetate. 3917
Lavalette, D. Triplet states of biphenylene. 225
Lawton, J. B. Polyanions and their complexes. VII. Interaction of methylene blue with cellulosic polyanions in heterogeneous systems. 688
Lee, Y. S. Ultrasonic shear wave study of the mechanical properties of a nematic liquid crystal. 2409
Lemaire, G. Radiolysis of water by tritium β-rays. Scavenging of hydrogen peroxide precursors. 1542
Lemmon, R. M. Hot-atom chemistry of carbon-14 in solid benzene at kinetic energies at or below 5 electron volts. 2521
Leniart, D. S. Powder ENDOR [electron nuclear double resonance] line shapes. Nuclear relaxation induced by motion of nearby electron spins. 2079
Leniart, D. S. Proton ENDOR [electron nuclear double resonance] of γ-irradiated Y-type zeolites. 2087
Leonard, A. J. Structural evolution of chromia. 1838
Leong, T. H. Electrical conductances and ionization behavior of sodium chloride in dioxane-water mixtures at 50°. 2294
Lepori, L. Volumetric properties of aqueous solutions of organic compounds. I. Cyclic ethers and cyclic amines. 1338
Lepori, L. Volumetric properties of aqueous solutions of organic compounds. II. Chloride salts of cyclic amines. 1343
Lepoutre, G. Thermodynamic properties of hydrated and ammoniated electrons. 683
Le Roy, R. J. Quantum mechanical tunneling in hydrogen atom abstraction for solid acetonitrile at 77-87°K. 546
LeRoy, R. L. Hydrogen displacement in butane by fast molecular tritium collisions. [Comments]. 2937
Lesigne, B. Pulsed radiolysis and flash photolysis of iodates in aqueous solution. 302
Lesigne, B. Direct effect in the radiolysis of 0.4 M sulfuric acid. 3676
Lett, R. G. Mass spectrometry study of microwave discharges in hydrogen-carbon monoxide-argon mixtures. 2941
Leung, C. Polywater, an organic contaminant. Reply to comments. 457
Leva, G. Volumetric properties of aqueous solutions of organic compounds. II. Chloride salts of cyclic amines. 1343
Levay, B. Effect of charge-transfer complex formation on the positronium-iodine reaction. 1951
Levi, H. W. Ion and isotopic exchange among solids. 1317
Levine, H. S. Formation of vapor nuclei in high temperature melts. 2609
Levine, S. Role of the diffuse layer in water-in-oil microemulsions. 876
Levy, A. Disulfur and the lower oxides of sulfur in hydrogen sulfide flames. 1925
Levy, J. B. Bistrifluoromethyl peroxide. II. Kinetics of the decomposition to carbonyl fluoride and trifluoromethyl hypofluorite 3480

Levy, O. Limiting behavior of alkylammonium salts in benzene. 1752

Levy, P. W. Kinetics of defect and radiolytic product formation in single crystal sodium bromate determined from color-center measurements. 3751

Lewis, G. G. Ionic-covalent interactions and glass formation in molten acetates. Cobalt(II) as a spectroscopic probe. 1035

Lewis, L. Thermodynamics of hydrogen bond formation between phenol and some diazine N-oxides. 3502

Leyte, J. C. Irreversible potentiometric behavior of isotactic poly(methacrylic acid). 2559

Li, P. C. Solid state spectra and conductivities of the potassium salts of anthracene. 1026

Lias, S. G. Ion-molecule reactions in ethane. 3919

Lichtin, N. N. Electron and hydrogen atom attachment to aromatic carbonyl compounds in aqueous solution. Absorption spectra and dissociation constants of ketyl radicals. 2072

Liebermann, E. Thermodynamics of the acetic acid-triethylamine system. 2764

Lilie, J. Pulse radiolysis and polarography. II. Use of an on-line computer in the determination of the half-wave potentials of short-lived inorganic radicals. 1487

Lilie, J. Lifetime of trifluoromethyl radical in aqueous solution. 2517

Lin, D. P. Optical bleaching effects on the paramagnetic relaxation of trapped electrons in methyltetrahydrofuran at 77°K. 636

Lin, D. P. Paramagnetic relaxation study of spatial distribution of trapped radicals in γ-irradiated alkaline ice and organic glasses at 4.2°K. 1226

Lin, I. J. Hydrophile-lipophile balance (hlb) of fluorocarbon surfactants and its relation to the critical micelle concentration (cmc). 2019

Lin, M. C. Chemical lasers produced from $O(^1D)$ atom reactions. III. Hydrogen chloride elimination lasers from the $O(^1D) + CH_nCl_{4-n}$ (n = 1, 2, and 3) reactions. 811

Lin, M. C. Chemical lasers produced from $O(^1D)$ atom reactions. IV. Competitive eliminations of hydrogen chloride and hydrogen fluoride from the vibrationally excited chlorofluoromethanol dichlorofluoromethanol, and chlorodifluoromethanol. 1425

Lin, M. C. Chemical lasers produced from $O(^1D)$ atom reactions. V. Carbon monoxide stimulated emission from flash-initiated O_3 + XCN systems. 1429

Lin, M-L. Hydrogen bonding interactions of p-chlorophenol with aliphatic amines. 587

Lin, S. H. Magnetic circular dichroism of molecules in dense media. I. Theory. 1844

Lin, W. C. Electron spin resonance study of nitrile and other radicals trapped in γ-irradiated single crystals of cyanoacetic acid. 3377

Lindenbaum, S. Effect of dimethyl sulfoxide, urea, guanidine hydrochloride, and sodium chloride on hydrophobic interactions. Heats of dilution of tetrabutylammonium bromide and lithium bromide in mixed aqueous solvent systems. 3050

Linder, C. Persistent electrical polarization in polyelectrolyte membranes. 3434

Lindgren, B. J. Infrared spectra of the oxides and carbonates of silver. 940

Lindner, W. Activity coefficient of n-heptane in 4,4′-dihexyloxyazoxybenzene liquid crystal. 596

Lindqvist, L. Solvent effects on acetophenone photoreduction studied by laser photolysis. 821

Lingertat, H. Polywater, an organic contaminant. Reply to comments. 457

Lintermans, J. Hot-atom chemistry of carbon-14 in solid benzene at kinetic energies at or below 5 electron volts. 2521

Liotta, C. L. Thermodynamics of acid-base equilibriums. II. Ionization of m- and p-hydroxybenzotrifluoride and the concept of fluorine double bond-no bond resonance. 1909

Lippits, G. J. M. Association of crystal violet in aqueous solutions. 1772

Lisle, J. B. Nitrogen and boron spin-lattice relaxation in borazole. 2871

Lissi, E. Bromine atom catalyzed oxidation of carbon monoxide. 1416

Lissi, E. Reaction of hydrogen peroxide with nitrogen dioxide and nitric oxide. 1919

Litvan, G. G. Adsorption isotherm and surface area determination below the triple point. 2584

Liu, M. T. H. Thermal decomposition of 3-halo-3-phenyldiazirine in solution. 797

Livingston, R. Paramagnetic resonance study of liquids during photolysis. XIV. Pyridine, pyrazine, pyrimidine, and pyridazine. 3348

Lizardi, L. R. Equilibrium studies by electron spin resonance. I. Free nitrobenzene anion radical. 1439

Lizardi, L. R. Equilibrium studies by electron spin resonance. II. Nitrobenzene free ion-ion pair equilibrium. 2058

Logan, J. Higher excited states in metal-ammonia solutions. I. The 2s state. 2738

Lok, M. T. Spectra of Na^-, K^-, and e^-_{solv} in amines and ethers. 2975

Lomax, A. Electron spin resonance study of the geometry of 9-phenylacridine. 3958

Long, F. A. Isotope effects on hydroxide ion in aqueous solution. 362

Loos, K. R. Spectroscopic studies of zeolite synthesis. 3388

Lopp, I. G. Detection and identification of gas phase free radicals by electron spin resonance spin trapping. 2056

LoSurdo, A. Proton magnetic resonance in concentrated aqueous solutions of tetraalkylammonium bromides and inorganic halides at 25 and 65°. 130

LoSurdo, A. Temperature dependence of the apparent and partial molal volumes of concentrated aqueous electrolyte solutions of tetraalkylammonium bromides, cetyltrimethylammonium bromide, and ammonium and lithium bromides. 1333

Loutfy, R. O. Correlations between the electrochemical and spectroscopic behavior of some benzophenones and thiobenzophenones. 1650

Loutfy, R. O. Correlations between the electrochemical and spectroscopic behavior of some benzophenones and thiobenzophenones. 1650

Love, A. L. Nuclear magnetic resonance rate studies of hindered rotation in methyl N-acetylsarcosinate. 853

Loyd, R. J. Paramagnetism and semiconductivity in doped charge-transfer complexes. 1849

Lucas, M. Nuclear magnetic resonance chemical shift of the water proton in aqueous tetraalkylammonium halide solutions at various temperatures. 1455

Lucas, M. Solubility of helium and methane in aqueous tetrabutylammonium bromide solutions at 25 and 35°. 3068

Lucas, M. Influence of a hard-sphere solute on water structure. 4030

Ludlum, K. H. Structure and orientation of phenols chemisorbed on γ-alumina. 2882

Luks, K. D. Rice-Allnatt transport theory. 2133

Lund, A. Electron spin resonance studies on irradiated heterogeneous systems. VIII. Radical cation formation from toluene. 1721

Lund, A. Electron spin resonance studies on irradiated heterogeneous systems. IX. Anisotropy of the g factor and the hyperfine coupling constant of the benzene cation in the adsorbed state. 1727

Lund, A. Free radical formation in hydrocarbon crystals by γ irradiation. II. Relative yields of isomeric alkyl by electron spin resonance. 1411

Lunsford, J. H. Electron paramagnetic resonance of SO_2-on magnesium oxide. 323

Lunsford, J. H. Electron paramagnetic resonances study of the Cu^+-NO complex in a Y-type zeolite. 1546

Lunsford, J. H. Electron paramagnetic resonance spectra of amino radicals formed by γ irradiation of ammoniated zeolites. 2716

Lunsford, J. H. Electron paramagnetic resonance study of copper(II)-ammonia complexes in Y-type zeolites. 2860

Luria, M. Photochemistry of benzene in oxygenated aqueous solution in the B_{2u} first excited singlet state. 165

Lutz, H. Solvent effects on acetophenone photoreduction studied by laser photolysis. 821

Lutze, W. Ion and isotopic exchange among solids. 1317

Lyerla, J. R. Jr. Influence of internal motion on the carbon-13 relaxation times of methyl carbons. 3213

McAllister, J. W. Oxidation of carbon at the surface of nickel. 968

McAlpine, I. Comparison of the radiolysis of liquid bromotrifluoromethane with the radiolysis of liquid trifluoroiodomethane. 2070

McCaffrey, E. F. Kinetic studies of the catalytic activity of alkaline earth oxides in 2-propanol decomposition. 3372

McCoy, L. R. Catalytic polarographic current of a metal complex. VIII. Effect of weakly complexing supporting electrolytes. 1170

MacDonald, H. C. Jr. Catalytic polarographic current of a metal complex. VIII. Effect of weakly complexing supporting electrolytes. 1170

McDonald, R. L. Far-infrared spectra of tertiary ammonium salts. 339

McDowell, C. A. Photoelectron spectra of methyl mercaptan, dimethyl sulfide, thiophenol, and α-toluenethiol. Bonding between sulfur and carbon. 1030

McDowell, M. V. Intermediates in the reactions of alkane and cycloalkane molecular ions with water vapor. 1517

Macedo, P. B. Conductivity relaxation in a concentrated aqueous electrolyte solution. 3287

McEwan, M. J. Mass spectrometric observations on the reaction of hydrogen atoms with iodine cyanide. 1392

McFeely, F. R. Vaporization kinetics of hydrogen-bonded liquids. 914

Mcgee, T. H. Thermal decomposition of cyclobutanone. 963

McGrath, P. W. Kinetic study of the reaction of methylene radicals with dimethylsilane. Decomposition of chemically activated trimethylsilane and methylethylsilane. 459

McGuire, R. F. Energy parameters in polypeptides. V. Empirical hydrogen bond potential function based on molecular orbital calculations. 375

Machi, S. Radiation-induced polymerization of pure styrene at low temperature. 930

Machulla, H. J. Influence of rotational conformation on the stereochemical course of hot halogen for halogen substitution in liquid 2,3-dichlorobutane. 501

Maciel, G. E. Additivity in the carbon-13 chemical shifts of 1,2-disubstituted ethanes. 1466

Maciel, G. E. Carbon-13-carbon-13 coupling constants. VI. Homonuclear double resonance experiments for carbon-13 nuclear magnetic resonance assignments. 2972

McIntosh, R. Dielectric evidence of two-dimensional condensation of halides adsorbed on nonporous sodium chloride. 2535

Mackay, R. A. Solvent dependence of charge-transfer spectra of 1-(p-substituted benzyl)-4-carbomethoxypyridinium iodides. 603

MacKnight, A. Application of significant structures theory to some hydrocarbon liquids. 731

MacKnight, A. K. Significant structure liquid theory of the alkali metals over the normal melting to boiling range. 1612

McLaughlin, E. Monoisotopic mass spectra of borane derivatives. 1860

McLean, R. A. N. Photoelectron spectra of methyl mercaptan, dimethyl sulfide, thiophenol, and α-toluenethiol. Bonding between sulfur and carbon. 1030

McNeel, M. L. Evaluation of the nuclear magnetic resonance total line shape analysis of uncoupled, exchanging two-site systems. 71

MacNeil, K. A. G. Ion-molecule reactions in gaseous acetone. 409

McNicol, B. D. Spectroscopic studies of zeolite synthesis. 3388

Maeda, H. Theory for the dependence of pH on polyelectrolyte concentration. 3445

Magee, J. L. Triplet formation in ion recombination in spurs. 3801

Magill, J. H. Molecular movements and phase transitions in solids. Tetrakis(trimethylsilyl)methane. 4037

Maguire, J. A. Spectroscopic study of the propionitrile-iodine molecular complex. 2098

Mahlman, H. A. Elementary processes in the radiolysis of aqueous sulfuric acid solutions. Determinations of both G_{OH} and G_{SO_4}. 1265

Mahlman, H. A. Elementary processes in the radiolysis of aqueous nitric acid solutions. Determination of both G_{OH} and G_{NO_3}. 2680

Mains, G. J. Quenching of $^3P_1$ mercury atoms by isotopic aromatic molecules. 2665

Mains, G. J. Reactions of photochemically produced hydrogen atoms at energies below 1.8 electron volts. 3337

Mains, G. J. Chemical kinetics of the pyrolysis of hydrogen deuteride. 3538

Malatesta, V. Electronic and electron spin resonance spectra of the anion radicals of phenyl-and diphenylethylenes. 3960

Malinowski, E. R. Substituent effects. IX. Correlation of carbon-13, proton, and fluorine-19 nuclear magnetic resonance chemical shifts of some aromatic compounds by pairwise additivity. 1593

Mallmann, A. J. Infrared spectra of the oxides and carbonates of silver. 940

Malone, S. D. Photochemical behavior of cobalt complexes containing macrocyclic (N_4) ligands. Oxidation-reduction chemistry of dihalogen radical anions. 2223

Mandel, M. Association of crystal violet in aqueous solutions. 1772

Mann, R. F. Kinetics of adsorption of carbon monoxide on alumina. 2349

Manning, G. S. Correlation of solute permeability and reflection coefficient for rigid membranes with high solvent content. 393

Manocha, A. S. Torsional frequencies and enthalpies of intramolecular hydrogen bonds of o-halophenols. 1553

Mansfield, W. W. Exchange of water molecules at air-water interfaces. 1505

Marciaq-Rousselot, M. M. Nuclear magnetic resonance chemical shift of the water proton in aqueous tetraalkylammonium halide solutions at various temperatures. 1455

Marcotte, R. E. Radiation chemistry of carbon tetrafluoride-carbon tetrachloride mixtures in the gas phase. 3734

Marcoux, L. Potential-dependent chronoamperometry. EC reaction. 1666

Marcoux, L. Potential-dependent chronoamperometry. Disproportionation followed by an irreversible chemical reaction. 3254

Marcoux, L. S. Electron spin resonance study of the geometry of 9-phenylacridine. 3958

Marinsky, J. A. Osmotic properties of polystyrenesulfonates. II. Donnan equilibrium. 1881

Mark, H. B. Jr. Catalytic polarographic current of a metal complex. VIII. Effect of weakly complexing supporting electrolytes. 1170

Markovits, G. Y. Thermochemistry of halide exchange in an anion-exchange resin. 680

Markusch, P. Chemistry of recoiling silicon atoms. V. Product-forming reactions in phosphine-silane mixtures. 1352

Maroni, V. A. Structural studies of stannous chloride-potassium chloride melts by Raman spectroscopy. 2796

Marshall, W. L. Further description of complete equilibrium constants. 720

Marshall, W. L. Electrical conductance and ionization behavior of sodium chloride in dioxane-water solutions at 300° and pressures to 4000 bars. 1053

Martin, R. B. Conformations of isocitrate in solution. 3073

Martire, D. E. Activity coefficient of n-heptane in 4,4′-dihexyloxyazoxybenzene liquid crystal. 596

Mason, R. P. Electron spin resonance spectra of zwitterion radicals and isoelectronic anion radicals. 2479

Mastroianni, M. J. Effect of dimethyl sulfoxide, urea, guanidine hydrochloride, and sodium chloride on hydrophobic interactions. Heats of dilution of tetrabutylammonium bromide and lithium bromide in mixed aqueous solvent systems. 3050

Matsuda, S. Gas-phase homogeneous catalysis in shock waves. III. Oxidation of carbon monoxide by oxygen in the presence of nickel carbonyl. 2833

Matsushige, T. Chemical effects due to low-energy electron impact on thin films of cyclohexane and n-hexane at 77°K. 1255

Matteoli, E. Kinetic study of the hydration reaction of 2-, 3-, and 4-pyridinecarboxaldehyde. 2959

Matthews, R. W. Elementary processes in the radiolysis of aqueous sulfuric acid solutions. Determinations of both G_{OH} and G_{SO_4}. 1265

Matthews, R. W. Elementary processes in the radiolysis of aqueous nitric acid solutions. Determination of both G_{OH} and G_{NO_3}. 2680

Maurus, J. K. Circular dichroism of sensitizing dye aggregates. 2982

Mayorga, G. D. Adsorption in mordenite. I. Calculation of adsorption potentials of nonpolar molecules. 1641

Mayorga, G. D. Adsorption in mordenite. II. Gas chromatographic measurement of limiting heats of adsorption of nonpolar molecules. 1647

Mays, R. Nitrogen and boron spin-lattice relaxation in borazole. 2871

Meany, J. E. Spontaneous and general base-catalyzed iodination of pyruvic acid and alkyl pyruvates. Activation parameters and solvent deuterium isotope effects. 3121

Meisel, D. Concentration effects on primary processes in the radiation chemistry of aqueous solutions. 3677

Meisels, G. G. Precise measurements of W, the average energy required for ion pair formation. II. Alcohols and water. 3842

Melera, A. Electron spectroscopy for chemical analysis (ESCA) studies on catalysts. Rhodium on charcoal. 2525

Mellon Inst. Sci. Electron spin resonance spectra of di- and trimethylaminium radicals. 2857

Melquist, J. L. Isotope effects in proton transfer from general acids to carbon bases. 2951

Melton, C. E. Formation of, by termolecular reactions, and bond dissociation energy, structure, and bond length for OH^-H_2O and O^-H_2O. 3116

Mentienne, F. Structure effect on the fading rate of photochromic 3-substituted benzothiazolinic spiropyrans. 3554

Menzinger, M. Hydrogen displacement in butane by fast molecular tritium collisions. [Comments]. 2937

Merryman, E. L. Disulfur and the lower oxides of sulfur in hydrogen sulfide flames. 1925

Meschi, D. J. Scattering a molecular beam as a result of intrabeam collisions. 2947

Mestdagh, M. M. Proton mobility in solids. IV. Study of proton motion in the decationated Y zeolite by nuclear magnetic resonance. 1220

Metz, D. J. Radiation-induced polymerization of pure styrene at low temperature. 930

Metzger, J. Structure effect on the fading rate of photochromic 3-substituted benzothiazolinic spiropyrans. 3554

Meyer, B. Extended Hueckel calculations on the color of sulfur chains and rings. 2274

Meyer, B. Infrared spectra of S_4. 3968

Meyer, J. A. Rate constants for quenching of molecular nitrogen ($A^3\Sigma_u^+$) in active nitrogen. 1

Mezaki, R. Catalytic hydrogenation of propylene. Verification of maximum rate. 943

Michaud, P. Reaction of the excited oxygen atoms O($^1D_2$) with cyclopentane. 1375

Micka, T. A. Kinetic studies of the catalytic activity of alkaline earth oxides in 2-propanol decomposition. 3372

Miksch, G. Thermodynamics of the acetic acid-triethylamine system. 2764

Miles, H. T. Restricted rotation about the exocyclic carbon-nitrogen bond in cytosine derivatives. 64

Mille, Y. Laser-induced gas breakdown. Spectroscopic and chemical studies. 31

Miller, D. G. Mutual-diffusion coefficients at 25° in the system silver nitrate-water. 1853

Miller, I. F. Persistent electrical polarization in polyelectrolyte membranes. 3434

Miller, J. E. Medium effects of urea and guanidine hydrochloride on the volume changes produced by protonation of carboxylate groups. 2778

Miller, J. R. Time-dependent scavenging of trapped electrons in 2-methyltetrahydrofuran glass at 77°K. 2641

Miller, J. R. Wavelength dependence of photobleaching of trapped electrons in 3-methylpentane glass. 2341

Miller, R. L. Electronic structure of furanquinones. II. Emission spectra of dinaphtho[2,1:2′,3′]furan-8,13-dione and dinaphtho[1,2:2′,3′]furan-7,12-dione. 2240

Miller, W. G. Differential scanning calorimetric studies of the system poly-γ-benzyl-α,L-glutamate-dimethylformamide. 1081

Millward, G. E. Kinetic analysis of the shock wave decomposition of 1,1,1,2-tetrafluoroethane. 292

Minasz, R. J. Solvent effects in organic chemistry. XIV. Solvation of sodium salts in glycerol acetate binaries by sodium-23 nuclear magnetic resonance spectroscopy and thermodynamics. 2474

Minday, R. M. Mobility of excess electrons in liquid hydrocarbon mixtures. 442

Minton, A. P. Relations between crystal structure, molecular electronic polarizability, and refractive properties of ice I. 886

Misono, M. Kinetic study of n-butene isomerization over supported aluminum and magnesium sulfates. 44

Mital, R. L. Magnetochemical studies on diphenyldialkoxysilanes. 1579

Miyatani, D. Effects of neutron radiation on the catalytic activities of lithium-doped copper, nickel, and copper-nickel. 2625

Miyoshi, K. Conductance and ion pair formation of bis(2,9-dimethyl-1,10-phenanthroline)copper(I) perchlorate. I. In normal alcohols and ketones. 3029

Moan, J. Mechanisms of photobleaching of trapped electrons in ethylene glycol-water glass. 3366

Mohanty, R. K. Excess partial molal heat capacities of n-tetraamylammonium bromide in water from 10 to 80° and in aqueous tert-butyl alcohol solvent system at 30° and the effects on the water structure. 2577

Momany, F. A. Energy parameters in polypeptides. V. Empirical hydrogen bond potential function based on molecular orbital calculations. 375

Momicchioli, F. Fluorescence and absorption spectra of polyphenyls. Theoretical study on the band shape. 3983

Monahan, A. R. Dimerization of a copper(II)-phthalocyanine dye in carbon tetrachloride and benzene. 446

Monahan, A. R. Association of copper(II), vanadyl, and zinc(II) 4,4′,4″,4‴-tetraalkylphthalocyanine dyes in benzene. 1994

Moore, J. H. Jr. Investigation of the low energy singlet-triplet and singlet-singlet transitions in ethylene derivatives by ion impact. 1130

Moore, L. S. Intermolecular forces in gases of associating substances. 890

Morcos, I. Electrocapillary phenomena at the stress-annealed pyrolytic graphite electrode. 2750

Morgan, C. U. Thermal growth of the formyl radical at 87°K in a 50% methanol-water matrix. 494

Morgan, L. O. Proton magnetic relaxation in N-methyl-γ-butyrolactam and hexamethylphosphoric triamide solutions containing manganese(II) ions. 1973

Morimoto, J. Y. Photochemistry of the copper(II)-malonate system. Sensitized reaction. 1387

Morosi, G. Electronic and electron spin resonance spectra of the anion radicals of phenyl-and diphenylethylenes. 3960

Morrison, H. A. Alkylbenzene luminescence. 3566

Mortier, W. J. Location of univalent cations in synthetic zeolites of the Y and X type with varying silicon to aluminum ratio. II. Dehydrated potassium exchanged forms. 650

Moshuk, G. Electron spin resonance studies of the electron-transfer equilibrium β-ethylnaphthalenide + α-ethylnaphthalene ↔ β-ethylnaphthalene + α-ethylnaphthalenide. 1734

Mothes, K. G. Application of electron cyclotron resonance technique in studies of electron capture processes in the thermal energy range. 3758

Moynihan, C. T. Conductivity relaxation in a concentrated aqueous electrolyte solution. 3287

Moynihan, C. T. Ultrasonic and Brillouin scattering study of viscoelastic relaxation in a concentrated aqueous calcium nitrate solution. 3495

Mozumder, A. Formation of solvated electrons in dilute solutions of polar molecules in nonpolar solvents. 3824

Mukerjee, P. Size distribution of small and large micelles. Multiple equilibrium analysis. 565

Mukherjee, L. M. Standard potential of the ferrocene-ferricinium electrode in pyridine. Evaluation of proton medium effect. 243

Mukhopadhyay, A. K. Hypochromism and exciton interaction in halofluorescein dyes. 3970

Mulac, W. A. Reaction of cyanogen radicals with ammonia. 1931

Mullens, J. Specific interactions of anilines with water. 4011

Muller, J. H. Ion-solvent interactions. Effect on ionic aggregation in the system sodium tetra-n-butylaluminate-cyclohexane-tetrahydrofuran. 3472

Muller, N. Investigation of micelle structure by fluorine magnetic resonance. VI. Quaternary ammonium salts. 3012

Muller, N. Kinetics of micelle dissociation by temperature-jump techniques. Reinterpretation. 3017

Munjal, A. K. Thermally stimulated conductivity of γ-irradiated triethylamine and 3-methylpentane glasses. 2781

Murphy, W. F. Raman spectra and an assignment of the vibrational stretching region of water. 1147

Myers, A. L. Thermodynamic consistency test for adsorption of liquids and vapors on solids. 3412

Myers, A. L. Analogy between adsorption from liquids and adsorption from vapors. 3415

Myers, K. High-resolution x-ray emission study of central atom-ligand bonding in phosphorus oxyanions. 3975

Nagasawa, M. Transport phenomena of polyelectrolytes in solution under electric field. 2286

Naito, S. Identification of reaction intermediates by microwave spectroscopy. Catalytic reactions between propylene and deuterium over zinc oxide. 2184

Nakanishi, K. Diffusion in mixed solvents. III. Iodine in nonpolar solutions. Evidence for charge-transfer interaction. 2470

Nakato, Y. Photoionization and Rydberg states of tetraaminoethylenes in organic solutions. 2105

Naleway, C. A. Ab initio studies of the interactions of an electron and two water molecules as a building block for a model of the hydrated electron. 3905

Namiki, A. Electronic spectra of trapped electrons in organic glasses at 4°K. III. Effect of an electron scavenger in ethanol. 3744

Nash, C. P. Solutions of N-substituted amino acids. IV. Tautomerism in N,N-dibutyl-α-, β-, and γ-amino acids. 4033

Navon, G. Nuclear magnetic resonance study of the solvation of europium(III) ions in water-acetonitrile mixtures. 1449

Neiss, M. A. Photochemical reactions of borazine with ammonia and methyl bromide. 2630

Nelson, D. A. Ketyl radicals of benzoylpyridines. 3200

Nelson, W. H. Comparison of measured optical anisotropy values with those calculated by means of two δ-function-potential models. 1502

Nemethy, G. Structure of liquid water. Statistical thermodynamic theory. 3229

Neta, P. Effect of ionic dissociation of organic compounds on their rate of reaction with hydrated electrons. 630

Neta, P. Electron spin resonance and pulse radiolysis studies of the reactions of OH and O^- radicals with aromatic and olefinic compounds. 847

Neta, P. Electron spin resonance study of radicals produced by the reactions of hydrated electrons with unsaturated acids. 1957

Neta, P. Electron spin resonance study of radicals produced in irradiated aqueous solutions of 5-halouracils. 2399

Neta, P. Effect of ionic dissociation of organic compounds on their rate of reaction with hydrogen atoms. 2673

Neta, P. Electron spin resonance spectra of di- and trimethylaminium radicals. 2857

Neta, P. pK_a of the $^+H_3NCHCOOH$ radical 3507

Newman, R. D. Polymer-solvent interactions from gas-liquid partition chromatography. 1492

Nichol, L. W. Effects of pressure and thermodynamic nonideality on the sedimentation equilibrium of chemically reacting systems. Results with lysozyme at pH 6.7 and 8.0. 777

Nichol, L. W. Overspeeding technique in relation to sedimentation equilibrium. 2740

Nichol, L. W. Effect of charge in the sedimentation equilibrium of polymerizing protein systems. 3429

Nicholas, J. B. Reactions of energetic positronium atoms in solutions. 1124

Nicholas, P. P. Steric interactions in tert-butylethylenes observed through proton carbon-13 satellite spectra. 2877

Nichols, C. Electron spin resonance study of several DNA base cation radicals produced by photoionization. 3571

Nielsen, S. O. Transient electrons in pulse-irradiated crystalline water and deuterium oxide ice. 1000

Nielson, D. Magnetic circular dichroism of ferrocene and substituted ferrocenes. d-d Transitions. 511

Nika, G. G. Exchange reaction of methane-d_4 with hydrogen chloride. 2809

Niki, T. Chemical kinetics of the pyrolysis of hydrogen deuteride. 3538

Nilsson, G. Transient electrons in pulse-irradiated crystalline water and deuterium oxide ice. 1000

Nishioka, M. Catalytic activity of cold-worked and quenched gold for the decomposition of hydrogen peroxide. 1907

Noble, B. Pyrolysis of 1,1-difluoroethane. 1680

Noda, I. Transport phenomena of polyelectrolytes in solution under electric field. 2286

Noda, M. Electronic spectra of trapped electrons in organic glasses at 4°K. III. Effect of an electron scavenger in ethanol. 3744

Noersjamsi, S. Solubility study of silver halides in molten calcium nitrate tetrahydrate. 2759

Noll, L. Calorimetric study of association of diketopiperazine in water. 3065

Nordine, P. C. Quasi-equilibrium analysis of the reaction of atomic and molecular fluorine with tungsten. Reply [to comments]. 2930

Noyes, R. M. Ultraviolet spectra of single and double molecules of gaseous bromine. 1017

Obenauf, R. H. Jr. Mass spectrometric study of the reaction of dicyanoacetylene with oxygen atoms. 269

Obenauf, R. H. Jr. Mass spectrometric study of the reaction of dicyanoacetylene with active nitrogen. 2643

Obi, K. Rate constants for the reactions of deuterium atoms with silanes. 3911

O'Brien, T. J. P. Potential-dependent chronoamperometry. EC reaction. 1666

O'Brien, W. D. Jr. Ultrasonic absorption mechanisms in aqueous solutions of bovine hemoglobin. 528

O'Connell, J. P. Intermolecular forces in gases of associating substances. 890

O'Connor, M. E. Effects of mannitol and sorbitol on water at 25°. 3077

Odiorne, T. J. Chemical ionization mass spectrometry using tetramethylsilane. 3217

Oestvold, T. Thermochemistry of fused halide systems. Enthalpies of mixing of the alkaline earth halides with the alkali halides. 1616

Ogren, P. J. Radical concentration growth in irradiated solid systems. Simple model involving competitive radical production, thermal decay, and radiation-induced decay. 1324

Okabe, H. Determination of the heat of formation of diazirine by photon impact. 3504

Okamoto, K. Effects of neutron radiation on the catalytic activities of lithium-doped copper, nickel, and copper-nickel. 2625

Olfky, R. S. Bisdifluoraminoalkanes. Mass spectral decomposition of isomeric propanes. 60

Olsen, D. K. Cyclization and decomposition of 4-penten-1-yl radicals in the gas phase. 1089

Olsen, R. K. Nuclear magnetic resonance rate studies of hindered rotation in methyl N-acetylsarcosinate. 853

Ong, E. L. Spectrophotometric and thermodynamic study of donor-acceptor complexes of carbazole. 2102

Ono, M. Electron spin resonance study of the far-ultraviolet photolysis of some inorganic and organic compounds. 2061

Oosawa, F. Theory for the dependence of pH on polyelectrolyte concentration. 3445

Orbach, N. Primary processes in excited charge-transfer systems. 1133

Orttung, W. H. Temperature dependence of the Kerr constant of water. 216

Oshima, K. Studies of transition phenomena of some organic solids by electrical conductivity measurement at low temperature. 115

Oshima, K. Transition phenomena of some organic solids by electrical conductivity measurement at low temperature. Reply to the comment. 2799

Oswal, S. L. Use of exponential six potential in the statistical theory of solutions. 3005

Oszust, J. Infrared spectra and dipole moments of hydrogen-bonded complexes. III. Adducts of 2,6-dichloro-4-nitrophenol with pyridine bases. 2112

Otterbach, J. Kinetic analysis and mechanism of chlorine-38 and bromine-82 recoil reactions in $K_2[ReBr_6]/K_2[ReCl_6]$ mixed crystals. 2499

Otto, K. Studies of surface reactions of nitric oxide by isotope labeling. IV. Reaction between nitric oxide and ammonia over copper surfaces at 150-200°. 37

Ottolenghi, M. Primary processes in excited charge-transfer systems. 1133

Ottolenghi, M. Biphotonic ionization processes in nonpolar solutions of N,N,N′,N′-tetramethyl-p-phenylenediamine. 2229

Ottolenghi, M. Pulse radiolysis of sodium metaphosphate glasses. 203

Ozaki, M. Photoionization and Rydberg states of tetraaminoethylenes in organic solutions. 2105

Pacansky, J. Anomalous isotope shifts in the vibrational spectrum of hydrogen cyanide in argon matrixes. 454

Pace, I. Dissociation constant of the 9-anthroic acidium cation in the lowest excited singlet state. 1996

Padrick, T. D. Hydrogen fluoride elimination chemical laser from deuterated N,N-difluoromethylamine. 3125

Pagano, R. E. Physical chemistry of lipid films at the air-water interface. I. Intermolecular energies in single-component lipid films. 1231

Pagano, R. E. Physical chemistry of lipid films at the air-water interface. II. Binary lipid mixtures. Principles governing miscibility of lipids in surfaces. 1238

Pagano, R. E. Physical chemistry of lipid films at the air-water interface. III. Condensing effect of cholesterol. Critical examination of mixed-film studies. 1244

Pagsberg, P. Transient electrons in pulse-irradiated crystalline water and deuterium oxide ice. 1000

Pak, K. Photochemistry of nitrosobenzene. 1087

Palombo, R. Ionic association of potassium perchlorate in sulfolane-water mixtures from conductance measurements at 25°. 2923

Paniccia, F. Redox mechanisms in an ionic matrix. Kinetics of the reaction $2O_2^- + H_2O = 2OH^- + 1.5O_2$ in molten alkali nitrates. 422

Pao, Y. C. Systematics of (n,γ)-activated hot iodine-128 reactions in gaseous methane and halomethanes. Energy Degradation factor. 2685

Papez, R. J. Ion pairing in alkali metal durosemiquinone solutions. 1012

Parlange, J. Y. Diffusion-controlled condensation and evaporation in wedge-shaped pores. 2543

Partridge, A. Anion exchange in aqueous-organic solvent mixtures. II. 1040

Patterson, D. Pressure effects in polymer solution phase equilibriums. I. Lower critical solution temperature of poly(isobutylene) and poly(dimethylsiloxane) in lower alkanes. 1206

Patterson, D. Pressure effects in polymer solution phase equilibriums. II. Systems showing upper and low critical solution temperatures. 1214

Patterson, L. K. Pulse radiolysis studies of 5-halouracils in aqueous solutions. 2392

Patterson, L. K. Production of halide ion in the radiolysis of aqueous solutions of the 5-halouracils. 2386

Patton, J. E. Gas-chromatographic reactor study of the kinetics of dicyclopentadiene dissociation. 2159

Pauchaeult, J. Direct effect in the radiolysis of 0.4 M sulfuric acid. 3676

Payne, R. Dielectric properties and relaxation in ethylene carbonate and propylene carbonate. 2892

Pearson, J. Irradiated single crystal clathrate of Dianin's compound and 1,2-dibromo-1,1-difluoroethane. Electron spin resonance observation of the Br_2^- radical 133

Pedone, C. X-ray study of the conformation of the molecule of 1,2-trans-cyclopentanedicarboxylic acid. 790

Peled, E. Concentration effects on primary processes in the radiation chemistry of aqueous solutions. 3677

Peleg, M. Raman spectroscopic investigation of the magnesium nitrate-water system. 1019

Pellerin, J. H. Investigation of micelle structure by fluorine magnetic resonance. VI. Quaternary ammonium salts. 3012

Penny, A. L. Reactions involving electron transfer at semiconductor surfaces. III. Dissociation of methyl iodide over zinc oxide. 2353

Peradejordi, F. Triplet states of biphenylene. 225

Perlmutter-Hayman, B. Kinetics of the hydrolysis of the dichromate ion. VI. Environmental influences on the acid-catalyzed reaction. 582

Pernikova, T. E. Polaron yields in low-temperature pulse radiolysis of chemically inert aqueous matrices. 3776

Peron, J. J. Low-temperature infrared study of sterically hindered associated alcohols. 864

Peron, J. J. Vibrational overtone study of association in liquid methanol. 869

Perone, S. P. Electroanalytical measurements of flash-photolyzed ferrioxalate. 830

Perotti, A. Electron spin resonance study of transient radicals in γ-irradiated organic inclusion compounds. II. Palmitic acid urea clathrate. 801

Perumareddi, J. R. d^2 and d^8 Quadrate energy levels including spin-orbit perturbation. 3401

Peter, F. A. Effect of ionic dissociation of organic compounds on their rate of reaction with hydrated electrons. 630

Peters, C. R. Factors influencing reverse osmosis rejection of organic solutes from aqueous solution. 4006

Peterson, D. L. Adsorption in mordenite. I. Calculation of adsorption potentials of nonpolar molecules. 1641

Peterson, D. L. Adsorption in mordenite. II. Gas chromatographic measurement of limiting heats of adsorption of nonpolar molecules. 1647

Peterson, H. T. Activity coefficient of n-heptane in 4,4'-dihexyloxyazoxybenzene liquid crystal. 596

Petrakis, L. Adsorbed species. II. Electron spin resonance study of thianthrene and other sulfur heterocyclics adsorbed on oxide surfaces. 1443

Petrucci, S. Ultrasonic relaxation in calcium nitrate hydrated melts. 1507

Pettijohn, R. R. Reactions of iodine with olefins. III. Radiative neutron capture induced reactions of iodine-128 with gaseous ethylene and propylene. 3342

Pezzatini, G. Influence of specific adsorption of reactant and product upon charge-transfer processes in voltammetry. Tl^{3+}/Tl^{+} couple in 1 M perchloric acid on smooth and platinized platinum. 976

Phillips, D. Quenching of the excited states of benzene and substituted benzenes by olefins. 3668

Phillips, D. Photochemistry of trifluoromethylbenzenes. III. 1,4-Bis(trifluoromethyl)benzene. 823

Phillips, D. Photochemistry of the fluorotoluenes. II. Quenching of the excited states. 2967

Phillips, G. O. Polyanions and their complexes. VII. Interaction of methylene blue with cellulosic polyanions in heterogeneous systems. 688

Phillips, L. F. Quantum yields in the 58.4-nm photolyses of ammonia and water. 298

Phillips, L. F. Mass spectrometric observations on the reaction of hydrogen atoms with iodine cyanide. 1392

Pierotti, R. A. Modifications to a precision adsorption apparatus. Interaction of the inert gases with boron nitride. 3171

Pietrzak, T. Model for the simulation of the electron spin resonance spectra of nitroxide-type probe molecules in a nematic mesophase. 672

Pikaev, A. K. Solvated electrons in irradiated concentrated alkaline methanol and water-methanol mixtures. 3765

Pikal, M. J. Effect of dimethyl sulfoxide, urea, guanidine hydrochloride, and sodium chloride on hydrophobic interactions. Heats of dilution of tetrabutylammonium bromide and lithium bromide in mixed aqueous solvent systems. 3050

Pikal, M. J. Isotope effect in tracer diffusion. Comparison of the diffusion coefficients of $^{24}Na^+$ and $^{22}Na^+$ in aqueous electrolytes. 3038

Pilling, G. Viscosity of concentrated aqueous solutions of tetraalkylammonium bromides. 1902

Pimentel, G. C. Hydrogen fluoride elimination chemical laser from deuterated N,N-difluoromethylamine. 3125

Plumb, R. C. Columns of liquid bearing a constrained chemical activity gradient. 1637

Pochan, J. M. Nitrogen-14 nuclear quadrupole coupling and the nitrogen localized electron distribution in diazirine. 2249

Pohl, H. A. Solid state spectra and conductivities of the potassium salts of anthracene. 1026

Pohland, A. E. Electron spin resonance studies of cation radicals in trifluoromethanesulfonic acid. 1504

Pollard, G. Infrared and Raman spectra of group I nitrate aggregates in carbon dioxide matrixes and glassy thin films. 1826

Popov, A. I. Nitrogen-14 nuclear magnetic resonance study of 1,5-disubstituted tetrazoles. 2403

Porter, R. F. Photochemical reactions of borazine with ammonia and methyl bromide. 2630

Porter, R. S. Thermal transitions and phase relations for binary mixtures of cholesteryl esters. 3089

Posner, A. M. Radioisotope determination of the surface concentrations of calcium and phosphorus on hydroxylapatite in aqueous solution. 900

Potashnik, R. Primary processes in excited charge-transfer systems. 1133

Pott, G. T. Spectroscopic studies of zeolite synthesis. 3388

Potter, A. E. Jr. Rates of interaction of vibrationally excited hydroxyl (v = 9) with diatomic and small polyatomic molecules. 1511

Potzinger, P. Ethylene as an actinometer in the wavelength region 147-185 nanometers. 138

Poziomek, E. J. Solvent dependence of charge-transfer spectra of 1-(p-substituted benzyl)-4-carbomethoxypyridinium iodides. 603

Prausnitz, J. M. Solubilities of gases in liquids at elevated temperatures. Henry's constants for hydrogen, methane, and ethane in hexadecane, bicyclohexyl, and diphenylmethane. 598

Prausnitz, J. M. Gas solubilities from a perturbed hard-sphere equation of state. 601

Prausnitz, J. M. Polymer-solvent interactions from gas-liquid partition chromatography. 1492

Premovic, P. I. Electron spin resonance study of γ-irradiated single crystal of ammonium oxalate monohydrate. 3274

Prendergast, D. F. Kinetic oscillations in the oxidation of 2,4-pentanedione by bromate ion, catalyzed by manganese(II) 2185

Price, F. P. Transitions in mesophase-forming systems. III. Transformation kinetics and textural changes in cholesteryl nonanoate. 276

Price, F. P. Transitions in mesophase forming systems. IV. Transformation behavior and pretransition effects in p-azoxyanisole. 2605

Priore, D. Manometric study of the oxygen-peroxide-superoxide reaction in nitrate melts. 2841

Pritchard, G. O. Reaction of trifluoromethyl radicals with hexafluoroacetone imine. 487

Pritchard, G. O. Half-quenching pressures in the association of methyl radicals-d_0 and -d_3. 2196

Probstein, R. F. Electrokinetic salt rejection in hyperfiltration through porous materials. Theory and experiment. 4015

Pucheault, J. Radiolysis of water by tritium β-rays. Scavenging of hydrogen peroxide precursors. 1542

Pupezin, J. Vapor pressure isotope effect in aqueous systems. I. Water-water-d_2 (-64° to 100°) and water-water^{18}-0 (-17° to 16°). Ice and liquid. II. Alkali metal chloride solution in water and water-d^2 (-5° to 100°). 743

Purkayastha, A. Scaled particle theory for nonelectrolyte solution of dilute solid solutes. 2138

Quach, A. Statistical thermodynamics of the glass transition and the glassy state of polymers. 416

Quickert, K. A. Mechanism to explain the methylidene emission at 4330 Ang. in oxygen atom-acetylene systems. 825

Quirk, J. P. Radioisotope determination of the surface concentrations of calcium and phosphorus on hydroxylapatite in aqueous solution. 900

Quist, A. S. Raman spectra of molten alkali metal carbonates. 1565

Quist, A. S. Raman spectra of tetrafluoroberyllate ion in molten sodium fluoride and lithium fluoride to 686°. 78

Rabani, J. Pulse radiolysis of sodium metaphosphate glasses. 203

Rabani, J. Oxidation of aqueous bromide ions by hydroxyl radicals. Pulse radiolytic investigation. 312

Rabani, J. Pulse radiolysis of the aqueous ferro-ferricyanide system. 1. Reactions of OH, HO_2, and O_2^- radicals. 3703

Rabinovitch, B. S. Competitive thermal unimolecular reactions of trans-cyclopropane-d_2. Collisional energy transfer. 1695

Rabinovitch, B. S. Energy transfer in thermal methyl isocyanide isomerization. Relative efficiency of mercury atoms. 1935

Rabinovitch, B. S. Comparisons of the RRK [Rice-Ramsperger-Kassel] and RRKM [Markus-Rice] theories of thermal unimolecular reaction. Energy distributions and the s parameter. 2418

Rabinovitch, B. S. Identity scrambling and isomerization networks in systems of excited alkyl radicals. 2507

Rack, E. P. Systematics of (n,γ)-activated hot iodine-128 reactions in gaseous methane and halomethanes. Energy Degradation factor. 2685

Rack, E. P. Reactions of iodine with olefins. III. Radiative neutron capture induced reactions of iodine-128 with gaseous ethylene and propylene. 3342

Rahman, A. Conductivity of sodium chloride and potassium chloride in polymer solutions and the obstruction effect. 1763

Rai, J. H. Differential scanning calorimetric studies of the system poly-γ-benzyl-α,L-glutamate-dimethylformamide. 1081

Rampazzo, L. Adsorption behavior of tetraphenylborate anions at a mercury electrode. 707

Ramsey, R. N. Modifications to a precision adsorption apparatus. Interaction of the inert gases with boron nitride. 3171

Ranck, K. M. Recoil tritium reactions with hexamethyldisilane in the gas phase. 1249

Rappoport, S. Effect of temperature in the radiolysis of paraffins. 3851

Ratajczak, H. Charge-transfer properties of the hydrogen bond. I. Theory of the enhancement of dipole moment of hydrogen-bonded systems. 3000

Ratajczak, H. Charge-transfer properties of the hydrogen bond. II. Charge-transfer theory and the relation between the enhancement of dipole moment and the ionization potential of hydrogen-bonded systems. 3991

Ratnasamy, P. Structural evolution of chromia. 1838

Ravi, A. Infrared spectra of hydrocarbons adsorbed on silica-supported metals. IV. Butenes on iridium. 2699

Ray, D. J. M. Epoxidation of alkenes in the gas phase. 3319

Read, A. J. Dissolution of copper in weakly acidic solutions. 3656

Read, J. F. Hydrogen-oxygen reaction on lanthanide oxides. II. Stoichiometric hydrogen-oxygen reaction on neodymium oxide, dysprosium oxide, and erbium oxide. 2199

Reddy, M. P. Effect of temperature on the γ radiolysis of aqueous solutions. 1273

Reeves, R. R. Photodissociation of nitrogen dioxide by pulsed laser light at 6943 Ang. 474

Regan, T. H. Kinetics and mechanism of decafluorobenzophenone photochemical reactions in cyclohexane, benzene, and alkyl aromatics. 3926

Regen, S. L. Nitrogen and boron spin-lattice relaxation in borazole. 2871

Reger, D. W. Solvent dependence of charge-transfer spectra of 1-(p-substituted benzyl)-4-carbomethoxypyridinium iodides. 603

Reilly, P. J. Heats of mixing aqueous electrolytes. IX. The reciprocal salt pair Mg^{2+}, $Na^{+}||Cl^{-}$, Br^{-}. 3474

Reisfeld, R. Quantum efficiencies and radiationless transitions of europium(III) in phosphate glasses. 1293

Revzin, A. New procedure for calculating the four diffusion coefficients for ternary systems from Gouy optical data. Application to data for the system potassium bromide-hydrobromic acid-water. 3419

Rhodes, K. A. Thermodynamics of acid-base equilibriums. II. Ionization of m- and p-hydroxybenzotrifluoride and the concept of fluorine double bond-no bond resonance. 1909

Rice, W. W. Hydrogen chloride chemical laser from hydrogen atom-chlorine azide reaction. 805

Richards, J. T. Excited states in the nanosecond pulse radiolysis and laser flash photolysis of N,N-dimethylaniline. 3805

Richelson, M. R. Ultrasonic relaxation in calcium nitrate hydrated melts. 1507

Richey, W. F. Stereochemistry of the silver-catalyzed epoxidation of olefins. 213

Richmond, A. B. Gas-phase thermolysis kinetics of small ring nitriles. 2817

Rigby, M. Van der Waals equation for nonspherical molecules. 2014

Riley, P. E. Crystal structures of hydrated and dehydrated thallium-exchanged zeolite A. 2593

Robinson, B. B. Efficiency of the electrochemiluminescent process. 1868

Robinson, E. A. Pulse radiolysis of solutions of stilbene. I. Evidence for triplet and singlet excited state formation. 3897

Robinson, G. D. Jr. Recoil and charging contributions to organic incorporation of radiobromine atoms following neutron activation. 3331

Robinson, J. S. Emission from aromatic radicals in ion recombination luminescence. 3710

Robinson, K. Role of the diffuse layer in water-in-oil microemulsions. 876

Rodgers, A. S. Comparison of stabilization energy and resonance energy as a measure of the delocalization energy in free radicals. 918

Roe, R-J. X-ray diffraction study of possible clustering in cesium salt of ethylene-acrylic acid copolymer. 1311

Roessler, K. Kinetic analysis and mechanism of chlorine-38 and bromine-82 recoil reactions in $K_2[ReBr_6]/K_2[ReCl_6]$ mixed crystals. 2499

Rogers, F. E. Thermochemistry of the Diels-Alder reaction. II. Heat of addition of several dienes to tetracyanoethylene. 106

Rohatgi, K. K. Hypochromism and exciton interaction in halofluorescein dyes. 3970

Rojo, E. A. Dealkylation of isopropylbenzene on γ-irradiated silica-alumina. Effect of various reagents on the active centers and on their yield. 3741

Rolinski, E. J. Mass spectrometric study of the vaporization of cuprous iodide. 2310

Romberger, K. A. New electrochemical measurements of the liquidus in the lithium fluoride-beryllium fluoride system. Congruency of lithium beryllium fluoride (Li_2BeF_4). 1154

Roos, B. Ester group. I. Ab initio calculations on methyl formate. 2430

Root, J. W. New primary process in the ultraviolet photolysis of methyl iodide. Direct photolysis to :CHI. 308

Rorabacher, D. B. Bicipital relaxation phenomena. 452

Rose, T. L. Production of triplet methylene in the reaction of carbon atoms with hydrogen. 1389

Rosenberg, J. L. Excited state dissociation rate constants in naphthols. 3558

Rosner, D. E. Dissolution lifetime of a hydrated solute sphere. 2017

Rosner, D. E. Quasi-equilibrium analysis of the reaction of atomic and molecular fluorine with tungsten. Reply [to comments]. 2930

Ross, R. A. Kinetic studies of the catalytic activity of alkaline earth oxides in 2-propanol decomposition. 3372

Rossi, A. R. Extended Hueckel calculations on polypeptide chains. IV. ϕ-ψ Energy surface for a tetrapeptide of poly-L-alanine. 2793

Rossiter, R. F. Dielectric relaxation of p-benzoquinones and $Me_{4-n}C(OMe)_n$ and $Me_{4-n}Si(OMe)_n$ (n = 1-4) in benzene solution. 525

Rowland, C. G. Existence of spin-forbidden predissociation in the mass spectrum of isocyanic acid. 2636

Rowland, F. S. Electronegativity effects in T-for-CH_2X substitutions for recoil tritium reactions with propyl fluoride. 187

Rowland, F. S. Temperature dependence of the reaction yields from recoil tritium reactions. II. Tritium atom addition to 1-butene and cis-2-butene. 190

Rowland, F. S. Reactions of fluorine-18 atoms with ethylene. 3509

Roy, C. R. Free-radical decay in γ-irradiated alkyl halide and hydrocarbon-alkyl halide glasses. 1405

Rozett, R. W. Monoisotopic mass spectra of borane derivatives. 1860

Rubin, K. Tetracyanomethane. X-ray diffraction and differential scanning calorimetry study from -150 to +160°. 3973

Rudman, R. Tetracyanomethane. X-ray diffraction and differential scanning calorimetry study from -150 to +160°. 3973

Ruf, A. Effect of temperature in the radiolysis of paraffins. 3851

Ruff, I. Transfer diffusion. III. Kinetics and mechanism of the triiodide-iodide exchange reaction. 162

Ruff, I. Transfer diffusion. IV. Numerical test of the correlation between prototrope mobility and proton exchange rate of H_3O^+ and OH^- ions with water. 2954

Ruff, I. Transfer diffusion. V. Kinetics and mechanism of the exchange reaction between bromide and tribromide ions. 2957

Ryu, J. Electrode reduction kinetics of carbon dioxide in aqueous solution. 3278

Rzad, S. J. Radiolysis of liquid 2,2,4-trimethylpentane. Kinetics of scavenging processes. 2374

Rzad, S. J. Radiolysis of liquid 2,2,4-trimethylpentane. Effect of charge scavengers on product formation. 2381

Rzad, S. J. Application of charge scavenging kinetics to the formation of excited states in irradiated solutions of aromatics in cyclohexane. 3722

Saalfeld, F. E. Bisdifluoraminoalkanes. Mass spectral decomposition of isomeric propanes. 60

Saalfeld, F. E. Intermediates in the reactions of alkane and cycloalkane molecular ions with water vapor. 1517

Safarik, I. Model calculations of secondary α-deuterium isotope effects in addition reactions to olefinic double bonds. 3613

Sakata, T. Electric conduction of the aluminum-auramine-stannic oxide system. 1655

Saleh, J. M. Oxidation of metal films by nitrous oxide. 2530

Saleh, J. M. Interaction of arsine ith evaporated metal films. 2851

Sallach, R. A. Initial reaction of nitrogen with zirconium at 1440°. 2156

Salmon, G. A. Pulse radiolysis of solutions of stilbene. I. Evidence for triplet and singlet excited state formation. 3897

Saluja, P. P. S. Ionic solvation numbers from compressibilities and ionic vibration potentials measurements. 2140

Saluja, P. P. S. Approximate calculations of the heats and entropies of hydration according to various models. 2298

Samat, A. Structure effect on the fading rate of photochromic 3-substituted benzothiazolinic spiropyrans. 3554

Sambhi, M. S. Spectrophotometric and thermodynamic study of donor-acceptor complexes of carbazole. 2102

Samuni, A. Precursors of the metal-complexed hydroperoxyl radical. 2207

Sancier, K. M. Temperature dependence of the electron spin resonance spectra of zinc oxide powder. 2527

Sandberg, R. G. Kinetics of acid dissociation-ion recombination of aqueous methyl orange. 4023

Sandhu, H. S. Rate constants for the reactions of deuterium atoms with silanes. 3911

Sandorfy, C. Low-temperature infrared study of sterically hindered associated alcohols. 864

Sandorfy, C. Vibrational overtone study of association in liquid methanol. 869

Sandstrom, J. Barriers to rotation around the amide bond and the central carbon-carbon bond in tetrabenzyloxamide and its monothio and dithio analogs. 642

Santos, M. C. Transference numbers of potassium chloride and ionic conductances in ethylene glycol at 25°. 712

Sarkar, A. Osmotic properties of polystyrenesulfonates. II. Donnan equilibrium. 1881

Sarma, T. S. Thermodynamics of transfer of tetrabutylammonium bromide from water to aqueous urea solutions and the effects on the water structure. 1366

Sarner, S. F. Gas-phase thermolysis kinetics of small ring nitriles. 2817

Saroff, H. A. Action of hemoglobin. Cooperative and Bohr effects. 1597

Sartorio, R. Dissipative structures and diffusion in ternary systems. 2050

Sato, M. Electron spin resonance evidence for the photosensitized dissociation of hydrogen molecules on vanadium oxide. 2637

Sauer, M. C. V. Reactions of acetone and hydrogen peroxide. II. Higher adducts. 1283

Sawada, K. Visible-light effects on electronic absorption bands of some cation radicals produced by photoionization at 77°K. 639

Scala, A. A. Vacuum ultraviolet photolysis of cyclohexanone. 615

Schaaf, D. W. Mass spectrometric study of the vaporization of cuprous bromide. 3271

Schatz, G. Chemiluminescence excited by atomic fluorine. 3586

Scheider, W. Two-body diffusion problem and applications to reaction kinetics. 349

Scheraga, H. A. Energy parameters in polypeptides. V. Empirical hydrogen bond potential function based on molecular orbital calculations. 375

Scheraga, H. A. Structure of liquid water. Statistical thermodynamic theory. 3229

Schilling, K. M. Ultraviolet photochemistry of formatopentaamminecobalt(III) ion in aqueous solution. Hydrogen atom formation and oxygen → carbon linkage isomerization. 2492

Schindler, R. N. Application of electron cyclotron resonance technique in studies of electron capture processes in the thermal energy range. 3758

Schlegel, J. M. Manometric study of the oxygen-peroxide-superoxide reaction in nitrate melts. 2841

Schleifer, A. Thermal decomposition of cyclobutanone. 963

Schmidt, L. D. Mobility of excess electrons in liquid hydrocarbon mixtures. 442

Schmitz, K. S. Role of orientation constraints and rotational diffusion in bimolecular solution kinetics. 534

Scholes, G. Pulse radiolysis of aqueous thiocyanate solutions. Nature of the intermediate transient species. 1537

Schoonheydt, R. A. Electron paramagnetic resonance of SO_2-on magnesium oxide. 323

Schor, R. CNDO [complete neglect of differential overlap]/2 calculation on the helical conformations of a tetrapeptide of glycine. III. phi-psi. Energy surface. 670

Schor, R. Extended Hueckel calculations on polypeptide chains. IV. ϕ-ψ Energy surface for a tetrapeptide of poly-L-alanine. 2793

Schuler, R. H. Competitive electron-scavenging experiments in the radiolysis of hydrocarbons. Kinetics of the reactions of secondary ions. 987

Schuler, R. H. Production of halide ion in the radiolysis of aqueous solutions of the 5-halouracils. 2386

Schuler, R. H. Lifetime of trifluoromethyl radical in aqueous solution. 2517

Schuler, R. H. Effect of ionic dissociation of organic compounds on their rate of reaction with hydrogen atoms. 2673

Schuler, R. H. Lifetime distribution function for geminate ion pairs and its importance to the kinetics of ionic reactions in the radiolysis of hydrocarbon solutions. 3812

Schulman, S. G. Electronic spectral study of the ionizations of the naphthalene monosulfonic acids. 508

Schulman, S. G. Dissociation constant of the 9-anthroic acidium cation in the lowest excited singlet state. 1996

Schultes, E. Application of electron cyclotron resonance technique in studies of electron capture processes in the thermal energy range. 3758

Schultz, A. W. Interaction of neighboring groups in maleic acid copolymers. 1767

Schurr, J. M. Role of orientation constraints and rotational diffusion in bimolecular solution kinetics. 534

Schwartz, M. E. Ab initio studies of the interactions of an electron and two water molecules as a building block for a model of the hydrated electron. 3905

Schwartz, P. M. Efficiency of the electrochemiluminescent process. 1868

Schwarz, H. A. Ranges of photoinjected electrons in dielectric liquids. 3794

Scott, E. J. Y. Kinetics of the cobalt-catalyzed autoxidation of toluene in acetic acid. Role of cobalt. 1520

Scott, R. M. Hydrogen-bonded complex-ion-pair equilibriums in 3,4-dinitrophenol-amine-aprotic solvent systems. 1989

Scott, R. M. Hydrogen bonding interactions of p-chlorophenol with aliphatic amines. 587

Scudder, J. A. Effect of pressure on charge-transfer complexes in solution. II. Complexes formed between ions and between ions and neutral molecules. 249

Seely, G. R. Chlorophyll-poly(vinylpyridine) complexes. IV. Transfer of energy to a complex of pyrochlorophyll with DTNB [5,5′-dithiobis(2-nitrobenzoic acid)]. 172

Seff, K. Crystal structures of hydrated and dehydrated thallium-exchanged zeolite A. 2593

Seff, K. Crystal structure of an ammonia sorption complex of zeolite 4A. 2597

Seff, K. Crystal structure of a sulfur sorption complex of zeolite 4A. 2601

Sellers, N. G. Theoretical models for acid-base equilibrium data in nonaqueous solvents. 3618

Selwyn, J. E. Aggregation of equilibriums of xanthene dyes. 762

Servis, K. L. Nuclear magnetic resonance studies of methanol-boron trifuloride complexes. 329

Seshadri, K. S. Adsorbed species. II. Electron spin resonance study of thianthrene and other sulfur heterocyclics adsorbed on oxide surfaces. 1443

Setser, D. W. Rate constants for quenching of molecular nitrogen ($A^3\Sigma_u^+$) in active nitrogen. 1

Setser, D. W. Rate constants, threshold energies, and energy partitioning for three and four centered hydrogen chloride elimination reactions of 1,1,2-trichloroethane-1-d_1. 283

Setser, D. W. Nonequilibrium unimolecular reactions and collisional deactivation of chemically activated fluoroethane and 1,1,1-trifluoroethane. 954

Sevilla, M. D. Electron spin resonance study of several DNA base cation radicals produced by photoionization. 3571

Sevilla, M. D. Reactions of the cation and anion radicals of several DNA bases. 3577

Shafrin, E. G. Effect of temperature on wetting of high- and low-energy solid surfaces. 3259

Shapira, D. Photolysis of hydroxylamine in aqueous solution. 180

Shapiro, J. S. Kinetic isotope effects in the reaction of methyl radicals with molecular hydrogen. 1669

Sheets, R. Isotope effect in the decomposition of ammonia on tungsten surfaces. 970

Sheets, R. W. Promoted adsorption of pyridine on nickel. 972

Shelef, M. Studies of surface reactions of nitric oxide by isotope labeling. IV. Reaction between nitric oxide and ammonia over copper surfaces at 150-200°. 37

Sheppard, N. Infrared spectra of hydrocarbons adsorbed on silica-supported metals. IV. Butenes on iridium. 2699

Shida, T. Electronic absorption spectra of excess electrons in molecular aggregates. I. Trapped electrons in γ-irradiated amorphous solids at 77°K. 3683

Shida, T. Electronic absorption spectra of excess electrons in molecular aggregates. II. Solvated electrons. 3691

Shieh, D. J. Magnetic circular dichroism of molecules in dense media. I. Theory. 1844

Shimada, O. Dissociative electron attachment to dimethyl ether in irradiated 3-methylpentane glass. 3747

Shimamoto, N. Transport phenomena of polyelectrolytes in solution under electric field. 2286

Shimoda, H. Electric conduction of the aluminum-auramine-stannic oxide system. 1655

Shin, H. K. Excitation of molecular vibration on collision. Simultaneous vibrational and rotational transitions in hydrogen + argon at high collision velocities. 2006

Shinoda, K. Physicochemical properties of aqueous solutions of fluorinated surfactants. 909

Shoemaker, D. P. Crystal structures of hydrated and dehydrated thallium-exchanged zeolite A. 2593

Shooter, D. Annealing and other variables which affect observed decay rates of trapped electrons in 3-methylpentane glass. 3167

Shore, L. Proton magnetic resonance studies of the structure of water in Dowex 50W. 578

Shoup, R. R. Restricted rotation about the exocyclic carbon-nitrogen bond in cytosine derivatives. 64

Shoup, R. R. Evaluation of the nuclear magnetic resonance total line shape analysis of uncoupled, exchanging two-site systems. 71

Shranin, Yu. I. Polaron yields in low-temperature pulse radiolysis of chemically inert aqueous matrices. 3776

Shroff, G. H. Diffusion of acetic acid dimers and their homomorphs. 2463

Shubin, V. N. Polaron yields in low-temperature pulse radiolysis of chemically inert aqueous matrices. 3776

Shuhler, T. A. Phase diagrams of liquid crystal solvents used in nuclear magnetic resonance studies. 925

Sibirskaya, G. K. Solvated electrons in irradiated concentrated alkaline methanol and water-methanol mixtures. 3765

Silver, M. Hot electron injection into dense methane, carbon monoxide, and carbon dioxide. 3890

Silverman, J. Radiation-induced polymerization of pure styrene at low temperature. 930

Simeral, L. Additivity in the carbon-13 chemical shifts of 1,2-disubstituted ethanes. 1466

Simha, R. Statistical thermodynamics of the glass transition and the glassy state of polymers. 416

Simic, M. Electron spin resonance and pulse radiolysis studies of the reactions of OH and O^- radicals with aromatic and olefinic compounds. 847

Simic, M. Acid-base properties of the radicals produced in the pulse radiolysis of aqueous solutions of benzoic acid. 1398

Simic, M. Electron and hydrogen atom attachment to aromatic carbonyl compounds in aqueous solution. Absorption spectra and dissociation constants of ketyl radicals. 2072

Simic, M. pK_a of the $^+H_3NCHCOOH$ radical. 3507

Simonaitis, R. Bromine atom catalyzed oxidation of carbon monoxide. 1416

Simonetta, M. Electronic and electron spin resonance spectra of the anion radicals of phenyl-and diphenylethylenes. 3960

Simons, J. W. Kinetic study of the reaction of methylene radicals with dimethylsilane. Decomposition of chemically activated trimethylsilane and methylethylsilane. 459

Simons, J. W. Kinetics of vibrationally hot propane produced by methylene insertion into ethane. 607

Simpson, L. M. Photochemical production of hot hydrogen and deuterium atoms. Reactions with hydrogen halides and halogens. 2801

Singh, P. Preparation and structure of bromobis(2-(2-aminoethyl)pyridine)copper(II) bromide. 2887

Sinha, B. P. Oxidation kinetics of 2-dimethylaminoethanethiol hydrochloride by ferricyanide ion in acid medium. 3641

Sircar, S. Thermodynamic consistency test for adsorption of liquids and vapors on solids. 3412

Sircar, S. Analogy between adsorption from liquids and adsorption from vapors. 3415

Skell, P. S. Potential surfaces for the addition of methylene and difluoromethylene to ethylene and isobutene. 664

Skinner, G. B. Comparisons of the RRK [Rice-Ramsperger-Kassel] and RRKM [Markus-Rice] theories of thermal unimolecular reaction. Energy distributions and the s parameter. 2418

Skinner, J. F. Electrolyte viscosities in associated solvents. 434

Slager, T. L. Infrared spectra of the oxides and carbonates of silver. 940

Sloan, A. E. Vibration analyses and barrier to internal rotation of 1,1-dichloroethane and 1,1-dichloroethane-d_4. 3591

Slutsky, L. J. Proton-transfer kinetics in the aminobenzoic acids. 1327

Smail, T. Electronegativity effects in T-for-CH_2X substitutions for recoil tritium reactions with propyl fluoride. 187

Smedley, S. Ultrasonic relaxation in calcium nitrate tetrahydrate melts. 1506

Smejtek, P. Hot electron injection into dense methane, carbon monoxide, and carbon dioxide. 3890

Smid, J. Reactivities of ion pairs and free ions in proton abstraction reactions. Reaction between polystyryl carbanion salts and triphenylmethane. 695

Smid, J. Ion-pair aggregation in solutions of complexes of carbanion salts and macrocyclic polyethers. 2152

Smith, B. L. Raman scattering in sodium-liquid ammonia solutions. 2481

Smith, D. F. Jr. Thermodynamics of acid-base equilibriums. II. Ionization of m- and p-hydroxybenzotrifluoride and the concept of fluorine double bond-no bond resonance. 1909

Smith, D. W. Matrix infrared spectra and bonding in the di- and triiodomethyl radicals. 2718

Smith, M. B. Calculation of $\Delta H_d{}^\circ{}_{(g)} - \Delta H_d{}^\circ{}_{(l)}$ for dissociating dimers via the "dissociation-vaporization" rule. $\Delta H_d{}^\circ{}_{(l)}$ of trimethylaluminum. 2933

Smith, N. O. Solubility and partial molar properties of helium in water and aqueous sodium chloride from 25 to 100° and 100 to 600 atmospheres. 1195

Smith, P. Electron paramagnetic resonance spectroscopic study of the photoinitiated polymerization of alkyl methacrylates. 3141

Smith, W. S. Reactions of recoil chlorine atoms with cis and trans olefins. 2711

Smyrl, N. Infrared and Raman spectra of group I nitrate aggregates in carbon dioxide matrixes and glassy thin films. 1826

Smyrl, N. Alkali metal nitrate glass transition temperatures from vapor deposited films. 3093

Snead, C. C. Association of formic acid in carbon tetrachloride solution. 774

Snider, N. S. Dielectric evidence of two-dimensional condensation of halides adsorbed on nonporous sodium chloride. 2535
Sobczyk, L. Infrared spectra and dipole moments of hydrogen-bonded complexes. III. Adducts of 2,6-dichloro-4-nitrophenol with pyridine bases. 2112
Solomon, B. S. Fluorescence quenching by benzoic acid. 3563
Somorjai, G. A. Vaporization kinetics of hydrogen-bonded liquids. 914
Sonin, A. A. Electrokinetic salt rejection in hyperfiltration through porous materials. Theory and experiment. 4015
Sonin, A. A. Ion transport through layered ion exchange membranes. 3996
Sonnessa, A. J. Thermodynamic and spectral properties of molecular complexes of iodine with several aminopyridines. 1895
Spedding, F. H. Thermodynamics of the association of aqueous europium(III) and sulfate ions. 1887
Spedding, F. H. Effect of high pressure on the formaton of aqueous $EuSO_4^+$ at 25°. 2925
Spedding, P. L. Basic modes of transport in molten salts. 1348
Spiker, R. C. Jr. Argon matrix Raman and infrared spectra and vibrational analysis of ozone and the oxygen-18 substituted ozone molecules. 3208
Spink, C. H. Apparent hydration numbers of alcohols in aqueous solution. 1660
Spiro, M. Transference numbers of potassium chloride and ionic conductances in ethylene glycol at 25°. 712
Spitzer, K. Extended Hueckel calculations on the color of sulfur chains and rings. 2274
Sprague, E. D. Quantum mechanical tunneling in hydrogen atom abstraction for solid acetonitrile at 77-87°K. 546
Srinivasan, R. Photochemical addition of benzene to bicyclo[2.2.1]hept-2-ene (norbornene). 15
Stafford, F. E. Mass spectrometric determination of the heat of formation of ethynyl radical, C_2H, and of some related species. 1913
Stanislaus, A. Kinetics of adsorption of carbon monoxide on alumina. 2349
Starkie, H. C. Electron spin resonance detection of Sn^{3+} and Pb^{3+} complexes in γ-irradiated stannous, plumbous, and plumbic salts. 141
Steel, C. Photochemistry of azoisopropane in the 2000-Ang region. 1685
Steen, H. B. Reactivities of solvated electrons in ethylene glycol-water glass. 2217
Steen, H. B. Mechanisms of photobleaching of trapped electrons in ethylene glycol-water glass. 3366
Stein, G. Photochemistry of benzene in oxygenated aqueous solution in the B_{2u} first excited singlet state. 165
Stein, G. Radiative and nonradiative pathways in solutions. Excited states of the europium(III) ion. 1093
Steiner, W. A. Mass spectrometry study of microwave discharges in hydrogen-carbon monoxide-argon mixtures. 2941
Steinfeld, J. I. Aggregation of equilibriums of xanthene dyes. 762
Stern, J. H. Effects of mannitol and sorbitol on water at 25°. 3077
Stern, K. H. Alkali ion mobility and exchange equilibriums in silica glass. 1072
Stevens, G. Fluorescence of the uranyl ion in electron-irradiated sulfuric acid solutions. 3698
Stevens, G. C. Radiolysis of aqueous methane solutions. 3863
Stevens, R. D. Electron paramagnetic resonance spectroscopic study of the photoinitiated polymerization of alkyl methacrylates. 3141
Stevens, T. L. Association of trifluoroacetic acid in vapor and in organic solvents. 2039
Stevenson, G. R. Equilibrium studies by electron spin resonance. I. Free nitrobenzene anion radical. 1439
Stevenson, G. R. Equilibrium studies by electron spin resonance. II. Nitrobenze free ion-ion pair equilibrium. 2058
Stevenson, G. R. Thermodynamic parameters for the cyclooctatetraene anion radical disproportionation as a function of ion pairing in hexamethylphosphoramide. 2176
Stevenson, J. Gas-phase reaction of perchloric acid with methane. 1795
Stevenson, P. E. CNDO-CI [complete neglect of differential overlap-configuration interaction] studies of the effects of multiple substitution on the electronic spectrum of p-benzoquinone. 2424
Stevovic, J. Kinetics of adsorption of mineral acids on alumina. 3625
Stickney, R. E. Quasi-equilibrium analysis of the reaction of atomic and molecular fluorine with tungsten. [Comments]. 2930
Stoecklin, G. Influence of rotational conformation on the stereochemical course of hot halogen for halogen substitution in liquid 2,3-dichlorobutane. 501
Stoecklin, G. Kinetic analysis and mechanism of chlorine-38 and bromine-82 recoil reactions in $K_2[ReBr_6]/K_2[ReCl_6]$ mixed crystals. 2499
Stone, W. E. Proton mobility in solids. IV. Study of proton motion in the decationated Y zeolite by nuclear magnetic resonance. 1220
Stone, W. E. E. Methanol-silica gel system. II. Molecular diffusion and proton exchange from pulse proton magnetic resonance data. 3078
Stork, W. H. J. Association of crystal violet in aqueous solutions. 1772
Storvick, T. S. Transport properties of polar gases. Collision integrals for the Kihara spherical core plus dipole-dipole potential. 1470
Strathmann, H. Low-pressure ultrafiltration of sucrose and raffinose solutions with anisotropic membranes. 238
Straub, T. S. Isotope effects in proton transfer from general acids to carbon bases. 2951
Strauss, U. P. Dilatometric studies of counterion binding by polycarboxylates. 254
Strauss, U. P. Interaction of neighboring groups in maleic acid copolymers. 1767
Strausz, O. P. Model calculations of secondary α-deuterium isotope effects in addition reactions to olefinic double bonds. 3613
Strausz, O. P. Rate constants for the reactions of deuterium atoms with silanes. 3911
Stroyer-Hansen, T. Infrared spectra of S_4. 3968
Strumeyer, B. Thermodynamic stability of perylene-iodine charge-transfer complexes from measurements of iodine vapor absorption. 921
Stymne, H. CNDO [complete neglect of differential overlap]/2 calculation on the helical conformations of a tetrapeptide of glycine. III. phi-psi. Energy surface. 670
Su, Y. Y. Unimolecular processes subsequent to recoil tritium reactions with spiropentane. 2187
Subramanian, S. Near-infrared spectral studies on the effects of perchlorate and tetrafluoroborate ions on water structure. 84
Subramanian, S. Near-infrared spectroscopic study of the interactions between water and acetone. Reply to comments. 452
Sujdak, R. J. Lifetime of trifluoromethyl radical in aqueous solution. 2517
Sukigara, M. Electric conduction of the aluminum-auramine-stannic oxide system. 1655
Sullivan, P. D. Electron spin resonance studies of dialkoxydialkylbenzenes. Evidence for some unusual rearrangements in sulfuric acid. 3943
Summers, W. A. Jr. Viscosity effects on the photohydration of pyrimidines. 3137
Sun, S. F. Intrinsic viscosities of bovine serum albumin in propyl alcohol-water mixtures. 128
Sundararajan, S. Photoredox chemistry of bis(2,9-dimethyl-1,10-phenanthroline)copper(II) complexes in aqueous and methanolic media. 1528
Sunder, S. Excess partial molal heat capacities of n-tetraamylammonium bromide in water from 10 to 80° and in aqueous tert-butyl alcohol solvent system at 30° and the effects on the water structure. 2577
Sung, N. H. Resolution of components of the optical rotation tensor of collagen. 2935
Suryanarayanan, K. Photolysis of solid dimethylnitramine. Nitrogen-15 study and evidence for nitrosamide rearrangement. 496
Sutcliffe, B. T. Theoretical study of hyperfine coupling constants of some σ radicals based on the INDO [intermediate neglect of differential overlap] method. 553
Sutcliffe, H. Comparison of the radiolysis of liquid bromotrifluoromethane with the radiolysis of liquid trifluoroiodomethane. 2070
Svejda, P. Electron spin resonance study of adsorption stabilization of photolytic trifluoromethyl radicals on zeolites. 2690
Sweeney, W. V. Electron spin resonance spectroscopy of the bisdithiooxalatonitrosyl iron anion. 49
Swinehart, J. H. Equilibrium and kinetic properties of 9,10-phenanthrenequinone-3-sulfonate in aqueous solutions. 1875
Swinehart, J. H. Kinetic study of the monomer-dimer equilibrium in aqueous vanadium(IV) tetrasulfophthalocyanine solutions. 2343
Sworski, T. J. Elementary processes in the radiolysis of aqueous sulfuric acid solutions. Determinations of both G_{OH} and G_{SO_4}. 1265
Sworski, T. J. Elementary processes in the radiolysis of aqueous nitric acid solutions. Determination of both G_{OH} and G_{NO_3}. 2680
Symons, M. C. R. Electron spin resonance detection of Sn^{3+} and Pb^{3+} complexes in γ-irradiated stannous, plumbous, and plumbic salts. 141
Symons, M. C. R. Paramagnetic centers in or on various oxides. 3095
Szwarc, M. Electron spin resonance studies of the electron-transfer equilibrium β-ethylnaphthalenide + α-ethylnaphthalene ↔ β-ethylnaphthalene + α-ethylnaphthalenide. 1734
Szwarc, M. Aggregation of salts of thianthrene radical cations. 3468
Tabata, Y. Studies of transition phenomena of some organic solids by electrical conductivity measurement at low temperature. 115
Tabata, Y. Transition phenomena of some organic solids by electrical conductivity measurement at low temperature. Reply to the comment. 2799
Takada, Y. Effects of neutron radiation on the catalytic activities of lithium-doped copper, nickel, and copper-nickel. 2625
Takagi, H. Free-radical intermediates in the reaction of the hydroxyl radical with dialkyl sulfoxides. 135
Takahashi, H. Study of the nature of active sites on zeolites by the measurement of heat of immersion. II. Effects of silica/alumina ratio to electrostatic-field strength of calcium-exchanged zeolites. 110
Takahashi, T. Transport phenomena of polyelectrolytes in solution under electric field. 2286
Takaki, U. Ion-pair aggregation in solutions of complexes of carbanion salts and macrocyclic polyethers. 2152
Takeuchi, T. Effects of neutron radiation on the catalytic activities of lithium-doped copper, nickel, and copper-nickel. 2625
Tam, J. W. O. Solutions of N-substituted amino acids. IV. Tautomerism in N,N-dibutyl-α-, β-, and γ-amino acids. 4033
Tamai, Y. Experimental study of the relation between contact angle and surface roughness. 3267
Tamaru, K. Identification of reaction intermediates by microwave spectroscopy. Catalytic reactions between propylene and deuterium over zinc oxide. 2184
Tamir, M. Biphotonic ionization processes in nonpolar solutions of N,N,N′,N′-tetramethyl-p-phenylenediamine. 2229
Tamura, H. Reduction of methylene blue on illuminated titanium dioxide in methanolic and aqueous solutions. 3460
Tan, H-S. Reaction of ethyl radicals with nitric oxide. Nitrosoethane and triethylhydroxylamine formation. 3303
Tanaka, K. Photocatalytic reactions on zinc oxide. III. Hydrogenation of ethylene. 1394
Tanaka, K. Photocatalytic reaction on zinc oxide. II. Oxidation of carbon monoxide with nitrous oxide and oxygen. 1807

Tanaka, K. Adsorbed oxygen species on zinc oxide in the dark and under illumination. 3184

Tanaka, M. Infrared spectra of carbon monoxide chemisorbed on iron at low temperature. 3180

Tanford, C. Micelle shape and size. 3020

Tang, Y. N. Recoil tritium reactions with hexamethyldisilane in the gas phase. 1249

Tang, Y-N. Unimolecular processes subsequent to recoil tritium reactions with spiropentane. 2187

Tang, Y-N. Reactions of recoil chlorine atoms with cis and trans olefins. 2711

Taniguchi, H. Free-radical intermediates in the reaction of the hydroxyl radical with dialkyl sulfoxides. 135

Tarpley, A. R. Jr. High-resolution carbon-13 nuclear magnetic resonance spectra and substituent effects for monohalobenzenes. 515

Tarpley, A. R. Jr. Steric interactions in tert-butylethylenes observed through proton carbon-13 satellite spectra. 2877

Tawn, D. N. Emission from aromatic radicals in ion recombination luminescence. 3710

Taylor, D. R. Structure and orientation of phenols chemisorbed on γ-alumina. 2882

Taylor, R. W. Bicipital relaxation phenomena. 452

Teather, G. G. Spectral shifts of trapped electrons in alkane glasses at 76°K. 3847

Tehan, F. J. Spectra of Na^-, K^-, and e^-_{solv} in amines and ethers. 2975

Tellinghuisen, J. B. Quantum yields in the 58.4-nm photolyses of ammonia and water. 298

Testa, A. C. Photochemistry of nitrosobenzene. 1087

Testa, A. C. Photochemistry of phenylimidazoles. 3362

Teter, M. P. Bronsted acid sites on porous glass from membrane potentials. 3633

Tetreau, C. Triplet states of biphenylene. 225

Theodorou, I. E. Dielectric properties and relaxation in ethylene carbonate and propylene carbonate. 2892

Thoma, R. E. New electrochemical measurements of the liquidus in the lithium fluoride-beryllium fluoride system. Congruency of lithium beryllium fluoride (Li_2BeF_4). 1154

Thomas, H. E. Modifications to a precision adsorption apparatus. Interaction of the inert gases with boron nitride. 3171

Thomas, J. K. Reactions of electrons in glycerol. 1700

Thomas, J. K. Excited states in the nanosecond pulse radiolysis and laser flash photolysis of N,N-dimethylaniline. 3805

Thomas, J. K. Picosecond observations of some ionic and excited state processes in liquids. 3856

Thomas, V. G. Hot-atom reactions of iodine in the liquid phase induced by x-ray resonance absorption. 2639

Thompson, L. G. External heavy atom effect on the phosphorescence spectra of some halonaphthalenes. 221

Tiepel, E. W. Partial molal volumes of gases dissolved in electrolyte solutions. 3044

Timmons, R. B. Hydrolysis of triethylethoxysilane at the silica-carbon tetrachloride interface. 3192

Toby, S. Reaction of trifluoromethyl radicals with hexafluoroacetone imine. 487

Tokousbalides, P. Fluorescence spectra and lifetimes of Sm^{3+} in phosphoryl chloride-tin tetrachloride. 3397

Tomimoto, S. Photoinduced ionic dissociation of tetracyanobenzene-α-methylstyrene complex. 1419

Tomkins, R. P. T. Nuclear magnetic resonance study of acid-base interactions for the chloranil electrode system in acetonitrile. 246

Tondre, C. Ultrasonic studies of proton transfers in solutions of poly(lysine) and poly(ornithine). Implications for the kinetics of the helix-coil transition of polypeptides and for the ultrasonic absorption of proteins. 1737

Tondre, C. Apparent molal volumes of polyelectrolytes in aqueous solutions. 3451

Toriyama, K. Thermal decomposition of 3-halo-3-phenyldiazirine in solution. 797

Toriyama, K. Electron spin resonance study of nitrile and other radicals trapped in γ-irradiated single crystals of cyanoacetic acid. 3377

Toriyama, K. Electron spin resonance evidence for the carbon-fluorine bond rupture by dissociative electron attachment. 1824

Toyoguchi, Y. Reduction of methylene blue on illuminated titanium dioxide in methanolic and aqueous solutions. 3460

Trachtman, M. Quenching of $^3P_1$ mercury atoms by isotopic aromatic molecules. 2665

Treinin, A. Photolysis of hydroxylamine in aqueous solution. 180

Trindle, C. Mixed basis scheme for the rapid computation of molecular electronic energy in the SCF-LCAO-(STO [Slater-type orbitals])-MO formalism, and its application to the lithium superoxide molecule. 2995

Truong, T. B. Negative species formed in γ- or ultraviolet-irradiated nonpolar glasses. 3894

Tsang, W. Hydrocarbon decomposition. 6. Thermal decomposition of 3,4-dimethylhexane, 2,2,3-trimethylpentane, tert-butylcyclohexane, and related hydrocarbons. 143

Tsao, C-W. New primary process in the ultraviolet photolysis of methyl iodide. Direct photolysis to :CHI. 308

Tschuikow-Roux, E. Kinetic analysis of the shock wave decomposition of 1,1,1,2-tetrafluoroethane. 292

Tseung, A. C. C. Kinetics of oxygen reduction on graphite/cobalt-iron oxide electrodes with coupled heterogeneous chemical decomposition of hydrogen peroxide. 3646

Tsubomura, H. Photoionization and Rydberg states of tetraaminoethylenes in organic solutions. 2105

Tsuji, K. Infrared optical constants and absorption intensities of naphthalene single crystal. 260

Tsutsumi, K. Study of the nature of active sites on zeolites by the measurement of heat of immersion. II. Effects of silica/alumina ratio to electrostatic-field strength of calcium-exchanged zeolites. 110

Turkevich, J. Laser Raman spectroscopy of surfaces. 2325

Turner, J. B. Vibrational spectra and structure of organogermanes. XII. Normal vibrations and free rotation in p-chlorophenylgermane and p-fluorophenylgermane. 1558

Turner, P. J. Nuclear magnetic resonance study of acid-base interactions for the chloranil electrode system in acetonitrile. 246

Tuttle, T. R. Jr. Solvent effect on metal hyperfine constants in alkali metal radical anion ion pairs. 2866

Uchtman, V. A. Structural investigations of calcium binding molecules. I. Crystal and molecular structures of ethane-1-hydroxy-1,1-diphosphonic acid monohydrate, $C(CH_3)(OH)(PO_3H_2)_2 \cdot H_2O$. 1298

Uchtman, V. A. Structural investigations of calcium binding molecules. II. Crystal and molecular structures of calcium dihydrogen ethane-1-hydroxy-1,1-diphosphonate dihydrate, $CaC(CH_3)(OH)(PO_3H)_2 \cdot 2H_2O$. Implications for polynuclear complex formation. 1304

Ueda, T. Effective fixed charge density governing membrane phenomena. IV. Further study of activity coefficients and mobilities of small ions in charged membranes. 2447

Uhlmann, D. R. Viscous flow in simple organic liquids. 2317

Ullman, R. Hydrodynamic interaction of segmented rodlike molecules. Comparison among three approximations. 1755

Uytterhoeven, J. B. Location of univalent cations in synthetic zeolites of the Y and X type with varying silicon to aluminum ratio. II. Dehydrated potassium exchanged forms. 650

Uytterhoeven, J. B. Identification of the A-type hydroxyls on silica surfaces. 1434

Van Cauwelaert, F. H. Identification of the A-type hydroxyls on silica surfaces. 1434

Van Hook, W. A. Vapor pressure isotope effect in aqueous systems. I. Water-water-d_2 (-64° to 100°) and water-water^{18}-0 (-17° to 16°). Ice and liquid. II. Alkali metal chloride solution in water and water-d^2 (-5° to 100°). 743

Van Hook, W. A. Vapor pressure isotope effect in aqueous systems. III. Vapor pressure of HOD (-60 to 200°). 3040

Van Paemel, C. Electron spin resonance study of several DNA base cation radicals produced by photoionization. 3571

Van Paemel, C. Reactions of the cation and anion radicals of several DNA bases. 3577

Vansant, E. F. Electron paramagnetic resonance spectra of amino radicals formed by γ irradiation of ammoniated zeolites. 2716

Vansant, E. F. Electron paramagnetic resonance study of copper(II)-ammonia complexes in Y-type zeolites. 2860

Varga, J. A. Strong crystalline field perturbation calculations for d^3,d^7 pentacoordinate complexes. I. Trigonal bipyramid. 2907

Vasaros, L. Influence of rotational conformation on the stereochemical course of hot halogen for halogen substitution in liquid 2,3-dichlorobutane. 501

Vasvari, G. Sequence studies in liquid-phase hydrocarbon oxidation. I. Alcohol-ketone transition in the oxidation of ethylbenzene. 2785

Vedrine, J. C. Powder ENDOR [electron nuclear double resonance] line shapes. Nuclear relaxation induced by motion of nearby electron spins. 2079

Vedrine, J. C. Proton ENDOR [electron nuclear double resonance] of γ-irradiated Y-type zeolites. 2087

Velapoldi, R. A. Quantum efficiencies and radiationless transitions of europium(III) in phosphate glasses. 1293

Veljkovic, S. Kinetics of adsorption of mineral acids on alumina. 3625

Villermaux, J. Laser-induced gas breakdown. Spectroscopic and chemical studies. 31

Vincent-Geisse, J. Infrared spectra of nitrous oxide adsorbed on sodium type A synthetic zeolite. 945

Vinogradov, G. A. Polaron yields in low-temperature pulse radiolysis of chemically inert aqueous matrices. 3776

Vinogradov, S. N. Hydrogen-bonded complex-ion-pair equilibriums in 3,4-dinitrophenol-amine-aprotic solvent systems. 1989

Vitagliano, V. Dissipative structures and diffusion in ternary systems. 2050

Vladimiroff, T. First-order perturbation theory in the LCAO approximation. Case of an ionic crystal in a magnetic field. 3993

Volman, D. H. Rate constant for the reaction of HO_2 with carbon monoxide. 3301

Voltz, R. Formation of excited singlet states in irradiated aromatic liquids. 3867

Vorachek, J. H. Methylene produced by vacuum-ultraviolet photolysis. IV. Energy distribution for the reaction $C_3H_8+h\nu$ (123.6 nm) = $CH_2+C_2H_6$. 9

Vouros, P. Chemical ionization mass spectrometry using tetramethylsilane. 3217

Waage, E. V. Competitive thermal unimolecular reactions of trans-cyclopropane-d_2. Collisional energy transfer. 1695

Waddington, D. J. Epoxidation of alkenes in the gas phase. 3319

Wade, W. H. Adsorption on flat surfaces. III. Adsorption of branched-chain alcohols. 675

Wagner, L. C. Study of ionization processes by the angular distribution technique. Silver cloride system. 2819

Walker, D. C. Cerenkov reabsorption spectroscopy for subnanosecond pulse radiolysis studies. 3780

Walker, M. S. Electronic structure of furanquinones. II. Emission spectra of dinaphtho[2,1:2′,3′]furan-8,13-dione and dinaphtho[1,2:2′,3′]furan-7,12-dione. 2240

Walkley, J. Scaled particle theory for nonelectrolyte solution of dilute solid solutes. 2138

Wallace, S. C. Cerenkov reabsorption spectroscopy for subnanosecond pulse radiolysis studies. 3780

Walters, E. A. Isotope effects on hydroxide ion in aqueous solution. 362

Wang, F-M. Energy transfer in thermal methyl isocyanide isomerization. Relative efficiency of mercury atoms. 1935

Warneck, P. Reaction of ozone with carbon monoxide. 1514

Warrick, P. Jr. Viscosity effects on ion-recombination kinetics. Bromocresol green in water-glycerol mixtures. 1184

Wasgestian, H. F. Evidence against the doublet hypothesis. Photolysis of hexacyanochromate(III) in dimethylformamide. 1947

Wasserman, B. Aggregation of salts of thianthrene radical cations. 3468

Wasserman, E. Electron spin resonance of triplet nitrenes from aryl isocyanates. 3570

Watanabe, T. Electronic absorption spectra of excess electrons in molecular aggregates. I. Trapped electrons in γ-irradiated amorphous solids at 77°K. 3683

Watanabe, T. Electronic absorption spectra of excess electrons in molecular aggregates. II. Solvated electrons. 3691

Watkins, A. R. Electron-transfer mechanism of fluorescence quenching in polar solvents. I. Dicyanobenzene as quencher. 469

Watkins, A. R. Electron transfer mechanism of fluorescence quenching in polar solvents. II. Tetracyanoethylene and tetracyanobenzene as quenchers. 3132

Watkins, K. W. Cyclization and decomposition of 4-penten-1-yl radicals in the gas phase. 1089

Webber, L. M. Effect of hydrogen adsorption on the electron paramagnetic resonance spectra of catalysts containing chromium oxide. 2694

Webber, S. E. External heavy atom effect on the phosphorescence spectra of some halonaphthalenes. 221

Webster, B. C. Stabilized cluster. Molecular model for the solvated electron. 3714

Webster, K. Electron spin resonance evidence for dissociative electron capture in γ-irradiated phosphate esters. 2848

Wehry, E. L. Photoredox chemistry of bis(2,9-dimethyl-1,10-phenanthroline)copper(II) complexes in aqueous and methanolic media. 1528

Weiner, S. C. Catalytic hydrogenation of propylene. Verification of maximum rate. 943

Weller, A. Electron-transfer mechanism of fluorescence quenching in polar solvents. I. Dicyanobenzene as quencher. 469

Weller, A. Electron transfer mechanism of fluorescence quenching in polar solvents. II. Tetracyanoethylene and tetracyanobenzene as quenchers. 3132

Wen, W. Y. General solution for the sequence of two competitive-consecutive second-order reactions. 704

Wen, W. Y. Ultraviolet spectra of single and double molecules of gaseous bromine 1017

Wen, W-Y. Thermodynamics of transfer of three tetraalkylammonium bromides from water to aqueous urea solutions at 25°. 1369

Wendorff, J. H. Transitions in mesophase-forming systems. III. Transformation kinetics and textural changes in cholesteryl nonanoate. 276

Wendorff, J. H. Transitions in mesophase forming systems. IV. Transformation behavior and pretransition effects in p-azoxyanisole. 2605

Wennerstrom, H. Ester group. I. Ab initio calculations on methyl formate. 2430

Westenberg, A. A. Steady-state intermediate concentrations and rate constants. HO_2 results. 1586

Westenberg, A. A. Measurement of the rate constant for $H + H_2CO \rightarrow H_2 + HCO$ at 297-652°K. 2213

Westenberg, A. A. Relative rate constants for $O + HCO \rightarrow OH + CO$ and $O + HCO \rightarrow H + CO_2$. 2215

Weston, R. E. Jr. Kinetic isotope effects in the reaction of methyl radicals with molecular hydrogen. 1669

Wettermark, G. CNDO [complete neglect of differential overlap]/2 calculation on the helical conformations of a tetrapeptide of glycine. III. phi-psi. Energy surface. 670

Wexler, S. Hydrogen displacement in butane by fast molecular tritium collisions. [Reply to] comments. 2939

Whillans, D. W. Photoreactions in aqueous solutions of thymine, pH 12. 489

White, G. Bisdifluoraminoalkanes. Mass spectral decomposition of isomeric propanes. 60

White, J. M. Oxidation of carbon at the surface of nickel. 968

White, J. M. Photochemistry of ethanethiol at 254 and 214 nm. 2668

White, R. D. Proton-transfer kinetics in the aminobenzoic acids. 1327

White, R. D. Kinetics of acid dissociation-ion recombination of aqueous methyl orange. 4023

Whitesides, G. M. Nitrogen and boron spin-lattice relaxation in borazole. 2871

Whitten, D. G. Measurement of excited singlet yields in γ-radiolysis of benzene and ketones. Radiation-induced "type II" elimination of 4-methyl-4-phenyl-2-pentanone. 198

Widman, R. P. Temperature effects in the intersystem crossing process of anthracene. 1524

Willard, J. E. Free-radical decay in γ-irradiated alkyl halide and hydrocarbon-alkyl halide glasses. 1405

Willard, J. E. Elementary processes in the photochlorination of 3-methylpentane glass at 77-97°K. 1800

Willard, J. E. Wavelength dependence of photobleaching of trapped electrons in 3-methylpentane glass. 2341

Willard, J. E. Time-dependent scavenging of trapped electrons in 2-methyltetrahydrofuran glass at 77°K. 2641

Willard, J. E. Chemical reactions on γ-irradiated silica gel and porous Vycor glass. 3158

Willard, J. E. Annealing and other variables which affect observed decay rates of trapped electrons in 3-methylpentane glass. 3167

Willey, D. G. Thermodynamic study of solutions with liquid crystal solvents by gas-liquid partition chromatography. 99

Willi, A. V. Kinetic dueterium isotope effects in the reactions of methyl iodide with azide and acetate ions in aqueous solution. 427

Williams, D. J. Ultraviolet adsorption spectra of polyphosphate solutions. 3673

Williams, F. Quantum mechanical tunneling in hydrogen atom abstraction for solid acetonitrile at 77-87°K. 546

Williams, F. Electron spin resonance evidence for dissociative electron capture in γ-irradiated phosphate esters. 2848

Williams, F. Investigation of the structure of the hydrated electron based on unpaired electron densities calculated by the INDO [intermediated neglect of differential overlap] method. 3838

Williams, F. Reversible line broadening in the electron spin resonance spectra of tert-butyl radicals in γ-irradiated crystalline tert-butyl isothiocyanate. 1792

Williams, M. B. Oxidation pathways of 2 2′-benzothiazolinone azines. I. Electrochemistry. 1178

Williams, R. L. Reactions of fluorine-18 atoms with ethylene. 3509

Wilson, W. W. Quasi-elastic light scattering from two-component mixtures. 2744

Winkler, C. A. Quantum yields in the 58.4-nm photolyses of ammonia and water. 298

Wirth, H. E. Proton magnetic resonance in concentrated aqueous solutions of tetraalkylammonium bromides and inorganic halides at 25 and 65°. 130

Wirth, H. E. Temperature dependence of the apparent and partial molal volumes of concentrated aqueous electrolyte solutions of tetraalkylammonium bromides, cetyltrimethylammonium bromide, and ammonium and lithium bromides. 1333

Wirth, H. E. Apparent molal volumes of sodium chloride and magnesium chloride in aqueous solution. 3488

Wirth, H. E. Volume changes on mixing solutions of magnesium chloride and sodium chloride. 3491

Witt, J. D. Vibration analyses and barrier to internal rotation of 1,1-dichloroethane and 1,1-dichloroethane-d_4. 3591

Wold, S. Temperature dependence of the heat capacity of activation $(\Delta C_p^{\pm})$ for solvolysis reactions in water. 369

Wolff, H. Hydrogen bonding and complex formation of dimethylamine. Infrared investigations on the NH stretching vibration bands. 871

Won, C. M. Kinetic dueterium isotope effects in the reactions of methyl iodide with azide and acetate ions in aqueous solution. 427

Wood, R. H. Heats of mixing aqueous electrolytes. IX. The reciprocal salt pair $Mg^{2+}, Na^+||Cl^-, Br^-$. 3474

Woolf, L. A. Multicomponent diffusion in a system consisting of a strong electrolyte solute at low concentrations in an ionizing solvent. 1166

Woolley, E. M. Molecular association of hydrogen bonding solutes. Phenol in cyclohexane and benzene. 3058

Worley, S. D. Rates of interaction of vibrationally excited hydroxyl ($v = 9$) with diatomic and small polyatomic molecules. 1511

Wu, M. C. R. Comparison of stabilization energy and resonance energy as a measure of the delocalization energy in free radicals. 918

Wyatt, J. R. Mass spectrometric determination of the heat of formation of ethynyl radical, C_2H, and of some related species 1913

Wyckoff, J. C. Apparent hydration numbers of alcohols in aqueous solution. 1660

Yager, W. A. Electron spin resonance of triplet nitrenes from aryl isocyanates. 3570

Yakatan, G. J. Electronic spectral study of the ionizations of the naphthalene monosulfonic acids. 508

Yamabe, S. Molecular orbital calculation of chemically interacting systems. Bimolecular nucleophilic substitution. 232

Yamada, H. Infrared optical constants and absorption intensities of naphthalene single crystal. 260

Yamazaki, T. Electronic absorption studies of the radical complex between perylene and tetracene cations. 1549

Yanagida, R. Y. Crystal structure of an ammonia sorption complex of zeolite 4A. 2597

Yang, G. C. Electron spin resonance studies of cation radicals in trifluoromethanesulfonic acid. 1504

Yannas, I. V. Resolution of components of the optical rotation tensor of collagen. 2935

Yayanos, A. A. Apparent molal volume of glycine, glycolamide, alanine, lactamide, and glycylglycine in aqueous solution at 25° and high pressures. 1783

Yeager, E. Concentration dependence of ionic vibration potentials. Consequences for the determination of ionic partial molal volumes. 1086

Yeager, E. Ultrasonic relaxation in calcium nitrate tetrahydrate melts. 1506

Yeatts, L. B. Electrical conductance and ionization behavior of sodium chloride in dioxane-water solutions at 300° and pressures to 4000 bars. 1053

Yencha, A. J. Hydrogen displacement in butane by fast molecular tritium collisions. [Comments]. 2937

Yoneda, Y. Kinetic study of n-butene isomerization over supported aluminum and magnesium sulfates. 44

Yoneyama, H. Reduction of methylene blue on illuminated titanium dioxide in methanolic and aqueous solutions. 3460

Yoong, M. Systematics of (n,γ)-activated hot iodine-128 reactions in gaseous methane and halomethanes. Energy Degradation factor. 2685

Yoshida, H. Dissociative electron attachment to dimethyl ether in irradiated 3-methylpentane glass. 3747

Yu, T-Y. Ionic reactions in monosilane. Radiation chemistry implications. 3321

Yung, D. Electrokinetic salt rejection in hyperfiltration through porous materials. Theory and experiment. 4015

Zagari, A. Dissipative structures and diffusion in ternary systems. 2050

Zainal, H. Reactions involving electron transfer at semiconductor surfaces. IV. Zinc oxide promoted photoreductions in aqueous solutions at neutral pH. 2362

Zambonin, P. G. Redox mechanisms in an ionic matrix. Kinetics of the reaction $20_2^- + H_2O = 2OH^- + 1.50_2$ in molten alkali nitrates. 422

Zana, R. Ultrasonic studies of proton transfers in solutions of poly(lysine) and poly(ornithine). Implications for the kinetics of the helix-coil transition of

polypeptides and for the ultrasonic absorption of proteins. 1737
Zana, R. Apparent molal volumes of polyelectrolytes in aqueous solutions. 3451
Zana, R. Concentration dependence of ionic vibration potentials. Consequences for the determination of ionic partial molal volumes. 1086
Zarnegar, B. M. Measurement of excited singlet yields in γ-radiolysis of benzene and ketones. Radiation-induced "type II" elimination of 4-methyl-4-phenyl-2-pentanone. 198
Zecchina, A. Infrared study of surface properties of α-chromia. IV. Pyridine and heavy water adsorption on oxygen-covered surface. 571
Zehavi, D. Oxidation of aqueous bromide ions by hydroxyl radicals. Pulse radiolytic investigation. 312
Zehavi, D. Pulse radiolysis of the aqueous ferro-ferricyanide system. 1. Reactions of OH, HO_2, and O_2^- radicals. 3703
Zeldes, H. Paramagnetic resonance study of liquids during photolysis. XIV. Pyridine, pyrazine, pyrimidine, and pyridazine. 3348
Zeman, L. Pressure effects in polymer solution phase equilibriums. I. Lower critical solution temperature of poly(isobutylene) and poly(dimethylsiloxane) in lower alkanes. 1206
Zeman, L. Pressure effects in polymer solution phase equilibriums. II. Systems showing upper and low critical solution temperatures. 1214
Zhestkova, T. P. Solvated electrons in irradiated concentrated alkaline methanol and water-methanol mixtures. 3765
Zimbrick, J. D. Concentrated electron scavenger effects on the yields of trapped species in γ-irradiated alkaline glass. 1962
Zisman, W. A. Effect of temperature on wetting of high- and low-energy solid surfaces. 3259
Zorman, G. Reactions of the cation and anion radicals of several DNA bases. 3577
Zubler, E. G. Adsorption effects in tungsten-oxygen-bromine reaction. 320
Zuiderweg, L. H. Irreversible potentiometric behavior of isotactic poly(methacrylic acid). 2559
Zwolinski, B. J. Molecular structure and shear viscosity. Isomeric hexanes. 3295

KEYWORD INDEX *to Volume 76, 1972*

Ab initio hydrated electron 3905
Absorbance flash photolyzed oxalatoiron 2618
Absorption charge transfer complex 249
Absorption coeff molecule dense media 1844
Absorption naphthalene 260
Absorption polyphenyl 3983
Absorption spectra solvated electron 2931
Absorption spectra trapped electron 3847
Absorption ultrasound dioxane water 1571
Absorption water interface polemic 1505
Abstraction reaction butene oxygen 3311
Acceptor donor adduct 3532
Acceptor donor complex carbazole 2102
Acetate amyl decompn kinetics 3917
Acetate glass ionic covalent interaction 1035
Acetate glycerol soln 2474
Acetate methyl iodide 427
Acetate soln water activity 90
Acetic acid chloroform water 2050
Acetic acid dimer diffusion 2463
Acetic acid ethylamine thermodn 2764
Acetic acid trifluoro assocn 2039
Acetone gaseous ion mol 409
Acetone imine hexafluoro trifluoromethyl radical 487
Acetone peroxide mechanism 1283
Acetone polystyrene soln 1214
Acetone pulse irradiated 26
Acetone water complex polemic 452
Acetone water IR polemic 449
Acetonitrile hydrogen atom abstraction 546
Acetophenone photoredn 821
Acetylene cyano nitrogen reaction 2643
Acetylene dicarboxylate radical protonation 1957
Acetylene dicyano oxygen atom 269
Acetylene oxygen system emission 825
Acid amino soln 4033
Acid base equil 3618
Acid base equil thermodn 1909
Acid base interaction chloranil 246
Acid base recombination bromcresol green 1184
Acid catalyzed hydrolysis dichromate 582
Acid catalyzed isomerization 44
Acid cyanoacetic irradn ESR 3377
Acid dissocn methyl orange 4023
Acid equil maleate 1957
Acid olefin proton exchange 2951
Acid site Bronsted glass 3633
Acid sulfuric radiolysis product 3676
Acidity benzoic acid radicals 1398
Acidity napthol excited 3558
Aconitase mechanism 3073
Aconitic acid ionization const 3073
Acridine radical anion phenyl ESR 3958
Acridine Red aggregation equil 762
Acrylate ethylene copolymer 1311
Acrylate radical ESR 1957
Acrylic acid molar vol 3451
Acrylic copolymer dimerization 1311
Acrylonitrile elec conductivity 115
Actinometer UV photolysis ethylene 138
Activation conformation amide 2178
Activation energy hydrogen transfer 1581
Activation energy proton transfer 1327
Activation energy pyrolysis 3538
Activation energy thermal curves 162
Activation heat capacity sovolysis 369
Activation parameter pyruvate iodination 3121
Active nitrogen quenching rate 1
Active site zeolite 110
Activity coeff 2447
Activity coeff heptane dihexyloxyazoxybenzene 596
Activity coeff medium phenylborate 2024
Activity coeff polystyrenesulfonate 1881
Activity coeffs org solute 99
Activity free energy mixing 2764
Activity gradient soln column 1637
Activity ion computer simulation 1758
Activity osmotic pressure polyelectrolyte 3445
Activity solvent polystyrene 1492
Activity water soln 90
Addn alkene methyl isotope effect 3613
Addn butene oxygen 3311
Addn diene tetracyanoethylene 106
Addn hydrated electron 2072
Adduct donor acceptor 3532
Adsorbed haloalkane dielec property 2535
Adsorbed hydrocarbon metal IR 2699
Adsorption alc alumina 675
Adsorption app inert gas 3171
Adsorption arsine iron nickel 2851
Adsorption carbon monoxide alumina 2349
Adsorption effect voltammetry 976
Adsorption effects reactions 320
Adsorption gas water interface 2769
Adsorption iodomethane zinc oxide 2353
Adsorption ion electrode 2915
Adsorption isotherm detn 2584
Adsorption liq 3412 3415
Adsorption mordenite gas chromatog 1647
Adsorption mordenite nonpolar mol 1641
Adsorption nitrous oxide zeolite 945
Adsorption oxygen zinc oxide 3184
Adsorption pyridine nickel 972
Adsorption tetraphenylborate mercury 707
Adsorption thianthrene oxide 1443
Adsorption water lysozyme 2987
Adsorption water silica 3188
Adsorption water vapor 2280
Aggregation equil xanthene dye 762
Aggregation ion pair soln 2152
Aggregation methylene blue 4026
Aggregation phthalocyanine dye 446
Aggregation sensitizing dye CD 2982
Air effect xenon trioxide irradn 3909
Alanine tetrapeptide energy surface 2793
Albumin borine serum 128
Albumin bovine serum light scattering 2744
Alc adsorption alumina 675
Alc fluoride ion coordination 1775
Alc hydration aq soln 1660
Alc IR hydrogen bonding 2562
Alc isopropyl 3372
Alc perchlorate cond solvation 3029
Alc solvated electron 3780
Alc solvated electron absorption 2931
Alc water ion pair formation 3842
Alcs photolysis UV 2061
Alcs sterically hindered assocd 864
Alk earth halide heat mixing 1616
Alk glass irradn electron scavenger 1962
Alk ice electron mobility 1509
Alk ice paramagnetic relaxation 1226
Alkali carbonate molten Raman 1565
Alkali chloride soln vapor pressure 743
Alkali halide heat mixing 1616
Alkali halide structure liq theory 1612
Alkali ion mobility glass 1072
Alkali metal cadmium halide melt 1831
Alkali metal hyperfine coupling 2866
Alkali metal ion pairing 1012
Alkali metal nitrate glass transition 3093
Alkali methanol solvated electron 3765
Alkali nitrate molten 422
Alkali perchlorate methanol assocn 2920
Alkaline earth oxide catalysts 3372
Alkane glass trapped electron 3847
Alkane mol ion water vapor 1517
Alkane polyisobutylene soln 1206
Alkane THF hyperfine coupling 2866
Alkene addn methyl isotope effect 3613
Alkene addn methylene stereochem 664
Alkene benzene singlet quenching 3668
Alkene epoxidation gas phase 3319
Alkene iodine hot atom reaction 3342
Alkyl chloride adsorption 2535
Alkyl phosphate irradn ESR 2848
Alkyl pyruvate iodination 3121
Alkyl radical electron scavenger 2848
Alkyl radical isomerization 2507
Alkylammonium bromide PMR 130
Alkylammonium bromide soln viscosity 1902
Alkylammonium partial molal vol 1333
Alkylammonium salt benzene system 1752
Alkylbenzene excited singlet 3867
Alkylbenzene luminescence 3566
Allnatt Rice transport theory 2133
Alloy free energy mixing 1202
Allyl pi zinc oxide 2184
Alumina alc adsorption 675
Alumina carbon monoxide adsorption 2349
Alumina mineral acid reaction 3625
Alumina phenol chemisorption spectrum 2882
Aluminum electrode auramine 1655
Aluminum trimethyl dimer dissocn 2933
Amide rotation barrier 642 2178
Amine alkali metal soln 2975
Amine aq molal vol 1338
Amine arom pulse radiolysis 20
Amine chlorophenol hydrogen bond 587
Amine copper complex zeolite EPR 2860
Amine cyclic molal vol 1343
Amine ethyl glass cond 2781
Amine fluoro chem laser 3125
Amine nitrophenol aprotic solvent 1989
Amine nitrophenol complex bonding 3991
Amine poly ultrasonic absorption 334
Aminium methyl ion EPR 2857
Amino acid selectivity membrane 1872
Amino acid soln 4033
Amino radical EPR 2716
Aminoalkane fluoro decompn 60
Aminoborazine photoprodn 2630
Aminoethonethiol oxidn ferricyanide 3641
Aminoethylene photoionization 2105
Aminoethylpyridine copper complex magnetic 2707
Aminoethylpyridine copper complex structure 2887
Aminopyridine iodine complex thermodn 1895
Amminerhodium aquation photo 1937
Ammonia borazines photoreaction 2630
Ammonia copper complex zeolite EPR 2860
Ammonia cyanogen radical reaction 1931
Ammonia decompn isotope effect 970
Ammonia deuterated radiolysis 3812
Ammonia metal soln energy level 2738
Ammonia nitric oxide reaction 37
Ammonia photolysis 298
Ammonia scavenger methylpentane radiolysis 2381
Ammonia sodium Raman 2481
Ammonia sorption complex zeolite 2597
Ammoniated electron thermodn 683
Ammoniated zeolite irradn EPR 2716
Ammonium alkyl bromide soln 1902
Ammonium bromide alkyl urea soln 1369
Ammonium bromide amyl soln 2577
Ammonium bromide butyl soln 2582
Ammonium bromide PMR 130
Ammonium halide alkyl extn 1775
Ammonium nitrate decompn catalysis 2844
Ammonium nitrobenzyl methyl radical 2479
Ammonium oxalate hydrate irradn 3274
Ammonium perchlorate thermal decompn 3545
Ammonium quaternary bromide thermodn 1366
Ammonium salt benzene system 1752
Ammonium salt dielec property 1999
Ammonium salt molal vol 1333
Ammonium tertiary salt IR 339
Amyl acetate decompn kinetics 3917
Anhydride maleic copolymer magnesium 254
Aniline nitro structure 3597
Aniline nitrosomethyl soln photoredn 2362
Aniline water interaction 4011
Anion exchange heterovalent 2459
Anion exchange resin halide exchange 680
Anion exchange solvent mixt 1040
Anion radical cyclooctatetraene disproportionation 2176
Anion radical DNA irradn 3577
Anion radical ESR 1439 2479
Anion radical phenylbenzylidenemalononitrile ESR 3384
Anion radical sulfur dioxide 323
Anionic fluoro detergents 909
Anisotropic membrane ultrafiltration 238
Anisotropy optical calcn 1502

Anodic substitution reaction 3254
Anomalous water contaminant IR 457
Anomalous water IR polemic 456
Anthracene diethylaniline complex photolysis 1133
Anthracene intersystem crossing 1524
Anthracene potassium salt IR Raman 1026
Anthroate prototropism fluorescence 1996
Antimony monophosphide thermodn 2336
App adsorption inert gas 3171
Aq org glass photocond 3830
Aq soln irradn ESR 1706
Aq soln structure 2045
Aquation amminerhodium photo 1937
Argon effect xenon trioxide irradn 3909
Argon hydrogen carbon monoxide discharge 2941
Argon hydrogen collision 2006
Argon matrix spectra zone 3208
Argon oxygen reaction kinetics 2653
Arom amine pulse radiolysis 20
Arom cyclohexane irradn electron scavenging 3722
Arom hydrocarbon dimer cation 1119
Arom hydrocarbon fluorescence quenching 3132
Arom liqs excited singlet 3867
Arom oxygen hydroxide radical 847
Arom PMR zwitterionic micellar soln 1460
Arom solid state photoionization 2236
Arom substituent effect NMR 1593
Aromatic compd mercury quenching 2665
Arsine adsorption iron nickel 2851
Assocd solvent electrolyte viscosity 434
Assocd sterically hindered alcs 864
Assocg substance intermol force 890
Assocn alkali perchlorate methanol 2920
Assocn crystal violet soln 1772
Assocn diketopiperazine water 3065
Assocn formic acid 774
Assocn hydrogen bond solutes 3058
Assocn ionic reaction vol 895
Assocn metal phthalocyanine 1994
Assocn methanol 869
Assocn micelle 565
Assocn potassium perchlorate water 2923
Assocn thermodn europium sulfate 1887
Assocn trifluoroacetic acid 2039
Atom hydrogen reaction photolysis 3337
Atomic hydrogen org compd reaction 2673
Attachment electron radiation interaction 3730
Attenuated total reflection naphthalene 260
Attenuation ultrasonic molybdate polymer 1575
Auger effects hot atoms 2639
Auger electron spectroscopy silver 1289
Auramine photocond 1655
Autoxidn ethylbenzene 2785
Autoxidn toluene cobalt catalyzed 1520
Azeotrope ethylamine acetic acid 2764
Azide benzoyl photolysis ESR 3570
Azide chlorine hydrogen reaction 805
Azide methyl iodide 427
Azine benzothiazolinone oxidn 1178
Azine oxide phenol interaction 3502
Azobenzene liq crystal chromatog 99
Azobisisobutyronitrile photoinitiator polymn 3141
Azoethane photolysis 3303
Azoisopropane photochemistry 1669 1685
Azoxyanisole pretransition effect 2605
Azoxybenzene heptane activity coeff 596
Band shape polyphenyl theory 3983
Barbituric acid chloro irradn ESR 2399
Barrier amide rotation 2178
Barrier potential rotation fluoronitrosomethane 3099
Base acid equil 3618
Base acid equil thermodn 1909
Benzanthracene pulse radiolysis 1119
Benzene addn bicycloheptene 15
Benzene alkyl luminescence 3566
Benzene alkylammonium salt system 1752
Benzene aq radiolysis 1273
Benzene bombardment carbon 14 2521
Benzene cyano fluorescence quenching 3132
Benzene donor acceptor complex 1982
Benzene dye dimerization 446
Benzene ethyl autoxidn 2785
Benzene fluorescence quenching mercury 2665
Benzene halo NMR 515
Benzene hexane cyclohexane diffusion 2572
Benzene irradn excited singlet 3867
Benzene nitro butyl radical 2479
Benzene phenol system 3058
Benzene photochem 165
Benzene radical cation ESR 3943
Benzene radiolysis 198
Benzene singlet quenching olefin 3668
Benzene spectrum ESR 1727
Benzene thermodn props 731
Benzene trifluoromethyl photochem 823
Benzilate vanadyl EPR 3951
Benzoic acid fluorescence quenching naphthalene 3563
Benzoic acid proton transfer 1327
Benzoic acid pulse radiolysis 1398
Benzophenone electrochem 1650
Benzophenone fluoro photochem reaction 3926
Benzoquinone charge transfer complex 1849
Benzoquinone soln dielec relaxation 525
Benzoquinone UV substituent effect 2424
Benzothiazolinone azine oxidn 1178
Benzotrifluoride hydroxy ionization 1909
Benzoyl azide photolysis ESR 3570
Benzoylpyridine radical UV 3200
Benzyl carbomethoxypyridinium iodide spectrum 603
Benzyl chloride ethanol radiolysis 3744
Benzyne addn ethylene mechanism 656
Beryllate fluoro Raman 78
Beryllium lithium fluoride system 1154
Biacetyl sensitizer hexaamminecobalt photodecompn 1105
Bicipital relaxation equil reaction 452
Bicycloheptene addn benzene 15
Bimol nucleophilic substitution 232
Biol system soln column 1637
Biphenylene triplet 225
Biphotonic ionization methyl phenylenediamine 2229
Bleaching optical glass 3830
Bohr effect hemoglobin 1597
Bombardment benzene carbon 14 2521
Bond dissocn energy 2332
Bond energy carbon hydrogen 3314
Bond energy peroxide 3480
Bond ester butyl formate 3582
Bond formation hydrogen thermodn 3502
Bond hydrocarbon soly water 2754
Bond hydrogen intramol enthalpy 1553
Bond length water complex 3116
Bonding nitrophenol amine complex 3991
Borane deriv mass spectrum 1860
Borane kinetics ketene reaction 3532
Borate tetraphenyl adsorption mercury 707
Borazine photochemistry 2630
Borazole PMR spectra 2871
Borine serum albumin 128
Boron nitride adsorption gas 3171
Boron relaxation borazole 2871
Boron sulfide vapor pressure 2035
Boron trifluoride methanol NMR 329
Bovine serum albumin light scattering 2744
Breakdown gas laser induced 31
Bremsstrahlung laser gas breakdown 31
Brillouin scattering viscoelastic relaxation 3495
Bromate oxidn pentanedione kinetics 2185
Bromate sodium defect formation 3751
Bromcresol green acid base recombination 1184
Bromide alkylammonium soln viscosity 1902
Bromide chloride magnesium sodium 3474
Bromide cobalt complex racemization 119
Bromide copper vapor UV 1632
Bromide cuprous vaporization 3271
Bromide exchange transfer diffusion 2957
Bromide lithium heat diln 3050
Bromide oxidn hydroxyl radicals 312
Bromide potassium system diffusion 3419
Bromide radiolysis 1815
Bromide silver soly nitrate 2759
Bromide tetraalkylammonium heat soln 1369
Bromide tetraalkylammonium PMR 130
Bromide tetraamylammonium aq heat capacity 2577
Bromide tetraamylammonium soln conductance 1049
Bromide tetrabutylammonium soln 3068
Bromide tetrabutylammonium soln thermodn 2582
Bromine catalyzed reaction 1416
Bromine mol UV 1017
Bromine neutron activation 3331
Bromine oxygen tungsten reaction 320
Bromine radical ESR clathrate 133
Bromine 82 recoil reaction 2499
Bromofluoromethane radiolysis 2070
Bromouracil pulse radiolysis 2386 2392
Bronsted acid site glass 3633
Bronsted coeff iodination 3121
Bubble nucleation kinetics 2609
Buckingham potential soln theory 3005
Butadiene transition 1130
Butane irradn olefin oxygen 1260
Butane reaction tritium 2937 2939
Butene addn tritium 190
Butene fluoro isomerization 2829
Butene iridium adsorption IR 2699
Butene isomer recoil chlorine 2711
Butene isomerization kinetics 44
Butene oxygen addn 3311
Butyl alc hydration 1660
Butyl formate NMR 3582
Butylammonium bromide thermodn 1366
Butylethylene NMR steric effect 2877
Butyne photolysis 1112
Butyrate vanadyl EPR 3951
Butyrolactam proton magnetic relaxation 1973
Cadmium halide melt 1831
Cadmium salt soln position lifetime 1124
Calcium binding mol structure 1298 1304
Calcium exchanged zeolite 110
Calcium hydroxylapatite surface concns 900
Calcium nitrate aq viscoelastic relaxation 3495
Calcium nitrate hydrate ultrasonic relaxation 1506 1507
Calcium nitrate silver soly 2759
Calcium nitrate soln 3244
Calorimetry differential scanning tetracyanomethane 3973
Capture electron 3758
Carbanion polystyryl 695
Carbazole charge transfer complex 1849
Carbazole donor acceptor complex 2102
Carbene iodo photolysis 308
Carbide cerium bond dissocn 2332
Carbomethoxypyridinium benzyl iodide spectrum 603
Carbon atom reaction hydrogen 1389
Carbon dioxide matrix nitrate aggregate 1826
Carbon dioxide methanol interaction 2170
Carbon dioxide redn kinetics 3278
Carbon dioxide silver interaction 1289
Carbon dioxide vibrational relaxation 3108
Carbon hydrogen bond energy 3314
Carbon iron oxygen nucleation 2609
Carbon methyl relaxation 3213
Carbon monoxide adsorption alumina 2349
Carbon monoxide hydrogen argon discharge 2941
Carbon monoxide iron chemisorption 3180
Carbon monoxide oxidn 1416 1807
Carbon monoxide oxygen reaction 3527
Carbon monoxide ozone reaction 1514
Carbon monoxide reaction hydroperoxo 3301
Carbon monoxide stimulated emission 1429
Carbon NMR relaxation isodurene 281
Carbon oxide hot electron 3890
Carbon oxide oxidn ir 2833
Carbon oxidn nickel surface 968
Carbon sulfide anion radical 1706
Carbon tetrachloride dye dimerization 446
Carbon tetrachloride fluorine reaction 947
Carbon tetrachloride silica interface 3192
Carbon tetrachloride soln formic acid 774
Carbon tetrachloride suspension silica 3188
Carbon tetrahalides radiation chemistry 3734
Carbon 13 double resonance 2972
Carbon 14 benzene bombardment 2521
Carbon 14 counting 3603
Carbonate alkali molten Raman 1565
Carbonate org dielec property 2892
Carbonate silver IR 940
Carbonium ion styrene polymn 930
Carbonyl monoolefin excitation 478
Carboxylate hydroxy vanadyl EPR 3951
Carboxylate interaction copolymer 1767
Carboxylate protonation vol 2778
Carboxymethylcellulose molar vol 3451
Catalysis ammonium nitrate decompn 2844
Catalysis pentanedione oxidn manganese 2185
Catalyst chromia EPR 2694
Catalyst impurity ozone reaction 1514
Catalyst laser Raman 2325
Catalyst neutron irradn 2625
Catalyst photo zinc oxide 1394
Catalyst rhodium electron spectroscopy 2525
Catalytic activity gold 1907
Catalytic decompn isopropyl alc 3372
Catalytic polarog current metal complex 1170
Catalytic thermal oxidn 1807
Cation radical DNA ESR 3571
Cation radical DNA irradn 3577
Cavity surface area solvent 2754
CD ferrocenes 511
CD sensitizing dye aggregation 2982
Cell concn transference 1758
Cellulosic polyanion dye complex 688
Cerenkov reabsorption spectroscopy 3780
Cerium palladium bond dissocn 2332
Cerium sulfate aq radiolysis 1273

Cesium acrylate copolymer 1311
Cesium iodide viscosity solvents 434
Cetomacrogol soln cond 1763
Charge density chelate 3029
Charge effect sedimentation equil 3429
Charge surface tension pyrolytic graphite 2750
Charge transfer chem reaction kinetic 1666
Charge transfer complex 1982
Charge transfer complex halogen spectra 3220
Charge transfer complex intermol 2452
Charge transfer complex iodine 1951
Charge transfer complex paramagnetism 1849
Charge transfer complex soln 249
Charge transfer hydrogen bond 3000 3991
Charge transfer interaction 2470
Charge transfer intermol 2405
Charge transfer laser photolysis 1133
Charge transfer pyridinium iodide 603
Charge transfer tetracene perylene 1549
Charged membrane hyperfiltration 3638
Chelate charge density 3029
Chem ionization mass spectrometry 3217 3917
Chem laser 1429
Chem laser hydrogen chloride 805
Chem laser hydrogen fluoride 3125
Chem laser hydrogen halide 1425
Chemiluminescence excitation atomic fluorine 3586
Chemisorption carbon monoxide IR 3180
Chemisorption phenol alumina spectrum 2882
Chloranil electrode acetonitrile NMR 246
Chloride alkali soln vapor pressure 743
Chloride alkyl adsorption 2535
Chloride bromide magnesium sodium 3474
Chloride copper vapor UV 1632
Chloride eutectic system 904
Chloride hydrogen chem laser 805 1425
Chloride ion coordination phenol 1775
Chloride magnesium PMR 130
Chloride magnesium sodium vol 3488 3491
Chloride phosphorus tin samarium fluorescence 3397
Chloride potassium transference no 712
Chloride silver ionization 2819
Chloride silver soly nitrate 2759
Chloride sodium elec conductance 2294
Chloride sodium helium soln 1195
Chloride sodium soln cond 1053
Chloride soln cond 1763
Chloride tin potassium complex 2796
Chlorine azide hydrogen reaction 805
Chlorine recoil olefin isomer 2711
Chlorine 38 recoil reaction 2499
Chloroaniline distribution cyclohexane water 4011
Chlorocyanobenzoquinone charge transfer complex 1849
Chloroethane elimination threshold energy 283
Chloroethane IR 3591
Chloroethylene isomerization 2829
Chloroform water acetic acid 2050
Chloromethane oxygen laser 811
Chloromethane silica interface 3192
Chloromethane suspension silica 3188
Chlorophenol amine hydrogen bond 587
Chlorophyll energy transfer 172
Chlorouracil pulse radiolysis 2386 2392
Cholesteryl ester thermal transition 3089
Cholesteryl nonanoate 276
Choline deriv selectivity membrane 1872
Chroman bromo fluoroethane clathrate ESR 133
Chromate hexacyano photoactive state 1947
Chromatog gas mordenite adsorption 1647
Chromatog gas reactor 2159
Chromatog peak shape 2586
Chromatog soln thermodn 99
Chromatog solvent activity 1492
Chromia catalyst EPR 2694
Chromia IR surface property 571
Chromia structure 1838
Chromium hydroxide drying 1838
Chronoamperometry potential dependent 1666 3254
Chronoamperometry theory 2439
Chronocoulometry theory 2439
Circular dichroism molecule 1844
Cis trans isomerization complex 3934
Cis trans olefin recoil chlorine 2711
Clathrate bromine radical ESR 133
Clathrate urea Palmitic acid 801
Cluster stabilized 3714
Clustering acrylic copolymer 1311
Cobalt catalyzed autoxidn toluene 1520
Cobalt chloride decompn catalyst 2844
Cobalt complex macrocyclic ligand 2223
Cobalt complex sensitized photodecompn 1105
Cobalt DMF soln NMR 1968
Cobalt ethylenediamine complex racemization 119
Cobalt formato pentaammine photolysis 2492
Cobalt iron oxide electrode 3646
Cobalt probe glass 1035
Coil helix transition polyglutamate 3464
Cold worked gold thermoemf 1907
Collagen film optical rotation 2935
Collision energy cyclopropane isomerization 1695
Collision integral spherical core 1470
Collision intrabeam 2947
Collision mol vibration 2006
Collision proton hydrogen bromide 1321
Collision relaxation carbon dioxide 3108
Collisional deactivation fluoroethane 954
Color center potassium lead 1202
Color center sodium bromate 3751
Column soln activity gradient 1637
Competitive consecutive reaction kinetics 704
Complex charge transfer halogen spectra 3220
Complex charge transfer iodine 1951
Complex charge transfer paramagnetism 1849
Complex chlorophyll polymer 172
Complex copper magnetic susceptibility 2707
Complex dimethylamine 871
Complex dipole moment enhancement 3991
Complex donor acceptor carbazole 2102
Complex donor acceptor spectrum 1982
Complex formation water 3116
Complex iodine aminopyridine thermodn 1895
Complex perylene thermodn stability 921
Complex polyanion dye thermodn 688
Complex soln pressure effect 249
Complex tetracene perylene 1549
Complexed metal hydroperoxyl radical 2207
Compressibility soln 2140
Comproportionation kinetics violene 701
Computer simulation junction potential 1758
Concn cell transference 1758
Concn gradient fluid layer 783
Cond alkali perchlorate methanol 2920
Cond anthracene potassium salt 1026
Cond charge transfer complex 1849
Cond dimethylphenanthroline copper perchlorate 3029
Cond elec measurement 2116
Cond elec obstruction 1763
Cond potassium perchlorate assocn 2923
Cond relaxation electrolyte soln 3287
Cond sodium chloride soln 1053
Cond sodium salt formamide 3034
Cond thermal monat gas 1743
Cond thermally stimulated glass 2781
Cond transfer number hydroxide 2954
Condensation wedge shaped pore 2543
Conductance elec sodium chloride 2294
Conductance fluidity electrolyte soln 3244
Conductance ion pair 2452
Conductance potassium chloride 712
Conductance tetraamylammonium bromide soln 1049
Conduction elec auramine 1655
Conduction sodium potassium glass 1072
Conduction transport mode 1348
Conductivity elec transitions 115
Conformation alanine tetrapeptide energy 2793
Conformation amide barrier 2178
Conformation cyclopentanedicarboxylic acid 790
Conformation helical glycine tetrapeptide 670
Conformation isocitrate soln NMR 3073
Conformation methyl formate LCAO MO 2430
Conformation polymethacrylic acid pH 2559
Conformation rotational 501
Consecutive competitive reaction kinetics 704
Contact angle surface roughness 3267
Contaminant org polywater IR 457
Convection cell fluid layer 783
Copper catalyst neutron irradn 2625
Copper chloride decompn catalyst 2844
Copper complex magnetic susceptibility 2707
Copper complex structure 2887
Copper dimethylphenanthroline perchlorate cond 3029
Copper dissoln acid soln 3656
Copper halide vapor UV 1632
Copper iodide vaporization mass spectrometry 2310
Copper malonate photochemistry 1387
Copper nitric oxide zeolite EPR 1546
Copper phenanthroline photolysis 1528
Copper phthalocyanine assocn 1994
Copper phthalocyanines dimerization 446
Counterion binding polycarboxylate dilatometry 254
Counting carbon 14 3603
Coupling quadrupole nitrogen diazirine 2249
Crit micelle concn NMR 3012
Crit micelle concn surfactant 2019
Crit polymer soln temp 1206 1214
Cross section electron capture 3758
Cross section proton hydrogen bromide 1321
Crystal field perturbation calcns 2907
Crystal structure cyclopentanedicarboxylic acid 790
Crystal structure ice 886
Crystal violet assocn soln 1772
Cumene cracking activity zeolite 110
Cumene dealkylation silica alumina 3741
Cupric oxide ammonia nitric oxide 37
Cuprous bromide vaporization 3271
Cyanatoferrate pulse radiolysis 3703
Cyanide hydrogen cryst IR 1140
Cyanide hydrogen deuterium 285
Cyanide hydrogen geometry polemic 2483
Cyanide hydrogen isotope IR 454
Cyanide hydrogen radiolysis ESR 3945
Cyanide iodine hydrogen reaction 1392
Cyanine dye aggregation 2982
Cyanoacetic acid irradn ESR 3377
Cyanoacetylene di oxygen atom 269
Cyanoacetylene nitrogen reaction 2643
Cyanobenzene fluorescence quenching 3132
Cyanobenzene methylstyrene complex 1419
Cyanobenzoquinone charge transfer complex 1849
Cyanochromate electrochem redn 2439
Cyanoethylene donor acceptor complex 1982
Cyanoethylene fluorescence quenching 3132
Cyanogen radical ammonia reaction 1931
Cyanomethane structure 3973
Cyclic amine molal vol 1343
Cyclic voltammetry theory 1160 2439
Cyclization pentenyl radical 1089
Cyclization photo phenylimidazole singlet 3362
Cycloalkane mol ion water vapor 1517
Cyclobutane phenyl photodissocn 3355
Cyclobutanecarbonitrile thermolysis 2817
Cyclobutanone decompn 963
Cyclohexane alc solvated electron 2931
Cyclohexane arom irradn electron scavenging 3722
Cyclohexane benzene hexane diffusion 2572
Cyclohexane film electron impact 1255
Cyclohexane phenol system 3058
Cyclohexane sodium tetrabutylaluminate THF system 3472
Cyclohexane water chloroaniline distribution 4011
Cyclohexanone UV photolysis 615
Cyclooctatetraene anion radical disproportionation 2176
Cyclopentadiene dissocn kinetics 2159
Cyclopentadiene hydrogen hot atom chemistry 1389
Cyclopentane singlet oxygen reaction 1375
Cyclopentanedicarboxylic acid conformation 790
Cyclopropane isomerization unimol 1695
Cyclopropane radiolysis butane 1260
Cyclotron resonance electron 3758
Cytosine restricted rotation 64
Cytosine rotation 71
Dealkylation cumene silica alumina 3741
Decationated zeolite proton motion 1220
Decay benzoylpyridine radical 3200
Decay trapped electron methylpentane 3167
Decay trapped electron tunneling 2641
Decompn ammonia isotope effect 970
Decompn ammonium nitrate catalysis 2844
Decompn catalytic 3372
Decompn catalytic isopropyl alc 3372
Decompn free radical sulfoxide 135
Decompn hydrocarbon 143
Decompn hydrogen peroxide catalysis 1907
Decompn isomerization tritium spiropentane 2187
Decompn kinetics amyl acetate 3917
Decompn kinetics tetrafluoroethane 292
Decompn methylsilanes 459
Decompn pentenyl radical 1089
Decompn peroxide fluoromethyl 3480
Decompn rate melting solid 2253
Decompn solid state kinetics 1474
Decompn thermal ammonium perchlorate 3545

Defect formation sodium bromate 3751
Dehydration isopropyl alc catalytic 3372
Dehydrogenation isopropyl alc catalytic 3372
Density alkylammonium bromide soln 1902
Density fixed charge 2447
Density viscosity sodium salt 3034
Desorption oxygen zinc oxide 3184
Deuterated ammonia radiolysis 3812
Deuterated ethanol soln structure 2562
Deuteration catalysis zinc oxide 2184
Deuteration propylene mechanism 2184
Deuteride kinetics pyrolysis hydrogen 3538
Deuterium atom silane reaction 3911
Deuterium effects methyl iodide reactions 427
Deuterium fluoride chem laser 3125
Deuterium hydrogen cyanide reaction 285
Deuterium isotope effect iodination 3121
Deuterium methyl radical quenching 2196
Deuterium oxide vapor pressure 3040
Deuterium vanadium x ray 927
Diat mol transition metal 2268
Diazine photoisomerization 2245
Diazirine decompn mechanism 797
Diazirine heat formation 3504
Diazirine nitrogen quadrupole coupling 2249
Dibenzodioxin ESR trifluoromethanesulfonic 1504
Diborane ion mol reaction 2467
Dichloroethylene isomer recoil chlorine 2711
Dichlorotetrafluoroacetone water polyglutamate 3464
Dichroism thin film 3390
Dichromate ion hydrolysis kinetics 582
Dicyanoacetylene oxygen atom 269
Dicyanobenzene fluorescence quenching 469
Dielec const assocn solvation 2920
Dielec const gradient soln 1062
Dielec const naphthalenide 2866
Dielec liq electron range 3794
Dielec property adsorbed haloalkane 2535
Dielec property ammonium salt 1999
Dielec property hydrogen cyanide 1140
Dielec property org carbonate 2892
Dielec relaxation solute 525
Dielec relaxation water adsorption 2987
Diels Alder thermochem 106
Diene tetracyanoethylene addn 106
Differential scanning calorimetry tetracyanomethane 3973
Diffraction electron mol motion 3099
Diffraction polyacrylate 1311
Diffuse layer microemulsion 876
Diffusion acetic acid dimer 2463
Diffusion coeff ternary system 3419
Diffusion const org solute 4006
Diffusion controlled condensation 2543
Diffusion electrolyte solute 1166
Diffusion limited reaction viscosity 1192
Diffusion mixed solvent 2470
Diffusion mol proton exchange 3078
Diffusion monat gas 1743
Diffusion problem two body 349
Diffusion radical kinetics 3008
Diffusion silver nitrate water 1853
Diffusion ternary system 2050
Diffusion transfer 162
Diffusion transfer exchange bromide 2957
Diffusive transport mode 1348
Digital simulation electrochemistry ESR cell 2550
Dihexyloxyazoxybenzene heptane activity coeff 596
Dihydrophenanthrene intermediate phenylimidazole photolysis 3362
Dihydropyrazine radical EPR 3348
Dihydropyridazine radical EPR 3348
Dihydropyrimidine radical EPR 3348
Diiodobenzene photoprodn 2639
Diiodomethyl radical matrix IR 2718
Dilatometry polycarboxylate counterion binding 254
Diln heat electrolyte 1608
Diln heat lithium bromide 3050
Dimer trimethylaluminum heat dissocn 2933
Dimerization acrylic copolymer 1311
Dimerization copper phthalocyanines 446
Dimerization metal phthalocyanine 1994
Dimerization purine reaction 2838
Dimethyl ether trapped electron photobleaching 3747
Dimethyl glutarate saponification kinetics 704
Dimethyl sulfide photoelectron spectrum 1030
Dimethylamine hydrogen bonding 871
Dimethylaminium ion EPR 2857
Dimethylaniline irradn singlet triplet 3805
Dimethylphenanthroline copper perchlorate cond 3029
Dioxane water pulse radiolysis 1279
Dioxane water solvent 1053
Dioxane water ultrasound absorption 1571
Dioxide carbon vibrational relaxation 3108
Dioxide nitrogen photodissocn 474
Dioxide sulfur anion radical 323
Dipolar relaxation NMR 53
Dipole moment enhancement complex 3991
Dipole moment hydrogen bond 3000
Dipole moment solute 525
Dipole phenol pyridine complex 2112
Dipole potential polar gas 1470
Discharge microwave mass spectrometry 2941
Disilane radiolysis silane 3321
Disproportionation cyclooctatetraene anion radical 2176
Disproportionation reaction 3254
Dissipative structure ternary system 2050
Dissocn acid methyl orange 4023
Dissocn cyclopentadiene kinetics 2159
Dissocn energy bond 2332
Dissocn energy water complex 3116
Dissocn fluorescence anthroate 1996
Dissocn heat trimethylaluminum dimer 2933
Dissocn ionic org compd 630
Dissocn ionic photoinduced 1419
Dissocn isocyanic acid formylium 2636
Dissocn methyl iodide kinetics 2353
Dissocn phenylcyclobutane photolysis 3355
Dissoln copper acid soln 3656
Dissoln lifetime hydrated solute 2017
Dissoln micelle kinetics relaxation 3017
Dissolved gas partial molal vol 3044
Dithionite thermal decompn 157
DMF polyglutamate thermal props 1081
DMF soln nickel NMR 1968
DMF soln nitrogen 14 NMR 1968
DNA cation radical ESR 3571
DNA cation radical irradn 3577
Donnan equil ion solvent 3445
Donnan equil polystyrenesulfonate 1881
Donnan Planck model 3633
Donor acceptor adduct 3532
Donor acceptor complex carbazole 2102
Donor acceptor complex spectrum 1982
Double resonance carbon 13 2972
Dowex 50W PMR 578
Drying chromium hydroxide 1838
DTNB chlorophyll complex 172
Durosemiquinone alkali ESR 1012
Dye halo fluorescein hypochromism 3970
Dye phthalocyanine assocn 1994
Dye phthalocyanine dimerization 446
Dye polyanion complex thermodn 688
Dye sensitizing aggregation CD 2982
Dye xanthene aggregation equil 762
Dysprosium oxide catalyst 2199
ECE mechanism 2439
ECE reaction pathway 3254
Elastic scattering ion 3883
Elec cond measurement 2116
Elec cond obstruction 1763
Elec cond org glass 2781
Elec cond org transition 2798 2799
Elec conductance sodium chloride 2294
Elec conduction auramine 1655
Elec conductivity transitions 115
Elec field transport phenomena 2286
Elec polarization polyelectrolyte membrane 3434
Electret formation polyelectrolyte membrane 3434
Electrocapillarity pyrolytic graphite 2750
Electrochem benzophenone 1650
Electrochem cell resistive effect 2550
Electrochem liquidus measurement 1154
Electrochem redn hexacyanochromate 2439
Electrochem selectivity ratio membrane 1872
Electrochemiluminescence efficiency 1868
Electrode chloranil acetonitrile NMR 246
Electrode cobalt iron oxide 3646
Electrode ferrocene ferricinium pyridine 243
Electrode ion adsorption 2915
Electrode kinetics oxygen redn 3646
Electrode reaction 1160
Electrolyte heat diln 1608
Electrolyte partial molal vol 1333
Electrolyte sodium diffusion coeff 3038
Electrolyte soln cond relaxation 3287
Electrolyte soln fluidity conductance 3244
Electrolyte soln structure 1062
Electrolyte solute diffusion 1166
Electrolyte viscosity assocd solvent 434
Electron attachment radiation interaction 3730
Electron capture 3758
Electron capture phosphate irradn 2848
Electron diffraction mol motion 3099
Electron excess mobility 3830
Electron excitation arom singlet 3867
Electron hot injection current 3890
Electron hydrated ab initio 3905
Electron hydrated absorption spectra 3780
Electron hydrated formation 3694
Electron hydrated org reaction 630
Electron hydrated pulse radiolysis 2072
Electron hydrated radical 1957
Electron hydrated spin density 3838
Electron hydrated thermodn 683
Electron impact cyclohexane film 1255
Electron irradn ice 1000
Electron irradn methane aq 3863
Electron irradn uranyl fluorescence 3698
Electron localized pulse radiolysis 3776
Electron mobility alk ice 1509
Electron mobility hydrocarbon 442
Electron photoinjected range liq 3794
Electron scavenger alk glass irradn 1962
Electron scavenging arom cyclohexane irradn 3722
Electron scavenging hydrocarbon radiolysis 987
Electron solvated absorption spectra 2931
Electron solvated electronic spectra 3691
Electron solvated glycerol spectra 1700
Electron solvated halide 3677
Electron solvated methanol water 3765
Electron solvated mol model 3714
Electron solvated optical spectra 2975 3876
Electron solvated polar mol 3824
Electron solvated reactivity 2217
Electron solvated sodium reaction 839
Electron spectroscopy rhodium catalyst 2525
Electron transfer equil ESR 1734
Electron transfer fluorescence quenching 469 3132
Electron transfer reaction 1160 2223
Electron transfer semiconductor surface 2353
Electron trapped absorption spectra 3847
Electron trapped decay methylpentane 3167
Electron trapped decay tunneling 2641
Electron trapped electronic spectra 3744
Electron trapped methylpentane glass 3747
Electron trapped methylpentane photobleaching 2341
Electron trapped methyltetrahydrofuran 636
Electron trapped solid state excitation 3366
Electron trapped theoretical spectra 3683
Electron trapping radiation chemistry 2726
Electronegativity effects 187
Electronic absorption bands 639
Electronic absorption spectrum complex 1549
Electronic configuration wave function 3401
Electronic energy molecular 2995
Electronic polarizability ice 886
Electronic spectra ethylene phenyl 3960
Electronic spectra excess electron 3683 3691
Electronic spectra trapped electron 3744
Electronic spectrum anthracene potassium 1026
Electronic structure furanquinones 2240
Electronic transition formaldehyde 1844
Elimination chloroethane threshold energy 283
Ellipsometry transmission thin layer 3390
Emission spectra furan quinone 2240
Emission stimulated carbon monoxide 1429
Emission x ray phosphorus oxyanion 3975
ENDOR phenylbenzylidenemalononitrile radical anion 3384
ENDOR powder line shape 2079
ENDOR proton zeolite 2087
Energy bond carbon hydrogen 3314
Energy bond peroxide 3480
Energy degradation recoil reactions 2685
Energy difference halophenol isomer 1553
Energy interaction mol 2123
Energy level metal ammonia soln 2738
Energy level quadrate 3401
Energy level structure glass 3830
Energy molecular electronic 2995
Energy parameters polypeptide 375
Energy partition elimination chloroethane 283
Energy surface alanine tetrapeptide 2793
Energy transfer chlorophyll 172
Energy transfer irradn water 3698
Energy transfer thermal isomerization 1935
Enthalpy butylammonium bromide 1366
Enthalpy formation carbazole complex 2102
Enthalpy hydrogen bond formation 3065
Enthalpy intramol hydrogen bond 1553
Enthalpy molar org solute 99
Enthalpy nitrobenzene ion equil 2058
Enthalpy peroxide superoxide reaction 2841
Enthalpy phenanthrenequinonesulfonate 1875

Enthalpy solvent transfer 2045
Enthalpy transfer sodium chloride 3077
Entropy adsorption hydrocarbon 2769
Entropy hydration ion 2298
Entropy nitrobenzene ion equil 2058
Entropy phenanthrenequinonesulfonate 1875
Entropy polymer solvent mixing 400
Entropy soln solid solute 2138
Enzyme kinetics orientation constraint 534
Enzyme reactions relaxation spectra 366
Epoxidation alkene gas phase 3319
Epoxidation olefins stereochem 213
EPR amino radical 2716
EPR chromia catalyst 2694
EPR copper ammonia complex zeolite 2860
EPR copper nitric oxide zeolite 1546
EPR heterocyclic radical EPR 3348
EPR photoinitiation polymn methacrylate 3141
EPR radiolysis methylamine 2857
EPR sulfur dioxide anion radical 323
EPR vanadyl carboxylate hydroxy 3951
Equation state approx 1479
Equation state hard sphere 601
Equation state hydrocarbon 2769
Equation state nonspherical mol 2014
Equil acid base thermodn 1909
Equil acid maleate 1957
Equil aggregation xanthene dye 762
Equil alkali ion exchange 1072
Equil anthroate prototropism 1996
Equil const calcn 720
Equil const complex formation 1549
Equil const disproportionation 2176
Equil const propionitrile iodine 2098
Equil const proton transfer 4033
Equil electron transfer ESR 1734
Equil micelle 565
Equil nitrobenzene ion enthalpy 2058
Equil phenanthrenequinonesulfonate 1875
Equil reaction bicipital relaxation 452
Equil salt rejection membrane 3638
Equil sedimentation polymg protein 3429
Equil sedimentation polymg system 777
Equil thioamide iodine complex 2405
Erbium oxide catalyst 2199
ESR alkali durosemiquinone 1012
ESR anion radical 1439
ESR bromine radical clathrate 133
ESR cell electrochemistry 2550
ESR cyanoacetic acid irradn 3377
ESR DNA cation radical 3571
ESR electron transfer equil 1734
ESR ethylene phenyl radical 3960
ESR gamma irradn oxalate 3274
ESR glycine radical reaction 3507
ESR heptanal perhydrotriphenylene 1008
ESR hydrogen cyanide radiolysis 3945
ESR hydrogen photodissocn 2637
ESR inclusion compd radical 801
ESR inorg radical soln 1710
ESR irradiated butyl isothiocyanate 1792
ESR irradiated heterogeneous system 1721 1727
ESR irradn alkyl phosphate 2848
ESR irradn aq soln 1706
ESR irradn halo uracil 2399
ESR irradn hydrocarbon crystal 1411
ESR methionine 1729
ESR nitrobenzene ion equil 2058
ESR nitroxides simulation model 672
ESR org radicals 553
ESR oxygen radical org 847
ESR paramagnetic intermediate redox 2207
ESR phenylacridine radical anion 3958
ESR phenylbenzylidenemalononitrile radical anion 3384
ESR photolysis UV 2061
ESR radical acrylate 1957
ESR radical cation benzene 3943
ESR rotational correlation time nitroxide 1858
ESR sodium triphenylacetate decompn 937
ESR thermal decompn mechanism 157
ESR thiooxalato nitrosyl iron 49
ESR tin 3 141
ESR triflucromethanesulfonic dibenzodioxin 1504
ESR trifluoromethyl radical sorbed 2690
ESR triplet nitrene 3570
ESR zinc oxide powder 2527
ESR zwitterion radical 2479
Ester bond butyl formate 3582
Ethane chloro IR Roman 3591
Ethane difluoro pyrolysis 1680
Ethane disubstituted NMR 1466
Ethane ion mol reaction gas 3919
Ethane methylene insertion 607
Ethane yield ethanethiol photolysis 2668
Ethanethiol amino oxidn ferricyanide 3641
Ethanethiol photochemistry 2668
Ethanol electron scavenger 3744
Ethanol hexane gamma irradn polemic 944
Ethanol hydration aq soln 1660
Ethanol iodine reaction 3314
Ethanol pulse radiolysis 3856
Ethanol soln deuterated structure 2562
Ethanol solvated electron spectra 3876
Ether alkali metal soln 2975
Ether aq molal vol 1338
Ether vinyl methyl copolymer 254
Ethyl iodide gamma irradn 1324
Ethyl radical nitric oxide reaction 3303
Ethylamine acetic acid thermodn 2764
Ethylamine glass elec cond 2781
Ethylamine paramagnetic relaxation 1226
Ethylbenzene autoxidn 2785
Ethylene acrylate copolymer 1311
Ethylene addn benzyne mechanism 656
Ethylene butyl steric effect 2877
Ethylene carbonate dielec property 2892
Ethylene chloro isomerization 2829
Ethylene copolymer hydrogen binding 254
Ethylene copolymer titrn 1767
Ethylene cyano fluorescence quenching 3132
Ethylene fluorine 18 reaction 3509
Ethylene glycol potassium chloride 712
Ethylene hydrogenation catalysis 2625
Ethylene hydrogenation kinetics 1394
Ethylene iodine hot atom reaction 3342
Ethylene ion impact spectroscopy 1130
Ethylene phenyl radical ESR 3960
Ethylene photolysis UV actinometer 138
Ethylene radiolysis butane 1260
Ethylene yield ethanethiol photolysis 2668
Ethylenediamine cobalt complex racemization 119
Ethylenesulfonic acid molar vol 3451
Ethylenethiourea iodine complex 2405
Ethylethoxysilane hydrolysis 3192
Ethylnaphthalene electron transfer 1734
Ethylpyridine amino complex magnetic 2707
Ethynyl radical mass spectrometry 1913
Europium ion excited state 1093
Europium ion solvation NMR 1449
Europium quantum efficiency fluorescence 1293
Europium sulfate assocn thermodn 1887
Europium sulfate ion formation 2925
Eutectic system potassium chloride 904
Evapn wedge shaped pore 2543
Excess electron mobility 3830
Exchange bromide transfer diffusion 2957
Exchange equil alkali ion 1072
Exchange halide anion exchange resin 680
Exchange hydrogen propene zeolite 3940
Exchange interfacial water polemic 1505
Exchange irradn hydrogen water 621
Exchange isotope solid 1317
Exchange methane hydrogen chloride 2809
Exchange proton naphthol 3558
Exchange rate proton water 2954
Exchange reaction iodide triiodide 162
Exchange resin halide exchange 680
Exchanged zeolite thallium structure 2593
Exciplex dimethylaniline photolysis 3805
Exciplex yield complex photolysis 1133
Excitation electron trapped solid state 3366
Excitation yield naphthalene irradn 2485
Excited borazine photodecompn 2630
Excited singlet arom liqs 3867
Excited singlet oxygen reaction 1375
Excited state europium ion 1093
Excited state pulse radiolysis 2485
Excited state quenching fluorotoluene 2967
Exciton bound ionized impurity 3771
Exciton interaction halofluorescein dye 3970
Exotherm polyglutamate DMF 1081
Extended Hueckel calcn polyalanine 2793
Extn tetraalkylammonium halide 1775
Faujasite synthesis 3388
Ferrate cyanato radiolysis 3703
Ferricinium ferrocene electrode pyridine 243
Ferricyanide oxidn aminoethonethiol 3641
Ferrioxalate flash photolysis 830
Ferrocene ferricinium electrode pyridine 243
Ferrocenes CD 511
Ferrous oxalate photoprodn 830
Film collagen optical rotation 2935
Film cyclohexane electron impact 1255
Film lipid interface 1238 1244
Film lipid intermol energy 1231
Film metal oxidn 2530
Film soap surface tension 3024
Film transmission ellipsometry 3390
Fixed charge density 2447
Flame hydrogen sulfide 1925
Flash photolysis ferrioxalate 830
Flash photolysis helium nitrogen 3518
Flash photolyzed oxalatoiron absorbance 2618
Flash spectra arom hydrocarbon 3132
Flow viscous org liq 2317
Fluid layer convection cell 783
Fluidity conductance electrolyte soln 3244
Fluorenyl salt complex 2152
Fluorescein halo dye hypochromism 3970
Fluorescence aminoethylene Rydberg 2105
Fluorescence anthroate prototropism 1996
Fluorescence irradn uranyl ion 3698
Fluorescence polyphenyl 3983
Fluorescence quantum efficiency europium 1293
Fluorescence quenching benzene olefin 3668
Fluorescence quenching electron transfer 469 3132
Fluorescence quenching mercury benzene 2665
Fluorescence quenching naphthalene benzoic acid 3563
Fluorescence samarium nonaq medium 3397
Fluorescence trifluoromethylbenzene 823
Fluoride hydrogen chem laser 1425 3125
Fluoride ion coordination alc 1775
Fluoride lithium beryllium system 1154
Fluoride molten tetrafluoroberyllate Raman 78
Fluorination tungsten analysis polemic 2930
Fluorination tungsten model analysis 2930
Fluorine atomic chemiluminescence excitation 3586
Fluorine carbon tetrachloride reaction 947
Fluorine NMR surfactant micelle 3012
Fluorine 18 ethylene reaction 3509
Fluoro surfactants 909
Fluoroacetate 1824
Fluoroacetic acid assocn 2039
Fluoroacetone imine trifluoromethyl radical 487
Fluoroamine methyl chem laser 3125
Fluoroaminoalkane mass spectra 60
Fluorobenzophenone photochem reaction 3926
Fluoroberyllate Raman molten fluoride 78
Fluorobutene isomerization 2829
Fluorocarbon surfactant math 2019
Fluoroethane collisional deactivation 954
Fluoroethane pyrolysis 1680
Fluoroethane tetra decompn 292
Fluoromethane radiolysis 2070
Fluoromethyl peroxide decompn 3480
Fluoromethylalkyl ammonium micelle structure 3012
Fluoronitrosomethane mol structure 3099
Fluorotoluene excited state quenching 2967
Fluorouracil pulse radiolysis 2386 2392
Force const tetrafluoroberyllate 78
Formaldehyde electronic transition 1844
Formaldehyde hydrogen reaction 2213
Formaldehyde oxygen reaction 2215
Formamide cond sodium salt 3034
Formate butyl NMR 3582
Formate methyl conformation LCAO MO 2430
Formation const carbazole complex 2102
Formation heat complex 1549
Formation heat diazirine 3504
Formato pentaammine cobalt photolysis 2492
Formic acid assocn 774
Formyl radical 494
Formylium dissocn isocyanic acid 2636
Fragmentation silver chloride 2819
Free energy mixing activity 2764
Free energy mixing alloy 1202
Free energy solvent transfer 2045
Free radical decay 1405
Free radical gas spectroscopy 2056
Free radical model water radiolysis 2733
Free radical stabilization energy 918
Free radical sulfoxide decompn 135
Furan quinone emission spectra 2240
Fused halide system thermochemistry 1616
Gamma irradiated org glass 1226
Gamma irradiated silica alumina 3741
Gamma irradiated silica gel 3158
Gamma irradiated zeolite ENDOR 2087
Gamma irradn benzene 1727
Gamma irradn cyanoacetic acid 3377
Gamma irradn ethanol hexane polemic 944
Gamma irradn ethyl iodide 1324
Gamma irradn hydrated electron 3694
Gamma irradn methane aq 3863
Gamma irradn methionine 1729
Gamma irradn methylpentane 3747
Gamma irradn methylpentane glass 3167
Gamma irradn org compd 630
Gamma irradn oxalate ESR 3274
Gamma irradn soln temp 1273
Gamma irradn water 2733
Gamma irradn xenon trioxide 3909
Gas adsorption 3415
Gas breakdown laser induced 31
Gas carbon tetrahalides irradn 3734

Gas chromatog mordenite adsorption 1647
Gas chromatog reactor 2159
Gas dissolved partial molal vol 3044
Gas free radical spectroscopy 2056
Gas intermol force 890
Gas irradn electron attachment 3730
Gas liq electronic transport 3890
Gas liq partition chromatog 99
Gas liq soly 598 601
Gas monat model potential 1743
Gas phase epoxidation alkene 3319
Gas polar transport property 1470
Gas reaction suprahigh pressure 2614
Gas soly methanol 2170
Gas water interface adsorption 2769
Geminate ion pairs radiolysis 3812
Germane halophenyl spectra 1558
Glass acetate ionic covalent interaction 1035
Glass alk irradn electron scavenger 1962
Glass alkali ion mobility 1072
Glass Bronsted acid site 3633
Glass energy level structure 3830
Glass metaphosphate pulse radiolysis 203
Glass methylpentane gamma irradn 3167
Glass methylpentane trapped electron 3747
Glass org contamination polywater 457
Glass org elec cond 2781
Glass org irradn neg species 3894
Glass org paramagnetic relaxation 1226
Glass polymer statistical thermodn 416
Glass thin film nitrate aggregate 1826
Glass transition alkali metal nitrate 3093
Glasses alkyl halide hydrocarbon 1405
Glutamate poly transition 3464
Glutarate dimethyl saponification kinetics 704
Glycerol acetate soln 2474
Glycerol solvated electron spectra 1700
Glycine molal vol 1783
Glycine platinum complex isomerization 3934
Glycine radiolysis radical reaction 3507
Glycine tetrapeptide helical conformation 670
Glycolamide molal vol 1783
Glycolate vanadyl EPR 3951
Gold catalytic activity 1907
Gold electrode ion adsorption 2915
Group IIa element catalysts 3372
Guanidine hydrochloride vol urea 2778
Halfwave potential inorg radical 1487
Halide alkali metal cadmium melt 1831
Halide alkali structure liq theory 1612
Halide alkyl hydrocarbon glasses 1405
Halide cobalt complex racemization 119
Halide copper vapor UV 1632
Halide exchange anion exchange resin 680
Halide hydrogen chem laser 1425
Halide hydrogen halogen photochem 2801
Halide lithium pyridine complex 53
Halide nitrate soly silver 2759
Halide solvated electron 3677
Halide system fused thermochemistry 1616
Halide tetraalkylammonium extn 1775
Halide tetraalkylammonium water structure 1455
Haloalkane adsorbed dielec property 2535
Halobenzene NMR substituent effect 515
Halogen charge transfer complex spectra 3220
Halogen hydrogen halide photochem 2801
Halogen substitution dichlorobutane stereochem 501
Halomethane iodine 128 recoil 2685
Halonaphthalenes phosphorescence 221
Halophenol hydrogen bond 1553
Halophenylgermane spectra 1558
Halorhenate potassium recoil reaction 2499
Halouracil pulse radiolysis 2386 2392
Hard sphere solute water structure 4030
Hard sphere state equation 601
Heat adsorption carbon dioxide 3278
Heat adsorption hydrocarbon 2769
Heat adsorption inert gas 3171
Heat adsorption nonpolar mol 1647
Heat capacity activation solvolysis 369
Heat capacity aq tetraamylammonium bromide 2577
Heat capacity butylammonium bromide 1366
Heat diln electrolyte 1608
Heat diln lithium bromide 3050
Heat dissocn trimethylaluminum dimer 2933
Heat formation complex 1549
Heat formation diazirine 3504
Heat formation ethynyl radical 1913
Heat hydration ion 2298
Heat immersion zeolite 110
Heat immersion zirconium oxide 1497
Heat mixing alk earth halide 1616
Heat mixing aq electrolyte 3474
Heat mixing molten salt 1629
Heat soln tetraalkylammonium bromide 1369
Helical conformation glycine tetrapeptide 670
Helium nitrogen flash photolysis 3518
Helium oxygen reaction rate 2653
Helium soly aq solns 3068
Helium soly water 1195
Helix coil kinetics polypeptide 1737
Helix coil transition polyglutamate 3464
Hemimellitene nuclear Overhauser effect 281
Hemoglobin Bohr effect 1597
Hemoglobin proton transfer 528
Henry const gas soln 598
Heptanal oxime 1819
Heptanal perhydrotriphenylene ESR 1008
Heptane dihexyloxyazoxybenzene activity coeff 596
Heterocycle substituent effect NMR 1593
Heterovalent anion exchange 2459
Hexaamminecobalt sensitized photodecompn 1105
Hexacyanochromate photoactive state 1947
Hexafluoroacetone imine trifluoromethyl radical 487
Hexafluoroacetone photolysis 2690
Hexamethyldisilane tritium recoil 1249
Hexamethylphosphotriamide manganese NMR 1973
Hexamethylphosphotriamide nitrobenzene alkali system 2058
Hexane chlorination 1800
Hexane cyclohexane benzene diffusion 2572
Hexane ethanol gamma irradn polemic 944
Hexane film electron impact 1255
Hexane isomeric kinematic viscosity 3295
Hindered rotation sarcosinate 853
Homogeneous reaction theory 1160
Hot atom chemistry benzene 2521
Hot atom chemistry cyclopentadiene hydrogen 1389
Hot atom chemistry x ray 2639
Hot atom fluorine 18 3509
Hot atom iodine reactions 2685
Hot atom reaction bromine 3331
Hot atom reaction iodine alkene 3342
Hot atom recoil reactions 2711
Hot electron injection current 3890
Hueckel calcn amide 2178
Hueckel calcn extended polyalanine 2793
Hueckel calcn sulfur 2274
Hydrate calcium nitrate ultrasonic relaxation 1506 1507
Hydrated ammonium salt dielec 1999
Hydrated electron ab initio 3905
Hydrated electron absorption spectra 3780
Hydrated electron formation 3694
Hydrated electron org reaction 630
Hydrated electron pulse radiolysis 2072
Hydrated electron spin density 3838
Hydrated electron thermodn 683
Hydrated solute dissoln lifetime 2017
Hydration alc aq soln 1660
Hydration heat entropy ion 2298
Hydration org solvent 2454
Hydration pairing ion 2459
Hydration photo pyrimidine viscosity 3137
Hydration pyridinecarboxaldehyde 2959
Hydration silica 3188
Hydrobromic acid system diffusion 3419
Hydrocarbon adsorbed metal IR 2699
Hydrocarbon alkyl halide glasses 1405
Hydrocarbon arom dimer cation 1119
Hydrocarbon crystal irradn ESR 1411
Hydrocarbon decompn 143
Hydrocarbon electron mobility 442
Hydrocarbon fluorescence quenching 469
Hydrocarbon liq structures theory 731
Hydrocarbon polyolefin mixing entropy 400
Hydrocarbon radiolysis electron scavenging 987
Hydrocarbon solns radiolysis 3812
Hydrocarbon soly water bond 2754
Hydrochloric acid ion pairing 3664
Hydrochloric acid polystyrenesulfonate system 1881
Hydrodynamic rodlike macromol 1755
Hydrogen adsorption chromia catalyst 2694
Hydrogen argon collision 2006
Hydrogen atom reaction 1124
Hydrogen atom reaction photolysis 3337
Hydrogen atomic org compd reaction 2673
Hydrogen binding polyacrylic acid 254
Hydrogen bond charge transfer 3991
Hydrogen bond chlorophenol amine 587
Hydrogen bond dipole moment 3000
Hydrogen bond formation enthalpy 3065
Hydrogen bond formation thermodn 3502
Hydrogen bond intramol enthalpy 1553
Hydrogen bond MO peptide 375
Hydrogen bond solutes mol assocn 3058
Hydrogen bonded complex equil 1989
Hydrogen bonded liq vaporization 914
Hydrogen bonding dimethylamine 871
Hydrogen bonding polypeptide 3464
Hydrogen bonding water IR 1228
Hydrogen breakdown laser 31
Hydrogen bromide proton reaction 1321
Hydrogen carbon atom reaction 1389
Hydrogen carbon bond energy 3314
Hydrogen carbon monoxide argon discharge 2941
Hydrogen chloride chem laser 805
Hydrogen chloride elimination laser 811
Hydrogen chloride methane exchange 2809
Hydrogen chlorine azide reaction 805
Hydrogen cyanide cryst IR 1140
Hydrogen cyanide deuterium reaction 285
Hydrogen cyanide geometry polemic 2483
Hydrogen cyanide isotope IR 454
Hydrogen cyanide radiolysis ESR 3945
Hydrogen displacement butane 2937 2939
Hydrogen exchange propene zeolite 3940
Hydrogen fluoride chem laser 3125
Hydrogen formaldehyde reaction 2213
Hydrogen halide chem laser 1425
Hydrogen halide halogen photochem 2801
Hydrogen hydroperoxo reaction rate 1586
Hydrogen iodide radiolysis 3812
Hydrogen iodine cyanide reaction 1392
Hydrogen kinetics pyrolysis deuteride 3538
Hydrogen mol photolysis ethylene 138
Hydrogen oxygen reaction 2199
Hydrogen oxygen reaction rate 3518
Hydrogen peroxide acetone 1283
Hydrogen peroxide decompn catalysis 1907
Hydrogen peroxide radiolysis precursor 1542
Hydrogen peroxide reaction 1919
Hydrogen photodissocn ESR 2637
Hydrogen photoyield ammonia water 298
Hydrogen reaction methyl kinetics 1669
Hydrogen spin density 3838
Hydrogen sulfide ethanethiol photolysis 2668
Hydrogen sulfide flame 1925
Hydrogen transfer activation energy 1581
Hydrogen transfer methylene 1581
Hydrogen water irradn exchange 621
Hydrogen yield ethanethiol photolysis 2668
Hydrogen yield water radiolysis 2733
Hydrogenation ethylene catalysis 2625
Hydrogenation kinetics ethylene 1394
Hydrogenation propylene intermediate 2184
Hydrogenation rate propylene 943
Hydrolysis dichromate ion kinetics 582
Hydrolysis ethylethoxysilane 3192
Hydrolysis phenyl ester 432
Hydrolysis thiazoline 1192
Hydronium hydroxide proton exchange 2954
Hydroperoxo hydrogen reaction rate 1586
Hydroperoxo metal complexed 2207
Hydroperoxo reaction carbon monoxide 3301
Hydroperoxy propane kinetics 1283
Hydroperoxyl radical metal complexed 2207
Hydrophile lipophile balance surfactant 2019
Hydrophobic interaction 3050
Hydropyridine radical EPR 3348
Hydroxide chromium drying 1838
Hydroxide hydronium proton exchange 2954
Hydroxide ion isotope effect 362
Hydroxide purine reaction kinetics 2838
Hydroxide radical arom olefin 847
Hydroxide water termol reaction 3116
Hydroxy silica surface 1434
Hydroxyisopropyl radical reaction 3348
Hydroxyl bromide ion reaction 1815
Hydroxyl polyat mol reaction 1511
Hydroxyl radicals bromide oxidn 312
Hydroxyl sulfuric acid radiolysis 1265
Hydroxyl yield nitric acid radiolysis 2680
Hydroxylamine photolysis aq soln 180
Hydroxylapatite calcium surface concns 900
Hyperfiltration charged membrane 3638
Hyperfiltration ion exchange membrane 2256
Hyperfiltration porous material 4015
Hyperfine coupling alkali metal 2866
Hyperfine parameter nitroxide 1858
Hypochromism fluorescein halo dye 3970
Hypophosphite x ray emission 3975
Ice alk electron mobility 1509
Ice alk paramagnetic relaxation 1226
Ice electron irradn 1000
Ice refractive index 886
Ice satn silver iodide 2280
Imine hexafluoroacetone trifluoromethyl radical 487
Immersion heat zeolite 110
Immersion heat zirconium oxide 1497

Impurity ionized bound exciton 3771
Indigo carmine soln photoredn 2362
Inert gas app adsorption 3171
Injection current hot electron 3890
Inorg crystal bound exciton 3771
Inorg radical halfwave potential 1487
Interaction carboxylate copolymer 1767
Interaction charge transfer 2470
Interaction energy mol 2123
Interface gas water adsorption 2769
Interface lipid film 1238 1244
Interface silica carbon tetrachloride 3192
Interfacial exchange water polemic 1505
Interfacial tension pyrolytic graphite 2750
Intermediate hydrogen peroxide redox 2207
Intermol charge transfer 2405
Intermol charge transfer complex 2452
Intermol energy lipid film 1231
Intermol force gas 890
Intermol potential liq 2133
Internal conversion bromine 3331
Internal motion methyl carbon relaxation 3213
Internal rotation barrier 551
Intersystem crossing phthalazine 3937
Intersystem crossing trifluoromethylbenzene 823
Intramol proton transfer 4033
Intrinsic viscosities albumin 128
Intrinsic viscosity macromol 1755
Iodate photolysis radiolysis 302
Iodide cobalt complex racemization 119
Iodide copper vaporization mass spectrometry 2310
Iodide lithium dissoln water 2017
Iodide methyl dissocn kinetics 2353
Iodide methyl photolysis 308
Iodide pyridinium charge transfer 603
Iodide silver ice satn 2280
Iodide silver soly nitrate 2759
Iodide sodium viscosity solvents 434
Iodide triiodide exchange reaction 162
Iodination pyruvic acid ester 3121
Iodine aminopyridine complex thermodn 1895
Iodine charge transfer complex 1951
Iodine cyanide hydrogen reaction 1392
Iodine ethanol reaction 3314
Iodine nonpolar soln 2470
Iodine perylene complex thermodn 921
Iodine propionitrile complex 2098
Iodine thioamide charge transfer 2405
Iodine 128 recoil reactions 2685
Iodobenzene x ray irradn 2639
Ion activity computer simulation 1758
Ion adsorption electrode 2915
Ion exchange membrane hyperfiltration 2256
Ion exchange membrane ion transport 3996
Ion exchange solid 1317
Ion formation europium sulfate 2925
Ion heat entropy hydration 2298
Ion impact spectroscopy ethylene 1130
Ion irradn solid benzene 2521
Ion mol gaseous reactions 409
Ion mol reaction 2467 3883
Ion mol reaction gas ethane 3919
Ion mol reaction silane 3321
Ion nitrobenzene equil enthalpy 2058
Ion pair aggregation soln 2152
Ion pair conductance 2452
Ion pair equil 1989
Ion pair formation alc water 3842
Ion pairing alkali metal 1012
Ion pairing anion radical 2176
Ion pairing hydration 2459
Ion pairing sodium sulfate 3664
Ion pairs geminate radiolysis 3812
Ion product const water 90
Ion radical sulfuric acid irradn 3676
Ion recombination bromcresol green 1184
Ion recombination luminescence radical 3710
Ion recombination methyl orange 4023
Ion recombination triplet prodn 3801
Ion repulsive force soln 1062
Ion solvation number 2140
Ion solvent interaction 3472
Ion transport ion exchange membrane 3996
Ion water structure 84
Ion yield irradiated solvent polemic 944
Ionic assocn reaction vol 895
Ionic conductance potassium chloride 712
Ionic covalent interaction acetate glass 1035
Ionic crystal magnetic field 3993
Ionic dissocn org compd 630
Ionic dissocn photoinduced 1419
Ionic molal vol polemic 1086
Ionic soln theory polemic 1229
Ionic styrene polymn 930
Ionization biphotonic methyl phenylenediamine 2229
Ionization chem mass spectrometry 3917
Ionization current nickel 63 decay 3842
Ionization hydroxybenzotrifluoride 1909
Ionization naphthol excited singlet 3558
Ionization potential charge transfer complex 3220
Ionization potential complex 3991
Ionization potential thiourea 2405
Ionization silver chloride 2819
Ionization sodium chloride 1053
Ionization solute equil 720
Ionization UV photolysis 2061
Ionized impurity bound exciton 3771
Ionizing solvent diffusion 1166
IR acetone water polemic 449
IR alkali carbonate 1565
IR assocd alcs 864
IR carbon monoxide chemisorption 3180
Ir carbon oxide oxidn 2833
IR chromia surface property 571
IR cryst hydrogen cyanide 1140
IR dimethylamine 871
IR hydrocarbon adsorbed metal 2699
IR hydrogen bonding alc 2562
IR hydrogen cyanide isotope 454
IR matrix diiodomethyl radical 2718
IR matrix spectra zone 3208
IR nitrous oxide zeolite 945
IR optical const naphthalene 260
IR polywater org contaminant 457
IR potassium salt anthracene 1026
IR prepn polywater polemic 456
IR silver oxide carbonate 940
IR spectra halophenylgermane 1558
IR spectra nitrate carbon dioxide 1826
IR sulfur tetramer 3968
IR tertiary ammonium salt 339
IR uranium oxide gaseous 648
IR water acetone complex 452
IR water adsorption silica 3188
IR water hydrogen bonding 1228
IR water monodeuterated polemic 3675
IR water structure 84
Iridium butene adsorption IR 2699
Iron carbon monoxide chemisorption 3180
Iron carbon oxygen nucleation 2609
Iron cobalt oxide electrode 3646
Iron nickel adsorption arsine 2851
Iron oxalato photochemistry 2618
Iron oxidn nitrous oxide 2530
Iron sulfate aq radiolysis 1273
Iron thiooxalato nitrosyl ESR 49
Irradiated gamma silica alumina 3741
Irradiated gamma silica gel 3158
Irradiated heterogeneous system ESR 1721 1727
Irradiated solvent ion yield polemic 944
Irradiation solvated electron 3765 3824
Irradn alk glass electron scavenger 1962
Irradn alkyl phosphate ESR 2848
Irradn ammoniated zeolite EPR 2716
Irradn aq methane 3863
Irradn aq soln 1710
Irradn aq soln ESR 1706
Irradn arom cyclohexane electron scavenging 3722
Irradn benzene excited singlet 3867
Irradn beta sulfuric acid 1542
Irradn butane olefin oxygen 1260
Irradn carbon tetrahalides gas 3734
Irradn cation radical DNA 3577
Irradn cyanoacetic acid ESR 3377
Irradn dioxane water pulse 1279
Irradn electron ice 1000
Irradn exchange hydrogen water 621
Irradn gamma methylpentane 3747
Irradn gamma methylpentane glass 3167
Irradn gamma soln temp 1273
Irradn gamma xenon trioxide 3909
Irradn gas electron attachment 3730
Irradn halo uracil ESR 2399
Irradn hydrated electron formation 3694
Irradn hydrocarbon crystal ESR 1411
Irradn ion solid benzene 2521
Irradn methanol ethanol spectra 3876
Irradn neutron catalyst 2625
Irradn org compd 630
Irradn org glass neg species 3894
Irradn oxalate ESR 3274
Irradn paraffin temp dependence 3851
Irradn solid radical concn 1324
Irradn spectra trapped electron 3683
Irradn styrene polymn 930
Irradn sulfuric acid aq 1265
Irradn sulfuric acid radical ion 3676
Irradn tin lead salt 141
Irradn triplet prodn mechanism 3801
Isobutane decompn amyl acetate 3917
Isocitrate conformation soln NMR 3073
Isocyanate aryl nitrene ESR 3570
Isocyanic acid predissocn polemic 2636
Isocyanide methyl thermal isomerization 1935
Isodurene relaxation carbon NMR 281
Isomer halophenol energy difference 1553
Isomer olefin recoil chlorine 2711
Isomeric hexane kinematic viscosity 3295
Isomeric yield hydrocarbon irradn 1411
Isomerization alkyl radical 2507
Isomerization chloroethylene 2829
Isomerization cyclopropane unimol 1695
Isomerization decompn tritium spiropentane 2187
Isomerization kinetics butene 44
Isomerization platinum glycine complex 3934
Isomerization propylene intermediate 2184
Isomerization thermal energy transfer 1935
Isopropyl alc decompn catalytic 3372
Isotherm adsorption detn 2584
Isothiocyanate butyl irradiated ESR 1792
Isotope effect ammonia decompn 970
Isotope effect deuterium iodination 3121
Isotope effect hydroxide ion 362
Isotope effect methyl addn alkene 3613
Isotope effect proton transfer 2951
Isotope effect vapor pressure 743 3040
Isotope effects methyl iodide reactions 427
Isotope exchange solid 1317
Isotope kinetic effect methyl 1669
Isotope labeled nitrogen reaction 37
Isotope shift hydrogen cyanide 2483
Junction potential computer simulation 1758
Kerr const water temp 216
Ketene kinetics borane reaction 3532
Ketone addn hydrated electron 2072
Ketones radiolysis 198
Ketyl benzoylpyridine UV 3200
Kihara spherical core 1470
Kinematic viscosity isomeric hexane 3295
Kinetic charge transfer chem reaction 1666
Kinetic isotope effect methyl 1669
Kinetics arsenidation metal surface 2851
Kinetics benzene photochem 165
Kinetics borane ketene reaction 3532
Kinetics bromate oxidn pentanedione 2185
Kinetics butene isomerization 44
Kinetics carbon monoxide oxidn 3527
Kinetics chloroethane elimination 283
Kinetics competitive consecutive reaction 704
Kinetics comproportionation violene 701
Kinetics cyclopentadiene dissocn 2159
Kinetics decompn amyl acetate 3917
Kinetics decompn tetrafluoroethane 292
Kinetics diffusion radical 3008
Kinetics electron org reaction 630
Kinetics enzyme orientation constraint 534
Kinetics hydrogen oxygen reaction 3518
Kinetics hydrogenation ethylene 1394
Kinetics hydrolysis dichromate ion 582
Kinetics hydrolysis ethylethoxysilane 3192
Kinetics hydroperoxy propane 1283
Kinetics hydroxyl bromide reaction 1815
Kinetics methyl bromide scavenger 2374
Kinetics methyl iodide dissocn 2353
Kinetics methyl iodide reactions 427
Kinetics methylene radicals dimethylsilane 459
Kinetics micelle dissoln relaxation 3017
Kinetics oxygen redn electrode 3646
Kinetics peroxide superoxide reaction 2841
Kinetics phenanthrenequinonesulfonate 1875
Kinetics phenylmethane carbanion abstraction 695
Kinetics photoredn reaction 2362
Kinetics proton transfer benzoate 1327
Kinetics proton transfer reaction 2951
Kinetics pyrolysis difluoroethane 1680
Kinetics pyrolysis hydrogen deuteride 3538
Kinetics radical decay glasses 1405
Kinetics reaction mineral acid 3625
Kinetics recoil reaction 2499
Kinetics redn carbon dioxide 3278
Kinetics solid state decompn 1474
Kinetics solvated electron decay 3765
Kinetics solvated electron reaction 1700
Kinetics toluene autoxidn 1520
Kinetics transformation cholesteryl nonanoate 276
Kinetics vibrationally hot propane 607
Krafft point surfactants 909
Lactate vanadyl EPR 3951
Lambda transition trimethylsilylmethane 4037
Lanthanide oxide catalyst 2199
Laser chem 1429
Laser chem hydrogen chloride 805
Laser chem hydrogen fluoride 3125
Laser chem hydrogen halide 1425
Laser hydrogen chloride elimination 811
Laser induced gas breakdown 31
Laser light beating spectroscopy 2744

Laser nitrogen dioxide photodissocn 474
Laser photolysis charge transfer 1133
Laser photolysis dimethylaniline 3805
Laser Raman spectroscopy melt 1831
Laser Raman surface 2325
Latex sphere light scattering 2744
Lattice nuclear spin relaxation 2079
LCAO approxn perturbation theory 3993
LCAO MO methyl formate conformation 2430
Lead acetate glass 1035
Lead oxidn nitrous oxide 2530
Lead potassium thermodn 1202
Lead salt soln position lifetime 1124
Lead silver arsine adsorption 2851
Lead 3 ESR 141
Leghemoglobin nitrogen xenon 591
Lifetime dissoln hydrated solute 2017
Lifetime excited singlet alkylbenzene 3566
Lifetime positron detn 1951
Lifetime trifluoromethyl radical 2517
Ligand field photochem rhodium 1937
Ligand macrocyclic cobalt complex 2223
Light scattering mixt 2744
Light scattering sp vol macromol 2437
Line shape ENDOR powder 2079
Lipid film interface 1238 1244
Lipid film intermol energy 1231
Lipophile hydrophile balance surfactant 2019
Liq adsorption 3412 3415
Liq crystal dihexyloxyazoxybenzene 596
Liq crystal mech property 2409
Liq crystal solvent NMR 925
Liq crystal solvent thermodn 99
Liq gas electronic transport 3890
Liq gas soly 598 601
Liq glass polymer thermodn 416
Liq intermol potential 2133
Liq junction potential computer simulation 1758
Liq photoinjected electron range 3794
Liq structure isomeric hexane 3295
Liq system tracer diffusion 2572
Liq theory structure alkali halide 1612
Liquidlike state adsorbate 2584
Liquidus measurement electrochem 1154
Lithium beryllium fluoride system 1154
Lithium bromide heat diln 3050
Lithium bromide PMR 130
Lithium doped catalyst irradn 2625
Lithium halide pyridine complex 53
Lithium iodide dissoln water 2017
Lithium nitrobenzene hexamethylphosphotriamide system 2058
Lithium perchlorate methanol assocn 2920
Luminescence alkylbenzene 3566
Luminescence ion recombination radical 3710
Lysozyme light scattering 2744
Lysozyme sedimentation equil 777
Lysozyme sedimentation overspeeding rotor 2740
Lysozyme water adsorption 2987
Macrocyclic ligand cobalt complex 2223
Macrocyclic polyether complex 2152
Macromol hydrodynamic rodlike 1755
Macromol solute specific vol 2437
Magnesium chloride PMR 130
Magnesium maleic anhydride copolymer 254
Magnesium nitrate water Raman 1019
Magnesium oxide sulfur dioxide 323
Magnesium sodium chloride bromide 3474
Magnesium sodium chloride vol 3488 3491
Magnesium sulfate ion pairing 3664
Magnetic circular dichroism molecule 1844
Magnetic field ionic crystal 3993
Magnetic susceptibility copper complex 2707
Magnetochem diphenyldialkoxysilane 1579
Maleate equil acid 1957
Maleic acid copolymer 1767
Maleic anhydride copolymer magnesium 254
Malonate copper photochemistry 1387
Malononitrile phenylbenzylidene radical anion ESR 3384
Mandelate vanadyl EPR 3951
Manganese butyrolactam NMR 1973
Manganese catalysis pentanedione oxidn 2185
Manganese DMF soln NMR 1968
Mannitol effect water 3077
Mass spectra dicyanoacetylene oxygens 269
Mass spectra fluoroaminoalkane 60
Mass spectra ion mol reaction 409
Mass spectrometer ionization 2819
Mass spectrometry chem ionization 3917
Mass spectrometry copper iodide vaporization 2310
Mass spectrometry ethynyl radical 1913
Mass spectrometry methylsilane 3217
Mass spectrometry microwave discharge 2941
Mass spectrometry water reaction 3116
Mass spectrum borane deriv 1860
Mass spectrum isocyanic acid polemic 2636
Math fluorocarbon surfactant 2019
Matrix IR vibrational model 454
Matrix isolated hydrogen cyanide 2483
Matrix spectra sulfur tetramer 3968
Matrix spectra zone argon 3208
Mech property nematic liq crystal 2409
Mechanism acetone peroxide 1283
Mechanism benzyne addn ethylene 656
Mechanism decompn diazirine 797
Mechanism intersystem crossing 1524
Mechanism methylidene emission 825
Mechanism nitric acid radiolysis 2680
Medium activity coeff phenylborate 2024
Melt transport mode 1348
Melt vapor nuclei 2609
Melting solid decompn rate 2253
Membrane anisotropic ultrafiltration 238
Membrane charged hyperfiltration 3638
Membrane electrochem selectivity ratio 1872
Membrane ion exchange hyperfiltration 2256
Membrane ion exchange ion transport 3996
Membrane phenomena 2447
Membrane polyelectrolyte elec polarization 3434
Membrane porous salt rejection 4015
Membrane potential porous glass 3633
Membrane rigid solute permeability 393
Mercaptan methyl photoelectron spectrum 1030
Mercury electrode ion adsorption 2915
Mercury quenching aromatic compd 2665
Mercury sensitized photoisomerization 2245
Mercury silica gel contact angle 3267
Mercury tetraphenylborate adsorption 707
Merocyanine photolysis spiropyran 3554
Mesophase forming system transition 2605
Mesophase forming systems 276
Mesophase nematic nitroxide ESR 672
Metal adsorbed hydrocarbon IR 2699
Metal ammonia soln energy level 2738
Metal complex polarog current 1170
Metal complexed hydroperoxyl radical 2207
Metal film oxidn 2530
Metal oxide ratio catalyst 2525
Metaphosphate glass pulse radiolysis 203
Methacrylate polymn photoinitiation EPR 3141
Methacrylic acid molar vol 3451
Methane aq irradn 3863
Methane hot electron 3890
Methane hydrogen chloride exchange 2809
Methane iodine 128 recoil 2685
Methane reaction kinetics 1795
Methane soly aq solns 3068
Methanes methoxymethyl dielec relaxation 525
Methanol alkali perchlorate assocn 2920
Methanol assocn 869
Methanol boron trifluoride NMR 329
Methanol hydration aq soln 1660
Methanol silica gel 3078
Methanol solvated electron spectra 3876
Methanol soly gas 2170
Methanol water solvated electron 3765
Methionine radical cation 1729
Methoxymethyl methanes dielec relaxation 525
Methyl addn alkene isotope effect 3613
Methyl bromide borazines photoreaction 2630
Methyl bromide scavenger methylpentane 2374
Methyl carbon relaxation 3213
Methyl formate conformation LCAO MO 2430
Methyl group substitution phenol 2882
Methyl iodide azide acetate 427
Methyl iodide dissocn kinetics 2353
Methyl iodide photolysis 308
Methyl iodo radical matrix IR 2718
Methyl isocyanide thermal isomerization 1935
Methyl orange acid dissocn 4023
Methyl phenylenediamine biphotonic ionization 2229
Methyl radical quenching pressure 2196
Methyl reaction hydrogen kinetics 1669
Methylamine radiolysis EPR 2857
Methylcyclohexane glass irradn 3894
Methylene addn alkene stereochem 664
Methylene blue aggregation 4026
Methylene blue polyanion complex 688
Methylene blue redn 3460
Methylene hydrogen transfer 1581
Methylene insertion ethane 607
Methylene prodn propane photolysis 9
Methylene radicals dimethylsilane kinetics 459
Methylene triplet state prodn 1389
Methylenecyclopropane UV photolysis 3153
Methylidene emission mechanism 825
Methylnaphthalene irradn singlet triplet 2485
Methylpentane glass elec cond 2781
Methylpentane glass gamma irradn 3167
Methylpentane glass irradn 3894
Methylpentane glass trapped electron 3747
Methylpentane liq radiolysis scavenger 2381
Methylpentane scavenger liq radiolysis 2374
Methylpentane trapped electron photobleaching 2341
Methylsilane mass spectrometry 3217
Methylsilanes decompn 459
Methyltetrahydrofuran paramagnetic relaxation 1226
Methyltetrahydrofuran trapped electron 636 2641
Micellar zwitterionic arom soln 1460
Micelle concn crit 909
Micelle dissoln kinetics relaxation 3017
Micelle shape surface area 3020
Micelle size distribution 565
Microemulsion water oil 876
Microwave discharge mass spectrometry 2941
Mineral acid kinetics reaction 3625
Mixing entropy polymer solvent 400
Mixing free energy alloy 1202
Mixing heat alk earth halide 1616
Mixing heat aq electrolyte 3474
Mixing heat molten salt 1629
Mixing vol chloride 3491
Mixt light scattering 2744
MO benzoquinone electronic spectra 2424
MO calcn ethylene phenyl radical 3960
MO chem interacting system 232
MO diat mol 2268
MO hydrogen bond peptide 375
MO LCAO methyl formate conformation 2430
MO naphthol ionization excited 3558
MO phosphorus oxyanion 3975
Mobility alkali ion glass 1072
Mobility electron alk ice 1509
Mobility excess electron 3830
Mobility hydronium hydroxide water 2954
Mobility small ion 2447
Model analysis fluorination tungsten 2930
Model free radical water radiolysis 2733
Model ion hydration 2298
Model potential monat gas 1743
Mol beam scattering 2947
Mol diffusion proton exchange 3078
Mol interaction energy 2123
Mol ion gaseous reactions 409
Mol ion reaction gas ethane 3919
Mol ion water vapor reaction 1517
Mol model solvated electron 3714
Mol movement methylsilylmethane 4037
Mol structure fluoronitrosomethane 3099
Mol structure isomeric hexane 3295
Mol vibration collision 2006
Mol wt distribution polystyrene 930
Mol wt polymer soly 1214
Molal vol chloride 3488
Molal vol dissolved gas 3044
Molal vol glycine 1783
Molal vol org aq soln 1338 1343
Molal vol partial electrolyte 1333
Molar vol polyelectrolyte 3451
Molecular electronic energy 2995
Molten alkali nitrate 422
Molten salt heat mixing 1629
Molybdate polymer ultrasonic attenuation 1575
Moment relation magnetic circular dichroism 1844
Monat gas model potential 1743
Monolayer carbon 14 counting 3603
Monomer dimer equil vanadium 2343
Monoolefin carbonyl excitation 478
Monophosphide antimony thermodn 2336
Monoxide carbon chemisorption IR 3180
Monoxide carbon oxidn 1807
Monoxide carbon reaction hydroperoxo 3301
Monoxide carbon stimulated emission 1429
Mordenite adsorption gas chromatog 1647
Mordenite adsorption nonpolar mol 1641
Motion mol electron diffraction 3099
Naphthalene donor acceptor complex 1982
Naphthalene fluorescence quenching benzoic acid 3563
Naphthalene IR optical const 260
Naphthalene irradn excitation yield 2485
Naphthalene pulse radiolysis 1119
Naphthalene scavenger trapped electron 2641

Naphthalenesulfonic acid ionization 508
Naphthalenide electron transfer 1734
Naphthalenide hyperfine coupling 2866
Naphthol excited singlet ionization 3558
Neg ion formation sodium 839
Neg species org glass irradn 3894
Neighboring carboxylate interaction 1767
Nematic liq crystal mech property 2409
Nematic mesophase nitroxide ESR 672
Neodymium oxide catalyst 2199
Nernst Planck equation stability 2256
Neutralization structure polymethacrylic acid 2559
Neutron activation bromine 3331
Neutron activation iodine 3342
Neutron irradn catalyst 2625
Nickel carbonyl oxidn oxygen 2833
Nickel catalyst neutron irradn 2625
Nickel chloride decompn catalyst 2844
Nickel DMF soln NMR 1968
Nickel iron adsorption arsine 2851
Nickel oxidn nitrous oxide 2530
Nickel pyridine adsorption 972
Nickel surface carbon oxidn 968
Nickel 2 polarog redn 1170
Nickel 63 decay alc water 3842
Nitramine dimethyl photolysis 496
Nitrate aggregate carbon dioxide matrix 1826
Nitrate alkali metal glass transition 3093
Nitrate alkali molten 422
Nitrate ammonium decompn catalysis 2844
Nitrate calcium aq viscoelastic relaxation 3495
Nitrate calcium hydrate ultrasonic relaxation 1506 1507
Nitrate calcium soln 3244
Nitrate halide silver soly 2759
Nitrate hydration 2454
Nitrate magnesium water Raman 1019
Nitrate silver water diffusion 1853
Nitrate sodium soln photoredn 2362
Nitrene triplet ESR 3570
Nitric acid radiolysis mechanism 2680
Nitric oxide ammonia reaction 37
Nitric oxide copper zeolite EPR 1546
Nitric oxide ethyl radical reaction 3303
Nitrile ring thermolysis 2817
Nitroaniline structure 3597
Nitrobenzene anion radical 1439
Nitrobenzene ion equil enthalpy 2058
Nitrogen active quenching rate 1
Nitrogen cyanoacetylene reaction 2643
Nitrogen dioxide photodissocn 474
Nitrogen helium flash photolysis 3518
Nitrogen heterocycle molal vol 1343
Nitrogen isotope labeled reaction 37
Nitrogen oxide gas reaction 2614
Nitrogen oxide reaction 1919
Nitrogen oxygen reaction rate 2653
Nitrogen quadrupole coupling diazirine 2249
Nitrogen relaxation borazole 2871
Nitrogen xenon leghemoglobin 591
Nitrogen zirconium reaction 2156
Nitrogen 14 NMR tetrazole 2403
Nitromethane radical trapping 1710
Nitrophenol amine aprotic solvent 1989
Nitrophenol amine complex bonding 3991
Nitrosamide rearrangement 496
Nitrosobenzene photoredn 1087
Nitrosomethylaniline soln photoredn 2362
Nitrosyl thiooxalato iron ESR 49
Nitrous oxide carbon monoxide reaction 1807
Nitrous oxide methane aq irradn 3863
Nitrous oxide methylpentane radiolysis 2381
Nitrous oxide oxidn metal 2530
Nitrous oxide zeolite IR 945
Nitroxide rotational correlation time ESR 1858
Nitroxides ESR simulation model 672
Nitryl chloride pyrolysis 2614
NMR aq tetraalkylammonium halide 1455
NMR butyl formate 3582
NMR butylethylene steric effect 2877
NMR carbon relaxation isodurene 281
NMR chloranil electrode acetonitrile 246
NMR conformation isocitrate soln 3073
NMR disubstituted ethane 1466
NMR DMF soln nickel 1968
NMR double resonance carbon 13 2972
NMR europium ion solvation 1449
NMR halobenzene substituent effect 515
NMR hindered rotation sarcosinate 853
NMR internal rotation 71
NMR manganese butyrolactam 1973
NMR methanol boron trifluoride 329
NMR nitrogen 14 tetrazole 2403
NMR quadrupolar dipolar relaxation 53
NMR relaxation methyl carbon 3213
NMR solvent phase diagram 925
NMR substituent effect arom 1593
NMR surfactant micelle structure 3012
NMR zeolite 1220
Nonanoate cholesteryl 276
Nonaq medium samarium fluorescence 3397
Nonaq solvent complex equil 3618
Nonequil unimol reaction 954
Nonpolar mol mordenite adsorption 1641
Nonpolar soln iodine 2470
Nonpolar solvent entropy soln 2138
Nonpolar system soly estn 601
Nonspherical mol equation state 2014
Norbornene photochem addn 15
Nuclear Overhauser effect hemimellitene 281
Nuclear quadrupole coupling diazirine 2249
Nuclear recoil technique 1389
Nuclear spin lattice relaxation 2079
Nuclei vapor melt 2609
Nucleophile phenyl ester 432
Nucleophilic substitution bimol 232
Obstruction elec cond 1763
Octanoate perfluoro 909
Oil water microemulsion 876
Olefin acid proton exchange 2951
Olefin addn methyl isotope effect 3613
Olefin benzene singlet quenching 3668
Olefin butane irradn oxygen 1260
Olefin cis trans recoil chlorine 2711
Olefin epoxidation gas phase 3319
Olefin iodine hot atom reaction 3342
Olefin mono carbonyl excitation 478
Olefin oxygen hydroxide radical 847
Olefin polymer mixing entropy 400
Olefins epoxidation stereochem 213
Optical anisotropy calcn 1502
Optical bleaching 636
Optical bleaching glass 3830
Optical const IR naphthalene 260
Optical rotation collagen film 2935
Optical spectra solvated electron 2975 3876
Org aq glass photocond 3830
Org aq solvent mixt 1040
Org carbonate dielec property 2892
Org compd hydrogen atomic reaction 2673
Org compd ionic dissocn 630
Org contaminant polywater IR 457
Org elec conductivity 115
Org glass elec cond 2781
Org glass irradn neg species 3894
Org glass paramagnetic relaxation 1226
Org glass trapped electron 3744
Org liq viscous flow 2317
Org solid transition 2798 2799
Org solute reverse osmosis rejection 4006
Org solvent hydration 2454
Orientation constraint kinetics enzyme 534
Orotic acid bromo irradn ESR 2399
Oscillator strength carbazole complex 2102
Osmotic pressure activity polyelectrolyte 3445
Osmotic property polystyrenesulfonate 1881
Overhauser effect hemimellitene 281
Overspeeding rotor lysozyme sedimentation 2740
Oxalate gamma irradn ESR 3274
Oxalato iron photochemistry 2618
Oxamide rotation barrier 642
Oxide carbon methanol interaction 2170
Oxide cobalt iron electrode 3646
Oxide deuterium vapor pressure 3040
Oxide ion water reaction 422
Oxide metal ratio catalyst 2525
Oxide nitric copper zeolite EPR 1546
Oxide nitrogen gas reaction 2614
Oxide nitrous zeolite IR 945
Oxide paramagnetic center 3095
Oxide photocatalytic reaction 1807
Oxide silver IR 940
Oxide stannic electrode auramine 1655
Oxide thianthrene adsorption 1443
Oxide uranium gaseous IR 648
Oxide zinc iodomethane adsorption 2353
Oxide zinc oxygen adsorption 3184
Oxide zinc powder ESR 2527
Oxide zinc promoted photoredn 2362
Oxide zirconium heat immersion 1497
Oxidn aminoethonethiol ferricyanide 3641
Oxidn benzothiazolinone azine 1178
Oxidn bromide hydroxyl radicals 312
Oxidn carbon monoxide 1416
Oxidn carbon nickel surface 968
Oxidn kinetics carbon monoxide 3527
Oxidn mechanism bromide ion 1815
Oxidn metal film 2530
Oxidn nickel carbonyl oxygen 2833
Oxidn pentanedione manganese catalysis 2185
Oxime heptanal 1819
Oxyanion phosphorus x ray emission 3975
Oxygen adsorption zinc oxide 3184
Oxygen argon reaction kinetics 2653
Oxygen atom dicyanoacetylene 269
Oxygen bromine tungsten reaction 320
Oxygen butane irradn olefin 1260
Oxygen butene addn 3311
Oxygen carbon monoxide reaction 1807 3527
Oxygen chloromethane laser 811
Oxygen electron attachment 3730
Oxygen excited singlet reaction 1375
Oxygen fluorine bond energy 3480
Oxygen formaldehyde reaction 2215
Oxygen hydrogen reaction 2199
Oxygen hydrogen reaction rate 3518
Oxygen nickel carbonyl oxidn 2833
Oxygen peroxide superoxide reaction 2841
Oxygen radical arom olefin 847
Oxygen redn kinetics electrode 3646
Oxygen water termol reaction 3116
Oxygen zirconium bubble nucleation 2609
Ozone carbon monoxide reaction 1514
Ozonide thermal decompn 2659
Pairing alkali metal ion 1012
Pairing hydration ion 2459
Pairwise additivity 1593
Palladium cerium bond dissocn 2332
Palladium oxidn nitrous oxide 2530
Palladium tungsten arsine adsorption 2851
Palmitic acid urea clathrate 801
Paraffin irradn temp dependence 3851
Paramagnetic center oxide 3095
Paramagnetic intermediate redox ESR 2207
Paramagnetic relaxation trapped radical 1226
Paramagnetism charge transfer complex 1849
Parametric relaxation trapped electrons 636
Partial molal properties helium 1195
Partial molal vol dissolved gas 3044
Partial molar enthalpy electrolyte 1608
Partial sp vol macromol 2437
Partition coeff org solute 4006
Peak shape chromatog 2586
Pentaammine formato cobalt photolysis 2492
Pentacoordinate complex 2907
Pentane methyl chlorination 1800
Pentane methyl glass cond 2781
Pentanedione oxidn manganese catalysis 2185
Pentanone methylphenyl 198
Pentenyl radical cyclization decompn 1089
Peptide energy parameter 375
Peptide glycine helical conformation 670
Perchlorate alkali methanol assocn 2920
Perchlorate ammonium thermal decompn 3545
Perchlorate dimethylphenanthroline copper cond 3029
Perchlorate hydration 2454
Perchlorate potassium assocn water 2923
Perchlorate thianthrene assocn spectra 3468
Perchlorate water structure 84
Perchloric acid reaction kinetics 1795
Perfluorocyclohexane 1824
Permanganate potassium soln photoredn 2362
Permeability measurement 2116
Permeability solute rigid membrane 393
Permittivity measurement 2116
Permselective liq membrane 1872
Peroxide acetone mechanism 1283
Peroxide fluoromethyl decompn 3480
Peroxide hydrogen decompn catalysis 1907
Peroxide hydrogen radiolysis precursor 1542
Peroxide hydrogen reaction 1919
Peroxide oxygen superoxide reaction 2841
Peroxide photolysis UV 2061
Peroxy radical cobalt 1385
Perturbation calcns crystal field 2907
Perturbation theory LCAO approxn 3993
Perylene complex thermodn stability 921
Perylene pulse radiolysis 1119
Perylene tetracene complex 1549
PH conformation polymethacrylic acid 2559
PH polyelectrolyte polymer concn 3445
Phase diagram solvent NMR 925
Phase diagram vanadium deuterium 927
Phase relation cholesteryl ester 3089
Phase transition methylsilylmethane 4037
Phenanthrenequinonesulfonate equil 1875
Phenanthroline dimethyl copper photolysis 1528
Phenol alumina chemisorption spectrum 2882
Phenol chloride ion coordination 1775
Phenol cyclohexane system 3058
Phenol diazine oxide interaction 3502
Phenol halo hydrogen bond 1553
Phenol nitro amine equil 1989
Phenol pyridine complex spectrum 2112
Phenols amine hydrogen bond 587

Phenyl ester nucleophile 432
Phenylarsonium medium activity coeff 2024
Phenylbenzylidenemalononitrile radical anion ESR 3384
Phenylborate medium activity coeff 2024
Phenylcyclobutane photolysis dissocn 3355
Phenylenediamine methyl biphotonic ionization 2229
Phenylenediamine nickel complex 1170
Phenylhydroxylamine photoprodn 1087
Phenylimidazole photolysis dihydrophenanthrene intermediate 3362
Phenylmethane carbanion abstraction kinetics 695
Phosphate alkyl irradn ESR 2848
Phosphate methyl UV 3673
Phosphate x ray emission 3975
Phosphine silane reaction 1352
Phosphite x ray emission 3975
Phosphonate alkyl calcium structure 1304
Phosphonic acid alkyl structure 1298
Phosphorescence halonaphthalenes 221
Phosphorescence phthalazine 3937
Phosphorescence spectroscopy zeolite synthesis 3388
Phosphoric telluric acid reaction 3625
Phosphorus oxide anion radical 1706
Phosphorus oxyanion x ray emission 3975
Phosphorus oxychloride samarium fluorescence 3397
Phosphorus surface concn hydroxylapatite 900
Photoactivation polaron solid state 3366
Photoactive state hexacyanochromate 1947
Photobleaching solid state polaron 3366
Photobleaching trapped electron methylpentane 2341 3747
Photocatalytic reaction oxide 1807
Photocatalytic reactions zinc oxide 1394
Photochem benzene 165
Photochem hydrogen halide halogen 2801
Photochem ligand field rhodium 1937
Photochem norbornene addn 15
Photochem reaction fluorobenzophenone 3926
Photochem trifluoromethyl benzene 823
Photochemistry azoisopropane 1669 1685
Photochemistry borazine 2630
Photochemistry copper malonate 1387
Photochemistry ethanethiol 2668
Photochemistry oxalato iron 2618
Photocond aq org glass 3830
Photocond auramine 1655
Photocond irradiated alk ice 1509
Photocyclization phenylimidazole singlet 3362
Photodecompn sensitized hexaamminecobalt 1105
Photodissocn hydrogen ESR 2637
Photodissocn nitrogen dioxide 474
Photodissocn phenylcyclobutane 3355
Photoelimination methylphenylpentanone 198
Photohydration pyrimidine viscosity effect 3137
Photoinduced ionic dissocn 1419
Photoinitiation polymn methacrylate EPR 3141
Photoinjected electron range liq 3794
Photoionization aminoethylene 2105
Photoionization arom solid state 2236
Photoionization cation radical prodn 639
Photoionization DNA cation radical 3571
Photoisomerization diazine 2245
Photolysis ammonia water 298
Photolysis azoethane 3303
Photolysis benzoyl azide isocyanate 3570
Photolysis butyne 1112
Photolysis copper phenanthroline 1528
Photolysis dimethylaniline exciplex 3805
Photolysis dimethylnitramine 496
Photolysis ethylene UV actinometer 138
Photolysis flash ferrioxalate 830
Photolysis formato pentaammine cobalt 2492
Photolysis hexafluoroacetone 2690
Photolysis hydroxylamine aq soln 180
Photolysis laser charge transfer 1133
Photolysis liq EPR 3348
Photolysis methyl iodide 308
Photolysis phenylcyclobutane dissocn 3355
Photolysis phenylimidazole dihydrophenanthrene intermediate 3362
Photolysis propane methylene prodn 9
Photolysis radiolysis iodate 302
Photolysis reaction hydrogen atom 3337
Photolysis solvated electron glycerol 1700
Photolysis spiropyran merocyanine 3554
Photolysis thymine 489
Photolysis UV cyclohexanone 615
Photolysis UV ionization 2061
Photolysis UV methylenecyclopropane 3153
Photolyzed flash oxalatoiron absorbance 2618
Photon impact diazirine 3504
Photoprodn diiodobenzene 2639
Photoprodn ethane 9
Photoprodn free radical gas 2056
Photoprodn sorbed trifluoromethyl radical 2690
Photoprodn sulfur trioxide 814
Photoredn acetophenone 821
Photoredn nitrosobenzene 1087
Photoredn zinc oxide promoted 2362
Photoyield hydrogen ammonia water 298
Phthalazine triplet absorption 3937
Phthalocyanine dye assocn 1994
Phthalocyanines copper dimerization 446
Phys property monat gas 1743
Pi bond carbon 3532
Picrate potassium soln cond 1049
Piperazine diketo assocn water 3065
Plasma gas breakdown laser 31
Platinum electrode thallium voltammetry 976
Platinum glycine complex isomerization 3934
PMR arom zwitterionic micellar soln 1460
PMR conformation amide 2178
PMR Dowex 50W 578
PMR spectra borazole 2871
PMR tetraalkylammonium bromide 130
Poisson distribution radioactive decay 3603
Polar gas transport property 1470
Polar mol solvated electron 3824
Polar solvent fluorescence quenching 3132
Polarizability electronic ice 886
Polarization elec polyelectrolyte membrane 3434
Polarization spectrometry thin film 3390
Polarog current metal complex 1170
Polarog pulse radiolysis inorg radical 1487
Polaron solid state photoactivation 3366
Polaron yield pulse radiolysis 3776
Polyacrylamide membrane elec polarization 3434
Polyacrylate x ray diffraction 1311
Polyacrylic acid hydrogen binding 254
Polyalanine extended Hueckel calcn 2793
Polyamine ultrasonic absorption 334
Polyanion dye complex thermodn 688
Polyat mol hydroxyl reaction 1511
Polycarboxylate counterion binding dilatometry 254
Polydimethylsiloxane alkane soln 1206
Polyelectrolyte membrane elec polarization 3434
Polyelectrolyte pH polymer concn 3445
Polyelectrolyte transport phenomena 2286
Polyether macrocyclic complex 2152
Polyglutamate DMF thermal props 1081
Polyglutamate helix coil transition 3464
Polyisobutylene alkane soln 1206
Polyisobutylene solvent activity 1492
Polylysine proton transfer 1737
Polymer chlorophyll complex 172
Polymer concn pH polyelectrolyte 3445
Polymer glass statistical thermodn 416
Polymer molybdate ultrasonic attenuation 1575
Polymer soln convection cell 783
Polymer soln thermodynamics 1206 1214
Polymer solvent entropy mixing 400
Polymethacrylic acid conformation pH 2559
Polymg protein sedimentation equil 3429
Polymg system sedimentation equil 777
Polymn methacrylate photoinitiation EPR 3141
Polyoxyethylene glycol cond 1763
Polypeptide energy parameters 375
Polypeptide helix coil kinetics 1737
Polyphenyl absorption fluorescence 3983
Polyphosphate UV chain length 3673
Polypropylene oxide propane soln 1214
Polystyrene methyl acetate soln 1214
Polystyrene mol wt distribution 930
Polystyrene solvent activity 1492
Polystyrenesulfonate membrane elec polarization 3434
Polystyrenesulfonate osmotic property 1881
Polystyryl carbanion proton abstraction 695
Polyvinyl alc membrane elec polarization 3434
Polyvinylpyrrolidone membrane elec polarization 3434
Polyvinylpyrrolidone soln cond 1763
Polywater IR prepn polemic 456
Polywater org contaminant IR 457
Pore wedge shaped condensation 2543
Porous glass membrane potential 3633
Porous material hyperfiltration 4015
Porous silica surface charge 2547
Positronium atom reaction soln 1124
Positronium iodine reaction 1951
Potassium anion optical spectra 2975
Potassium bromide system diffusion 3419
Potassium chloride eutectic system 904
Potassium chloride transference no 712
Potassium conduction glass 1072
Potassium exchanged zeolite structure 650
Potassium halorhenate recoil reaction 2499
Potassium iodide viscosity solvents 434
Potassium lead thermodn 1202
Potassium nitrobenzene hexamethylphosphotriamide system 2058
Potassium perchlorate assocn water 2923
Potassium permanganate soln photoredn 2362
Potassium picrate soln cond 1049
Potassium salt anthracene IR Raman 1026
Potassium tin chloride complex 2796
Potential barrier rotation chloroethane 3591
Potential barrier rotation fluoronitrosomethane 3099
Potential dependent chronoamperometry 3254
Potential dipole polar gas 1470
Potential intermol liq 2133
Potential ionic vibration 2140
Potential model monat gas 1743
Potential vibration ionic polemic 1086
Powder ENDOR line shape 2079
Predissocn isocyanic acid polemic 2636
Pressure carbon monoxide oxidn 3527
Pressure effect complex soln 249
Pressure quenching methyl radical 2196
Pressure vol temp steam 2901
Propane hydroperoxy kinetics 1283
Propane nitrophenyl methyl radical 2479
Propane photolysis methylene prodn 9
Propane polypropylene oxide soln 1214
Propane vibrationally hot kinetics 607
Propanol hydration aq soln 1660
Propanol pulse radiolysis 3856
Propene exchange hydrogen zeolite 3940
Propene iodine hot atom reaction 3342
Propene radiolysis butane 1260
Propionitrile iodine complex 2098
Propionitrile thianthrene assocn 3468
Propyl fluoride tritium reactions 187
Propylene carbonate dielec property 2892
Propylene carbonate water solvation 855
Propylene hydrogenation isomerization intermediate 2184
Propylene hydrogenation rate 943
Protein polymg sedimentation equil 3429
Protein ultrasonic absorption 1737
Proton abstraction 695
Proton ENDOR zeolite 2087
Proton exchange chloranil hydrochloranil 246
Proton exchange mol diffusion 3078
Proton exchange naphthol excited 3558
Proton exchange rate water 2954
Proton hydrogen bromide reaction 1321
Proton magnetic relaxation butyrolactam 1973
Proton motion zeolite 1220
Proton spin decoupled relaxation 1152
Proton transfer benzoic acid 1327
Proton transfer hemoglobin 528
Proton transfer intramol 4033
Proton transfer isotope effect 2951
Protonated amyl acetate decompn 3917
Protonation carboxylate vol 2778
Protonation glycine radical 3507
Protonation radical 1957
Prototropism anthroate fluorescence 1996

Pulse irradiated acetone 26
Pulse radiolysis arom amine 20
Pulse radiolysis arom hydrocarbon 1119
Pulse radiolysis benzoic acid 1398
Pulse radiolysis benzoylpyridine 3200
Pulse radiolysis bromide oxidn 312
Pulse radiolysis dimethylaniline 3805
Pulse radiolysis dioxane water 1279
Pulse radiolysis ethanol propanol 3856
Pulse radiolysis excited state 2485
Pulse radiolysis ferroferricyanide 3703
Pulse radiolysis glycine radical reaction 3507
Pulse radiolysis halouracil 2386 2392
Pulse radiolysis hydrated electron 2072
Pulse radiolysis metaphosphate glass 203
Pulse radiolysis oxygen radical org 847
Pulse radiolysis polarog inorg radical 1487
Pulse radiolysis polaron yield 3776
Pulse radiolysis stilbene 3897
Purine hydroxide reaction kinetics 2838
Pyrene diethylaniline complex photolysis 1133
Pyridine adsorption nickel 972
Pyridine adsorption oxygen covered surface 571
Pyridine aminoethyl complex magnetic 2707

Pyridine benzoyl pulse radiolysis 3200
Pyridine copper complex structure 2887
Pyridine iodine complex formation 1951
Pyridine lithium halide complex 53
Pyridine phenol complex spectrum 2112
Pyridinecarboxaldehyde hydration 2959
Pyridinium iodide charge transfer 603
Pyrimidine photohydration viscosity effect 3137
Pyrolysis difluoroethane 1680
Pyrolysis kinetics hydrogen deuteride 3538
Pyrolytic graphite electrocapillarity 2750
Pyruvic acid ester iodination 3121
Quadrate energy level 3401
Quadrupolar dipolar NMR 53
Quadrupole coupling nitrogen diazirine 2249
Quantum efficiency fluorescence europium 1293
Quantum efficiency photoredn reaction 2362
Quantum mech tunneling 546
Quantum mech tunneling electron 2641
Quantum yields ethanethiol photolysis 2668
Quasireversible electrode reaction 1160
Quaternary ammonium bromide PMR 130
Quaternary ammonium bromide thermodn 1366
Quaternary ammonium molal vol 1333
Quaternary ammonium salt dielec 1999
Quaternary ammonium surfactant NMR 3012
Quenched gold catalytic activity 1907
Quenching benzene singlet olefin 3668
Quenching excited state fluorotoluene 2967
Quenching fluorescence electron transfer 469 3132
Quenching fluorescence naphthalene benzoic acid 3563
Quenching mercury aromatic compd 2665
Quenching platinum complex isomerization 3934
Quenching pressure methyl radical 2196
Quenching rate active nitrogen 1
Quinoline sensitizer hexaamminecobalt photodecompn 1105
Quinone furan emission spectra 2240
Racemization cobalt ethylenediamine complex 119
Radiation chemistry alc water 3842
Radiation chemistry carbon tetrahalides 3734
Radiation chemistry resonance effects 2726
Radiation damage DNA 3577
Radiation interaction electron attachment 3730
Radiationless transition europium 1293
Radiative pathway soln 1093
Radical acrylate ESR 1957
Radical alkyl electron scavenger 2848
Radical alkyl isomerization 2507
Radical anion cyclooctatetraene disproportionation 2176
Radical anion ESR 1439
Radical anion phenylacridine ESR 3958
Radical anion phenylbenzylidenemalononitrile ESR 3384
Radical anion sulfur dioxide 323
Radical benzoylpyridine UV 3200
Radical cation benzene ESR 3943
Radical cation formation toluene 1721
Radical cation methionine 1729
Radical cation prodn photoionization 639
Radical cation thianthrene 3468
Radical complex electronic absorption 1549
Radical concn solid irradn 1324
Radical cyanogen reaction 1931
Radical diffusion kinetics 3008
Radical ESR irradn aq soln 1706
Radical ethyl nitric oxide reaction 3303
Radical free gas spectroscopy 2056
Radical free model water radiolysis 2733
Radical heterocycle EPR 3348
Radical hydroperoxyl metal complexed 2207
Radical inclusion compd ESR 801
Radical inorg halfwave potential 1487
Radical ion recombination luminescence 3710
Radical ion sulfuric acid irradn 3676
Radical methyl quenching pressure 2196
Radical photochem azoisopropane 1669 1685
Radical photolysis UV 2061
Radical reaction glycine radiolysis 3507
Radical stabilization energy 918
Radical styrene polymn 930
Radical trapped paramagnetic relaxation 1226
Radical trapping nitromethane 1710
Radical trifluoromethyl lifetime 2517
Radical trifluoromethyl sorbed photoprodn 2690
Radical zwitterion ESR 2479
Radicals benzoic acid properties 1398
Radicals hydroxyl bromide oxidn 312
Radicals org ESR 553
Radioactive decay Poisson distribution 3603
Radiolysis alkane trapped electron 3847
Radiolysis aq cerium sulfate 1273
Radiolysis aq methane 3863
Radiolysis benzene ketones 198
Radiolysis benzyl chloride ethanol 3744
Radiolysis bromide 1815
Radiolysis Cerenkov reabsorption spectra 3780
Radiolysis dimethylamine trimethylamine 2857
Radiolysis fluoromethane 2070
Radiolysis geminate ion pairs 3812
Radiolysis glycine radical reaction 3507
Radiolysis hydrocarbon electron scavenging 987
Radiolysis hydrogen cyanide ESR 3945
Radiolysis liq methylpentane scavenger 2374
Radiolysis methylpentane liq scavenger 2381
Radiolysis nitric acid mechanism 2680
Radiolysis photolysis iodate 302
Radiolysis product sulfuric acid 3676
Radiolysis pulse arom amine 20
Radiolysis pulse benzoylpyridine 3200
Radiolysis pulse dioxane water 1279
Radiolysis pulse ethanol propanol 3856
Radiolysis pulse excited state 2485
Radiolysis pulse ferroferricyanide 3703
Radiolysis pulse halouracil 2386 2392
Radiolysis pulse hydrated electron 2072
Radiolysis pulse metaphosphate glass 203
Radiolysis pulse polaron yield 3776
Radiolysis silane ion reaction 3321
Radiolysis thiocyanate aq soln 1537
Radiolysis water free radical model 2733
Radiolysis water tritium beta 1542
Radiolytic product sodium bromate 3751
Raffinose ultrafiltration 238
Raman chloroethane 3591
Raman laser surface 2325
Raman magnesium nitrate water 1019
Raman matrix spectra zone 3208
Raman molten alkali carbonate 1565
Raman potassium salt anthracene 1026
Raman sodium ammonia 2481
Raman spectra cadmium halide melt 1831
Raman spectra chloride complex 2796
Raman spectra halophenylgermane 1558
Raman spectra nitrate carbon dioxide 1826
Raman spectra sulfate 3664
Raman spectroscopy zeolite synthesis 3388
Raman tetrafluoroberyllate molten fluoride 78
Raman water 1147
Range photoinjected electron liq 3794
Rate const hydrogen transfer 1581
Rate const termol reaction 3116
Rate consts relaxation spectra 366
Reaction diffusion limited viscosity 1192
Reaction ethyl radical nitric oxide 3303
Reaction hydroxyl polyat mol 1511
Reaction iodine ethanol 3314
Reaction ion mol gas ethane 3919
Reaction kinetics diffusion problem 349
Reaction kinetics oxygen argon 2653
Reaction kinetics purine hydroxide 2838
Reaction kinetics solid state 2253
Reaction order thermal curves 162
Reaction rate hydroperoxo hydrogen 1586
Reaction rate hydroxyl 1511
Reaction theory unimol 2418
Reactive scattering ion 3883
Reactivity solvated electron 2217
Reactor gas chromatog 2159
Rearrangement cyclobutanecarbonitrile 2817
Recoil chlorine cis trans olefin 2711
Recoil reaction mechanism 2499
Recoil reactions iodine 128 2685
Recoil tritium hexamethyldisilane 1249
Recoil tritium reactions 187 190
Recoiling reaction silicon 1352
Recombination ion triplet prodn 3801
Redn hexacyanochromate 2439
Redn kinetics carbon dioxide 3278
Redn methylene blue 3460
Redox hydrogen peroxide intermediate 2207
Redox mechanism ionic matrix 422
Reflection coeff rigid membrane 393
Refractive index ice 886
Relaxation bicipital equil reaction 452
Relaxation boron nitrogen borazole 2871
Relaxation carbon NMR isodurene 281
Relaxation cond electrolyte soln 3287
Relaxation dielec solute 525
Relaxation dielec water adsorption 2987
Relaxation fluorescence anthroate 1996
Relaxation methyl carbon 3213
Relaxation micelle dissoln kinetics 3017
Relaxation nuclear spin lattice 2079
Relaxation paramagnetic trapped radical 1226
Relaxation quadrupolar dipolar NMR 53
Relaxation spectra enzyme reactions 366
Relaxation spectra molybdate polymer 1575
Relaxation spin decoupled proton 1152
Relaxation time zeolite 1220
Relaxation ultrasonic calcium nitrate hydrate 1506 1507
Relaxation vibrational carbon dioxide 3108
Relaxation viscoelastic aq calcium nitrate 3495
Repulsive force ion soln 1062
Resistive effect electrochem cell 2550
Resonance cyclotron electron 3758
Resonance effects radiation chemistry 2726
Resonance energy free radical 918
Reverse osmosis rejection org solute 4006
Rhenate halo recoil reaction 2499
Rhodamine dye aggregation equil 762
Rhodium catalyst electron spectroscopy 2525
Rhodium photochem ligand field 1937
Rice Allnatt transport theory 2133
Rice Ramsperger Kassel theory 2418
Rigid membrane solute permeability 393
RNase light scattering 2744
Rodlike hydrodynamic macromol 1755
Rotation amide barrier 2178
Rotation barrier amide 642
Rotation barrier internal 551
Rotation barrier potential 3591
Rotation hindered sarcosinate 853
Rotation internal NMR 71
Rotation potential barrier fluoronitrosomethane 3099
Rotation restricted cytosine 64
Rotational conformation 501
Rotational correlation time nitroxide ESR 1858
Rotational model nitroxide 1858
Rotor overspeeding lysozyme sedimentation 2740
Rubrene electrochemiluminescence efficiency 1868
Rydberg aminoethylene spectrum 2105
Salt effect vol 2778
Salt pH polymer concn 3445
Salt rejection porous membrane 4015
Salt soly product 2024
Samarium fluorescence nonaq medium 3397
Saponification dimethyl glutarate kinetics 704
Sarcosinate hindered rotation 853
Satn recovery relaxation time 1152
Scattering elastic ion 3883
Scattering light mixt 2744
Scattering mol beam 2947
Scavenger electron alk glass irradn 1962
Scavenger electron alkyl radical 2848
Scavenger electron ethanol 3744
Scavenger methylpentane liq radiolysis 2374 2381
Scavenger naphthalene trapped electron 2641
Scavenging electron arom cyclohexane irradn 3722
Second virial coeff steam 2901
Secondary ion reaction 987
Sedimentation equil polymg protein 3429
Sedimentation equil polymg system 777
Sedimentation lysozyme overspeeding rotor 2740
Sedimentation methylene blue aggregation 4026
Segment rodlike macromol 1755
Selectivity ratio electrochem membrane 1872
Selenide bound exciton 3771
Semicond charge transfer complex 1849
Semiconductor surface electron transfer 2353
Sensitization platinum complex isomerization 3934
Sensitizing dye aggregation CD 2982
Shear viscosity isomeric hexane 3295
Shock tube hydrocarbon decompn 143
Shock wave decompn tetrafluoroethane 292
Shock wave oxidn 2833
Shock wave reactions 285
Silane deuterium atom reaction 3911
Silane diphenyl dialkoxy magnetochem 1579
Silane ethylethoxy hydrolysis 3192
Silane methyl mass spectrometry 3217
Silane phosphine reaction 1352
Silane radiolysis ion reaction 3321
Silanes methoxymethyl dielec relaxation 525
Silanes methyl decompn 459

Silica alumina dealkylation cumene 3741
Silica carbon tetrachloride interface 3192
Silica gel gamma irradiated 3158
Silica gel mercury contact angle 3267
Silica laser Raman 2325
Silica surface charge 2547
Silica surface hydroxy 1434
Silica water adsorption 3188
Silicon recoiling reaction 1352
Siloxane alkane soln 1206
Silver catalyzed epoxidation 213
Silver chloride ionization 2819
Silver electrode ion adsorption 2915
Silver iodide ice satn 2280
Silver lead arsine adsorption 2851
Silver nitrate water diffusion 1853
Silver oxide carbonate IR 940
Silver soly halide nitrate 2759
Silver sulfur dioxide interaction 1289
Silylmethane mol movement 4037
Singlet excited arom liqs 3867
Singlet excited lifetime alkylbenzene 3566
Singlet excited oxygen reaction 1375
Singlet phenylimidazole photocyclization 3362
Singlet quenching benzene olefin 3668
Singlet quenching fluorotoluene 2967
Singlet triplet dimethylaniline irradn 3805
Singlet triplet naphthalene irradn 2485
Singlet triplet stilbene irradn 3897
Soap film surface tension 3024
Sodalite solid ion exchange 1317
Sodium ammonia Raman 2481
Sodium anion optical spectra 2975
Sodium bromate defect formation 3751
Sodium chloride elec conductance 2294
Sodium chloride enthalpy transfer 3077
Sodium chloride helium soln 1195
Sodium chloride soln cond 1053
Sodium conduction glass 1072
Sodium diffusion coeff 3038
Sodium iodide viscosity solvents 434
Sodium magnesium chloride bromide 3474
Sodium magnesium chloride vol 3488 3491
Sodium neg ion formation 839
Sodium nitrate soln photoredn 2362
Sodium nitrobenzene hexamethylphosphotriamide system 2058
Sodium perchlorate methanol assocn 2920
Sodium polystyrenesulfonate membrane elec polarization 3434
Sodium salt density viscosity 3034
Sodium salt soln position lifetime 1124
Sodium salt solvation 2474
Sodium sulfate forms stability 737
Sodium sulfate ion pairing 3664
Sodium tetrabutylaluminate cyclohexane THF system 3472
Solid irradn radical concn 1324
Solid isotope exchange 1317
Solid solute entropy soln 2138
Solid state arom photoionization 2236
Solid state decompn kinetics 1474
Solid state photoactivation polaron 3366
Solid state reaction kinetics 2253
Solid surface wetting temp 3259
Soln aq structure 2045
Soln column activity gradient 1637
Soln complex pressure effect 249
Soln compressibility 2140
Soln cond polyvinylpyrrolidone 1763
Soln ion pair aggregation 2152
Soln ionic theory polemic 1229
Soln phenanthrenequinonesulfonate 1875
Soln polymer thermodynamics 1206 1214
Soln radiative pathway 1093
Soln statistical theory 3005
Soln tetrabutylammonium bromide thermodn 2582
Soln thermodn 4030
Soln thermodn chromatog 99
Solute hydrated dissoln lifetime 2017
Solute ionization equil 720
Solute macromol specific vol 2437
Solute permeability rigid membrane 393
Solvated electron absorption spectra 2931
Solvated electron electronic spectra 3691
Solvated electron glycerol spectra 1700
Solvated electron halide 3677
Solvated electron methanol water 3765
Solvated electron mol model 3714
Solvated electron optical spectra 2975 3876
Solvated electron polar mol 3824
Solvated electron reactivity 2217
Solvated electron sodium reaction 839
Solvation alc perchlorate cond 3029
Solvation dielec const assocn 2920
Solvation europium ion 1449
Solvation number ion 2140
Solvation sodium salt 2474
Solvation trityl ion 695
Solvation water propylene carbonate 855
Solvent activity polystyrene 1492
Solvent assocd electrolyte viscosity 434
Solvent dioxane water 1053
Solvent effect dimerization 446
Solvent effect nucleophile phenyl ester 432
Solvent effects acetophenone photoredn 821
Solvent fluorescence aminoethylene 2105
Solvent ion interaction 3472
Solvent liq crystal NMR 925
Solvent mixt anion exchange 1040
Solvent nonaq complex equil 3618
Solvent polymer entropy mixing 400
Solvent spectroscopy for UV 2703
Solvent transfer enthalpy 2045
Solvolysis reactions water 369
Soly fluoro detergents 909
Soly gas liq 598 601
Soly helium aq solns 3068
Soly helium water 1195
Soly hydrocarbon water bond 2754
Soly methanol gas 2170
Soly product salt 2024
Soly silver halide nitrate 2759

Sorbitol effect water 3077
Sorption complex ammonia zeolite 2597
Sorption complex sulfur zeolite 2601
Specific vol macromol solute 2437
Spectra emission furan quinone 2240
Spectra halogen charge transfer complex 3220
Spectra laser gas breakdown 31
Spectra phthalocyanine assocn 1994
Spectra relaxation enzyme reactions 366
Spectra thianthrene perchlorate assocn 3468
Spectral correlation charge transfer complex 3220
Spectral sensitizing dye CD 2982
Spectrometry mass chem ionization 3917
Spectrometry mass ethynyl radical 1913
Spectrophotometry aminopyridine iodine complex 1895
Spectrophotometry carbazole complex 2102
Spectroscopy alcs pulse radiolysis 3856
Spectroscopy electron rhodium catalyst 2525
Spectroscopy free radical gas 2056
Spectroscopy propionitrile iodine complex 2098
Spectrum donor acceptor complex 1982
Spectrum phenol alumina chemisorption 2882
Spectrum phenol pyridine complex 2112
Spectrum radiolysis hydrated electron 2072
Spectrum Rydberg aminoethylene 2105
Spherical core collision integral 1470
Spin adduct free radical trap 2056
Spin decoupled proton relaxation 1152
Spin density hydrated electron 3838
Spin forbidden predissocn polemic 2636
Spin lattice relaxation 2079
Spin orbit perturbation energy level 3401
Spiropentane tritium decompn isomerization 2187
Spiropyran photolysis merocyanine 3554
Stability Nernst Planck equation 2256
Stability sodium sulfate forms 737
Stability thermodn perylene complex 921
Stabilization energy free radical 918
Stable trifluoromethyl radical sorbed 2690
Stannic oxide electrode auramine 1655
State equation approx 1479
State equation hard sphere 601
State excited pulse radiolysis 2485
State photoactive hexacyanochromate 1947
Statistical theory soln 3005
Statistical thermodn polymer glass 416
Statistical thermodn water structure 3229
Steam second virial coeff 2901
Stereochem epoxidation olefins 213
Stereochem halogen substitution dichlorobutane 501
Stereochem methylene addn alkene 664
Steric effect butylethylene NMR 2877
Sterically hindered assocd alcs 864
Sticking coeff nitrogen zirconium 2156
Stilbene irradn triplet singlet 3897
Stimulated emission carbon monoxide 1429
Structure alkyl phosphonic acid 1298
Structure aq soln 2045
Structure cadmium halide melt 1831
Structure calcium binding mol 1304
Structure chromia 1838
Structure copper complex 2887
Structure deuterated ethanol soln 2562
Structure electrolyte soln 1062
Structure electronic furanquinones 2240
Structure liq theory alkali halide 1612
Structure neutralization polymethacrylic acid 2559
Structure nitroaniline 3597
Structure tetracyanomethane 3973
Structure thallium exchanged zeolite 2593
Structure water complex 3116
Structure water Dowex 50W 578
Structure water hard sphere solute 4030
Structure water IR 84
Structure water statistical thermodn 3229
Structure water tetraalkylammonium halide 1455
Structure zeolite 650 2597 2601
Structures theory hydrocarbon liq 731
Styrene irradn polymn 930
Styrene tetracyanobenzene complex 1419
Styrenesulfonic acid molar vol 3451
Substituent effect benzoquinone UV 2424
Substituent effect NMR arom 1593
Substituent effect NMR halobenzene 515
Substitution halogen dichlorobutane stereochem 501
Substitution nucleophilic bimol 232
Sucrose ultrafiltration 238
Sulfate cerium aq radiolysis 1273
Sulfate europium assocn thermodn 1887
Sulfate europium ion formation 2925
Sulfate iron aq radiolysis 1273
Sulfate sodium forms stability 737
Sulfate sulfuric acid radiolysis 1265
Sulfide boron vapor pressure 2035
Sulfide carbon anion radical 1706
Sulfide dimethyl photoelectron spectrum 1030
Sulfide hydrogen flame 1925
Sulfite thermal decompn 157
Sulfolane water assocn perchlorate 2923
Sulfonate perfluoro 909
Sulfonic acid naphthalene ionization 508
Sulfophthalocyanine vanadium soln 2343
Sulfoxide decompn free radical 135
Sulfur dioxide anion EPR 323
Sulfur dioxide photooxidn 814
Sulfur dioxide silver interaction 1289
Sulfur hexafluoride methylpentane radiolysis 2381
Sulfur Hueckel calcn 2274
Sulfur sorption complex zeolite 2601
Sulfur tetramer IR UV 3968
Sulfur trioxide anion radical 1706
Sulfur trioxide photoprodn 814
Sulfuric acid aq irradn 1265
Sulfuric acid beta irradn 1542
Sulfuric acid radiolysis product 3676
Superoxide oxygen peroxide reaction 2841
Surface area cavity solvent 2754
Surface area detn 2584
Surface area micelle shape 3020
Surface concns calcium hydroxylapatite 900
Surface energy alanine tetrapeptide 2793
Surface laser Raman 2325
Surface property chromia IR 571
Surface roughness contact angle 3267
Surface semiconductor electron transfer 2353
Surface tension charge pyrolytic graphite 2750
Surface tension soap film 3024
Surface tension surfactants 909
Surfactant hydrophile lipophile balance 2019
Surfactant micelle structure NMR 3012
Susceptibility magnetic copper complex 2707
Synthesis zeolite 3388
Tautomerism amino acid 4033
TCNQ charge transfer complex 1849
Telluric phosphoric acid reaction 3625
Telluride bound exciton 3771
Temp dependence paraffin irradn 3851
Temp effects intersystem crossing 1524
Temp gamma irradn soln 1273
Temp pressure vol steam 2901
Temp wetting solid surface 3259
Termol reaction water 3116
Ternary system diffusion coeff 3419
Tertiary ammonium salt IR 339
Tetraalkylammonium bromide heat soln 1369
Tetraalkylammonium halide extn 1775
Tetraalkylammonium halide water structure 1455
Tetraamylammonium bromide aq heat capacity 2577
Tetraamylammonium bromide soln conductance 1049
Tetrabutylaluminate sodium cyclohexane THF system 3472
Tetrabutylammonium bromide heat diln 3050
Tetrabutylammonium bromide soln 3068
Tetrabutylammonium bromide soln thermodn 2582
Tetrabutylammonium durosemiquinone ESR 1012
Tetracene perylene complex 1549

Tetrachloride carbon fluorine reaction 947
Tetracyanoethylene diene addn 106
Tetracyanomethane structure 3973
Tetrafluoroborate water structure 84
Tetrahydrofurans trapped electrons 636
Tetramethylphenylenediamine glass irradn 3894
Tetrapeptide alanine energy surface 2793
Tetraphenylborate adsorption mercury 707
Tetraphenylboride hydration 2454
Tetrazole nitrogen 14 NMR 2403
Thallium exchanged zeolite structure 2593
Thallium salt soln position lifetime 1124
Thallium voltammetry perchloric acid 976
Theory ionic soln polemic 1229
Theory unimol rate 342
Thermal catalytic oxidn 1807
Thermal cond monat gas 1743
Thermal decompn ammonium perchlorate 3545
Thermal decompn mechanism ESR 157
Thermal decompn ozonide 2659
Thermal isomerization energy transfer 1935
Thermal props polyglutamate DMF 1081
Thermal reactions 342
Thermal relaxation anthroate 1996
Thermal transition cholesteryl ester 3089
Thermally stimulated cond glass 2781
Thermochem Diels Alder 106
Thermodn acid base equil 1909
Thermodn aminopyridine iodine complex 1895
Thermodn antimony monophosphide 2336
Thermodn assocn europium sulfate 1887
Thermodn carbazole complex 2102
Thermodn ethylamine acetic acid 2764
Thermodn lead potassium 1202
Thermodn peroxide superoxide reaction 2841
Thermodn polyanion dye complex 688
Thermodn soln column 1637
Thermodn solvent transfer 2045
Thermodn stability perylene complex 921
Thermodn statistical polymer glass 416
Thermodynamics polymer soln 1214
Thermodynamics soln polymer 1206
Thermoemf cold worked gold 1907
Thermoluminescence arom hydrocarbon 3710
Thermolysis cyclobutanecarbonitrile 2817
THF alkane hyperfine coupling 2866
THF methyl paramagnetic relaxation 1226
THF sodium tetrabutylaluminate cyclohexane system 3472
Thianthrene adsorption oxide 1443
Thianthrene perchlorate assocn spectra 3468
Thiazoline hydrolysis 1192
Thioamide iodine charge transfer 2405
Thiobenzophenone electrochem 1650
Thiocyanate aq soln radiolysis 1537
Thiocyanate butyl radical interaction 1792
Thiooxalato nitrosyl iron ESR 49
Thiooxamide rotation barrier 642
Thiophenol photoelectron spectrum 1030
Thiourea diphenyl iodine complex 2405
Third law thermodn sodium sulfate 737
Threshold energy chloroethane elimination 283
Thymine photolysis 489
Tin chloride samarium fluorescence 3397
Tin potassium chloride complex 2796
Tin salt soln position lifetime 1124
Tin 3 ESR 141
Titanium oxide methylene blue redn 3460
Titrn ethylene copolymer 1767
Toluene autoxidn cobalt catalyzed 1520
Toluene fluoro excited state quenching 2967
Toluene radical cation formation 1721
Toluenethiol photoelectron spectrum 1030
Torsional frequency hydrogen bond 1553
Tracer diffusion liq system 2572
Trans cis olefin recoil chlorine 2711
Transfer diffusion 162
Transfer diffusion exchange bromide 2957
Transfer electron semiconductor surface 2353
Transfer number cond hydroxide 2954
Transfer proton acid benzoic 1327
Transfer proton intramol 4033
Transference concn cell 1758
Transference no potassium chloride 712
Transformation kinetics cholesteryl nonanoate 276
Transition ethylene 1130
Transition helix coil polyglutamate 3464
Transition mesophase forming system 2605
Transition metal diat mol 2268
Transition org solid 2798 2799
Transition phase methylsilylmethane 4037
Transition thermal cholesteryl ester 3089
Transmission ellipsometry thin layer 3390
Transport mode melt 1348
Transport phenomena polyelectrolyte 2286
Transport property polar gas 1470
Transport props chloride system 904
Transport theory Rice Allnatt 2133
Trapped electron absorption spectra 3847
Trapped electron decay methylpentane 3167
Trapped electron decay tunneling 2641
Trapped electron electronic spectra 3683
Trapped electron matrix 3830
Trapped electron methylpentane glass 3747
Trapped electron methylpentane photobleaching 2341
Trapped electron methyltetrahydrofuran 636
Trapped electron solid state excitation 3366
Trapped radical paramagnetic relaxation 1226
Trapping electron radiation chemistry 2726
Trifluoroacetic acid assocn 2039
Trifluoroacetic acid thianthrene assocn 3468
Trifluoromethanesulfonic ESR dibenzodioxin 1504
Trifluoromethyl benzene photochem 823
Trifluoromethyl radical lifetime 2517
Trifluoromethyl radical photoprodn sorbed 2690
Trigonal bipyramid crystal field 2907
Triiodomethyl radical matrix IR 2718
Trimethylaluminum dimer heat dissocn 2933
Trimethylaminium ion EPR 2857
Trioxide sulfur photoprodn 814
Triphenylacetate decompn 937
Triphenylene perhydro trapped heptanal 1008
Triplet absorption phthalazine 3937
Triplet biphenylene 225
Triplet energy path 478
Triplet methylene prodn 1389
Triplet nitrene ESR 3570
Triplet prodn ion recombination 3801
Triplet quenching fluorotoluene 2967
Triplet singlet dimethylaniline irradn 3805
Triplet singlet naphthalene irradn 2485
Triplet singlet stilbene irradn 3897
Triplet yield complex photolysis 1133
Tritium beta water radiolysis 1542
Tritium reaction butane 2937 2939
Tritium recoil hexamethyldisilane 1249
Tritium recoil reactions 187 190
Tritium spiropentane decompn isomerization 2187
Trityl ion solvation 695
Tungsten fluorination analysis polemic 2930
Tungsten fluorination model analysis 2930
Tungsten oxidn nitrous oxide 2530
Tungsten oxygen bromine reaction 320
Tungsten palladium arsine adsorption 2851
Tungsten surface ammonia decompn 970
Two body diffusion problem 349
Ultrafiltration anisotropic membrane 238
Ultrasonic absorption polyamine 334
Ultrasonic absorption protein 1737
Ultrasonic relaxation calcium nitrate hydrate 1506 1507
Ultrasound absorption dioxane water 1571
Ultrasound mech property liq crystal 2409
Ultrasound viscoelastic relaxation 3495
Unimol cyclopropane isomerization 1695
Unimol decompn tritium spiropentane 2187
Unimol rate theory 342
Unimol reaction theory 2418
Uracil halo irradn ESR 2399
Uranium oxide gaseous IR 648
Uranyl irradn fluorescence 3698
Urea clathrate Palmitic acid 801
Urea soln tetraalkylammonium bromide 1369
Urea vol guanidine hydrochloride 2778
UV actinometer photolysis ethylene 138
UV aminopyridine iodine complex 1895
UV benzoquinone substituent effect 2424
UV benzoylpyridine radical 3200
UV bromine mol 1017
UV copper halide vapor 1632
UV ethylene phenyl radical 3960
UV europium sulfate 1887
UV for solvent spectroscopy 2703
UV ionization photolysis 2061
UV photolysis cyclohexanone 615
UV photolysis formatopentaamminecobalt 2492
UV photolysis methylenecyclopropane 3153
UV polyphosphate chain length 3673
UV sulfur tetramer 3968
Vacuum UV photolysis methylenecyclopropane 3153
Valence isomerization trifluoromethylbenzene 823
Van der Waals equation 2014
Vanadium deuterium x ray 927
Vanadium monomer dimer equil 2343
Vanadium oxide photodissocn hydrogen 2637
Vanadyl hydroxy carboxylate EPR 3951
Vanadyl phthalocyanine assocn 1994
Vapor adsorption 3412 3415
Vapor deposition alkali nitrate 3093
Vapor nuclei melt 2609
Vapor pressure boron sulfide 2035
Vapor pressure isotope effect 743 3040
Vapor pressure polymer soln 1214
Vaporization copper iodide mass spectrometry 2310
Vaporization cuprous bromide 3271
Vaporization dissocn enthalpy dimer 2933
Vaporization kinetics liq 914
Vibration hydrogen cyanide polemic 2483
Vibration potential ionic 2140
Vibration potential ionic polemic 1086
Vibrational analysis zone 3208
Vibrational model matrix IR 454
Vibrational relaxation carbon dioxide 3108
Vinyl acetate elec conductivity 115
Vinyl methyl ether copolymer 254
Violene radical ion 701
Virial coeff monat gas 1743
Virial coeff second steam 2901
Viscoelastic relaxation aq calcium nitrate 3495
Viscosities intrinsic albumin 128
Viscosity alkylammonium bromide soln 1902
Viscosity density sodium salt 3034
Viscosity diffusion limited reaction 1192
Viscosity effect photohydration pyrimidine 3137
Viscosity electrolyte assocd solvent 434
Viscosity ion recombination kinetic 1184
Viscosity kinematic isomeric hexane 3295
Viscosity macromol 1755
Viscosity monat gas 1743
Viscosity ternary liq system 2572
Viscous flow org liq 2317
Vol ionic assocn reaction 895
Vol molal ionic polemic 1086
Vol molal org aq soln 1343
Vol partial molal electrolyte 1333
Vol pressure temp steam 2901
Vol specific macromol solute 2437
Vol urea guanidine hydrochloride 2778
Voltammetry adsorption effect 976
Vycor glass gamma irradiated 3158
Water acetone complex polemic 452
Water acetone IR complex 449
Water adsorption lysozyme 2987
Water adsorption oxygen covered surface 571
Water adsorption silica 3188
Water anomalous contaminant IR 457
Water anomalous IR polemic 456
Water carbon dioxide relaxation 3108
Water dichlorotetrafluoroacetone polyglutamate 3464
Water dioxane pulse radiolysis 1279
Water dioxane solvent 1053
Water dioxane ultrasound absorption 1571
Water gas interface adsorption 2769
Water heavy water transfer 2045
Water hydrated electron 3905
Water hydrocarbon soly bond 2754
Water hydrogen irradn exchange 621
Water interfacial exchange polemic 1505
Water ion product const 90
Water IR hydrogen bonding 1228
Water IR monodeuterated polemic 3675
Water irradn energy transfer 3698
Water Kerr const temp 216
Water lithium iodide dissoln 2017
Water magnesium nitrate Raman 1019
Water mannitol sorbitol effect 3077
Water methanol solvated electron 3765
Water oil microemulsion 876
Water photolysis 298
Water photolysis UV 2061
Water polaron pulse radiolysis 3776
Water proton exchange rate 2954
Water radiolysis free radical model 2733
Water radiolysis tritium beta 1542
Water Raman 1147
Water silver nitrate diffusion 1853
Water solvation propylene carbonate 855
Water structure Dowex 50W 578
Water structure hard sphere solute 4030
Water structure IR 84
Water structure statistical thermodn 3229
Water structure tetraalkylammonium halide 1455
Water structure tetrabutylammonium bromide 2582
Water sulfolane assocn perchlorate 2923
Water termol reaction 3116

Water vapor adsorption 2280
Wave function electronic configuration 3401
Wenzel relation contact angle 3267
Wetting solid surface temp 3259
X ray diffraction polyacrylate 1311
X ray emission phosphorus oxyanion 3975
X ray hot atom chemistry 2639
X ray vanadium deuterium 927
Xanthene dye aggregation equil 762
Xenon nitrogen leghemoglobin 591
Xenon trioxide gamma irradn 3909
Xylene effect alkylbenzene luminescence 3566
Xylene thermodn props 731
Yield excitation naphthalene irradn 2485
Yield polaron pulse radiolysis 3776
Yields nitric acid radiolysis 2680
Yields quantum ethanethiol photolysis 2668
Zeolite active site 110
Zeolite ammoniated irradn EPR 2716
Zeolite copper amine complex EPR 2860
Zeolite copper nitric oxide 1546
Zeolite exchange hydrogen propene 3940
Zeolite nitrous oxide IR 945
Zeolite proton ENDOR 2087
Zeolite proton motion 1220
Zeolite structure 650 2597 2601
Zeolite synthesis 3388
Zeolite thallium exchanged structure 2593
Zeolite trifluoromethyl radical sorbed 2690
Zinc chloride eutectic system 904
Zinc oxide deuteration catalysis 2184
Zinc oxide iodomethane adsorption 2353
Zinc oxide oxygen adsorption 3184
Zinc oxide photocatalytic reactions 1394
Zinc oxide powder ESR 2527
Zinc oxide promoted photoredn 2362
Zinc phthalocyanine assocn 1994
Zinc salt soln position lifetime 1124
Zirconium nitrogen reaction 2156
Zirconium oxide heat immersion 1497
Zirconium oxygen bubble nucleation 2609
Zone argon matrix spectra 3208
Zwitterion radical ESR 2479
Zwitterionic micellar arom soln 1460

Here is the ideal way to obtain the ***most reliable reference data available today!*** *All you need is a subscription to the new*

JOURNAL OF PHYSICAL AND CHEMICAL REFERENCE DATA

published by the American Chemical Society and the American Institute of Physics for the National Bureau of Standards.

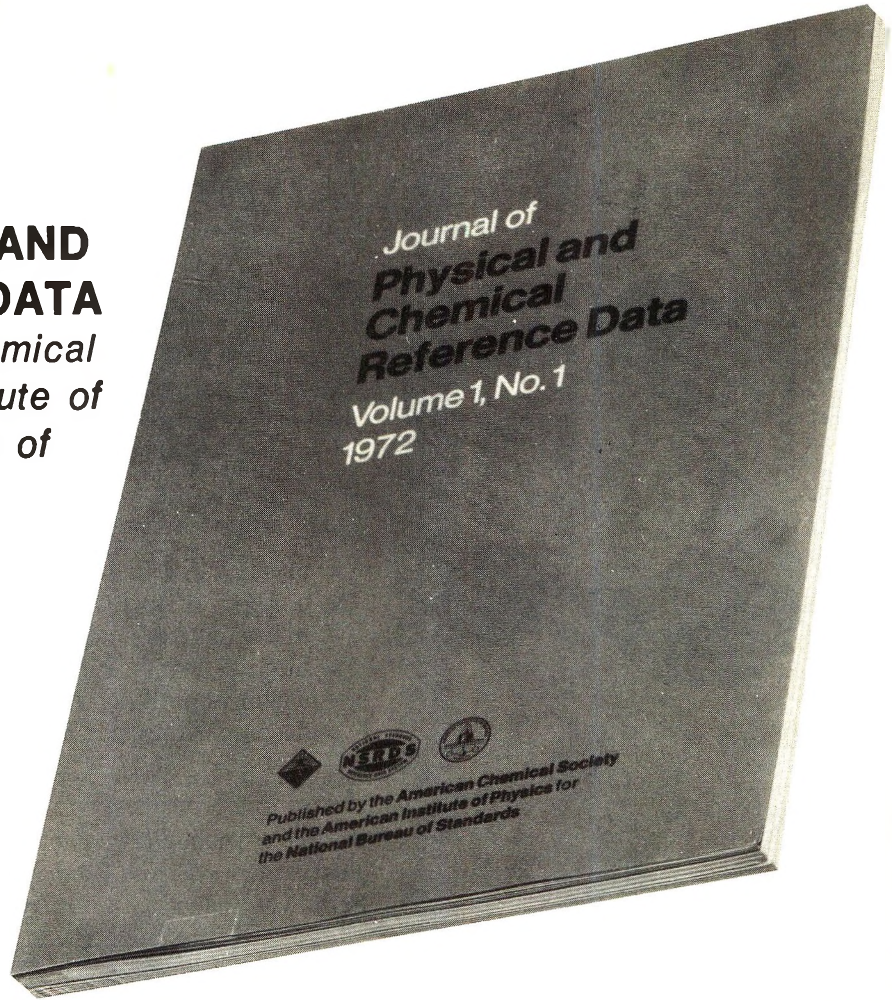
Journal of
Physical and
Chemical
Reference Data
Volume 1, No. 1
1972
NSRDS
Published by the American Chemical Society
and the American Institute of Physics for
the National Bureau of Standards

The *Journal of Physical and Chemical Reference Data* fills an important gap in the literature of the physical sciences. Its subject matter is the quantitative numerical data of physics and chemistry. As the new publication vehicle of the National Standard Reference Data System, the *Journal* will contain carefully evaluated data, with recommended values and uncertainty limits chosen by experts in each field. Critical commentary on methods of measurement and sources of error, as well as full references to the original literature, will be an integral part of each compilation.

Examples of some of the critical compilations scheduled for publication in the four issues of Volume I (1972) include:

- Tables of Molecular Vibrational Frequencies, Part 5, T. Shimanouchi
- Gaseous Diffusion Coefficients, by T. R. Marrero and E. A. Mason
- The Spectrum of Molecular Oxygen, by P. Krupenie
- Thermal Conductivity of the Elements, by C. Y. Ho, R. W. Powell and P. E. Liley
- Selected Values of Critical Supersaturation for Nucleation of Liquids from the Vapor, by G. M. Pound
- Gas Phase Reaction Kinetics of the Hydroxyl Radical, by W. E. Wilson, Jr.
- Selected Values of Heats of Combustion and Heats of Formation of Organic Compounds Containing the Elements CHNOPS, by E. S. Domalski
- Microwave Spectra of Molecules of Astrophysical Interest: Formaldehyde, Formamide, Thio-Formaldehyde, by D. R. Johnson, F. J. Lovas and W. H. Kirchhoff

Future compilations are expected to cover areas such as the following:

Band gaps in semiconductors
Nuclear moments
Atomic energy levels and transition probabilities
Diffusion in metals
Electron swarm data
Elastic constants of metals
Surface tension of liquids
Properties of molten salts
Activity coefficients of electrolytes
Equation of state of atmospheric gases
Ionization and appearance potentials

The *Journal of Physical and Chemical Reference Data* is intended to be a definitive source of reliable data on physical and chemical properties. Just fill in the order form at the bottom of this page to receive this invaluable reference source.

JOURNAL OF PHYSICAL AND CHEMICAL REFERENCE DATA
AMERICAN CHEMICAL SOCIETY
1155 Sixteenth Street, N.W.
Washington, D.C. 20036

Yes, I would like to receive the JOURNAL OF PHYSICAL AND CHEMICAL REFERENCE DATA at the one-year rate checked below:

	U.S.	Canada	PUAS	Other Countries
AIP and ACS members	$20.00	$20.00	$23.00	$23.00
Nonmembers	$60.00	$60.00	$63.00	$63.00

Bill me ☐ Bill company ☐ Payment enclosed ☐

Name ____________________

Street ____________ Home ☐ Business ☐ ____________

City ____________ State ________ Zip ________

JP 72

Nonequilibrium Systems In Natural Water Chemistry

ADVANCES IN CHEMISTRY
SERIES No. 106

Thirteen papers from a symposium by the Division of Water, Air, and Waste Chemistry of the American Chemical Society, chaired by J. D. Hem.

Which is more important: efficient exploitation of our natural resources or a stable ecosystem? What is the relationship between a wide variety of life forms and a healthy environment? What do geology and groundwater flow patterns have to do with the chemical composition of water? How may one predict when a lake will reach equilibrium or tell how long it has supported life?

This volume features:

- principles of water pollution control
- methods of analysis for dissolved chemicals
- mathematical models
- discussion of stratified lakes
- chemical processes in a carbonate aquifer
- decomposition and racemization of amino acids

342 pages with index Cloth (1971) $11.00
Postpaid in U.S. and Canada; plus 40 cents elsewhere.
Set of L.C. cards with library orders upon request.

Other books in the ADVANCES IN CHEMISTRY SERIES on water chemistry include:

No. 105 Anaerobic Biological Treatment Processes
Nine papers survey the state of the art of this natural process for waste treatment, with three papers on methane fermentation, others on process control and design. Considers volatile acid formation, toxicity, synergism, antagonism, pH control, heavy metals, light metal cations.
196 pages with index Cloth (1971) $9.00

No. 79 Adsorption from Aqueous Solution
Fifteen papers discuss thermodynamic and kinetic aspects of adsorption phenomena and the results of studies on a variety of adsorbate-adsorbent systems.
212 pages with index Cloth (1968) $10.00

No. 73 Trace Inorganics in Water
Research reports; analytical developments including atomic absorption, flame emission, and neutron activation; and broad reviews, such as effects of trace inorganics on the ice-water system and the role of hydrous manganese and iron oxides on fixing metals in soils and sediments.
396 pages with index Cloth (1968) $12.50

No. 67 Equilibrium Concepts in Natural Water Systems
Sixteen papers represent the collaboration of aquatic chemists, analytical chemists, geologists, oceanographers, limnologists, and sanitary engineers, working with simplified models to produce fruitful generalizations and valuable insights into the factors that control the chemistry of natural systems.
344 pages with index Cloth (1967) $11.00

No. 38 Saline Water Conversion—II
Fourteen papers from two symposia; includes recovery of minerals from sea water, minimizing scale formation, wiped thinfilm distillation, diffusion still, solar flash evaporation, osmosis, electrodialysis (3 paper), research in Israel, hydrate process.
199 pages Paper (1963) $8.00

No. 27 Saline Water Conversion
Thermodynamics of desalting, solvent extraction, freezing, centrifugal phase barrier recompression distillation, multistage flash evaporation, ion exchange, osmosis, and electrochemical demineralization.
246 pages Paper (1960) $9.00

Order from: **Special Issues Sales, American Chemical Society**
1155 Sixteenth St., N.W., Washington, D.C. 20036

what's happening

on the frontiers

of chemical research?

ACCOUNTS OF CHEMICAL RESEARCH LETS YOU KNOW...

in short, critical articles

that cover all areas *of*

chemical research.

Whether you are a practicing chemist, professor or student, you want to keep up with the latest developments. Yet few of you have the time to read thoroughly all the journals of primary publications. ACCOUNTS fills the gap.

Written by investigators active in the fields reviewed, ACCOUNTS' concise, brief articles place recent developments in perspective—and relate them to earlier work and their probable future significance.

Once you start relying on ACCOUNTS to keep you informed, you'll wonder how you got along without its monthly arrival.

Complete and mail back the form below. We'll prove how valuable this publication can be to you.

American Chemical Society / 1155 Sixteenth Street, N.W., Washington, D.C. 20036

Please send me ACCOUNTS OF CHEMICAL RESEARCH at the following subscription rates:

ACS members:	☐ U.S. $ 5.00	☐ Canada, PUAS $ 9.00	☐ Other Nations $10.00
Nonmembers:	☐ U.S. $15.00	☐ Canada, PUAS $19.00	☐ Other Nations $20.00

Name ____________________ Title ____________________

Employer ____________________

Address: ☐ Home ☐ Business ____________________

City ____________________ State/Country ____________________ Zip ________

Nature of employer's business? ☐ Manufacturing or processing ☐ Academic ☐ Government

☐ Other ____________________

(Please indicate)

Note: Subscriptions at ACS Member Rates are for personal use only.

☐ I am an ACS member ☐ I am not an ACS member

Payment must be made in U.S. currency, by international money order, UNESCO coupons, U.S. bank draft; or order through your book dealer.

Need to know about…

The most advanced theory?

Then read such articles as: "Relation between Structure and Retention Time of Sterols in Gas Chromatography" and "Ion Association between Indicators and Indifferent Electrolytes".

The latest applications?

Then read such articles as: "Gas Chromatography of Volatiles from Breath and Urine" and "Identification of Dangerous Drugs by Isobutane Chemical Ionization Mass Spectrometry".

Newest chemicals and reagents?

Then read such articles as: "Clinical Test Kits for Enzymes, Phosphorus and Calcium Determinations, Narcotics Detection, Mercury and Lead Determinations" and "Ultrapure Chemicals: Enzymes, Refractory Metals, Organics, Other Metals".

All are found in ANALYTICAL CHEMISTRY.

Each month you receive information that is fresh, current and relevant to your needs. Brand new ideas are introduced. One of them might be the answer to one of your problems.

Two other good reasons for starting your ANALYTICAL CHEMISTRY subscription now are the 1971-72 LABORATORY GUIDE to Instruments, Equipment and Chemicals and the valuable ANNUAL REVIEWS issue.

The 500-page LABORATORY GUIDE gives you 20,000 separate entries with more than 1000 manufacturers selling over 600 products.

The special ANNUAL REVIEWS issue presents authoritative researchers reviewing the latest methodology and applications of analytical chemistry.

ANALYTICAL CHEMISTRY

American Chemical Society / 1155 Sixteenth Street, N.W., Washington, D.C. 20036

Please send me ANALYTICAL CHEMISTRY at the following subscription rate:

ACS members:	☐ U.S. $5.00	☐ Canada $ 9.00	☐ PUAS $ 9.00	☐ Other Nations $10.00
Nonmembers:	☐ U.S. $7.00	☐ Canada $11.00	☐ PUAS $19.00	☐ Other Nations $20.00

Note: Subscriptions at ACS Member Rates are for personal use only.

NAME ____________________ POSITION ____________________

ADDRESS ____

CITY ____________________ STATE/COUNTRY ____________________ ZIP __________

YOUR COMPANY ____________________ NATURE OF COMPANY'S BUSINESS ____________________

☐ **I am an ACS member** ☐ **I am not an ACS member** ☐ **Bill me for $**__________

☐ Payment enclosed in the amount of $__________ (payable to American Chemical Society)